CORRELATIONS BETWEEN COMPRESSIVE, FLEXURAL, AND TENSILE BEHAVIOR OF SELF-CONSOLIDATING FIBER REINFORCED CONCRETE

BY

Waleed Tameemi

Submitted to the graduate degree program in Civil Engineering
and the Graduate Faculty of the University of Kansas in partial fulfillment
of the requirements for the degree of MASTER OF SCIENCE (Civil Engineering).

_____
Chairperson

_____

_____

_____

_____
Committee Members

Date Defended: _____

The Thesis Committee for Waleed Tameemi
certifies that this is the approved version of the following thesis:

CORRELATIONS BETWEEN COMPRESSIVE, FLEXURAL, AND TENSILE BEHAVIOR OF SELF-CONSOLIDATING FIBER REINFORCED CONCRETE

_____
Chairperson

Date approved: _____

ABSTRACT

Self-consolidating fiber reinforced concrete (SCFRC) is a hybrid concrete that is both self-compacting and fiber reinforced. Use of SCFRC in reinforced concrete members has been shown to result in improved behavior under shear, flexure, and compression relative to conventional reinforced concrete.

The aim of this study was to investigate relationships between the compressive and tensile responses of SCFRC as well as relationships between measured compressive and flexural behavior. Such relationships would simplify characterization of the mechanical behavior of SCFRCs based on a relatively limited number of standard tests. A secondary objective was to quantify and report the effect of introducing different volume fractions of four types of steel fiber to SCCs with compressive strengths of 6 and 10 ksi. Four different hooked-end steel fibers were used in this study at volume fractions between 0.5% and 1.5%.

Results showed that the post-peak slope in compression and the post-cracking flexural and tensile strengths all increased as fiber volume fraction increased, whereas properties up to development of cracking (or peak strength in the case of compression) were not affected by use of fibers. Among the parameters investigated, it was shown that the post-peak compressive response was most closely correlated with the post-crack peak strength in flexure and the flexural strength corresponding to a mid-span deflection of 0.04 in. It was also found that the within-batch coefficient of variation of post-crack peak tensile and flexural loads decreased significantly when T_{50} was at least 1.0 second, from an average of 40% to 13%. Of the fibers investigated, the RC-80/30-BP had the greatest impact on mechanical performance for a given volume fraction and the 3D RC-55/30-BG fiber had the least.

To my parents, Ali and Inam

Thank you for your never-ending understanding and pulling me through the most difficult times

To whom I owe so much

My lovely wife Afnan and my daughter Rahf for their infinite love and support

Thank you for always being there for me

To my brother Khalid and my sisters

To other family and friends

Thank you for always giving me your love and support

ACKNOWLEDGEMENTS

First of all, I would like to express my deepest gratitude to the Almighty God for giving me strength to carry out this research. I want to express my sincere gratitude to my advisor and my Master's committee chair Dr. Rémy Lequesne for his continued knowledgeable advising, contributing to my learning experience, and encouraging me throughout this research. I would like to specially thank the other two members of my Master's committee: David Darwin and Andres Lepage, for their much-appreciated help in supporting, guiding and instructing me during this project, as well as my years of study at the University of Kansas.

I would like to thank all other faculty members and staff of the Department of Civil Engineering for their contributions and encouragement. I acknowledge David Woody, Matthew Maksimowicz and all people who helped during the research at KU Lab for their labor and technical assistance. I would like to thank all the people who contributed to the development of this research. To my classmates for giving me hope and cheering me up in the bad times. I give thanks to the Higher Committee for Education Development in Iraq for providing me this scholarship. I acknowledge BEKAERT Corporation, Midwest Concrete Material, Grace Chemical, and Gerdau for donating materials used in this study. The opinions expressed in this report are those of the authors and do not necessarily represent the views of the sponsors.

TABLE OF CONTENTS

LIST OF TABLES

LIST OF FIGURES

CHAPTER 1: INTRODUCTION

1.0 – General

Reinforced concrete is the number one structural material in the world with billions of tons of annual production. It is used to construct the majority of infrastructure, including bridges, dams, and power plants. Concrete has excellent compression strength, but its tensile strength is much lower. Commonly, reinforcing steel (steel rods) are used to reinforce members where tensile strength is required. Unfortunately, there are issues associated with reinforcing steel use such as installation time, construction cost, corrosion and reinforcement congestion. Steel fibers, when used as a partial replacement for ordinary reinforcement, can simplify construction. Use of steel fiber reinforced concrete (SFRC) as a replacement for wire mesh or non-structural steel reinforcing bars is increasingly common because SFRC reduces the construction time and produces concrete with fewer or no visible cracks (Vondran, 1991; Hockenberry & Lopez, 2012).

In addition to improved constructability, use of fiber reinforced concrete (FRC) can improve the behavior of structural members. Steel fibers have been shown to improve the behavior of concrete under shear, tension, flexure, and compression stresses. In addition, adding fiber to concrete improves the bond between concrete and reinforcing steel under cyclic loading (Hota, 1997; Otter & Naaman, 1988; Mindess, 1995).

Unfortunately, introducing fibers to conventional concrete reduces its workability, which is considered a barrier to use in practice (Liao, Chao, Park, & Naaman, 2006). This can be overcome by using self-consolidating concrete (SCC) instead of ordinary concrete as the base for FRC. Self-consolidating fiber reinforced concrete (SCFRC) combines the properties of self-consolidating concrete (SCC) with the characteristics of FRC (Liao, Chao, Park, & Naaman,

2006). SCFRC has a considerably flowable, non-segregating cement-based matrix. It spreads into place, fills the formwork, and flows around the reinforcing steel without need for mechanical consolidation in typical concrete structures (ACI Committee 237, 2007). SCFRC has been used in several applications, including, precast concrete, dams, bridges, industrial floors, deep foundations, and structures designed to resist seismic demands.

1.1 – Research Objectives

The aim of this study was to develop relationships between compression test results (compression stress vs. longitudinal strain) and tensile test results (tensile stress vs. crack width) as well as relationships between results from compression and flexural tests (flexural load vs. mid-span net deflection). These relationships would make it easier for engineers to characterize the mechanical behavior of SCFRC for modeling or design based on a relatively limited number of standard tests. A secondary objective was to quantify and report the effect of introducing different volume fractions of four types of steel fiber to SCCs with compressive strengths of 6 and 10 ksi.

1.2 – Scope

The behavior of SCFRC with different volume fractions (0, 0.5, 0.75, 1.0, and 1.5%) of four types of hooked end steel fibers was tested under compression, flexure, and tension and the results are reported. Reported properties include compression strength, modulus of elasticity, post-peak slope, compression stress-longitudinal strain behavior, and compression stress-lateral strain response. Flexural strength, flexural load-crack width behavior, flexural load-net deflection behavior, flexural load-support rotation behavior, tensile strength, and tensile stress-crack width behavior are also reported. Fresh-state properties of the SCFRC, including slump flow, visual

stability index, T_{50}, J-ring slump flow, concrete density, and air content were also documented and are reported. Preliminary analyses are presented that were aimed at relating the post-peak slope in compression to key features of the measured tensile and flexural responses.

1.3 – Hypothesis

Because concrete cylinders often fail as a result of splitting cracks, the resistance provided by fibers to crack opening can improve the post-peak response of concrete cylinders under compression. It is therefore expected that the post-peak response of SCFRC in compression can be related to the tensile stress-crack opening behavior and flexural response of the SCFRC.

Based on previous work, it is expected that introducing fibers to SCC will reduce the workability, flowability, and the passability of SCFRC. Addition of fibers is not likely to affect the mechanical properties before cracking occurs, but it is expected to increase the concrete toughness after cracking. Improvements in the strength, toughness, and cracking behavior are expected to be linked to increases in the fiber volume fraction and aspect ratio.

1.4 – Research Significance

To facilitate the use of FRC in design, there is a need for simple and robust methods for characterizing the response of the material to stress. If successful, this study will provide a means of relating the post-peak compressive response of FRC, which is difficult to measure, to the measured response of FRC in tensile or flexural tests, which are relatively easy to conduct. The aim is a significant simplification of the testing required to characterize the mechanical behavior of a particular FRC. In addition, the current study will provided detailed data regarding the effect of different volume fractions of various types of hooked end steel fibers on the properties of freshly

mixed SCFRC (workability, flowabilty, stability, and passability) as well as the mechanical and physical properties (toughness, ductility, and cracking behavior).

1.5 – Organization of Thesis

This thesis has six chapters and four appendices. The first chapter describes the topic and motivation for the study of SCFRC. The second chapter summarizes a brief review of the related literature that provides a basis for the presented study. The third chapter describes the experimental program with details of material properties, mixture proportions, mixing procedures, specimen construction, and test methods. Chapter Four reports the properties of freshly mixed concrete such as slump flow, visual stability index, T_{50}, J-ring slump flow, concrete density, and air content. In addition, the results of compression, tensile, and flexure tests are reported in Chapter Four. Chapter five presents an analysis of the test results. A summary and conclusions are described in chapter six. Detailed test results are presented in the Appendices.

CHAPTER 2: LITERATURE REVIEW

2.0 – Introduction

This chapter offers an overview of previous studies on self-consolidating fiber reinforced concrete (SCFRC). A brief review of the history, advances, and applications of SCFRC are presented in the chapter. This section gives an overview of the properties of freshly mixed SCFRC, and summarizes the mechanical characteristics of the material.

2.1 – History

2.1.1 – History of Fiber Reinforced Concrete

Use of fibers in construction is not a recent breakthrough. Egyptians and Babylonians used straw as reinforcement in adobe bricks (ACI Committee 544, 1996). In 1874, metallic waste was added to concrete as reinforcement (Minelli, 2005) and asbestos strips were used in concrete in the 1900s. However, fiber reinforced concrete (FRC) did not become a focus of the research community until the 1950s. By the 1960s, FRC with glass, synthetic, and steel fibers had been tested. In that decade, straight steel fiber was first used to reinforce mortar and plain concrete (Balaguru & Shah, 1992). In the second half of the 1970s, the European market started producing steel fiber reinforced concrete (SFRC), but there were no recommendations or standards for their use by engineers. Partially due to the lack of standards, adoption of SFRC by the market has been slow (Ross, 2008). Figure 2.1 illustrates the timeline of design and test methods that have been adopted for FRC (Ross, 2008).

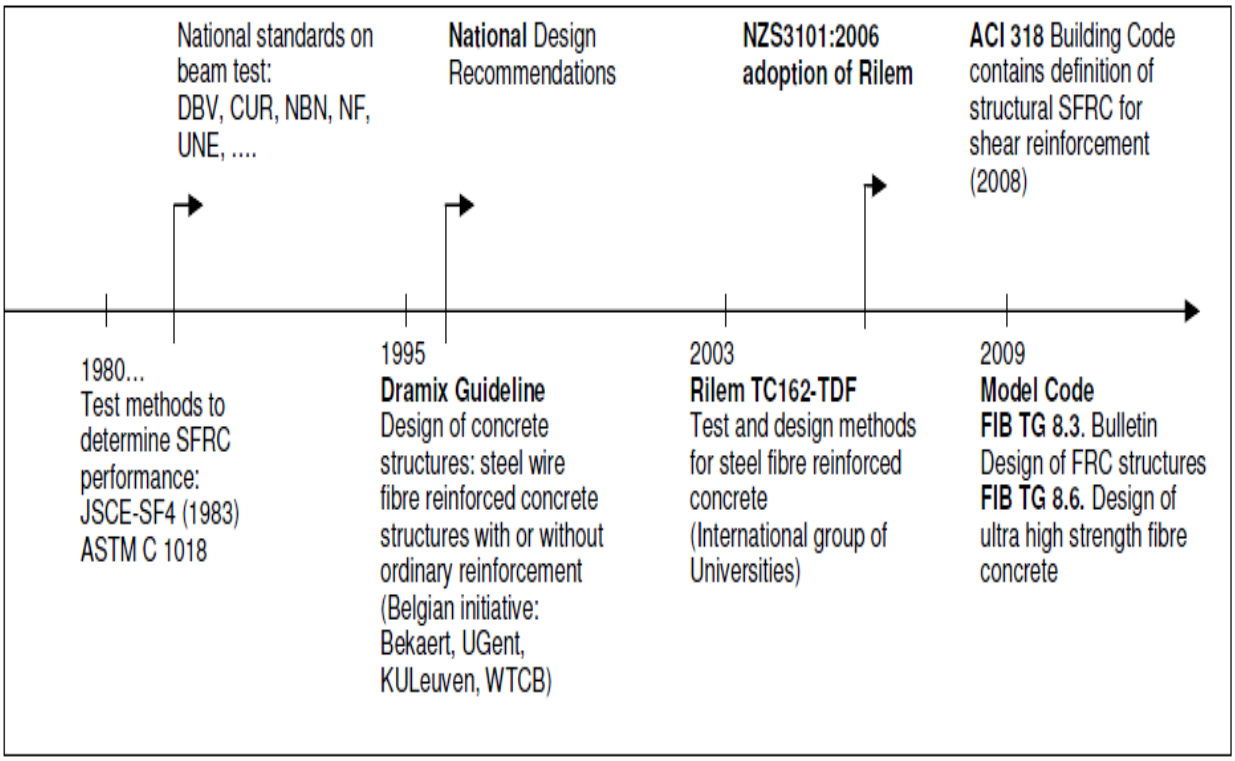

Figure 2.1 –FRC timeline of design and test methods (Ross, 2008).

2.1.2 – History of Self Consolidating Concrete

Self-consolidating concrete (SCC) was first developed in the late 1980s in Japan, for the purpose of ensuring compaction of concrete in dense reinforcement regardless of the construction work quality (ACI Committee 237, 2007; Gencel, Brostowb, Datashvili, & Thedford, 2011). As new chemical admixtures and cementitious materials that improve the quality and lower the cost of SCC have entered the marketplace, use of SCC has become somewhat common in construction.

2.1.3 – Development of Self Consolidating Fiber Reinforced Concrete

New generations of additives such as superplasticizers (SPs), which improve concrete plasticity, and viscosity modifying agents (VMAs), which adjust concrete viscosity and prevent

segregation, have been developed and added successfully to SCFRCs. Those new additives make achieving high strength concrete possible without any reduction in concrete workability. Fine cementitious materials such as fly ash, blast furnace slag, silica fumes, and limestone fines have also been developed that improve SCFRCs. For example, addition of fine cementitious materials reduces voids, which tends to enhance the fiber-matrix bond (Barnes, 2007).

Adding fibers to cementitious composites reduces the matrices workability, especially if the cementitious composites contain coarse aggregates. Ritchie and Rahman (1973), and Luke et al. (1973) examined the impact that adding steel fiber had on concrete workability. They found that concrete workability decreased steadily with the increase of steel fiber content. They found that a 3% fiber volume fraction of steel fibers decreased the slump by 12%, while 8% volume fraction of steel fiber reduces the slump by 70%. Liao et al (2006) investigated the effect of adding 1.2 inch long hooked end steel fibers in volume fractions ranging between 1.5% to 2% to SCCs of compression strengths ranging between 5 ksi to 9.5 ksi. They developed a mixture design for a tensile-strain hardening self-consolidating FRC that was used as a basis for the mixture designs used in this study.

SCCs are highly affected by the mixing steps and the time each step takes. In addition, minor changes in the mixing procedure as well as the sequence of mixing may significantly affect the freshly mixed concrete's properties (Liao, Chao, Park, & Naaman, 2006). Researchers have done many studies to improve SCC production processes. Traditionally, using standard mixing approaches and undeveloped fibers (straight and smooth steel fibers) led to fiber segregation and fiber balling. Using glued steel fibers, special mixing processes, and unique placing methods to minimize segregation and to distribute fibers uniformly, are considered significant advances in FRC (Naaman A. E., 2003).

2.2 – Types of Fibers

Use of different types of fibers has been shown to have multiple advantages, including reduced crack widths, improved concrete toughness, prevention of concrete spalling during fires, and reduced plastic shrinkage cracking (LÖFGREN, 2005). The three primary types of fiber materials are synthetic (carbon, polypropylene, polyester, and nylon), steel, natural (such as wood based), and glass. Figure 2.2 shows several types of commercial fibers. Steel fibers are the most commonly used fiber for structural applications. Only Spectra (polyethylene fiber), twisted steel fiber, and hooked end steel fiber have been successfully used to produce high-performance fiber reinforced concrete (HPFRC) with fiber volume fractions less than 2% (Setkit, 2012).

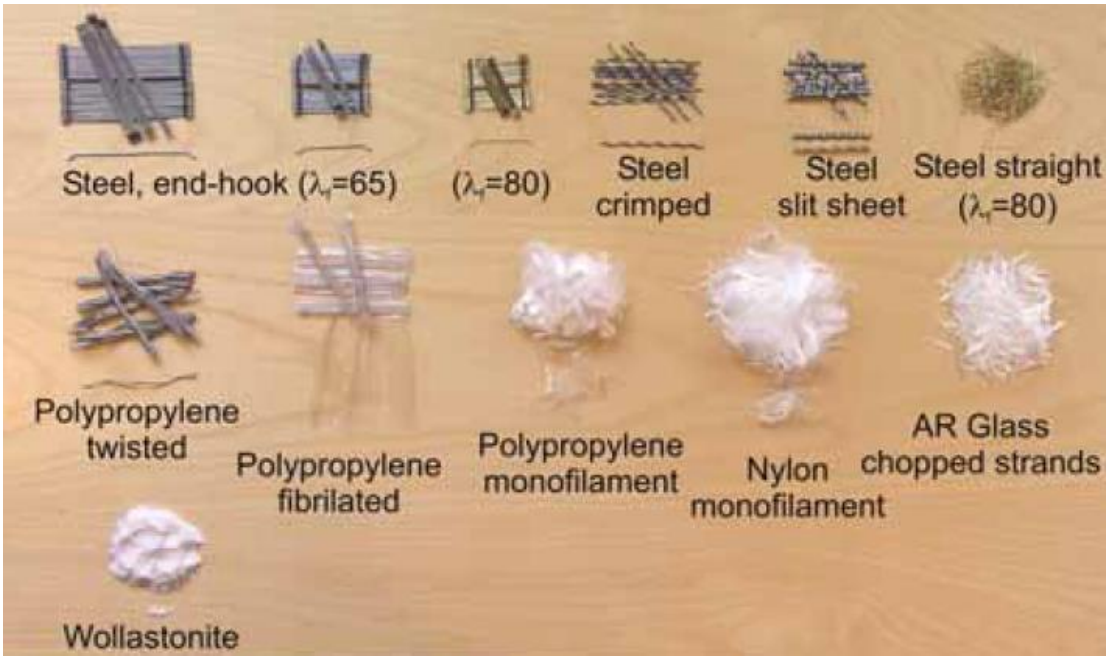

Figure 2.2 – Several types of the available fibers (LÖFGREN, 2005).

Steel fibers are added to FRCs to improve toughness, ductility, and other properties (Hockenberry & Lopez, 2012). To improve the anchorage of steel fibers in concrete, steel fibers come in several different shapes, including smooth and straight, twisted, crimped, coiled, indented,

with paddled ends, with hooked ends, or with buttoned ends. Some common shapes of steel fibers are shown in Figure 2.3.

According to Naaman (2003), fibers must have several characteristics in order to be effective in FRCs. One of the most important characteristics of a fiber is its aspect ratio, defined as the ratio of length to diameter. Commonly, steel fiber aspect ratios range between 20 and 100 though it can easily exceed 100 for fine fibers (Trub, 2011). Fibers with large aspect ratios have a larger ratio of surface area to cross-sectional area, which makes them more capable of developing their full strength through bond with the matrix. Also, fibers with large aspect ratios tend to have a small volume; so, for the same volume of fibers, those with large aspect ratios will have a larger number of individual fibers. Also, the tensile strength of fibers must be much greater than the matrix capacity (about 2 to 3 orders of magnitude). Third, the bond strength between the fiber and matrix must be greater than the matrix cracking strength. Fourth, the elastic modulus of the fibers should be at least three times that of the matrix. In addition, fibers must have enough ductility; it is not desirable for fibers to fracture. Finally, the thermal coefficient and the Poisson's ratio of fibers should be in the same order as the matrix.

The quantity of fibers in a mixture is often expressed as a portion of the total composite volume, referred to herein as the fiber volume fraction. Practical fiber volume fractions range between 0.25% and 3% for steel fibers (Trub, 2011).

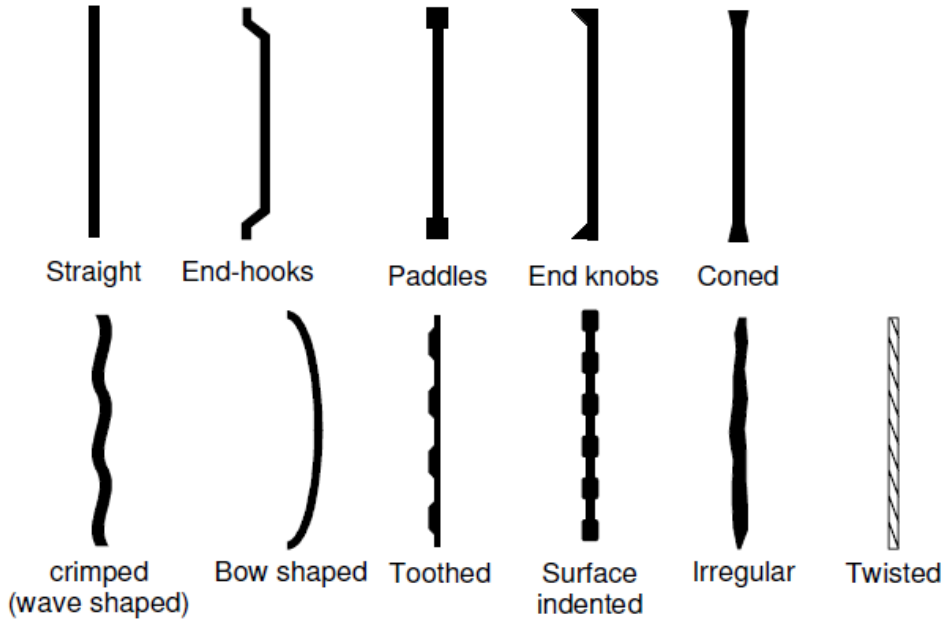

Figure 2.3 – Some of the standard shapes of steel fibers (LÖFGREN, 2005).

2.3 – Classification of Fiber Reinforced Concrete Based on Mechanical Behavior

ACI Committee 544 defines FRC as a matrix made of cementitious materials, aggregates, and discontinuous discrete fibers (ACI Committee 544, 1996). As shown in Figure 2.4, FRC can be classified on the basis of its response to flexural and direct tensile loads response (Naaman & Reinhardt, 2005). The term "high-performance fiber reinforced concrete (HPFRC)" has been used to refer to FRC that develops a post-cracking tensile strength higher than the first cracking strength (strain hardening) and also typically develops multiple cracks instead of a single large crack. Other FRCs that exhibit higher flexural strength after first cracking are referred to deflection-hardening FRCs (T.Mastsumoto & Mihashi, 2002). It is common for deflection hardening composites to exhibit the tensile strain softening response shown in Figure 2.5.

HPFRCs have been shown to have the most significant impact on structural behavior (Parra-Montesinos G. J., 2005). When HPFRC is used, the spacing between cracks and crack

widths are smaller than those expected in a similar structure construected with a non-strain-hardening material (Naaman A. E., 2008).

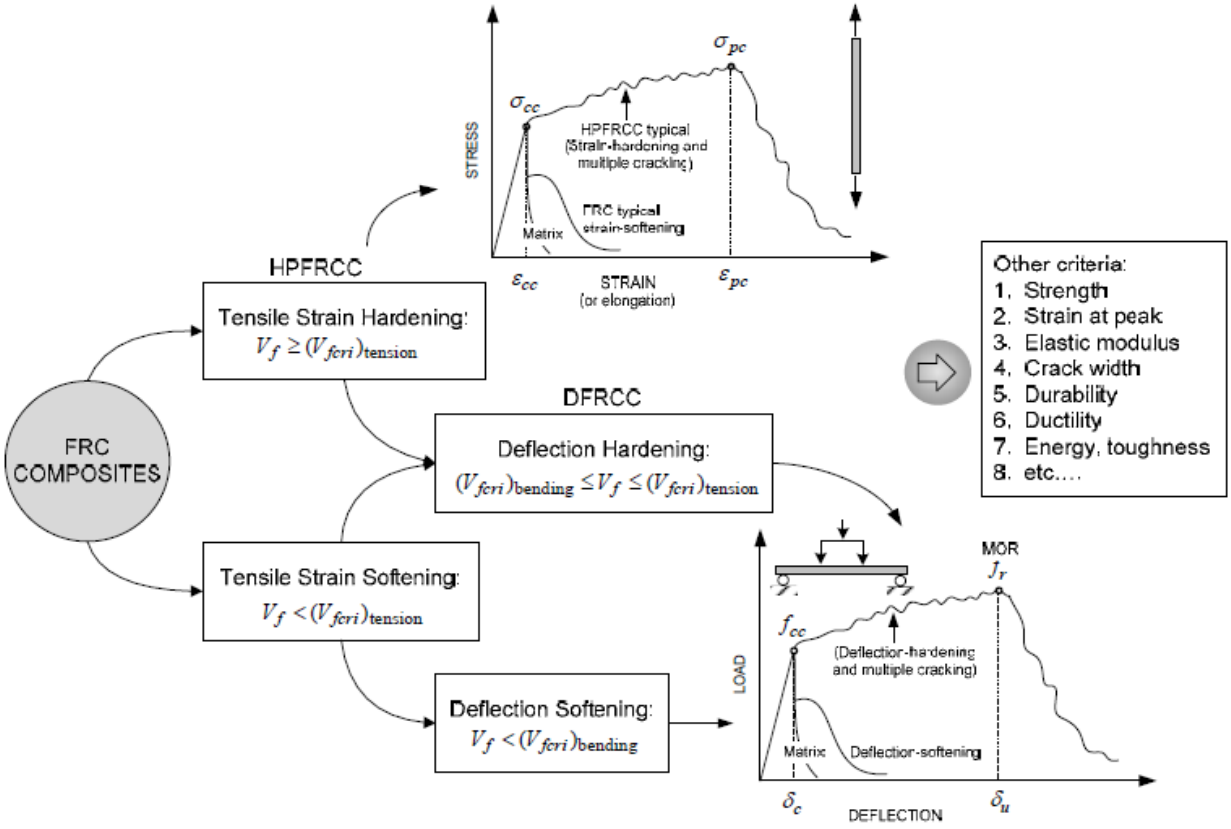

Figure 2.4 – Classification of FRCs on the basis of tensile stress-strain response and the flexural load-net deflection response (Naaman & Reinhardt, 2005).

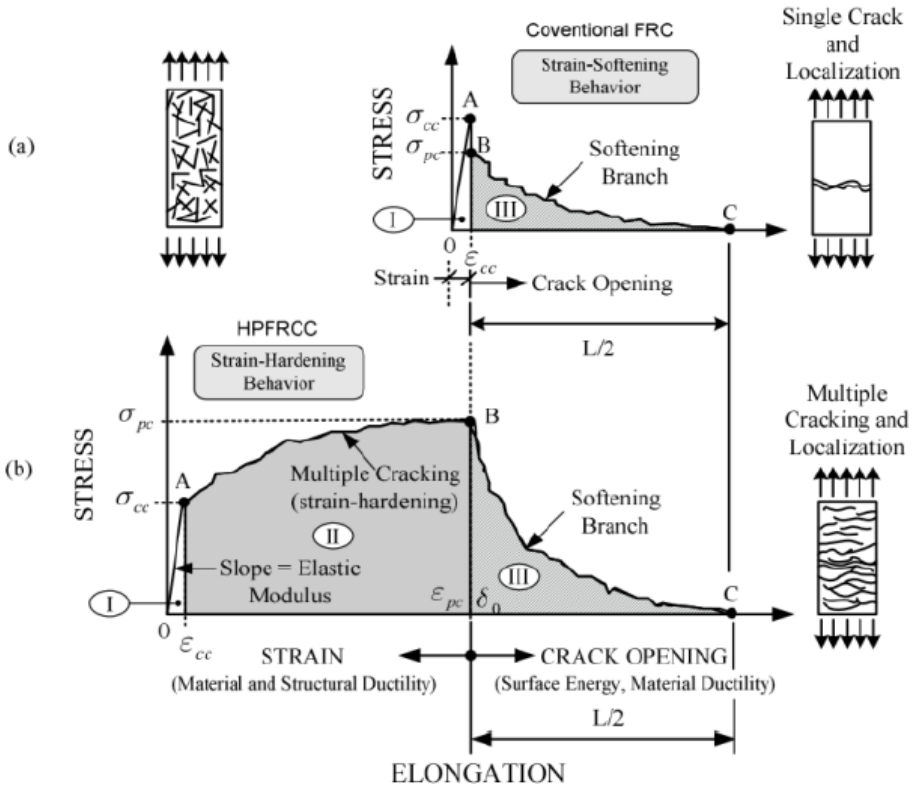

Figure 2.5 – HPFRCs and FRCs response under tensile stresses (Naaman A. E., 2008).

Although not investigated in this study, there are other classifications of FRCs. A common class of FRCs are referred to as ultra high-performance fiber reinforced concrete (UHPFRC), which commonly has a compression strength between 22-32 ksi (150-220 MPa) (Trub, 2011). UHPFRC combines the properties of high strength concrete and the characteristics of FRC (Yu, Spiesz, & Brouwers, 2013). Fibers are introduced to UHPFRCs to prevent sudden failure by increasing the concrete toughness and ductility (Astarlioglu & Krauthammer, 2014). The ultra high-performance can be achieved by using a large quantity of cement and fine materials such as fly ash and/or silica fume to achieve maximum packing density (FHWA, 2013). In addition, a smaller coarse aggregates nominal size, a low water-cement ratio (0.16-0.20), and a superplasticizer (SP) are necessary to produce UHPFRC (FHWA, 2013).

2.4 – Structural Applications of FRC

Although FRC has become common in slabs and other flatwork where crack control is the primary design consideration, use of FRC has been shown to be advantageous in several structural applications, as described below.

2.4.1 – Members under Cyclic Loads

Use of HPFRC in concrete structures that are exposed to seismic activities can be advantageous. Typically, structures that are expected to undergo inelastic displacement reversals have congested reinforcement that is required to confine and reinforce the concrete, but that makes concrete placement difficult. An investigation conducted by Parra-Montesinos and Chompreda (2007) showed that flexural members with polyethylene high-performance fiber reinforced concrete (PHPFRC) and without transverse reinforcement have larger damage tolerance and greater drift capacities in comparison to conventionally reinforced concrete. The same investigation also showed that HPFRC is capable of sustaining high shear stresses and provide buckling restraint to the longitudinal reinforcement.

2.4.2 – Coupling Beams

The overall behavior and constructability of coupling beams, which are subjected to high shear stresses and deformation demands in a seismic event, can be improved by using HPFRC instead of conventional concrete (Canbolat, Parra-Montesinos, & Wight., 2005). Canbolat, Parra-Montesinos, and Wight (2005) investigated four short HPFRC coupling beams with length to depth ratios of 1.0. They reported that using HPFRCs improved the deformation capacity and toughness

of the beams, reduced the reinforcement requirements, and improves the damage tolerance by distributing damage over multiple cracks.

2.4.3 – Shotcrete

Shotcrete, which is defined by ACI 506R (2005) as "mortar or concrete pneumatically projected at high velocity onto a surface," can contain fibers (Vondran, 1991). If supplied in a sufficient quantity, fibers can replace wire-mesh reinforcement in shotcrete applications (Vondran, 1991). An advantage to using fibers as reinforcement in shotcrete applications is to prevent shadows, which are air voids and sand pockets behind reinforcing bars that can lead to corrosion issues and surface cracks. Figure 2.6 illustrates the difference between using steel fibers and reinforcing bars as reinforcement in shotcrete applications. Another reason for using FRC in shotcrete applications is to reduce the casting time and costs.

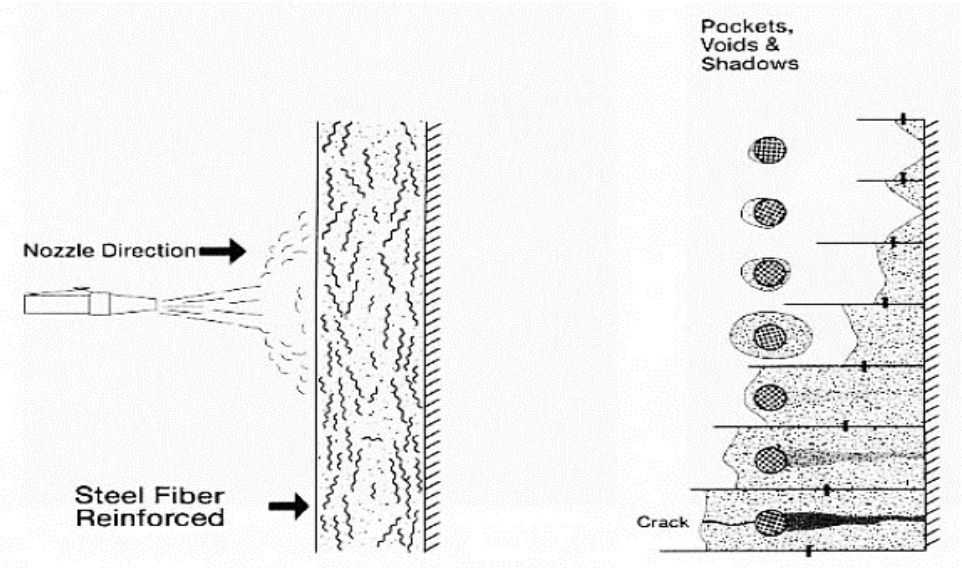

Figure 2.6 – Comparison between fibers and reinforcing steel in shotcrete (Vondran, 1991).

2.4.4 – Low-Rise Structural Walls

Use of HPFRCs in low-rise structural walls that are subjected to earthquake-type cyclic loads has been shown to allow a reduction in web shear reinforcement and result in an increase in damage tolerance. A study conducted by Parra-Montesinos and Kim (2004) of the use of HPFRCCs in low-rise structural walls with a height-to-length ratio of 1.5, using two different HPFRCCs, show that the FRC can resist about 70% of the total shear stresses.

2.4.5 – Precast Concrete

SCFRCs have been used for many years in precast concrete applications to enhance the resistance of precast concrete units to corrosion and cracking. Using SCFRCs in precast concrete improves its performance in aggressively corrosive environments and increases its resistance to impact shock. In addition, SCFRCs tend to reduce the width of cracks, including settlement cracks, bed cracks, pattern cracks, surface cracks, and cracks that occur due to handling of the units.

For example, in the 1970s, the U.S. Army Corps of Engineers made 600 units of precast dolosse, twisted H-shaped units, which had 80 to 120 lbs/yd^3 of steel fibers as their primary reinforcement. Only two of them were fractured during transportation. After 14 years of exposure to the Pacific Ocean, the Corps reported that no evidence of fiber corrosion was found in the precast steel fiber reinforced dolosse. In contrast, the U.S. Army Corps reported that 80 percent of the traditional reinforced precast dolosse units disintegrated within a few years due to corrosion exacerbated by plastic settlement cracks (Vondran, 1991).

2.4.6 – Beam–Column Connections

Using HPFRCs in beam-column connections increases the shear strength, bond strength between the matrix and the reinforcement, and overall damage tolerance of the connection. A study by Parra-Montesinos (2005) concluded that using HPFRCs for beam-column connections increases the confinement of the longitudinal reinforcement in that region which allows for a reduction in the required transverse reinforcement and an increase in the required minimum spacing of the transverse reinforcement.

2.4.7 – Other applications of FRC

FRCs have been used in several other applications, especially in those where limitation of crack widths is important but placement of reinforcement is difficult. Several of these other applications are shown in Figure 2.7.

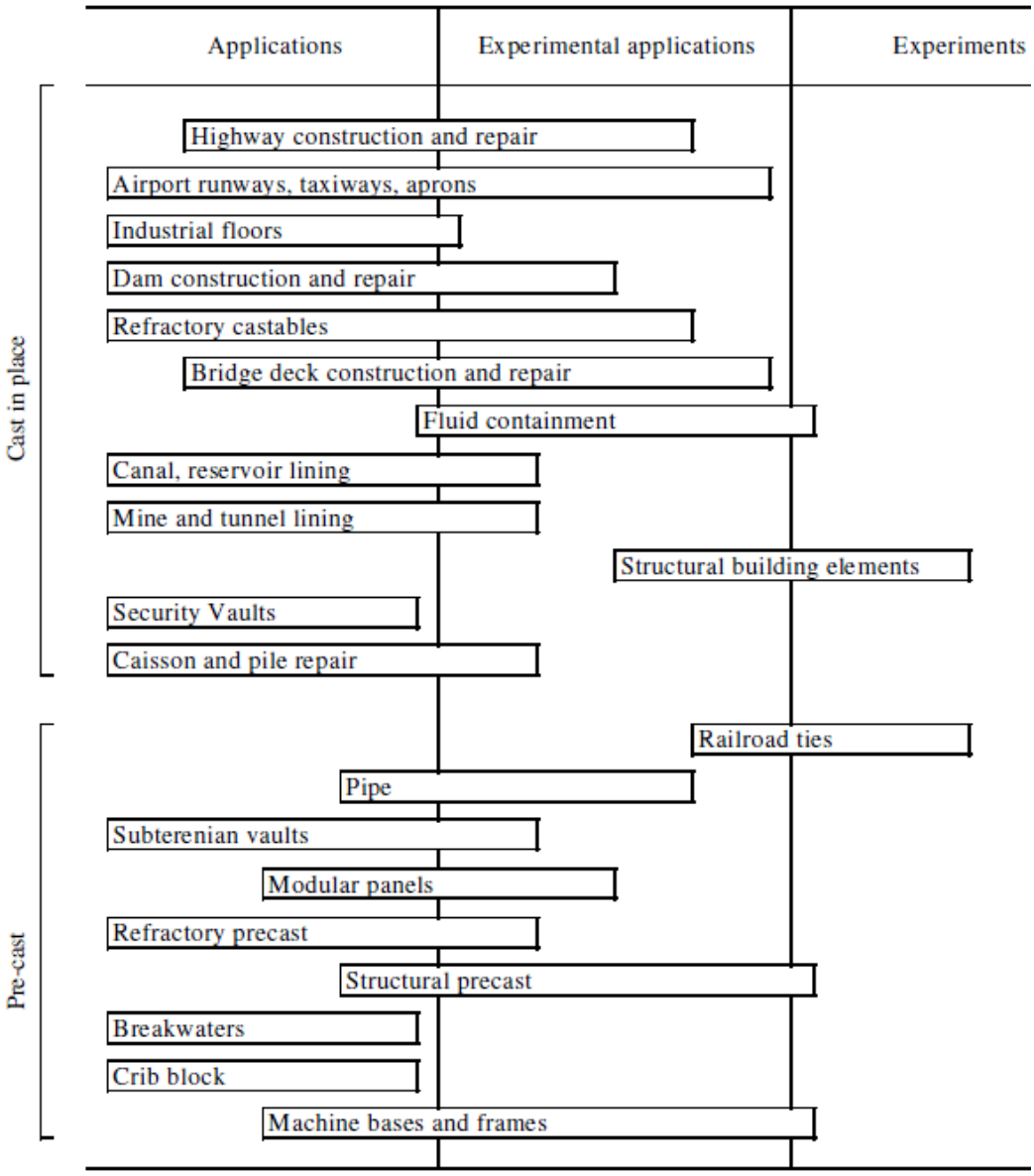

Figure 2.7 – SFRC main applications (Zollo, 1985).

2.5 – Properties of Freshly Mixed SCFRC

As discussed in Section 2.1.3, the workability of concrete tends to be reduced when fibers are added to the mixture. However, this limitation can be overcome through use of chemical admixtures that increase the workability of fresh concrete. This improved workability is the primary advantage of using SCFRC instead of conventional FRC.

Certain fiber properties are known to affect the workability of the mixture. Gru¨newald and Walraven (2001) reported that there are direct relationships between the fiber factor (the product of fiber aspect ratio and volume fraction) and the concrete workability as illustrated in Figure 2.8. Similarly, (Liao, Chao, Park, & Naaman, 2006) showed that the higher the aspect ratio is, the lower the dosage of fiber that can be added for a given target workability. A study that was produced by Bentur and Mindess (1990) shows the effect of different fiber lengths (0.8, 1.6, and 2.4 inches) and different fiber content (1-3%) of polypropylene fiber on the concrete slump as shown in Figure 2.9.

A problem associated with producing SCFRC is fiber balling, which is commonly caused by using high coarse aggregates content (usually more than 55% of the total combined aggregates) and/or over mixing (Yurtseven, 2004). Many studies show that the risk of balling increases as the fiber stiffness decreases and as the fiber diameter decreases. Several solutions are available to control balling such as using pre-glued fibers and/or using special mixing procedures (Naaman & Reinhardt, 1995).

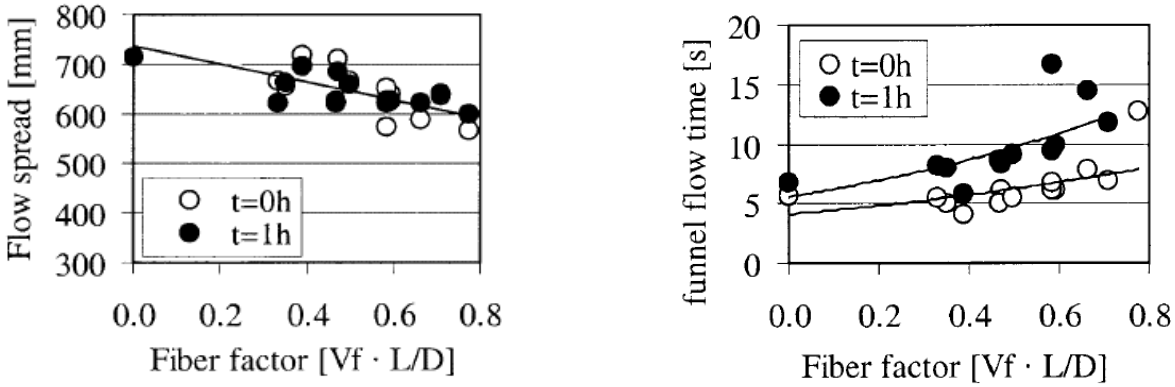

Figure 2.8 – The effect of fiber factors on the workability of SCC (Gru¨newald & Walraven, 2001).

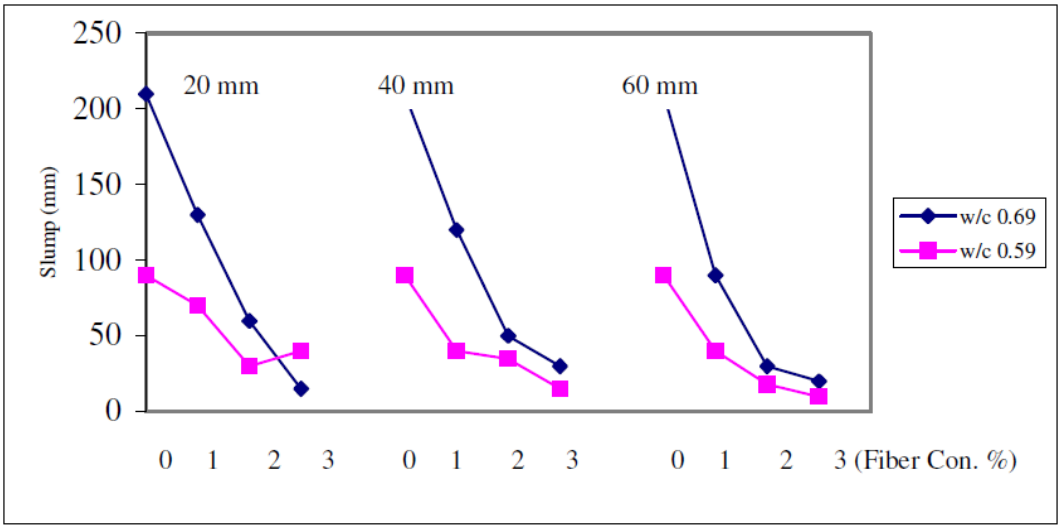

Figure 2.9 – The effect of fiber length and the content of polypropylene fiber on concrete slump (Yurtseven, 2004).

Although fiber properties influence workability, properties of the matrix have a greater effect on the concrete workability when fiber volume fractions are 0.5-2% (Barnes, 2007). Figure 2.10 shows the relationships between the measured slump, paste volume fraction, and fiber content. As illustrated in Figure 2.11, the maximum size of coarse aggregate also influences the distribution of fibers and should influence the choice of fiber length (Liao, Chao, Park, & Naaman, 2006; Johnston, 1996; Mangat & Swamy, 1974). ACI Committee 544 recommends that the fiber length be no longer than 2-4 times the maximum size of coarse aggregate, whereas Vandewalle (1993) suggests using fibers with a length larger the maximum size of coarse aggregates.

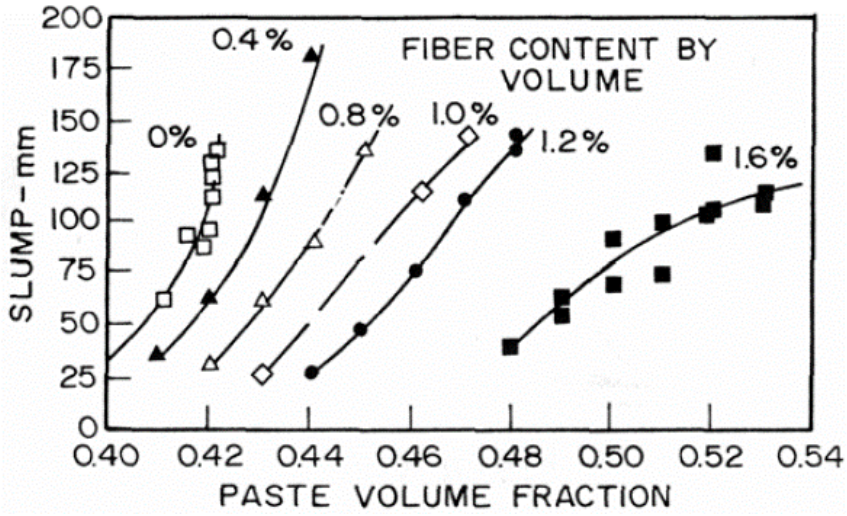

Figure 2.10 – The effect of paste volume on the workability of SFRCCs (Johnston, 2001).

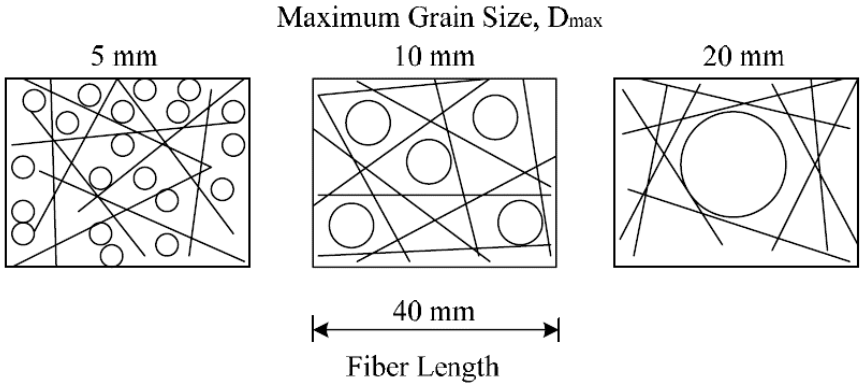

Figure 2.11 – The effect of maximum size of coarse aggregates on the fiber length and distribution (Johnston, 1996).

The maximum practical fiber volume fraction is a function of matrix properties. Narayanan and Kareem-Palanjian (1982) showed that increases in the fine/coarse aggregate ratio, fiber content can increase due to an increase in the amount of the paste, which fills the void between fibers and aggregates. A study by Mangat and Swamy (1974) showed that the coarse aggregate content affects the maximum steel fiber content. In their study, they used straight steel fibers with aspect ratio 100 (1.0 in. length and 0.01 in. diameter) and crushed aggregates with a nominal maximum

aggregate size of 0.4 inch. They found that the maximum allowable fiber content decreased as coarse aggregate content increased (Figure 2.12).

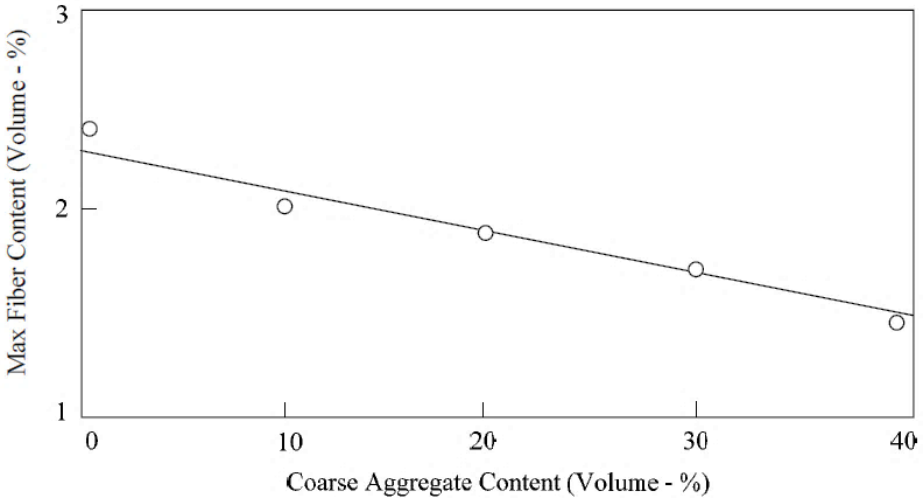

Figure 2.12 – The relationship between the coarse aggregates content and the maximum content of the steel fiber (Mangat & Swamy, 1974).

2.6 – Mixing Procedures

There are many methods available for introducing steel fibers to concrete mixtures. Compared with the conventional concrete mixing procedures, SCC is highly affected by the mixing steps and the time each step takes. In addition, minor changes in the mixing process as well as the sequence of mixing may significantly affect the properties of freshly mixed concrete. Furthermore, depending on the sequence and content of the added fibers, identical mixtures that are prepared with identical techniques might lead to different properties of SCC (Liao, Chao, Park, & Naaman, 2006). Moreover, the mixing duration should be kept as short as possible in order to prevent segregation (Gencel, Brostowb, Datashvili, & Thedford, 2011). This section provides several mixing procedures that have been used successfully in several studies.

The ACI Committee 544 (1998) published two successful mixing methods of making SFRCs. In both of these methods, the fiber should be added to a fluid mix to prevent balling of the fibers and to ensure dispersion of the steel fibers. The first procedure, which has been used successfully by many ready-mix concrete producers, is efficient when using a transit mix truck. It requires the following steps: First, the wet mixture is prepared without any fiber so that it has a slump that is at least one to two inches higher than the desired slump of the SFRC. Then the fiber shall be added gradually, perhaps by dumping the fiber through a four-inch mesh screen. After adding all fibers, the mixing speed is slowed for about thirty to forty revolutions of the drum.

The second method of the ACI Committee 544 (1998) can be done by charging a central mixer or transit mix truck with fiber and aggregates at the same time. Following the regular mixing manner, fibers should be added via a conveyor belt with the aggregates addition. If possible, the operator should elongate the time it takes to add fibers and aggregates to the mix. Furthermore, fibers shall not be introduced as clumps because they remain as clumps after mixing. In addition, the mixing drum has to be rotated fast enough to mix the fibers efficiently as they are introduced. If glued fibers are used, not more than thirty fibers per bundle is allowed. The fiber bundles can also be introduced to the mixture at the end to eliminate the balling risk. This procedure is successfully used for the majority of fibrous concrete projects.

Naaman, Alkhairi, and Hammoud, (1993) used the following steps during the mixing process: in the beginning, one must add and mix the aggregates for one minute. Next, the cementitious materials are added and mixed for another minute. After that, 75% of the water and the superplasticizer must be introduced slowly. Then the air entraining agent and the corrosion inhibitor (if used), should be mixed with the remaining 20% of the water. The operator shall mix the matrix for a few minutes to ensure a proper and uniform mix. Finally, the fibers are added to

the concrete through a sieve (0.5-inches-square openings) to guarantee arbitrary distribution of the fibers, eliminate fiber balling, and prevent segregation. Altogether, this mixing procedure takes about five to six minutes.

Liao et al (2006) proposed a mixing procedure for producing SCFRCs that is summarized in several steps. The cementitious materials and the fine aggregates are mixed for thirty seconds; then, half of the premixed liquid (Water+SP+VMA) must be added. A quarter of the remaining premixed liquid (Water+SP+VMA) should be poured in and mixed for one minute. Then, 1/8, 1/16, and all of the remaining liquid can be added with one minute of mixing time between each addition. After one minute of mixing, the coarse aggregates shall be introduced to the mixture. The operator can start adding the steel fibers slowly after two minutes of mixing. After addition of the fibers and mixing for three minutes, mixing can be stopped. The total mixing time of this technique is ten minutes and thirty seconds.

Sahmaran, Yurtseven, and Yaman (2005), and Sahmaran and Yaman (2007) used a different mixing technique in their experimental studies of FRCs. They used fiber with a volume fraction of about 0.8%. They used the following steps: the first step is the dry-mixing of the fine aggregates, coarse aggregates, and fibers for thirty seconds. Then, the operator must add the cement, the limestone powder and 1/3 of the total water amount. After 1.5 minutes of mixing, he or she shall add the premixed liquid (2/3 of the water with SP). The total mix time for all batches is five minutes.

Brodowski (2005) has proposed a mixing procedure of producing SCCs by using up to 2% of fiber content. The following steps are required to achieve satisfactory results: the first step, the coarse aggregates, the fine aggregates, and the steel fibers should be mixed for four minutes. Then, half of the water must be introduced into the mix in a one-minute interval. After that, half of the

fly ash and the cement can be added. Next, the operator must add a quarter of the water. After one minute of mixing, he or she can add the last quarter of water with a quarter of the fly ash amount. Then, a quarter of the SP, the rest of the cement, and fly ash can be introduced to the mix. After that, the operator must add the rest of the SP, and mix for two more minutes. He or she shall mix until all the fibers are completely separated. This procedure takes about eight to ten minutes.

Gru¨newald (2006) used fiber with a volume fraction of 1.5%, and a pan mixer. His procedure requires the following steps: first, the operator shall mix the cementitious materials and the fine aggregates for ten seconds. Then, the pre-mixed liquids (water and SP) must be introduced to the mixture, and then mixed for 110 seconds. After that, the coarse aggregates must be added and mixed for one minute. Next, the operator has to wait for one minute allowing the SP to activate, and mix for thirty seconds. Finally, he or she shall add the fibers slowly and mix for ninety seconds. Further mixing may be required to dissolve the glued fiber bundles. This procedure requires about six to eight minutes.

2.7 – Mechanical Properties of FRC

The following section offers a brief description of the most important mechanical properties of FRC. Characteristics such as strength, stress-strain behavior, modulus of elasticity, and toughness, as well as a brief discussion of some results found in the literature are reported.

In general, there is no significant improvement in the elastic region (before cracking) from addition of fibers to cement-based materials. In addition, small fiber volume fractions have a negligible effect on the compression strength and the modulus of elasticity (Barnes, 2007). Introducing fibers to concrete can, however, result in significantly improved post-cracking behavior.

2.7.1 – Compression Strength

In plain concrete and FRC with fiber volume fractions less than 1% the stress-strain relationship can be represented by a line up to approximately 30% of the compression strength, followed by a period of gradual softening up to the concrete compression strength. Beyond the compression strength, the stress-strain relationship exhibits strain softening until failure occurs (Williamson, 1974; Wafa & Ashour, 1992). Adding steel fibers tends to reduce the post-peak slope of the stress-strain relationship, resulting in a response to compression like that of well confined concrete, as illustrated in Figure 2.13 (LÖFGREN, 2005).

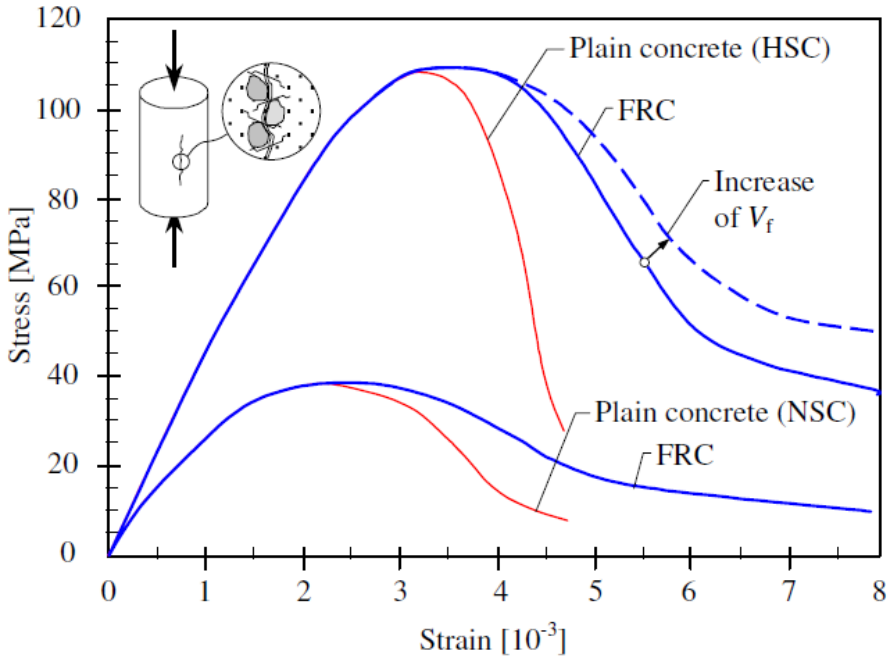

Figure 2.13 – Schematic description the behavior of plain concrete and FRC under compression stresses (LÖFGREN, 2005).

Although small volume fractions of fibers do not affect the compressive strength, large fiber volume fractions can. For these mixtures, it has been shown that the orientation of fibers influences the concrete compression strength (Fanella & Naaman, 1985; Homrich & Naaman,

1987; Ezeldin, Balaguru, & Perumalsamy, 1992; Balaguru & Najm, 2004; Li & Mishra, 1992). When fibers are oriented perpendicularly to the loading direction, fibers are more efficient in reducing cracks propagation and sliding (Barnes, 2007). Homrich and Naaman (1987) recorded that about 50% higher strength can be achieved by orienting fibers perpendicular to the loading direction instead of orienting them parallel to the loading direction. Fanella and Naaman (1985), and Balaguru and Najm (2004) reported that the strength increases by 0-50% when steel fibers (Dramix fibers) are oriented randomly, while Naaman, Otter, and Najm (1991) found that adding hooked end steel fibers with volume fractions 9-11% in making SIFCON increases the strength in the range of 300-400%. Several results from previous studies of compression strength of FRC are listed in Table 2.1.

Table 2.1 – Results of several studies of compression tests found in the literature compared by Barnes (2007).

Reference	Matrix	Fiber Type	Age (days)	V_f	Aspect Ratio (l/φ)	f_c (ksi)	f_{cf} (ksi)	f_{cf}/f'_c
Hughes and Fattuhi (1977)	concrete	hooked steel	30	1.5%	114	6.2	5.7	0.92
			190			7.7	6.2	0.81
Williamson (1974)	concrete	straight steel	28	1.0%	41	8.8	8.9	1.01
	mortar					8.5	8.1	0.95
	concrete			1.5%		8.8	9.2	1.05
	mortar					8.5	8.1	0.95
	concrete			2.0%		8.8	9.8	1.11
	mortar					8.5	7.8	0.92
Naaman and Fanella (1985)	mortar	straight steel		1.0%	83	7.2	8	1.11
				2.0%		8.5	9	1.06
				3.0%		9.9	10.6	1.07
Li (1992)	mortar with silica fume	hooked steel		3.0%	40			1.10
				6.0%				1.25
Ezeldin and Balaguru (1992)	concrete	hooked steel		0.4%	75	5.2	6.9	1.33
				0.6%		5.2	6.5	1.25
				0.8%		5.2	6.2	1.19
Naaman , Otter, Najm (1991)	mortar	hooked steel	240	11.0%	80	4.8	15	3.13
Mansur and Chin (1999)	concrete with silica fume	hooked steel	28	1.0%	60	10	11.5	1.15
				1.0%		12.4	11.6	0.94
				1.5%		15	15	1.00
Balaguru and Najm (2004)	mortar with silica fume	hooked steel	35	3.0%	60	8.6	12.6	1.47
				3.5%		8.6	10.9	1.27

2.7.2 – Tensile Strength

As defined previously, HPFRC is a class of FRC materials that exhibit tensile strain hardening, or increased tensile strength after cracking. In contrast, plain concrete and conventional FRC exhibit the greatest strength at first cracking, and therefore they exhibit strain-softening, as shown in Figure 2.14.

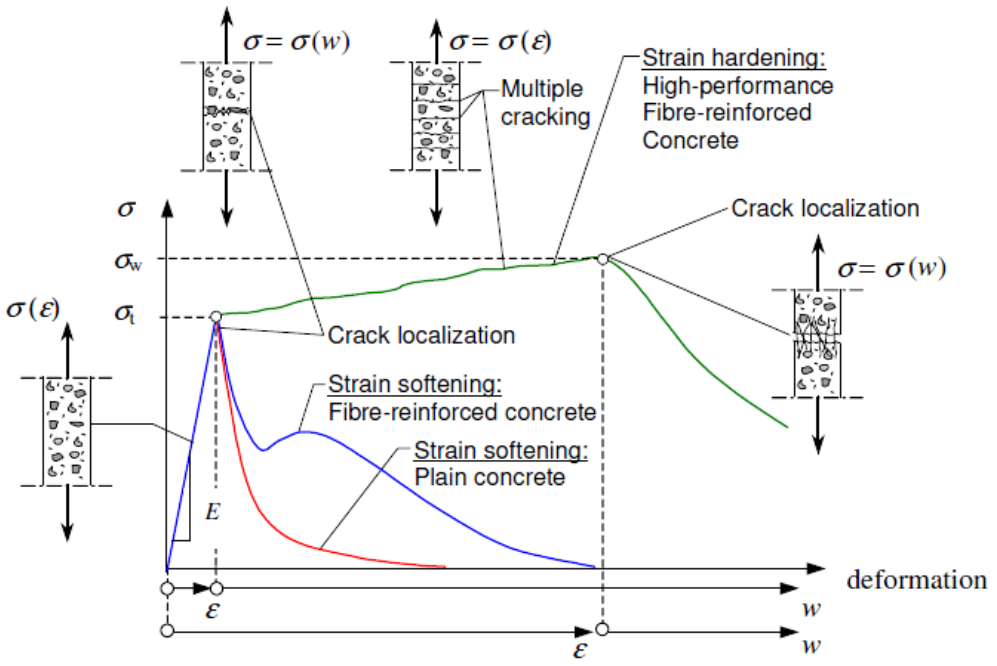

Figure 2.14 – Classification of FRCs based on their behavior under tensile stresses (LÖFGREN, 2005).

It has been well reported that adding steel fibers increases the concrete tensile strength (Johnston & Coleman, 1973; Homrich & Naaman, 1995; Balaguru & Najm, 2004). Using small fiber volume fractions (1-2%) increases the tensile strength by about 10% (Barnes, 2007). Naaman and Chandrangsu (2003) used 2% volume fraction of twisted steel fiber with fly ash to achieve strain hardening. Balaguru and Najm (2004) achieved a 10% higher tensile strength by using 1.5% volume fraction of hooked end steel fibers, while Johnston and Coleman (1973) produced a 30% higher tensile strength by using 6% volume fraction of hooked end steel fiber. In addition, adding polymer fibers slightly increases the concrete ultimate tensile strength. Balaburu and Khajuria (1996), and Kao (2005) also found that adding polymer fibers slightly increases early ages tensile strength, but there is no significant effect on long term tensile strength. Table 2.2 shows results from tensile strength tests found in the literature.

Table 2.2 – Results of tensile strength tests found in the literature that were compared by Barnes (2007).

Reference Number	Matrix	Fiber Type	Age (days)	V_f	Aspect Ratio	f_t (psi)	f_{tc} (psi)	f_{ut} (psi)	f_{tc}/f_t	f_{ut}/f_{tc}	f_{ut}/f_t
Johnston and Coleman (1973)	mortar	straight steel	30-180	2.0%	31						1.01
					63						1.04
					94						1.14
				4.0%	31						1.04
					63						1.11
					94						1.27
				6.0%	31						1.04
					63						1.18
					94						1.34
Naaman and Chandrangsu (2003)	mortar with fly ash	twisted steel[a]		2.0%	100		447	837		1.87	
		twisted steel[b]					417	858		2.06	
Naaman and Otter (1991)	mortar with fly ash	hooked steel[c]	150	15.6%	80			5250			
				16.7%				6100			
Naaman and Homrich (1987)	slurry (cement and fly ash)	hooked steel[c]	60	12.4%	60		1400	2280		1.63	
				13.8%				2340			
Li, Li, and Chang (1998)	concrete with silica fume	hooked steel		2.0%	60	580	616	616	1.06	1.00	1.34
				3.0%		580	711	711	1.23	1.00	1.34
				6.0%		580	870	1305	1.50	1.50	1.34
				3.5%	100	580	870	1196	1.50	1.37	1.34
Wafa and Ashour[d] (1992)	concrete with silica fume	hooked steel	28	1.0%	75	797		1087			1.36
				1.5%		797		1450			1.82

where:

f_t = unreinforced cementitious composites tensile strength,
f_{tc} = reinforced cementitous composites tensile first cracking strength,
f_{ut} = reinforced cementitous composites ultimate tensile strength,
a: 25 x 25 mm (square cross-sectional dimensions),
b: 50 x 12.5 mm (rectangular cross-sectional dimensions),
c: fibers were oriented parallel to the loading direction,
d: using split cylinder test.

2.7.3 – Flexural Strength

Deformed steel fibers are more efficient in increasing concrete flexural strength than synthetic fibers (Yurtseven, 2004; Naaman & Chandrangsu, 2003) because synthetic fibers have a lower modulus of elasticity than steel fibers (Balaguru & Khajuria, 1996; Naaman & Chandrangsu, 2003). Naaman and Chandrangsu (2003) observed that using twisted steel fiber produces higher flexural strength than using synthetic (Spectra) fibers. In addition, concrete flexural strength is highly sensitive to the aspect ratio and volume fraction of the fibers (Yurtseven, 2004). Higher flexural strengths can be achieved by using higher aspect ratios (Johnston, 1973; Yurtseven, 2004). Using aspect ratios ranging from 30-120 enhances the concrete flexural strength by 10-80% (Barnes, 2007). Adding fibers with volume fractions less than 1.0% does not significantly affect the flexural strength beyond the first crack. By contrast, those volume fractions would greatly enhance the flexural post-cracking strength (Setkit, 2012). The effect of different volume fractions of hooked end steel fibers on concrete flexural strength is shown in Figure 2.15 (Balaguru, Narahari, & Patel, 1992). For reference, 200 lb/yd^3 of steel fibers is approximately equivalent to a fiber volume fraction of 1.5%.

For normal strength concrete, deformed steel fibers have more impact on concrete post-cracking flexural strength than straight steel fibers. A reason the improved behavior is the excellent mechanical bond developed between deformed steel fibers and concrete as shown in Table 2.3 (Ramakrishnan, Brandshaug, Coyle, & Schrader, 1980; Bentur & Mindess, 1990; Balaguru & Shah, 1992; Mindess, Chen, & Morgan, 1994).

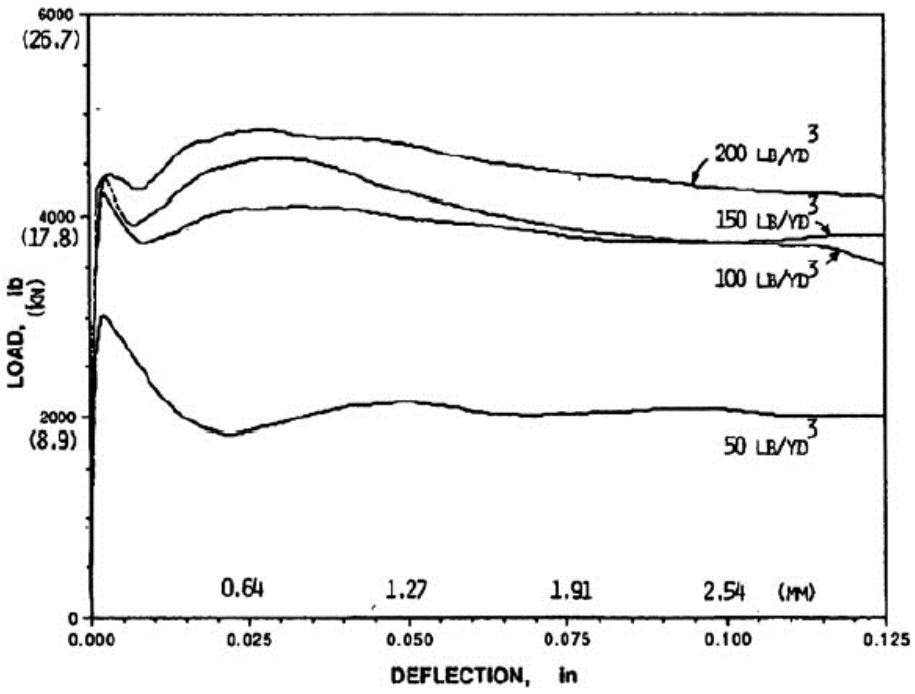

Figure 2.15 – The effect of volume fraction of hooked end steel fibers on concrete flexural strength (Balaguru, Narahari, & Patel, 1992).

2.7.4 – Shear Strength

One of the main advantages of introducing steel fibers to concrete is to enhance shear strength (Setkit, 2012; Kwak, Eberhard, Kim, & Kim, 2002), particularly those subjected to displacement reversals such as coupling beams and beam-column connections. Several researchers have investigated the effect of introducing steel fibers to concrete applications and the possibility of replacing part or all of the steel stirrups by steel fiber. Batson, Jenkins, and Spatney (1972), and Darwish (1987), and Swamy and Bahia (1985) studied the effect of adding steel fibers to concrete beams. They reported that adding fibers improved the shear resistance. Barragán (2002) reported that small volume fractions of steel fibers do not affect the cracking strength, but they significantly affect the toughness behavior after cracks occurred.

Table 2.3 – Flexural strength results for different types of steel fiber (Barnes 2007).

Reference Number	Matrix	Fiber Type	Age (days)	V_f	Aspect Ratio	$f_{rc\ (psi)}$	$f_{r\ (psi)}$	$f_{uf\ (psi)}$	f_r / f_{rc}	f_{uf} / f_r	f_{uf} / f_{rc}
Snyder and Lankard (1972)	mortar	straight steel		1.0%	100	900	1300	1400	1.44	1.08	1.56
				2.0%		900	1900	2400	2.11	1.26	2.67
				4.0%		900	2300	3100	2.56	1.35	3.44
Naaman and Chandrangsu (2003)	mortar with fly ash	twisted steel[a]		2.0%	100		901	1943		2.16	
		twisted steel[b]		2.0%	100		1420	2520		1.77	
Choi and Lee (2003)	concrete	ring type steel		0.2%		1990	2050	2050	1.03	1.00	1.03
				0.4%		1990	2260	2260	1.14	1.00	1.14
		hooked steel		0.8%	100	1990	2200	2400	1.11	1.09	1.21
Mindess and Chen (1994)	concrete	hooked steel	190	1.0%	60	653	840	1000	1.29	1.19	1.53
				1.5%		653	885	1060	1.36	1.20	1.62
Balaguru , Narahari and Patel(1992)	concrete	hooked steel	28	0.8%	60		796	796		1.00	
				1.5%			825	920		1.12	
Balaguru and Najm (2004)	mortar with silica fume	hooked steel	28-64	3.0%	60		1600	2050		1.28	
				3.8%			1740	2370		1.36	
Wafa and Ashour (1992)	concrete with silica fume	hooked steel	28	1.0%	75	1500	2260	2260	1.51	1.00	1.51
				1.5%		1500	2730	3145	1.82	1.15	2.10

Where:

f_{rc}: modulus of rupture of unreinforced matrix,
f_r: modulus of rupture of reinforced matrix,
f_{uf}: maximum bending stress,
a: 100 × 100 × 355 mm (b × w × l),
b: 75 × 12 × 305 mm (b × w × l).

Yang, Joh, and Kim (2011) investigated the effect of using steel fibers in 12 UHPFRC I-beams (depth 27.5 inches, compression strength 23-27.5 ksi) as a replacement for steel stirrups. They found that the ultimate shear resistance increased as the fiber volume fractions increased. Hockenberry and Lopez (2012) showed the same in their study of the effect of hooked end steel fibers on the performance of concrete beams subjected to shear. In addition, they showed that the shear capacity of the tested FRC beams was more than the limitations of ACI 318-08 by 50%.

2.7.5 – Toughness

An important property of FRC is the increased toughness (energy absorption capacity) observed in tests (Yurtseven, 2004). Toughness can refer to results from compression, tension, and flexural tests. All toughness measurements require testing by a satisfactorily stiff hydraulic machine. In order to eliminate energy loss after the first peak and to obtain reliable post-crack curves, a satisfactorily stiff hydraulic machine is required (Bentur & Mindess, 1990; Barr, Gettu, Al-Oraimi, & Bryars, 1996).

As an example, flexural toughness can be measured from the load versus mid-span deflection curves measured in a standard third-point bending test like that illustrated in Figure 2.16 (Sounthararajan, 2013). Toughness Index, which is a unitless value, can be defined as "the ratio of the amount of energy required to deflect a fibre concrete beam by a prescribed amount to the energy required to bring the fibre beam to the point of first crack," as shown in Figure 2.17 (ACI Committee 544 1988).

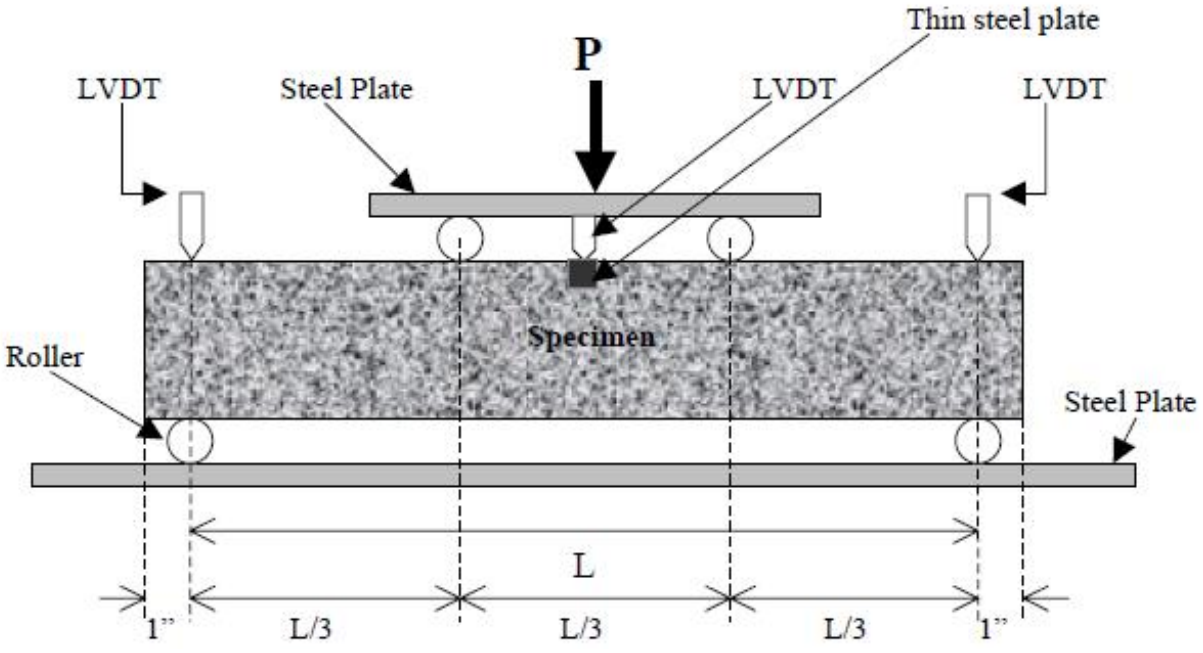

Figure 2.16 – Third point loading test arrangement (Guirola, 2001).

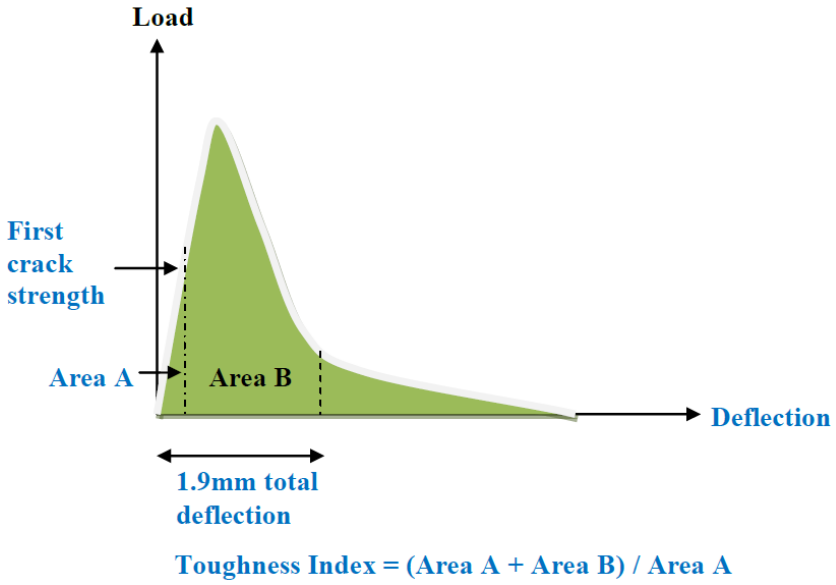

Figure 2.17 – Toughness Index according to ACI Committee 544 (Sounthararajan, 2013).

It has been reported that increasing fiber volume fractions increases the concrete toughness (Fanella & Naaman, 1985). In addition, using high aspect ratio of deformed steel fiber has been observed to improve the concrete toughness and ductility (Li, Li, Chang, & Mai, 1998; Bentur & Mindess, 1990; Balaguru & Shah, 1992).

CHAPTER 3: EXPERIMENTAL PROGRAM

3.0 – General

The primary purpose of the test program was to measure the response of various fiber reinforced concrete (FRC) mixtures under compression, tension, and flexure, and to study whether certain important features of each response (such as the post-peak slope in compression, which can be difficult to measure) can be related to certain features of the tension or bending test results.

Four different hooked steel fibers were used in this study at volume fractions that varied between 0.5% and 1.5%. Each mixture design had a target strength of either 6 or 10 ksi and a target spread of 25 inches without fibers to ensure adequate workability after addition of the steel fibers. A total of twenty-four concrete batches (6.75 ft^3 each) were prepared. Each batch was used to make five 6×12 inch cylinders for compression tests, five 6×6×20 inch beams for flexural tests, and five 6×6×20 inch rectangular prisms for direct tension tests. Several tests, such as ASTM C127 (standard test method for specific gravity and absorption of coarse aggregates), ASTM C128 (standard test method for specific gravity and absorption of fine aggregates), ASTM C136 (standard test method for sieve analysis of fine and coarse aggregates), and ASTM C117 (standard test method for materials finer than 75-μm sieve in mineral aggregates by washing) were performed to document the properties of the materials used in this study. For each batch, the temperature, unit weight, and air content were documented and slump flow, T_{50}, VSI, and J-ring slump flow tests were performed to determine the fresh-state properties of the mixtures. This chapter provides details regarding the materials that were used in the study, mixture designs, specimen preparation, and test procedures.

3.1 – Overview of Test Program

The test program (see Figure 3.1 and Table 3.1) included a series of batches with a target strength of 6 ksi (normal strength concrete) and a series with a target strength of 10 ksi (high strength concrete). Each series had a batch with no fibers that was used as a reference and several batches with different volume fractions (0.5, 0.75, 1.0, and 1.5%) of hooked-end steel fibers (fibers properties are presented in Tables 3.2). For each mixture, seven standard tests were conducted to characterize the fresh-state properties (discussed in Section 3.3). In addition, each batch was tested in compression (ASTM C39), flexure (ASTM C1609), and tension to determine the concrete properties in the hardened-state (discussed in Section 3.4).

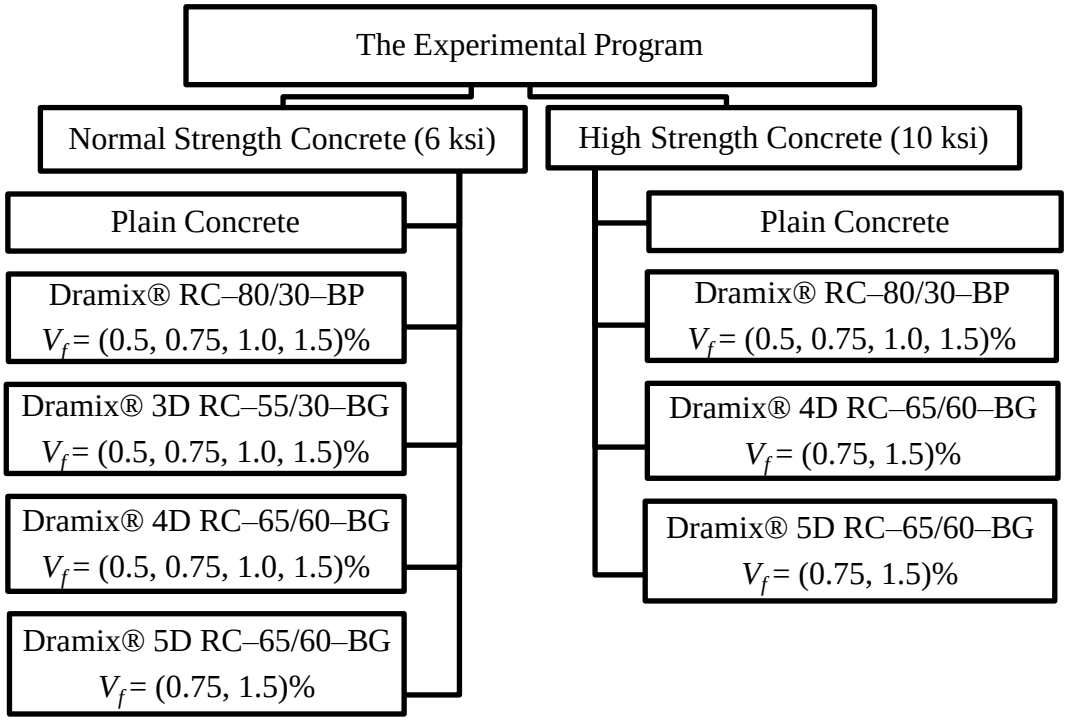

Figure 3.1 – Outline of the experimental program.

Table 3.1 – Fiber volume fraction and target compressive strength of each batch.

Batch ID	Fiber type	V_f (%)	$f`_c$ (ksi)
C 1	N/A	0	6
B 1	(RC-80/30-BP)	0.5	
B 2	(RC-80/30-BP)	0.75	
B 3	(RC-80/30-BP)	1.0	
B 4	(RC-80/30-BP)	1.5	
B 5	3D (RC-55/30-BG)	0.5	
B 6	3D (RC-55/30-BG)	0.75	
B 7	3D (RC-55/30-BG)	1.0	
B 8	3D (RC-55/30-BG)	1.5	
B 9	4D (RC-65/60-BG)	0.5	
B 10	4D (RC-65/60-BG)	0.75	
B 11	4D (RC-65/60-BG)	1.0	
B 12	4D (RC-65/60-BG)	1.5	
B 13	5D (RC-65/60-BG)	0.75	
B 14	5D (RC-65/60-BG)	1.5	
C 2	N/A	0	10
B 15	(RC-80/30-BP)	0.5	
B 16	(RC-80/30-BP)	0.75	
B 17	(RC-80/30-BP)	1.0	
B 18	(RC-80/30-BP)	1.5	
B 19	4D (RC-65/60-BG)	0.75	
B 20	4D (RC-65/60-BG)	1.5	
B 21	5D (RC-65/60-BG)	0.75	
B 22	5D (RC-65/60-BG)	1.5	

3.2 – Preparation of Specimens

3.2.1 – Formwork

Several types of molds were used for the experimental program. Five 6×12 inch cylindrical steel forms were used for casting specimens for the compression tests. Five 6×6×20 inch forms (four were made of steel, and one was made of wood) were used for casting the flexural test

specimens. Five 6×6×20 inch wood forms were used for casting the tensile test specimens (Figure 3.2). As shown, two #6 steel bars (16 inch length and 81.5 ksi yield strength) were placed along the centroidal axis of the specimen prior to casting. The bars protruded 6 inches beyond the ends of the concrete specimen to (as described later) faciliate loading of the specimen. The steel bars were not connected at the center in order to force the specimen to fail at that location.

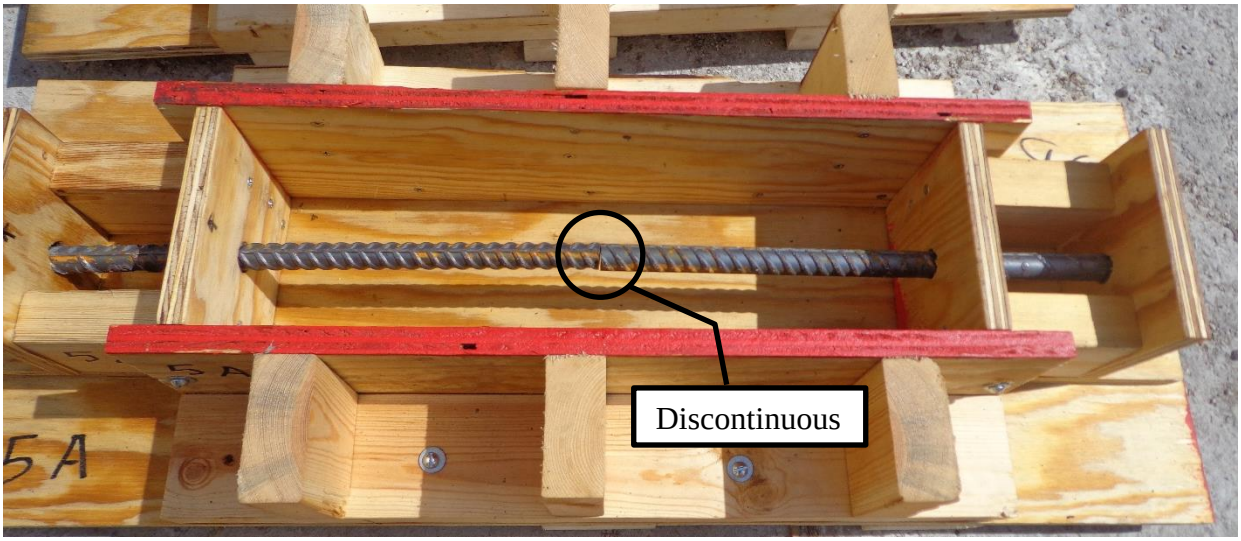

Figure 3.2 – A tension form.

3.2.2 – Mixture Proportions

The concrete mixtures used in this study incorporated the following materials:

1. Cement: ASTM type I Portland cement
2. Fly ash: Class C fly ash
3. Fine aggregate: Kansas River Sand (specific gravity of 2.62 and absorption of 0.46%)
4. Coarse aggregate: Kansas River Rock (½ inch nominal maximum size, specific gravity of 2.56, and absorption of 2.31%)
5. Chemical admixtures: Superplasticizer (ADVA® 195) and a viscosity modifying agent (VMAR® 3)

6. Fibers: Four types of hooked-end steel fibers were used (see Table 3.2 for details).

Table 3.2 – Characteristics of fibers used in this study.

Property	Fiber type			
	RC-80/30-BP	3D RC-55/30-BG	4D RC-65/60-BG	5D RC-65/60-BG
				
Bundling	glued	glued	glued	glued
End-deformation				
Length (mm)	30	30	60	60
Diameter (mm)	0.38	0.55	0.9	0.9
Aspect Ratio	79	55	65	65
Tensile Strength (N/mm2)	2300	1350	1500	2300
Young's Modulus (N/mm2)	210	210	210	210
Specific gravity	7.85	7.85	7.85	7.85
Relative Unit Cost[1]	2.0	1.0	1.0	1.1

[1] Source: Producer

Aside from the fiber volume fraction, which varied, two concrete mixtures were used in this study (Table 3.3). The first, which had a water-cementitious material ratio of 0.41, was used

to produce concrete with a target compressive strength of 6 ksi. The second, which had a water-cementitious material ratio of 0.29, was used to produce concrete with a target compressive strength of 10 ksi. The mixture proportions shown in Table 3.3 are based on both the fine and coarse aggregates being in a saturated surface dry (SSD) condition.

Table 3.3 – Concrete proportions per cubic yard.

Material	Batch ID	
	6 ksi	10 ksi
Type I Portland Cement (lbf)	627	1013
Class C Fly Ash (lbf)	549	253
Kansas River Sand (lbf)	1379	1436
Kansas River Rock (lbf)	752	844
Water (lbf)	482	367
VMAR 3 (mL)	4775	2700
ADVA® 195 (mL)	416	3300

3.2.3 – Mixing and Placing

Two different batching methods were used. The first procedure was used for small-scale batches (1.0 ft^3) early in the study aimed at developing the standard mixture designs. A second method was used for the larger batches (6.75 ft^3) used to cast the specimens for testing under compression, tension, and flexure.

Mixing Method 1

This method was based on Liao et al (2006). Prior to mixing, coarse aggregates were soaked in water for 24 hours and then dried with towels to achieve a saturated surface-dry condition (SSD) at the time of mixing. Fine aggregates were sampled (approximately 500 g sample size) and tested according to ASTM C70 to determine the free surface moisture content. All materials were weighed prior to mixing using a certified electronic scale with a precision of 0.01 lbs. An electrical pan mixer was used.

The mixing procedure, shown in Figures 3.3 to 3.7, was as follows: (1) Fine aggregate, cement, and fly ash were added and mixed for 1 minute, (2) Half of the water was added and mixed for 1 minute, (3) One quarter of the water was premixed with the superplasticizer and added and then mixed for 2 minutes, (3) The remaining water was premixed with the viscosity modifying admixture and added and then mixed for 2 minutes, (4) Coarse aggregate was added and mixed for 2 minutes, (5) Steel fibers were added slowly followed by 2 minutes of mixing, (6) The mixer was stopped for two minutes to allow for the water-soluble glue on the fibers to dissolve, and then the concrete was re-mixed for 2 minutes to further distribute the fibers. The temperature of the fresh concrete was measured according to ASTM C1064 (standard test method for temperature of freshly mixed hydraulic-cement concrete) after step 6.

Figure 3.3 – Step 1: Add the fine aggregate, cement, and fly ash and mix for 1 minute.

Figure 3.4 – Step 2: Add half of the water and mix for 1 minute.

Figure 3.5 – Steps 3 and 4: Add a quarter of the water after premixing with SP, and mix for 2 minutes, followed by the remaining water, premixed with VMA, and mix for 2 minutes.

Figure 3.6 – Step 4: Add the coarse aggregate and mix for 2 minutes.

Figure 3.7 – Steps 5 and 6: Slowly add the fibers, mix for 2 minutes, pause mixing for 2 minutes, and mix again for 2 minutes.

Mixing Method 2

The second mixing procedure was adapted from the first to allow for use of a larger drum mixer to accommodate larger batch sizes (6.75 ft^3 each). For each batch, the free surface moisture content was determined for both the fine and coarse aggregate using procedures from ASTM C70 or C566, to allow for adjustments to the amount of water added to the mixture.

The mixing procedure, shown in Figures 3.8 to 3.15, was as follows: (1) 90% of the water, premixed with SP, was mixed briefly with 50% of the coarse aggregate, (2) 50% of the cement and 50% of the fly ash were added and mixed for 2 minutes, (3) The remaining coarse aggregate, cement, and fly ash were added and mixed for 2 minutes, (4) 50% of the fine aggregate was added along with the remaining water, premixed with VMA, and mixed for 2 minutes, (5) The remaining fine aggregate was added and mixed for 2 minutes, (6) The steel fibers were added slowly and then mixed for 2 minutes, (7) The mixer speed was slowed down for 2 minutes to allow the water-soluble glue on the fibers to dissolve, and then the mixer speed was increased and allowed to blend the concrete until the fibers were well distributed (except that mixing was stopped after 20 minutes regardless of fiber distribution).

Figure 3.8 – Step 1: Add 90% of the water, premixed with SP, and mix with 50% of the coarse aggregate.

Figure 3.9 – Step 2: Add 50% of the cement and fly ash and mix for 2 minutes.

Figure 3.10 – Step 3: Add the remaining coarse aggregate, cement, and fly ash and mix for 2 minutes.

Figure 3.11 – Step 4: Add 50% of the fine aggregate.

Figure 3.12 – Step 4: Add the remaining water, premixed with VMA, and mix for 2 minutes.

Figure 3.13 – Step 5: Add the remaining fine aggregate and mix for 2 minutes.

Figure 3.14 – Step 6: Slowly add the steel fibers and mix for 2 minutes.

Figure 3.15 – Step 7: Slow or stop the mixer for two minutes and then mix for 20 minutes.

After mixing, tests (described in the following sections) were performed to document the fresh-state properties of the concrete. Concrete was placed in the forms using a 5-gallon bucket, as shown in Figure 3.16, that had been filled by pouring concrete directly out of the mixer. No vibration was used to avoid disturbing the fiber orientation.

Figure 3.16 – Concrete being poured into the forms.

3.2.4 – Curing

The freshly cast concrete specimens were covered with plastic sheets immediately after casting, as shown in Figure 3.17, to slow evaporation. Specimens were removed from the molds within 24 ± 8 hours after casting. Specimens were then labeled and placed in a curing room (in accordance to ASTM C511) until the testing date.

Figure 3.17 – Specimens after casting, covered with plastic sheets.

3.3 – Tests of Fresh-State Properties

3.3.1 – Slump Flow Test

The slump flow test was conducted for all batches following ASTM C1611 (standard test method for slump flow of self-consolidating concrete) to assess the horizontal free-flow characteristics of the concrete. The test method is similar to the slump test (ASTM C143) with some modifications. In the ASTM C1611 test, the average of two diameters measured perpendicular to each other is reported instead of the loss in height for the slump test of fresh concrete (ASTM C143). A mold that conforms to ASTM C143 specifications; a 30x30 inch non-absorbent, smooth, rigid base plate; strike-off bar as described in ASTM C173 (standard test method for air content of freshly mixed concrete by the volumetric method); and a metal roll-up measuring tape were necessary to perform the test. The following steps were adapted from ASTM C1611 specification requirements and were followed to obtain the slump flow for each batch:

- the base plate was leveled;
- the cone was placed at the center of the non-absorbent base plate;
- the slump cone was filled with fresh concrete following filling procedure type B (Inverted Mold);
- the extra concrete was struck-off by using the strike-off bar;
- concrete at the base of the mold was removed;
- the slump cone was slowly raised (3 ± 1 second) by a steady upward lift with no lateral or torsional motion allowing the concrete to flow freely;
- when the matrix stopped flowing, the average of two diameters (the largest diameter and a diameter perpendicular to it) was reported to the nearest 1⁄2 inch. The slump flow is the average of those diameters as shown in Figure 3.18.

According to ACI committee 237 (2007), concrete with a measured slump flow between 18 and 30 inches can be classified as a self-consolidating concrete (SCC).

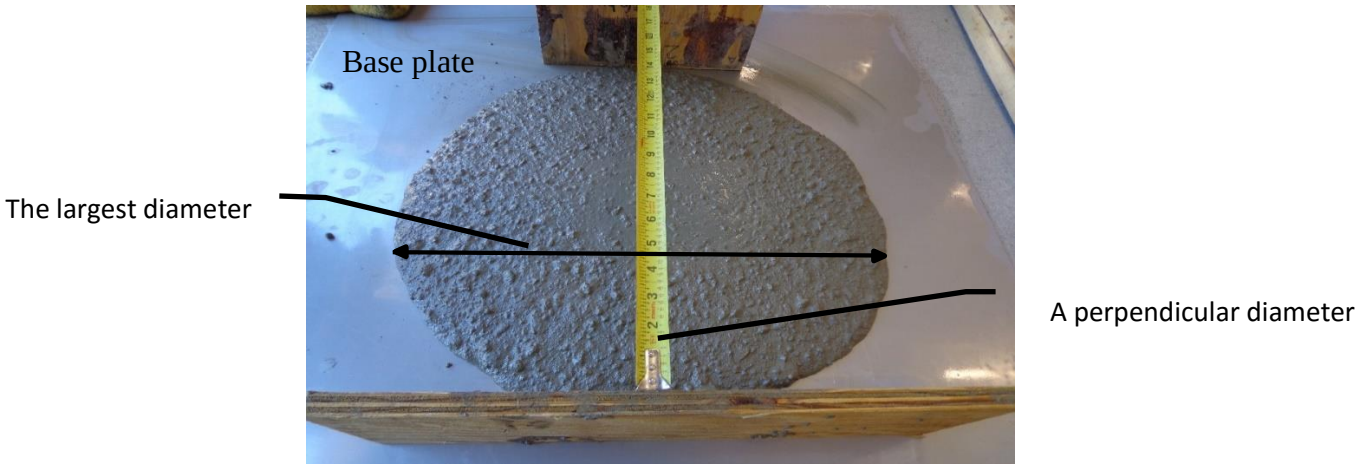

Figure 3.18 – The slump flow test (ASTM C1611).

3.3.2 – Visual Stability Index

The Visual Stability Index (VSI) is a qualitative assessment of the stability of each batch based on visual examination of the slump flow pie. Based on the definitions in Table 3.4 and Figures 3.19-3.22, a Visual Stability Index (VSI) of 0, 1, 2, or 3 was assigned to each mixture. A VSI of 2 or 3 indicates segregation possibility.

Table 3.4 – VSI values (ACI Committee 237, 2007; ASTM C1611, 2010).

VSI Value	Criteria
0 = Highly Stable	No evidence of bleeding or segregation
1 = Stable	No evidence of segregation and slight bleeding as a sheen on the concrete
2 = Unstable	A slight mortar halo ≤ 0.5 in. and/or aggregates pile
3 = Highly Unstable	A large mortar halo ≥ 0.5 in. and/or aggregates pile (clearly segregated)

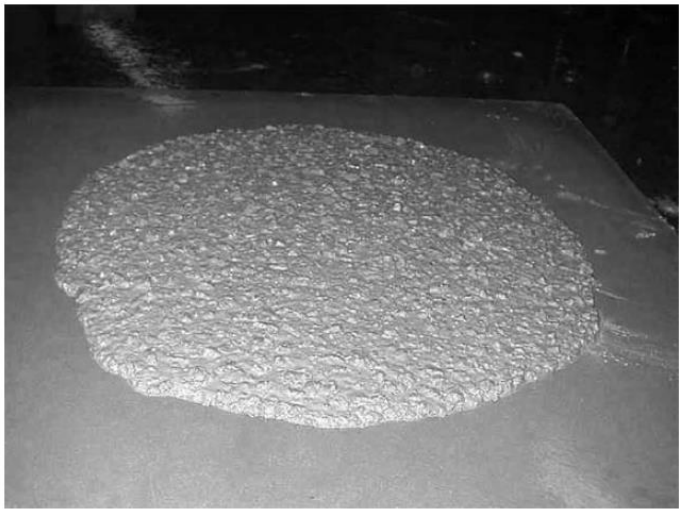

Figure 3.19 – Homogeneous concrete mass with no evidence of bleeding (VSI = 0) (ASTM C1611, 2010).

Figure 3.20 – Slight bleeding investigated as a sheen on the surface (VSI = 1) (ASTM C1611, 2010).

Figure 3.21 – Evidence of a water sheen mortar halo (VSI = 2) (ASTM C1611, 2010).

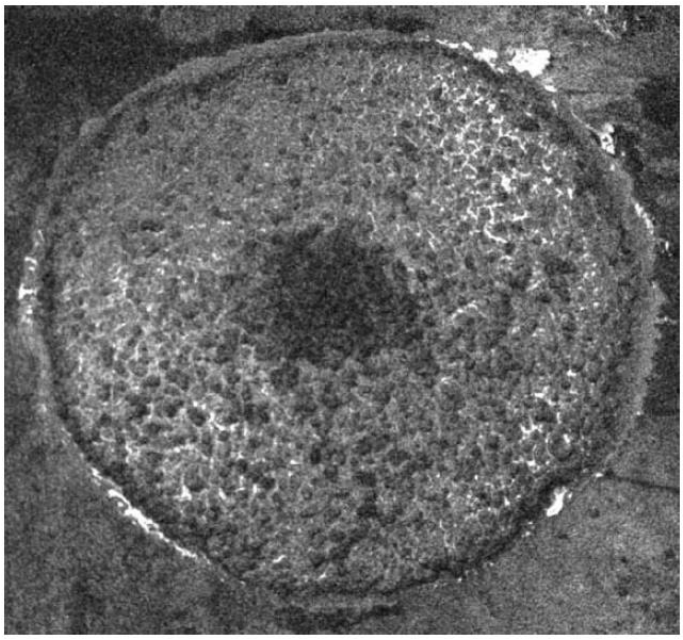

Figure 3.22 – Presence of a mortar halo with a concentration of coarse aggregates at the center (VSI = 3) (ASTM C1611, 2010).

3.3.3 – T_{50}

ACI 237R defines T_{50} as the time it takes the outer edge of the spreading concrete, resulting from the slump flow test, to reach a diameter of 20 inches (50 cm) from the time that the mold is first raised, as shown in Figure 3.23. T_{50} is a relative measure of the unconfined flow rate of SCCs. This test gives an indication of viscosity, where the larger the T_{50} time, the higher the viscosity. ACI 237R characterizes SCC mixtures with T_{50} time of 2 seconds or less as low viscosity SCCs, and mixtures of T_{50} greater than 5 seconds as high viscosity SCCs. This test was conducted for all batches at the same time as the slump flow tests.

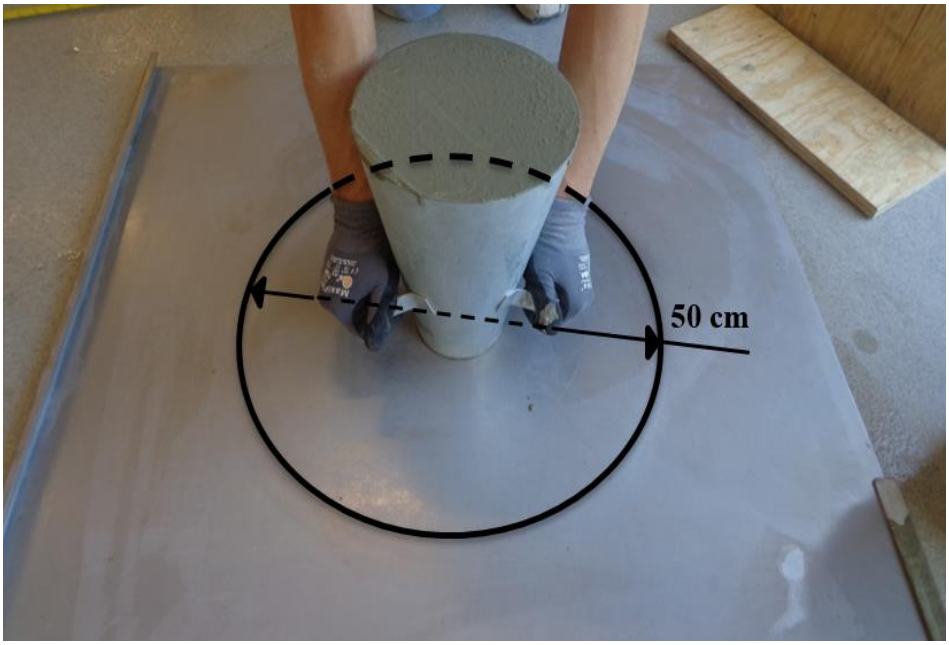

Figure 3.23 – T_{50} Test.

3.3.4 – J-ring Slump Flow Test

This test is used to characterize the passing ability of SCCs through reinforcement. The passing ability is an important property of SCC when it is used in members with congested reinforcement (ACI Committee 237, 2007). Typically, the higher the J-ring slump flow value, the faster and farther the SCC can travel under its own weight and through a steel reinforced formwork. This test was conducted for all batches to evaluate the effect of using different volume fractions of various types of hooked-end steel fiber on the passing ability (blocking assessment) of SCCs. The procedure was run as follows:

- after leveling a base plate, a cone was placed and firmly held down at the center of the base plate, and a J-ring was placed around the base of the cone;
- after filling the cone with fresh concrete, the extra concrete was removed by using a strike-off bar;

- the slump cone was slowly raised (3 ± 1 second) by a steady upward lift with no lateral or torsional motion allowing the concrete to flow freely;
- when the concrete stopped flowing, the average of two diameters (the largest diameter and a diameter perpendicular to it as shown in Figure 3.24) was reported to the nearest 1⁄2 inch. The reported J-ring slump flow is the average of the two diameters.

The passing ability of each batch was calculated as the difference between the slump flow and the J-ring slump flow results. Standard values for passing ability, as defined by (ASTM C1621, 2014), are given in Table 3.5.

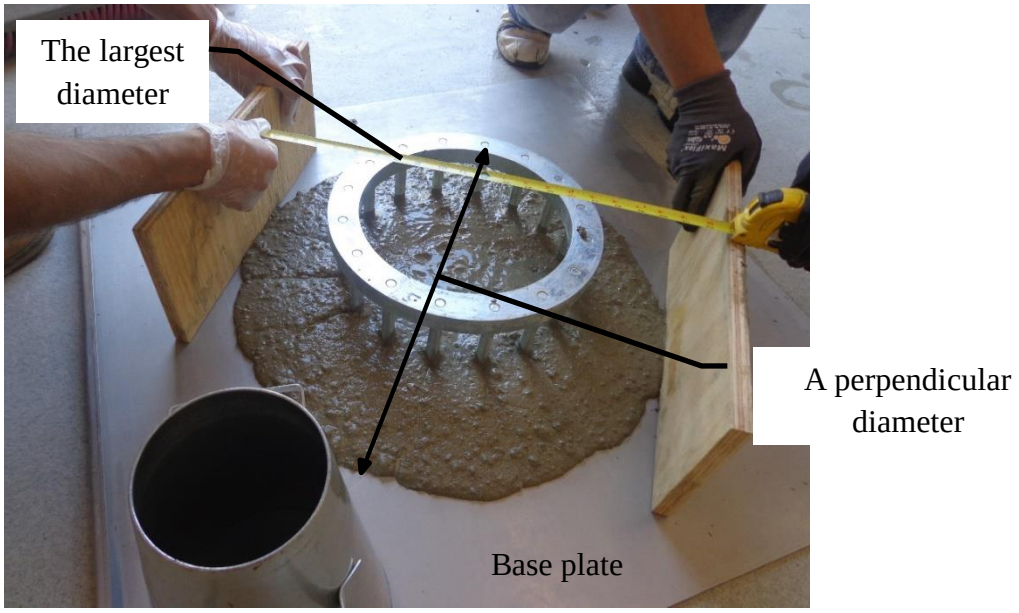

Figure 3.24 – J-ring slump flow test (ASTM C1611).

Table 3.5 – Typical passing ability values (ASTM C1621, 2014).

Passing Ability (in.)	Blocking Assessment
0 - 1	No visible blocking
> 1 - 2	Minimal to noticeable blocking
> 2	Noticeable to extreme blocking

3.3.5 – Concrete Density

The density of each batch was measured following ASTM C138 (standard test method for density (unit weight), yield, and air content (gravimetric) of concrete) procedures, except that no rodding or vibration was performed. The test required a balance accurate to 0.1 lbs and a 1/4 ft^3 cylindrical steel container (the steel bowl used to conduct the air content test was used because the nominal maximum size of the coarse aggregates was less than 1 inch). The following steps were used to obtain the concrete density:

- the mass of the empty container was determined (M_m);
- the concrete was poured into the container in one layer and without any rodding, vibration, or tapping;
- the concrete top surface was finished smoothly using a 14 × 14 × ¼ inch flat square glass plate;
- after cleaning all the external sides of the measure, the mass of the concrete and the measure (M_c) was reported.

The concrete density was then calculated as $(M_c - M_m)/(0.25\ \text{ft}^3)$.

3.3.6 – Air Content

The air content of each batch was routinely measured after measuring the concrete density. The test was performed in accordance with ASTM C231 standard specifications (the pressure method) except no rodding or vibration was performed (the concrete was placed into the bowl in one layer without any a rodding, vibration, or tapping). The test required a type B vertical air meter as shown in Figure 3.25, a 1.25 lbs rubber head mallet, a 12×3/4×1/8 inch metal strike-off bar, a

15×15×1/4 inch flat strike-off glass plate, and a trowel. The air content was calculated for each mixture to the nearest 0.1%.

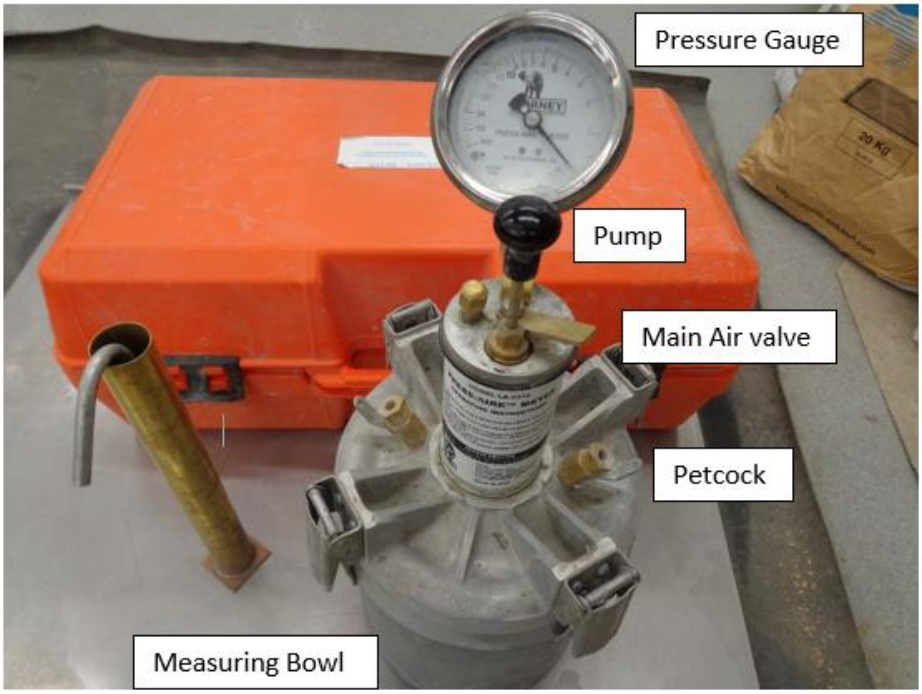

Figure 3.25 – An ASTM type B vertical air meter.

3.3.7 – Temperature

The temperature was measured for all mixtures following ASTM C1064.

3.4 – Tests of Hardened-State Properties

3.4.1 – Deformation Measurement

An infrared-based non-contact position sensor was used to determine deformations in the compression, flexure, and tension tests. It was used to determine the longitudinal and transverse strains in the compression tests; the mid-span net deflections, the primary crack width, and the support rotations in the flexure tests; and the crack widths in the direct tension tests. Figure 3.26 shows a typical position sensor.

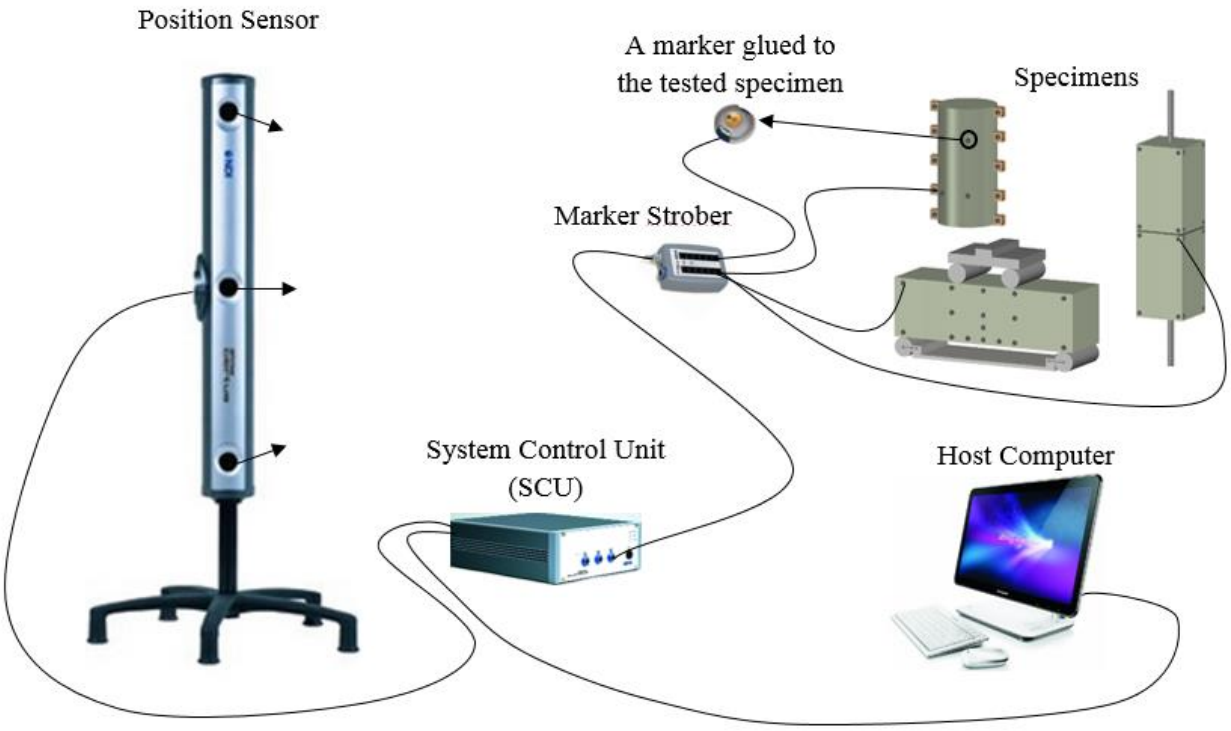

Figure 3.26 – Optical position track system.

3.4.2 – Uniaxial Compression Test

This test was conducted according to ASTM C39 (standard test method for compressive strength of cylindrical concrete specimens) on 6x12 inch cylindrical concrete specimens. Specimens were prepared and cured as described previously, and the ends of the specimens were ground smooth using an electrical grinder prior to testing. A hydraulic machine with a capacity of 600 kip was used to apply compression at the loading rates shown in Table 3.6. Testing was terminated after the post-peak strength decreased to less than 20% of the peak strength.

An infrared-based non-contact position sensor was used to measure the deformation of the cylinders. Sixteen markers were glued to the specimen, as shown in Figure 3.27. Markers numbered 5 and 6, which were located at mid-height, were used to calculate the lateral stains. Markers numbered 3, 4, 7, and 8 were used to calculate the longitudinal strains until one of the

four markers was dislodged due to cracking. After cracking, markers 15 and 16, which were fixed to the loading platens, were used to calculate the longitudinal strains.

Table 3.6 – Compression test loading rates.

The compression stress as a percent of the target peak stress (%)	Loading rate (in./min)
0-5	0.100
5-50	0.015
50-100	0.006[a]
100-50[pc]	0.006[a]
50[pc]-20[pc]	0.020

Notes:
[pc]: post-peak stress.
[a]: the loading rate is according to ASTM C39 specifications.

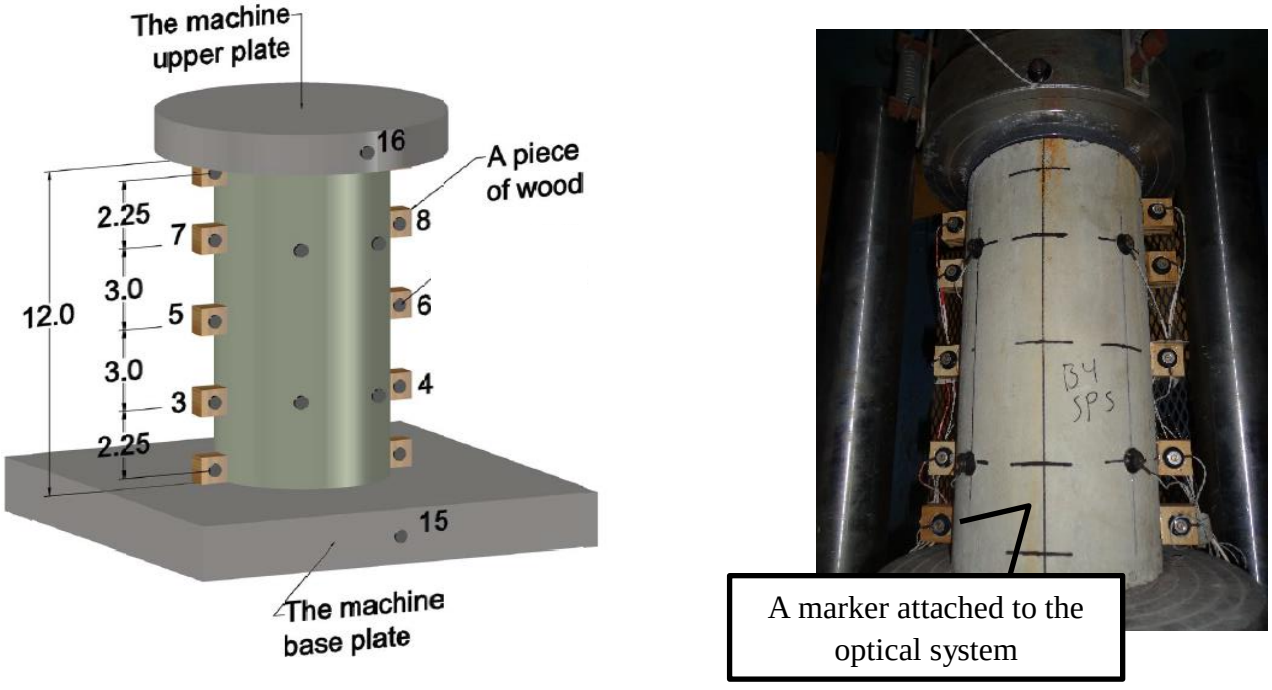

Figure 3.27 – A typical compression specimen.

After testing, the fracture type was noted in accordance with ASTM C39 specifications (illustrated in Figure 3.28). The concrete compression strength, static modulus of elasticity, and post-peak slope were calculated using Eq. 3-1 through 3-3. Note that Eq. 3-2 is different from that required by ASTM C469 for calculation of modulus of elasticity, which requires E_c be calculated between points corresponding to strains of 0.000050 and $\epsilon_{40\%}$. It is believed this change did not cause a systematic bias in the results given the linearity of the response to initial loading.

$$f_{cm} = \frac{P}{A} \tag{3-1}$$

$$E_c = \frac{\sigma_{40\%}}{\epsilon_{40\%}} \tag{3-2}$$

$$E_{PP} = \frac{-\sigma_{50\%}}{\epsilon_{50\%} - \epsilon_P} \tag{3-3}$$

where:

A = specimen cross-sectional area (in.^{2}),

E_c = modulus of elasticity (psi),

E_{PP} = post-peak slope (psi),

f_{cm} = compression strength (psi),

P = peak load (lbf),

$\epsilon_{40\%}$ = longitudinal strain produced by $\sigma_{40\%}$,

$\epsilon_{50\%}$ = longitudinal strain produced by $\sigma_{50\%}$,

ϵ_P = longitudinal strain at the peak,

$\sigma_{40\%}$ = prior-peak stress corresponding to 40 % of ultimate stress, (psi), and

$\sigma_{50\%}$ = post-peak stress corresponding to 50 % of ultimate stress, (psi).

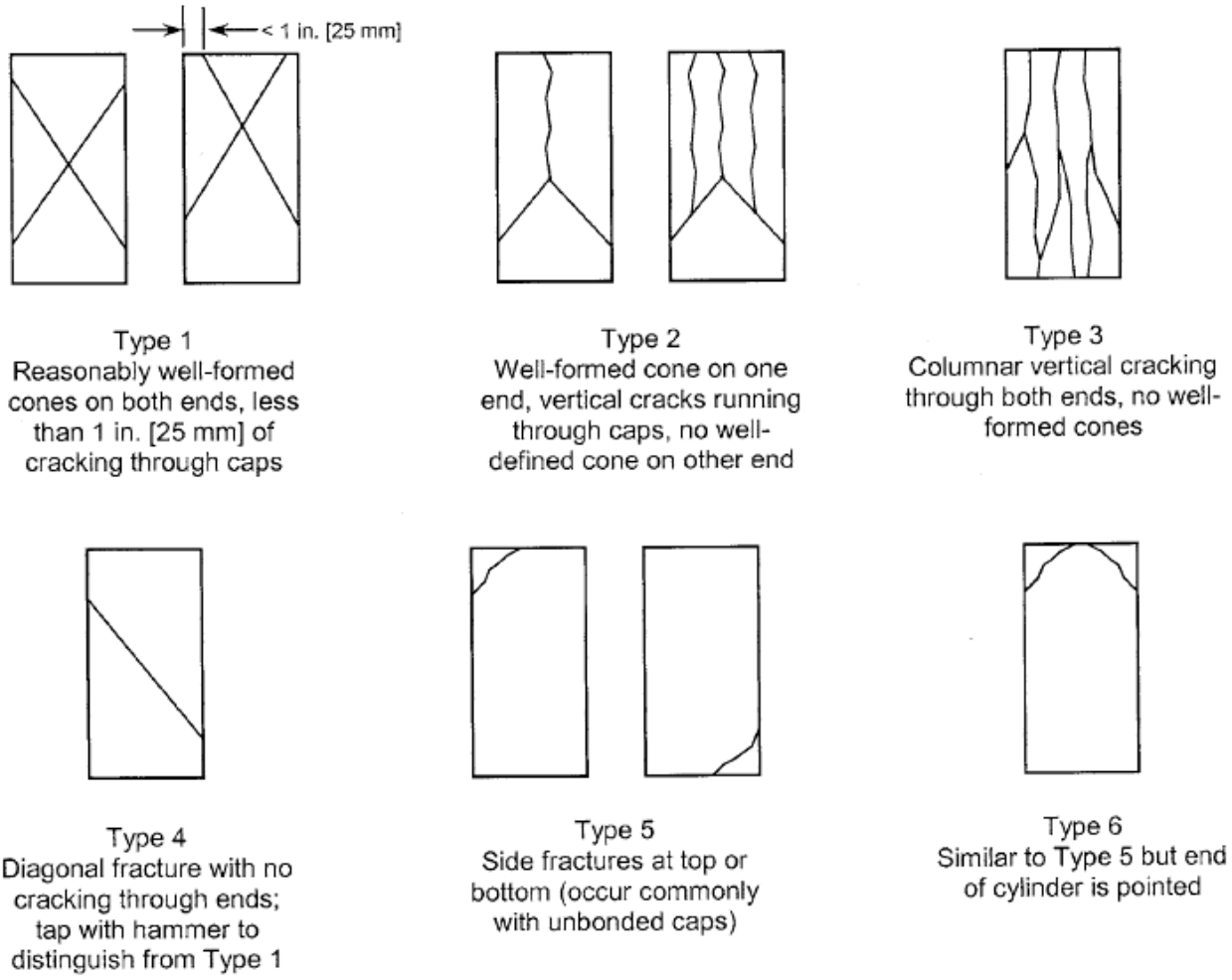

Figure 3.28 – Typical fracture patterns (ASTM C39, 2012).

3.4.3 – Flexure Test

For each batch, five 6×6×20 inch simply supported concrete beams were tested under third-point loading, as shown in Figure 3.29, according to ASTM C1609 (standard test method for flexural performance of fiber-reinforced concrete). A hydraulic machine with a capacity of 120 kip was used to load the specimens at the loading rates shown in Table 3.7. The test was terminated after the net deflection exceeded 0.15 inch. An infrared-based non-contact sensor was used to record specimen deformations. Sixteen markers, arranged as shown in Figure 3.30, were attached to each specimen. Markers 1, 5, 6, and 9 were used to calculate the mid-span deflection, markers

1, 3, 15, 5, 16, 7, and 9 were used to calculate the primary crack width, and markers 1, 2, 9, and 10 were used to calculate support rotations.

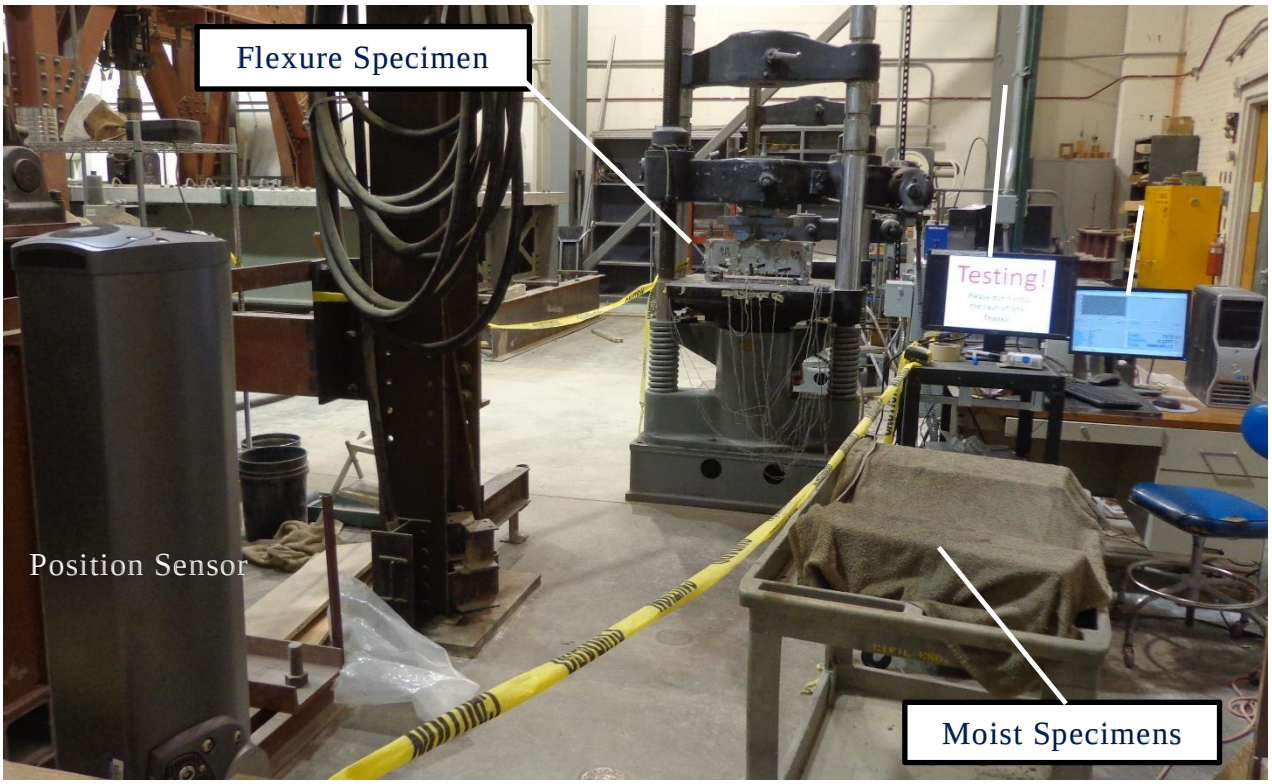

Figure 3.29 – The flexure test setup.

Table 3.7 – The loading rates of the flexure test.

The flexure stress as a percent of the first-peak stress (%)	Loading rate (in./min)
0-10	0.10
10-20	0.05
20-40	0.01
40-100	0.004
100-20p_1	0.012
Notes: 1) p_1: the first-peak strength.	

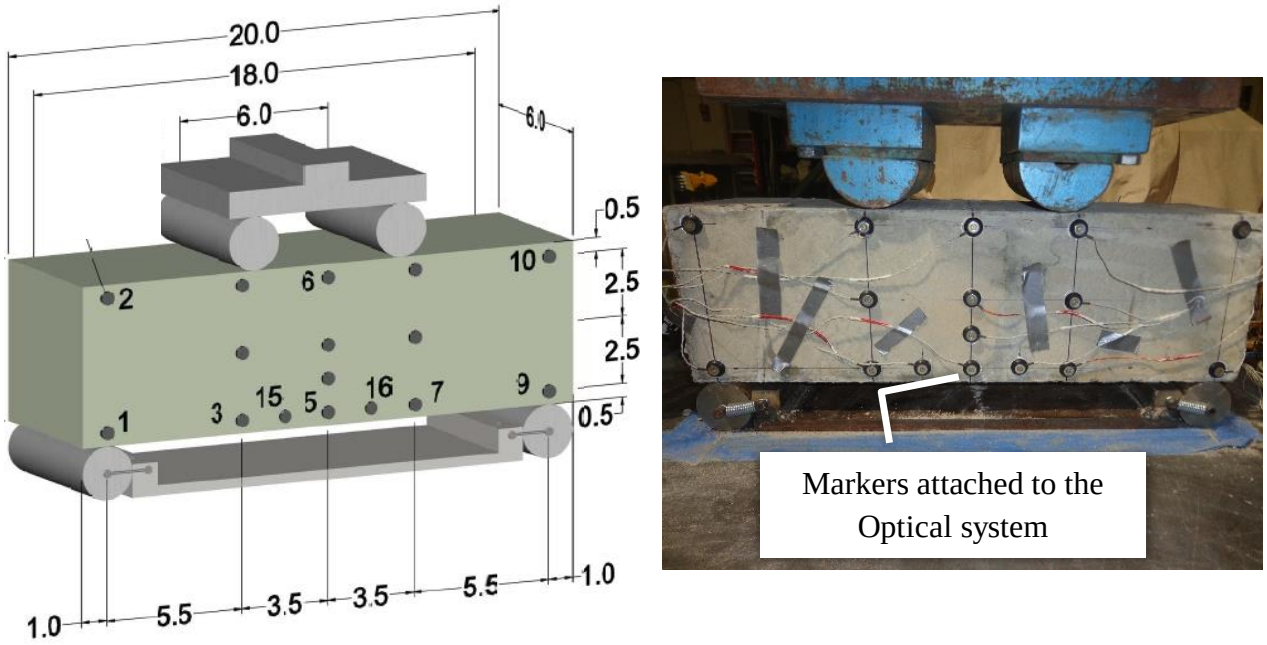

Figure 3.30 – A typical flexure specimen.

Figure 3.31 – A broken flexure beam.

Following the tests, the specimen was broken into two parts, shown in Figure 3.31, and the number of fibers exposed at the crack was counted. Results, in terms of load versus mid-span net deflection, primary crack width, and support rotations, are shown in Chapter 4 and Appendix C. The first-peak strength and the post-crack peak strength of each specimen were calculated using Eq. 3-4 and Eq. 3-5:

$$f_1 = \frac{P_1 L}{bd^2} \quad (3\text{-}4)$$

$$f_{\mathrm{pc}} = \frac{P_{\mathrm{pc}} L}{bd^2} \quad (3\text{-}5)$$

where:

b = average width of the specimen at the fracture (in.),

d = average depth of the specimen at the fracture (in.),

f_1 = first-peak (cracking) strength (psi),

f_{pc} = post-crack peak strength (psi),

L = span length, taken as 18 in.,

P_1 = first-peak (cracking) load (lbf), and

P_{pc} = post-crack peak load (lbf).

3.4.4 – Direct Tension Test

For each batch, five 6×6×20 inch concrete rectangular prisms were tested under tension to evaluate the tensile performance using parameters derived from the stress-crack width curves (Figure 3.32). As shown in Figures 3.33 and 3.34, each specimen had a 0.75 inch deep notch cut around its perimeter to force a crack to form at a known location. The specimens had a #6 bar passing through the center of the specimen that was discontinuous at the location of the notch. The reinforcing bar, which extended a minimum of 6 in. beyond the ends of the specimen, was used to load the specimen. A hydraulic machine with a capacity of 120 kip was used to load the specimens at the loading rates shown in Table 3.8. The test was terminated after the width of the crack exceeded 0.25 inch. An infrared-based non-contact position sensor was used to measure the width of the cracks. Sixteen markers were used to track the deformations in each specimen as shown in Figure 3.33.

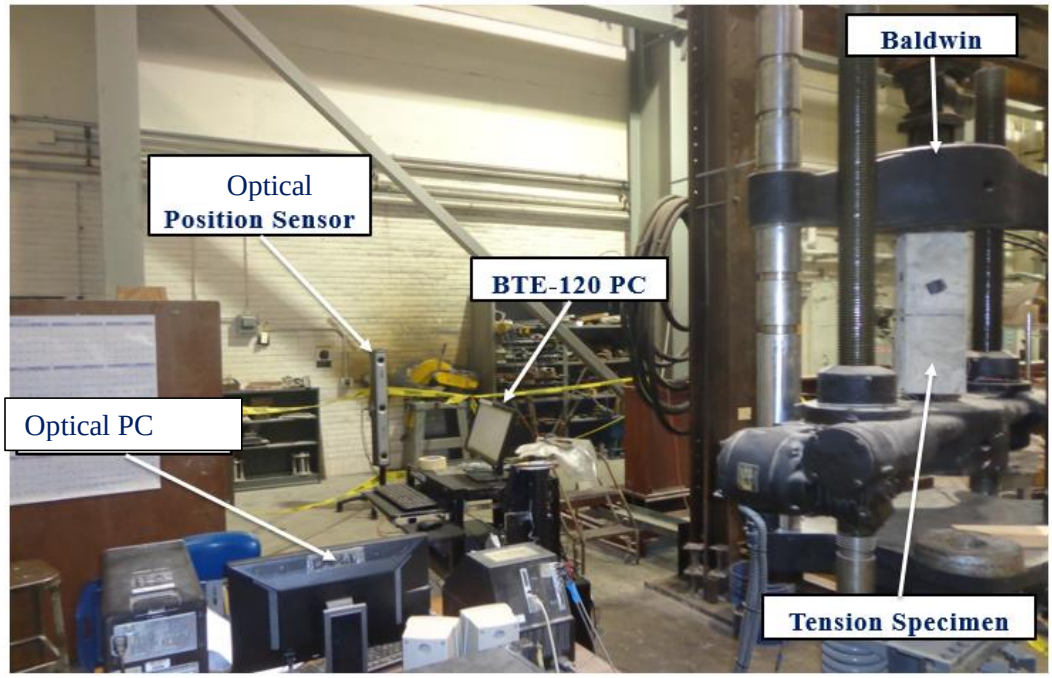

Figure 3.32 – The tension test setup.

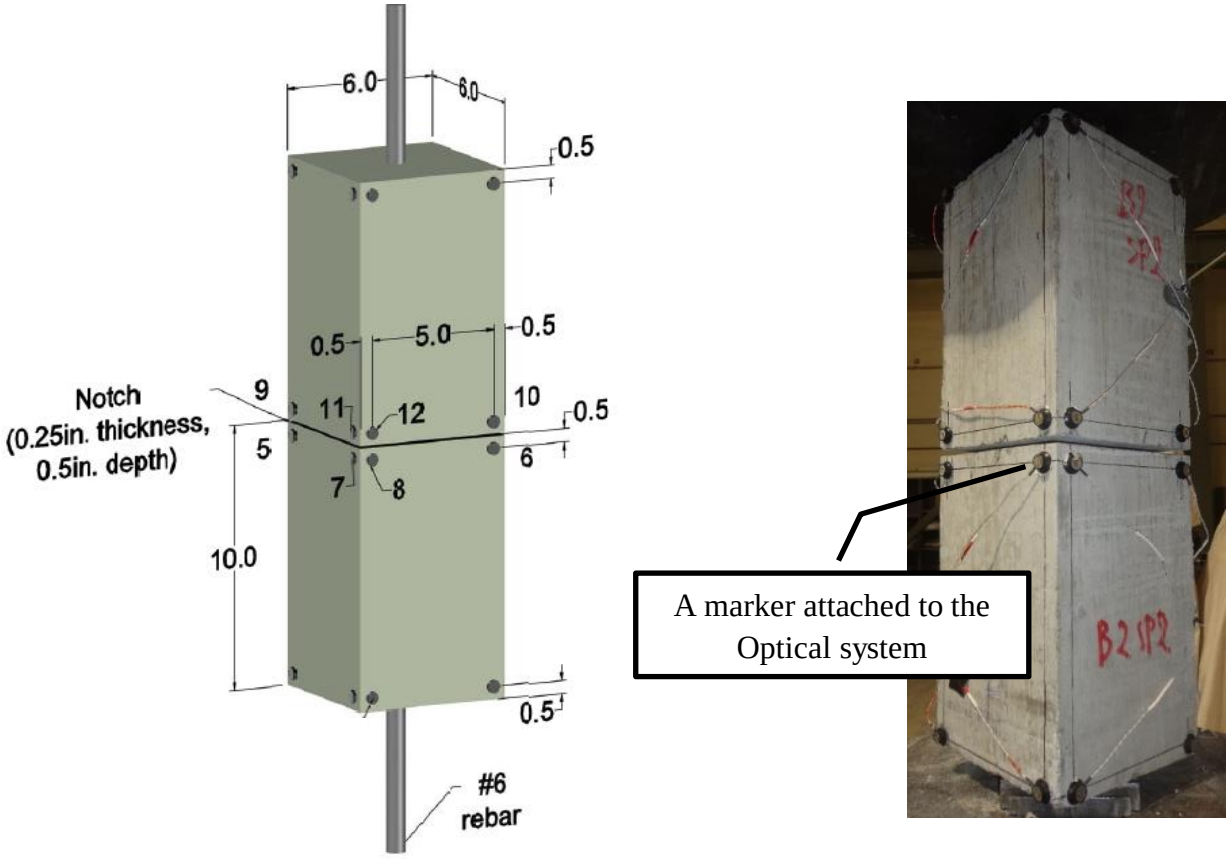

Figure 3.33 – A typical tension specimen.

Table 3.8 – The loading rates of the tension test.

The tensile stress as a percent of the first-peak stress (%)	Loading rate (in./min)
0-25	0.10
25-35	0.05
35-50	0.03
50-100	0.016
100-20p_1	0.016
Notes: 1) p_1: the first-peak strength.	

Figure 3.34 – Pre-notching a tension specimen.

Figure 3.35 – A broken tension specimen.

Following the tests, the specimen was broken into two parts (Figure 3.35) and the number of fibers crossing the failure surface was counted. The collected data was analyzed and the calculated tensile stress acting on the notched section was plotted versus crack width (see Chapter 4 and Appendix D). The area of the cracked section, first-peak tensile strength (σ_1), and post-crack peak strength (σ_{pc}) of each specimen were calculated using Eq. 3-6 through 3-8:

$$A = (b \times d) - A_{\#6} \tag{3-6}$$

$$\sigma_1 = \frac{P_1}{A} \tag{3-7}$$

$$\sigma_{\mathrm{pc}} = \frac{P_{\mathrm{pc}}}{A} \tag{3-8}$$

where:

A = cross sectional area at the cracked section (in.^{2}),

$A_{\#6}$ = cross sectional area of a #6 reinforcing bar (in.^{2}),

b = average width of the specimen at the fracture (in.),

d = average depth of the specimen at the fracture (in.),

P_1 = first-peak (cracking) load (lbf),

P_{pc} = post-crack peak load (lbf),

σ_1 = first-peak (cracking) stress (psi), and

σ_{pc} = post-crack peak stress (psi).

Due to small rotations, the crack width was not uniform across the cracked surface. To calculate an average crack width, it was assumed that the surfaces above and below the crack were rigid and that, therefore, the separation at the centroid of the cracked area represented the average crack width. The opening, ω, at the centroid of the section was calculated as follows. Figure 3.36, which shows a cross section of a tension specimen at the location of a crack, shows the locations (a, b, c, and d) where the opening of the crack at the surface could be calculated using measurements from the position tracking system (Figure 3.37). The crack openings calculated at c and d were averaged to find ω_1, the opening at the midpoint of line c-d (likewise for ω_2, the midpoint of line a-b). The crack width, ω, was then calculated using Eq. 3-9, which is based on the projection of a line passing through the midpoints of lines a-b and c-d.

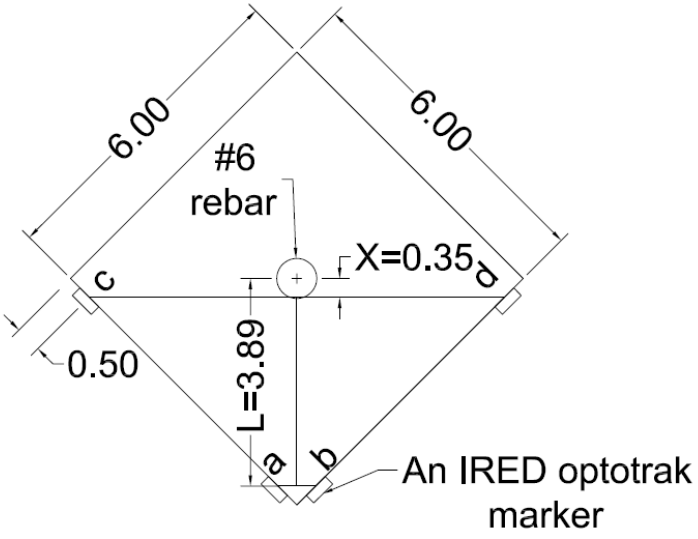

Figure 3.36 – A cross section of a tension specimen.

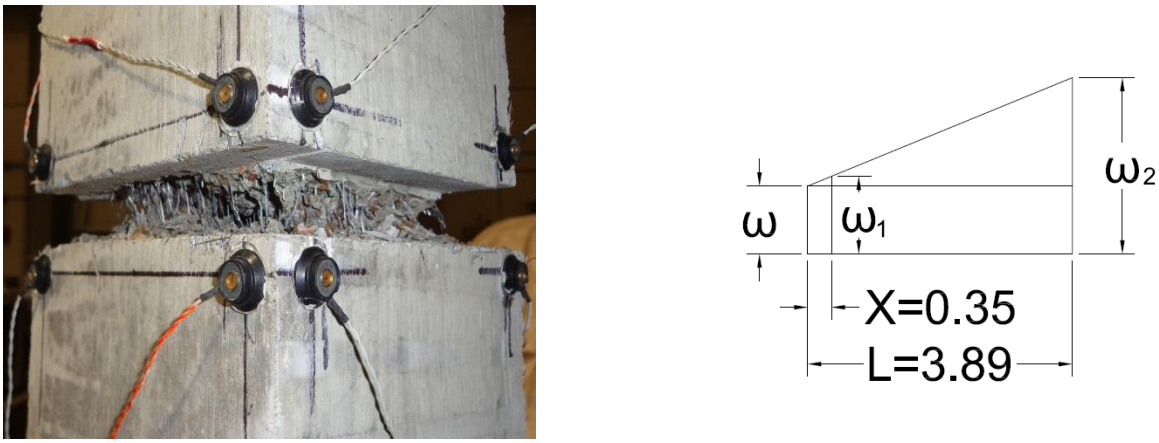

(a) **(b)**

Figure 3.37 – Close-up of crack opening and markers.

$$\omega = 1.1 \times \omega_1 - 0.1 \times \omega_2 \quad (3\text{-}9)$$

CHAPTER 4 TEST RESULTS

4.0 – General

This chapter is a summary of the experimental results. Detailed results are presented in Appendix A through D. The properties of freshly mixed self-consolidating fiber reinforced concrete (SCFRCs) such as temperature, density, air content, slump flow, Visual Stability Index (VSI), T_{50}, and J-ring slump flow are reported first. Then, the results of the uniaxial compression, flexural, and direct tension tests are summarized.

4.1 – Properties of Freshly Mixed SCFRCs

Each batch of SCFRC was tested for temperature, density, and air content (see Appendix A for detailed results). The concrete temperature, which was measured following ASTM C1064, ranged between 68 ºF and 89 ºF for control batch 1, control batch 2, and batch 1 to batch 19. The temperature of batch 20 to batch 22 ranged between 46 ºF and 58 ºF.

Concrete density, which was measured following ASTM C138, ranged between 139.0 lb/ft^3 and 144.8 lb/ft^3 for mixtures with a target compressive strength, f_c', of 6 ksi (control batch 1 as well as batch 1 to batch 14). The concrete density of mixtures with f_c' = 10 ksi (control batch 2 as well as batch 15 to batch 22) ranged between 145.4 lb/ft^3 and 151.2 lb/ft^3. As the target concrete compressive strength increased, the concrete density increased because of the lower water-to-cement ratio. There was also a slight trend of increased density with increased fiber volume fraction, likely due to the relatively high specific gravity of the fibers, but the difference was negligible.

The concrete air content, which was measured following the ASTM C231 standard test, ranged between 1% and 2.8% for all mixtures except for batch 4 which had an air content of 3.9%. As shown in Figures 4.1 and 4.2, air content tended to slightly increase as fiber volume fraction increased and as the water cement ratio decreased.

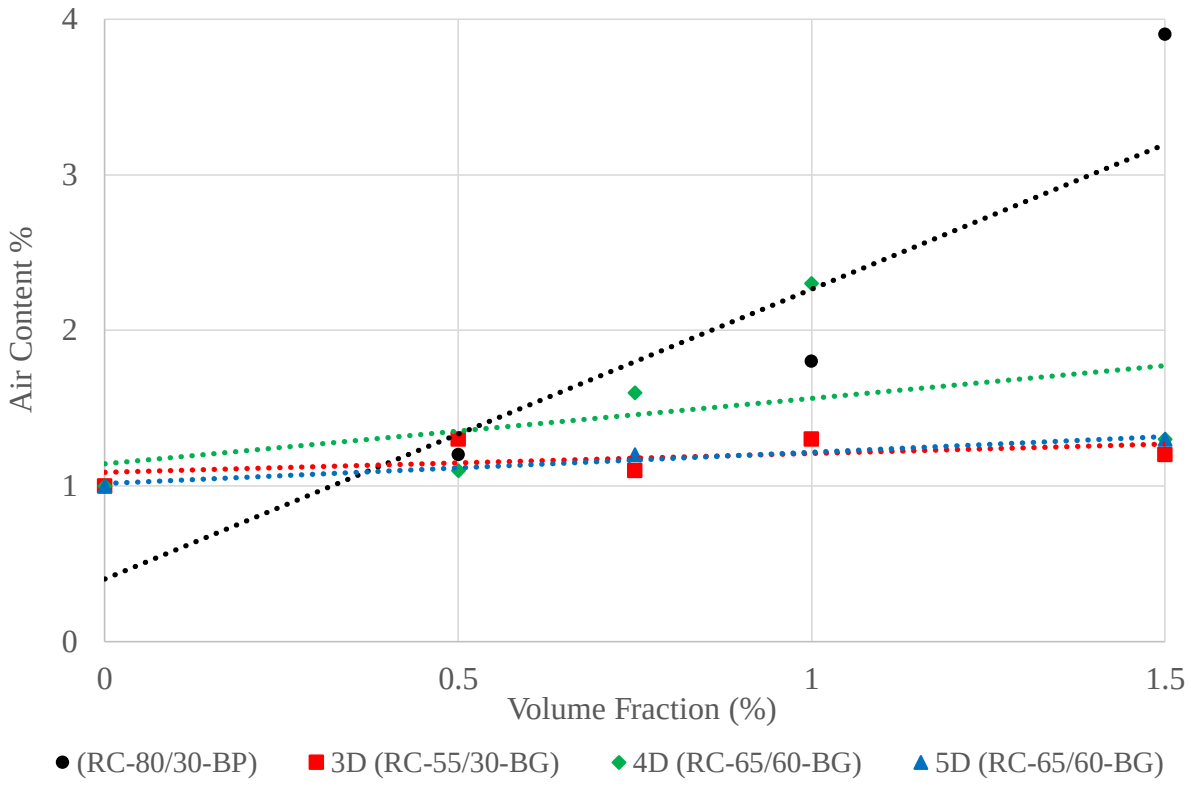

Figure 4.1 – Air content vs. fiber volume fraction ($f_c' = 6$ ksi).

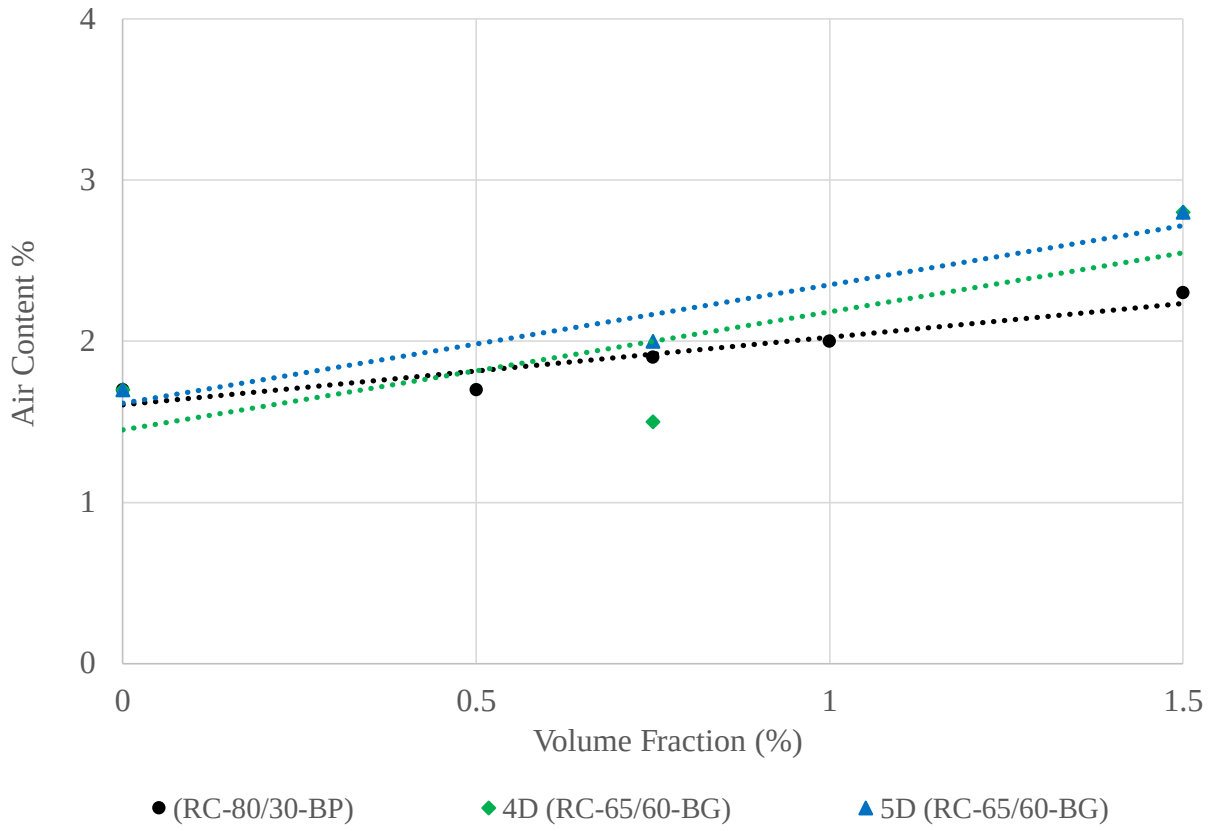

Figure 4.2 – Air content vs. fiber volume fraction ($f_c' = 10$ ksi).

Slump flow and J-ring slump flow tests were conducted for each batch (detailed results are given in Appendix A). Although the target slump flow was 25 inches, the slump flow measured in accordance with ASTM C1611 ranged between 20 inches and 27.5 inches for mixtures with $f_c' = 6$ ksi. The slump flow for mixtures with $f_c' = 10$ ksi ranged between 22.5 inches and 29.5 inches except for mixture 16, which had a slump flow of 30.5 inch. Results from the J-ring slump flow tests, which were conducted in accordance with ASTM C1621, ranged between 14.5 inches and 27 inches for mixtures with $f_c' = 6$ ksi. Measured J-ring slump flow results for the batches with $f_c' = 10$ ksi ranged between 20 inches and 27.5 inches. There was no target J-ring slump flow for this study.

As shown in Figures 4.3 through 4.6, the measured slump flow and J-ring slump flow decreased as the fiber volume fraction increased. Compared to the control batch results, the J-ring

slump flow test was more sensitive to fiber volume fraction than the slump flow test. For batches with a fiber volume fraction of 1.5%, mean J-ring slump flow results were 67% of the value measured for the control batch, whereas the slump flow was 80% of that measured for the control batch. Although the length of the 4D and 5D fibers (60 mm) is longer than the clear spacing of the J-ring bars (50 mm), the tests results did not conclusively show that batches with 4D and 5D fibers had a smaller J-ring slump flow than batches with shorter (30 mm) fibers.

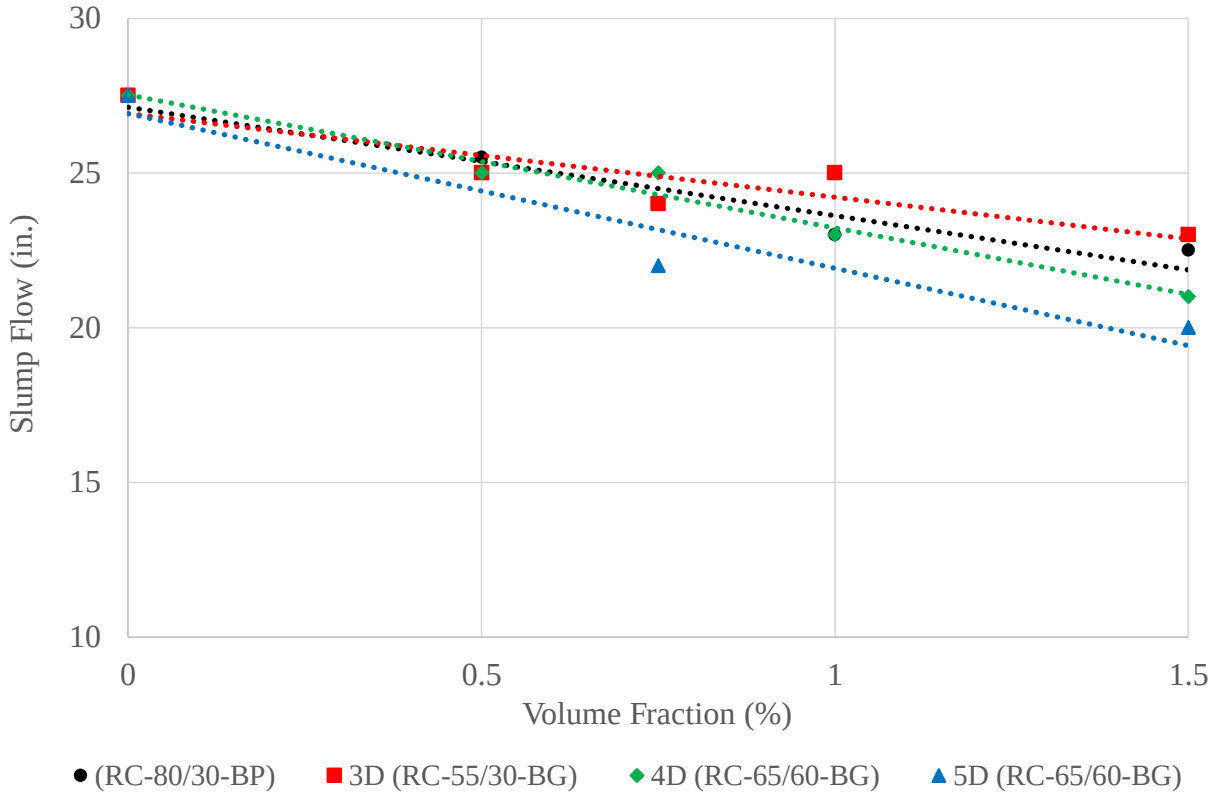

Figure 4.3 – Slump flow vs. fiber volume fraction ($f_c' = 6$ ksi).

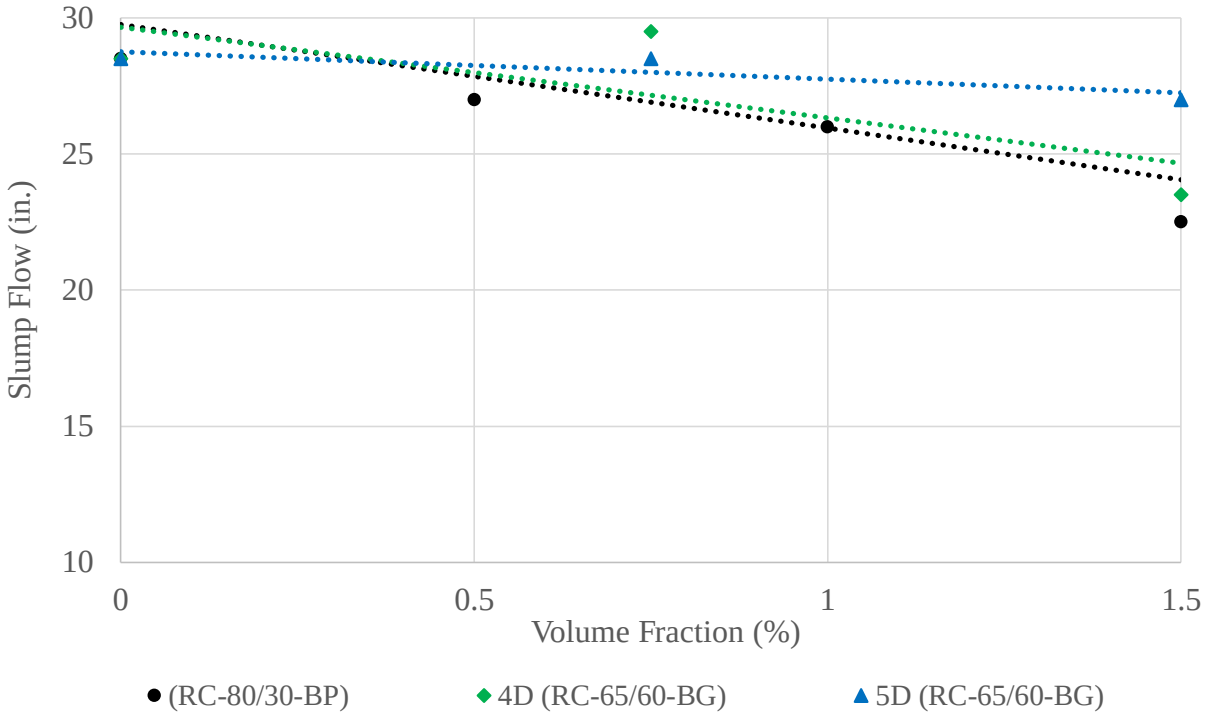

Figure 4.4 – Slump flow vs. fiber volume fraction ($f_c' = 10$ ksi).

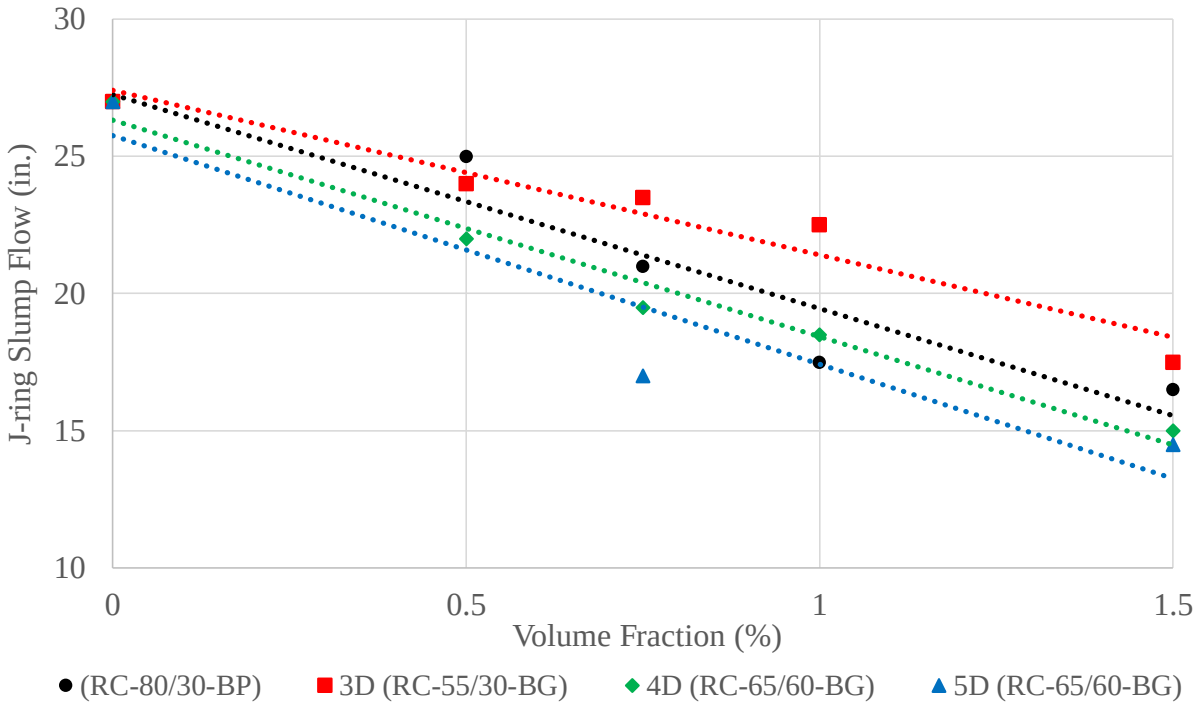

Figure 4.5 – J-ring slump flow vs. fiber volume fraction ($f_c' = 6$ ksi).

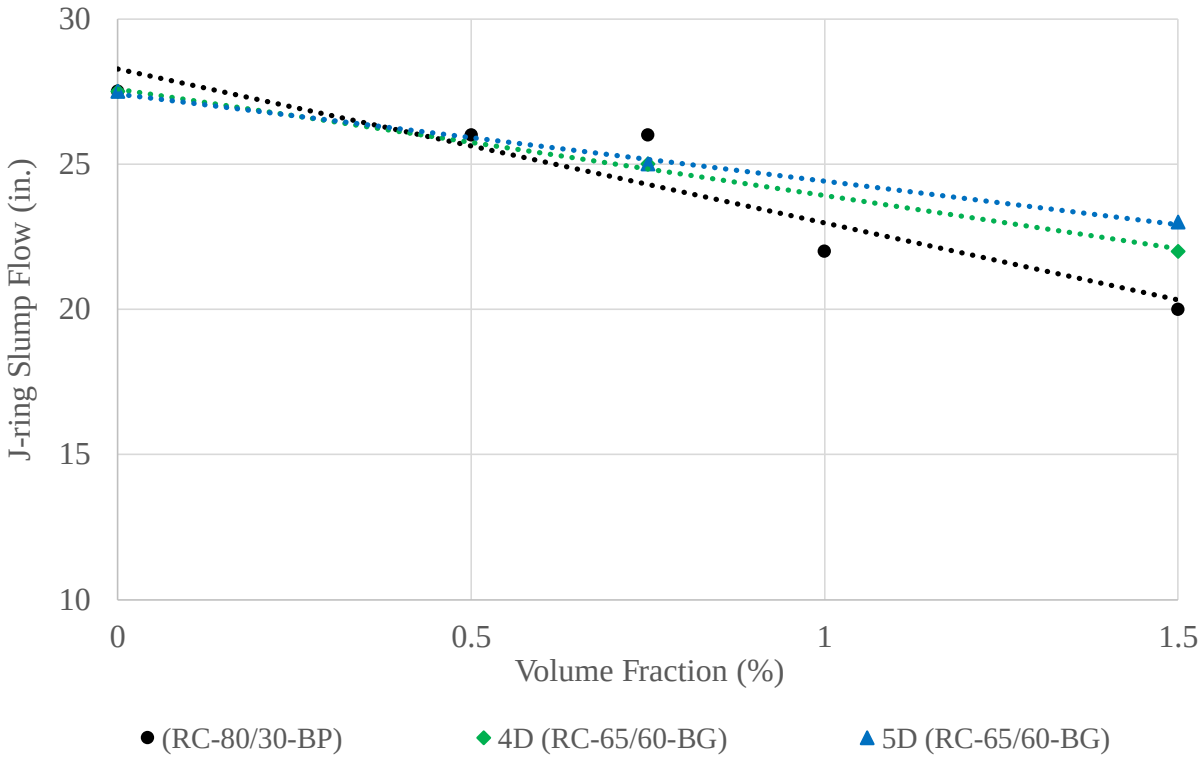

Figure 4.6 – J-ring **s**lump flow vs. fiber volume fraction ($f_c' = 10$ ksi).

Concrete mixtures were each assigned a Visual Stability Index (VSI) according to ASTM C1611. Assigned values were either 0 or 1 for all batches except for batches (7, 16, and 22) that had VSI of 2. It is not clear why three batches showed more bleeding/segregation than the others, as there is no correlation between VSI and fiber volume fraction, air content, temperature, or density in this study.

Finally, T_{50} was measured for each batch following ASTM C1611 procedures, with results ranging between 0.6 seconds and 0.95 seconds for mixtures with $f_c' = 6$ ksi. The T_{50} test results for batches with $f_c' = 10$ ksi ranged between 1.7 seconds and 3.4 seconds.

4.1.1 – Separation of Fiber Bundles

It was observed that the mixing time required to fully separate the bundles (or "packets") of fibers varied by fiber type. Fiber type RC-80/30-BP needed six minutes to qualitatively achieve complete separation, whereas fiber type 3D (RC-55/30-BG) needed more than 20 minutes. Because mixing time was limited to 20 minutes in this study, full separation of the fibers was not achieved for batches with this fiber type (3D (RC-55/30-BG)), as shown in Figure 4.7. Fiber type 4D (RC-65/60-BG) needed 15 minutes to be completely separated and fiber type 5D (RC-65/60-BG) needed 20 minutes to be entirely separated (as determined by visual inspection).

Figure 4.7 – Concrete with a 0.75% volume fraction of 3D (RC-55/30-BG) fibers after 15 minutes of mixing.

4.2 – Uniaxial Compression Test

This section is a summary of the uniaxial compression test results, which were obtained from tests conducted in accordance with the ASTM C39 standard test described in Chapter 3 (detailed results are presented in Appendix B). In this section, the measured stress-strain relationships are presented followed by a discussion of trends between fiber type and amount and concrete compressive strength, modulus of elasticity, and post-peak slope. Desciptions of the failures are reported at the end of this section.

4.2.1 – Stress-Strain Behavior

Figure 4.8 shows typical curves of stress versus longitudinal strain and identifies several parameters that were of interest in this study (plots of compression stress versus longitudinal and lateral strain are given in Appendix B for each specimen).

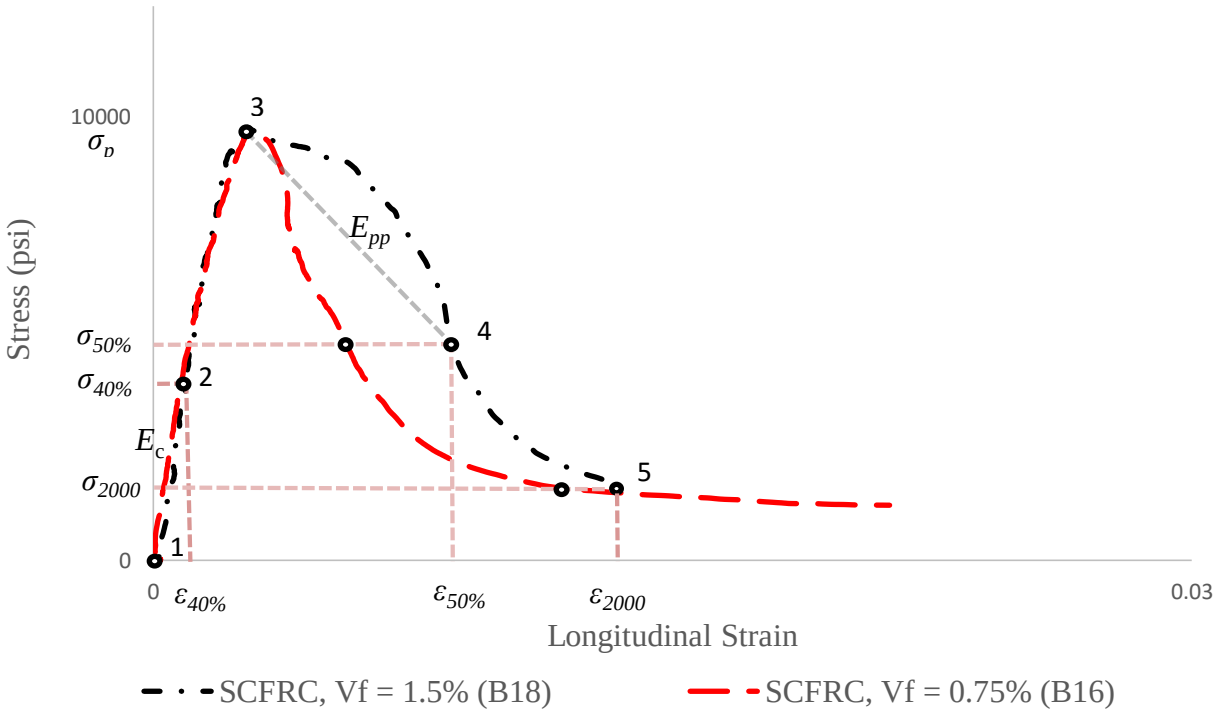

Figure 4.8 – Example plot of compression stress versus longitudinal strain (f_c` = 10 ksi and RC-80/30-BP).

To facilitate comparisons between test results, and thus allow study of the effect of introducing different volume fractions (0%, 0.5%, 0.75%, 1.0%, and 1.5%) and types of hooked steel fiber on the behavior of FRC under compression, a representative stress-longitudinal strain curve was constructed for each batch using the following procedure:

- The coordinates of five key points on the stress-longitudinal strain curve recorded for each specimen were identified. The five points were: the test start point (0,0), 40 percent of the peak strength on the ascending branch of the curve ($\sigma_{40\%}$, $\varepsilon_{40\%}$), the peak point (σ_p, ε_p), 50 percent of the peak strength on the descending branch ($\sigma_{50\%}$, $\varepsilon_{50\%}$), and the test end point at a stress of 2000 psi (σ_{2000}, ε_{2000}). These points are identified in Figure 4.8.
- A representative curve for the batch was constructed by averaging the coordinates of each of the five points, and linking them with line segments.

Representative stress-longitudinal strain curves are given in Figures 4.9 and 4.10 for all batches with $f_c' = 6$ ksi and fiber volume fractions of 0.75% and 1.5%. Similar plots are shown in Figures 4.11 and 4.12 batches of concrete with $f_c' = 10$ ksi. These figures show the ascending branch of the curves was not affected by the use of fibers, but, as expected, the slope of the descending branch tended to increase as fiber volume fraction increased. Fiber type RC-80/30-BP, with an aspect ratio of 79, had the greatest effect on the post-peak behavior, whereas fiber type 3D RC-55/30-BG, with an aspect ratio of 55, had the lowest influence. Fiber types 5D RC-65/60-BG and 4D RC-65/60-BG, which have an aspect ratio of 65, had similar effects on the post-peak behavior, with fiber type 5D RC-65/60-BG having a slightly stronger influence. The post-peak slope therefore tended to increase (become less negative) as the fiber volume fraction increased.

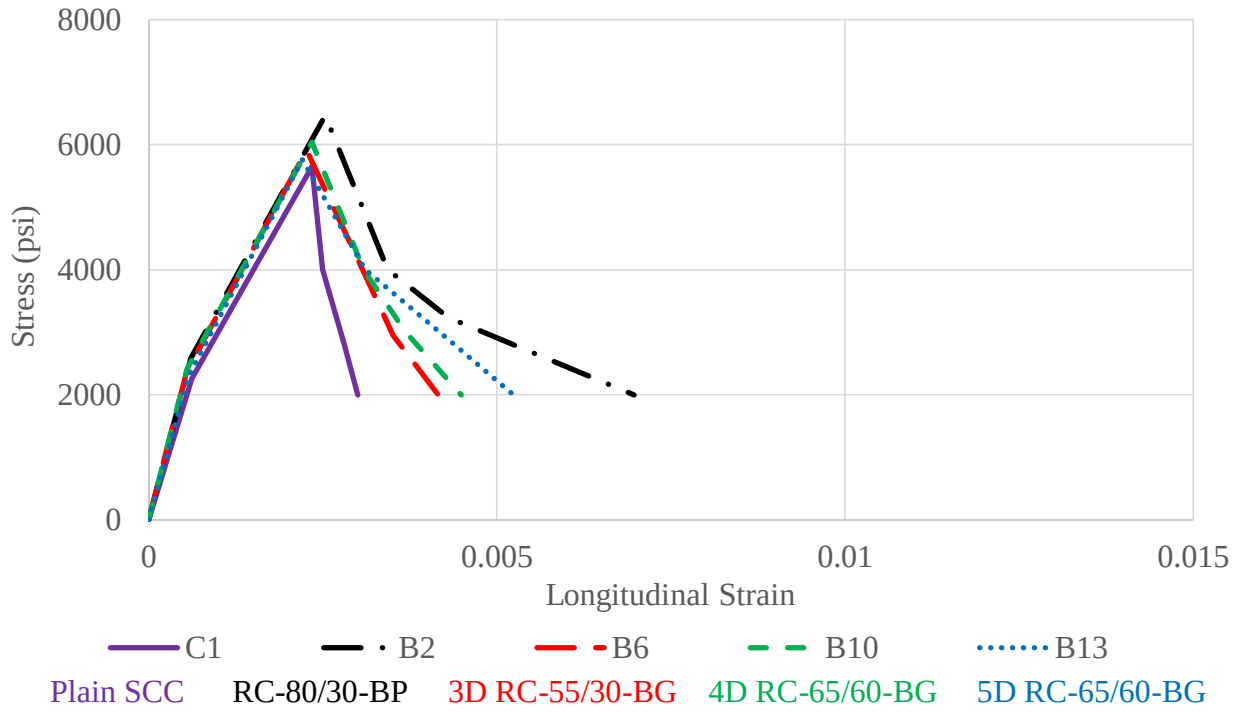

Figure 4.9 – Compression stress vs. longitudinal strain curves of 0.75% fiber volume fraction ($f_c' = 6$ ksi).

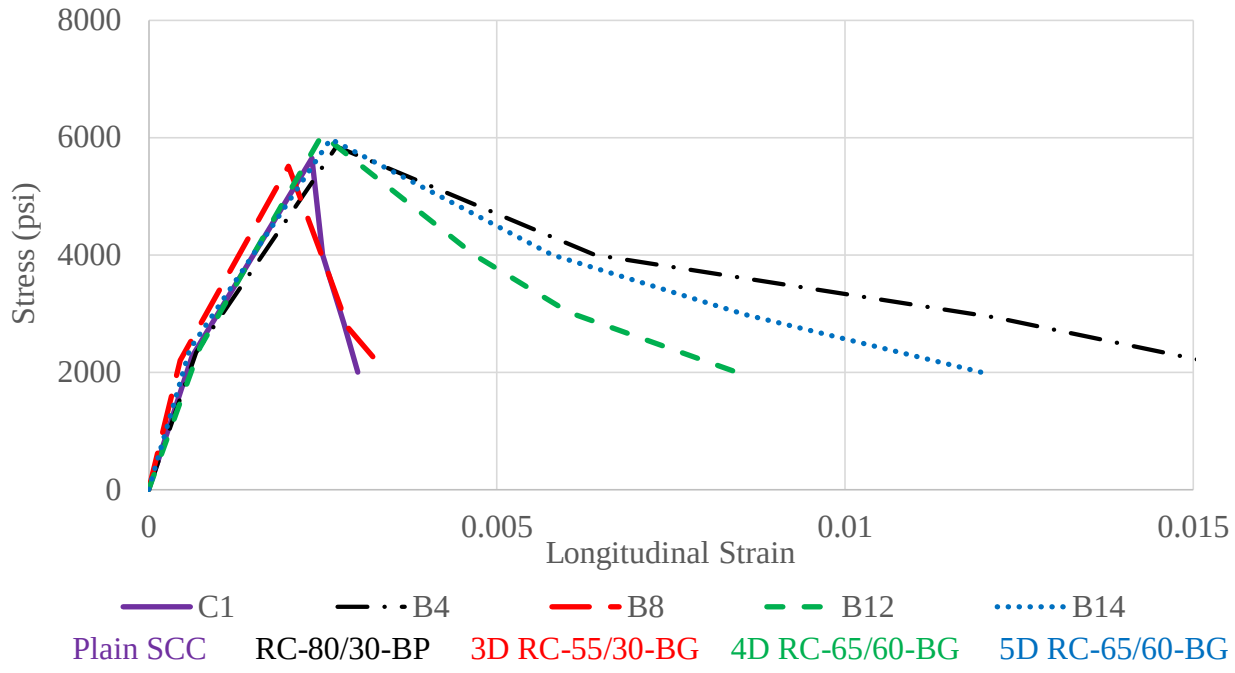

Figure 4.10 – Compression stress vs. longitudinal strain curves of 1.5% fiber volume fraction ($f_c' = 6$ ksi).

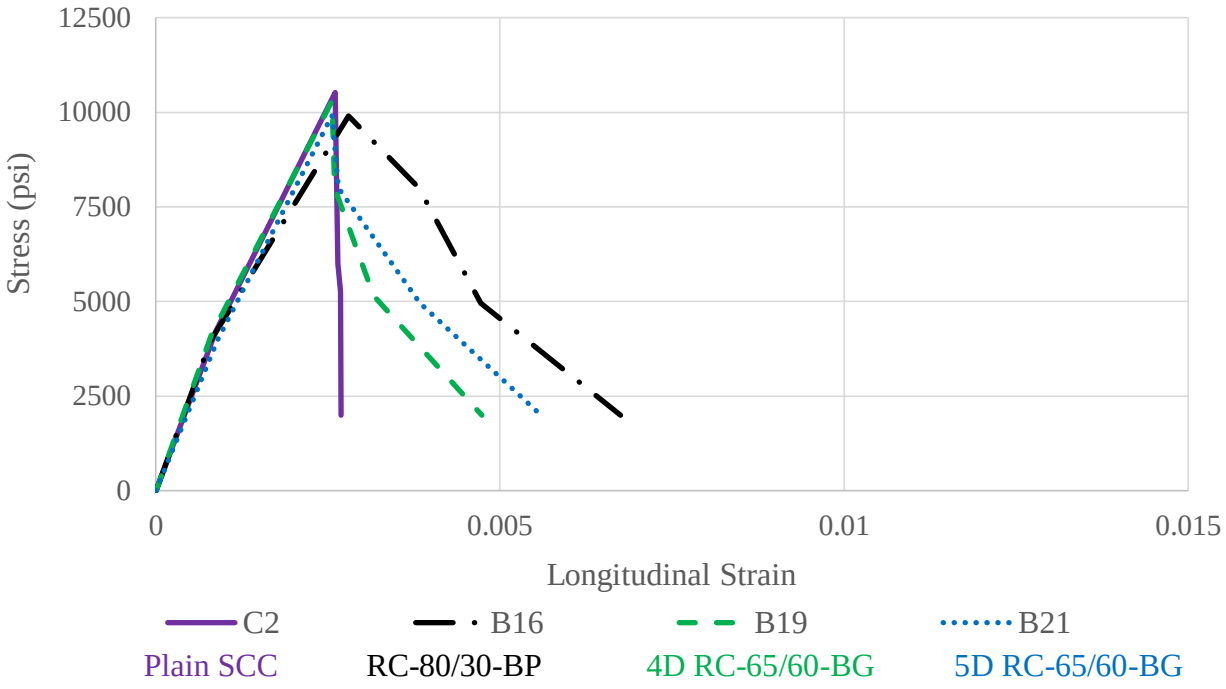

Figure 4.11 – Compression stress vs. longitudinal strain curves of 0.75% fiber volume fraction ($f_c' = 10$ ksi).

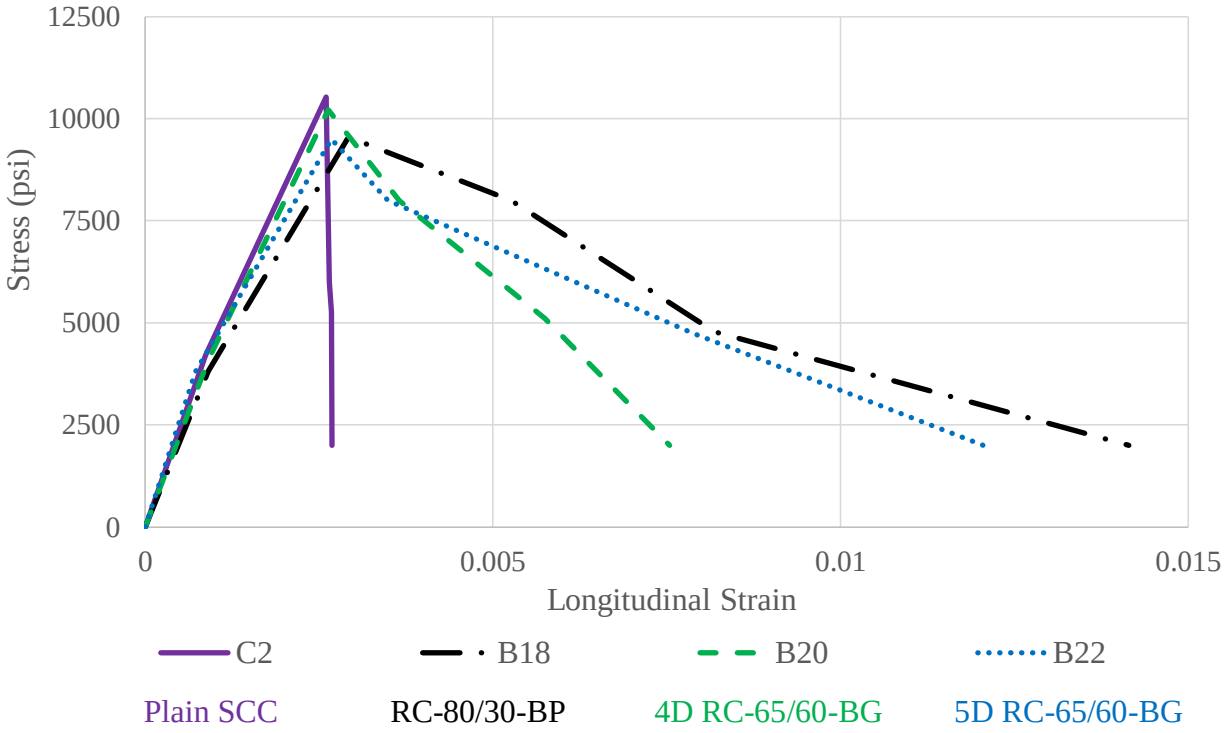

Figure 4.12 – Compression stress vs. longitudinal strain curves of 1.5% fiber volume fraction ($f_c' = 10$ ksi).

4.2.2 – Compressive Strength

The compressive strength of each specimen was calculated using Equation 3-1 (the ordinate of point 3 in Figure 4.8). The mean, standard deviation (*SD*), and coefficient of variation (*COV*) of the compressive strengths from each batch were calculated and are given in Table 4.1. The mean compressive strengths (f_{cm}) at 28 days ranged between 5490 psi and 6650 psi for batches with f_c' of 6 ksi. The mean compressive strength at 28 days of batches with f_c' of 10 ksi ranged between 9450 psi and 10,480 psi. The coefficient of variation for batches with $f_c' = 6$ ksi ranged between 1.3% and 5.2% except for batch 4 (*COV* = 9.4%) and batch 13 (*COV* = 8.8%). The coefficient of variation for batches with $f_c' = 10$ ksi ranged between 1.0% and 5.6%.

Figures 4.13 and 4.14 show the mean compressive strength calculated for each batch plotted versus fiber volume fraction. The type of fiber used in each batch is identified. There is no trend between fiber type or volume fraction and concrete compressive strength.

4.2.3 – Modulus of Elasticity

The modulus of elasticity of each specimen was calculated as the slope between points 1 and 2 in Figure 4.8 (Equation 3-2). The mean and the coefficient of variation of the modulus of elasticity of each batch are given in Table 4.2. The modulus of elasticity ranged between 3310 ksi and 4990 ksi for concrete with $f_c' = 6$ ksi, and between 4290 ksi and 5250 ksi for concrete with $f_c' = 10$ ksi. The coefficient of variation of the modulus of elasticity ranged between 3% and 18% for concrete with $f_c' = 6$ ksi except for batch 4 (*COV* = 33%), and between 4% and 16% for concrete with $f_c' = 10$ ksi.

Figures 4.15 and 4.16 show the mean modulus of elasticity calculated for each batch plotted versus fiber volume fraction. The type of fiber used in each batch is identified. There is no trend between fiber type or volume fraction and modulus of elasticity.

Table 4.1 – The mean, standard deviation, and coefficient of variation of the compression strength of each mixture.

Batch ID	Fiber type	V_f (%)	f_{cm} (psi)	$SD(f_{cm})$ (psi)	$COV(f_{cm})$
C 1	N/A	0	5710	240	4.2%
B 1	(RC-80/30-BP)	0.5	5490	260	4.7%
B 2	(RC-80/30-BP)	0.75	6460	210	3.3%
B 3	(RC-80/30-BP)	1.0	6340	205	3.3%
B 4	(RC-80/30-BP)	1.5	5760	540	9.4%
B 5	3D (RC-55/30-BG)	0.5	6370	235	3.7%
B 6	3D (RC-55/30-BG)	0.75	5920	305	5.2%
B 7	3D (RC-55/30-BG)	1.0	6140	245	4.0%
B 8	3D (RC-55/30-BG)	1.5	5520	190	3.5%
B 9	4D (RC-65/60-BG)	0.5	6200	245	4.0%
B 10	4D (RC-65/60-BG)	0.75	6050	310	5.2%
B 11	4D (RC-65/60-BG)	1.0	6650	90	1.3%
B 12	4D (RC-65/60-BG)	1.5	6050	200	3.3%
B 13	5D (RC-65/60-BG)	0.75	5770	510	8.8%
B 14	5D (RC-65/60-BG)	1.5	5980	85	1.4%
C 2	N/A	0	10480	380	3.6%
B 15	(RC-80/30-BP)	0.5	9970	215	2.1%
B 16	(RC-80/30-BP)	0.75	9910	100	1.0%
B 17	(RC-80/30-BP)	1.0	10100	335	3.3%
B 18	(RC-80/30-BP)	1.5	9490	440	4.6%
B 19	4D (RC-65/60-BG)	0.75	10320	580	5.6%
B 20	4D (RC-65/60-BG)	1.5	10240	290	2.8%
B 21	5D (RC-65/60-BG)	0.75	9800	415	4.2%
B 22	5D (RC-65/60-BG)	1.5	9450	270	2.9%

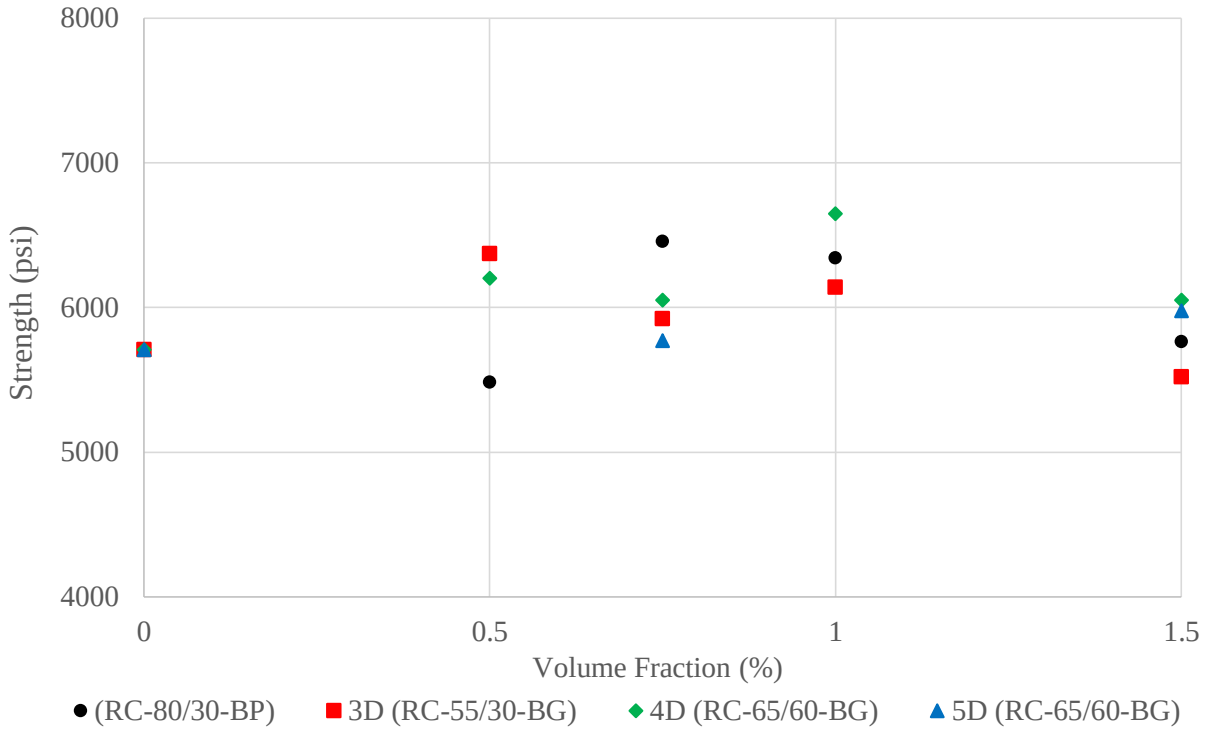

Figure 4.13 – Compression strength vs. fiber volume fraction ($f_c' = 6$ ksi).

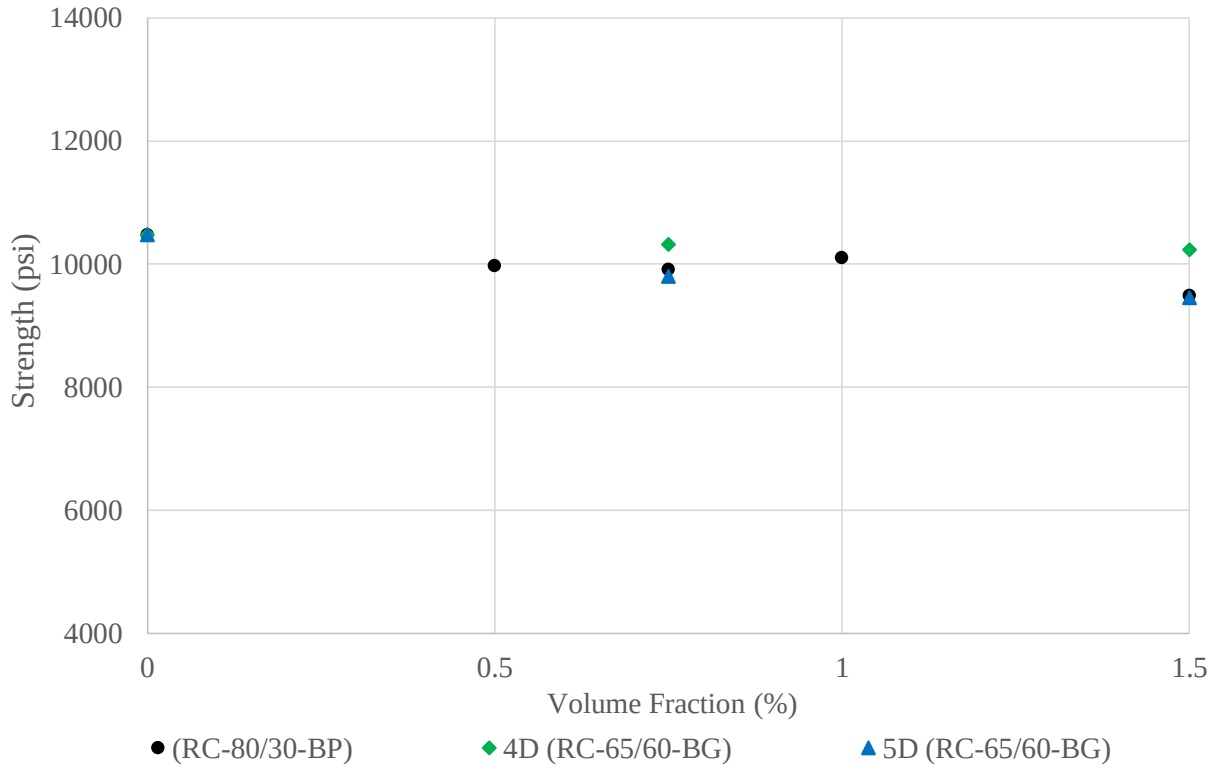

Figure 4.14 – Compression strength vs. fiber volume fraction ($f_c' = 10$ ksi).

Table 4.2 – The mean and the coefficient of variation of the modulus of elasticity of all batches.

Batch ID	Fiber type	V_f (%)	$E_c \times 10^3$ (ksi)	*COV*
C 1	N/A	0	3.69	12%
B 1	(RC-80/30-BP)	0.5	3.84	3%
B 2	(RC-80/30-BP)	0.75	4.14	16%
B 3	(RC-80/30-BP)	1.0	3.97	14%
B 4	(RC-80/30-BP)	1.5	4.00	33%
B 5	3D (RC-55/30-BG)	0.5	3.69	8%
B 6	3D (RC-55/30-BG)	0.75	4.45	18%
B 7	3D (RC-55/30-BG)	1.0	3.59	12%
B 8	3D (RC-55/30-BG)	1.5	4.99	12%
B 9	4D (RC-65/60-BG)	0.5	3.48	13%
B 10	4D (RC-65/60-BG)	0.75	4.43	12%
B 11	4D (RC-65/60-BG)	1.0	3.74	10%
B 12	4D (RC-65/60-BG)	1.5	3.31	7%
B 13	5D (RC-65/60-BG)	0.75	4.03	9%
B 14	5D (RC-65/60-BG)	1.5	4.08	11%
C 2	N/A	0	4.92	6%
B 15	(RC-80/30-BP)	0.5	4.80	4%
B 16	(RC-80/30-BP)	0.75	5.18	9%
B 17	(RC-80/30-BP)	1.0	4.78	5%
B 18	(RC-80/30-BP)	1.5	4.29	4%
B 19	4D (RC-65/60-BG)	0.75	5.14	7%
B 20	4D (RC-65/60-BG)	1.5	4.56	13%
B 21	5D (RC-65/60-BG)	0.75	4.87	8%
B 22	5D (RC-65/60-BG)	1.5	5.25	16%

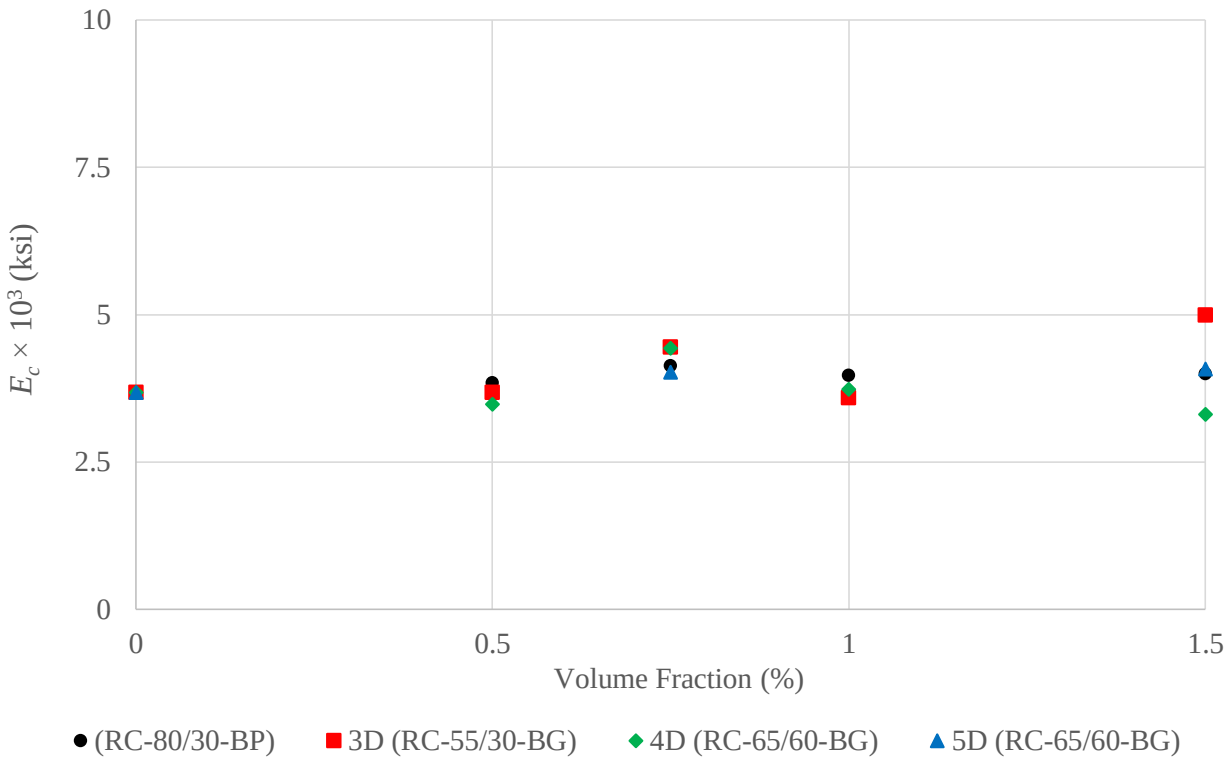

Figure 4.15 – Modulus of elasticity vs. fiber volume fraction ($f_c' = 6$ ksi).

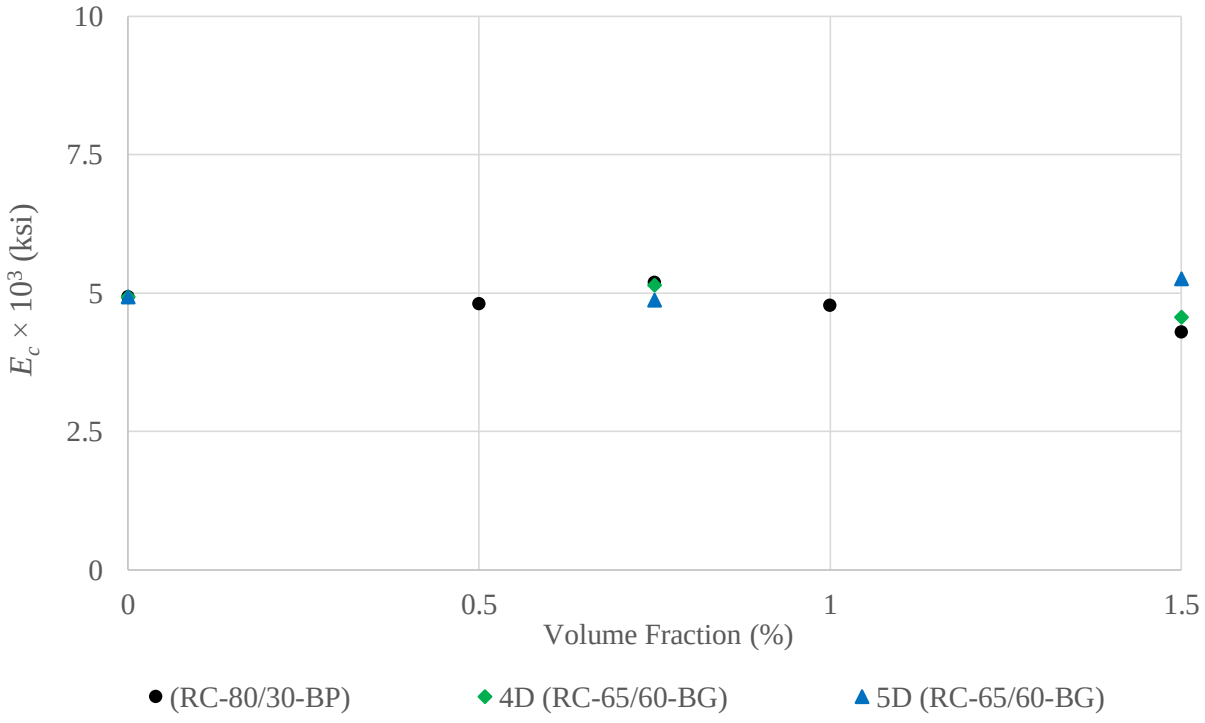

Figure 4.16 – Modulus of elasticity vs. fiber volume fraction ($f_c' = 10$ ksi).

4.2.4 – Post-Peak Slope

The post-peak slope of each specimen was calculated as the slope between points 3 and 4 of the recorded stress-strain relationship (Figure 4.8) using equation 3-3. Calculated values are given in Table 4.3. The post-peak slope for batches with $f_c' = 6$ ksi ranged between -0.38×10^6 psi and -6.18×10^6 psi, and between -0.91×10^6 psi and -3.88×10^6 psi for batches with $f_c' = 10$ ksi, except for control batch 2 (-16.12×10^6 psi) and batch 19 (-8.47×10^6 psi). The coefficient of variation of the post-peak slope ranged between 9% and 94% for batches with $f_c' = 6$ ksi and between 18% and 91% for batches with $f_c' = 10$ ksi, except for batch 22 (110%). For both strengths of concrete, batches with the longer fibers (4D RC-65/60-BG and 5D RC-65/60-BG) tended to have a larger coefficient of variation of the post-peak slope. For calculation of both the average post-peak slope and COV, specimens with behavior that appeared to be an outlier were omitted. The specimens that were considered and omitted are identified in Appendix B.

Figures 4.17 and 4.18 show the mean E_{pp} calculated for each batch plotted versus volume fraction. The type of fiber used in each batch is identified. As shown, the post-peak slope tended to increase as the fiber volume fraction increased. However, for a given increment in fiber volume fraction, there appears to be a diminishing effect on the post-peak slope. This is most pronounced for batches with the 3D fibers (3D RC-55/30-BG and RC-80/30-BP); the post-peak slope observed for batches with a volume fraction of 0.5% was not much different than for batches with a volume fraction of 1.5%. The exception to this trend are the batches with fiber type 4D RC-65/60-BG, which had more scattered results.

In Figures 4.17 and 4.18, there is also a trend between mean Epp and fiber type. As observed previously, batches with fiber type RC-80/30-BP, with an aspect ratio of 79, showed the greatest change in the post-peak behavior, whereas those with fiber type 3D RC-55/30-BG, with

an aspect ratio of 55, showed the least. Batches with fiber types 5D RC-65/60-BG and 4D RC-65/60-BG, which have an aspect ratio of 65, had similar post-peak behavior (fiber type 5D RC-65/60-BG resulted in a slightly more gradual loss of strength than fiber type 4D RC-65/60-BG).

Table 4.3 – The mean and coefficient of variation of the compression post-peak slopes.

Batch ID	Fiber type	V_f (%)	$E_{pp} \times 10^6$ (psi)	*COV*
C 1	N/A	0	-6.18	18%
B 1	(RC-80/30-BP)	0.5	-1.10	34%
B 2	(RC-80/30-BP)	0.75	-1.56	9%
B 3	(RC-80/30-BP)	1.0	-0.94	36%
B 4	(RC-80/30-BP)	1.5	-0.38	48%
B 5	3D (RC-55/30-BG)	0.5	-3.35	33%
B 6	3D (RC-55/30-BG)	0.75	-2.94	37%
B 7	3D (RC-55/30-BG)	1.0	-2.78	80%
B 8	3D (RC-55/30-BG)	1.5	-3.23	23%
B 9	4D (RC-65/60-BG)	0.5	-5.73	94%
B 10	4D (RC-65/60-BG)	0.75	-2.77	47%
B 11	4D (RC-65/60-BG)	1.0	-4.09	15%
B 12	4D (RC-65/60-BG)	1.5	-1.81	34%
B 13	5D (RC-65/60-BG)	0.75	-2.41	82%
B 14	5D (RC-65/60-BG)	1.5	-0.50	90%
C 2	N/A	0	-16.12	18%
B 15	(RC-80/30-BP)	0.5	-3.85	38%
B 16	(RC-80/30-BP)	0.75	-2.58	37%
B 17	(RC-80/30-BP)	1.0	-1.86	54%
B 18	(RC-80/30-BP)	1.5	-0.91	37%
B 19	4D (RC-65/60-BG)	0.75	-8.47	91%
B 20	4D (RC-65/60-BG)	1.5	-1.64	87%
B 21	5D (RC-65/60-BG)	0.75	-3.88	69%
B 22	5D (RC-65/60-BG)	1.5	-0.91	110%

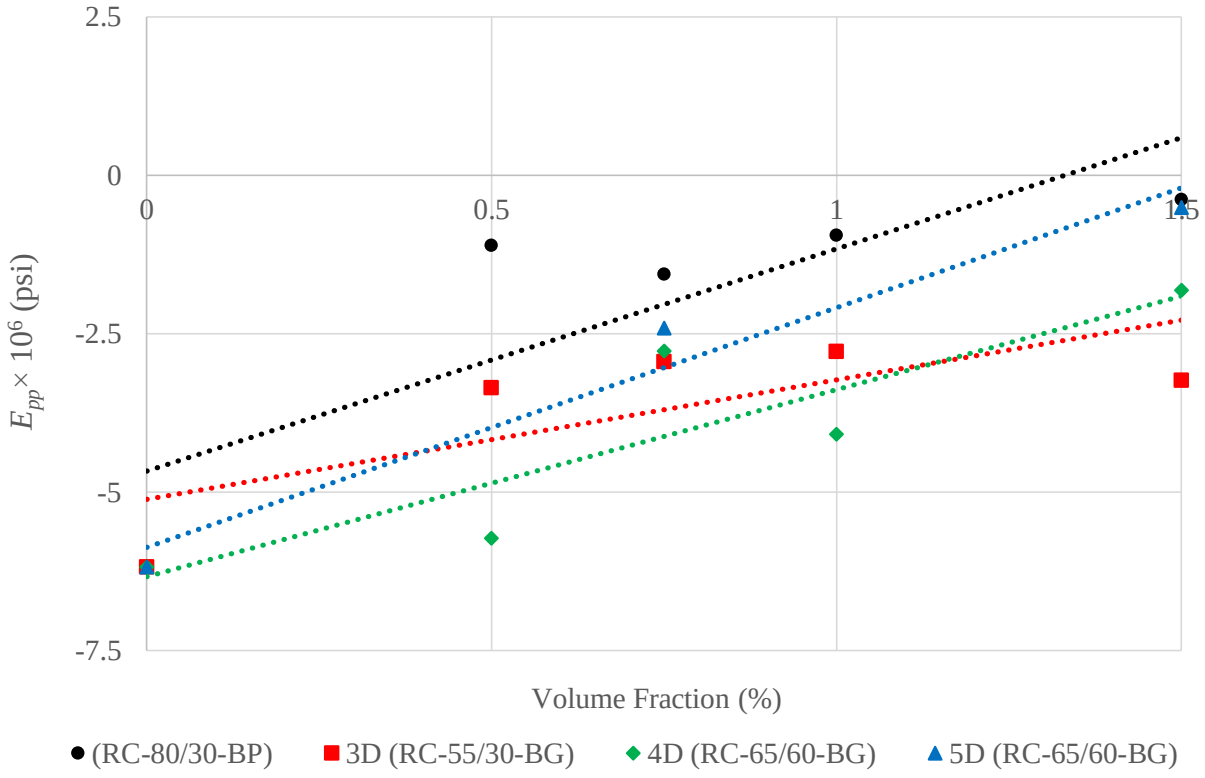

Figure 4.17 – Compression post-peak slope vs. fiber volume fraction ($f_c' = 6$ ksi).

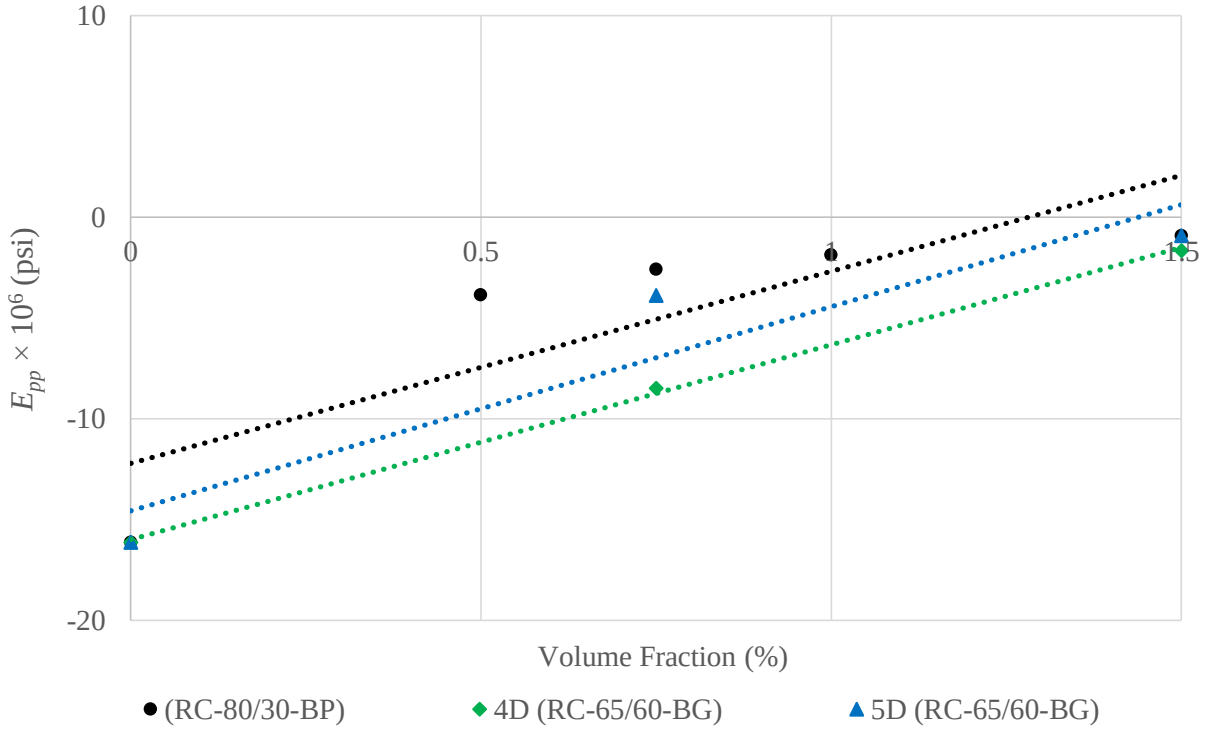

Figure 4.18 – Compression post-peak slope vs. fiber volume fraction ($f_c' = 10$ ksi).

4.2.5 – Description of Failure

Specimens with low fiber volume fractions (0% and 0.5%) had a tendency to fail in a brittle manner as shown in Figure 4.19. In addition, the tendency for sudden failure increased as the concrete compression strength increased (concrete with $f_c' = 10$ ksi had a higher tendency for sudden failure than concrete with $f_c' = 6$ ksi).

The failure of each specimen was characterized as one of the typical failure modes described in Chapter 3, and are presented in Appendix B. Type 2 failure, which can be described as a well-formed cone at one end and vertical cracks initiated from the other end, and type 3 failure, which is a columnar failure with vertical cracks initiating from both ends, occurred most commonly for cylinders with high fiber volume fractions (1% and 1.5%) as shown in Figures 4.20 and 4.21. Cone failures (type 1), occurred most commonly for specimens with low fiber volume fractions (0.5% and 0.75%), as well as plain concrete, as shown in Figure 4.22. Shear failures (type 4 failure), which can be described as a dominant diagonal crack with no cracks at the ends, occurred in some specimens as illustrated in Figure 4.23.

Cracking and damage to the cylinders frequently dislodged markers, making it difficult to record lateral deformations throughout the tests.

Figure 4.19 – Compression sudden (brittle) failure (f_c` = 6 ksi plain concrete; C1 SP5).

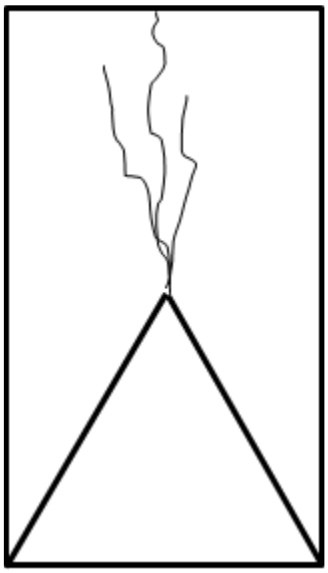

Figure 4.20 – Type 2 failure, shear-columnar failure, (f_c` = 10 ksi; V_f = 0.75% of 5D (RC-65/60-BG); B21 SP3).

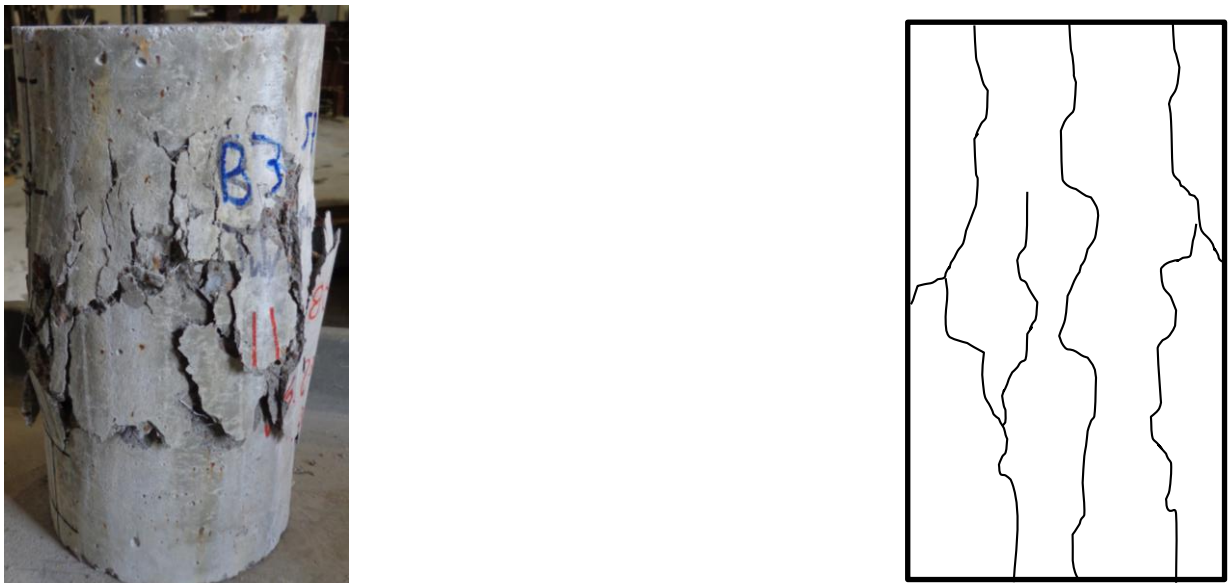

Figure 4.21 – Type 3 failure, columnar failure, (f_c` = 6 ksi; V_f = 1.0% of RC-80/30-BP; B3 SP1).

Figure 4.22 – Type 1 failure, cone failure, (f_c` = 6 ksi; V_f = 1.0% of 3D RC-55/30-BG; B7 SP1).

Figure 4.23 – Type 4 failure, shear failure, (f_c` = 6 ksi; V_f = 1.5% of RC-80/30-BP; B4 SP3).

4.3 – Flexure Test

This section summarizes results from the flexure tests, which were conducted in acordance with the ASTM C1609 standard. Detailed results are presented in Appendix C. First, the load-deflection behavior is described, followed by the relationship between load and primary crack width. The first-peak load (P_1) recorded in each test is then discussed as well as the post-crack peak load (P_{pc}). Finally, the relationship between the applied load and support rotations is summerized, followed by general descriptions of the failure modes.

4.3.1 – Load-Deflection Behavior

As discussed previously in Chapter 3, an infrared-based non-contact position sensor was used to record specimen deformations. Eight markers (named 1, 5, 6, 9, 13, and 14), were used to calculate mid-span net deflections. Figure 4.24 shows a plot of load versus mid-span net deflection for two typical test results. The initial slope and cracking load are similar for both specimens, but

the post-cracking response is different. The red curve carries less load after cracking, which is referred to as a deflection softening response. The black curve exhibits a period of deflection hardening, characterized by higher loads after cracking and formation of multiple cracks, followed by a deflection softening response after the peak.

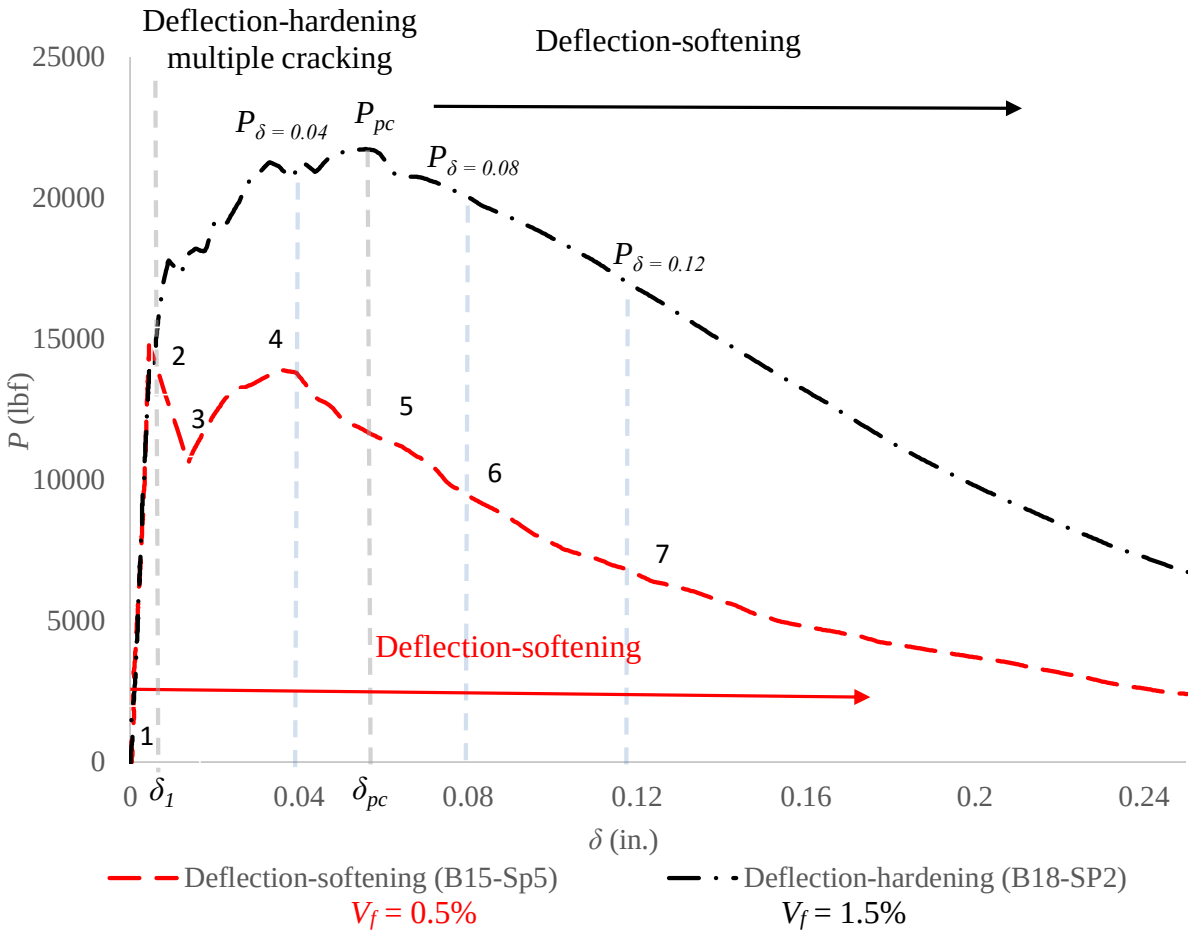

Figure 4.24 – Example plot of flexure load vs. mid-span net deflection (f_c` = 10 ksi and RC-80/30-BP).

To facilitate comparisons between test results, and thus allow study of the effect of introducing different volume fractions (0%, 0.5%, 0.75%, 1.0%, and 1.5%) and types of hooked steel fiber on the flexural behavior of FRC, a representative load-deflection curve was constructed for each batch using the following procedure:

- The coordinates of seven key points on the load-deflection curve recorded for each specimen were identified. The points were: the test start point (0,0), the first-peak load or the first-crack point (P_1,δ_1), the drop point (P_2,δ_2), the post-crack peak point (P_{pc},δ_{pc}), the point at a deflection of 0.04 inch ($P_{\delta = 0.04}$, 0.04 in.), the point at a deflection of 0.08 inch ($P_{\delta = 0.08}$, 0.08 in.), and the point at a deflection of 0.12 inch ($P_{\delta = 0.12}$, 0.12 in.). These points are identified in Figure 4.24.
- A representative curve for the batch was constructed by averaging the coordinates of each of the seven points, and linking them with line segments.

Representative plots of load versus mid-span deflection are given in Figures 4.25 and 4.26 for all batches with $f_c' = 6$ ksi and fiber volume fractions of 0.75% and 1.5%. Similar plots are shown in Figures 4.27 and 4.28 batches of concrete with $f_c' = 10$ ksi. It can be observed that fiber type 3D RC-55/30-BG had the lowest impact on load-deflection behavior. The other three fiber types showed similar behavior for the cases shown, except for that the RC-80/30-BP fibers performed much better than the others for a volume fraction of 0.75% in concrete with $f_c' = 6$ ksi.

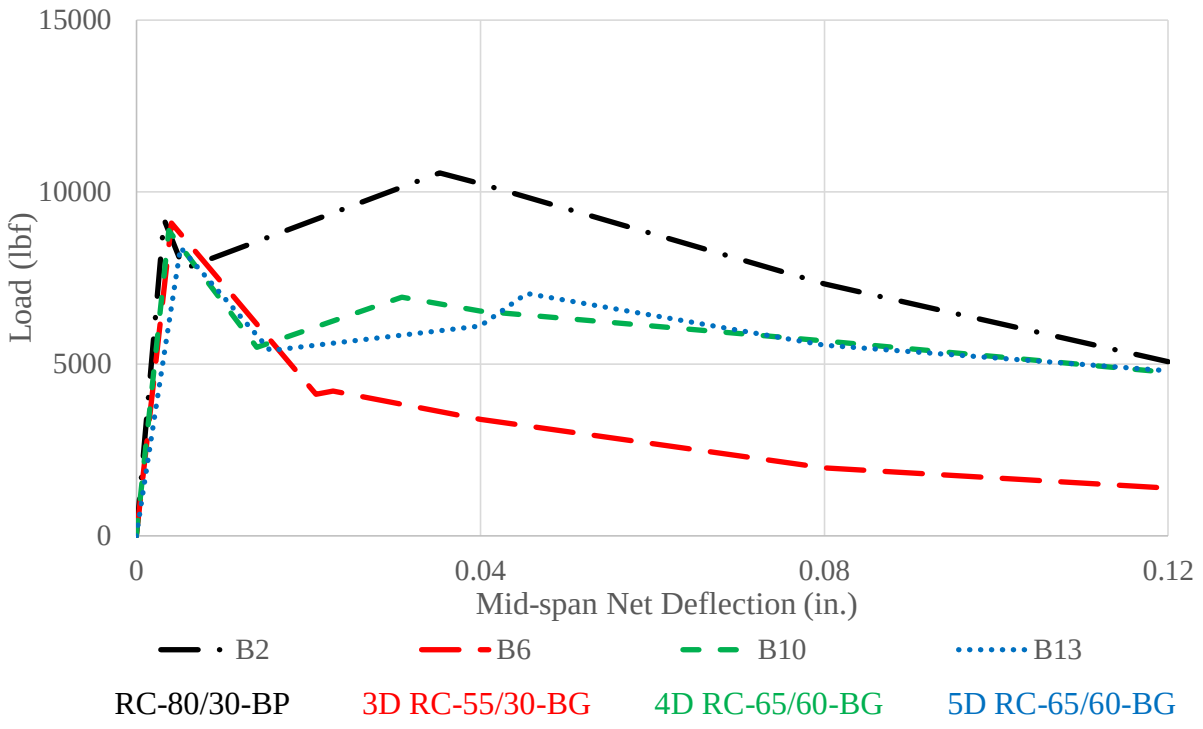

Figure 4.25 – Load vs. mid-span net deflection curves of 0.75% volume fraction ($f_c' = 6$ ksi).

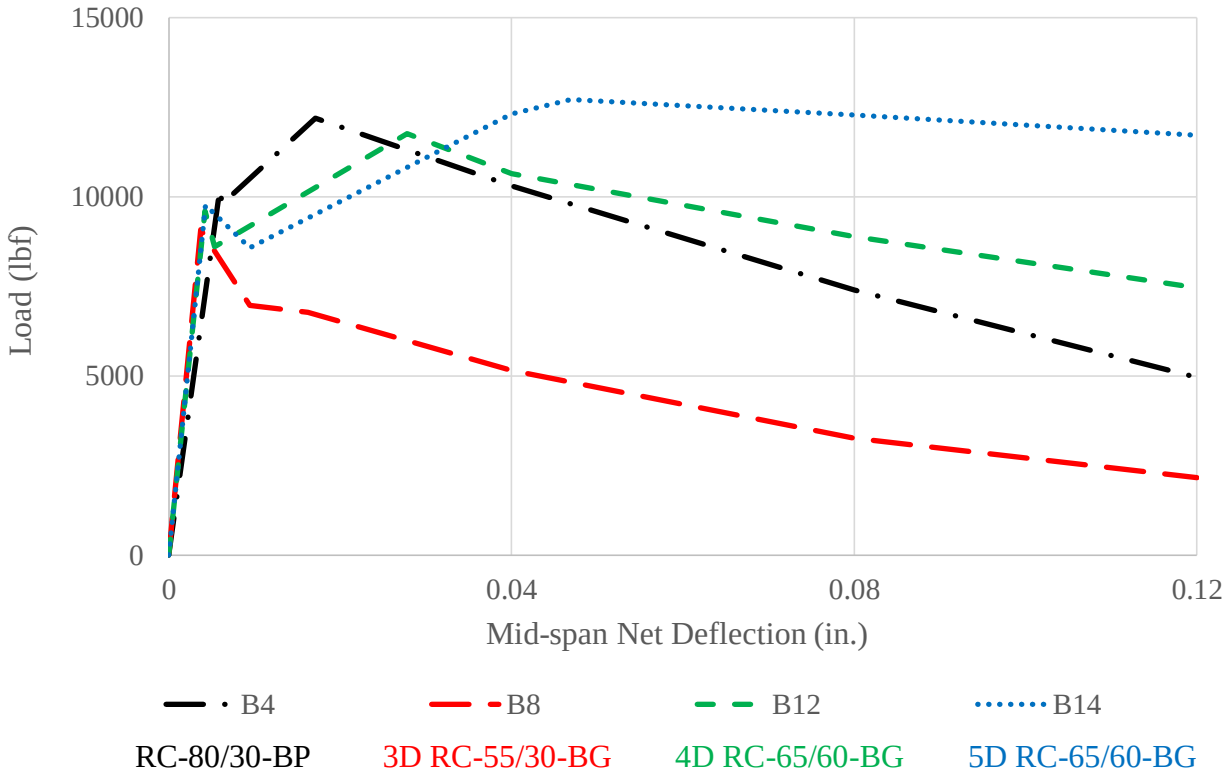

Figure 4.26 – Load vs. mid-span net deflection curves of 1.5% volume fraction ($f_c' = 6$ ksi).

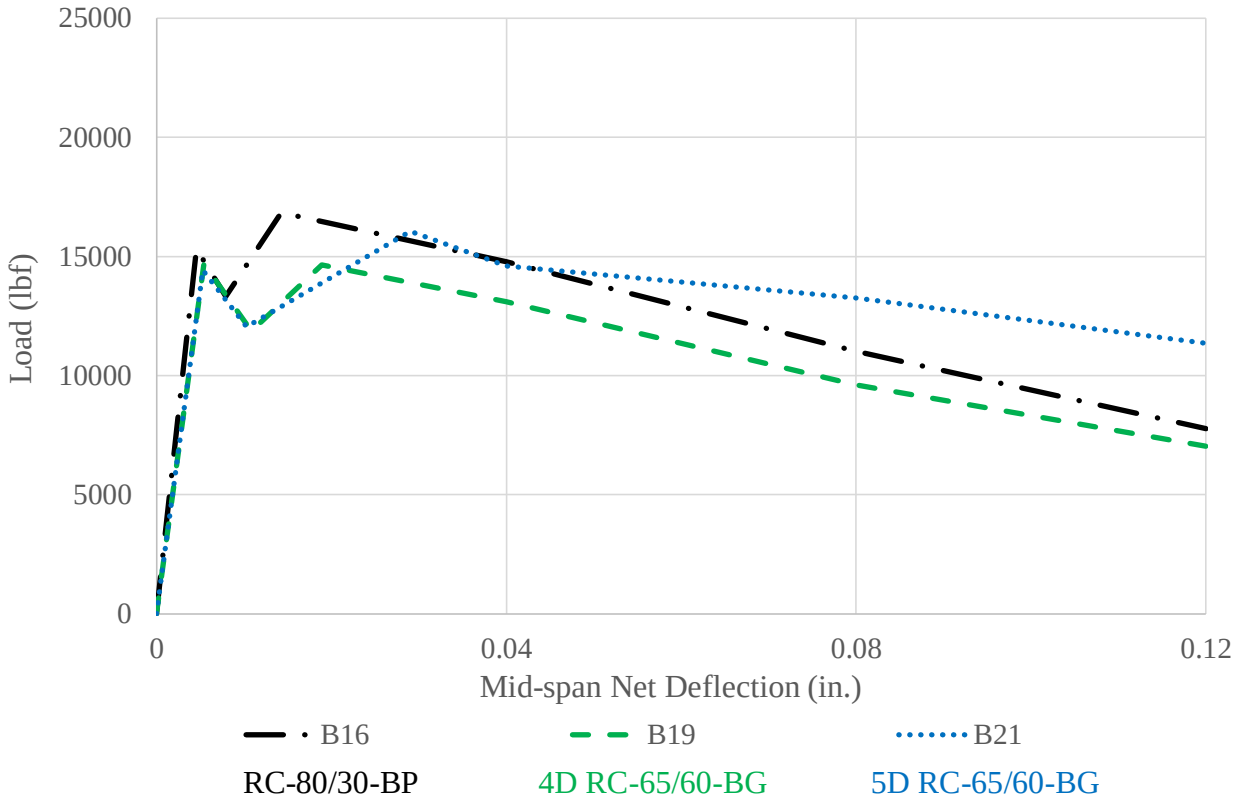

Figure 4.27 – Load vs. mid-span net deflection curves of 0.75% volume fraction ($f_c' = 10$ ksi).

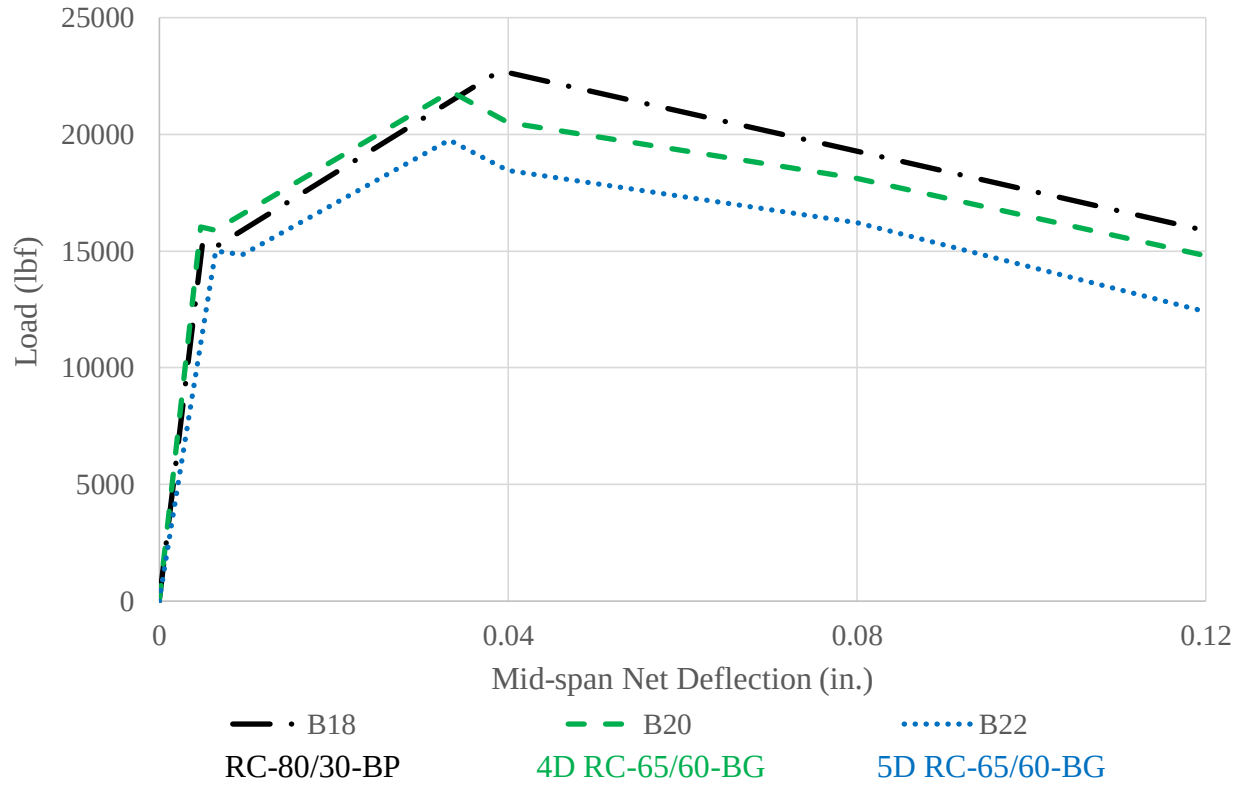

Figure 4.28 – Load vs. mid-span net deflection curves of 1.5% volume fraction ($f_c' = 10$ ksi).

4.3.2 – Load-Primary Crack Width Behavior

Figure 4.29 shows a plot of load versus primary crack width for two typical test results. Although several cracks may have formed during a test, the location of the dominant crack was identified after testing, and the width of that crack was calculated throughout the test as the distance between the two markers closest to the crack mouth (Figure 4.30).

As shown, the crack width was zero until the crack formed. As with Figure 4.29, the red curve carries less load after cracking and is referred to as a deflection softening response. The black curve has a period of deflection hardening, characterized by higher loads after cracking and formation of multiple cracks, followed by a deflection softening response after peak.

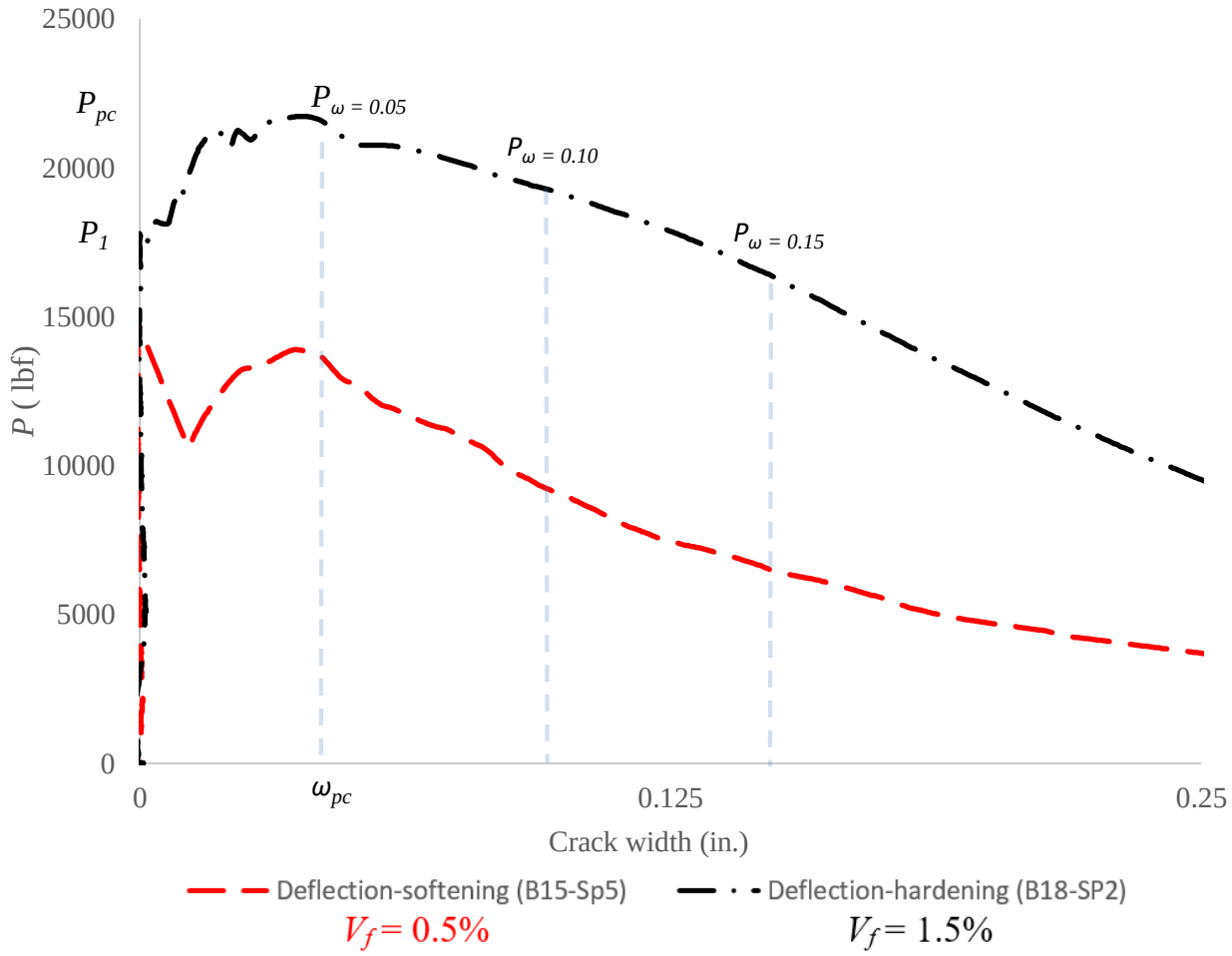

Figure 4.29 – Example plot of flexure load vs. primary crack width (f_c` = 10 ksi and RC-80/30-BP).

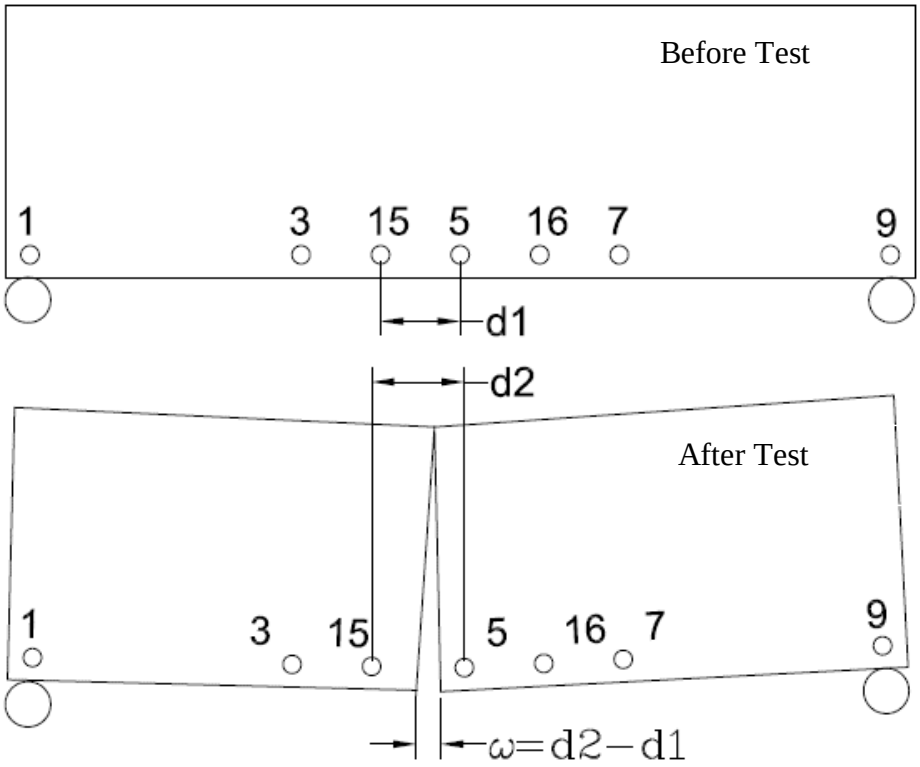

Figure 4.30 – Crack width calculation.

4.3.3 – First-Peak Strength

The first-peak strength (σ_1), which refers to the stress caused by bending along the bottom face of the beam when the first crack formed, was calculated using equation 3-4. Calculated values ranged between 620 psi and 890 psi for concrete with $f_c' = 6$ ksi and between 1155 psi and 1285 psi for concrete with $f_c' = 10$ ksi, except for batch 17, which had a first-peak strength of 980 psi. Table 4.4 summarizes the first-peak strength (σ_1) and the first-peak load (P_1) of all batches. Figures 4.31 and 4.32, which show plots of σ_1 versus fiber volume fraction, show that the fibers had a negligible effect on the first-peak flexural strength.

Table 4.4 – The first peak strength.

Batch ID	Fiber type	V_f (%)	σ_1 (psi)	P_1 (lbf)
C 1	N/A	0	720	8890
B 1	(RC-80/30-BP)	0.5	620	7540
B 2	(RC-80/30-BP)	0.75	715	8900
B 3	(RC-80/30-BP)	1.0	730	8700
B 4	(RC-80/30-BP)	1.5	890	10230
B 5	3D (RC-55/30-BG)	0.5	785	9760
B 6	3D (RC-55/30-BG)	0.75	755	9100
B 7	3D (RC-55/30-BG)	1.0	755	9360
B 8	3D (RC-55/30-BG)	1.5	735	9080
B 9	4D (RC-65/60-BG)	0.5	740	9180
B 10	4D (RC-65/60-BG)	0.75	735	8890
B 11	4D (RC-65/60-BG)	1.0	760	9460
B 12	4D (RC-65/60-BG)	1.5	775	9610
B 13	5D (RC-65/60-BG)	0.75	675	8390
B 14	5D (RC-65/60-BG)	1.5	770	9770
C 2	N/A	0	1190	14820
B 15	(RC-80/30-BP)	0.5	1160	14460
B 16	(RC-80/30-BP)	0.75	1230	15320
B 17	(RC-80/30-BP)	1.0	980	15560
B 18	(RC-80/30-BP)	1.5	1215	15250
B 19	4D (RC-65/60-BG)	0.75	1185	14700
B 20	4D (RC-65/60-BG)	1.5	1285	15990
B 21	5D (RC-65/60-BG)	0.75	1155	14420
B 22	5D (RC-65/60-BG)	1.5	1185	15010

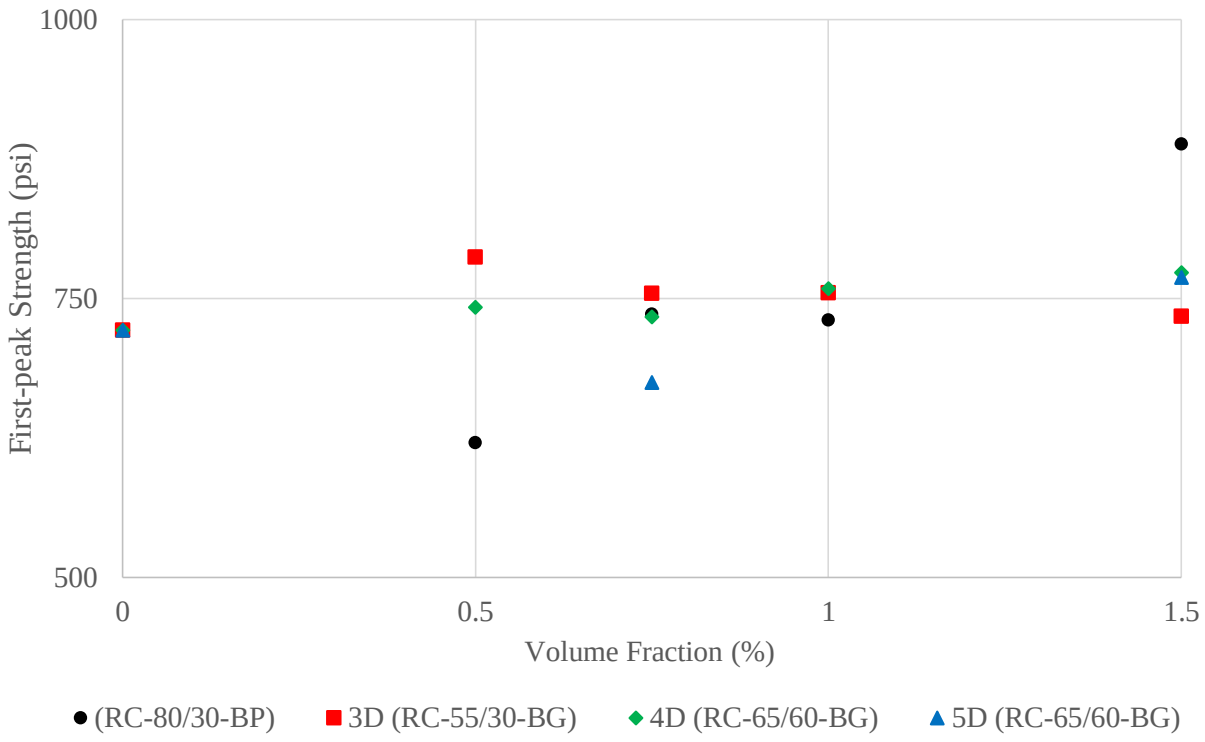

Figure 4.31 – First-peak flexural strength vs. fiber volume fraction ($f_c' = 6$ ksi).

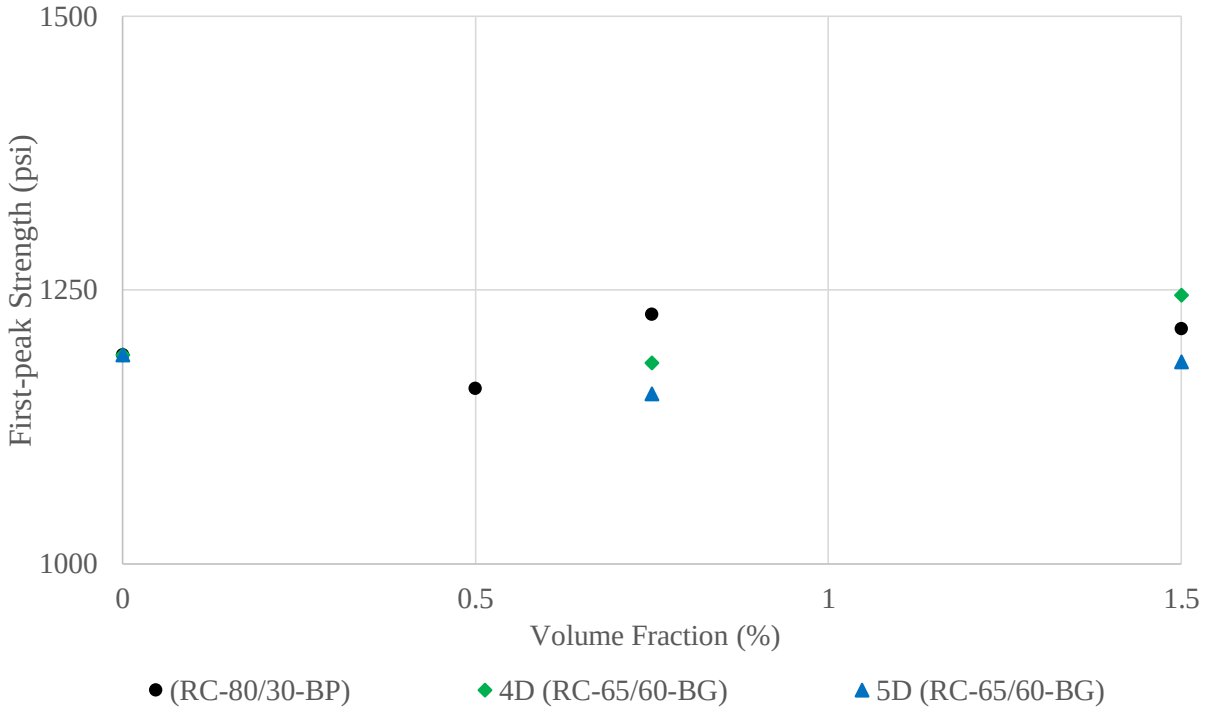

Figure 4.32 – First-peak flexural strength vs. fiber volume fraction ($f_c' = 10$ ksi).

4.3.4 – Post-Crack Peak Strength

The post-crack peak flexural strength (σ_{pc}) was calculated as described in Chapter 3 using equation 3-5. The post-crack peak strengths (σ_{pc}) and the post-crack peak loads (P_{pc}) along with their coefficients of variation, the corresponding mid-span net deflections, and the corresponding primary crack widths are given in Table 4.5. Figures 4.33 and 4.34 show plots of σ_{pc} versus fiber volume fraction for batches with $f_c' = 6$ and 10 ksi, respectively.

Fiber properties and fiber volume fractions significantly affected the post-crack peak strength. Plain concrete had zero post-crack peak strength because it failed immediately after the first crack. The post-crack peak strength increased as fiber volume fraction increased and as fiber aspect ratio increased. The post-crack peak strength ranged between 165 psi and 1020 psi for concrete with $f_c' = 6$ ksi (the coefficient of variation ranged between 11% and 60% except for batch 5, which had a coefficient of variation of 84%). The post-crack peak strength ranged between 1055 psi and 1810 psi for concrete with $f_c' = 10$ ksi (the coefficient of variation ranged between 5% and 23%). These values for coefficient of variation are higher than anticipated and may be indicative of issues with distribution and orientation of fibers.

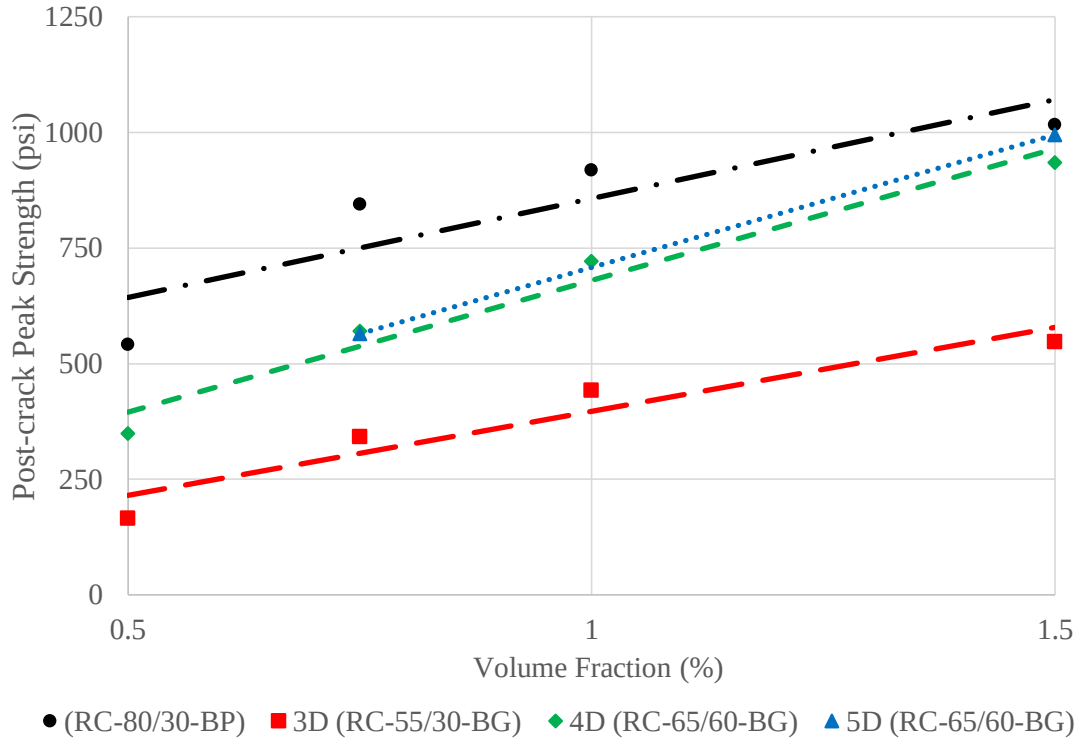

Figure 4.33 – Post-crack peak flexural strength vs. fiber volume fraction ($f_c' = 6$ ksi).

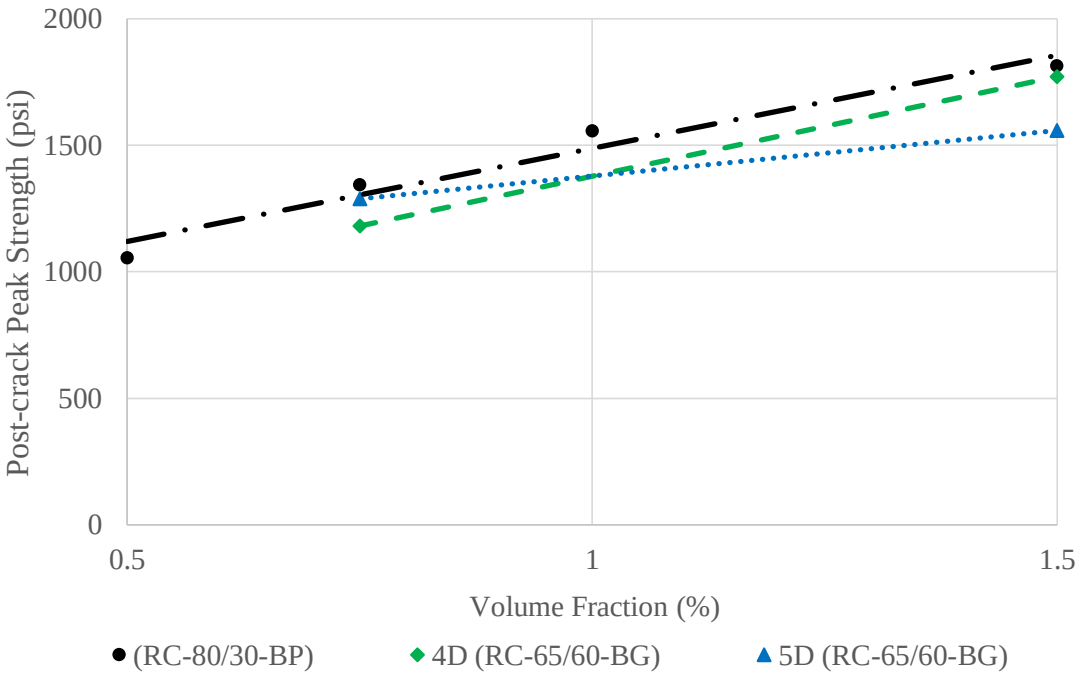

Figure 4.34 – Post-crack peak flexural strength vs. fiber volume fraction ($f_c' = 10$ ksi).

Table 4.5 – The post-crack peak strengths, deflections, and crack widths.

Batch ID	Fiber type	V_f (%)	σ_{pc} (psi)	P_{pc} (lbf)	*COV* of P_{pc}	δ_{pc} (in.)	ω_{pc} (in.)
C 1	N/A	0					
B 1	(RC-80/30-BP)	0.5	540	6560	41%	0.03	0.04
B 2	(RC-80/30-BP)	0.75	730	10180	14%	0.03	0.03
B 3	(RC-80/30-BP)	1.0	920	11070	17%	0.03	0.03
B 4	(RC-80/30-BP)	1.5	1020	12200	11%	0.02	0.01
B 5	3D (RC-55/30-BG)	0.5	165	2050	84%	0.06	0.10
B 6	3D (RC-55/30-BG)	0.75	340	4210	52%	0.02	0.04
B 7	3D (RC-55/30-BG)	1.0	445	5495	41%	0.02	0.03
B 8	3D (RC-55/30-BG)	1.5	550	6770	13%	0.02	0.02
B 9	4D (RC-65/60-BG)	0.5	350	4360	54%	0.06	0.07
B 10	4D (RC-65/60-BG)	0.75	570	6940	60%	0.03	0.05
B 11	4D (RC-65/60-BG)	1.0	720	9070	59%	0.02	0.04
B 12	4D (RC-65/60-BG)	1.5	935	11760	37%	0.03	0.03
B 13	5D (RC-65/60-BG)	0.75	565	7050	45%	0.05	0.05
B 14	5D (RC-65/60-BG)	1.5	995	12720	55%	0.05	0.06
C 2	N/A	0					
B 15	(RC-80/30-BP)	0.5	1055	13170	11%	0.03	0.03
B 16	(RC-80/30-BP)	0.75	1340	16840	5%	0.01	0.01
B 17	(RC-80/30-BP)	1.0	1555	19520	11%	0.02	0.03
B 18	(RC-80/30-BP)	1.5	1810	22730	11%	0.04	0.02
B 19	4D (RC-65/60-BG)	0.75	1180	14640	8%	0.02	0.02
B 20	4D (RC-65/60-BG)	1.5	1715	21360	19%	0.03	0.02
B 21	5D (RC-65/60-BG)	0.75	1290	16060	8%	0.03	0.03
B 22	5D (RC-65/60-BG)	1.5	1560	19760	23%	0.03	0.03

4.3.5 – Load vs. Support Rotations

Four markers (named 1, 2, 9, and 10) were used to calculate support rotations using an infrared-based non-contact position sensor, as discussed in section 3.4.3. The rotation of the left support was determined using the coordinates of markers 1 and 2, whereas markers 9 and 10 were used to calculate the rotation of the right support (Figure 4.35).

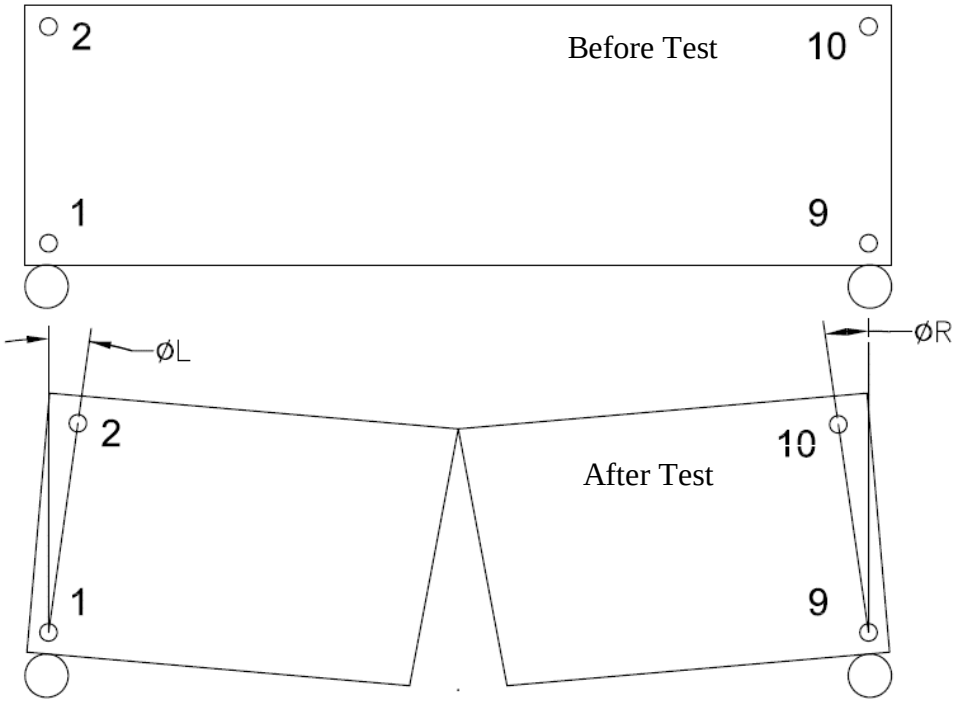

Figure 4.35 – Support rotations calculation.

Figure 4.36 shows a plot of load versus support rotations for fiber type RC-80/30-BP [different volume fractions (0.5%, 0.75%, 1.0%, and 1.5%)] and $f_c' = 10$ ksi. The initial slope and cracking load are similar for all specimens, but the post-cracking response is different (loads at similar rotation tended to increase as fiber volume fraction increased).

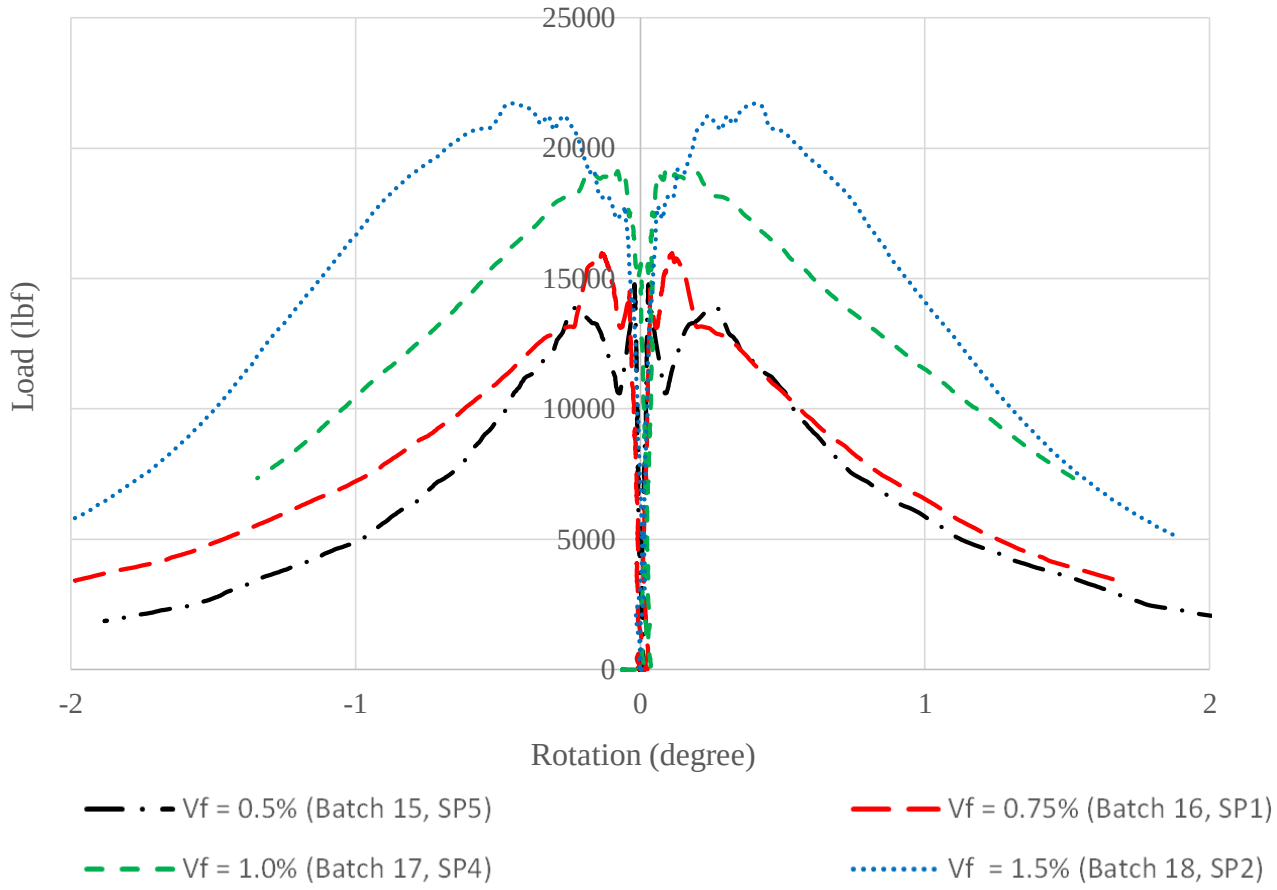

Figure 4.36 – Example plot of load vs. support rotations (f_c` = 10 ksi; RC-80/30-BP).

4.3.6 – Description of Failure

For specimens with plain concrete and low fiber volume fractions (0.5% and 0.75%), it was common to have only one crack form during the test (Figure 4.37). Specimens with fiber volume fractions of 1% and 1.5%, with the exception of those with fiber type 3D RC-55/30-BG, typically developed multiple flexural cracks prior to failure (Figures 4.38 and 4.39). Most of the flexural specimens were cracked within the middle third of the span where the shear force was nominally zero and the moment was maximum. However, some specimens were cracked outside

the middle portion. This was most common in specimens with fiber volume fractions of 1.0% and 1.5% that developed multiple cracks (Figure 4.38).

The behavior of the fibers at the primary crack was dominated by pullout and not fracture, as judged by visual inspection after testing and shown in Figure 4.40. The fibers exposed after testing at the primary crack were counted and are reported in Appendix C. Some specimens with $f_c' = 10$ ksi developed cracks above the supports (Figure 4.41) that are believed to be related to bearing.

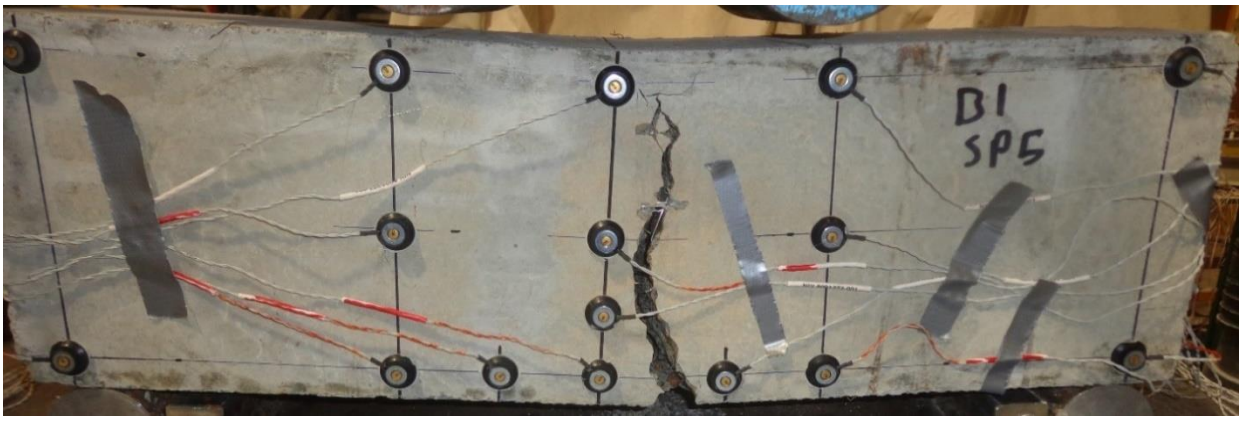

Figure 4.37 – Single crack developed at the middle portion of a flexural specimen (f_c` = 6 ksi; V_f = 0.5% of RC-80/30-BP; B1 SP5).

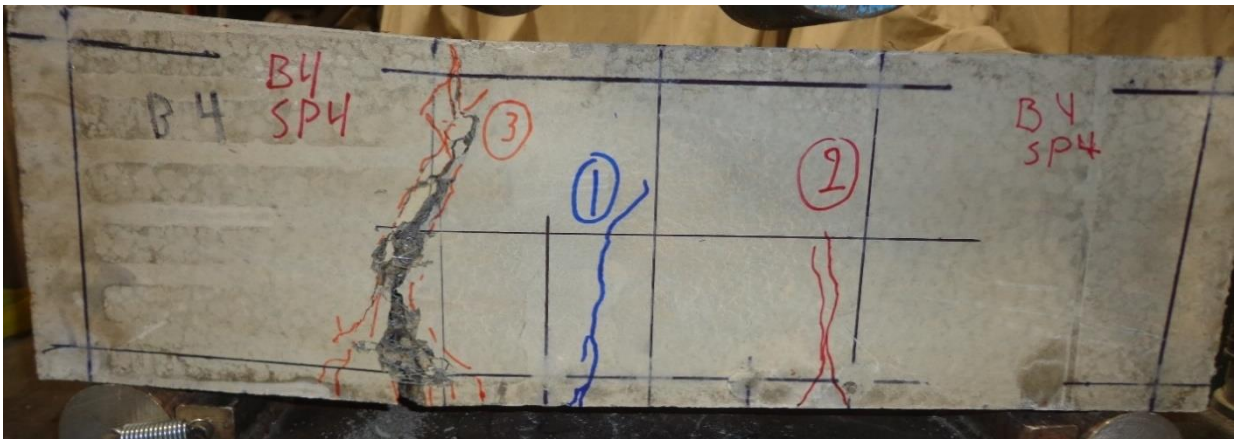

Figure 4.38 – Cracks developed outside the middle third of a flexural specimen (f_c` = 6 ksi; V_f = 1.5% of RC-80/30-BP; B4 SP4).

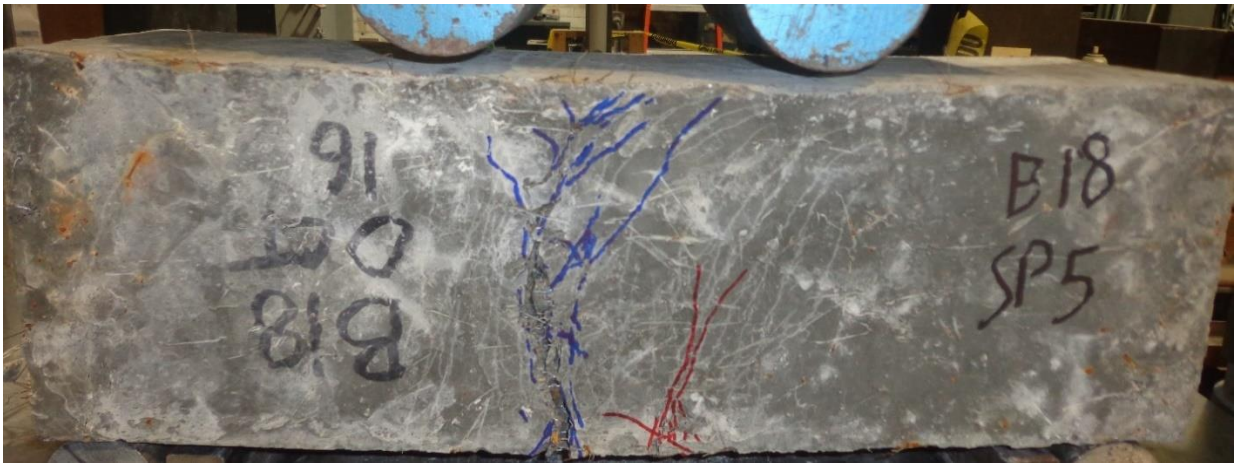

Figure 4.39 – Multiple flexural cracks (f_c` = 10 ksi; V_f = 1.5% of RC-80/30-BP; B18 SP5).

Figure 4.40 – Fiber pullout failure in a flexure specimen (f_c` = 6 ksi; V_f = 1.5% of 4D (RC-65/60-BG); B12 SP1).

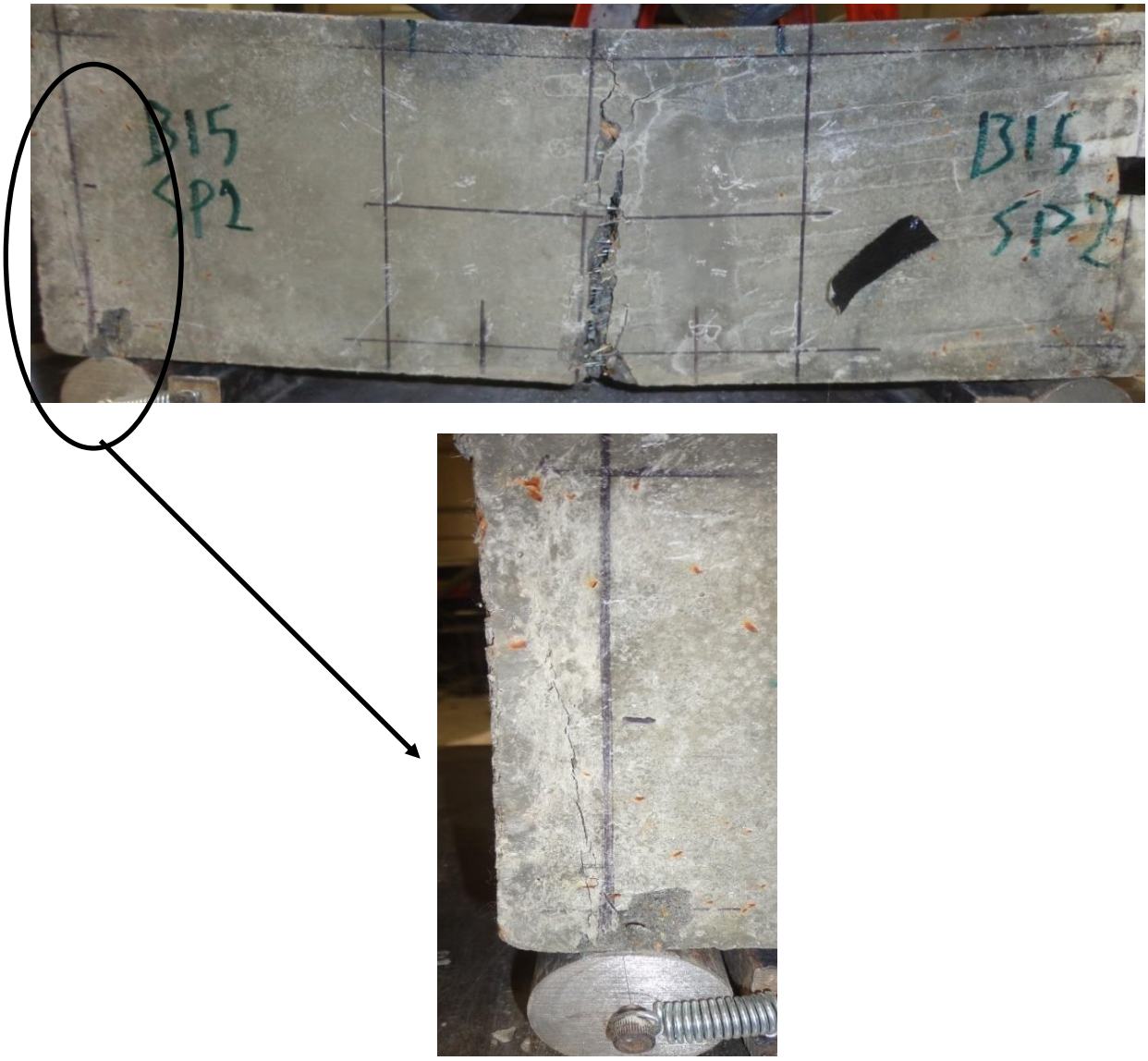

Figure 4.41 – Bearing crack developed in a flexure specimen (f_c` = 10 ksi; V_f = 0.5% of RC-80/30-BP; B15 SP2).

4.4 – Direct Tension Test

This section summarizes results from the tension tests. Detailed results are presented in Appendix D. First, the stress-crack width behavior is described. The first-peak strength (σ_1) recorded in each test is then discussed, as well as the post-crack peak strength (σ_{pc}), followed by general descriptions of the failure modes.

4.4.1 – Stress-Crack Width Behavior

An infrared-based non-contact position sensor was used to record specimen deformations. Eight markers (named 5, 6, 7, 8, 9, 10, 11, and 12) were used to calculate the crack width, as discussed in section 3.4.4. Figure 4.42 shows a plot of stress versus crack width for two typical test results (fiber type RC-80/30-BP with f_c` = 6 ksi). The initial slope and cracking stress are similar for both specimens, but the post-cracking response is different. The red curve (V_f = 0.75%) carries less stress after cracking, which is referred to as a strain softening response. The black curve (V_f = 1.5%) exhibits a period of strain hardening, characterized by higher stress after cracking and formation of multiple cracks, followed by a strain softening response after the peak.

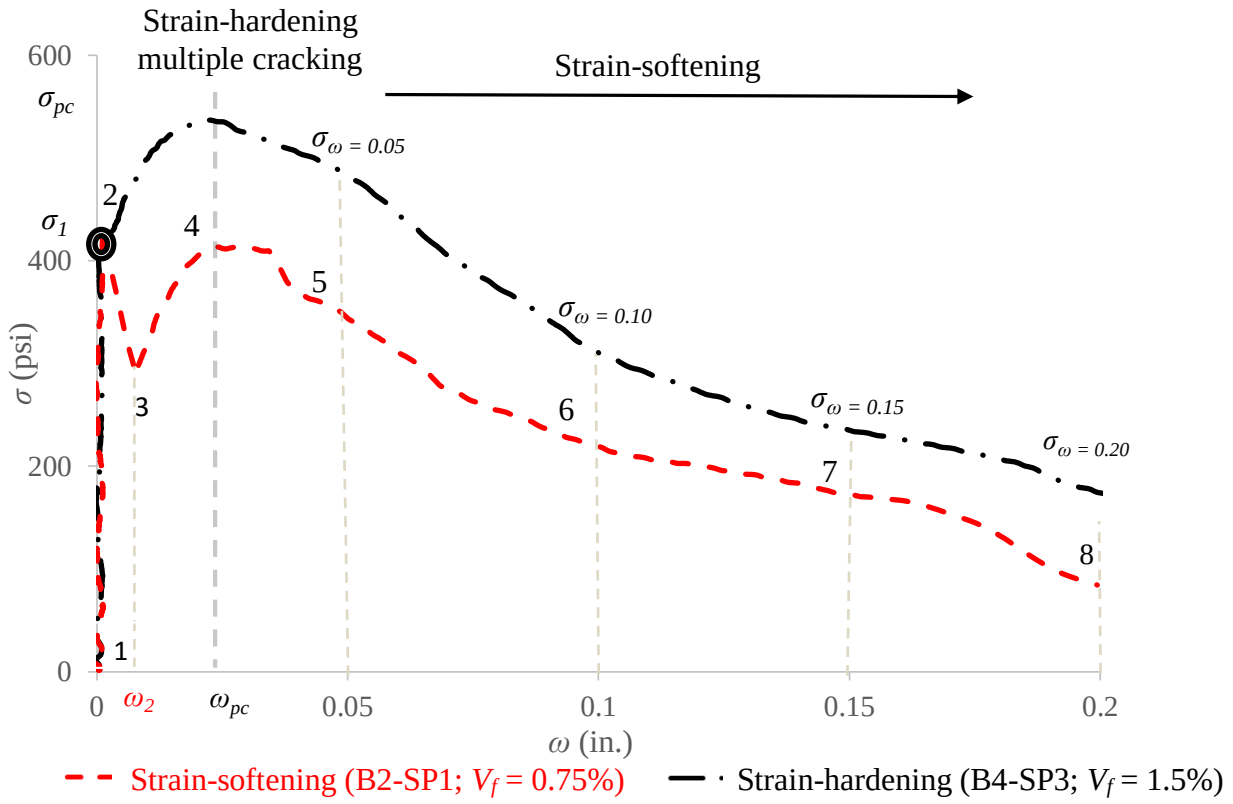

Figure 4.42 – Example plot of tensile stress vs. crack width (f_c` = 6 ksi and RC-80/30-BP).

To facilitate comparisons between test results, and thus allow study of the effect of introducing different volume fractions (0%, 0.5%, 0.75%, 1.0%, and 1.5%) and types of hooked steel fiber on the tension behavior of FRC, a representative stress-crack width curve was constructed for each batch using the following procedure:

- The coordinates of eight key points on the stress-crack width curve recorded for each specimen were identified. The points were: the test start point (0,0), the first-peak or the first-crack point (σ_1,ω_1), the drop point (σ_2,ω_2), the post-crack peak point (σ_{pc},ω_{pc}), the point at crack width equal to 0.05 inch ($\sigma_{\omega = 0.05}$, 0.05, in.), the point at crack width equal to 0.10 inch ($\sigma_{\omega = 0.10}$, 0.10 in.), the point at crack width equal to 0.15 inch ($\sigma_{\omega = 0.15}$, 0.15 in.), and the point at crack width equal to 0.20 inch ($\sigma_{\omega = 0.20}$, 0.20 in.). These points are identified in Figure 4.42.
- A representative curve for the batch was constructed by averaging the coordinates of each of the eight points, and linking them with line segments.

Representative plots of stress versus crack width are given in Figures 4.43 and 4.44 for all batches with $f_c' = 6$ ksi and fiber volume fractions of 0.75% and 1.5%. Similar plots are shown in Figures 4.45 and 4.46 for all batches with $f_c' = 10$ ksi. It can be observed that fiber type 3D RC-55/30-BG had the lowest impact on stress-crack width behavior. The other three fiber types showed similar behavior for the cases shown, except for that the RC-80/30-BP fibers performed much better than the others for a volume fraction of 0.75% in concrete with $f_c' = 6$ ksi.

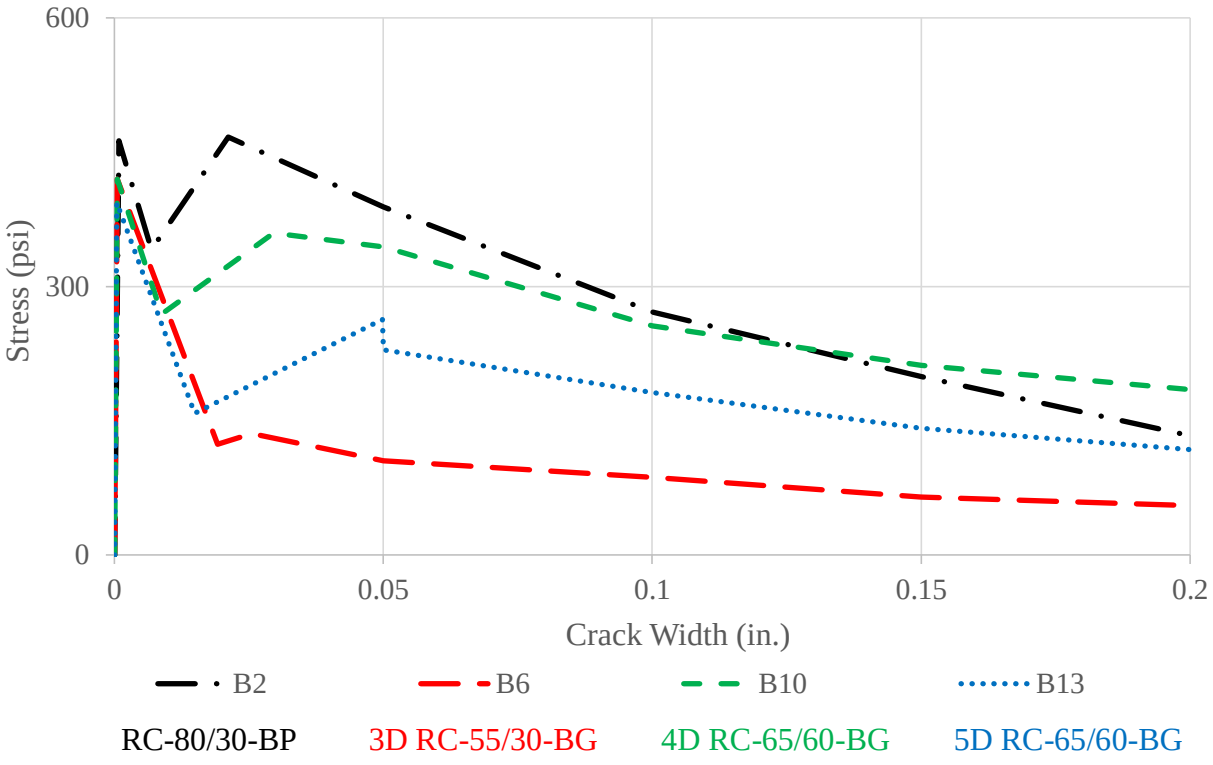

Figure 4.43 – Stress-crack width curves of 0.75% volume fraction ($f_c' = 6$ ksi).

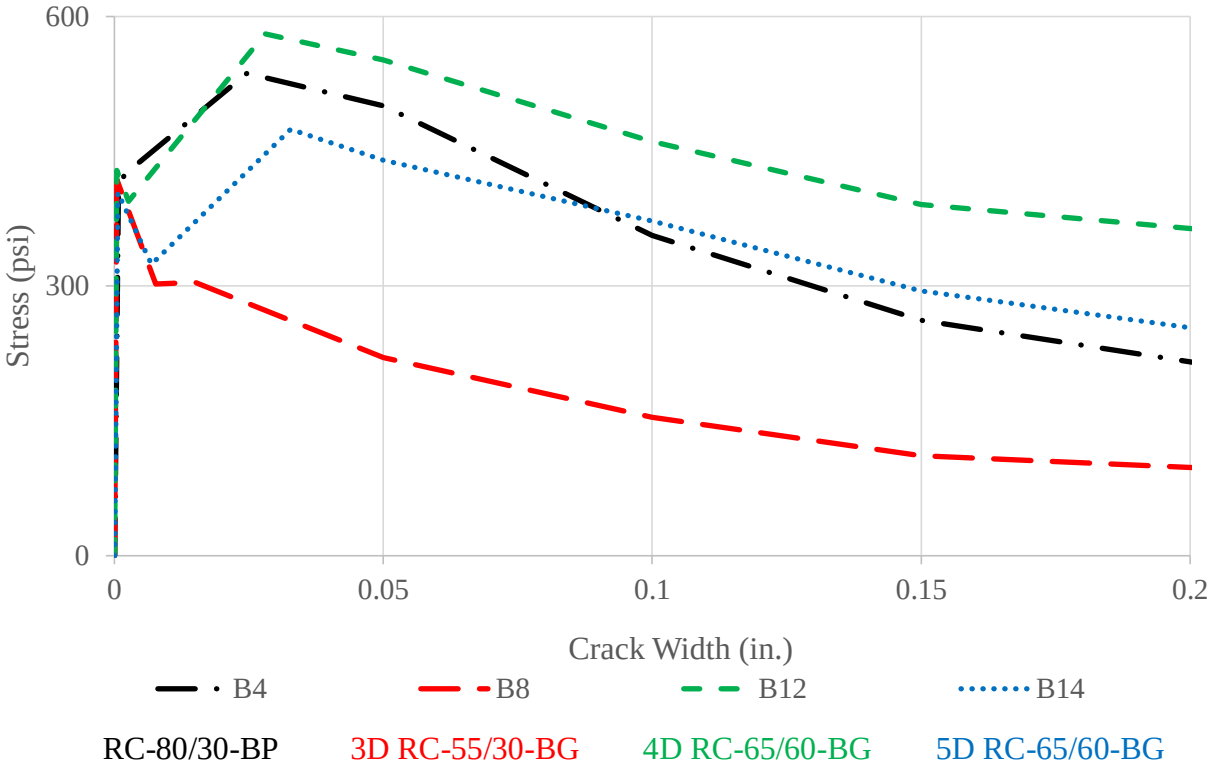

Figure 4.44 – Stress-crack width curves of 1.5% volume fraction ($f_c' = 6$ ksi).

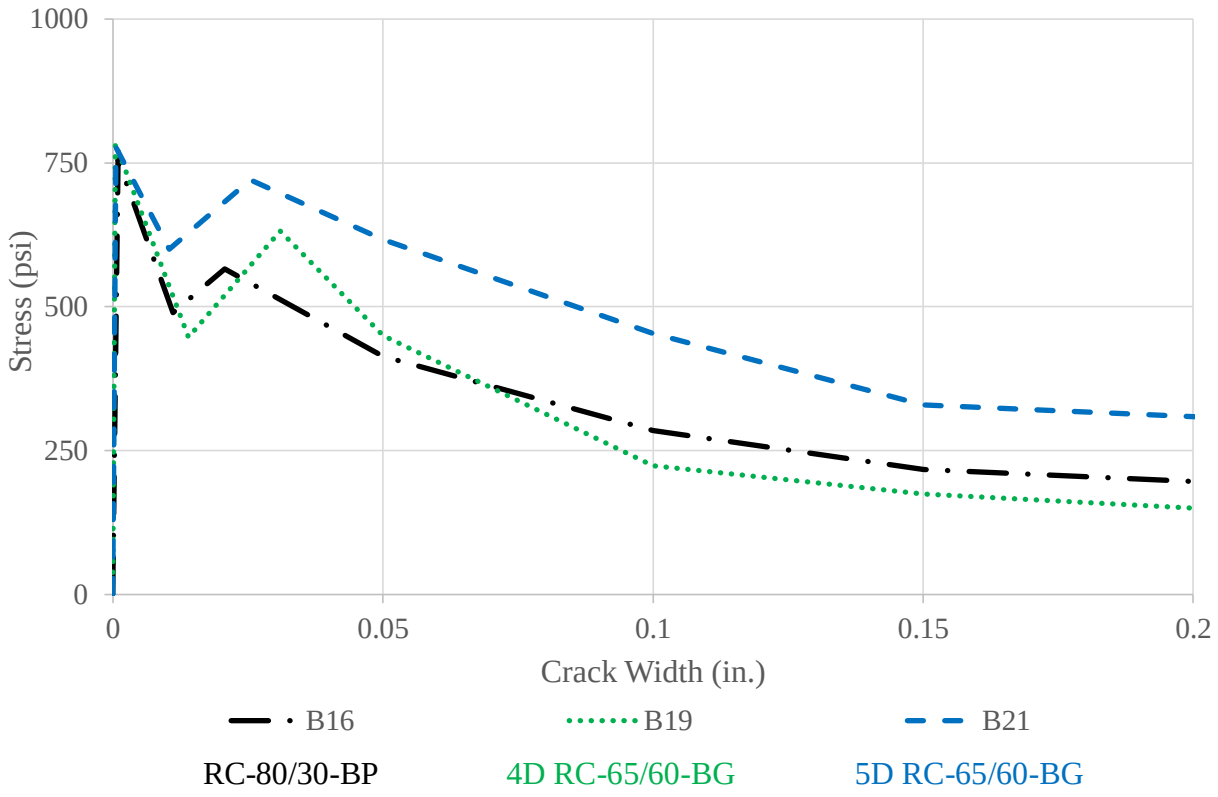

Figure 4.45 – Stress-crack width curves of 0.75% volume fraction ($f_c' = 10$ ksi).

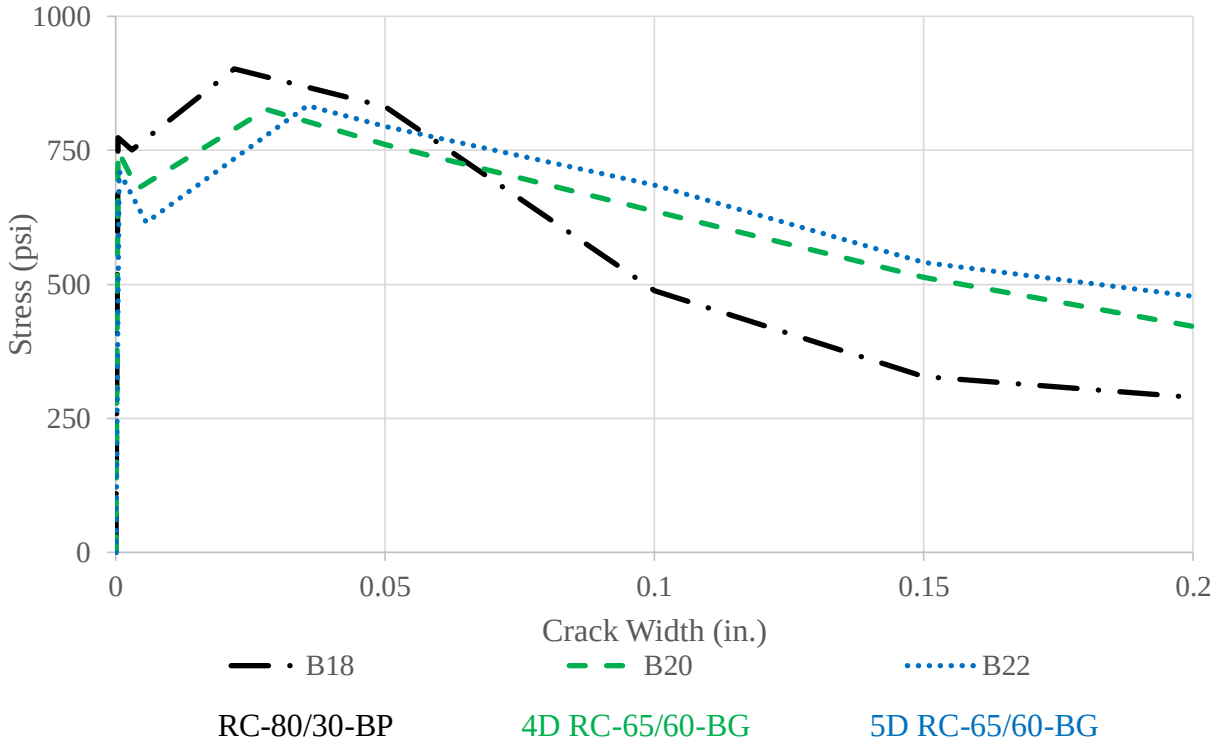

Figure 4.46 – Stress-crack width curves of 1.5% volume fraction ($f_c' = 10$ ksi).

4.4.2 – First-Peak Strength

The first-peak strength (the ordinate of point 2 in Figure 4.42) was calculated using equation 3-7. Calculated values ranged between 390 psi and 465 psi for concrete with $f_c' = 6$ ksi and between 685 psi and 820 psi for concrete with $f_c' = 10$ ksi. Table 4.6 summarizes the first-peak strength (σ_1) and the corresponding crack width of all batches. Figures 4.47 and 4.48, which show plots of σ_1 versus fiber volume fraction, show that the fibers had a negligible effect on the first-peak tensile strength.

4.4.3 – Post-Crack Peak Strength

The post-crack peak strength (σ_{pc}) was calculated using equation 3-8. The post-crack peak strengths (σ_{pc}), along with their coefficients of variation and the corresponding crack widths, are given in Table 4.7. Figures 4.49 and 4.50 show plots of σ_{pc} versus fiber volume fraction for batches with $f_c' = 6$ and 10 ksi, respectively.

Fiber properties and fiber volume fraction significantly affected the post-crack peak strength. Plain concrete had zero post-crack peak strength because it failed immediately after the first crack. The post-crack peak strength increased as fiber volume fraction increased and as fiber aspect ratio increased. The post-crack peak strength ranged between 130 psi and 590 psi for concrete with $f_c' = 6$ ksi (the coefficient of variation ranged between 3% and 54% except for batch 5, which had a post-crack peak strength equal to 60 psi and a coefficient of variation equal to 126%). The post-crack peak strength ranged between 490 psi and 885 psi for concrete with $f_c' = 10$ ksi (the coefficient of variation ranged between 5% and 33%).

Table 4.6 – The tensile first-peak strength.

Batch ID	Fiber type	V_f (%)	σ_1 (psi)
C 1	N/A	0	465
B 1	(RC-80/30-BP)	0.5	410
B 2	(RC-80/30-BP)	0.75	465
B 3	(RC-80/30-BP)	1.0	440
B 4	(RC-80/30-BP)	1.5	405
B 5	3D (RC-55/30-BG)	0.5	465
B 6	3D (RC-55/30-BG)	0.75	420
B 7	3D (RC-55/30-BG)	1.0	420
B 8	3D (RC-55/30-BG)	1.5	420
B 9	4D (RC-65/60-BG)	0.5	390
B 10	4D (RC-65/60-BG)	0.75	420
B 11	4D (RC-65/60-BG)	1.0	455
B 12	4D (RC-65/60-BG)	1.5	430
B 13	5D (RC-65/60-BG)	0.75	395
B 14	5D (RC-65/60-BG)	1.5	405
C 2	N/A	0	685
B 15	(RC-80/30-BP)	0.5	745
B 16	(RC-80/30-BP)	0.75	755
B 17	(RC-80/30-BP)	1.0	820
B 18	(RC-80/30-BP)	1.5	745
B 19	4D (RC-65/60-BG)	0.75	750
B 20	4D (RC-65/60-BG)	1.5	760
B 21	5D (RC-65/60-BG)	0.75	775
B 22	5D (RC-65/60-BG)	1.5	710

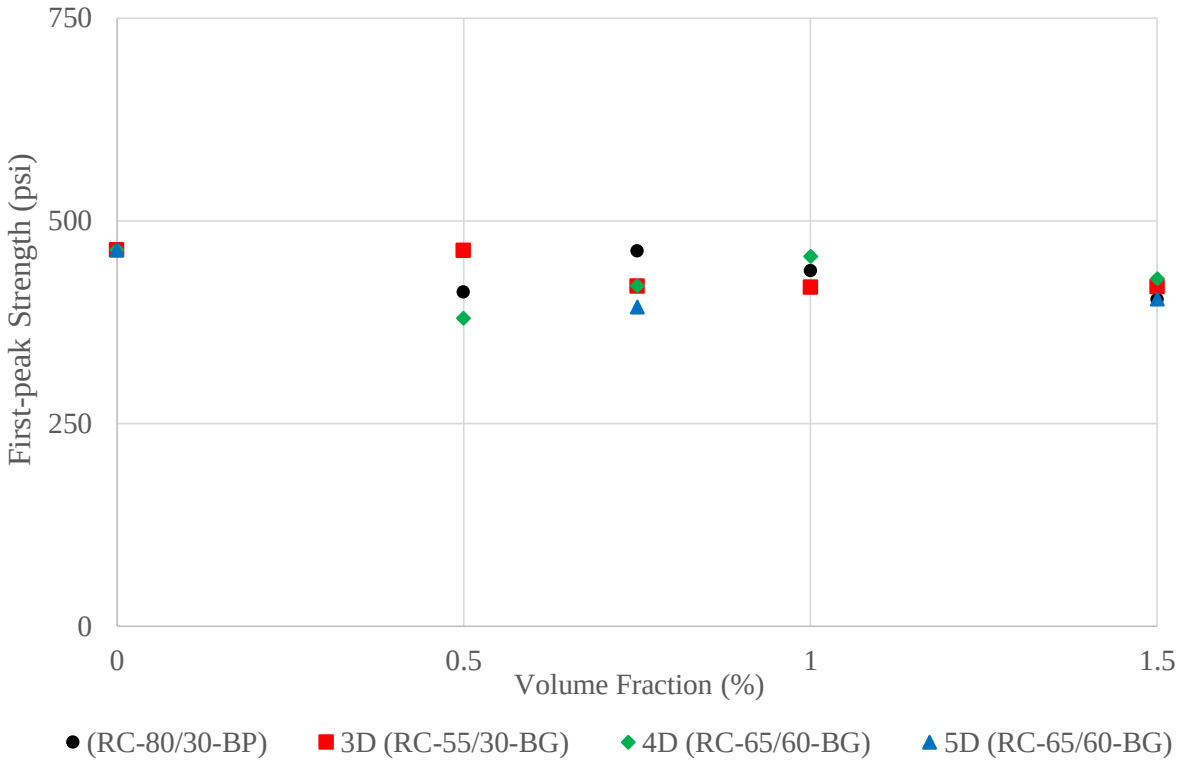

Figure 4.47 – First-peak tensile strength vs. fiber volume fraction ($f_c' = 6$ ksi).

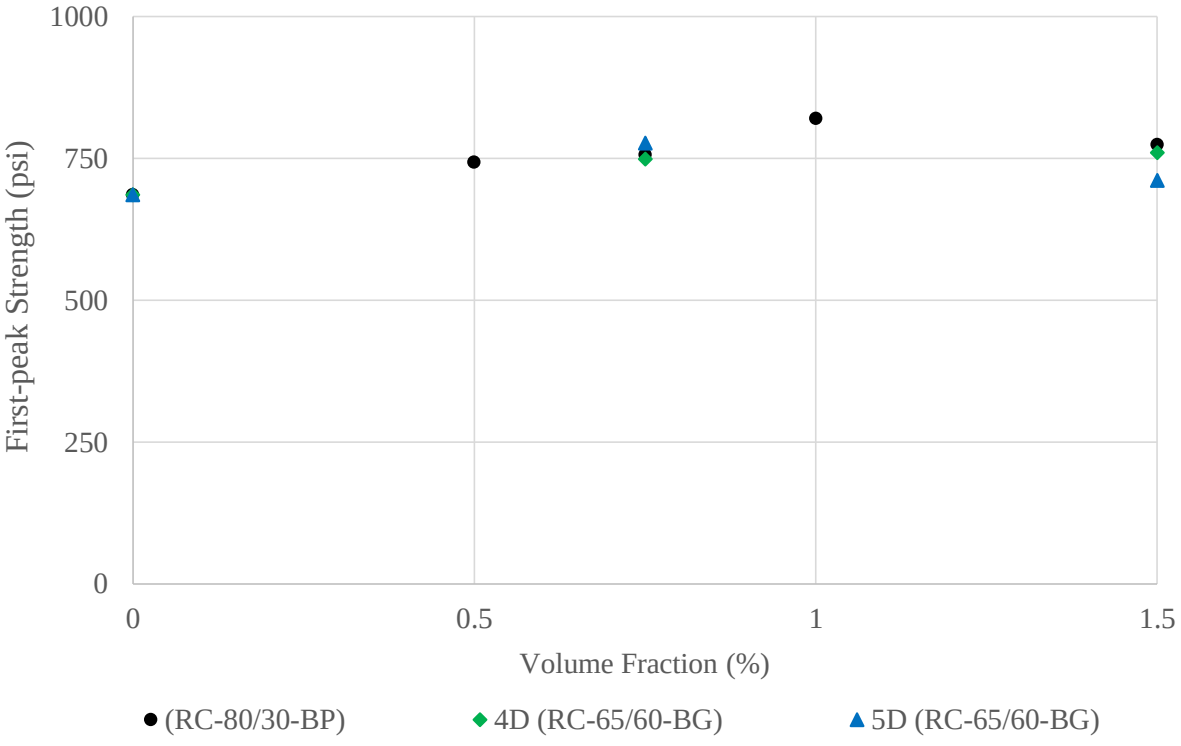

Figure 4.48 – First-peak tensile strength vs. fiber volume fraction ($f_c' = 10$ ksi).

Table 4.7 – The post-crack peak tensile strengths, coefficient of variations, and crack widths.

Batch ID	Fiber type	V_f (%)	σ_{pc} (psi)	$COV(\sigma_{pc})$	ω_{pc} (in.)
C 1	N/A	0			
B 1	(RC-80/30-BP)	0.5	225	35%	0.04
B 2	(RC-80/30-BP)	0.75	455	9%	0.02
B 3	(RC-80/30-BP)	1.0	460	11%	0.02
B 4	(RC-80/30-BP)	1.5	535	3%	0.02
B 5	3D (RC-55/30-BG)	0.5	60	126%	0.06
B 6	3D (RC-55/30-BG)	0.75	130	39%	0.03
B 7	3D (RC-55/30-BG)	1.0	215	49%	0.02
B 8	3D (RC-55/30-BG)	1.5	255	54%	0.01
B 9	4D (RC-65/60-BG)	0.5	285	25%	0.04
B 10	4D (RC-65/60-BG)	0.75	380	20%	0.03
B 11	4D (RC-65/60-BG)	1.0	475	23%	0.03
B 12	4D (RC-65/60-BG)	1.5	590	27%	0.03
B 13	5D (RC-65/60-BG)	0.75	260	47%	0.05
B 14	5D (RC-65/60-BG)	1.5	470	36%	0.03
C 2	N/A	0			
B 15	(RC-80/30-BP)	0.5	490	10%	0.03
B 16	(RC-80/30-BP)	0.75	545	9%	0.02
B 17	(RC-80/30-BP)	1.0	885	5%	0.02
B 18	(RC-80/30-BP)	1.5	865	9%	0.02
B 19	4D (RC-65/60-BG)	0.75	595	31%	0.03
B 20	4D (RC-65/60-BG)	1.5	790	33%	0.03
B 21	5D (RC-65/60-BG)	0.75	720	12%	0.03
B 22	5D (RC-65/60-BG)	1.5	835	13%	0.04

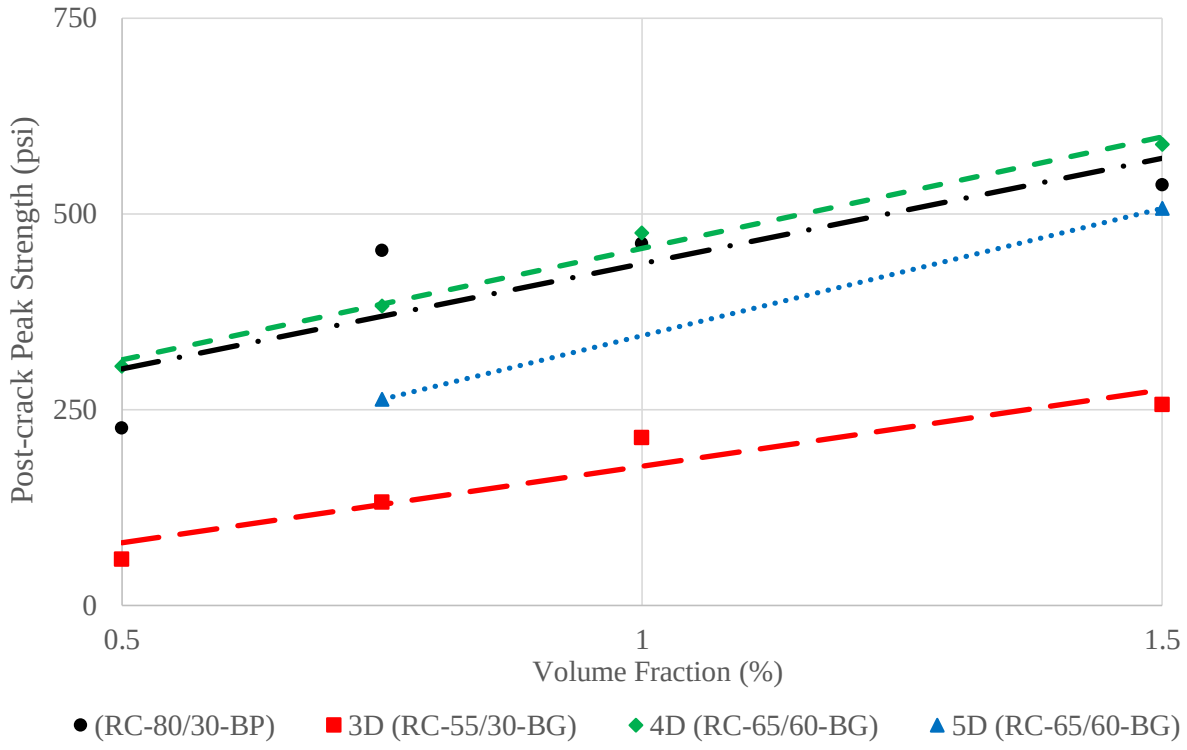

Figure 4.49 – The post-crack peak tensile strength vs. fiber volume fraction ($f_c' = 6$ ksi).

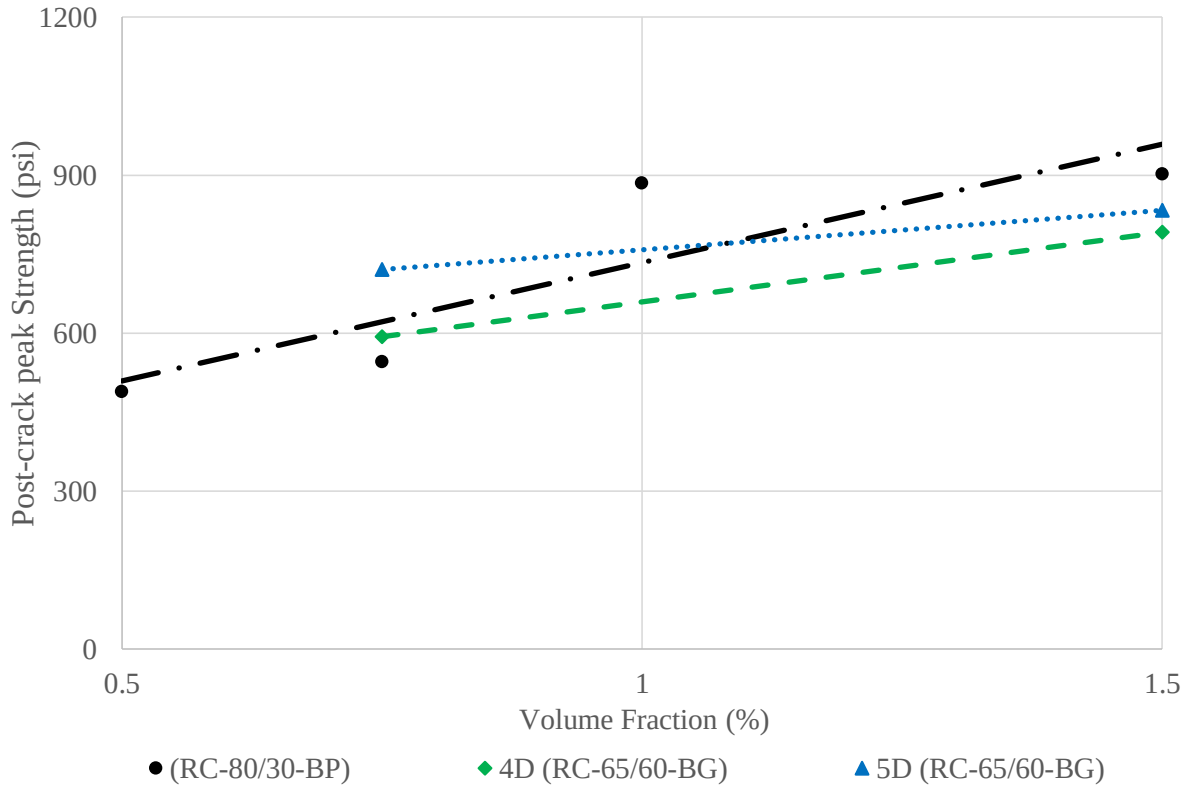

Figure 4.50 – The post-crack peak tensile strength vs. fiber volume fraction ($f_c' = 10$ ksi).

4.4.4 – Description of Failure

For specimens with plain concrete and low fiber volume fractions (0.5% and 0.75%), it was common to develop cracks at the pre-notched middle portion where the stresses were maximum (Figure 4.51). Some specimens with high volume fraction (1.0% and 1.5%) of fibers 4D (RC-65/60-BG) and 5D (RC-65/60-BG) (fiber length 60 mm) typically developed cracks inside and outside the middle portion (Figure 4.52).

The behavior of the fibers at the crack was dominated mainly (more than 90%) by fiber pullout, as judged by visual inspection after testing and shown in Figure 4.53. The fibers exposed after testing at the primary crack were counted and are reported in Appendix D.

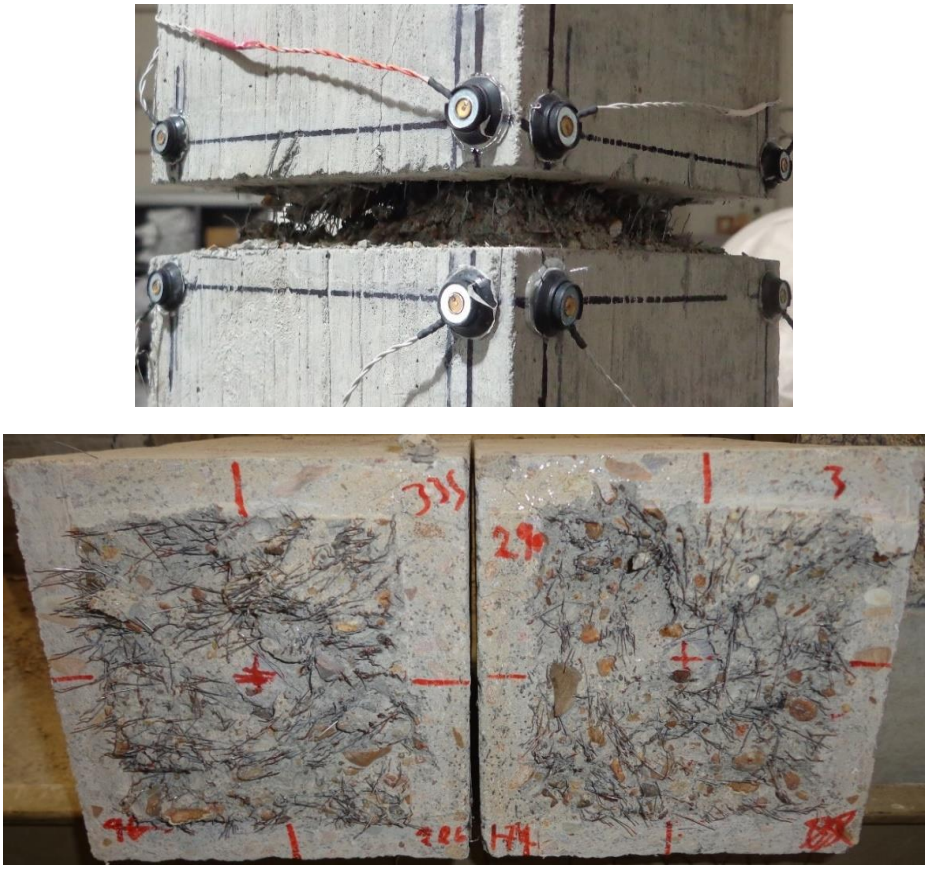

Figure 4.51 – Typical failure of tension specimen (f_c` = 6 ksi; V_f = 1.5% of RC-80/30-BP; B4 SP5).

Figure 4.52 – Failure outside the pre-notched middle portion (f_c` = 10 ksi; V_f = 1.5% of 4D RC-65/60-BG; B20 SP1).

Figure 4.53 – Fiber pullout failure in a tension specimen (f_c` = 6 ksi; V_f = 1.5% of 4D RC-65/60-BG; B12 SP3).

CHAPTER 5: DISCUSSION OF RESULTS

5.0 – General

This chapter is a discussion of the results presented in Chapter 4. The properties of the self-consolidating fiber reinforced concrete (SCFRCs) in the fresh-state are disscused first. Results from the uniaxial compression tests, the flexure tests, and the direct tension tests are then discussed. Finally, results from compression, tension, and flexural tests are correlated.

5.1 – SCFRCs in the Fresh-State

5.1.1 – Slump Flow

As previously shown in Chapter 4, measured slump flow decreased as fiber volume fraction increased. Table 5.1 summarizes the effect of different hooked end steel fibers of various volume fractions (0%, 0.5%, 0.75%, 1.0%, and 1.5%) on concrete workability and concrete passing ability.

Table 5.1 – Concrete workability assessment.

Batch ID	Fiber Type	V_f (%)	Reduction in Slump Flow	Reduction in J-ring Flow	Passing Ability (in.)	Blocking Assessment[1]
C 1	N/A	0			0.5	No visible blocking
B 1	(RC-80/30-BP)	0.5	-7%	-7%	0.5	No visible blocking
B 2	(RC-80/30-BP)	0.75	-13%	-22%	3.0	Noticeable to extreme blocking
B 3	(RC-80/30-BP)	1.0	-16%	-35%	5.5	Noticeable to extreme blocking
B 4	(RC-80/30-BP)	1.5	-18%	-39%	6.0	Noticeable to extreme blocking
B 5	3D (RC-55/30-BG)	0.5	-9%	-11%	1.0	No visible blocking
B 6	3D (RC-55/30-BG)	0.75	-13%	-13%	0.5	No visible blocking

B 7	3D (RC-55/30-BG)	1.0	-9%	-17%	2.5	Noticeable to extreme blocking
B 8	3D (RC-55/30-BG)	1.5	-16%	-35%	5.5	Noticeable to extreme blocking
B 9	4D (RC-65/60-BG)	0.5	-9%	-19%	3.0	Noticeable to extreme blocking
B 10	4D (RC-65/60-BG)	0.75	-9%	-28%	5.5	Noticeable to extreme blocking
B 11	4D (RC-65/60-BG)	1.0	-16%	-31%	4.5	Noticeable to extreme blocking
B 12	4D (RC-65/60-BG)	1.5	-24%	-44%	6.0	Noticeable to extreme blocking
B 13	5D (RC-65/60-BG)	0.75	-20%	-37%	5.0	Noticeable to extreme blocking
B 14	5D (RC-65/60-BG)	1.5	-27%	-46%	5.5	Noticeable to extreme blocking
C 2	N/A	0			1.0	No visible blocking
B 15	(RC-80/30-BP)	0.5	-5%	-5%	1.0	No visible blocking
B 16	(RC-80/30-BP)	0.75	7%	-5%	4.5	Noticeable to extreme blocking
B 17	(RC-80/30-BP)	1.0	-9%	-20%	4.0	Noticeable to extreme blocking
B 18	(RC-80/30-BP)	1.5	-21%	-27%	2.5	Noticeable to extreme blocking
B 19	4D (RC-65/60-BG)	0.75	4%	-9%	4.5	Noticeable to extreme blocking
B 20	4D (RC-65/60-BG)	1.5	-18%	-20%	1.5	Minimal to noticeable blocking
B 21	5D (RC-65/60-BG)	0.75	0%	-9%	3.5	Noticeable to extreme blocking
B 22	5D (RC-65/60-BG)	1.5	-5%	-16%	4.0	Noticeable to extreme blocking

[1] Rating according to ASTM C1621 based on calculated Passing Ability

The extent of the reduction in measured slump flow is shown for different volume fractions and types of fibers in Figures 5.1 ($f_c' = 6$ ksi) and 5.2 ($f_c' = 10$ ksi), which show the percent change in slump flow relative to the control batch plotted versus volume fraction. Batches with the 30 mm long "3D" fibers (fiber types RC-80/30-BP and 3D RC-55/30-BG) had similar reductions in slump

flow, with reductions up to approximately 20% for volume fractions of 1.5%. Batches with the 60 mm long "4D" and "5D" fibers (fiber types 4D RC-65/60-BG and 5D RC-65/60-BG) had similar reductions in workability to the batches with the "3D" fibers. Although these longer fibers appear to more adversely affect workability in Figure 5.1 ($f_c' = 6$ ksi), there is an opposite trend in Figure 5.2 ($f_c' = 10$ ksi). It is not clear from this data whether fiber length or hook shape influence measured slump flows.

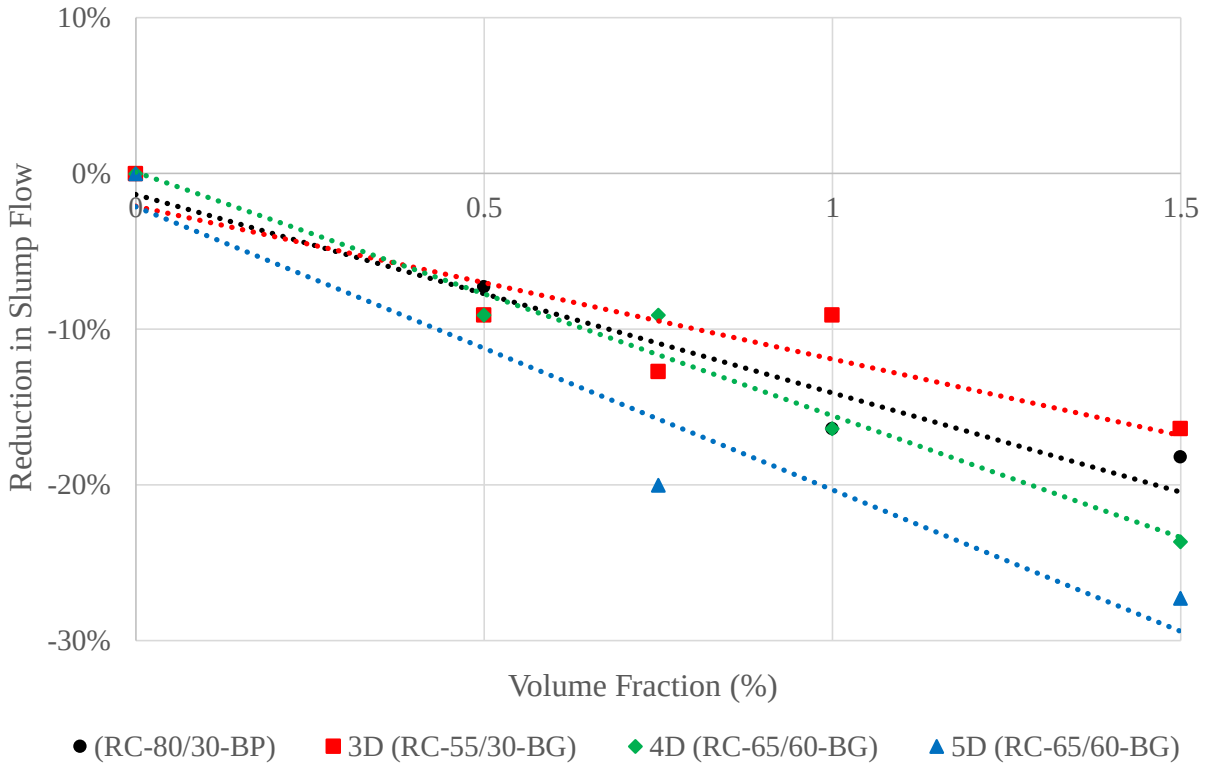

Figure 5.1 – Percent reduction in slump flow vs. volume fraction ($f_c' = 6$ ksi).

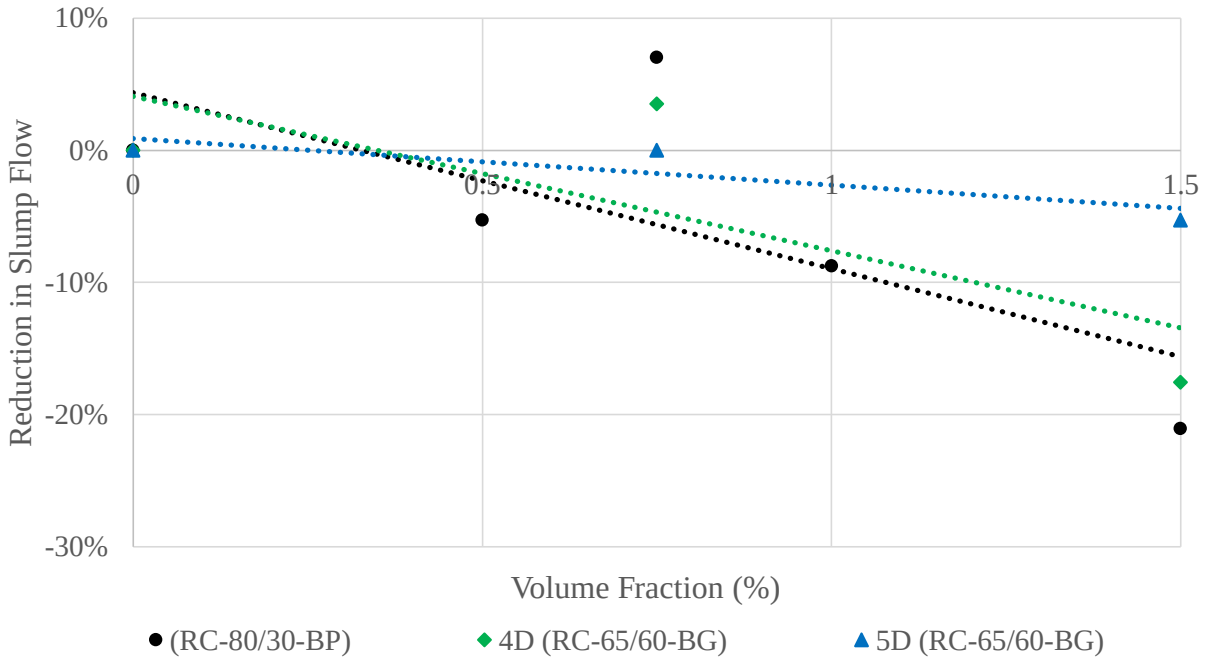

Figure 5.2 – Percent reduction in slump flow vs. volume fraction ($f_c' = 10$ ksi).

5.1.2 – J-Ring Slump Flow

The reduction in concrete workability in terms of J-ring slump flow is shown for different volume fractions and types of fibers in Figures 5.3 ($f_c' = 6$ ksi) and 5.4 ($f_c' = 10$ ksi), which show the percent change in J-ring slump flow relative to the control batch plotted versus fiber volume fraction. J-ring slump flow decreased as the volume fraction of fibers increased. The measured J-ring slump flow, which presents the concrete workability in the presence of reinforcement, was reduced by approximately 40% in batches with $f_c' = 6$ ksi and a fiber volume fraction of 1.5%, and 20% in batches with $f_c' = 10$ ksi and a fiber volume fraction of 1.5%. These results indicate that the J-ring slump flow test is much more sensitive to inclusion of fibers than the slump flow test. The J-ring slump flow test results show similar trends between types of fibers as the slump flow tests.

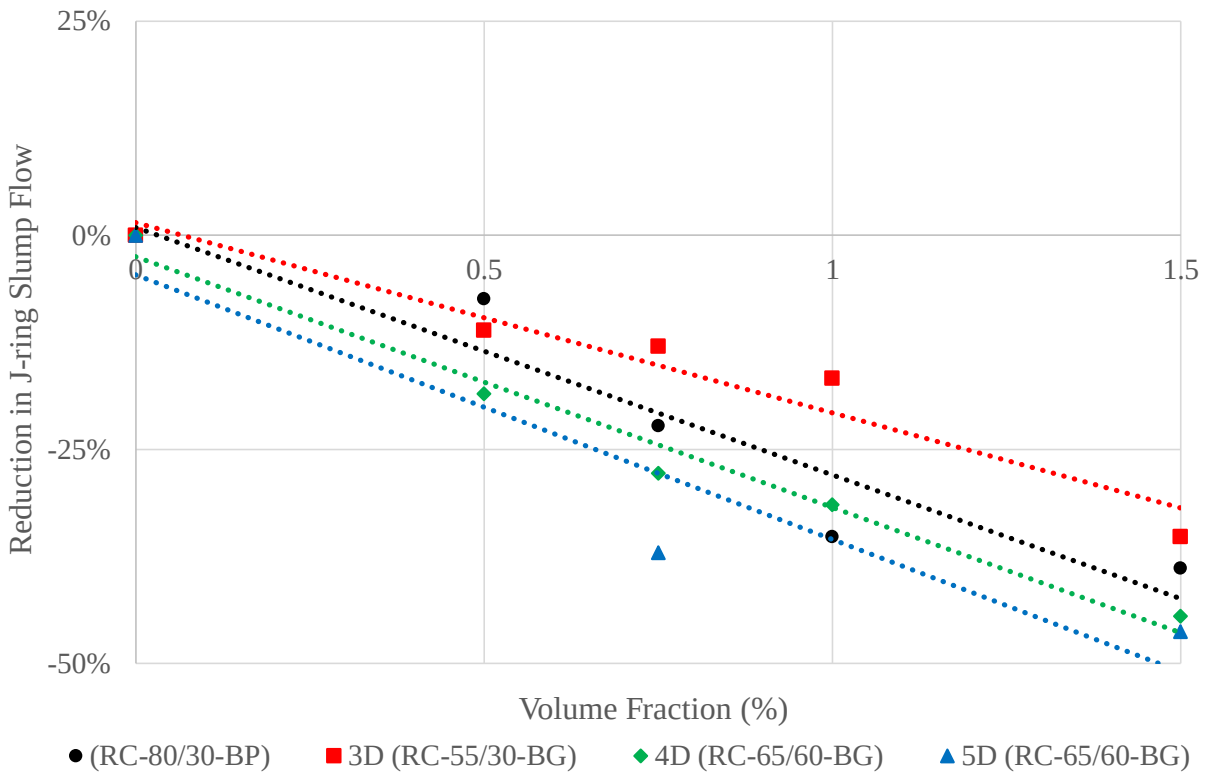

Figure 5.3 – Percent reduction in J-slump flow vs. volume fraction ($f_c' = 6$ ksi).

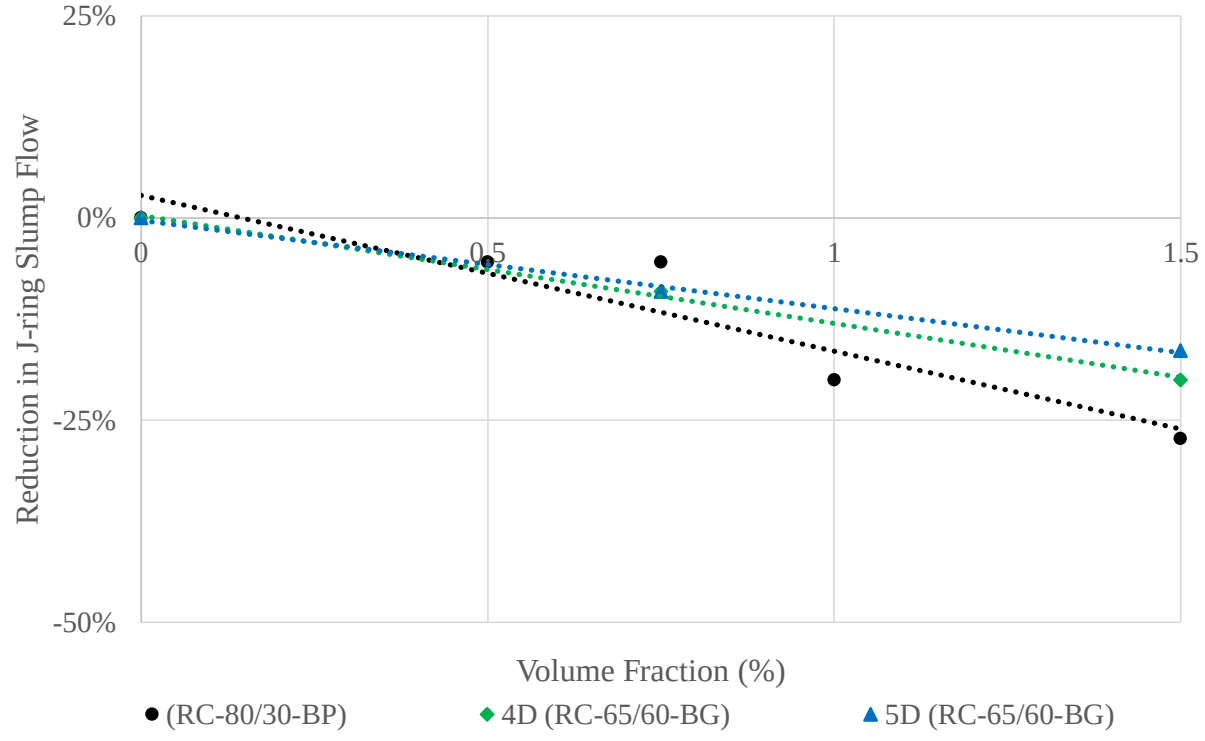

Figure 5.4 – Percent reduction in J-slump flow vs. volume fraction ($f_c' = 10$ ksi).

5.1.3 – Passing Ability

Concrete passing ability, which is the difference between concrete slump flow and J-ring slump flow results, increased as fiber volume fraction increased. This is shown in Figures 5.5 ($f_c' =$ 6 ksi) and 5.6 ($f_c' = 10$ ksi), which show the calculated passing ability plotted versus fiber volume fraction. As discussed in Chapter 3, the ASTM 1621 standard states concrete with a passing ability of 2 or greater has noticeable to extreme blocking. Although the control batches with no fibers exhibited a passing ability of 0.5 in. and 1.0 in. ($f_c' = 6$ and 10 ksi respectively), most batches of concrete with a fiber volume fraction of 0.75% and all batches with fiber volume fractions of 1.0% and 1.5%, had passing abilities greater than 2. However, given that all batches were highly workable and few showed clear evidence of segregation, it seems unreasonable to reject fiber reinforced concrete mixtures for having a passing ability greater than 2. There was no clear trend between fiber type and passing ability in this dataset.

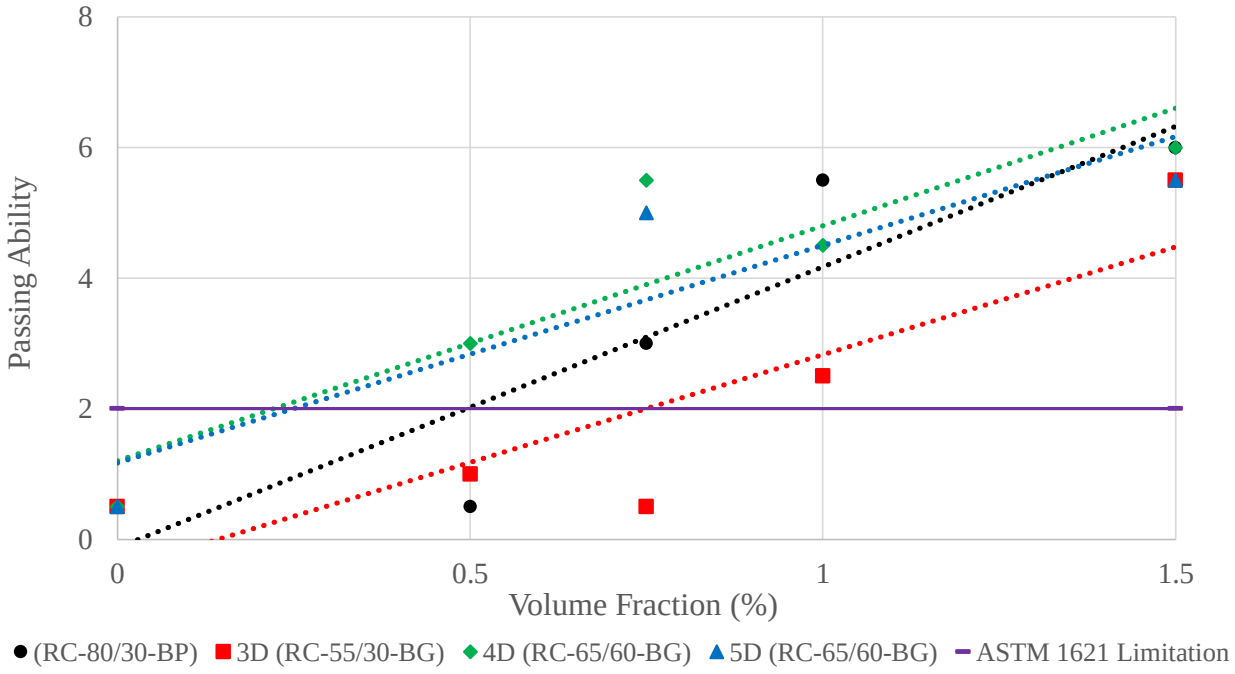

Figure 5.5 – Passing ability vs. volume fraction ($f_c' = 6$ ksi).

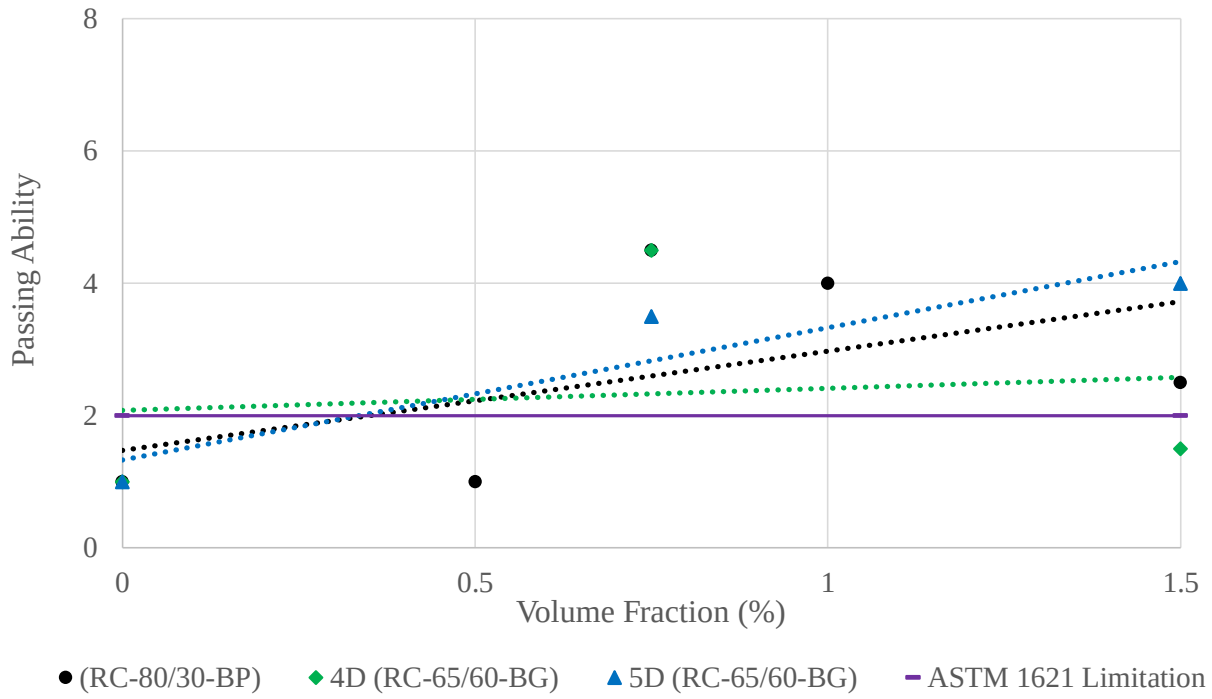

Figure 5.6 – Passing ability vs. volume fraction ($f_c' = 10$ ksi).

5.1.4 – T_{50}

Although, as shown in Appendix A, most batches of concrete in this study had a visual stability index of 0 or 1 (this is a qualitative evaluation of segregation conducted as part of the standard slump flow test, and values of 0 and 1 indicate little to no segregation), several batches of concrete exhibited a high variability in post-cracking behavior (see Chapter 4). This highly variable post-peak behavior was associated with a high variability in the number of fibers located at the dominant crack.

The T_{50} test, which is a measure of concrete viscosity, was shown to be related to this highly variable post-peak behavior (see Table 5.2). Figures 5.7, 5.8, and 5.9 show the coefficient of variation for the peak post-cracking flexural load, peak post-cracking tension stress, and compressive post-peak slope, respectively, plotted versus the measured T_{50} value for each batch.

Table 5.2 – Measured T_{50} values and coefficients of variation for the peak post-cracking flexural strength (P_{pc}), peak post-cracking tensile strength (σ_{pc}), and slope of the descending branch of the compressive stress-strain response (E_{pp}).

Batch ID	Fiber Type	V_f (%)	T_{50} (sec.)	$COV(P_{pc})$	$COV(\sigma_{pc})$	$COV(E_{pp})$
C 1	N/A	0	0.7			18%
B 1	(RC-80/30-BP)	0.5	0.8	41%	35%	34%
B 2	(RC-80/30-BP)	0.75	0.9	14%	9%	9%
B 3	(RC-80/30-BP)	1.0	0.95	17%	11%	36%
B 4	(RC-80/30-BP)	1.5	0.95	11%	3%	48%
B 5	3D (RC-55/30-BG)	0.5	0.8	84%	126%	33%
B 6	3D (RC-55/30-BG)	0.75	0.6	52%	39%	37%
B 7	3D (RC-55/30-BG)	1.0	0.7	41%	49%	80%
B 8	3D (RC-55/30-BG)	1.5	0.9	13%	54%	23%
B 9	4D (RC-65/60-BG)	0.5	0.9	54%	25%	94%
B 10	4D (RC-65/60-BG)	0.75	0.7	60%	20%	47%
B 11	4D (RC-65/60-BG)	1.0	0.8	59%	23%	15%
B 12	4D (RC-65/60-BG)	1.5	0.9	37%	27%	34%
B 13	5D (RC-65/60-BG)	0.75	0.8	45%	47%	82%
B 14	5D (RC-65/60-BG)	1.5	0.8	55%	36%	90%
C 2	N/A	0	2.2			18%
B 15	(RC-80/30-BP)	0.5	2.3	11%	10%	38%
B 16	(RC-80/30-BP)	0.75	1.9	5%	9%	37%
B 17	(RC-80/30-BP)	1.0	2.6	11%	5%	54%
B 18	(RC-80/30-BP)	1.5	3.2	11%	9%	37%
B 19	4D (RC-65/60-BG)	0.75	2.0	8%	31%	91%
B 20	4D (RC-65/60-BG)	1.5	3.4	18%	33%	87%
B 21	5D (RC-65/60-BG)	0.75	2.1	8%	12%	69%
B 22	5D (RC-65/60-BG)	1.5	1.7	23%	13%	110%

The coefficients of variation for the peak post-cracking load from both the flexure and tension tests are large for batches with T_{50} values less than 1, with an average coefficient of variation of approximately 40%. For batches with a T_{50} value greater than 1, the average coefficient

of variation for the peak post-cracking load from both the flexure and tension tests was 13%. Therefore, larger T_{50} values were correlated with decreased variability in peak post-cracking flexural and tensile strength. A T_{50} value of 1 may be a useful minimum when evaluating SCFRC mixtures.

As shown in Figure 5.9, T_{50} values were not correlated with variability in the slope of the descending branch of the compressive stress-strain response.

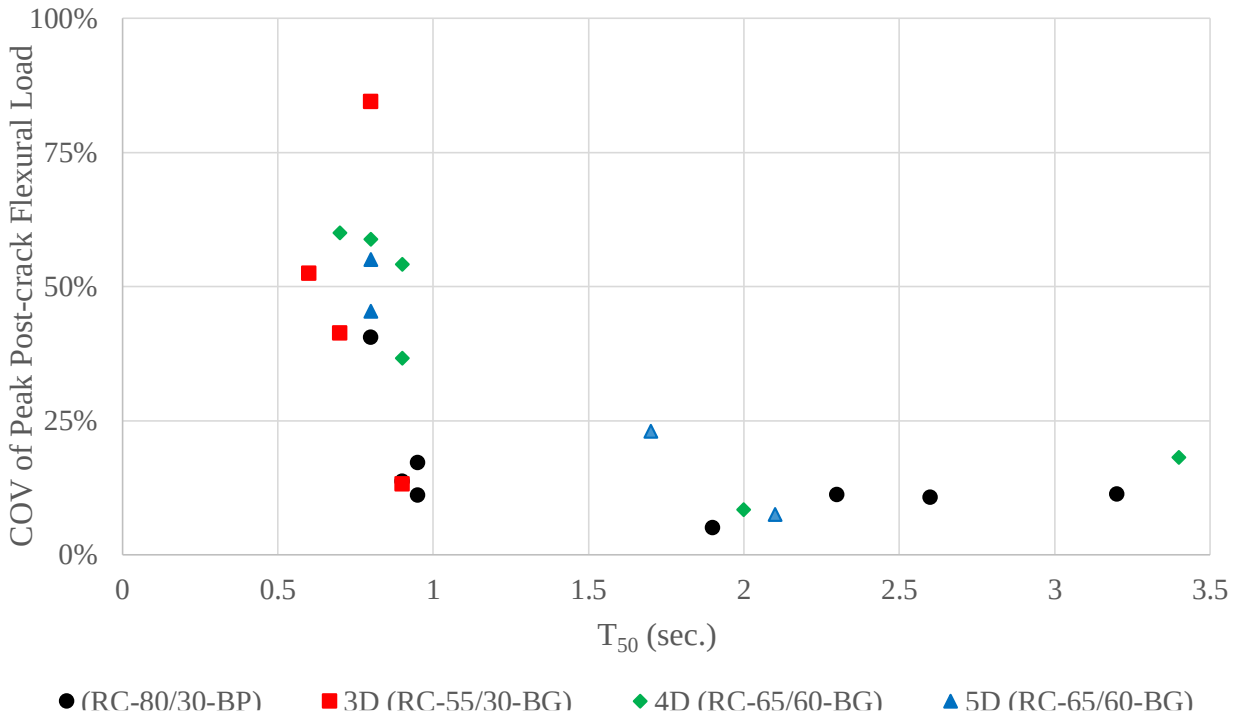

Figure 5.7 – T_{50} vs. coefficient of variation of the post-crack peak flexural load.

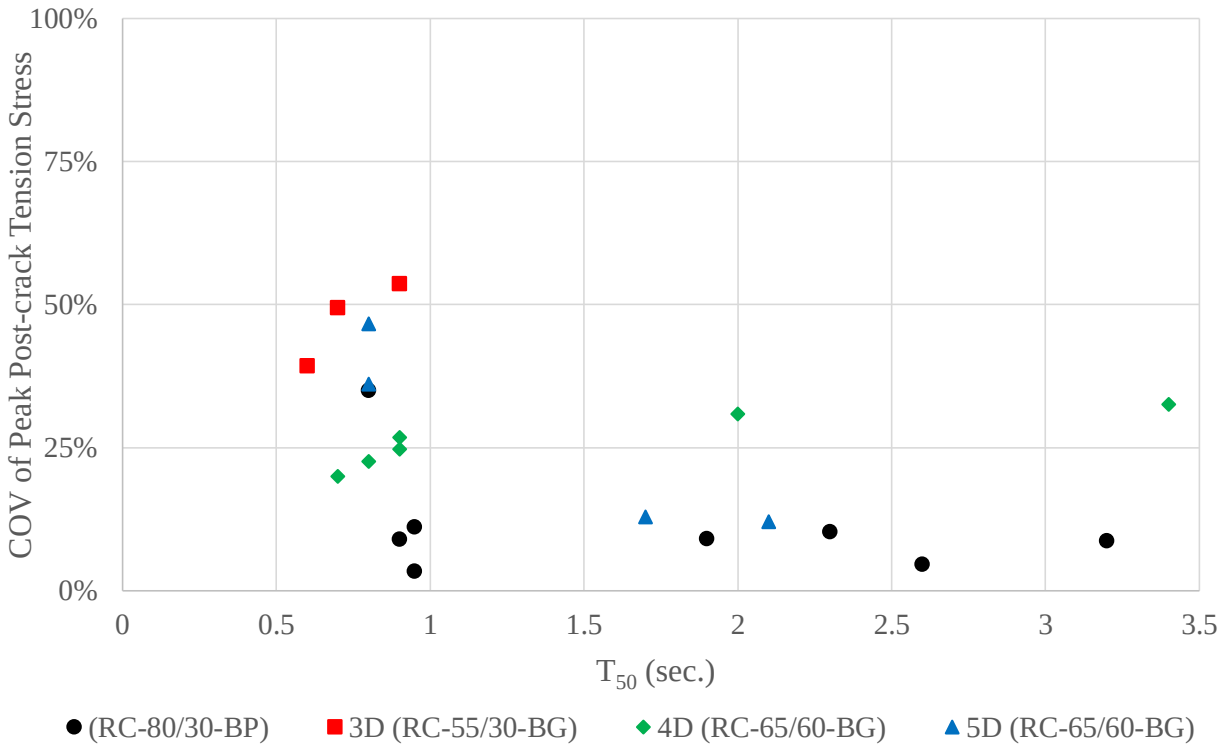

Figure 5.8 – T_{50} vs. the coefficient of variation of the post-crack peak tensile stress.

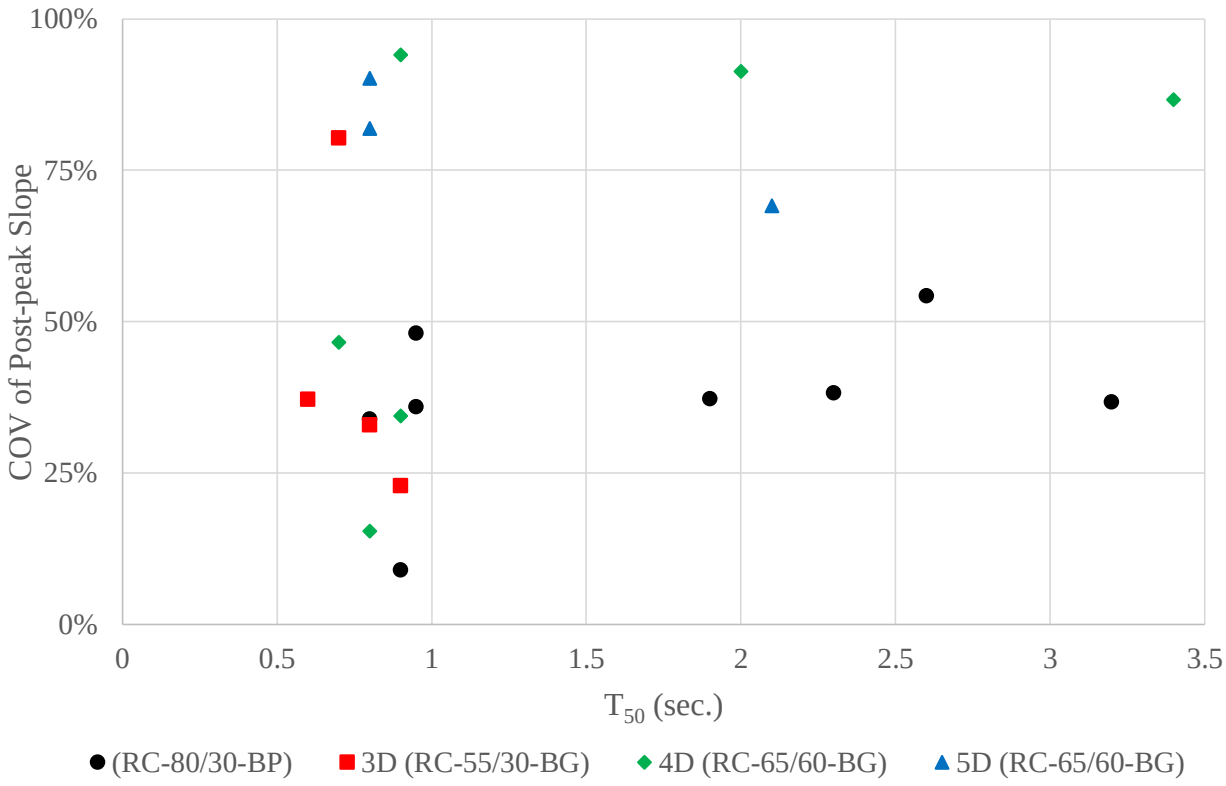

Figure 5.9 – T_{50} vs. the coefficient of variation of the post-peak compression slope.

5.1.5 – Fiber Separation

As previously described in Chapter 4, some fibers were not completely separated after mixing. This was particularly true for batches with fiber type 3D RC-55/30-BG, which had large fiber bundles (5 or more fibers per bundle) after 20 minutes of mixing, as shown in Figure 4.7. It is likely the bundles of fibers limited the distribution of fibers and somewhat compromised the performance of these mixtures in subsequent testing (although it is not clear to what extent). As shown in Figures 5.10 and Figure 5.11, which show plots of load versus deflection in bending tests and stress versus crack width in tension tests, respectively, no batch with 3D RC-55/30-BG fiber reinforced concrete (V_f = 0.5%, 0.75%, 1.0%, or 1.5%) developed deflection hardening nor strain hardening. Moreover, batches with 3D RC-55/30-BG fibers exhibited the most brittle post-peak response in compression, as shown in Figure 5.12, which shows compression stress plotted versus longitudinal strain for each batch with 3D RC-55/30-BG fibers. Inspection of specimens after testing showed that the 3D RC-55/30-BG fibers typically pulled out instead of fracturing (less than 10% of fibers fractured); therefore, the fiber strength was not the cause of the relatively poor performance.

It was also observed that in batches with fiber type 4D RC-65/60-BG and type 5D RC-65/60-BG, there were some small fiber bundles (2-3 fibers) after the mixing process. Given that the number of bundles was relatively small, these small fiber bundles are believed to have had negligible effects on compression, flexure, and tension behavior of SCFRCs.

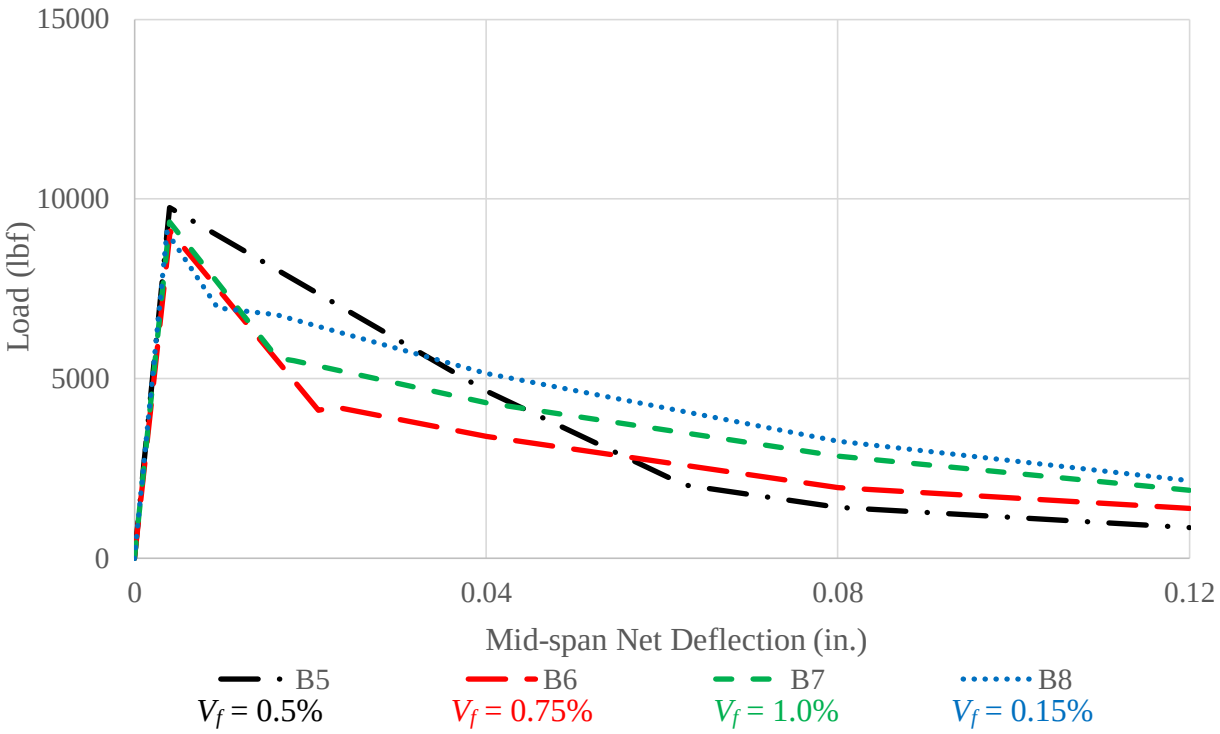

Figure 5.10 – Load-deflection response of batches with 3D RC-55/30-BG fibers tested in accordance with ASTM C1609.

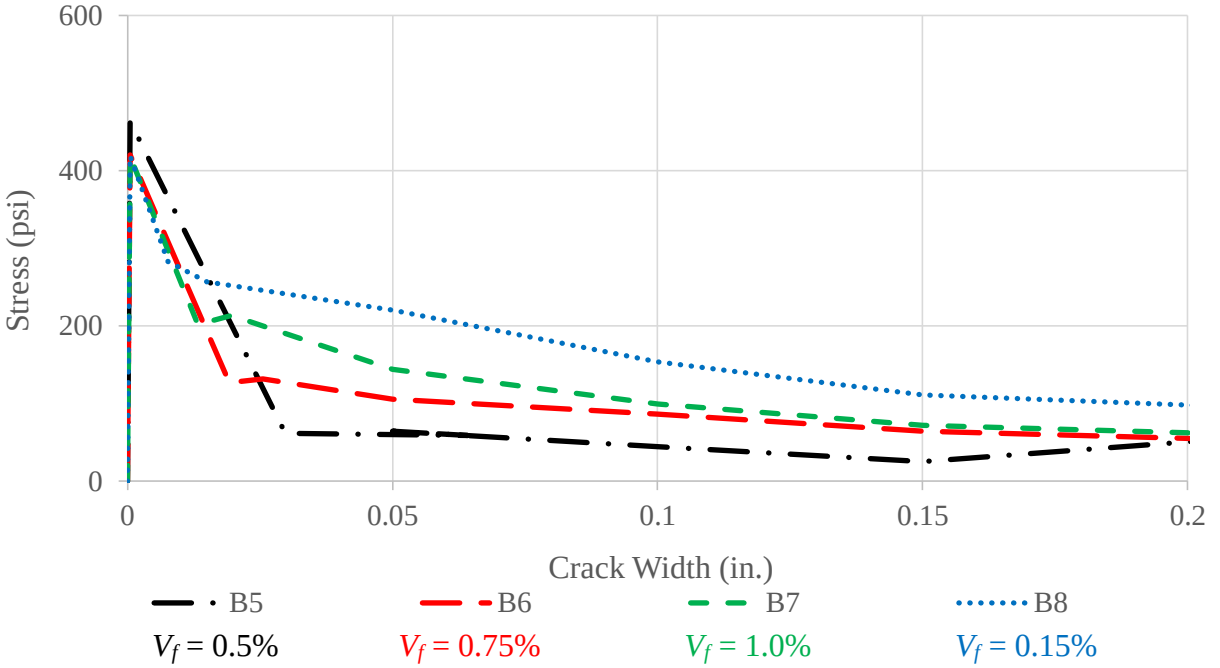

Figure 5.11 – Stress-crack width response of batches with 3D RC-55/30-BG fibers tested in tension.

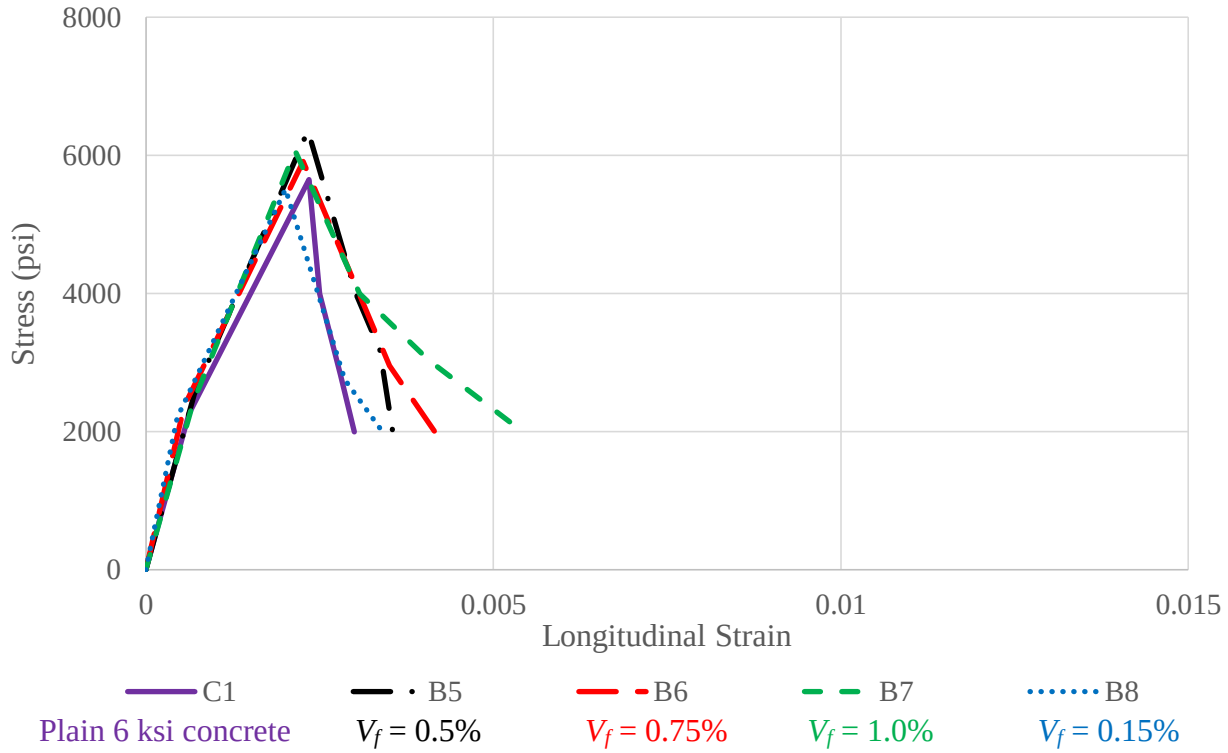

Figure 5.12 – Compression stress-longitudinal strain response of batches with 3D RC-55/30-BG fibers.

5.2 – Compression Behavior

5.2.1 – Compression Strength

The relatively large ("macro-") fibers used in this study had a negligible effect on concrete compression strength, as shown previously in Chapter 4. Likewise, there is no clear relationship between compression strength and air content in this series of tests. This is illustrated in Figures 5.13 and 5.14, which show average compressive strength plotted versus air content for concrete with $f_c' = 6$ and 10 ksi, respectively. The only exception may be batch 4 (f_c` = 6 ksi; RC-80/30-BP; V_f = 1.5%), which had a relatively low compression strength (f_{cm} = 5760 psi) and high air content (3.9%).

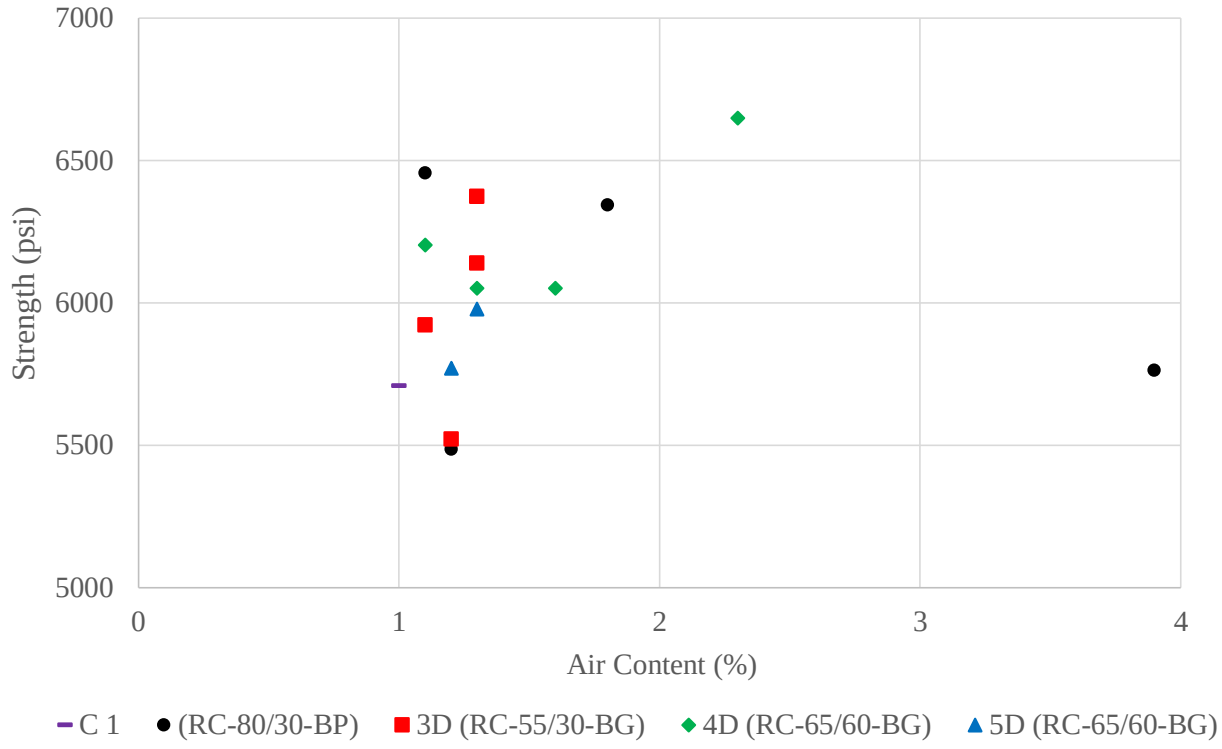

Figure 5.13 – Compression strength vs. air content ($f_c' = 6$ ksi).

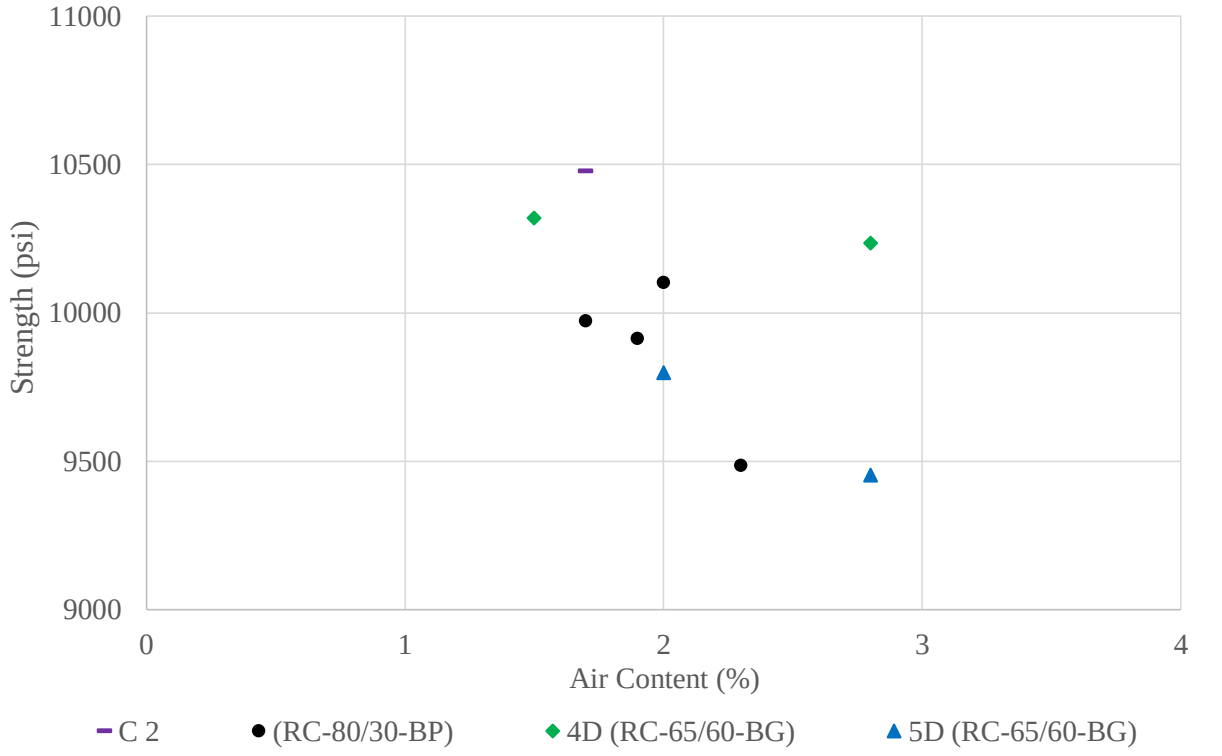

Figure 5.14 – Compression strength vs. air content ($f_c' = 10$ ksi).

5.2.2 – Modulus of Elasticity

As shown in Chapter 4, use of fibers had a negligible effect on the modulus of elasticity of the concrete. However, as expected, there was a relationship between the measured modulus of elasticity and concrete compressive strength. Figure 5.15 shows the measured modulus of elasticity plotted versus concrete compressive strength. Both the modulus and strength values plotted in Figure 5.15 are an average of the values measured for each batch of concrete. The relationship between elastic modulus and compressive strength given in the ACI Building Code ($E_c = 57\sqrt{f_c'}$) is also plotted. In general, the measured values of modulus were less than calculated using the ACI Building Code equation.

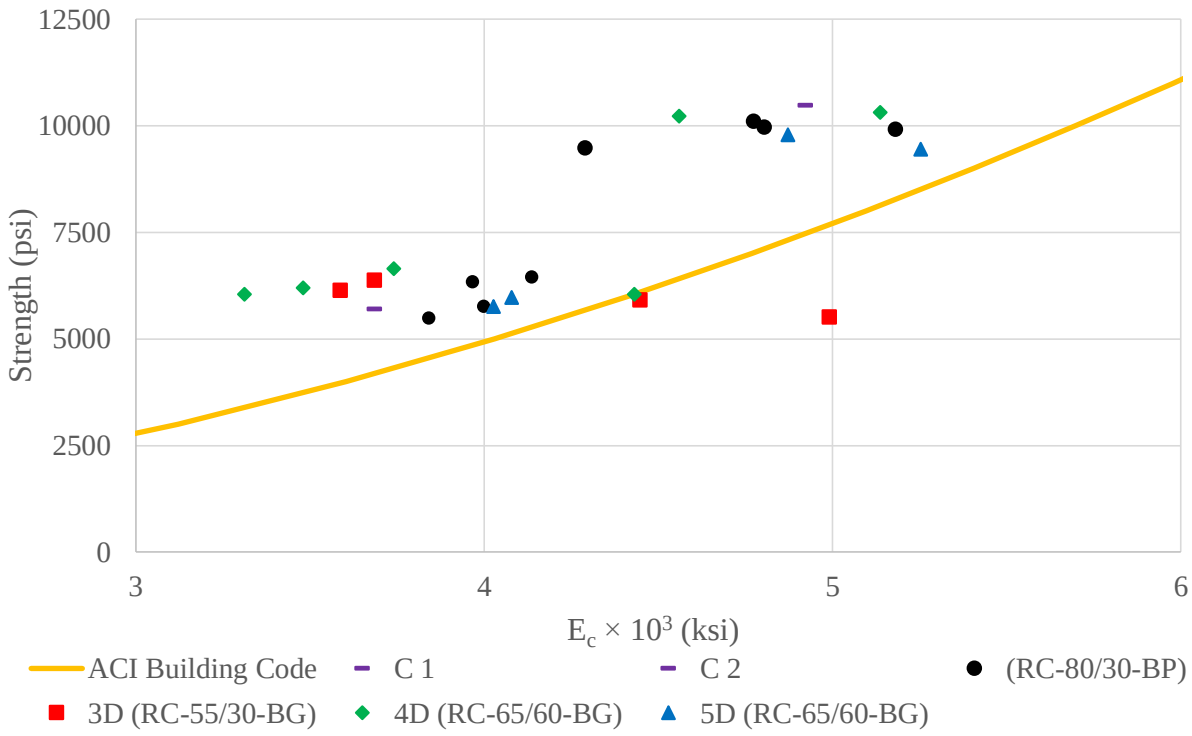

Figure 5.15 – Compression strength vs. modulus of elasticity.

5.2.3 – Post-Peak Slope

The post-peak slope of the specimens tested under compression, E_{pp}, was defined as the slope of the line drawn from the peak of the stress-strain diagram to a point on the curve representing a 50% loss of strength. Plain concrete has a brittle post-peak response characterized by a steep post-peak decline in strength (see reference batches C1 and C2). In SCFRCs, fibers resist the opening and propagation of cracks and thus allow for a more gradual loss of strength (E_{pp}, which is negative, increases and becomes closer to zero when fibers are used). This increase in E_{pp} results in an increased area under the compression stress versus longitudinal strain curve (toughness). As shown below, increases in E_{pp} were affected by fiber content and fiber properties. It is likely that fiber orientation is also important, but that was not quantified in this study.

The calculated average E_{pp} for each batch is given in Table 5.3 as well as the percentage change in E_{pp} relative to the control batch. The percentage change in E_{pp} is plotted versus fiber volume fraction in Figures 5.16 and 5.17 ($f_c' = 6$ and 10 ksi respectively). Percentage change was calculated as the difference between the post-peak slope of each batch and the post-peak slope of the control batch divided by the post-peak slope of the control batch; a change of 0% indicates the average slope was equal to the control and a change of 100% represents a horizontal slope. As shown, the calculated E_{pp} was sensitive to the fiber volume fraction, with change in E_{pp} of up to 100% observed for batches with a volume fraction of 1.5%. However, change in slope were not proportional to volume fraction. It appears from this limited sample that use of a fiber volume fraction of 0.75% results in a similar average E_{pp} as a fiber volume fraction of 1.5%. Furthermore, as shown in Table 4.3, the coefficient of variation for E_{pp} within each batch was similar for batches with fiber volume fractions of 0.75 and 1.5%.

Table 5.3 – The percentage change in post-peak slope of concrete under compression.

Batch ID	Fiber Type	V_f (%)	$E_{pp} \times 10^6$ (psi)	Change in E_{pp} (%)
C 1	N/A	0	-6.18	0
B 1	(RC-80/30-BP)	0.5	-1.10	82
B 2	(RC-80/30-BP)	0.75	-1.56	75
B 3	(RC-80/30-BP)	1.0	-0.94	85
B 4	(RC-80/30-BP)	1.5	-0.38	94
B 5	3D (RC-55/30-BG)	0.5	-3.35	46
B 6	3D (RC-55/30-BG)	0.75	-2.94	52
B 7	3D (RC-55/30-BG)	1.0	-2.78	55
B 8	3D (RC-55/30-BG)	1.5	-3.23	48
B 9	4D (RC-65/60-BG)	0.5	-5.73	7
B 10	4D (RC-65/60-BG)	0.75	-2.77	55
B 11	4D (RC-65/60-BG)	1.0	-4.09	34
B 12	4D (RC-65/60-BG)	1.5	-1.81	71
B 13	5D (RC-65/60-BG)	0.75	-2.41	61
B 14	5D (RC-65/60-BG)	1.5	-0.50	92
C 2	N/A	0	-16.12	0
B 15	(RC-80/30-BP)	0.5	-3.85	76
B 16	(RC-80/30-BP)	0.75	-2.58	84
B 17	(RC-80/30-BP)	1.0	-1.86	88
B 18	(RC-80/30-BP)	1.5	-0.91	94
B 19	4D (RC-65/60-BG)	0.75	-8.47	47
B 20	4D (RC-65/60-BG)	1.5	-1.64	90
B 21	5D (RC-65/60-BG)	0.75	-3.88	76
B 22	5D (RC-65/60-BG)	1.5	-0.91	94

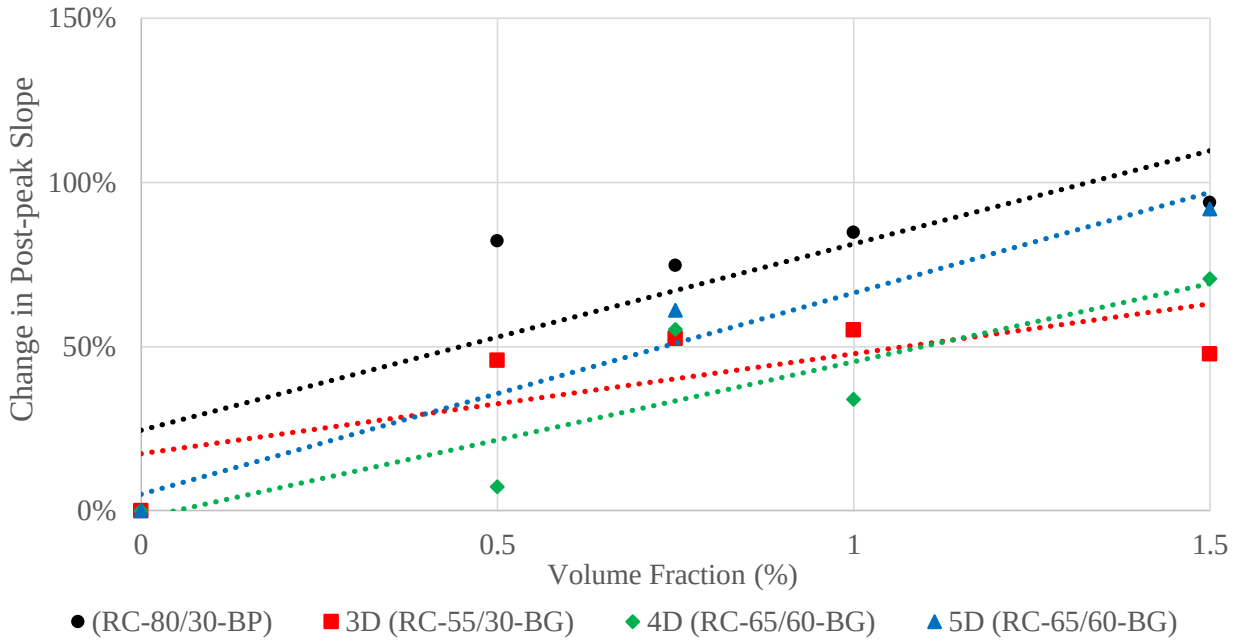

Figure 5.16 – The percentage change in post-peak slope of concrete under compression vs. fiber volume fraction ($f_c' = 6$ ksi).

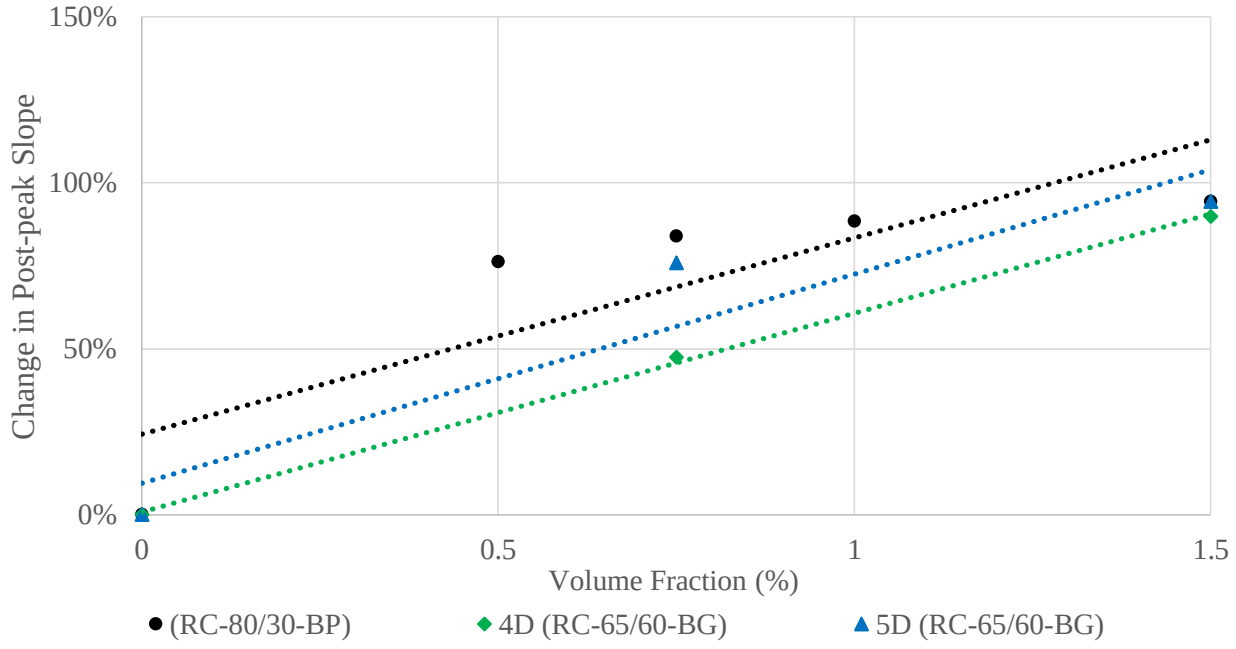

Figure 5.17 – The percentage change in post-peak slope of concrete under compression vs. fiber volume fraction ($f_c' = 10$ ksi).

As illustrated in Figures 5.16 and 5.17, as well as Table 5.3, use of fiber type 3D (RC-55/30-BG) had the lowest impact on concrete post-peak slope. This fiber, which is 30 mm long, has an aspect ratio of 55, and a relatively low minimum tensile strength of 200 ksi, increased the post-peak slope by 48% (relative to plain concrete) using a volume fraction of 1.5% in concrete with $f_c' = 6$ ksi. The low aspect ratio, as well as the bundles of fibers described in Chapters 4.1.1 and 5.1.5, are believed to have contributed to the comparatively poor performance of this fiber.

Fiber types 5D (RC-65/60-BG) and 4D (RC-65/60-BG) had similar effects on the post-peak slope, although use of fiber type 5D (RC-65/60-BG) did result in slightly better performance. Fiber types 5D (RC-65/60-BG) and 4D (RC-65/60-BG) are both 60 mm long and have an aspect ratio of 65, but they have different hook bend types (see Chapter 3) and minimum tensile strengths (330 and 220 ksi, respectively). With a fiber volume fraction of 1.5%, use of fiber type 5D (RC-65/60-BG) increased the post-peak slope of both 6 ksi and 10 ksi SCFRCs by 90% and use of fiber type 4D (RC-65/60-BG) increased the post-peak slope of 6 ksi and 10 ksi SCFRCs by 70% and 90%, respectively. It appears that the different hook configurations and tensile strength marginally increased the influence of the 5D (RC-65/60-BG) fibers on post-peak compressive response.

Finally, fiber type RC-80/30-BP, which has a length of 30 mm, an aspect ratio of 79, a hook configuration similar to that of the 3D (RC-55/30-BG) fiber, and a high tensile strength (330 ksi), had the greatest impact on the post-peak slope in compression. For both the concretes with $f_c' = 6$ and 10 ksi, this fiber increased the post-peak slope by about 75% with a fiber volume fraction of 0.5% and by 90% with a volume fraction of 1.5%. It appears that the high aspect ratio (79) and the high tensile strength of this fiber resulted in the improved post-peak response of the batches with this fiber. Furthermore, results from this small series of tests appear to indicate that

use of this fiber in a volume fraction of 1.5% may not provide a significant improvement in compressive behavior compared to mixtures with a fiber volume fraction of 0.5 to 0.75%.

5.3 – Flexural Behavior

5.3.1 – First Peak Strength and Deflection

As shown in Chapter 4 and Appendix C, use of fibers had a negligible effect on both the strength and deflection of the flexural specimens when the first crack developed.

5.3.2 – Post-Crack Peak Strength

The post-crack peak strength was significantly affected by fiber volume fraction and fiber properties. The average peak post-crack strength for each batch is reported in Table 5.4, as well as the ratio of the peak post-crack strength (σ_{pc}) to first crack strength (σ_{fc}). Figures 5.18 and 5.19 ($f_c' = 6$ and 10 ksi, respectively) show the ratio of σ_{pc} to σ_{fc} plotted versus fiber volume fraction. Deflection hardening, which refers to FRC mixtures that typically exhibit greater flexural strength after cracking than at cracking in standardized tests, can be used as a performance measure. Batches with a ratio of σ_{pc} to σ_{fc} greater than 1.0 exhibited, on average, a deflection hardening response.

Table 5.4 – Post-crack peak flexural strength.

Batch ID	Fiber Type	V_f (%)	σ_{pc} (psi)	Ratio of σ_{pc} to σ_{fc}
C 1	N/A	0	720	-
B 1	(RC-80/30-BP)	0.5	540	0.87
B 2	(RC-80/30-BP)	0.75	845	1.15
B 3	(RC-80/30-BP)	1.0	920	1.26
B 4	(RC-80/30-BP)	1.5	1015	1.14
B 5	3D (RC-55/30-BG)	0.5	165	0.21
B 6	3D (RC-55/30-BG)	0.75	340	0.45
B 7	3D (RC-55/30-BG)	1.0	445	0.59
B 8	3D (RC-55/30-BG)	1.5	545	0.75
B 9	4D (RC-65/60-BG)	0.5	350	0.47
B 10	4D (RC-65/60-BG)	0.75	570	0.78
B 11	4D (RC-65/60-BG)	1.0	720	0.95
B 12	4D (RC-65/60-BG)	1.5	935	1.21
B 13	5D (RC-65/60-BG)	0.75	565	0.84
B 14	5D (RC-65/60-BG)	1.5	995	1.29
C 2	N/A	0	1190	-
B 15	(RC-80/30-BP)	0.5	1055	0.91
B 16	(RC-80/30-BP)	0.75	1345	1.09
B 17	(RC-80/30-BP)	1.0	1555	1.58
B 18	(RC-80/30-BP)	1.5	1810	1.49
B 19	4D (RC-65/60-BG)	0.75	1180	1.00
B 20	4D (RC-65/60-BG)	1.5	1770	1.42
B 21	5D (RC-65/60-BG)	0.75	1290	1.11
B 22	5D (RC-65/60-BG)	1.5	1560	1.32

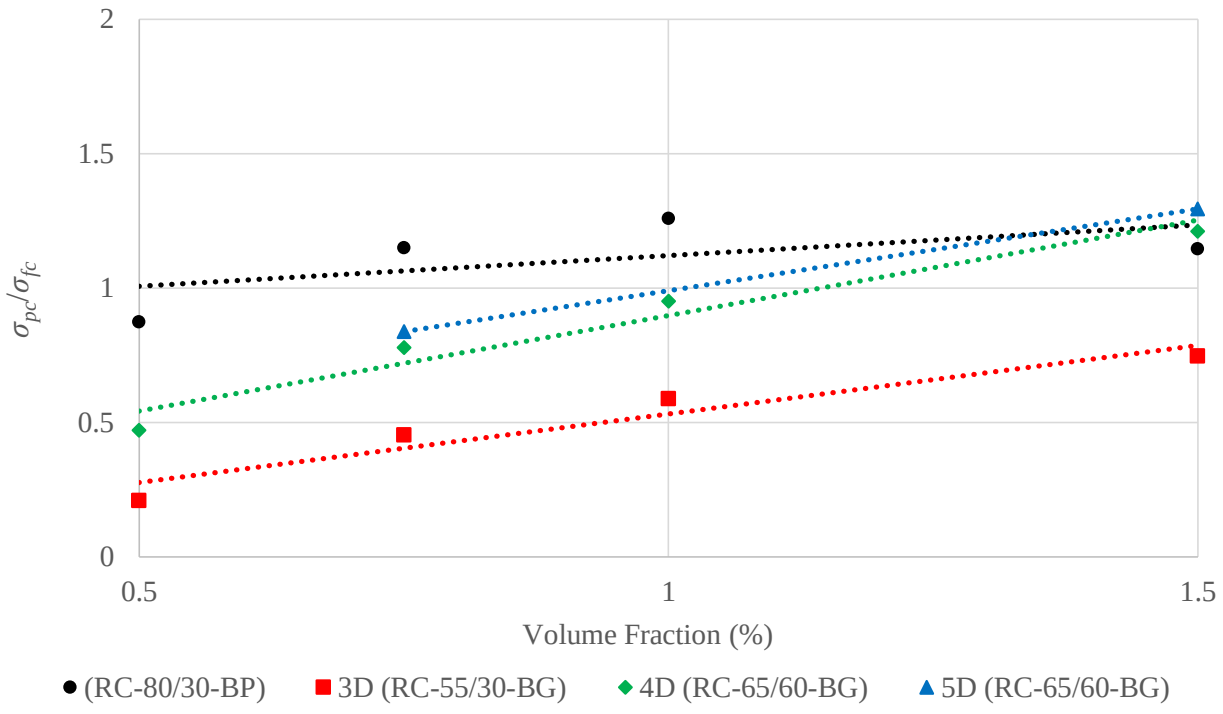

Figure 5.18 – Ratio of peak post-crack strength (σ_{pc}) to first crack strength (σ_{fc}) vs. fiber volume fraction ($f_c' = 6$ ksi).

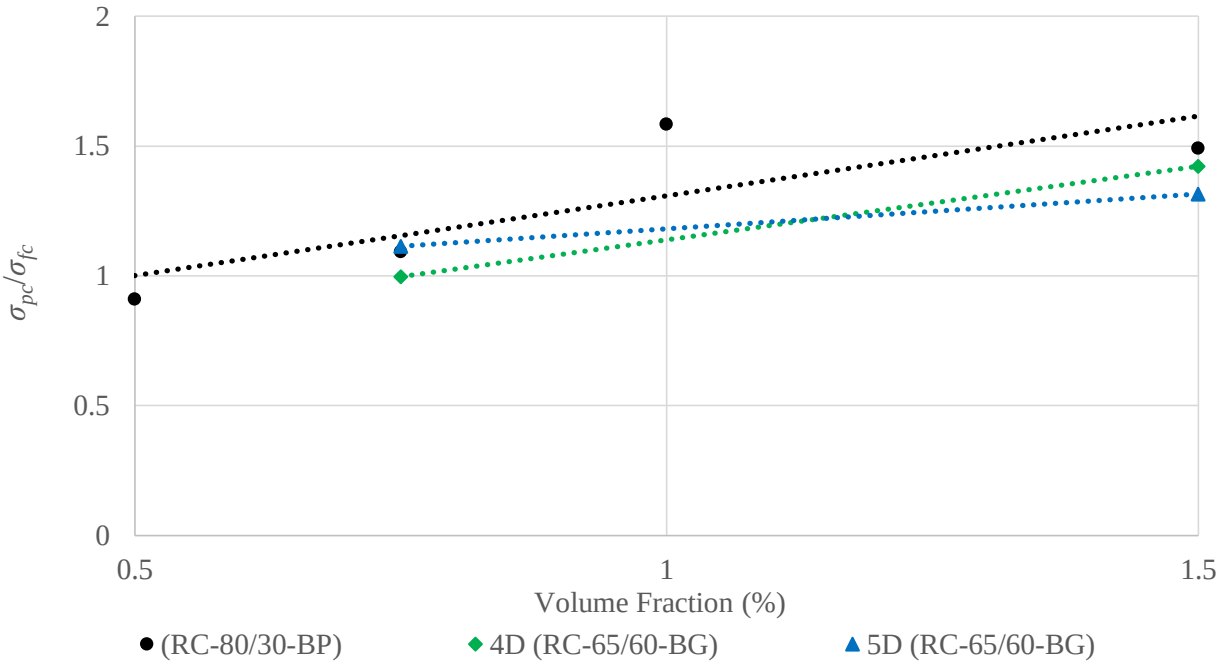

Figure 5.19 – Ratio of peak post-crack strength (σ_{pc}) to first crack strength (σ_{fc}) vs. fiber volume fraction ($f_c' = 10$ ksi).

As illustrated in Figure 5.18 and Figure 5.19, as well as Table 5.4, the relative performance of the fibers was similar to that in compression, with fiber type 3D (RC-55/30-BG), having the least influence on behavior and fiber type RC-80/30-BP having the greatest influence.

As can be seen in Figures 5.18 and 5.19, it was observed that batches with $f_c' = 10$ ksi tended to exhibit deflection hardening behavior at lower fiber volume fractions that batches with $f_c' = 6$ ksi. It appears that the higher f_c' tended to provide greater resistance to fiber pullout and thereby increased the resistance to crack opening provided by the fibers. This is consistent with the observed condition of the fibers, shown in Figure 4.40, after failure of the specimens. As shown, the fibers typically did not straighten as they pulled out (especially for the 4D and 5D fibers) indicating that breakout of the concrete occurred. It is reasonable to assume that increasing the concrete strength increased resistance to breakout of the concrete.

5.3.3 – Deflection Associated with Post-Crack Peak Strength

The deflection associated with the post-crack peak strength is plotted versus fiber volume fraction in Figures 5.20 and 5.21 ($f_c' = 6$ and 10 ksi, respectively). For concrete with

The average deflection at the post-crack peak for batches with $f_c' = 6$ ksi was 0.032 in. with the value ranging between 0.016 and 0.063 in. For batches with $f_c' = 10$ ksi, the average deflection was 0.030 in. with the value ranging between 0.014 and 0.039 in. This wide range in load-deflection behavior is likely because of fiber orientation and distribution, but these were not quantified.

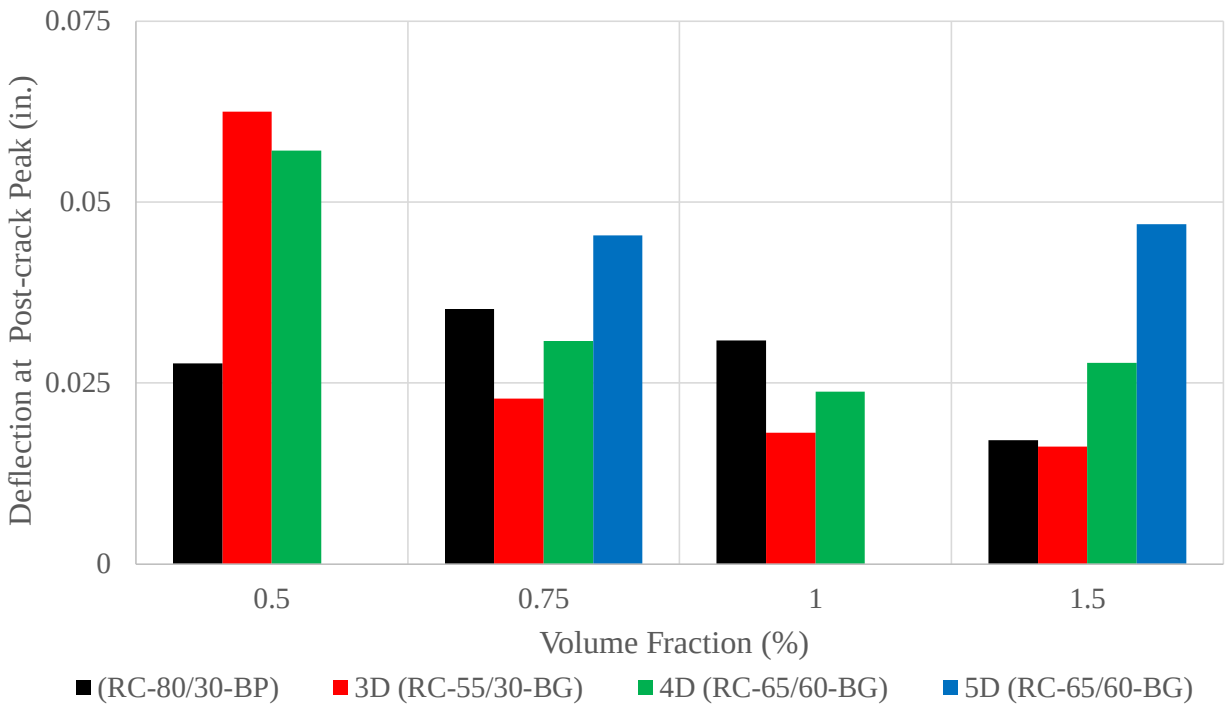

Figure 5.20 – Mid-span net deflection at the post-crack peak strength vs. fiber volume fraction ($f_c' = 6$ ksi).

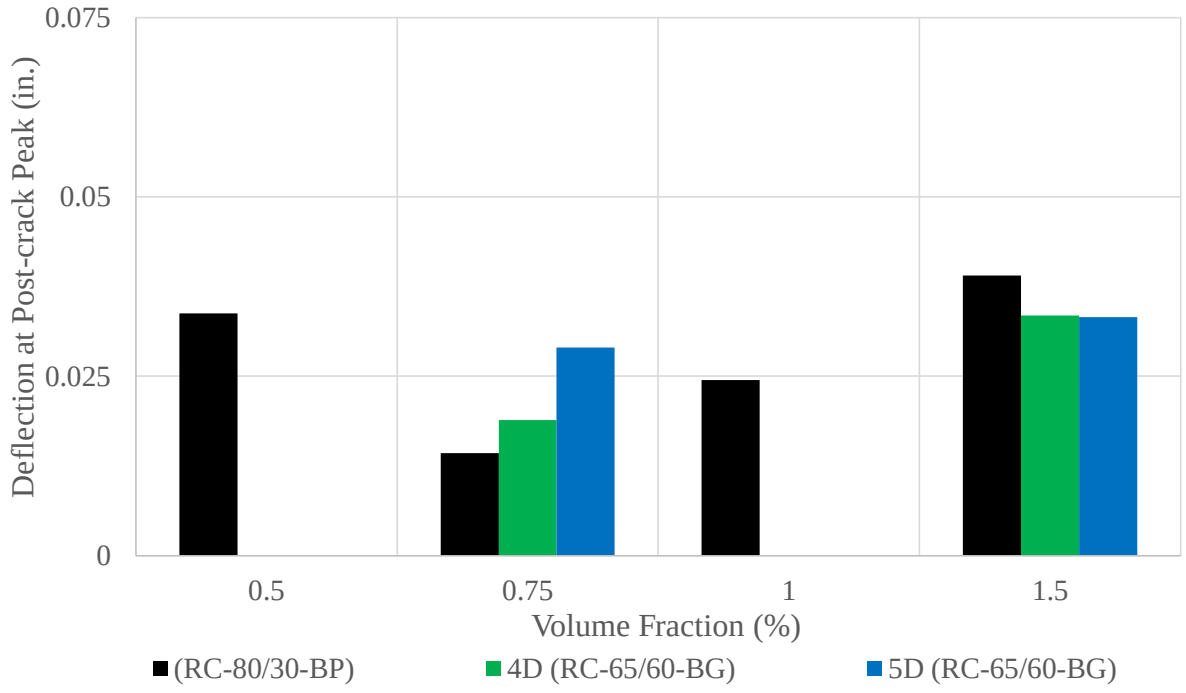

Figure 5.21 – Mid-span net deflection at the post-crack peak strength vs. fiber volume fraction ($f_c' = 10$ ksi).

5.3.4 – Load-Deflection Behavior

In addition to documenting the coordinates of the first cracking point and the peak post-cracking strength, an attempt was made to evaluate the effect of different fiber types and volume fractions on the shape of the load-deflection curve. This was done by comparing the calculated specimen strengths at mid-span deflections of 0.04, 0.08, and 0.12 in. Figures 5.22 through 5.27 show plots of specimen strength at these deflections versus fiber volume fraction.

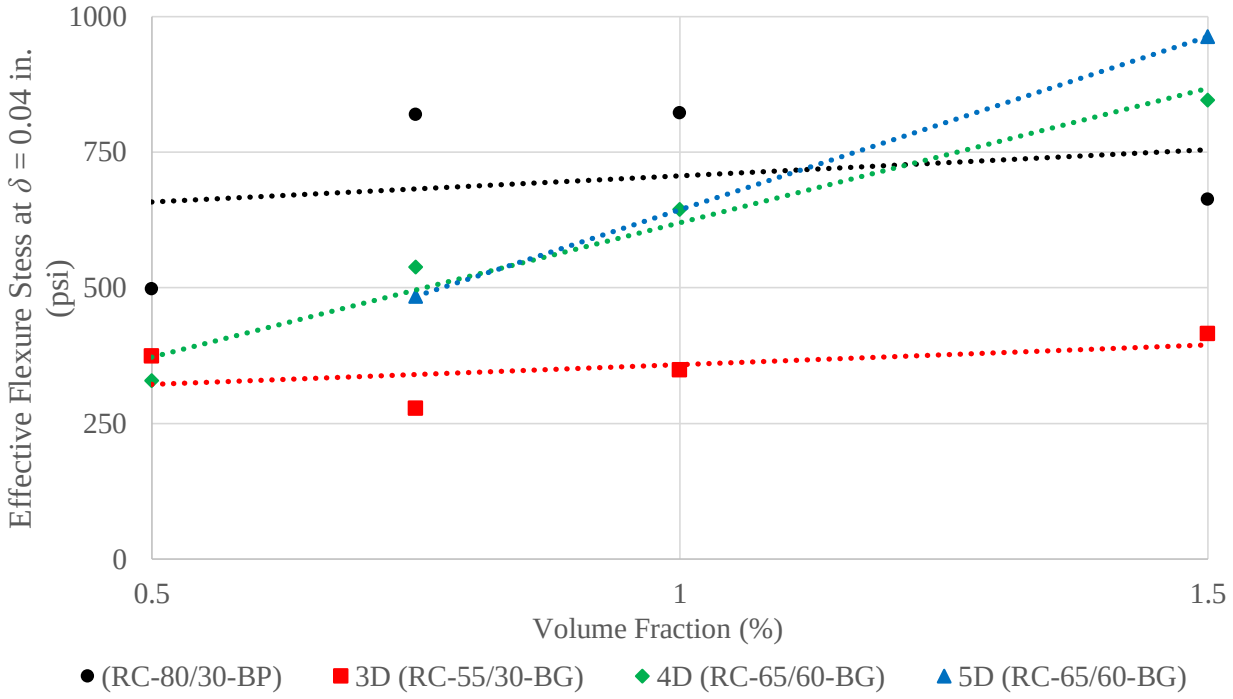

Figure 5.22 – Effective flexural stress at a deflection equal to 0.04 in. vs. fiber volume fractions ($f_c' = 6$ ksi).

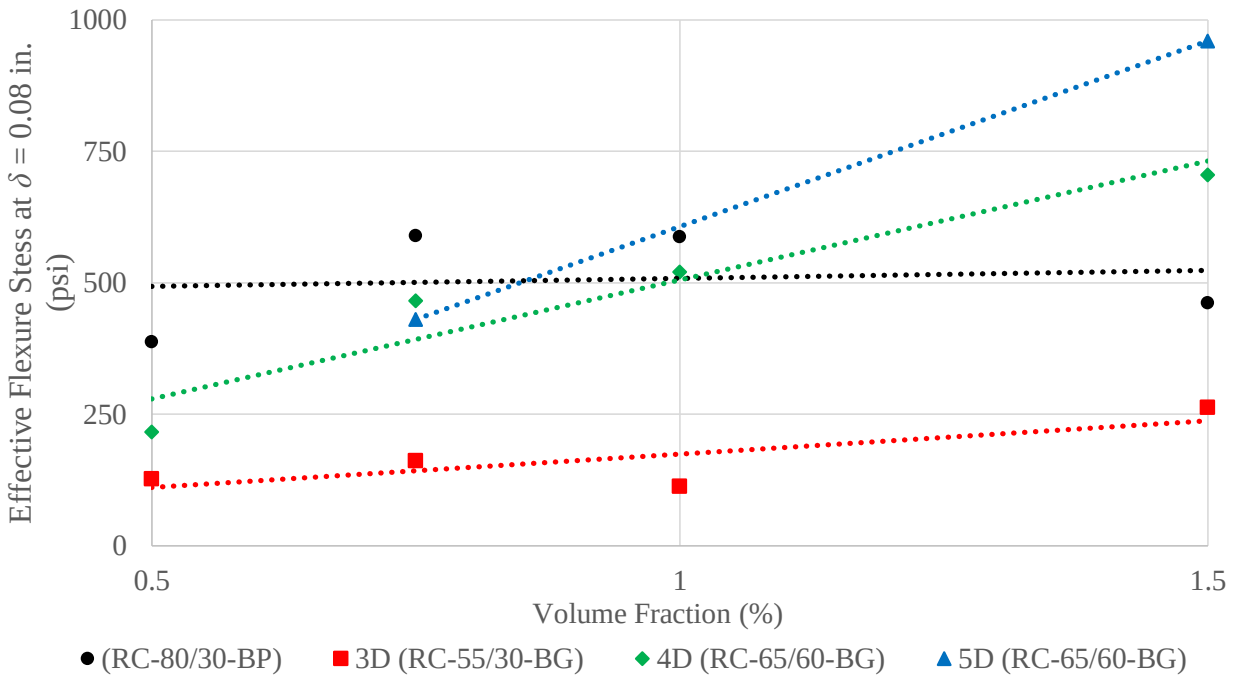

Figure 5.23 – Effective flexural stress at a deflection equal to 0.08 in. vs. fiber volume fractions ($f_c' = 6$ ksi).

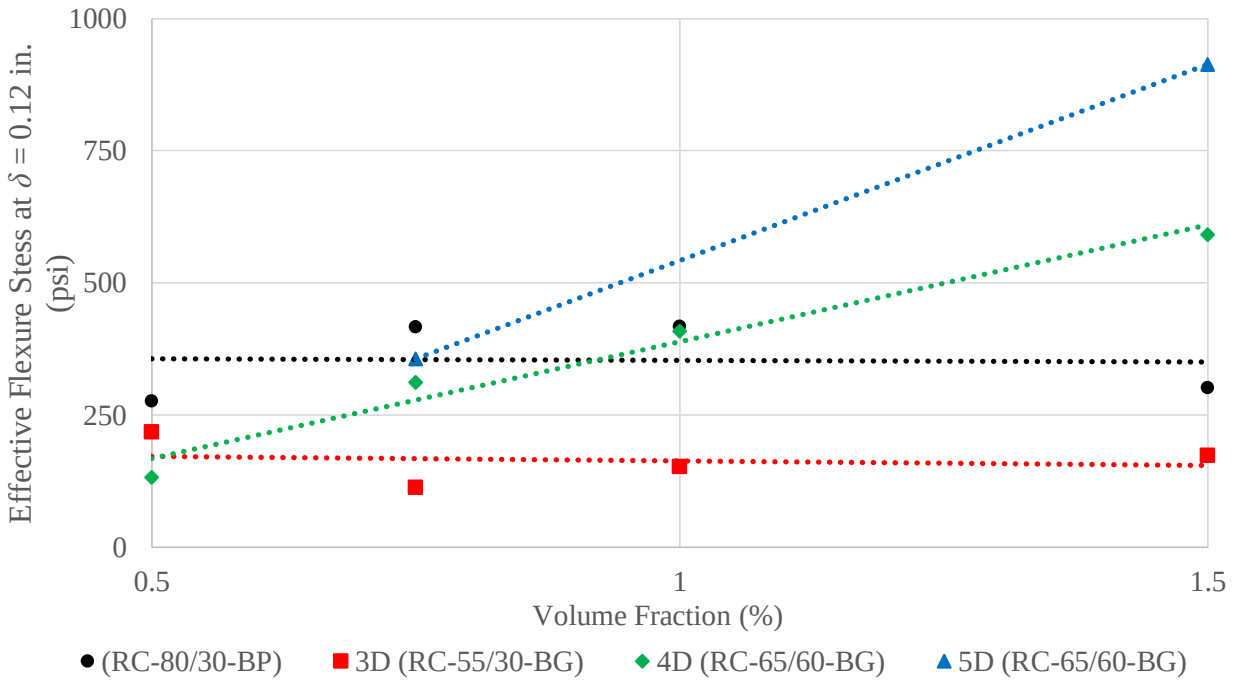

Figure 5.24 – Effective flexural stress at a deflection equal to 0.12 in. vs. fiber volume fractions ($f_c' = 6$ ksi).

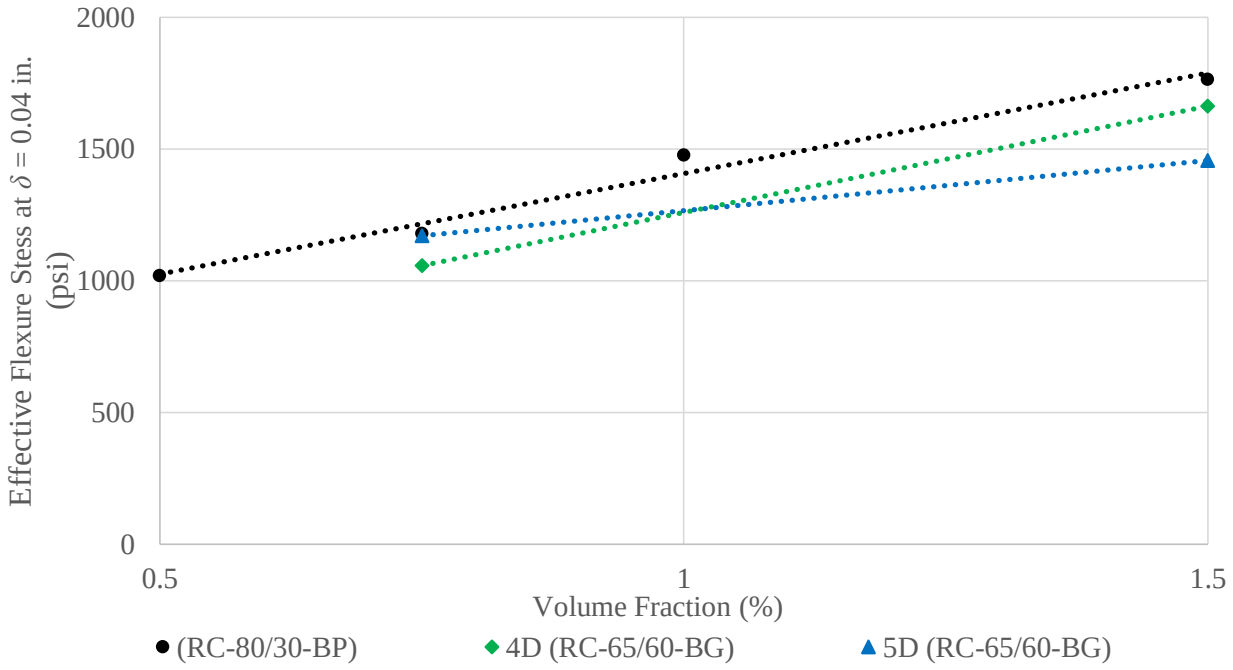

Figure 5.25 – Effective flexural stress at a deflection equal to 0.04 in. vs. fiber volume fractions ($f_c' = 10$ ksi).

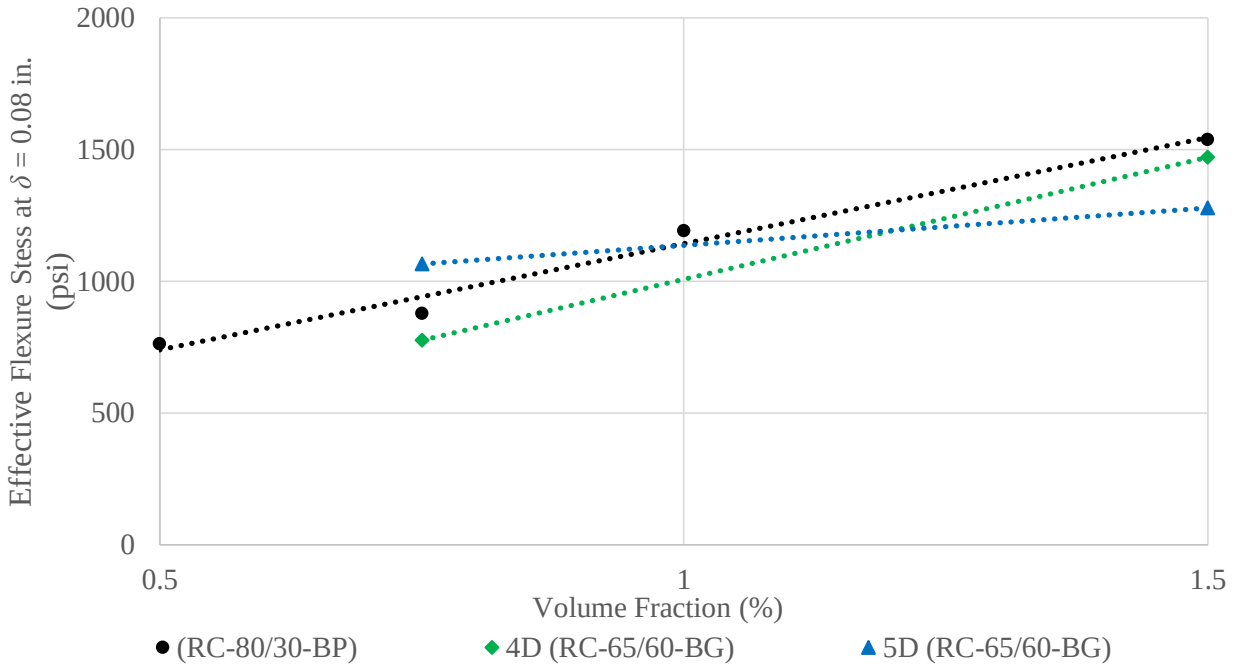

Figure 5.26 – Effective flexural stress at a deflection equal to 0.08 in. vs. fiber volume fractions ($f_c' = 10$ ksi).

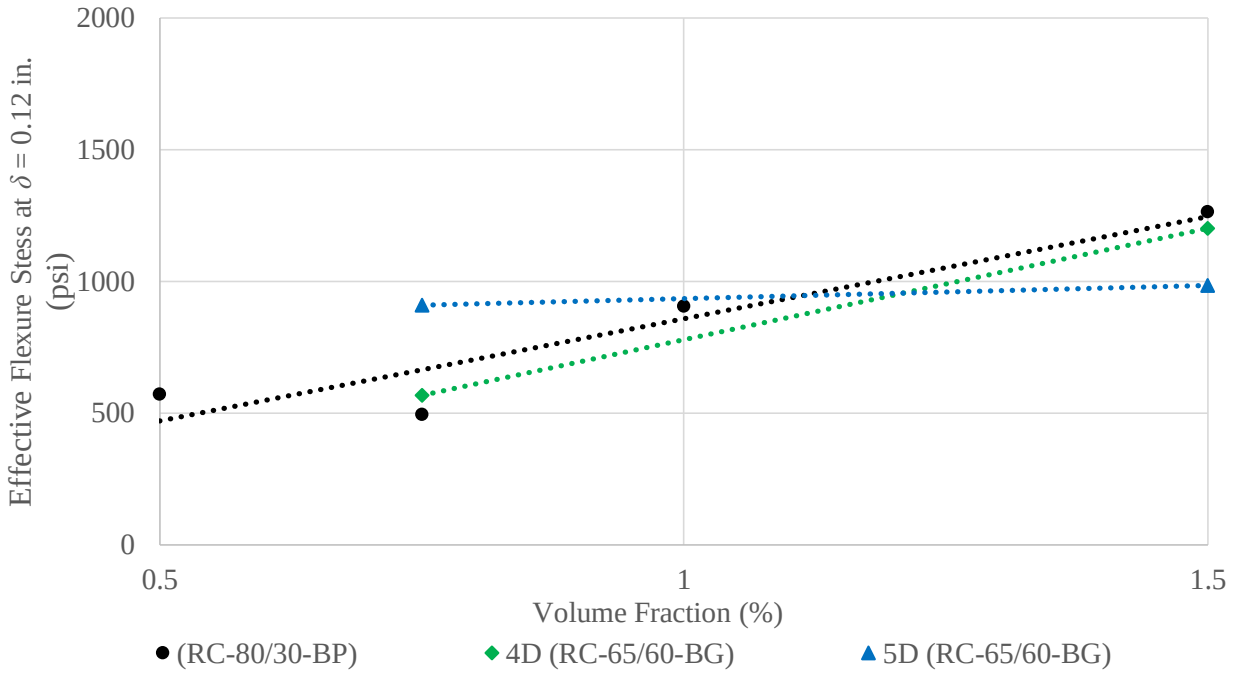

Figure 5.27 – Effective flexural stress at a deflection equal to 0.12 in. vs. fiber volume fractions ($f_c' = 10$ ksi).

5.3.5 – Load-Primary Crack Width Behavior

In addition to the effective stress versus deflection relationships, an attempt was made to report the relationship between effective stress and the width of the dominant crack (Appendix C). Figures 5.28 and 5.29 ($f_c' = 6$ and 10 ksi, respectively) show the crack width associated with the post-crack peak strength plotted versus fiber volume fraction. This particular crack width is of interest because the peak post-cracking strength typically corresponds to the beginning of damage localization at a single crack.

In Figures 5.28 and 5.29, there is a clear trend towards smaller average crack widths at the post-crack peak strength in the batches with $f_c' = 10$ ksi compared to those with $f_c' = 6$ ksi. However, other trends are obscured by the two following issues resulting from the chosen method

of presenting results: (1) the crack widths shown are averages taken for each batch, which may have included specimens exhibiting deflection hardening and deflection softening responses, and (2) many deflection softening specimens do not have a stable period of loading between first cracking and the peak post-cracking load (i.e., the first data point recorded after the instability associated with first cracking is often the peak post-cracking strength). It is likely the crack width measured for specimens with this behavior is more a function of the energy released at cracking than a critical crack width. Further research is necessary.

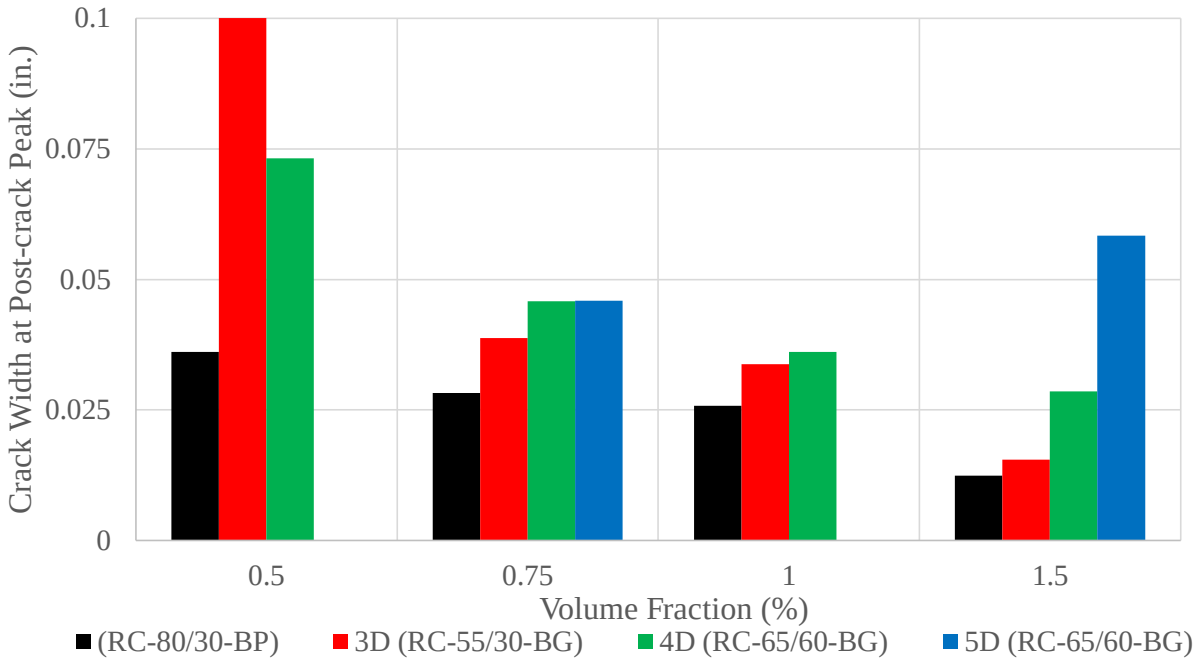

Figure 5.28 – Crack width at the post-crack peak vs. fiber volume fraction ($f_c' = 6$ ksi).

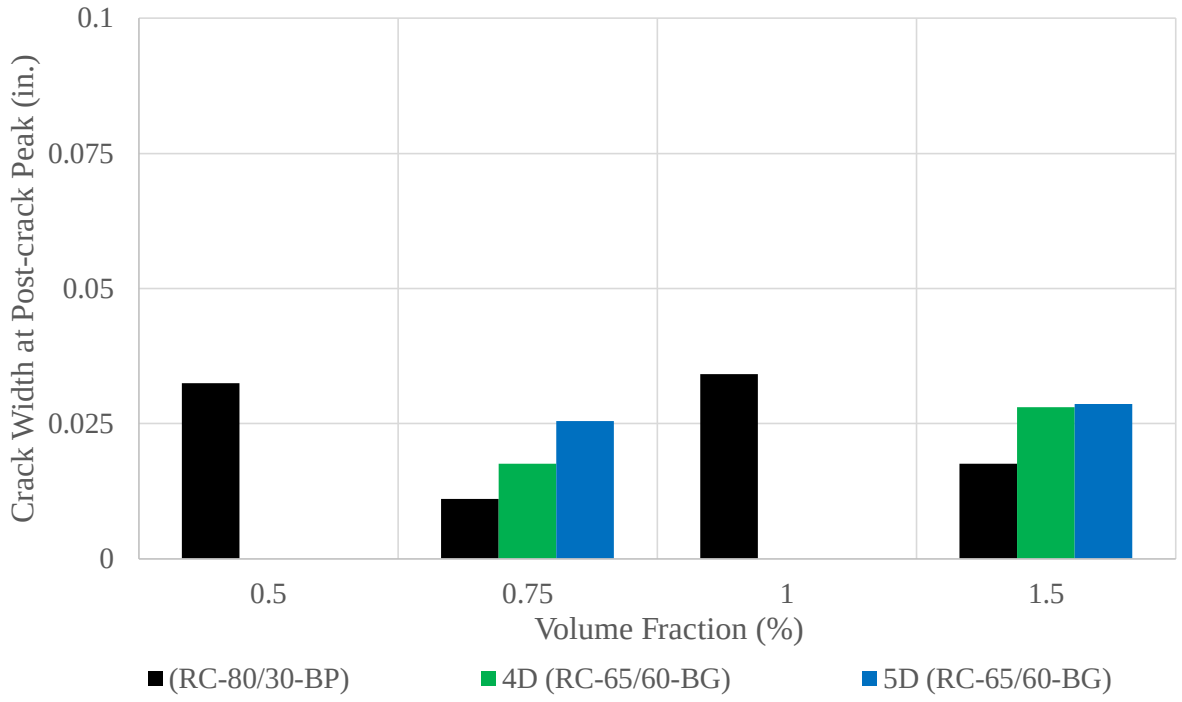

Figure 5.29 – Crack width at the post-crack peak vs. fiber volume fraction ($f_c' = 10$ ksi).

5.3.6 – Cracking over Beam Supports

In section 4.3.6, it was shown that some of the specimens with $f_c' = 10$ ksi developed cracks above the supports. A photo of one of the cracks is shown in Figure 5.30.

Figure 5.30 – Crack above the roller support (B15 SP2).

Calculation of the bearing capacity according to Chapter 22 of ACI 318-14 requires an assumption regarding the bearing area because the beam surface is flat and the support is a 2 in. diameter roller. Assuming a contact area of 0.25 by 6 in. and using a strength reduction factor of 1.0, the calculated bearing strength exceeds the support reactions in the reported tests. However, given that the crack appears to be a splitting crack and the bearing is between curved and flat surfaces, the cracking is analagous to that observed in a split cylinder test. Eq. 5-1 (modified from ASTM C496) was used to calaculate the maximum bearing load, F_b, assuming the splitting tensile strength is $6\sqrt{f_c'}$ and the splitting surface area is 6 by 6 in.

$$F_b = \frac{6\sqrt{f_c'}\cdot 6\text{ in.}\cdot 6\text{ in.}}{2} \tag{5-1}$$

The calculated F_b was 8.4 and 10.8 kip for $f_c' = 6$ and 10 ksi, respectively. These bearing loads correspond to total loads of 16.7 and 21.6 kip. Although no beams with $f_c' = 6$ ksi were subjected to loads exceeding 16.7 kip, several of the beams with $f_c' = 10$ ksi were loaded beyond 21.6 kip. This is consistent with test observations, which showed that no beams with $f_c' = 6$ ksi developed cracks above the supports but some of the specimens with concrete having $f_c' = 10$ ksi did. Although the analogy to split cylinder tests is imperfect, it may explain why beams with higher strengths were more susceptible to cracking at the support, and may suggest that use of roller supports with no bearing plate, as recommended by ASTM C1609, is not appropriate for beams with high concrete strength.

Although most beam forms were steel, one was made of wood. Use of the wood form appeared to slightly affect the initial stiffness of the flexural specimens, although the change was

minor (see the purple curve in Figure 5.31, which shows the load versus deflection response for beams cast in Batch 18).

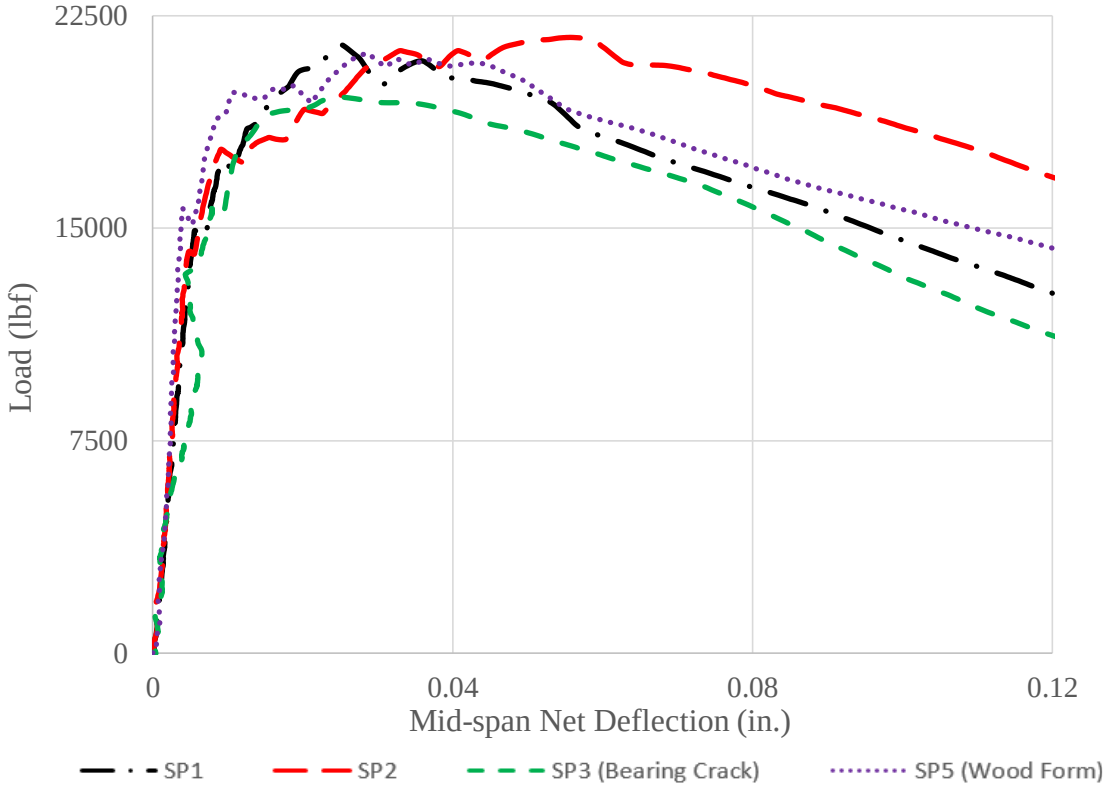

Figure 5.31 – Flexure load vs. primary crack width of batch 18 ($f`_c$=10 ksi; V_f=1.5%; Fiber: RC-80/30-BP).

5.4 – Tension Behavior

5.4.1 – First-Peak Strength and Crack Width

As shown in Chapter 4 and Appendix D, use of fibers had a negligible effect on the strength of the tension specimens when the first crack developed. Because the relative displacement between markers located on opposite faces of the notch was overwhelmingly due to opening of the crack, no deformation was measured prior to cracking.

5.4.2 – Post-Crack Peak Strength

The average peak post-crack strength for each batch is reported in Table 5.5, as well as the ratio of the peak post-crack strength (σ_{pc}) to first crack strength (σ_{fc}). Figures 5.32 and 5.33 ($f_c' = 6$ and 10 ksi, respectively) show the ratio of σ_{pc} to σ_{fc} plotted versus fiber volume fraction.

Table 5.5 – Post-crack peak tension strength.

Batch ID	Fiber Type	V_f (%)	σ_{pc} (psi)	Ratio of σ_{pc} to σ_{fc}
C 1	N/A	0	465	-
B 1	(RC-80/30-BP)	0.5	225	0.55
B 2	(RC-80/30-BP)	0.75	455	0.98
B 3	(RC-80/30-BP)	1.0	460	1.05
B 4	(RC-80/30-BP)	1.5	535	1.33
B 5	3D (RC-55/30-BG)	0.5	60	0.13
B 6	3D (RC-55/30-BG)	0.75	130	0.31
B 7	3D (RC-55/30-BG)	1.0	215	0.51
B 8	3D (RC-55/30-BG)	1.5	255	0.61
B 9	4D (RC-65/60-BG)	0.5	285	0.74
B 10	4D (RC-65/60-BG)	0.75	380	0.91
B 11	4D (RC-65/60-BG)	1.0	475	1.04
B 12	4D (RC-65/60-BG)	1.5	590	1.37
B 13	5D (RC-65/60-BG)	0.75	265	0.67
B 14	5D (RC-65/60-BG)	1.5	470	1.17
C 2	N/A	0	685	-
B 15	(RC-80/30-BP)	0.5	490	0.66
B 16	(RC-80/30-BP)	0.75	545	0.72
B 17	(RC-80/30-BP)	1.0	885	1.08
B 18	(RC-80/30-BP)	1.5	865	1.16
B 19	4D (RC-65/60-BG)	0.75	595	0.79
B 20	4D (RC-65/60-BG)	1.5	790	1.04
B 21	5D (RC-65/60-BG)	0.75	720	0.93
B 22	5D (RC-65/60-BG)	1.5	835	1.17

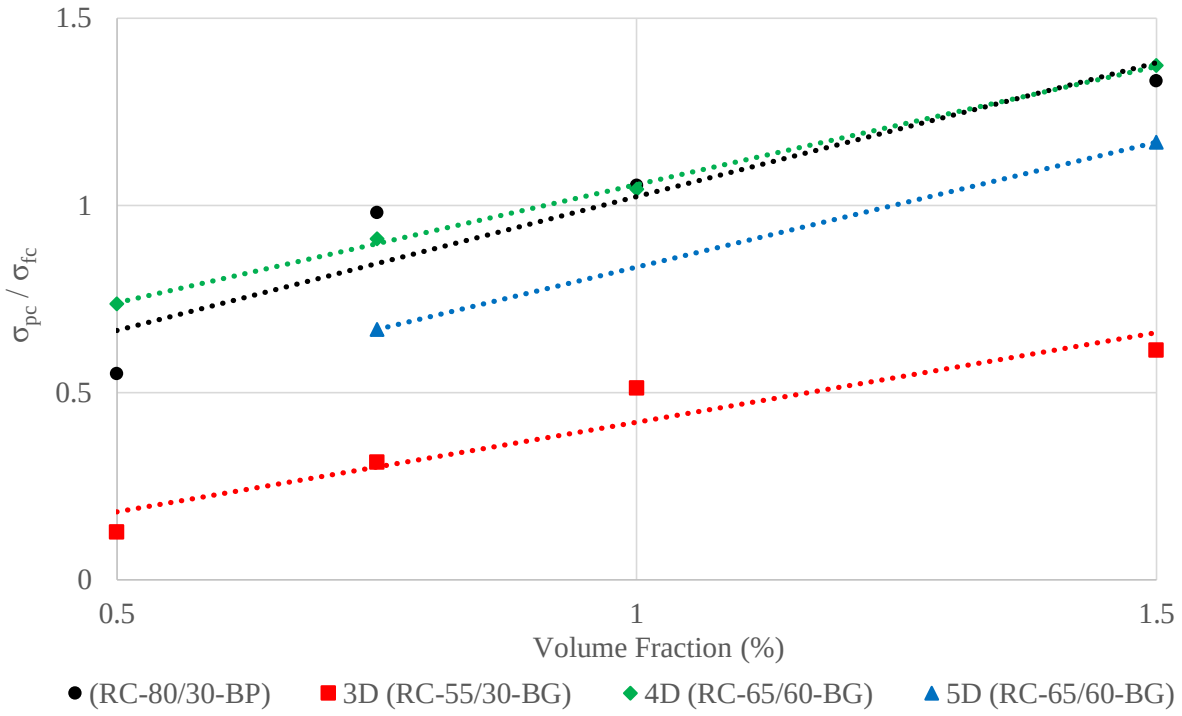

Figure 5.32 – Ratio of peak post-crack tensile strength (σ_{pc}) to first crack strength (σ_{fc}) vs. fiber volume fractions ($f_c' = 6$ ksi).

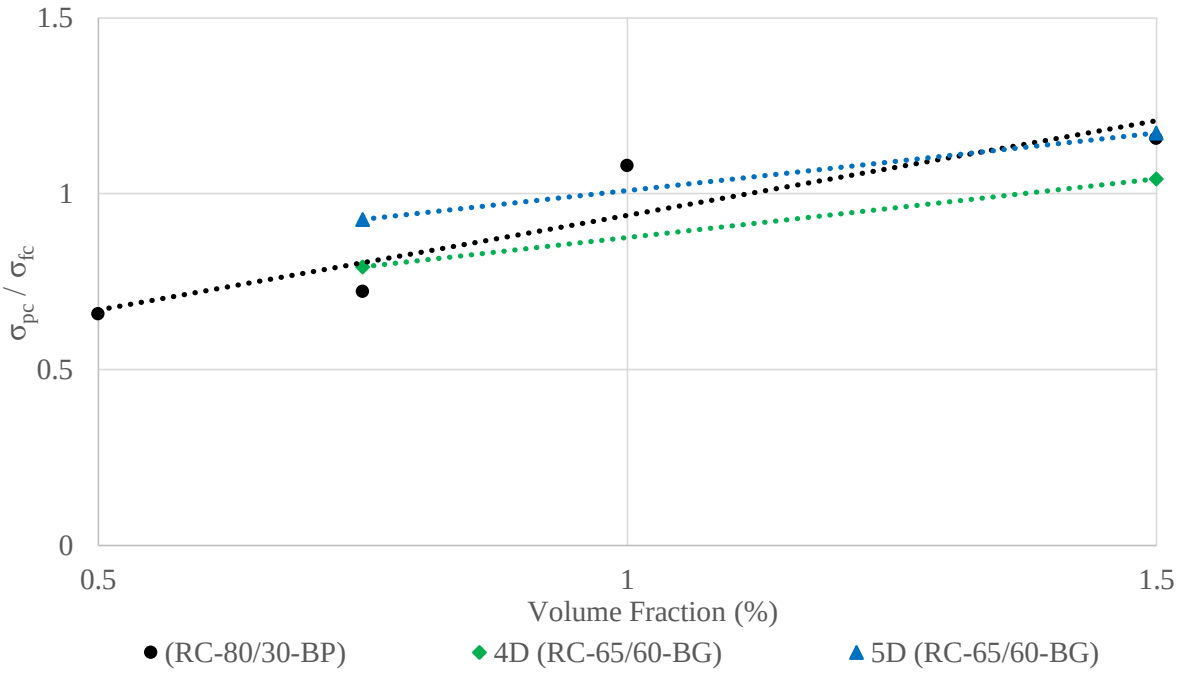

Figure 5.33 – Ratio of peak post-crack tensile strength (σ_{pc}) to first crack strength (σ_{fc}) vs. fiber volume fractions ($f_c' = 10$ ksi).

As illustrated in Figures 5.32 and 5.33, as well as Table 5.5, fiber type 3D (RC-55/30-BG) had the lowest effect on concrete post-crack peak strength. No specimens with volume fractions of up to 1.5% of this fiber developed strain hardening.

Fiber type 4D (RC-65/60-BG) and fiber type 5D (RC-65/60-BG) developed strain hardening by using a 1.5% fiber volume fraction. Fiber type 4D (RC-65/60-BG) showed better performance in enhancing the peak post-crack strength than fiber type 5D (RC-65/60-BG) with concrete of $f_c' = 6$ ksi, whereas with $f_c' = 10$ ksi, fiber type 5D showed higher performance than 4D. It was observed that specimens with fiber type 4D (RC-65/60-BG) and $f_c' = 10$ ksi had more fractured fibers, although the number of fractured fibers was still less than 10% of the total number of fibers. This suggests that the tensile strength of fiber type 4D had an effect on the performance of the batches with $f_c' = 10$ ksi.

Fiber type RC-80/30-BP, which has the highest tensile strength (330 ksi) and the highest aspect ratio (79), had the best performance in enhancing concrete post-crack peak strength. This fiber developed strain hardening using volume fraction of 1.0% and 1.5%.

5.4.3 – Crack Width Associated with Post-Crack Peak Strength

Figure 5.34 ($f_c' = 6$ ksi) and Figure 5.35 ($f_c' = 10$ ksi) show the average crack width associated with the peak post-crack strength plotted versus fiber volume fraction. In general, the average crack width at the post-crack peak was lower in batches with $f_c' = 10$ ksi than those with $f_c' = 6$ ksi. The average width was 0.031 inch for batches with $f_c' = 6$ ksi, with the value ranging between 0.015 inch and 0.064 inch. It was 0.027 inch for batches with $f_c' = 10$ ksi, with the value

ranging between 0.021 inch and 0.036 inch. This wide range is likely because of fiber orientation and fiber concentration across tension cracks.

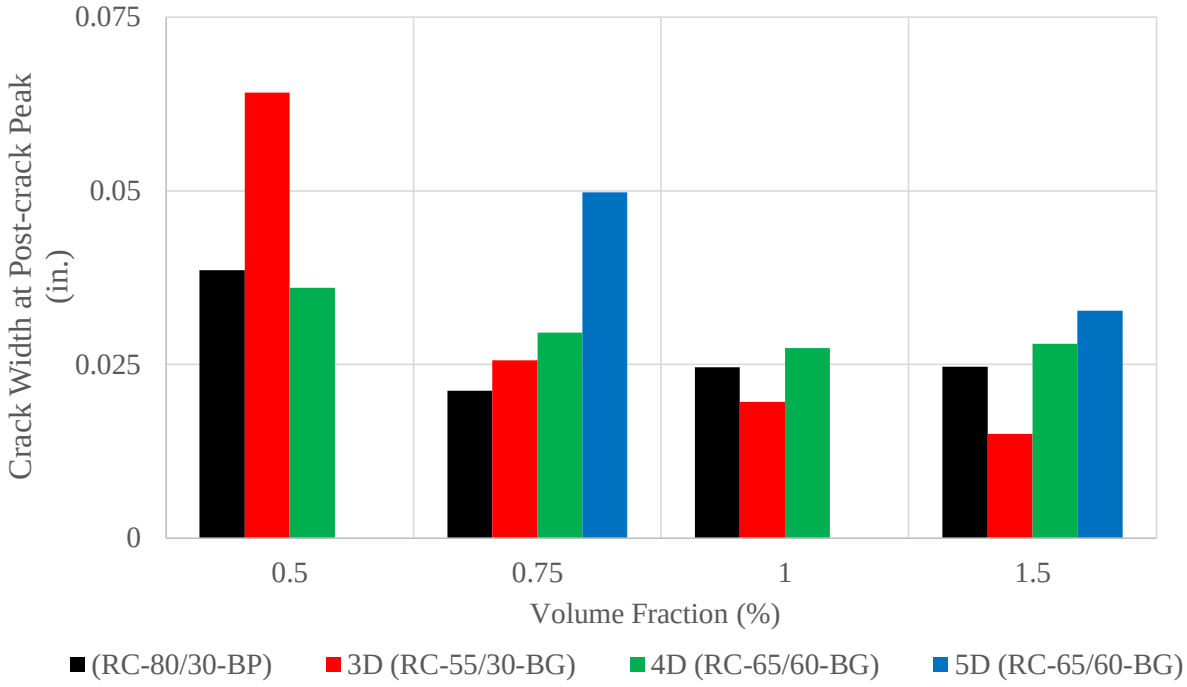

Figure 5.34 – Crack width at the post-crack peak vs. fiber volume fraction ($f_c' = 6$ ksi).

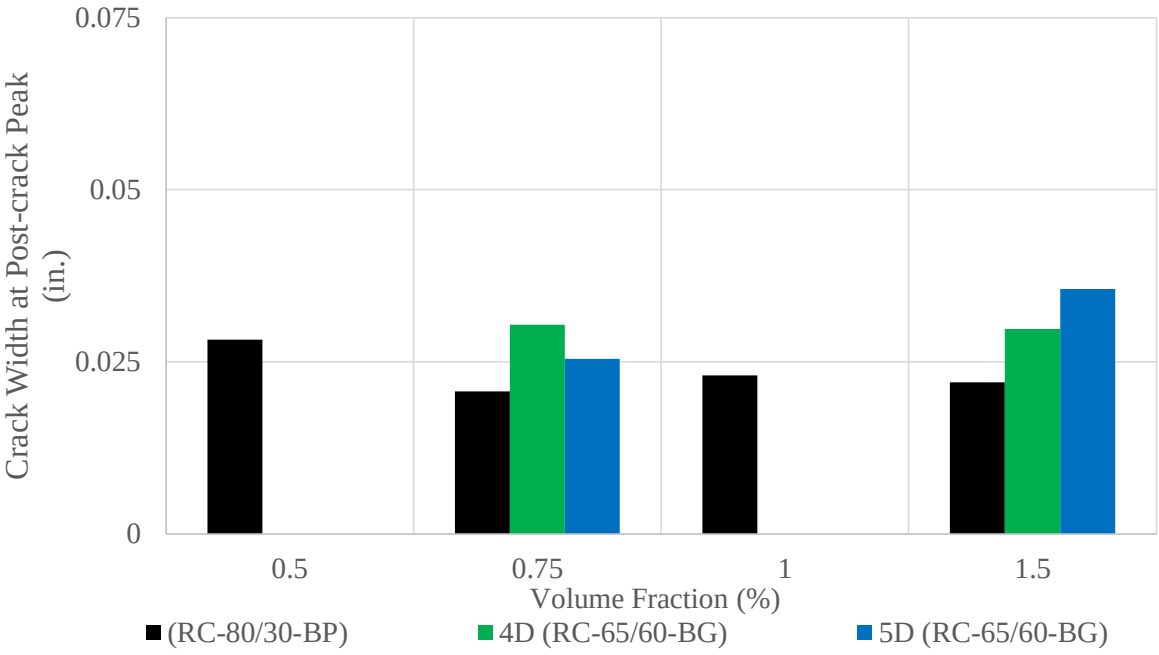

Figure 5.35 – Crack width at the post-crack peak vs. fiber volume fraction ($f_c' = 10$ ksi).

5.4.4 – Stress-Crack Width Behavior

Figures 5.37 through 5.42 show the average tensile stress calculated when the crack widths were 0.05, 0.10, and 0.15 in. plotted versus fiber volume fraction. These particular crack widths were selected because they are, according to the logic described below, close to the width of cracks expected to develop in 6 by 6 by 20 in. flexural specimens, loaded in accordance with ASTM C1609, at deflections of 0.04, 0.08, and 0.12 in.

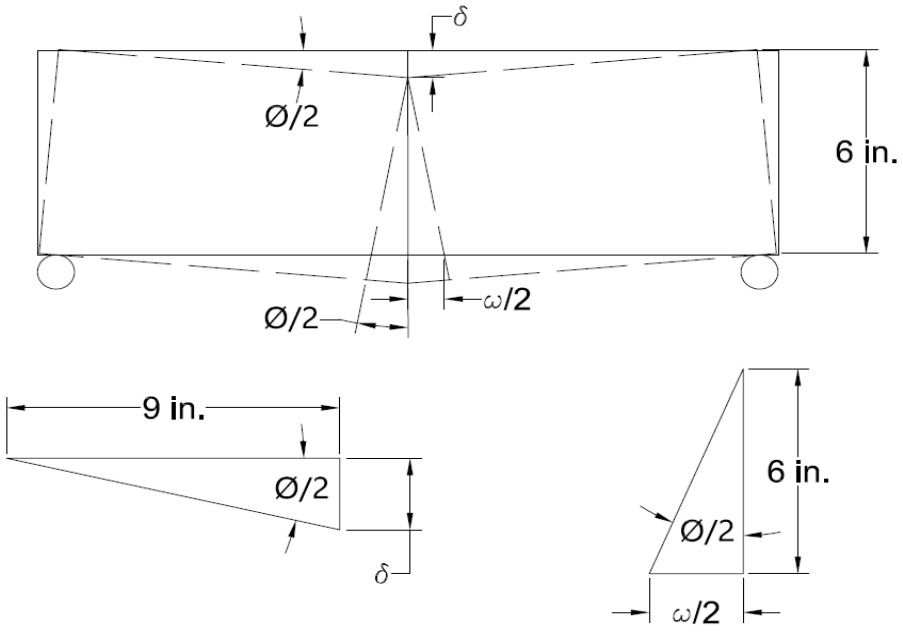

Figure 5.36 – The relationships between mid-span net deflection and crack width.

Assume that, as shown in Figure 5.36: (1) a single crack forms at exactly the center of the beam, (2) the crack extends from the bottom face of the beam to the top face of the beam, and (3) all beam deformation is attributable to opening of the crack. Given these assumptions, Eqs. 5-2 and 5-3 geometrically relate the rotation of the beam at the support to the mid-span beam deflection and mid-span crack width, respectively. By equating Eqs. 5-2 and 5-3, crack width and beam deflection can be related using Eq. 5-4.

$$\tan \emptyset/2 = \frac{\delta}{9} \quad (5\text{-}2)$$

$$\tan \emptyset/2 = \frac{\omega/2}{6} \quad (5\text{-}3)$$

$$\omega = \frac{4}{3}\delta \quad (5\text{-}4)$$

Where:

$\emptyset/2$: support rotation,

δ: mid-span net deflection,

ω: the crack width corresponding to mid-span deflection.

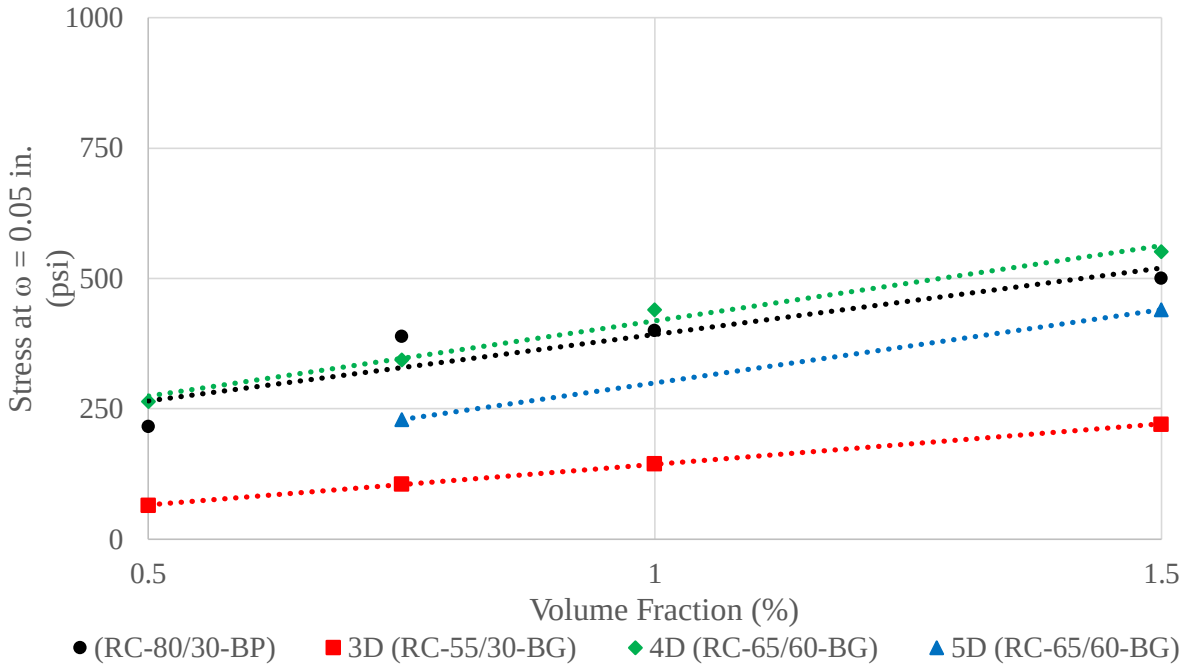

Figure 5.37 – Tension stress at crack width equal to 0.05 in. vs. fiber volume fraction ($f_c' = 6$ ksi).

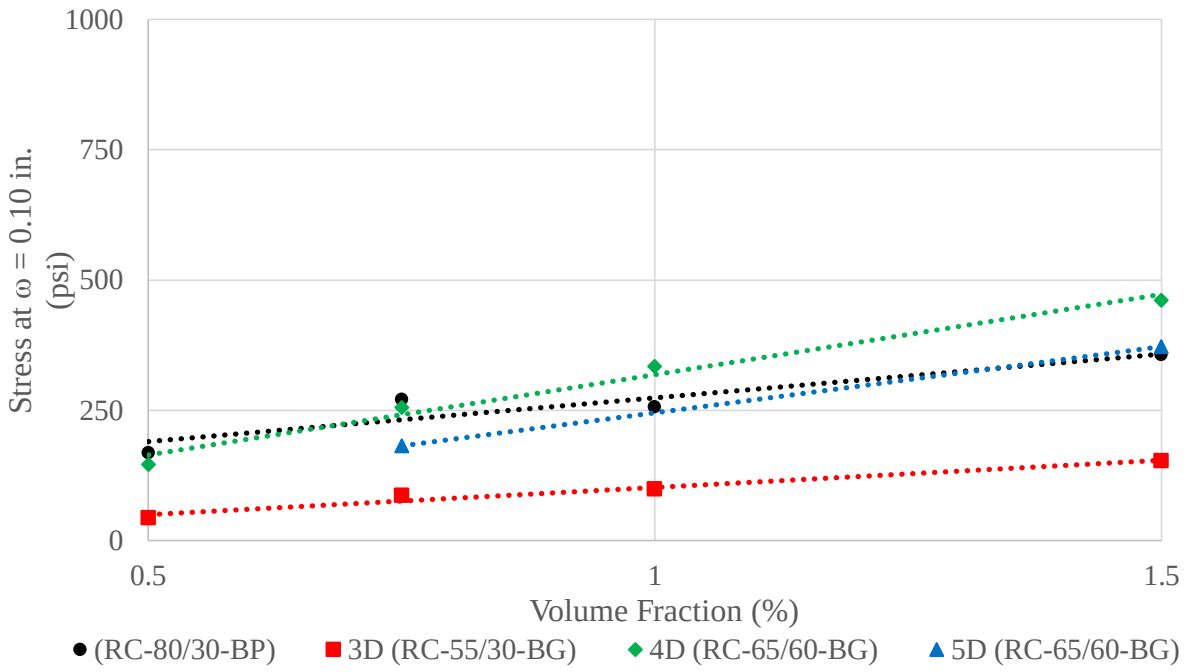

Figure 5.38 – Tension stress at crack width equal to 0.10 in. vs. fiber volume fraction ($f_c' = 6$ ksi).

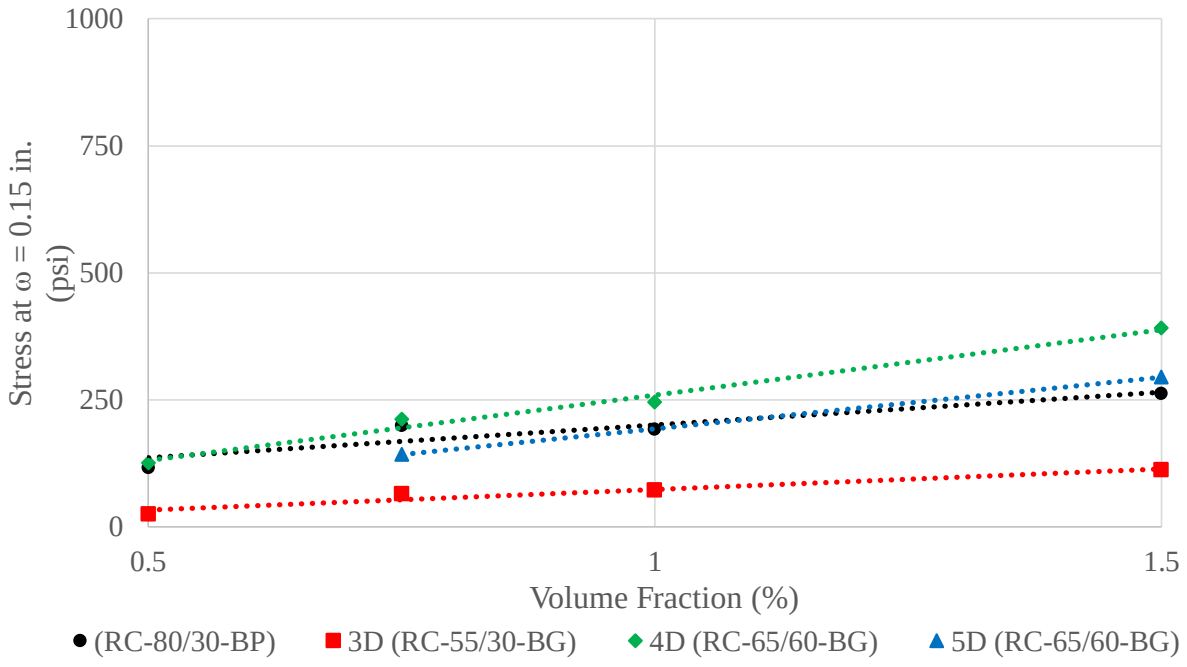

Figure 5.39 – Tension stress at crack width equal to 0.15 in. vs. fiber volume fraction ($f_c' = 6$ ksi).

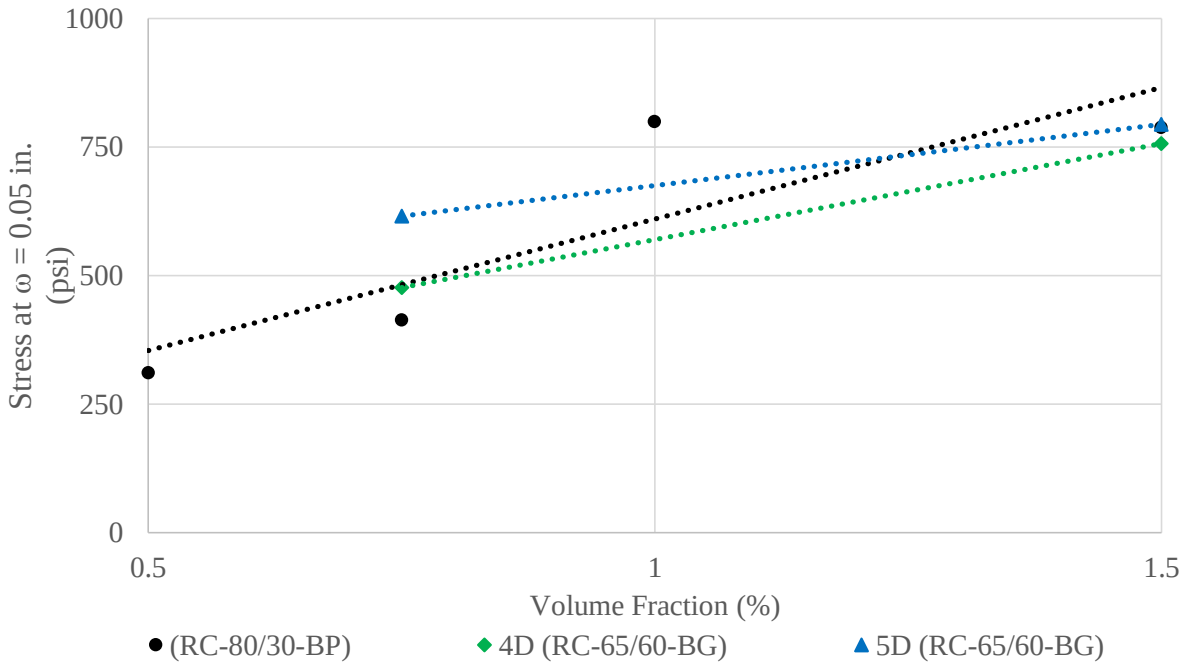

Figure 5.40 – Tension stress at crack width equal to 0.05 in. vs. fiber volume fraction ($f_c' = 10$ ksi).

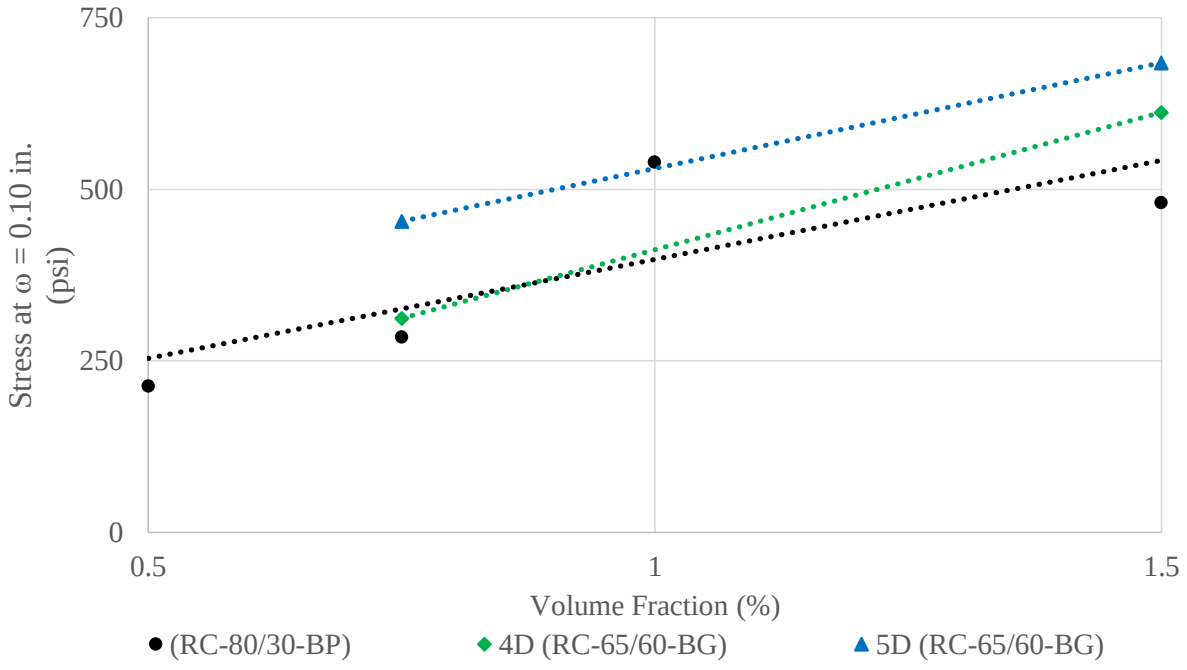

Figure 5.41 – Tension stress at crack width equal to 0.10 in. vs. fiber volume fraction ($f_c' = 10$ ksi).

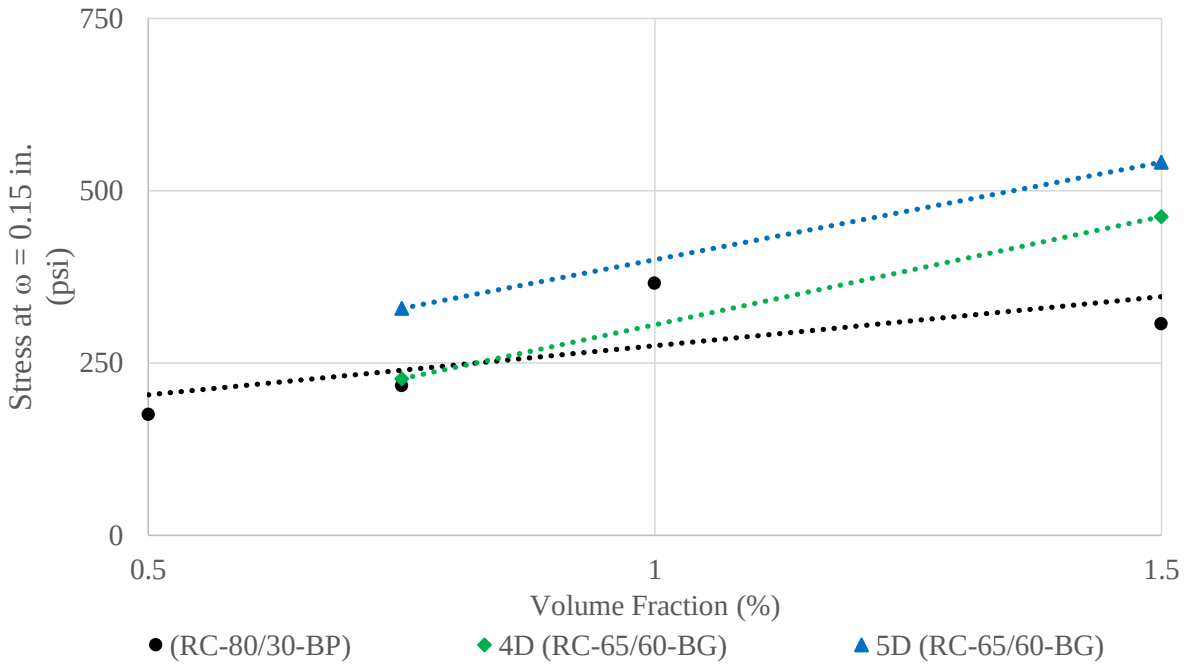

Figure 5.42 – Tension stress at crack width equal to 0.15 in. vs. fiber volume fraction ($f_c' = 10$ ksi).

5.5 – Compression, Flexure, and Tension Relationships

One of the main objectives of this study was to correlate the post-peak compressive response and the post-cracking flexural and tensile properties. These relationships would make it easier for engineers to characterize the mechanical behavior of SCFRCs for modeling or design based on a relatively limited number of standard tests. At the beginning of this section, the compressive and flexural results are related, followed by a discussion of results from the compression and tension tests.

5.5.1 – Compression-Flexure Relationships

As illustrated previously in this chapter, fiber content, as well as the mechanical and physical properties of the fiber, affected the compression behavior of SCFRCs. Fibers increased

concrete post-peak slope, which increased the compression toughness. Likewise, the flexural post-crack peak strength increased as fiber volume fraction increased, which increased concrete flexural toughness.

Several terms could be used to represent the post-peak flexural behavior of SCFRCs, such as the effective stress at the post-crack peak or at a deflection equal to 0.04, 0.08, or 0.12 in. Flexure loads (stress) corresponding to post-crack peak, as well as 0.04, 0.08 inch, and 0.12 inch mid-span deflection, can be used because they changed (increased) as fiber content increased and changed as fiber properties changed.

Figures 5.43 to 5.45 show the flexure load corresponding to post-crack peak plotted versus compression post-peak slope. Figures 5.46 to 5.48 show the flexure load corresponding to a mid-span deflection equal to 0.04 inch plotted versus compression post-peak slope. Similar plots are given for flexure loads corresponding to 0.08 inch and 0.12 inch mid-span deflections in Figures 5.49 and 5.50, respectively.

As shown, there is a significant amount of scatter in the data. However, if the R^2 value for the trend-line drawn through all of the results from batches with $f_c' = 6$ and 10 ksi is indicative of how closely the compression post-peak slope is correlated to each of the various parameters, the peak post-cracking strength and the flexural strength at a deflection of 0.04 in. appear to be most closely related to the post-peak slope in compression (Figures 5.45 and 5.48).

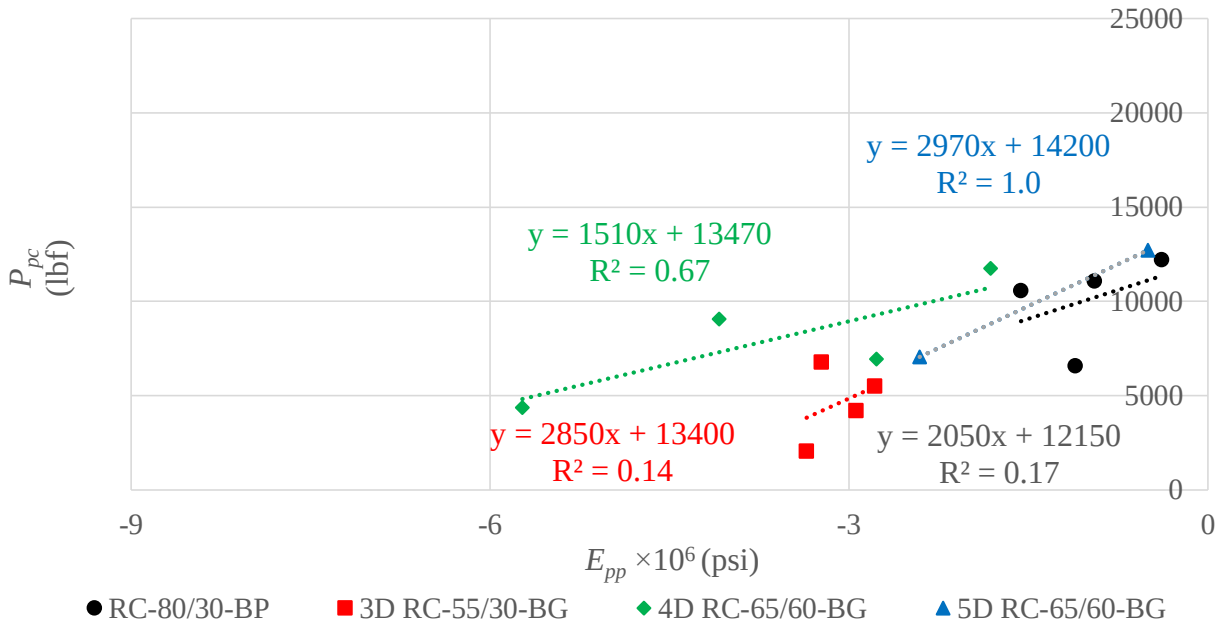

Figure 5.43 – Post-crack peak flexure load vs. compression post-peak slope ($f_c' = 6$ ksi).

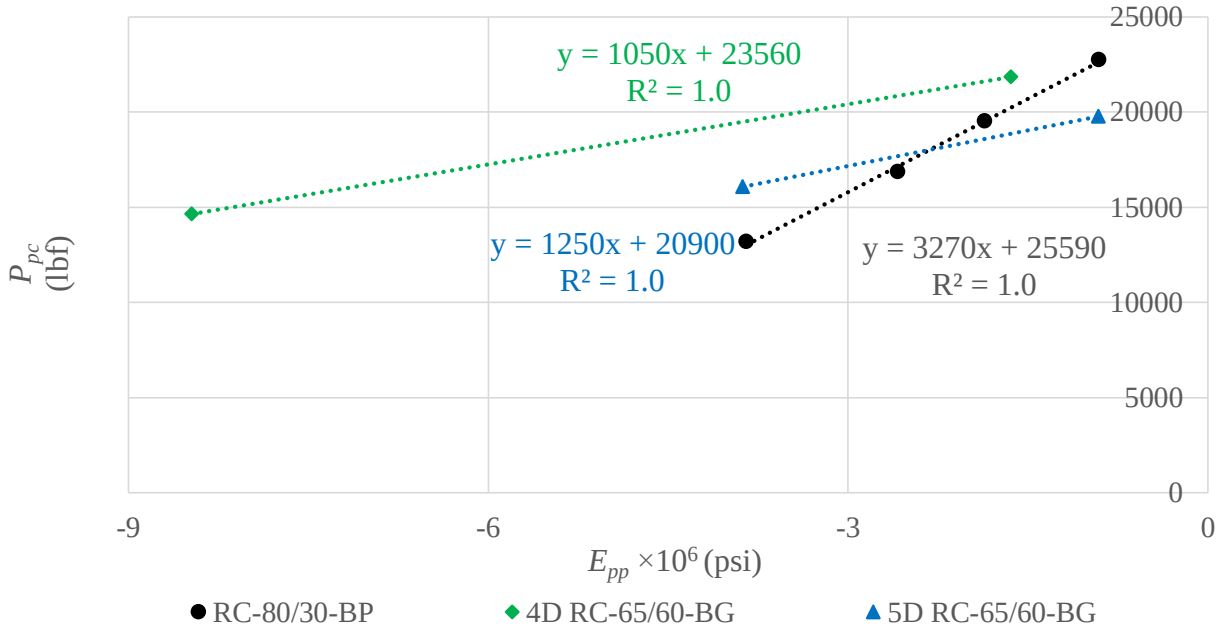

Figure 5.44 – Post-crack peak flexure load vs. compression post-peak slope ($f_c' = 10$ ksi).

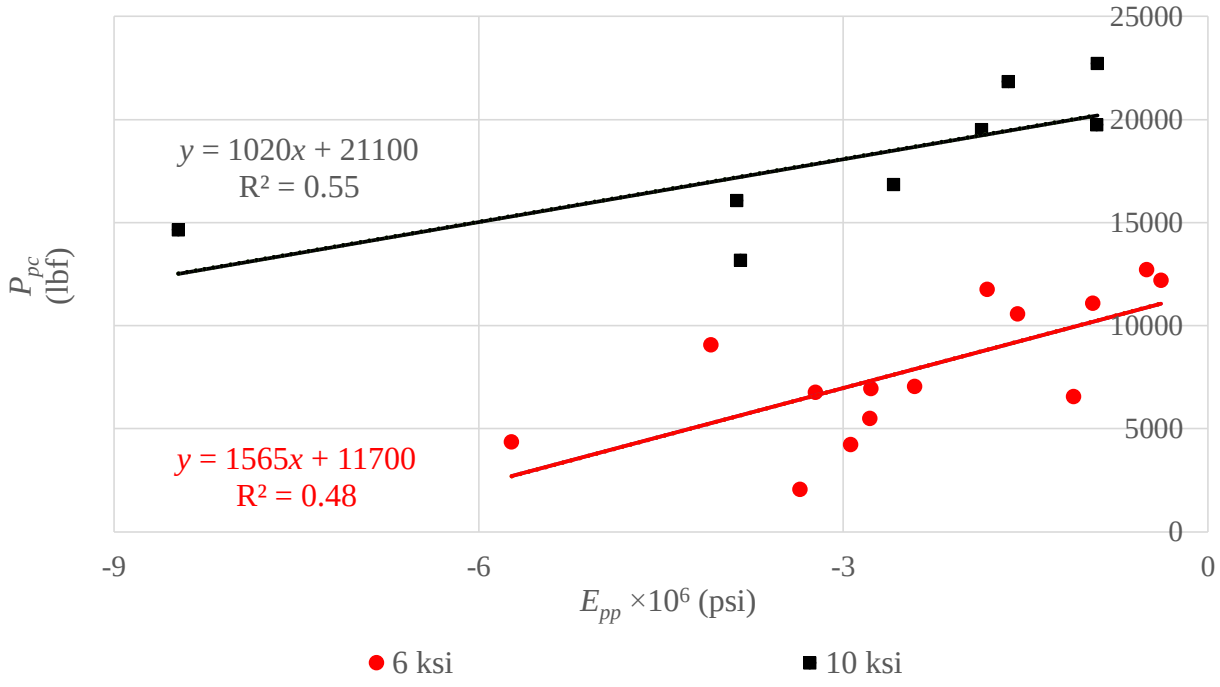

Figure 5.45 – Flexure load at post-crack peak vs. compression post-peak slope ($f_c' = 6$ ksi vs. $f_c' =$ 10 ksi).

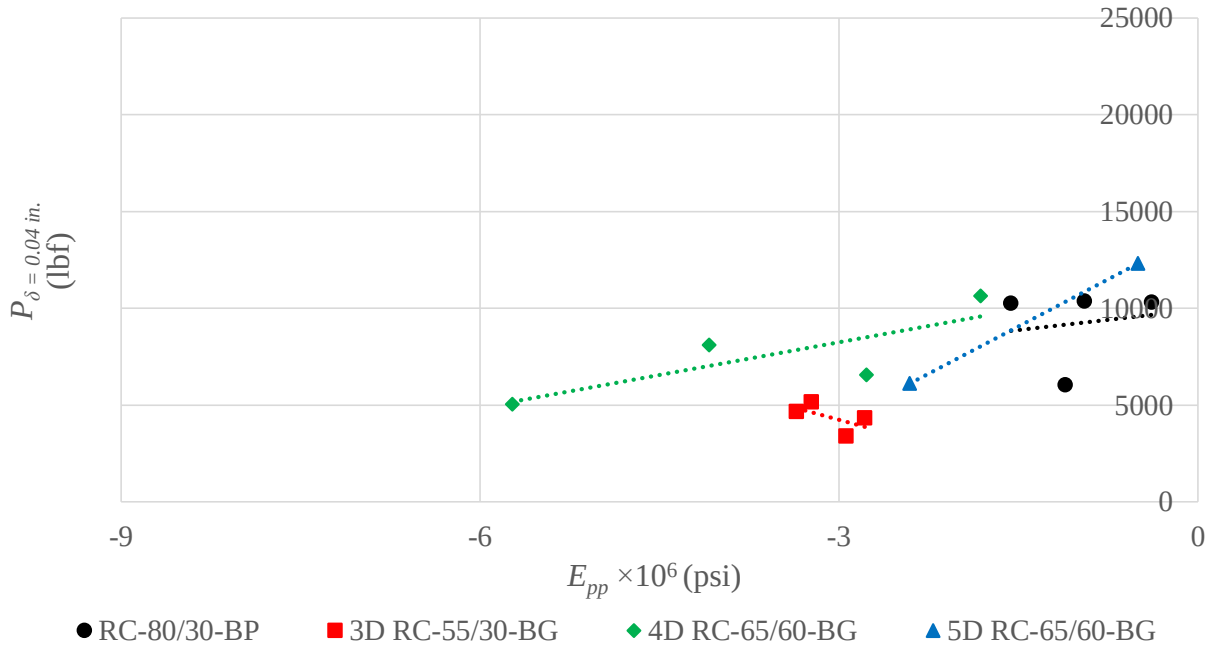

Figure 5.46 – Flexure load at 0.04 inch deflection vs. compression post-peak slope ($f_c' =$ 6 ksi).

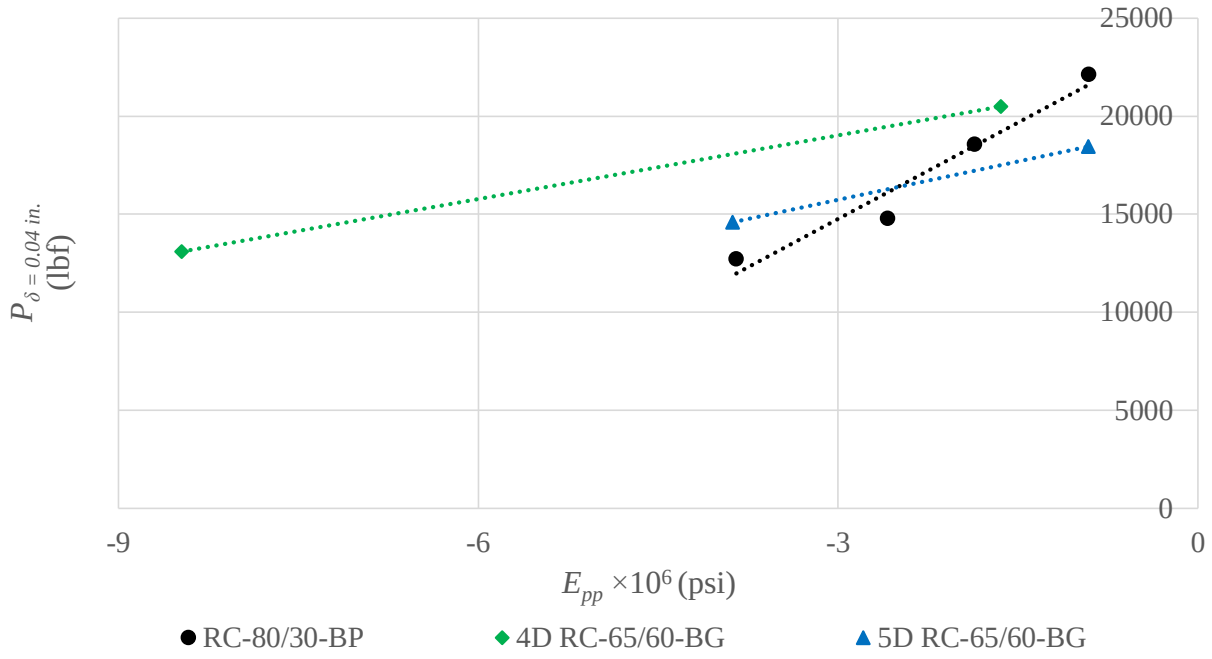

Figure 5.47 – Flexure load at 0.04 inch deflection vs. compression post-peak slope ($f_c' =$ 10 ksi).

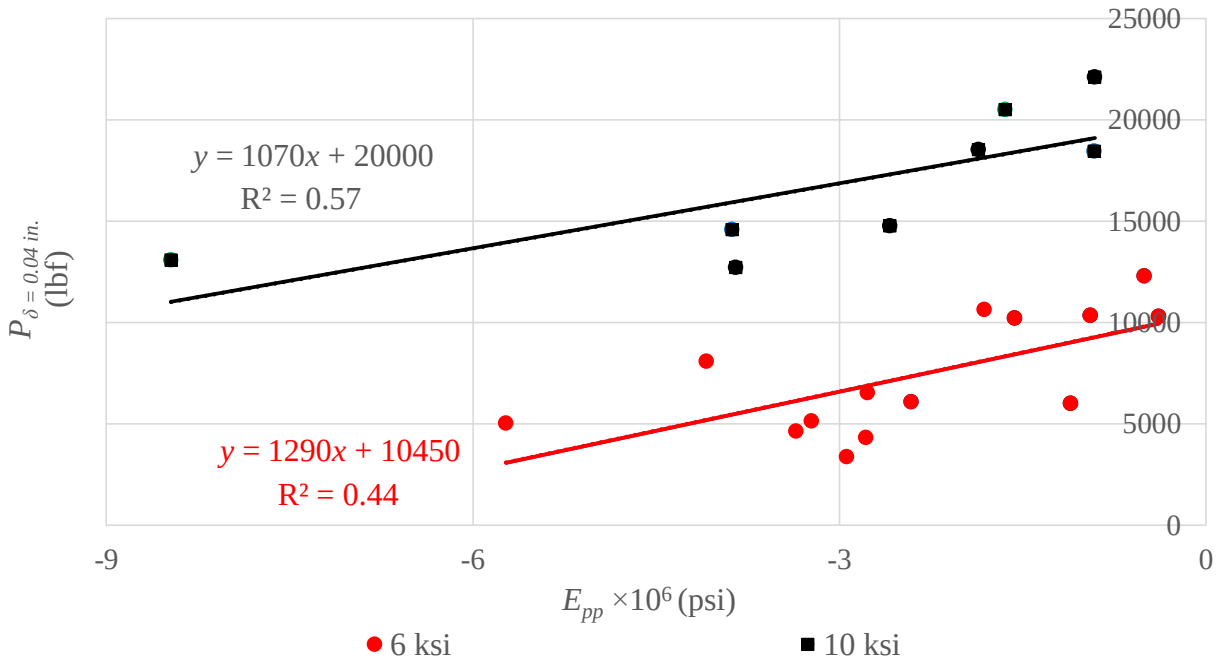

Figure 5.48 – Flexure load at 0.04 inch deflection vs. compression post-peak slope ($f_c' =$ 6 ksi vs. $f_c' =$ 10 ksi).

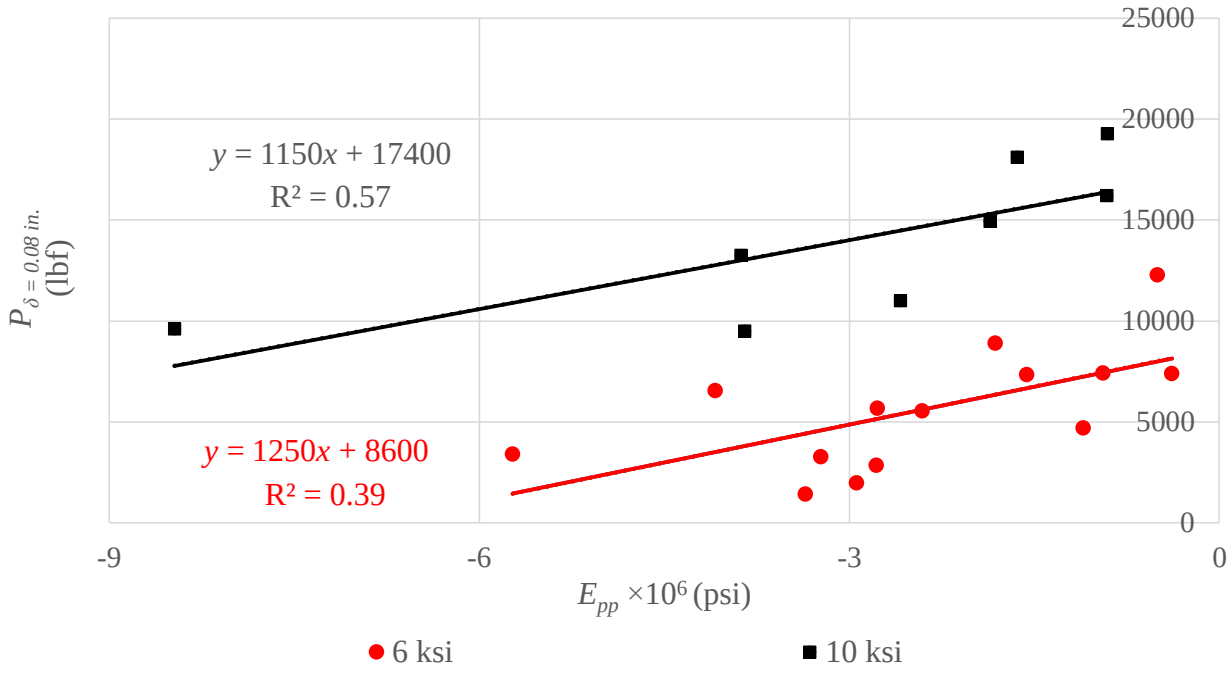

Figure 5.49 – Flexure load at 0.08 inch deflection vs. compression post-peak slope ($f_c' =$ 6 ksi vs. $f_c' =$ 10 ksi).

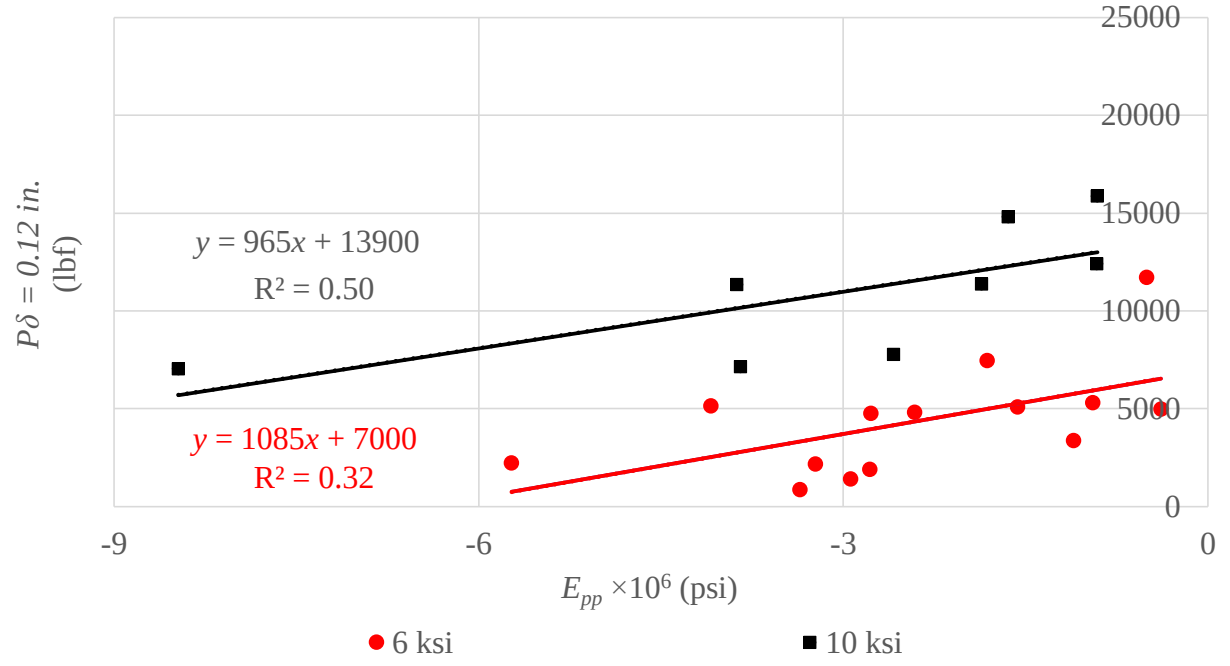

Figure 5.50 – Flexure load at 0.12 inch deflection vs. compression post-peak slope ($f_c' =$ 6 ksi vs. $f_c' =$ 10 ksi).

5.5.2 – Compression-Tension Relationships

Fiber content, as well as fiber mechanical and physical properties, had a significant effect on the concrete post-crack tension behavior, as shown in this chapter. The post-crack strengths increased as fiber volume fraction increased, which increased concrete tension toughness. The following show correlations between measures of post-cracking tension behavior and the compression post-peak response.

Several terms may be used to represent the tension behavior, such as the stress at the post-crack peak, the stress at crack width of 0.05 inch, the stress at crack width of 0.10 inch, and the stress at crack width of 0.15 inch. Figures 5.51 and 5.53 show the post-cracking peak tension stress plotted versus the compression post-peak slope. Figures 5.54 through 5.58 show the tension stress at crack widths of 0.05, 0.10, and 0.15 in. plotted versus the post-peak slope in compression. To the extent that R^2 values represent the correlation between the x- and y- axis values, the peak post-cracking tensile stress and the tensile stresses at crack widths of 0.05, 0.10, and 0.15 in. all are similarly correlated to the post-peak slope in compression.

None of the parameters from the tension tests are as well correlated to the post-peak compressive slope as the peak post-cracking flexural strength presented previously. The flexure test was also the easiest to perform in comparison to the compression and the tension tests.

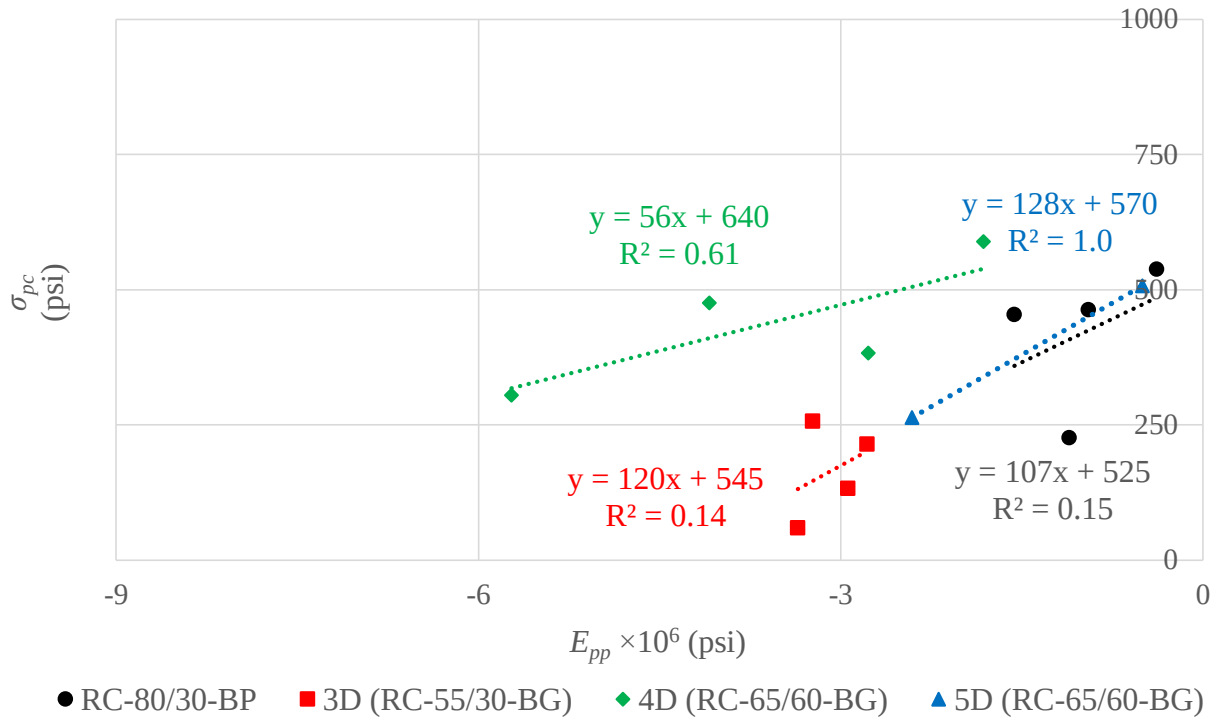

Figure 5.51 – Post-crack peak tension stress vs. compression post-peak slope ($f_c^{'} = 6$ ksi).

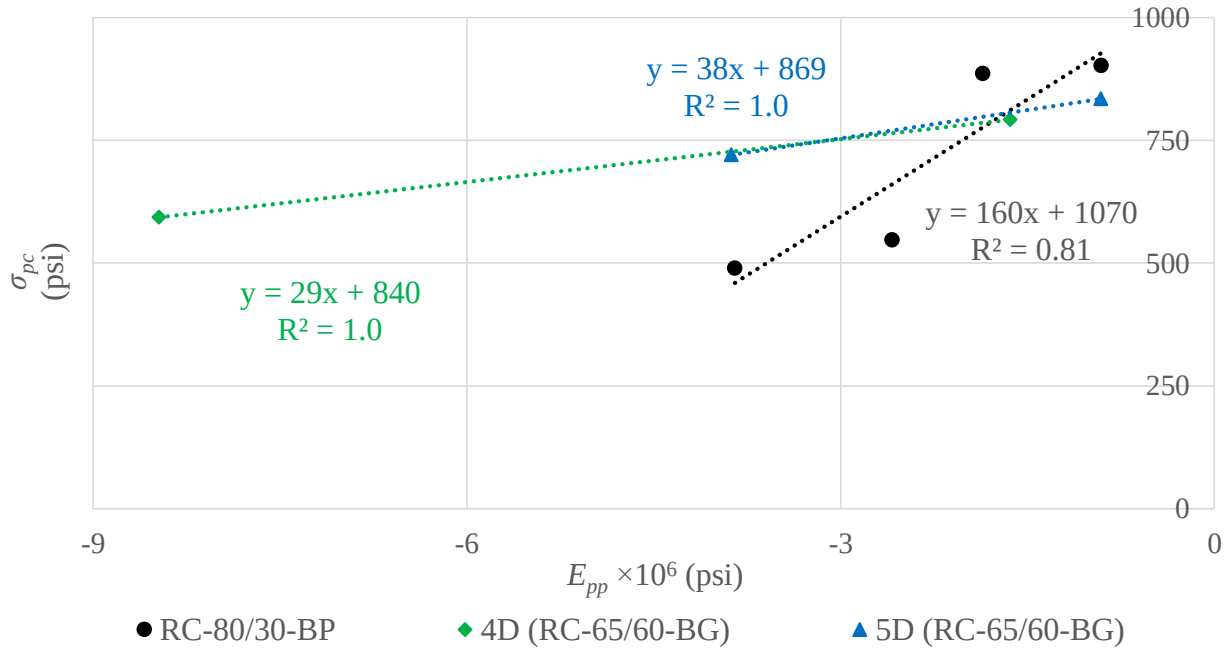

Figure 5.52 – Post-crack peak tension stress vs. compression post-peak slope ($f_c' = 10$ ksi).

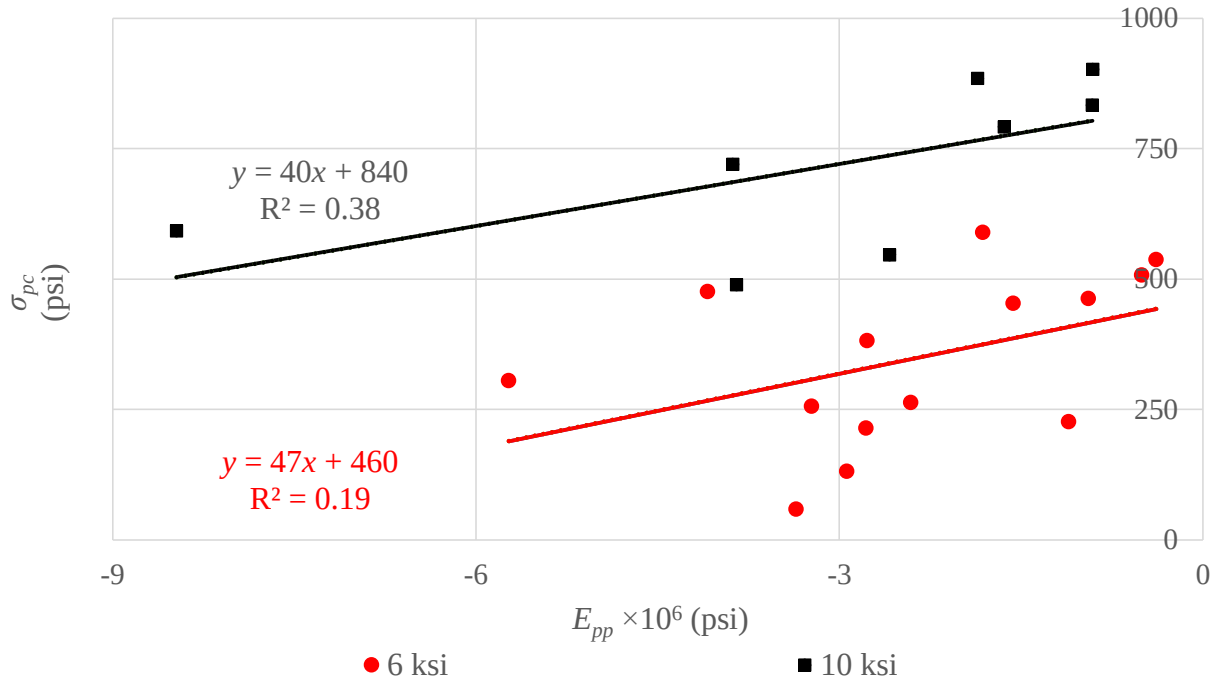

Figure 5.53 – Tension post-crack peak stress vs. compression post-peak slope ($f_c' = 6$ ksi vs. $f_c' =$ 10 ksi).

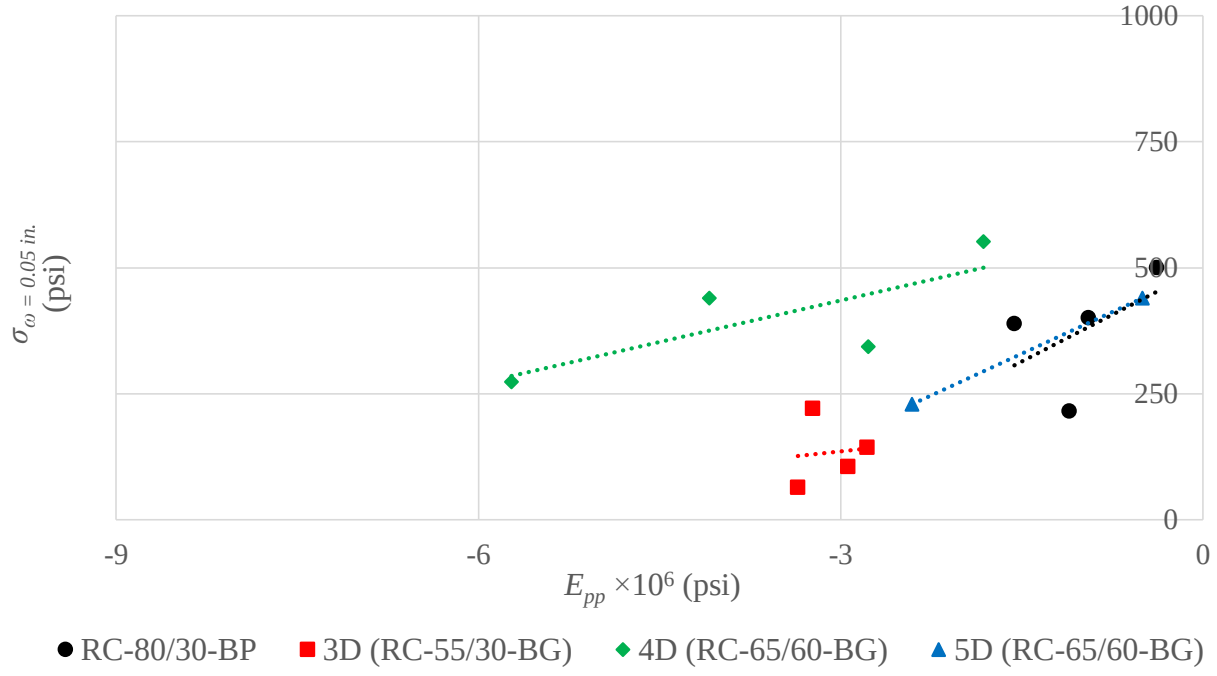

Figure 5.54 – Tension stress at 0.05 inch crack width vs. compression post-peak slope ($f_c^{'} = 6$ ksi).

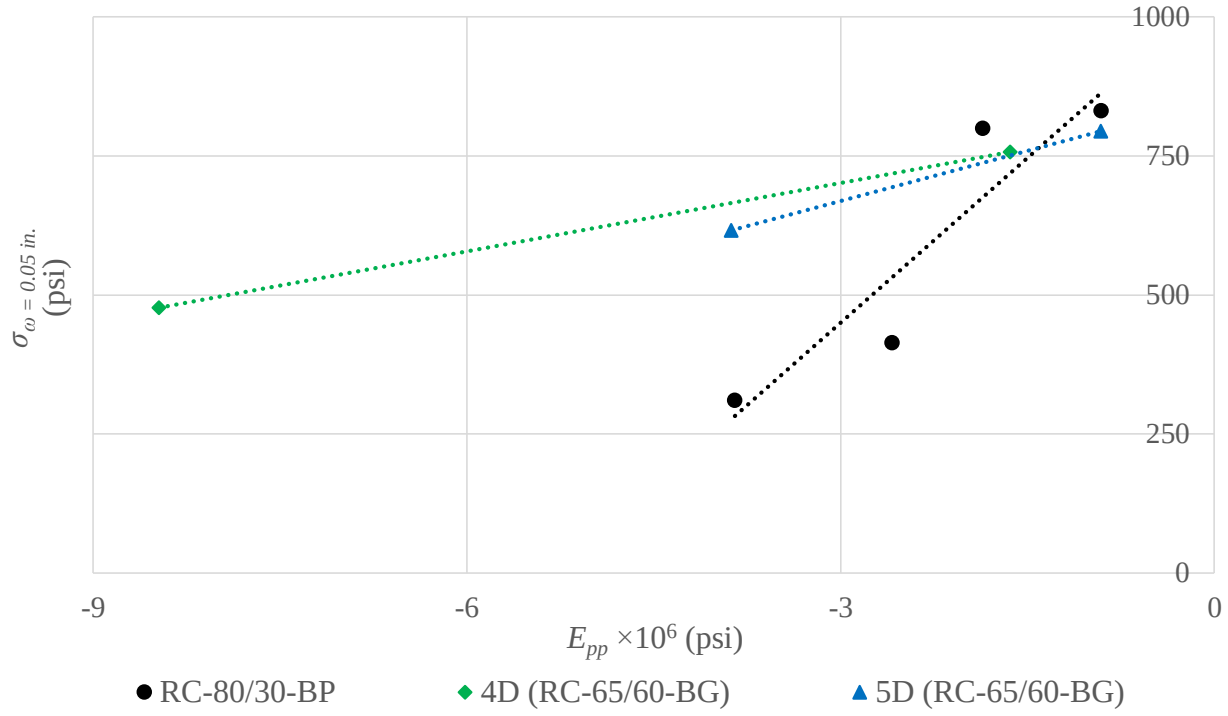

Figure 5.55 – Tension stress at 0.05 inch crack width vs. compression post-peak slope ($f_c' = 10$ ksi).

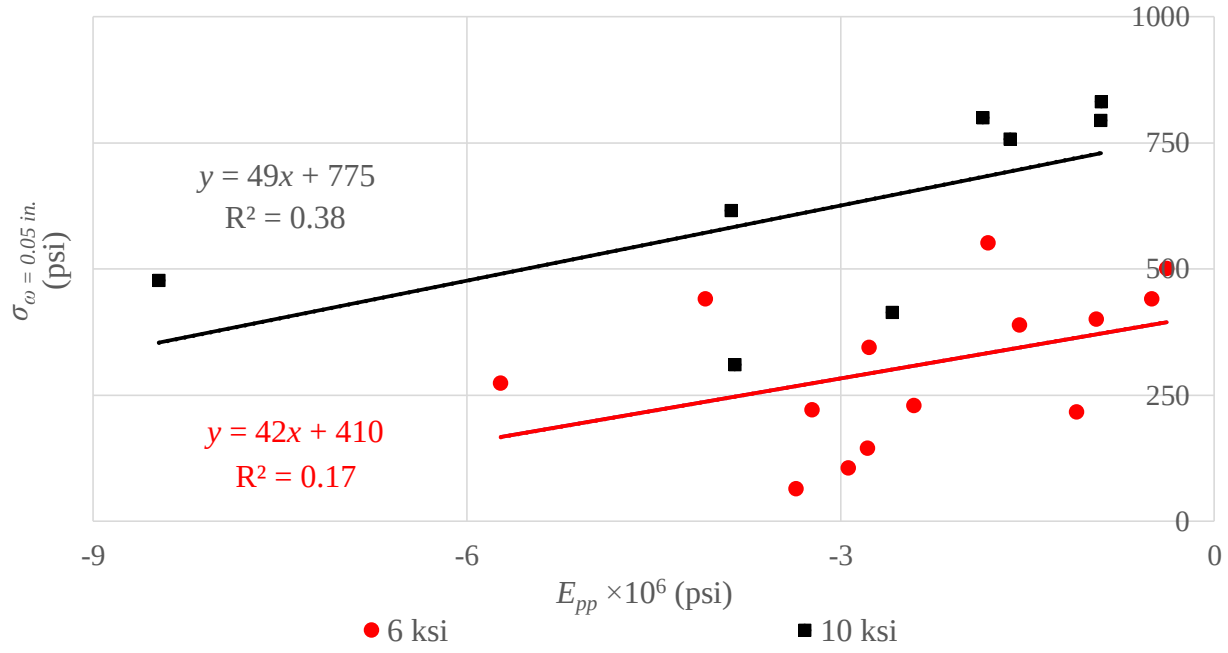

Figure 5.56 – Tension stress at 0.05 inch crack width vs. compression post-peak slope ($f_c' = 6$ ksi vs. $f_c' = 10$ ksi).

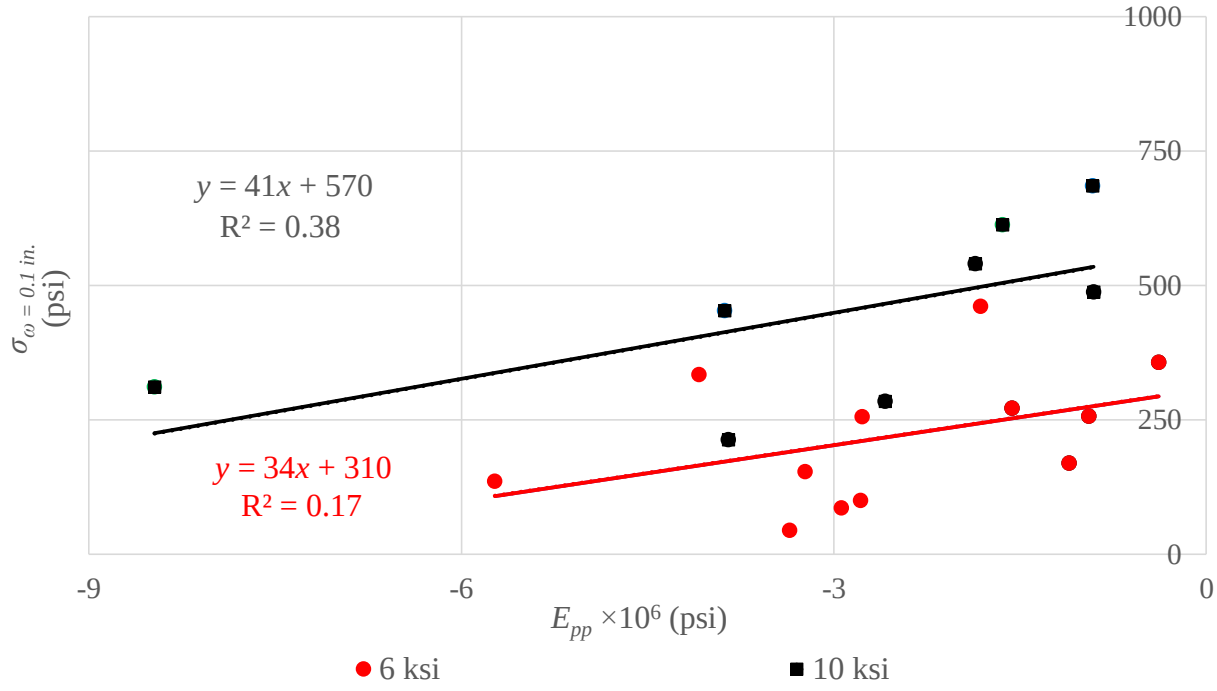

Figure 5.57 – Tension stress at 0.1 inch crack width vs. compression post-peak slope (f_c' = 6 ksi vs. f_c' = 10 ksi).

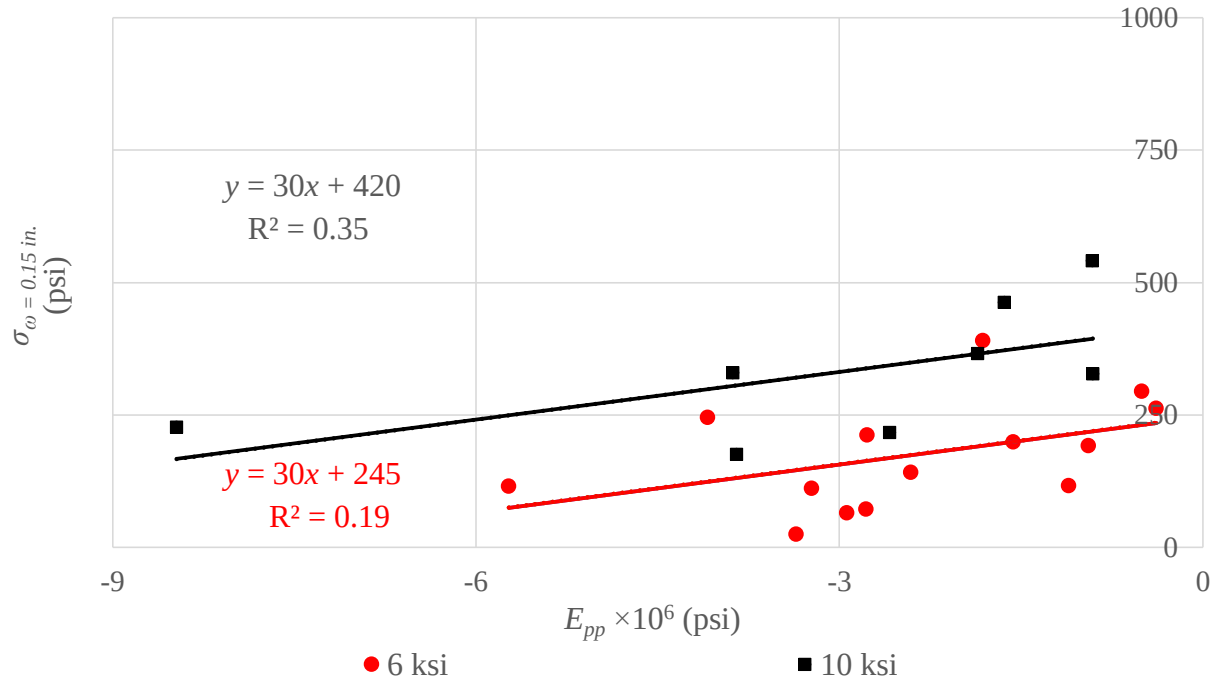

Figure 5.58 – Tension stress at 0.15 inch crack width vs. compression post-peak slope (f_c' = 6 ksi vs. f_c' = 10 ksi).

CHAPTER 6: SUMMARY AND CONCLUSIONS

6.1 – Summary

The aim of this study was to study the relationships between compression test results (compression stress vs. longitudinal strain) and tensile test results (tensile stress vs. crack width), as well as relationships between results from compression and flexural tests (flexural load vs. mid-span net deflection). A strong relationship between these results would facilitate characterization of the mechanical behavior of SCFRCs for modeling or design based on a relatively limited number of standard tests. A secondary objective was to quantify and report the effect of introducing different volume fractions of four types of steel fiber to self-consolidating concrete mixtures with target compressive strengths of 6 and 10 ksi.

Four different hooked-end-steel fibers were used in this study at volume fractions that varied between 0.5% and 1.5%. Each mixture had a target strength of either 6 or 10 ksi and a target spread of 25 inches without fibers to ensure adequate workability after the addition of steel fibers. As part of this study, twenty-four batches of concrete (6.75 ft^3 each) were prepared. Each was used to make five 6×12 inch cylinders for compression tests, five 6×6×20 inch beams for flexural tests, and five 6×6×20 inch rectangular prisms for direct tension tests.

The properties of SCFRCs in the fresh-state such as temperature, density, air content, slump flow, Visual Stability Index (VSI), T_{50}, and J-ring slump flow were reported and discussed for each mixture. Results from uniaxial compression, flexure, and direct tension were presented for each specimen. Test observations were also reported and discussed. Finally, the post-peak compression behavior was plotted versus the flexural post-crack response and the post-crack tension response to observe whether trends exist.

6.2 –Conclusions

a. The post-peak slope in compression and the post-cracking flexural and tensile strengths all increased with fiber volume fraction, whereas properties up to development of cracking (or peak strength in the case of compression) were not affected by use of fibers.

b. The relative performance of different fiber types was consistent among the flexural, tensile, and compressive tests.

c. The within-batch coefficient of variation of post-crack peak tensile and flexural loads decreased significantly when T_{50} was at least 1.0 second, from an average of 40% to 13%.

d. A preliminary analysis was done to determine which features of the post-cracking tensile and flexural test results were most closely correlated with the calculated post-peak slope in compression. Of the parameters investigated, the peak post-cracking flexural strength and the flexural strength at a mid-span deflection of 0.04 in. tended to have the most closely linear correlation with the post-peak slope in compression. However, there was significant scatter in the results.

6.3 – Other Findings

6.3.1 – Comparison between Fiber Types

a. Fiber RC-80/30-BP had the greatest effect on the mechanical behavior of SCFRC. Mixtures with this fiber exhibited tensile strain-hardening using a volume fraction of 1.0% and deflection-hardening in flexure with a volume fraction of 0.75%. Use of this fiber had the most significant effect on the post-peak slope in compression.

b. Fibers 5D RC-65/60-BG and 4D RC-65/60-BG were similarly effective at increasing the mechanical behavior of the materials. Mixtures with a volume fraction of 1.0% showed

deflection-hardening in flexure and those with a volume fraction of 1.5% showed a strain-hardening response in tension. It was observed that the 5D RC-65/60-BG fiber was somewhat more effective than the 4D RC-65/60-BG in concrete with a specified compressive strength of 10 ksi, perhaps due to greater resistance to concrete breakout.

c. Fiber 3D RC-55/30-BG had the smallest effect on the post cracking responses of the material. Mixtures with a volume fraction of 1.5% of this fiber exhibited neither strain-hardening nor deflection-hardening. The relatively poor performance of this fiber is likely partially due to incomplete dispersion of the fiber during the mixing process.

6.3.2 – Concrete Properties at Fresh-State

a. Measured slump flow for batches with $f_c' = 6$ ksi was reduced by 15-30%, relative to plain concrete, for batches with a fiber volume fraction of 1.5%. For the same fiber volume fraction, measured slump flow decreased by 5-20% for batches with $f_c' = 10$ ksi.

b. Mixtures with a fiber volume fraction of 0.5% or less had passing abilities less than 2 and most mixtures with 0.75% fiber volume fraction and all mixtures with 1.0% and 1.5% fiber volume fractions had passing abilities higher than 2.0. However, all batches were highly workable and few showed clear evidence of segregation.

6.3.3 – Uniaxial Compression Tests

a. Most specimens with low fiber volume fractions (0% and 0.5%) had a tendency to fail in a brittle manner, particularly as the concrete compression strength increased, except for specimens with fiber type RC-80/30-BP. In contrast, mixtures with high fiber volume fractions (0.75%, 1%, and 1.5%) showed gradual failures that are more typical of confined

concrete. Cone failure (type 1) occurred most commonly with specimens of low fiber volume fractions (0%, 0.5% and 0.75%). Shear-column failure (type 2) and column failure (type 3) occurred most commonly in specimens of high fiber volume fractions (1% and 1.5%). Shear failures (type 4 failure) occurred in only a few specimens.

b. The calculated post-peak slope was sensitive to the fiber volume fraction, with increases of up to 100% for batches with a volume fraction of 1.5%. However, increases in slope were not proportional to volume fraction. Use of a fiber volume fraction of 0.75% resulted in, on average, a 70% increase in post-peak slope.

6.3.4 – Flexural Tests

a. Some specimens with a target strength of 10 ksi developed vertical cracks above the supports. It is recommended that a flat plate be used between the roller supports and the specimen when specimens have a target compressive strength of 10 ksi or greater.

b. Post-test observation of the primary failure surface (crack) indicated that fiber pullout dominated the response of most specimens. Specimens with fiber type 3D (RC-55/30-BG) and fiber type 4D (RC-65/60-BG) exhibited the most fractured fibers, but in general only approximately 5% of the exposed fibers had fractured.

6.3.5 – Direct Tension Tests

a. Most specimens developed a single crack at the notch in the middle of the specimen. However, a few specimens with fiber volume fractions of 1.0% and 1.5% of fiber type 4D (RC-65/60-BG) and fiber type 5D (RC-65/60-BG) developed cracks outside the pre-notched portion after the first crack developed.

b. Post-test observation of the failure surface (crack) indicated that fiber pullout dominated the response of most specimens. However, specimens with fiber type 3D (RC-55/30-BG) and fiber type 4D (RC-65/60-BG) did have some fractured fibers (less than 10%).

c. The post-crack peak strength was sensitive to fiber concentration and fiber properties. As fiber volume fractions increased, the post-crack peak strength increased. Mixtures with fiber types 4D (RC-65/60-BG) and 5D (RC-65/60-BG) developed strain hardening using a 1.5% fiber volume fraction with mixtures of $f_c`$ = 6 ksi and 10 ksi. Mixtures with fiber type RC-80/30-BP developed strain hardening using volume fraction of 1.0% and 1.5% with mixtures of $f_c`$ = 6 ksi and 10 ksi. Non mixture with fiber type 3D (RC-55/30-BG) exhibited strain hardening.

d. The average maximum tension strength of 6 ksi SCFRCs ranged between 390 psi and 590 psi, while it ranged between 685 psi and 885 psi for 10 ksi SCFRCs.

6.4 – Recommendations for Future Study

a. Further analysis of the relationships between the tensile, compressive, and flexural responses is warranted.

b. Mixtures of SCFRCs of volume fractions ranging between 2% and 3% of various fibers, which may be feasible given the workability of the mixtures used herein, should be conducted to obtain more data for the observed relationships.

c. Because fiber types RC-80/30-BP and 5D (RC-65/60-BG) experienced pullout failure, using higher strength concrete (15 ksi and/or 20 ksi) might be feasible in future studies.

d. Additional testing of mixtures with T_{50} values of at least 1.0 should be conducted to evaluate whether the variability in the reported results is reduced.

e. Large-scale specimens need to be tested so that correlations between material behavior and structural response can be better correlated.

f. Numerical modelling of the compression, tension, and flexural behavior of SCFRCs will allow for the study of a wider range of variables.

g. Measuring the lateral strain of the concrete cylinders under compression was challenging after peak. Use of a new method in future studies is recommended if this result is of interest.

References

ACI Committee 237. (2007). *Self-Consolidating Concrete.* American Concrete Institute.

ACI Committee 544. (1996). State-of-the-Art Report on Fiber Reinforced Concrete. *American Concrete Institute*.

ACI Committee, 5. (1998). *Guide for Specifying, Proportioning, Mixing, Placing, and Finishing Steel Fiber Reinforced Concrete.* American Concrete Institute.

Adepegba, D., & Regan, P. E. (1981). Performance of Steel Fibre Reinforced Concrete in Axially Loaded Short Columns. *International Journal of Cement Composites and Lightweight Concrete*, 255-259.

Agarwal, B., & Brountman, L. (2006). Analysis and Performance of Fiber Composites. (3, Ed.) *JohnWiley and Sons*, 76-80.

Antunes, M. (2008). *Integration of optical tracking system for determination of the position and orientation of instruments during the surgery.* Coimbra: University of Coimbra.

Astarlioglu, S., & Krauthammer, T. (2014). Response of normal-strength and ultra-high-performance fiber-reinforced concrete columns to idealized blast loads. *ELSEVIER*.

ASTM C1018. (1992). *Standard Test Method for Flexural Toughness and First-Crack Strength of Fiber-Reinforced Concrete (Using Beam with Third Point Loading).* ASTM International.

ASTM C138. (2001). *Standard Test Method for Density (Unit Weight), Yield, and Air Content (Gravimetric) of Concrete.* ASTM International.

ASTM C1609. (2012). *Standard Test Method for Flexural Performance of Fiber-Reinforced Concrete (Using Beam With Third-Point Loading).* ASTM International.

ASTM C1611. (2010). *Standard Test Method for Slump Flow of Self Consolidating Concrete.* ASTM International.

ASTM C1621. (2014). Standard Test Method for Passing Ability of Self-Consolidating Concrete by J-Ring. *ASTM International*.

ASTM C231. (2010). *Standard Test Method for Air Content of Freshly Mixed Concrete by the Pressure Method.* ASTM International.

ASTM C39. (2012). *Standard Test Method for Compressive Strength of Cylindrical Concrete Specimens.* ASTM International.

ASTM C469. (2002). *Standard Test Method for Static Modulus of Elasticity and Poisson's Ratio of Concrete in Compression.* ASTM International.

Aulia, T. B. (2002). *Effects of Polypropylene Fibers on the Properties of High-Strength Concretes.* Leipzig Annual Civil Engineering Report.

Balaguru, P., & Khajuria, A. (1996, Sep). Properties of Polymeric Fiber- Reinforced Concrete. *Transportation Research Record*, 27-35.

Balaguru, P., & Najm, H. (2004, Aug). High Performance Fiber-Reinforced Concrete Mixture Proportions with High Fiber Volume Fractions. *ACI Materials Journal, 101*, 281-286.

Balaguru, P., & Ramakrishnan, V. (1987). Comparison of Slump Cone and V-B Tests as Measures of Workability for Fiber Reinforced and Plain Concrete. *9*, 3-11.

Balaguru, P., & Shah, S. (1992). Fiber Reinforced Cement Composites. *McGraw-Hill Inc*.

Balaguru, P., Narahari, R., & Patel, M. (1992, Dec.). Flexural Toughness of Steel Fiber Reinforced Concrete. *ACI Materials Journa*, *89*(6), 541-546.

Banthia, N., & Bindiganavile, V. (2007, April). Fiber Reinforced Shotcrete – Comparing the properties of dry- and wet-mix shotcrete reinforced with steel fibers. *Concrete International*, 53 58.

Barnes, A. J. (2007). *Uniaxial Compression and Flexural Behavior of High Performance Cementitious Composites (HPFRCC) "A Master thesis".* University of Wisconsin.

Barr, B., Gettu, R., Al-Oraimi, S. K., & Bryars, L. (1996). Toughness Measurementthe Need to Think Again. *Cement and Concrete Composites*, 281- 297.

BEKAERT. (2013). *Reinforcing your industrial floors.*

Bentur, A., & Mindess, S. (1990). *Fibre Reinforced Cementitious Composites.* London.

Brodowski, D. (2005). private communication with A.E. Naaman.

Canbolat, B., Parra-Montesinos, G., & J.K.Wight. (2004). Behavior of Precast High-Performance Fiber Reinforced Cement Composite Coupling Beams Under Large Displacement Reversals. *In Proceedings of the 13th world conference on earthquake engineering.* Vancouver, B.C., Canada.

Canbolat, B., Parra-Montesinos, G., & Wight., J. (2005). Experimental Study on Seismic Behavior of High-Performance Fiber-Reinforced Cement Composite Coupling Beams. *ACI Structural Journal, ,* 159–166.

Carreira, D., & Chu, K. (1981, May). Stress-Strain Relationship for Plain Concrete in Compression. *ACI, 78*, 171-177.

Dagar, K. (2012, April-June). SLURRY INFILTRATED FIBROUS CONCRETE (SIFCON). *International Journal of Applied Engineering and Technology, 2*, 99-100.

Dinh, H. H. (2009). *SHEAR BEHAVIOR OF STEEL FIBER REINFORCED CONCRETE BEAMS WITHOUT STIRRUP REINFORCEMENT " A PhD dissertation".* The University of Michigan.

Ezeldin, A., Balaguru, P., & Perumalsamy, N. (1992, Nov). Normal and High-Strength Fiber Reinforced Concrete under Compression. *ASCE Journal of Materials in Civil Engineering, 4*(4), 415-429.

Fanella, D. A., & Naaman, A. E. (1985, July 1). Stress-Strain Properties of Fiber Reinforced Mortar in Compression. *Journal of The American Concrete Institute, 82*(4), 475-483.

FHWA, U. D. (2013). *Ultra-High Performance Concrete.* State of the Art.

Gencel, O., Brostowb, W., Datashvili, T., & Thedford, M. (2011, February 11). Workability and Mechanical Performance of Steel Fiber-Reinforced Self-Compacting Concrete with Fly Ash. *Composite Interfaces*, 169–184.

Gru¨newald, S. (2006, June). Performance-based design of self-compacting fibre reinforced concrete," Ph.D. thesis.

Gru¨newald, S., & Walraven, J. C. (2001, May). Parameter-study on the influence of steel fibers and coarse aggregate content on the fresh properties of selfconsolidating concrete. *Cement and Concrete Research*, 1793–1798.

Guirola, M. (2001). *STRENGTH AND PERFORMANCE OF FIBER-REINFORCED CONCRETE COMPOSITE SLABS "Master Thesis".* Blacksburg, Virginia: Virginia Polytechnic Institute and State University.

Hockenberry, T., & Lopez, M. M. (2012). Performance of Fiber Reinforced Concrete Beams with and without Stirrups. *Journal of Civil Environmental and Architectural Engineering, 4*(1).

Homrich, J., & Naaman, A. (1987). Stress-Strain Properties of SIFCON in Compression. *American Concrete Institute*, 283-304.

Homrich, J., & Naaman, A. (1995). Micromechanical Models of Mechanical Response of HPFRCC. *In RILEM High Performance Fiber Reinforced Cement Composites 2*.

Hota, S. a. (1997). Bond Stress-Slip Response of Reinforcing Bars Embedded in FRC Matrices under Monotonic Cyclic Loading. *ACI Structural Journal, 95*(September-October 1997), 525-537.

Johnston, C. (1973). Steel Fiber Reinforced Mortar and Concrete: A Review of Mechanical Properties. *American Concrete Institute*.

Johnston, C. (1996). Proportioning, mixing and placement of fibre-reinforced cements and concretes," Production Methods and Workability of Concrete. (M. a. Bartos, Ed.) *E&FN Spon*, 155-179.

Johnston, C. (2001). Fiber-Reinforced Cements and Concretes.

Johnston, C., & Coleman, R. (1973). Strength and Deformation of Steel Fiber Reinforced Mortar in Uniaxial Tension," in Fiber Reinforced Concrete. *American Concrete Institute*, 177-194.

Kao, J. T. (2005). Investigation into the Use of Portland Cement Concrete with Fiber Additives for Bridge Decks in the State of Oklahoma. *University of Oklahoma*.

Krstulovic-Opara, N., & Al-Shannag, M. (1999, Feb). Slurry Infiltrated Mat Concrete (SIMCON) – Based Shear Retrofit of Reinforced Concrete Members. *ACI Structural Journal, 96*(1), 105-114.

Kwak, Y.-K., Eberhard, M. O., Kim, W.-S., & Kim, j. (2002 , Augest). Shear Strength of Steel Fiber-Reingorced Concrete Beams without Stirrups. *ACi Structural Journal*, 530-538.

Lequesne, R. D. (2011). *Behavior and Design of High-Performance Fiber-Reinforced Concrete Coupling Beams and Coupled-Wall Systems "A dissertation of Phd'.* Michigan: The University of Michigan.

Li, V. (1992, Feb.). Postcrack Scaling Relations for Fiber Reinforced Cementitious Composites. *ASCE Journal of Materials in Civil Engineering, 4*, 41-57.

Li, V., & Mishra, D. (1992). Micromechanics of Fiber Effect on the Uniaxial Compressive Strength of Cementitious Composites. *RILEM 4th Inter*.

Li, V., Mihashi, H., Wu, H., Alwan, J., Brincker, R., Horii, H., . . . Stang, H. (1995). *Micromechanical Models of Mechanical Response of HPFRCC.* In RILEM High Performance Fiber Reinforced Cement Composites 2.

Li, Z., Li, F., Chang, P., & Mai, Y. (1998). Uniaxial Tensile Behavior of Concrete Reinforced with Randomly Distributed Short Fibers. *ACI Materials Journa, 95*, 564-574.

Li., H. S. (2004). Classification of Fibre Reinforced Cementitious Materials for Structural Applications. 197-218.

Liao, W.-C., Chao, S.-H., Park, S.-Y., & Naaman, A. E. (2006). *Self-Consolidating High Performance Fiber Reinforced Concrete (SCHPFRC) - Preliminary Investigation.* Ann Arbor, USA: University of Michigan.

LÖFGREN, I. (2005). *Fibre-reinforced Concrete for Industrial Construction - a fracture mechanics approach to material testing and structural analysis "A PhD dissertation"*. Göteborg, Sweden: Chalmers University of Technology.

Mangat, P., & Motamedi Azari, M. (1985). Influence of Steel Fibre and Stirrup Reinforcement on the Properties of Concrete in Compression Members. *International Journal of Cement Composites and Lightweight Concrete, 7*(3), 183-192.

Mangat, P., & Swamy, R. (1974, September). Influence of fiber-aggregate interaction on some properties of steel fiber reinforced concrete. *Materials and Structures, 7*(5), 307-314.

Mindess, S., Chen, L., & Morgan, D. (1994, July). Determination of First-Crack Strength and Flexural Toughness of Steel Fiber-Reinforced Concrete. *Advanced Cement Based Materials, 1*(5), 201-208.

Minelli, F. (2005). *Plain and Fiber Reinforced Concrete Beams under Shear LoadingStructural Behavior and Design Aspects "A PhD dissertation".* Italy: University of Brescia.

Myers, D. S. (2006). *FIBER-REINFORCED CONCRETE AND BRIDGE DECK CRACKING 'A master thesis'.* Norman, Oklahoma: UNIVERSITY OF OKLAHOMA.

Naaman, A. (2003, November). Engineered Steel Fibers with Optimal Properties for Reinforcement of Cement Composites. *Journal of Advanced Concrete Technology, 1*, 241-252.

Naaman, A. E. (1985). Fiber Reinforcement for Concrete.

Naaman, A. E. (1998). New Fiber Technology. *Concrete International*, 57-62.

Naaman, A. E. (2003). *High Performance Fiber Reinforced Cement Composites.* Ann Arbor: University of Michigan.

Naaman, A. E. (2008). High-Performance Fiber Reinforced Cement Composites. *World Scientific*, 91-153.

Naaman, A. E., & Reinhardt, H. W. (1996). Characterization of High Performance Fiber Reinforced Cement Composites - HPFRCC. *International RILEM Workshop*.

Naaman, A. E., Alkhairi, F. M., & Hammoud, H. (1993). Mechanical Behavior of High Performance Concretes "High Early Strength Fiber Reinforced Concrete". *Strategic Highway Research Program "SHRP-C-366", 6*.

Naaman, A., & Chandrangsu, K. (2003). *Comparison of Tensile and Bending Response of Three High Performance Fiber Reinforced Composites," High Performance Fiber Reinforced Cement Composites.* Ann Arbor, Michigan: HPFRCC4 Workshop.

Naaman, A., & Reinhardt, H. (1995). High Performance Fiber Reinforced Cement Composites. *The Second International RILEM Workshop*, 2, 95, 172, 293, 430.

Naaman, A., & Reinhardt, H. (2005). Proposed classification of HPFRC composites based on their tensile response. *Material and Structures*, 1-13.

Naaman, A., Otter, D., & Najm, H. (1991, Nov). Elastic Modulus of SIFCON in Tension and Compression. *ACI Materials Journal, 88*, 603-612.

Narayanan, R., & Kareem-Palanjian, A. (1982). Factors influencing the workability of steel-fibre reinforced concrete. *16*.

Otter, D. E., & Naaman, A. E. (1988, Jul-Aug). Properties of Steel Fiber Reinforced. *ACI Materials Journal, 85*, 254-261.

Park, S., Lee, B., & Lim, Y. (1995). *Characterization of interfacial behavior.* he Second International RILEM Workshop.

Parra-Montesinos, G. J. (2005, September-October). High-Performance Fiber-Reinforced Cement Composites: An Alternative for Seismic Design of Structures. *ACI STRUCTURAL JOURNAL, 102*, 668-675.

Parra-Montesinos, G., & Chompreda, P. (2007). Deformation Capacity and Shear Strength of Fiber-Reinforced Cement Composite Flexural Members Subjected to Displacement Reversals. *Journal of Structural Engineering*, 421–431.

Parra-Montesinos, G., & Kim, K. (2004). Seismic Behavior of Low-Rise Walls Constructed With Strain-Hardening Fiber Reinforced Cement Composites. In Proceedings of the 13th world conference on earthquake engineering. Vancouver, B.C., Canada.

Parra-Montesinos, G., Peterfreund, S., & Chao., S. (2005). Highly Damage- Tolerant Beam–Column Joints Through Use of High-Performance Fiber- Reinforced Cement Composites. *ACI Structural Journal*, 487–495.

Ramakrishnan, V., Brandshaug, T., Coyle, W., & Schrader, E. K. (1980, May 1). A comparative Evaluation of Concrete Reinforced with Straight Steel Fibers and Fibers with Deformed Ends Glued Together into Bundles. *ACI Journal Proceeding, 77*(3), 135-143.

Ramseyer, C. (1999). *Investigation of Very Early Strength Concrete with Low Shrinkage Properties.* Norman, Oklahoma: University of Oklahoma Press.

Ritchie, A., & Rahman, T. (1973). The Effect of Fiber Reinforcements on the Rheological Properties of Concrete Mixes. *American Concrete Institute*, 29-44.

Ross, A. (2008). *Steel fibre reinforced concrete (SFRC) – Quality, performance and specification.* BOSFA (Bekaert OneSteel Fibres Australasia).

S., M. (1995, March 26-29). Fiber Reinforced Concrete: Challenges and Prospects. (M. Banthia N., Ed.)

Sahmaran, M., & Yaman, I. O. (2007, Jan). Hybrid fiber reinforced selfcompacting concrete with a high-volume coarse fly ash. *Construction and Building Materials 21.1*, 150-156.

Sahmaran, M., Yurtseven, A., & Yaman, I. O. (2005). Workability of hybrid fiber reinforced self-compacting concrete. *Building and Environment 40*, 1672–1677.

Setkit, M. (2012). *SEISMIC BEHAVIOR OF SLENDER COUPLING BEAMS CONSTRUCTED WITH HIGH-PERFORMANCE FIBER-REINFORCED CONCRETE A dissertation of Phd.* Michigan.

Soroushian, P., Khan, A., & Hsu, J.-W. (1992, November). Mechanical Properties of Concrete Materials Reinforced with Polypropylene or Polyethylene Fibers. *ACI Materials Journal, 89*, 535- 540.

Sounthararajan, A. S. (2013, March). Toughness characterization of steel fibre reinforced concrete – A review on various international standards. *Journal of Civil Engineering and Construction Technology, 4*(3), 65-69.

T.Mastsumoto, & Mihashi, H. (2002). Ductile Fiber Reinforced Cementitious Composites– Application and Evaluation. *JCI-DFRCC*, 59-66.

Trub, M. (2011). *Numerical Modeling of High Performance Fiber Reinforced Cementitious Composites.* Institute of Structural Engineering Swiss Federal Institute of Technology.

Vandewalle, L. (1993). Vezelversterkt Beton, Studiedag Speciale Betonsoorten en Toepassingen. *Universiteit Leuven, Departement Burgerlijke Bouwkunde*, 77-98.

Vondran, G. L. (1991, November). Applecation of Steel Fiber Reinforcred Concrete. *Concrete International*, 44-49.

Wafa, F., & Ashour, S. (1992, Dec). Mechanical Properties of High-Strength Fiber Reinforced Concrete. *ACI Materials Journal, 89*(6), 541-546.

Wight, J. K., & MacGregor, J. G. (2009). *Reinforced Concrete: Mechanics and Design* (6th ed.). Upper Saddle River: Pearson.

Wikipedia. (2009). *Fiber-reinforced concrete*. Retrieved from Wikipedia: http://en.wikipedia.org/wiki/Fiber-reinforced_concrete

Wikipedia. (2011). *High-performance fiber-reinforced cementitious composites*. Retrieved from Wikipedia: http://en.wikipedia.org/wiki/High-performance_fiber-reinforced_cementitious_composites

Williamson, G. R. (1974). "The Effect of Steel Fibers on the Compressive Strength of Concrete. *American Concrete Institute*, 195-207.

XIA, J. (2011). *ULTRA-HIGH PERFORMANCE FIBER REINFORCED CONCRETE IN BRIDGE DECK APPLICATIONS "A PhD dissertation".* Orlando, Florida: University of Central Florida.

Yang, I.-H., Joh, C., & Kim, B.-S. (2011). Shear behaviour of ultra-highperformance fibre-reinforced concrete beams without stirrups. *ICE-Magazine of Concrete Research, 11*, 979–993.

Yu, R., Spiesz, P., & Brouwers, H. (2013). Mix design and properties assessment of Ultra-High Performance Fibre Reinforced Concrete (UHPFRC). *ELSEVIER*.

Yurtseven, A. E. (2004). *DETERMINATION OF MECHANICAL PROPERTIES OF HYBRID FIBER REINFORCED CONCRETE " Master thesis"*. MIDDLE EAST TECHNICAL UNIVERSITY.

Zollo, R. (1985). An Overview of Progress in Applications of Steel Fibre Reinforced Concrete. *Swedish Cement and Concrete Research Institute*, 171-84.

Appendix A – Summary of Measured Fresh-State Concrete Properties

This appendix reports the measured properties of self-consolidating fiber reinforced concrete (SCFRC) in the fresh-state. Concrete temperature, density (ASTM C138) and air content (ASTM C231) are reported first (Table A.1). The results of the slump flow (ASTM C1611), Visual Stability Index (VSI), T_{50}, and J-ring slump flow tests (ASTM C1621) are then presented in this appendix (Table A.2).

Table A.1 – Temperature, density and air content of each mixture.

Batch ID	Fiber type	V_f (%)	Temperature (°F)	Density (lbf/ft^3)	Air content (%)
C 1	N/A	0	75	139.0	1.0
B 1	(RC-80/30-BP)	0.5	68	139.8	1.2
B 2	(RC-80/30-BP)	0.75	71	142.4	1.1
B 3	(RC-80/30-BP)	1.0	80	141.8	1.8
B 4	(RC-80/30-BP)	1.5	72	140.6	3.9
B 5	3D (RC-55/30-BG)	0.5	76	141.0	1.3
B 6	3D (RC-55/30-BG)	0.75	82	141.0	1.1
B 7	3D (RC-55/30-BG)	1.0	78	141.8	1.3
B 8	3D (RC-55/30-BG)	1.5	78	141.4	1.2
B 9	4D (RC-65/60-BG)	0.5	76	140.1	1.1
B 10	4D (RC-65/60-BG)	0.75	77	140.8	1.6
B 11	4D (RC-65/60-BG)	1.0	80	143.2	2.3
B 12	4D (RC-65/60-BG)	1.5	89	144.4	1.3
B 13	5D (RC-65/60-BG)	0.75	84	144.1	1.2
B 14	5D (RC-65/60-BG)	1.5	76	144.8	1.3
C 2	N/A	0	71	145.4	1.7
B 15	(RC-80/30-BP)	0.5	74	148.0	1.7
B 16	(RC-80/30-BP)	0.75	76	147.6	1.9
B 17	(RC-80/30-BP)	1.0	70	148.8	2.0
B 18	(RC-80/30-BP)	1.5	68	150.4	2.3
B 19	4D (RC-65/60-BG)	0.75	78	150.0	1.5
B 20	4D (RC-65/60-BG)	1.5	58	150.2	2.8
B 21	5D (RC-65/60-BG)	0.75	46	147.6	2.0
B 22	5D (RC-65/60-BG)	1.5	52	151.2	2.8

Table A.2 – Slump flow, VSI, T_{50}, and J-ring slump flow test results.

Batch ID	Fiber type	V_f (%)	Slump flow (in.)	J-ring slump flow (in.)	Passing Ability (in.)	VSI	T_{50} (sec.)
C 1	N/A	0	27.5	27.0	0.5	1	0.7
B 1	(RC-80/30-BP)	0.5	25.5	25.0	0.5	1	0.8
B 2	(RC-80/30-BP)	0.75	24.0	21.0	3.0	0	0.9
B 3	(RC-80/30-BP)	1	23.0	17.5	5.5	1	1.0
B 4	(RC-80/30-BP)	1.5	22.5	16.5	6.0	0	1.0
B 5	3D (RC-55/30-BG)	0.5	25.0	24.0	1.0	1	0.8
B 6	3D (RC-55/30-BG)	0.75	24.0	23.5	0.5	1	0.6
B 7	3D (RC-55/30-BG)	1	25.0	22.5	2.5	2	0.7
B 8	3D (RC-55/30-BG)	1.5	23.0	17.5	5.5	1	0.9
B 9	4D (RC-65/60-BG)	0.5	25.0	22.0	3.0	1	0.9
B 10	4D (RC-65/60-BG)	0.75	25.0	19.5	5.5	1	0.7
B 11	4D (RC-65/60-BG)	1	23.0	18.5	4.5	1	0.8
B 12	4D (RC-65/60-BG)	1.5	21.0	15.0	6.0	0	0.9
B 13	5D (RC-65/60-BG)	0.75	22.0	17.0	5.0	1	0.8
B 14	5D (RC-65/60-BG)	1.5	20.0	14.5	5.5	0	0.8
C 2	N/A	0	28.5	27.5	1.0	1	2.2
B 15	(RC-80/30-BP)	0.5	27.0	26.0	1.0	1	2.3
B 16	(RC-80/30-BP)	0.75	30.5	26.0	4.5	2	1.9
B 17	(RC-80/30-BP)	1	26.0	22.0	4.0	1	2.6
B 18	(RC-80/30-BP)	1.5	22.5	20.0	2.5	0	3.2
B 19	4D (RC-65/60-BG)	0.75	29.5	25.0	4.5	1	2.0
B 20	4D (RC-65/60-BG)	1.5	23.5	22.0	1.5	0	3.4
B 21	5D (RC-65/60-BG)	0.75	28.5	25.0	3.5	1	2.1
B 22	5D (RC-65/60-BG)	1.5	27.0	23.0	4.0	2	1.7

Figures A.1, A.2, A.3, A.4, A.5, and A.6 show the slump flow of control batch 1 (6 ksi reference batch), control batch 2 (10 ksi reference batch), batch 4 (6 ksi and V_f = 1.5% of RC-80/30-BP), batch 8 (6 ksi and V_f = 1.5% of 3D RC-55/30-BG), batch 12 (6 ksi and V_f = 1.5% of 4D RC-65/60-BG), and batch 14 (6 ksi and V_f = 1.5% of 5D RC-65/60-BG) respectively. Figures A.7, A.8, A.9, A.10, A.11, and A.12 present the J-ring slump flow of control batch 1, control batch 2, batch 4, batch 8, batch 12, and batch 14 respectively.

Figure A.1 – Slump flow of control batch 1 (6 ksi reference batch).

Figure A.2 – Slump flow of control batch 2 (10 ksi reference batch).

Figure A.3 – Slump flow of batch 4 (6 ksi and V_f = 1.5% of RC-80/30-BP).

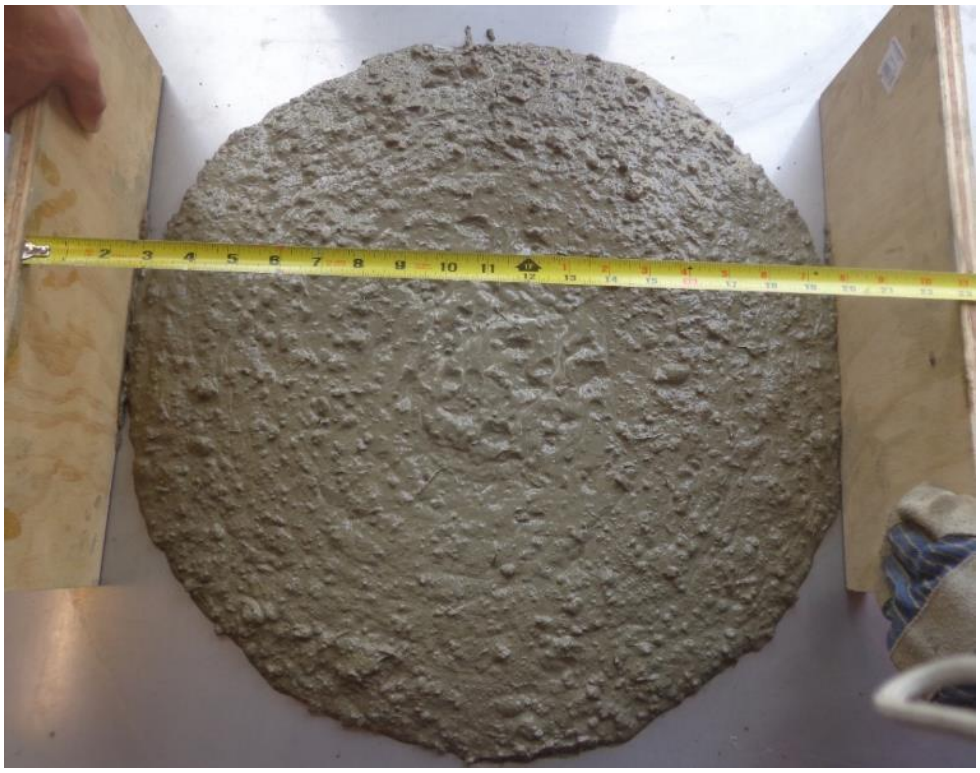

Figure A.4 – Slump flow of batch 8 (6 ksi and V_f = 1.5% of 3D RC-55/30-BG).

Figure A.5 – Slump flow of batch 12 (6 ksi and V_f = 1.5% of 4D RC-65/60-BG).

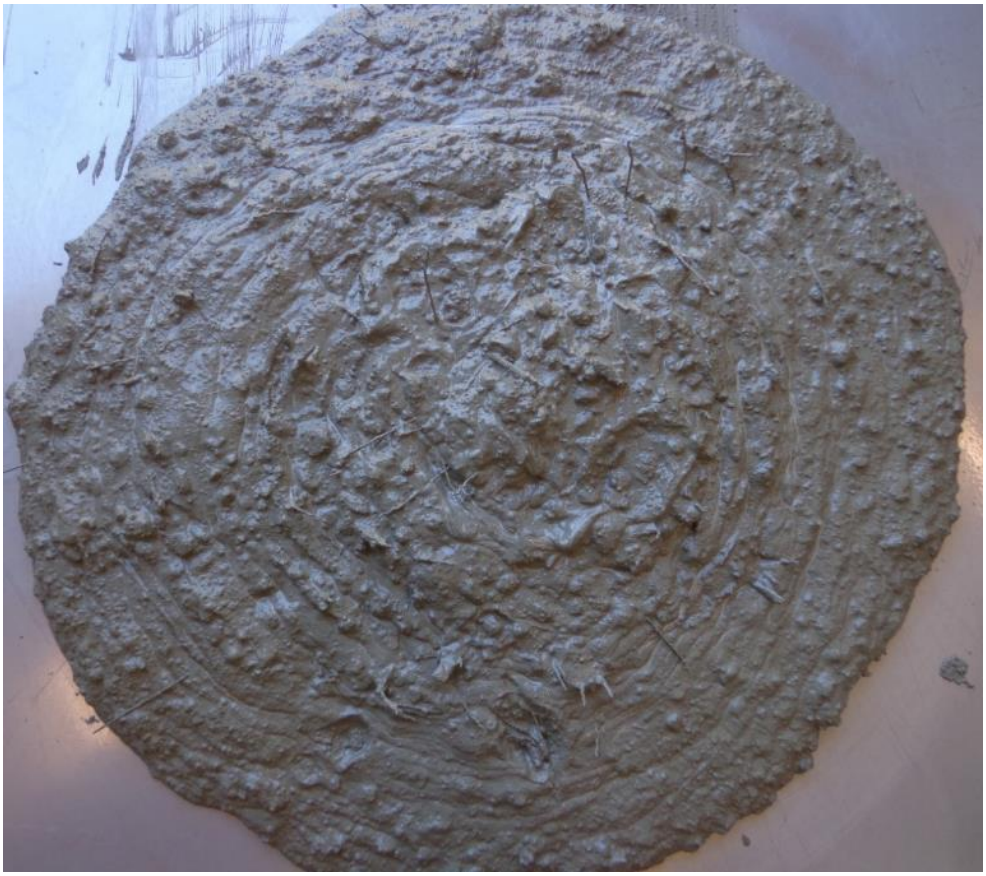

Figure A.6 – Slump flow of batch 14 (6 ksi and V_f = 1.5% of 5D RC-65/60-BG).

Figure A.7 – J-ring slump flow of control batch 1 (6 ksi reference batch).

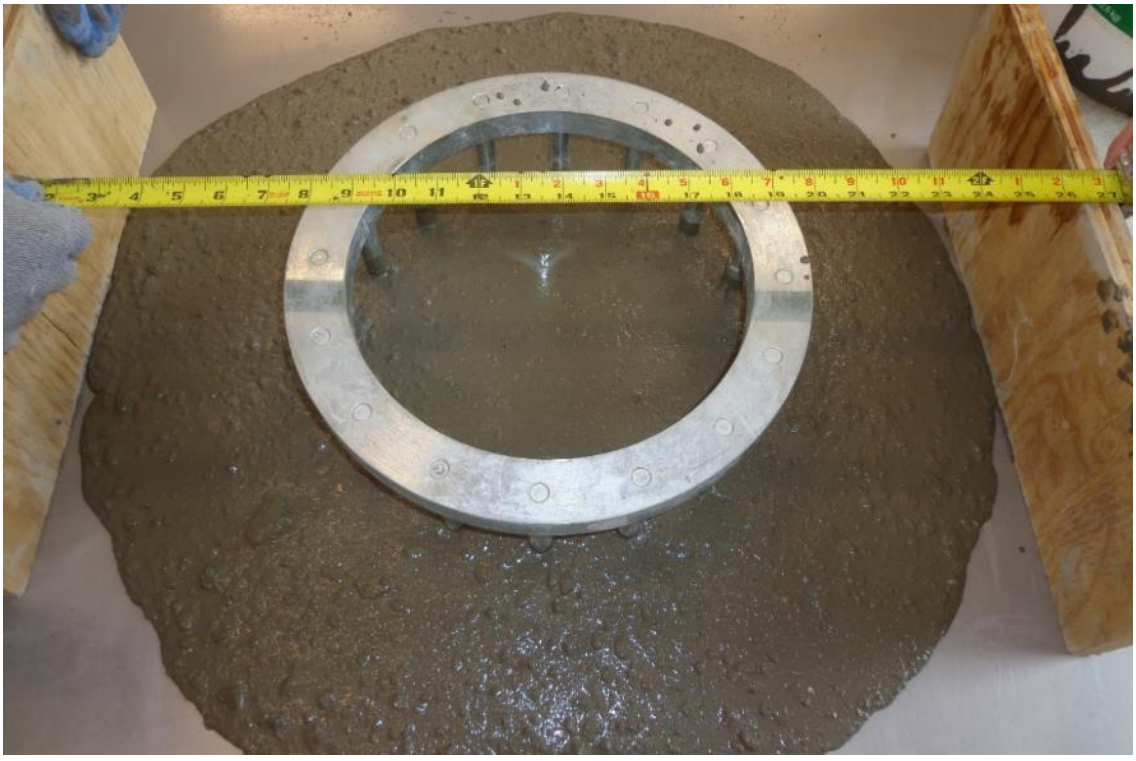

Figure A.8 – J-ring slump flow of control batch 2 (10 ksi reference batch).

Figure A.9 – J-ring slump flow of batch 4 (6 ksi and V_f = 1.5% of RC-80/30-BP).

Figure A.10 – J-ring slump flow of batch 8 (6 ksi and V_f = 1.5% of 3D RC-55/30-BG).

Figure A.11 – J-ring slump flow of batch 12 (6 ksi and V_f = 1.5% of 4D RC-65/60-BG).

Figure A.12 – J-ring slump flow of batch 14 (6 ksi and V_f = 1.5% of 5D RC-65/60-BG).

Appendix B – Summary of the Compression Test Results

Results from compression tests (ASTM C39) are presented in this appendix. The mean concrete compression strength, modulus of elasticity, and post-peak slope, as well as the coefficient of variation within each batch, are summarized in Table B.1. Plots of concrete stress versus longitudinal strain and lateral strain are also given for each batch. For each specimen, strain was calculated using data from the position sensor and not the test frame. The reason for this is illustrated in Figure B.1, which shows the difference between results from the infrared-based non-contact position sensor and the test frame.

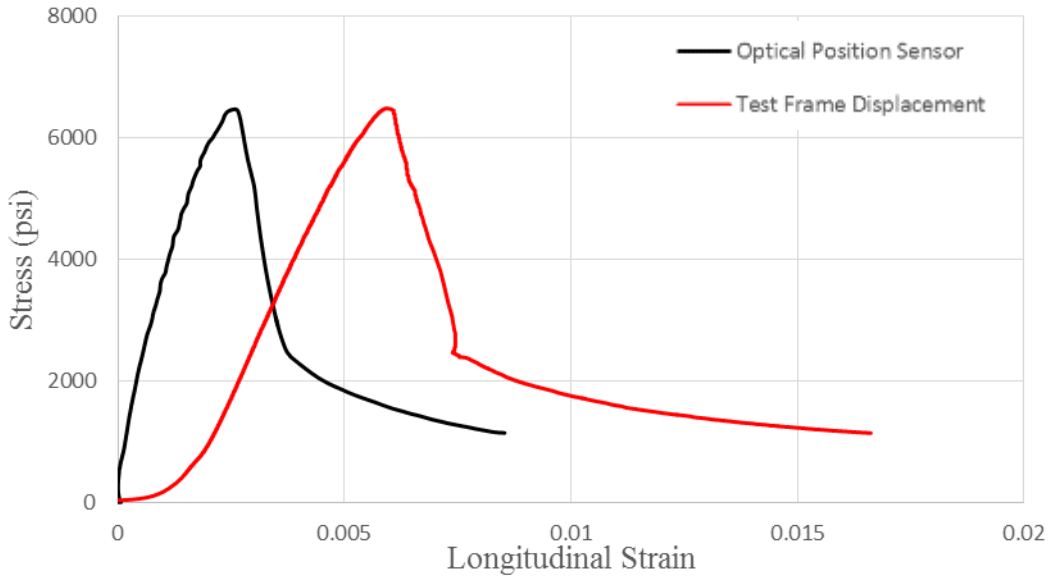

Figure B.1 – Stress vs. longitudinal strain, with strain calculated using data from the non-contact position sensor and test frame displacement.

Table B.1 – Compression test parameters.

Batch ID	Fiber type	V_f (%)	f_{cm} (psi)	COV (f_{cm})	$E_c \times 10^3$ (ksi)	COV (E_c)	E_{pp} (psi) × 10^6	COV (E_{pp})
C 1	N/A	0	5710	4.2%	3.69	12%	-6.18	18%
B 1	(RC-80/30-BP)	0.5	5490	4.7%	3.84	3%	-1.10	34%
B 2	(RC-80/30-BP)	0.75	6460	3.3%	4.14	16%	-1.56	9%
B 3	(RC-80/30-BP)	1.0	6340	3.3%	3.97	14%	-0.94	36%
B 4	(RC-80/30-BP)	1.5	5760	9.4%	4.00	33%	-0.38	48%
B 5	3D (RC-55/30-BG)	0.5	6370	3.7%	3.69	8%	-3.35	33%
B 6	3D (RC-55/30-BG)	0.75	5920	5.2%	4.45	18%	-2.94	37%
B 7	3D (RC-55/30-BG)	1.0	6140	4.0%	3.59	12%	-2.78	80%
B 8	3D (RC-55/30-BG)	1.5	5520	3.5%	4.99	12%	-3.23	23%
B 9	4D (RC-65/60-BG)	0.5	6200	4.0%	3.48	13%	-5.73	94%
B 10	4D (RC-65/60-BG)	0.75	6050	5.2%	4.43	12%	-2.77	47%
B 11	4D (RC-65/60-BG)	1.0	6650	1.3%	3.74	10%	-4.09	15%
B 12	4D (RC-65/60-BG)	1.5	6050	3.3%	3.31	7%	-1.81	34%
B 13	5D (RC-65/60-BG)	0.75	5770	8.8%	4.03	9%	-2.41	82%
B 14	5D (RC-65/60-BG)	1.5	5980	1.4%	4.08	11%	-0.50	90%
C 2	N/A	0	10480	3.6%	4.92	6%	-16.12	18%
B 15	(RC-80/30-BP)	0.5	9970	2.1%	4.80	4%	-3.85	38%
B 16	(RC-80/30-BP)	0.75	9910	1.0%	5.18	9%	-2.58	37%
B 17	(RC-80/30-BP)	1.0	10100	3.3%	4.78	5%	-1.86	54%
B 18	(RC-80/30-BP)	1.5	9490	4.6%	4.29	4%	-0.91	37%
B 19	4D (RC-65/60-BG)	0.75	10320	5.6%	5.14	7%	-8.47	91%
B 20	4D (RC-65/60-BG)	1.5	10240	2.8%	4.56	13%	-1.64	87%
B 21	5D (RC-65/60-BG)	0.75	9800	4.2%	4.87	8%	-3.88	69%
B 22	5D (RC-65/60-BG)	1.5	9450	2.9%	5.25	16%	-0.91	110 %

Batch **page**

Control 1: $f'_c = 6$ ksi

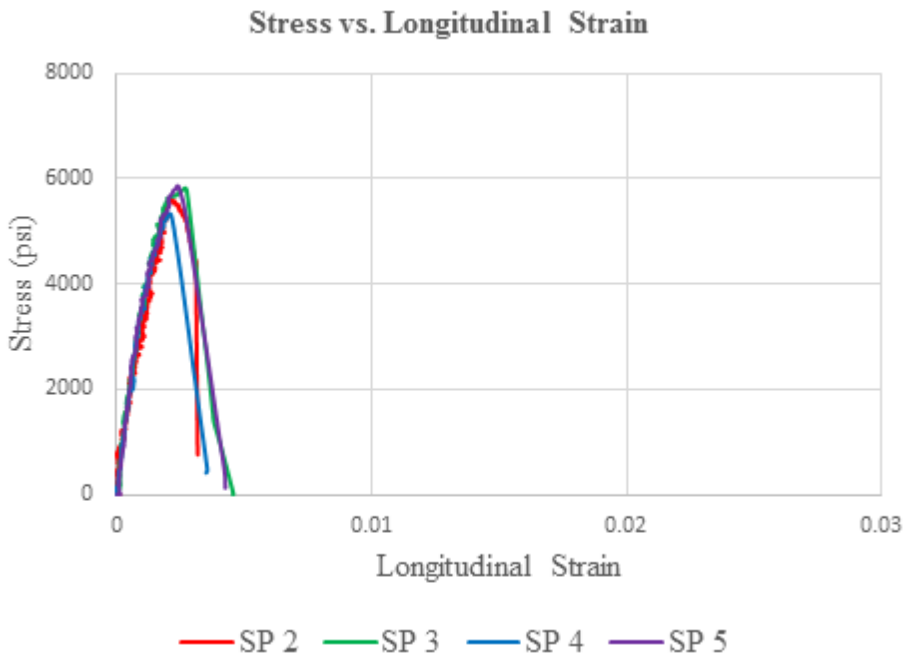

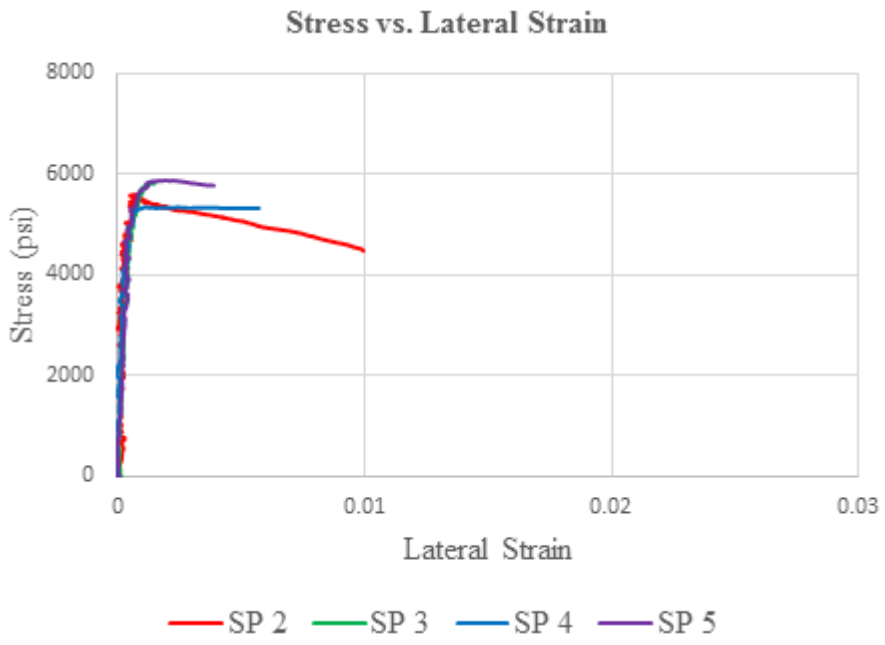

f_{cm} (psi)	$COV(f_{cm})$	$E_c \times 10^3$ (ksi)	$COV(E_c)$	$E_{pp} \times 10^6$ (psi)	$COV(E_{pp})$
5710	4.2%	3.69	12.2%	-6.18	17.7%
Comment: brittle failure, specimen 1 was not used in E_c and E_{pp} calculations.					

SP 1

Failure type: 3
Markers 3, 4, 5, 6, 7, 11, and 12 were dislodged after 1st crack.

SP 2

Failure type: 2
Markers 1, 2, 6, 7, 8, 12, and 13 were dislodged after 1st crack.

SP 3

Failure type: 4
Markers 2, 3, 10, 11, and 13 were dislodged after 1st crack.

SP 4

Failure type: 1
Markers 3, 4, 5, 6, 7, 8, 9, and 13 were dislodged after 1st crack.

SP 5

Failure type: 1
All markers, except for 1 and 11, were dislodged after 1st crack.

Batch 1: $f'_c = 6$ ksi; $V_f = 0.5\%$; Fiber: (RC-80/30-BP)

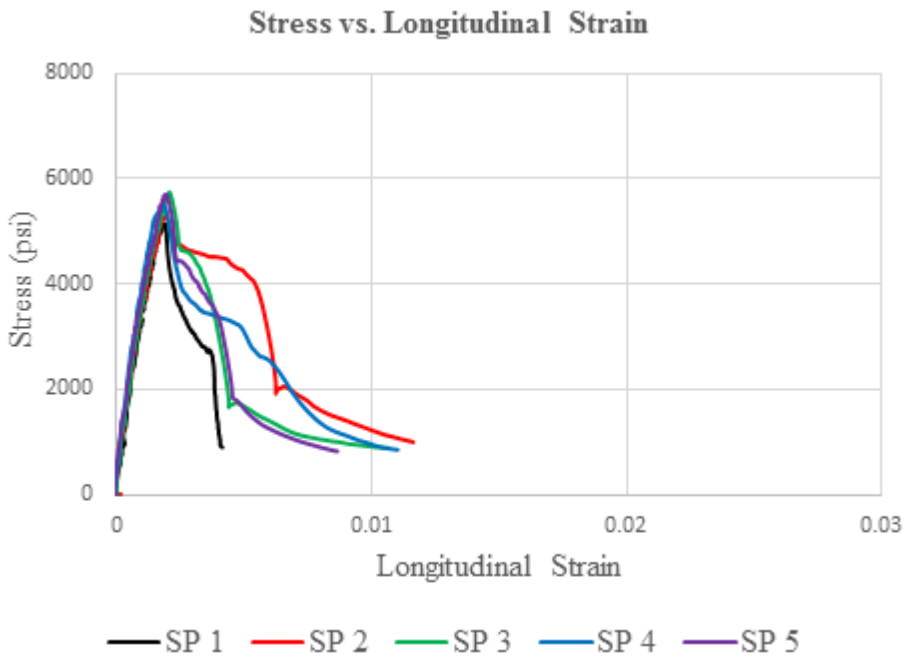

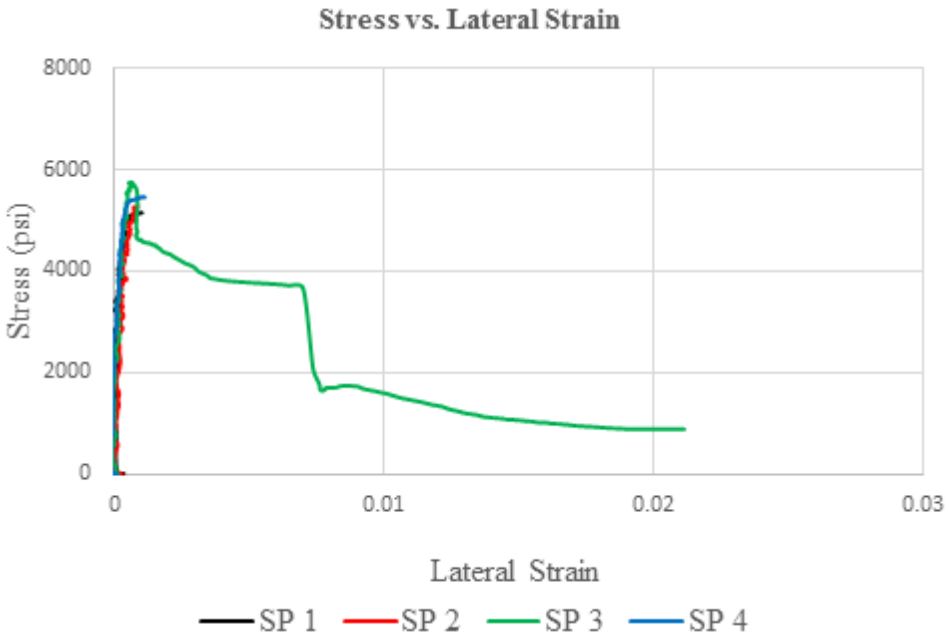

f_{cm} (psi)	$COV(f_{cm})$	$E_c \times 10^3$ (ksi)	$COV(E_c)$	$E_{pp} \times 10^6$ (psi)	$COV(E_{pp})$
5490	4.7%	3.84	3.1%	-1.10	33.9%
Comment: brittle failure.					

SP 1

Failure type: 1
Marker 5 was dislodged after 1st crack.

SP 2

Failure type: 2
Markers 3, 4, and 5 were dislodged after 1st crack.

SP 3

Failure type: 2
Markers 4 and 7 were dislodged after 1st crack.

SP 4

Failure type: 4 or 3
Markers 3 and 6 were dislodged after 1st crack.

SP 5

Failure type: 4 or 3
Markers 5 and 8 were dislodged after 1st crack.

Batch 2: $f`_c = 6$ ksi; $V_f = 0.75\%$; Fiber: (RC-80/30-BP)

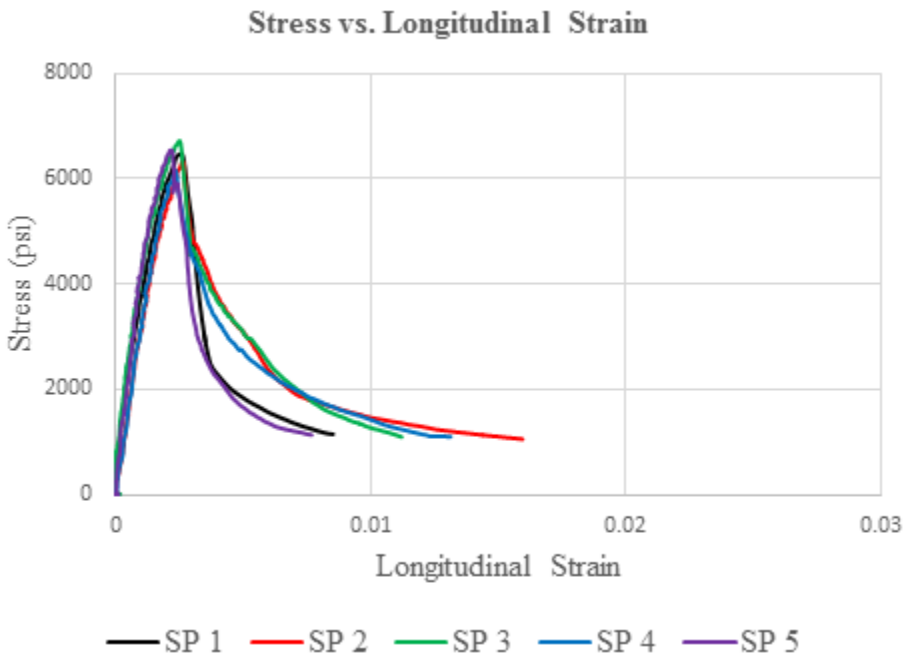

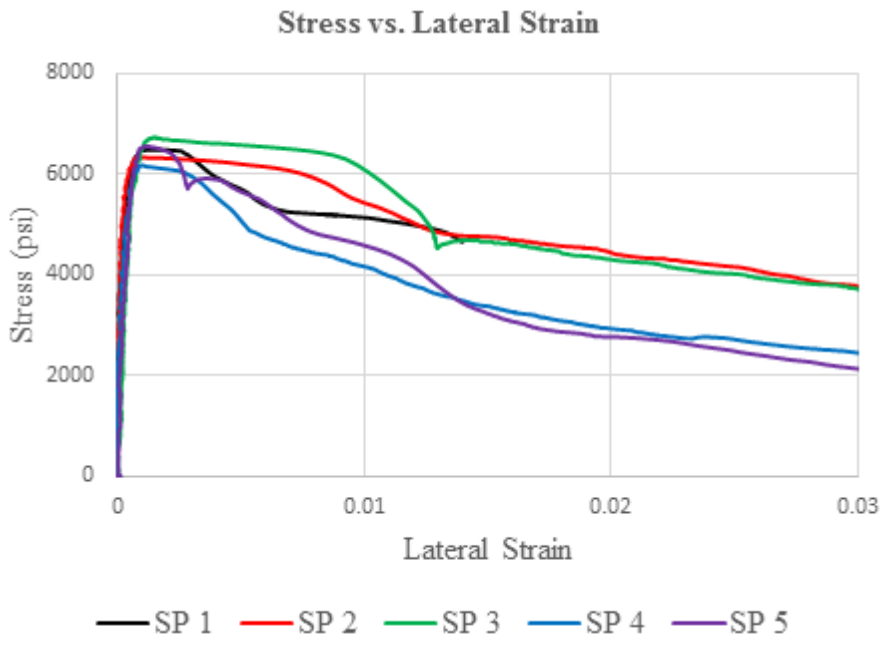

f_{cm} (psi)	$COV(f_{cm})$	$E_c \times 10^3$ (ksi)	$COV(E_c)$	$E_{pp} \times 10^6$ (psi)	$COV(E_{pp})$
6460	3.3%	4.14	15.6%	-1.56	8.9%
Comment: brittle failure, specimens 1 and 5 were not used in E_{pp} calculation.					

SP 1

Failure type: 2 or 4
Markers 9 and 11 were dislodged after 1st crack.

SP 2

Failure type: 2
Markers 5, 6, 7, and 13 were dislodged after 1st crack.

SP 3

Failure type: 3
Marker 10 was dislodged after 1st crack.

SP 4

Failure type: 3
Markers 4, 6, and 13 were dislodged after 1st crack.

SP 5

Failure type: 5
Markers 3, 10, and 12 were dislodged after 1st crack.

Batch 3: $f'_c = 6$ ksi; $V_f = 1.0\%$; Fiber: (RC-80/30-BP)

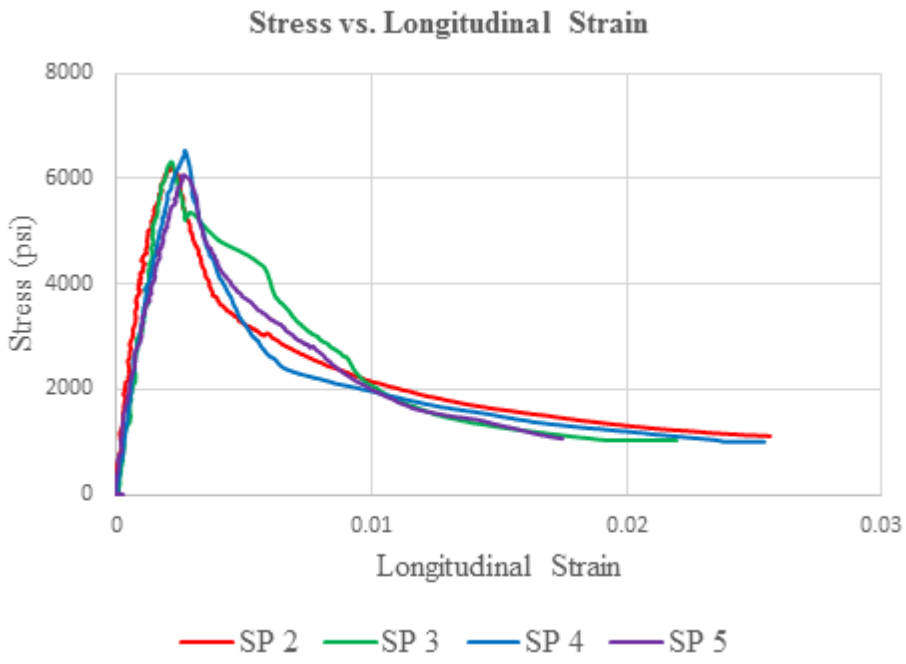

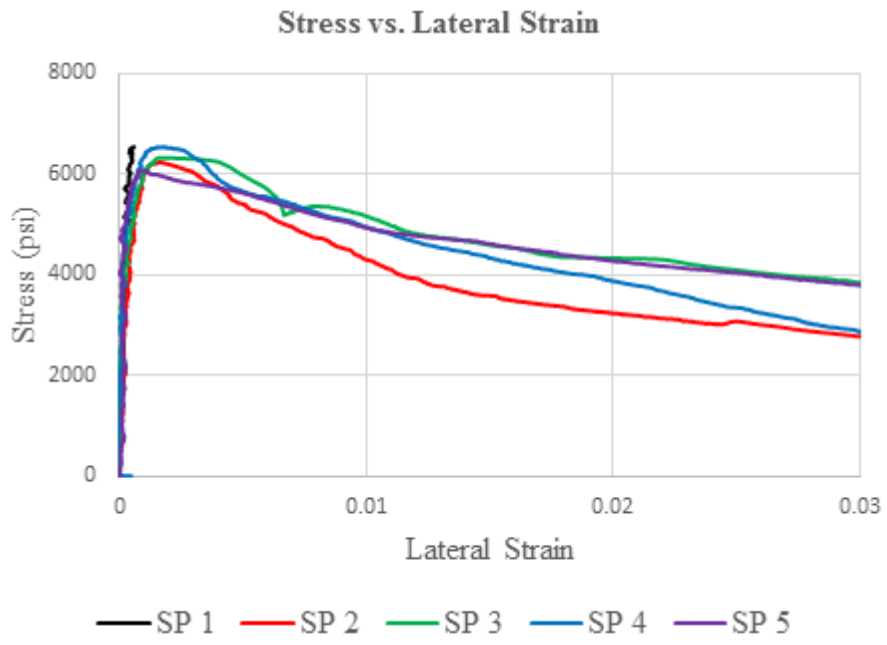

f_{cm} (psi)	$COV(f_{cm})$	$E_c \times 10^3$ (ksi)	$COV(E_c)$	$E_{pp} \times 10^6$ (psi)	$COV(E_{pp})$
6340	3.3%	3.97	14.3%	-0.94	35.9%
Comment: specimen 1 was not used in E_c and E_{pp} calculations.					

SP 1

Failure type: 3
Markers 3, 4, 6, and 12 were dislodged after 1st crack.

SP 2

Failure type: 3
Markers 1, 3, 8, 11, and 12 were dislodged after 1st crack.

SP 3

Failure type: 3

SP 4

Failure type: 2
Markers 3, 4, 6, 13, and 14 were dislodged after 1st crack.

SP 5

Failure type: 3
Markers 3 and 12 were dislodged after 1st crack.

Batch 4: $f'_c = 6$ ksi; $V_f = 1.5\%$; Fiber: (RC-80/30-BP)

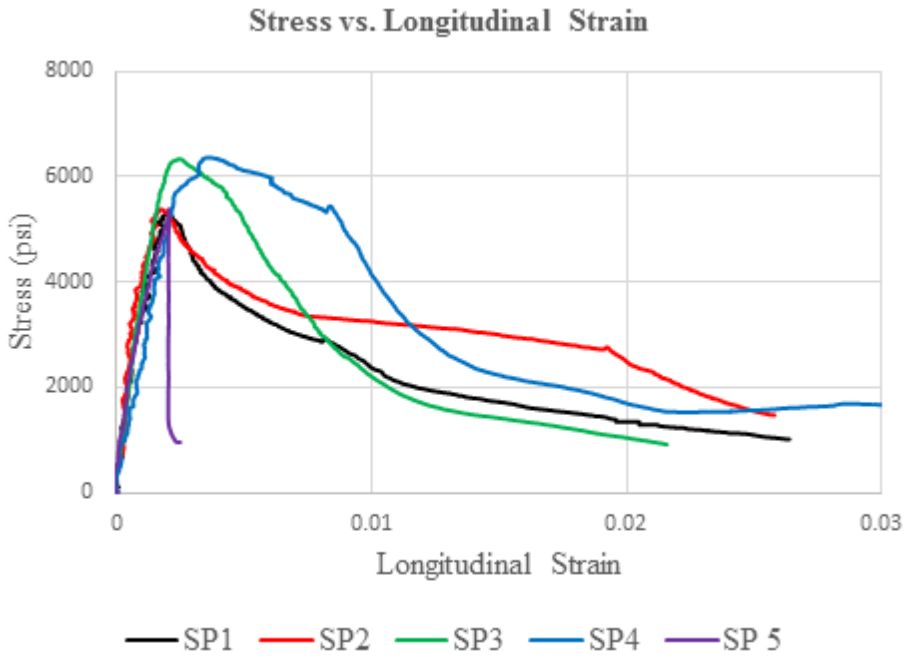

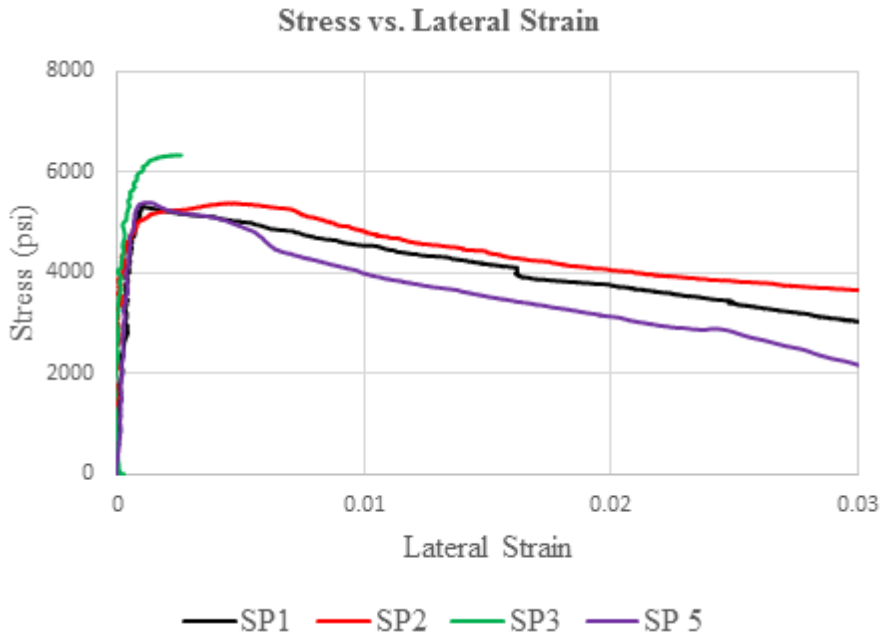

f_{cm} (psi)	$COV(f_{cm})$	$E_c \times 10^3$ (ksi)	$COV(E_c)$	$E_{pp} \times 10^6$ (psi)	$COV(E_{pp})$
5760	9.4%	4.00	33.4%	-0.38	48.0%
Comment: specimen 5 was not used in E_{pp} calculation.					

SP 1

Failure type: 3
Marker 4 was dislodged after 1st crack.

SP 2

Failure type: 2
Markers 5, 7, 10, and 13 were dislodged after 1st crack.

SP 3

Failure type: 4
Markers 4, 6, 7, and 9 were dislodged after 1st crack.

SP 4

Failure type: 4 or 3
Markers 5, 6, and 9 were dislodged after 1st crack.

SP 5

Failure type: 3
Marker 11 was dislodged after 1st crack.

Batch 5: $f'_c = 6$ ksi; $V_f = 0.5\%$; Fiber: 3D (RC-55/30-BG)

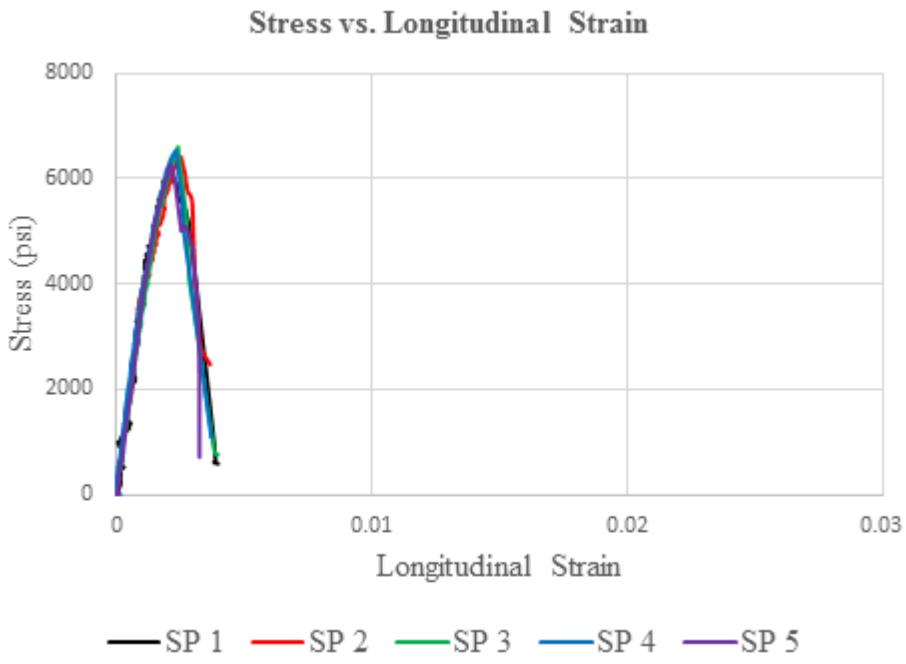

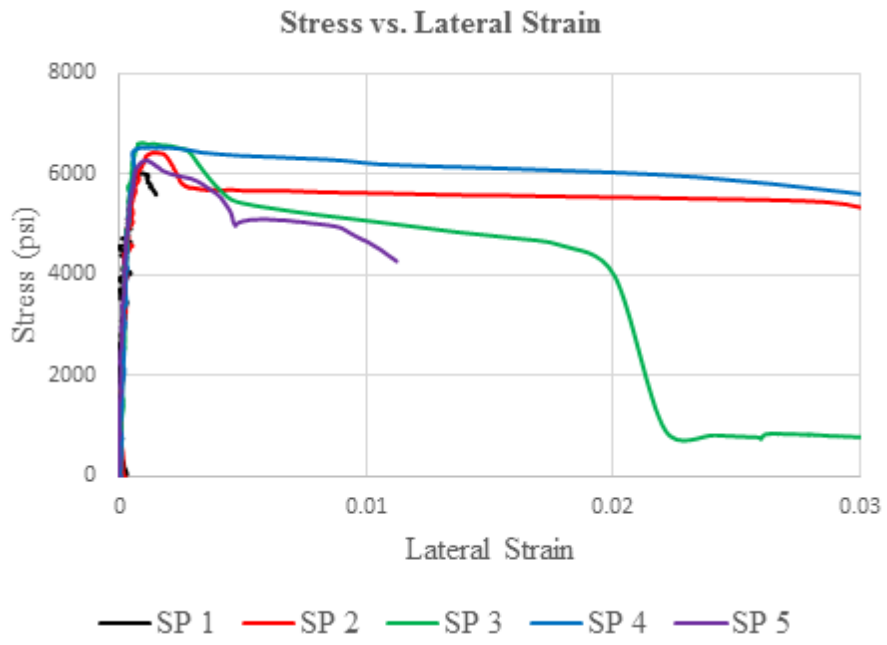

f_{cm} (psi)	$COV(f_{cm})$	$E_c \times 10^3$ (ksi)	$COV(E_c)$	$E_{pp} \times 10^6$ (psi)	$COV(E_{pp})$
6370	3.7%	3.69	8.4%	-3.35	32.8%
Comment: brittle failure, bundles of fiber.					

SP 1

Failure type: 3
Markers 4 and 11 were dislodged after 1st crack.

SP 2

Failure type: 2
Marker 4 was dislodged after 1st crack.

SP 3

Failure type: 3
Marker 11 was dislodged after 1st crack.

SP 4

Failure type: 3
Markers 3, 5, 6, 7, and 11 were dislodged after 1st crack.

SP 5

Failure type: 1
Marker 4 was dislodged after 1st crack.

Batch 6: $f`_c = 6$ ksi; $V_f = 0.75\%$; Fiber: 3D (RC-55/30-BG)

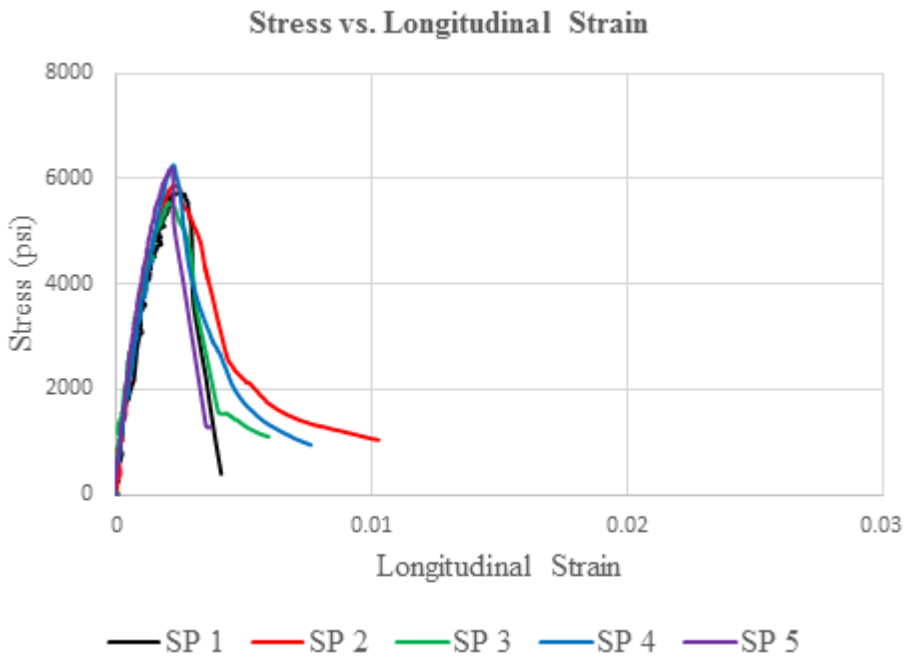

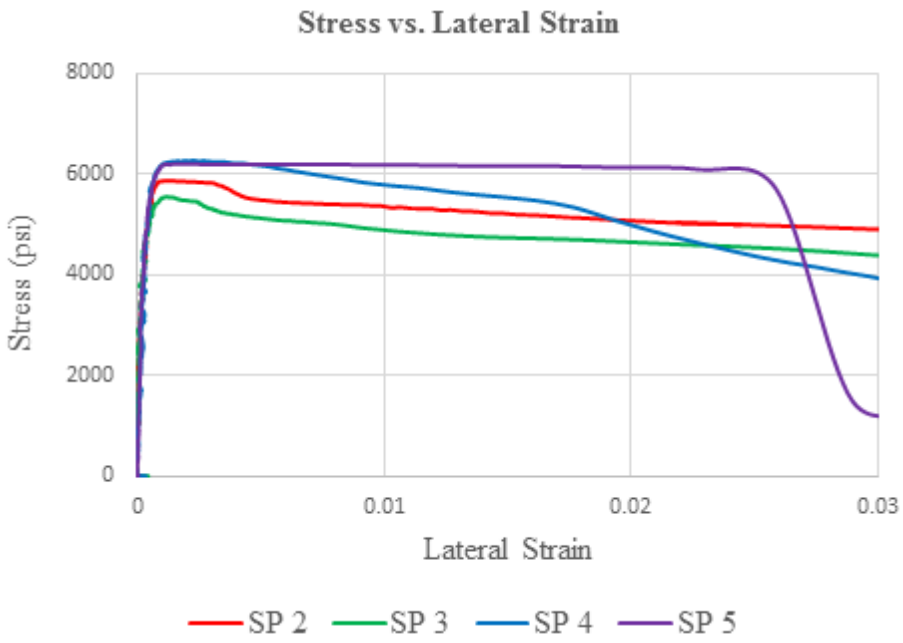

f_{cm} (psi)	$COV(f_{cm})$	$E_c \times 10^3$ (ksi)	$COV(E_c)$	$E_{pp} \times 10^6$ (psi)	$COV(E_{pp})$
5920	5.2%	4.45	18.1%	-2.94	37.1%
Comment: brittle failure, bundles of fiber, specimen 2 was not used in E_{pp} calculation.					

SP 1

Failure type: 1
Markers 4, 6, and 13 were dislodged after 1st crack.

SP 2

Failure type: 2
Markers 6 and 14 were dislodged after 1st crack.

SP 3

Failure type: 3

SP 4

Failure type: 3
Marker 12 was dislodged after 1st crack.

SP 5

Failure type: 3
Markers 1 and 9 were dislodged after 1st crack.

Batch 7: $f'_c = 6$ ksi; $V_f = 1.0\%$; Fiber: 3D (RC-55/30-BG)

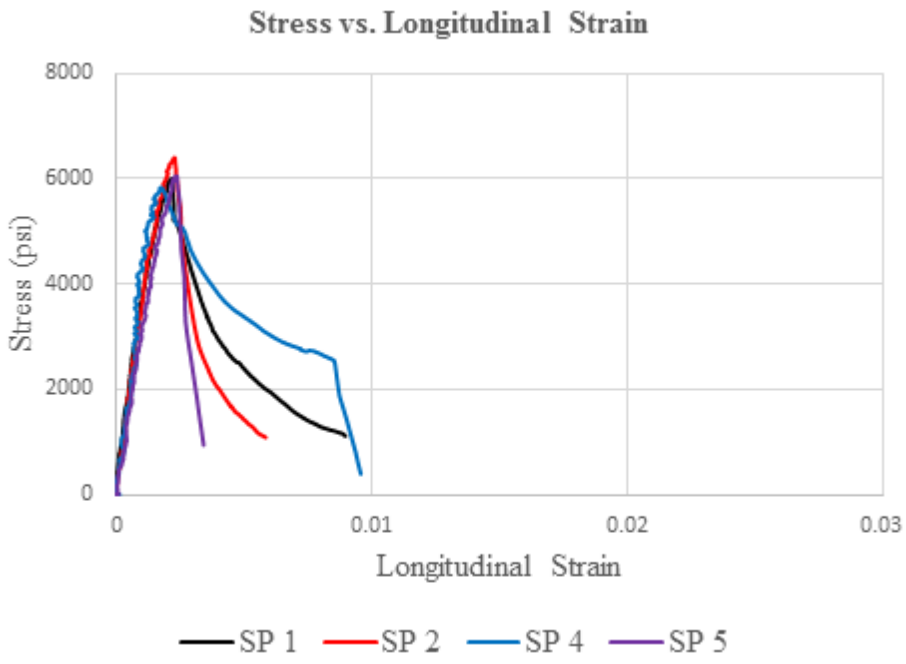

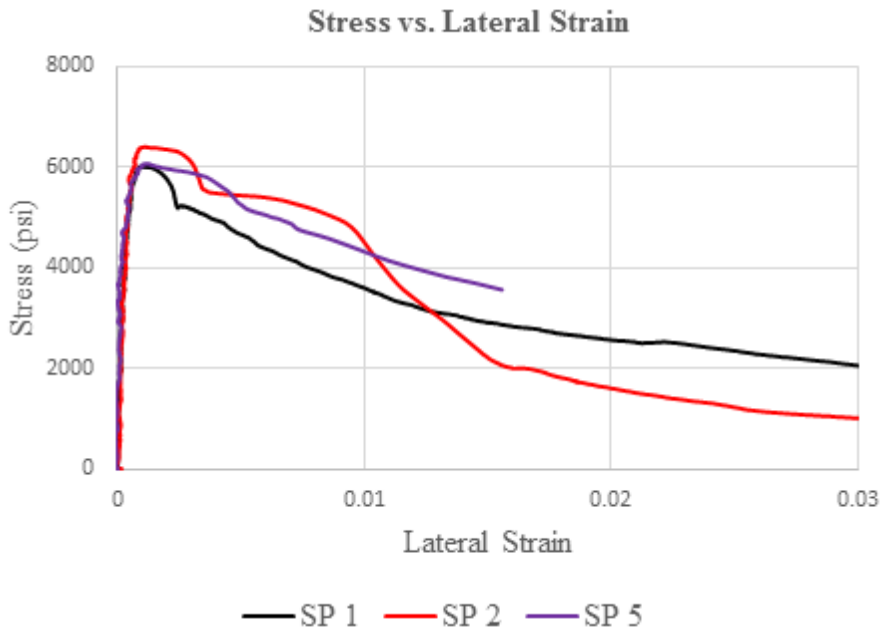

f_{cm} (psi)	$COV(f_{cm})$	$E_c \times 10^3$ (ksi)	$COV(E_c)$	$E_{pp} \times 10^6$ (psi)	$COV(E_{pp})$
6140	4.0%	3.59	11.8%	-2.78	80.3%
Comment: bundles of fiber, specimen 3 was not used in E_c and E_{pp} calculations.					

SP 1

Failure type: 3 or 4
Marker 13 was dislodged after 1st crack.

SP 2

Failure type: 2

SP 3

Failure type: 4

SP 4

Failure type: 1
Markers 5 and 6 were dislodged after 1st crack.

SP 5

Failure type: 3
Marker 7 was dislodged after 1st crack.

Batch 8: $f'_c = 6$ ksi; $V_f = 1.5\%$; Fiber: 3D (RC-55/30-BG)

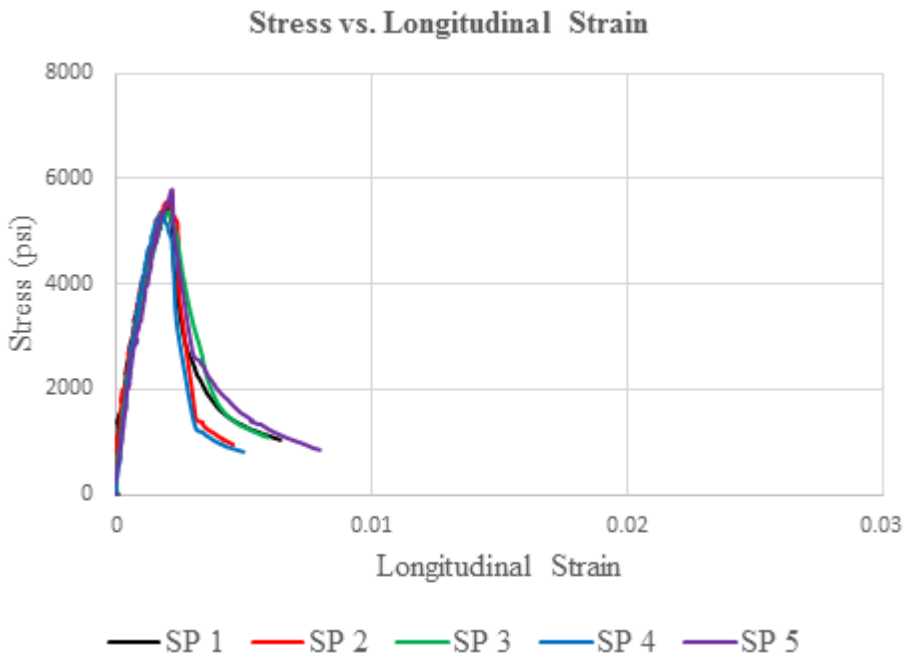

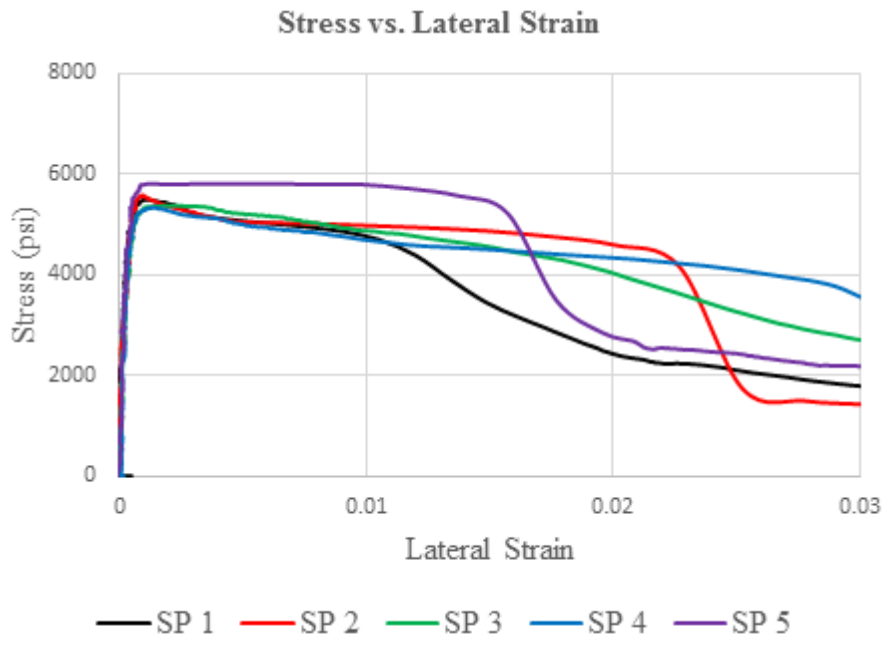

f_{cm} (psi)	$COV(f_{cm})$	$E_c \times 10^3$ (ksi)	$COV(E_c)$	$E_{pp} \times 10^6$ (psi)	$COV(E_{pp})$
5520	3.5%	4.99	12.5%	-3.23	22.8%
Comment: brittle failure, bundles of fiber.					

SP 1

Failure type: 3
Marker 12 was dislodged after 1st crack.

SP 2

Failure type: 3
Markers 6 and 14 were dislodged after 1st crack.

SP 3

Failure type: 3

SP 4

Failure type: 3
Marker 7 was dislodged after 1st crack.

SP 5

Failure type: 2

Batch 9: $f'_c = 6$ ksi; $V_f = 0.5\%$; Fiber: 4D (RC-65/60-BG)

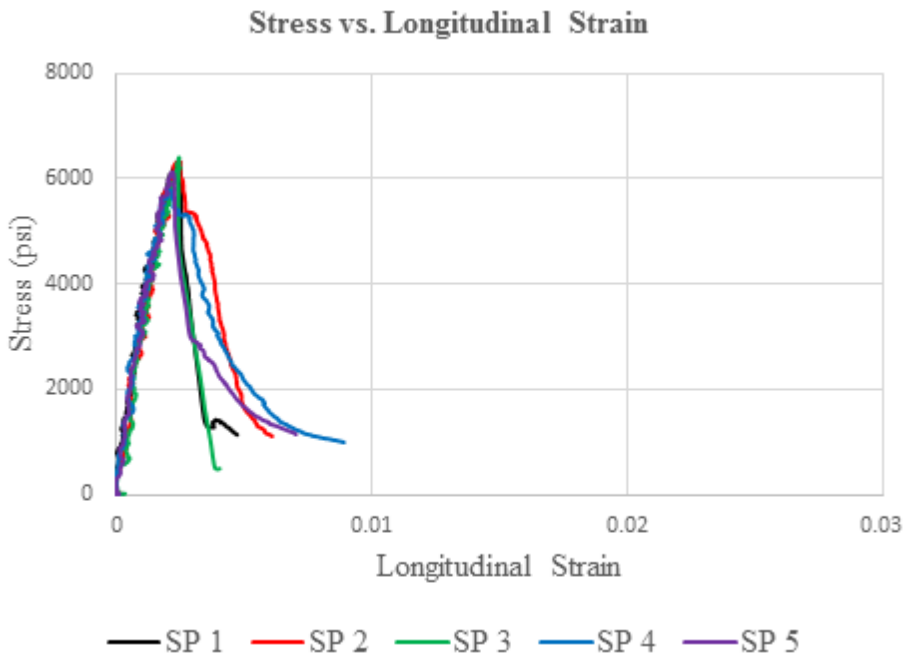

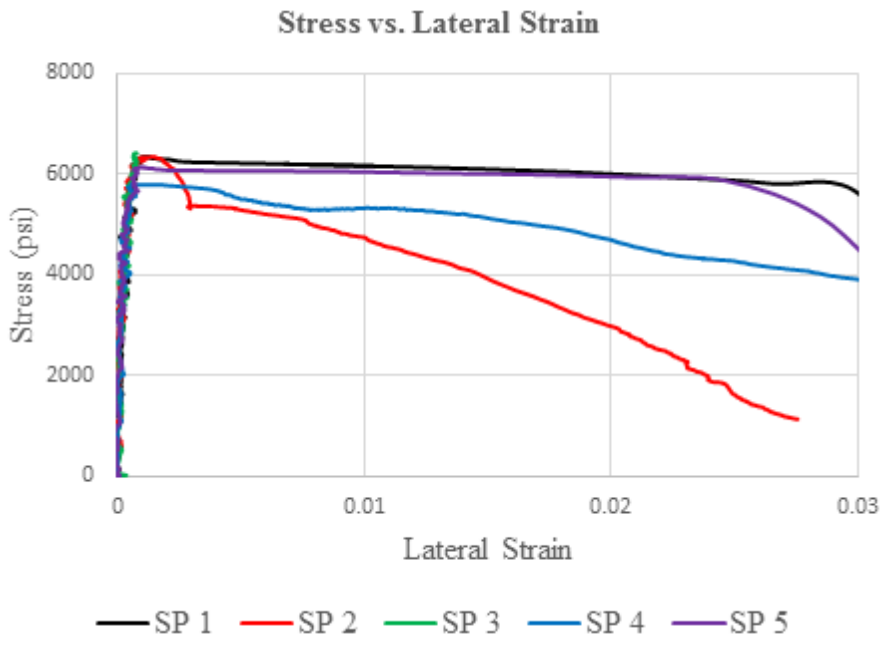

f_{cm} (psi)	$COV(f_{cm})$	$E_c \times 10^3$ (ksi)	$COV(E_c)$	$E_{pp} \times 10^6$ (psi)	$COV(E_{pp})$
6200	4.0%	3.48	13.2%	-5.73	94.0%
Comment: brittle failure, bundles of fiber.					

SP 1

Failure type: 1

SP 2

Failure type: 3
Markers 3 and 4 were dislodged after 1st crack.

SP 3

Failure type: 2
Markers 3, 5, 11, and 12 were dislodged after 1st crack.

SP 4

Failure type: 2

SP 5

Failure type: 3
Markers 5, 6, 8, 13, and 14 were dislodged after 1st crack.

Batch 10: $f'_c = 6$ ksi; $V_f = 0.75\%$; Fiber: 4D (RC-65/60-BG)

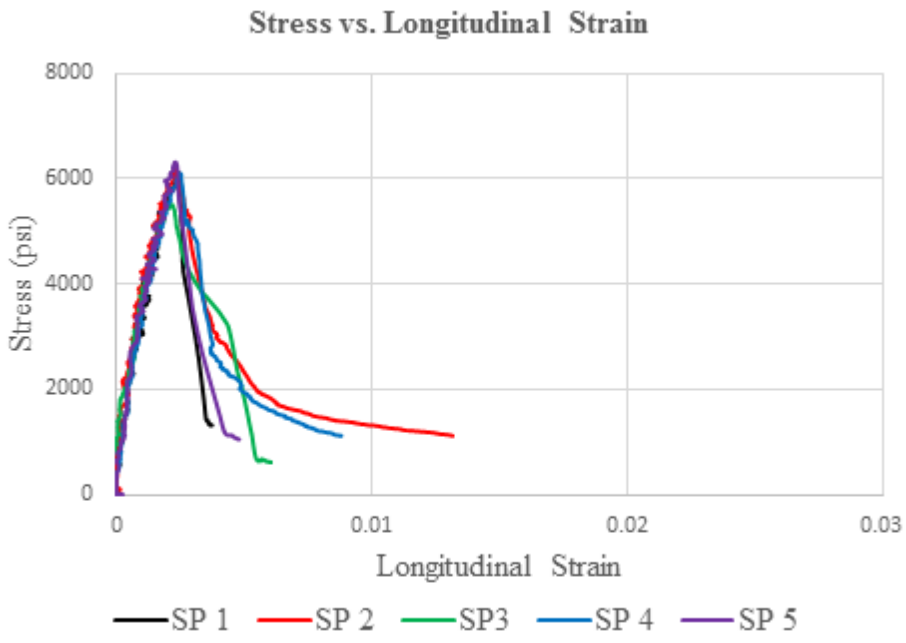

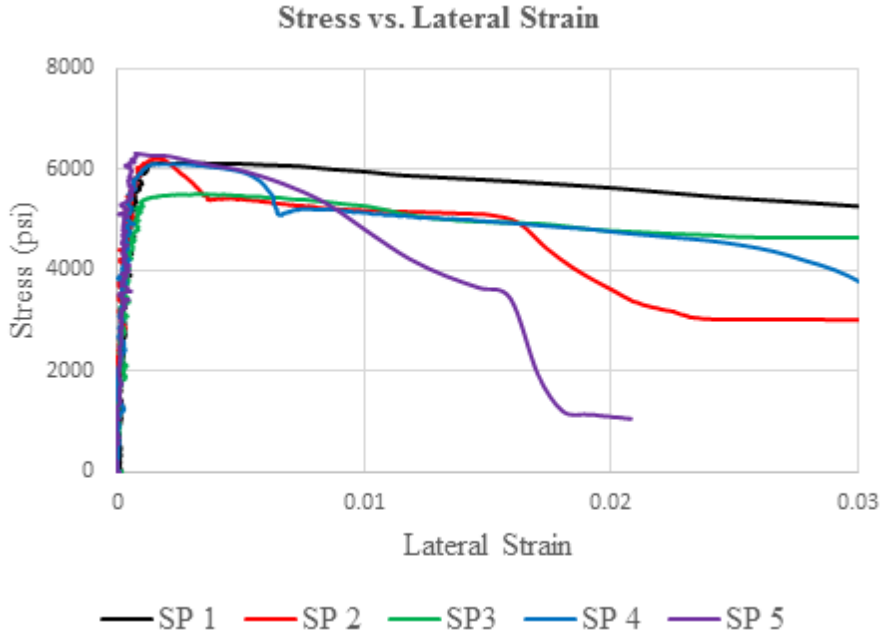

f_{cm} (psi)	$COV(f_{cm})$	$E_c \times 10^3$ (ksi)	$COV(E_c)$	$E_{pp} \times 10^6$ (psi)	$COV(E_{pp})$
6050	5.2%	4.43	12.5%	-2.77	46.5%
Comment: brittle failure.					

SP 1

Failure type: 3
Marker 8 was dislodged after 1st crack.

SP 2

Failure type: 2
Markers 6 and 8 were dislodged after 1st crack.

SP 3

Failure type: 4
Markers 5 and 12 were dislodged after 1st crack.

SP 4

Failure type: 2
Markers 5 and 11 were dislodged after 1st crack.

SP 5

Failure type: 3

Batch 11: $f'_c = 6$ ksi; $V_f = 1.0\%$; Fiber: 4D (RC-65/60-BG)

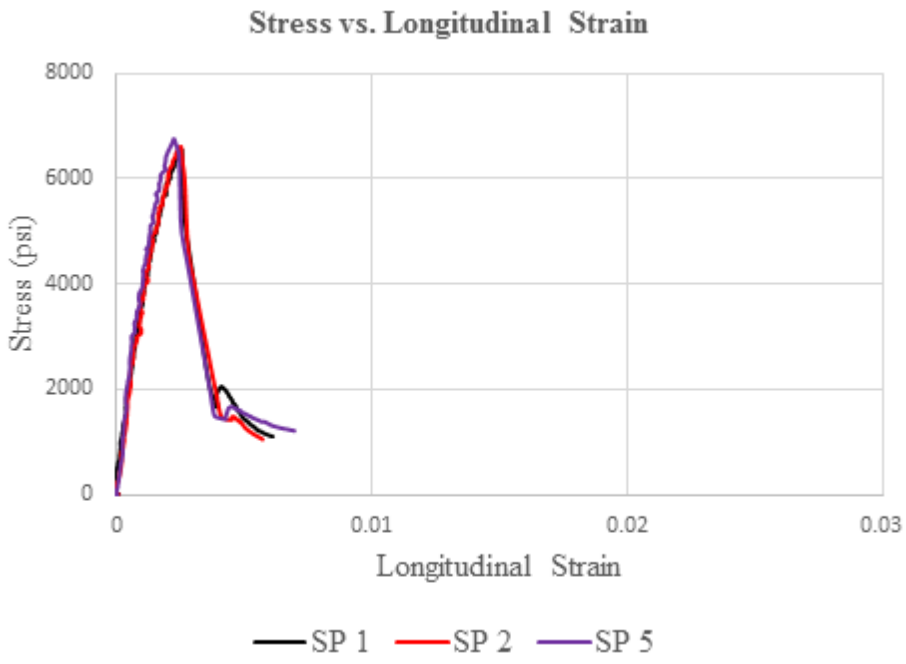

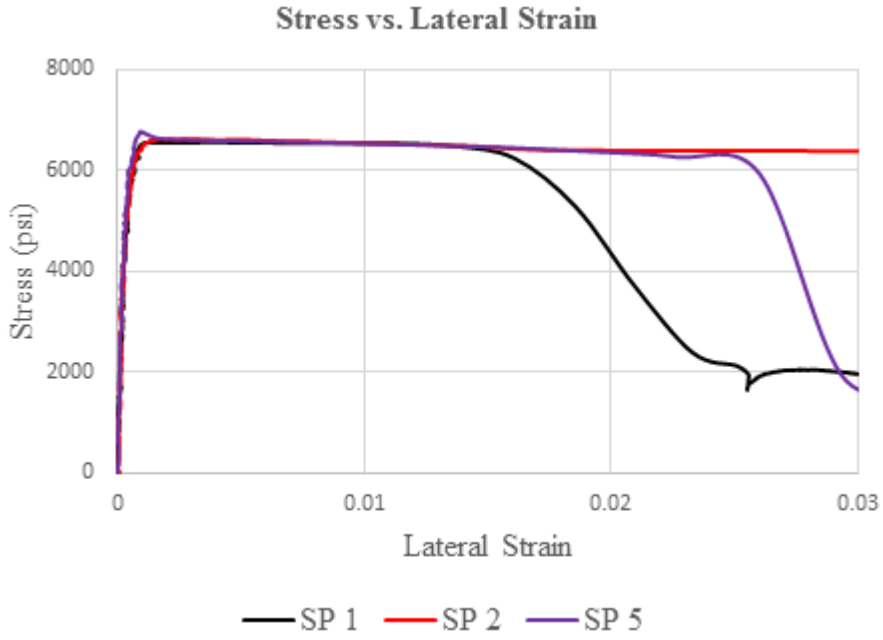

f_{cm} (psi)	$COV(f_{cm})$	$E_c \times 10^3$ (ksi)	$COV(E_c)$	$E_{pp} \times 10^6$ (psi)	$COV(E_{pp})$
6650	1.3%	3.74	10.4%	-4.09	15.4%
Comment: brittle failure, specimen 3 was not used in E_c and E_{pp} calculations, specimen 4 was not used in E_c calculation.					

SP 1

Failure type: 2

SP 2

Failure type: 3
Markers 6 and 7 were dislodged after 1st crack.

SP 3

Failure type: 3
Markers 5 and 11 were dislodged after 1st crack.

SP 4

Failure type: 2
Markers 4, 12, and 13 were dislodged after 1st crack.

SP 5

Failure type: 3

Batch 12: $f'_c = 6$ ksi; $V_f = 1.5\%$; Fiber: 4D (RC-65/60-BG)

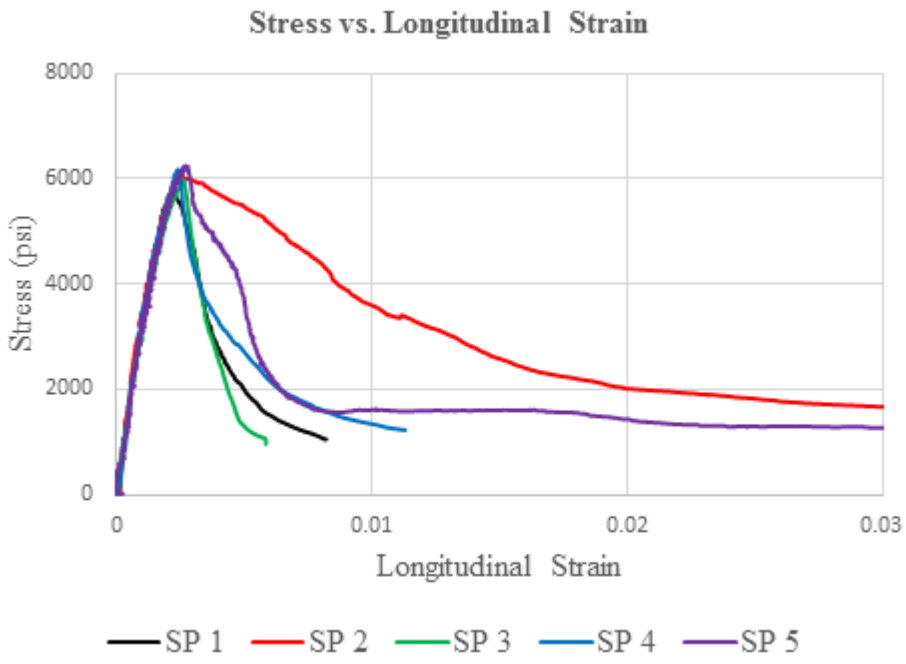

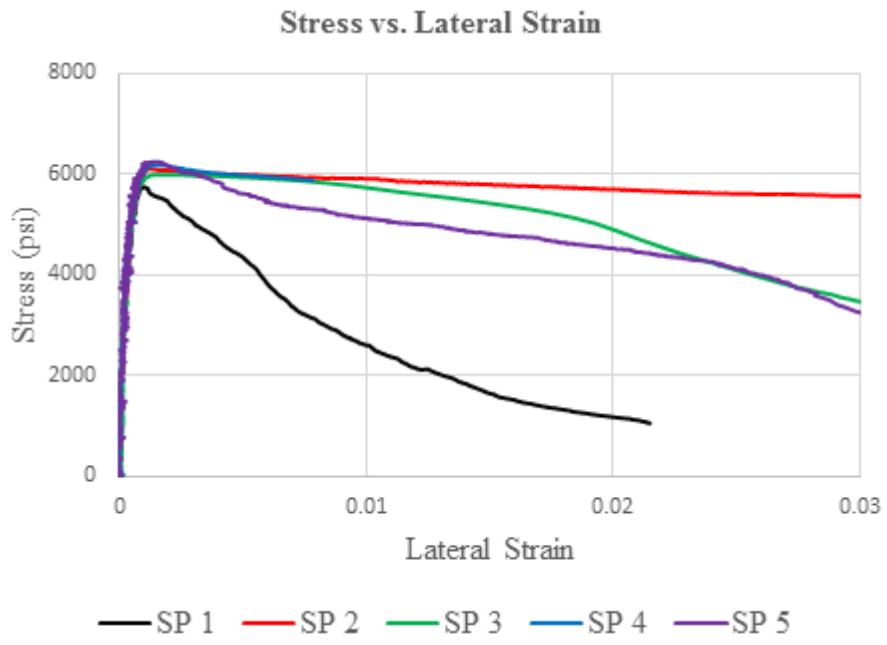

f_{cm} (psi)	$COV(f_{cm})$	$E_c \times 10^3$ (ksi)	$COV(E_c)$	$E_{pp} \times 10^6$ (psi)	$COV(E_{pp})$
6050	3.3%	3.31	6.7%	-1.81	34.3%
Comment: specimen 2 was not used in E_{pp} calculation.					

SP 1

Failure type: 4 or 3
Markers 4, 7, 12, and 13 were dislodged after 1st crack.

SP 2

Failure type: 3
Markers 3, 5, 8, and 14 were dislodged after 1st crack.

SP 3

Failure type: 3
Markers 3, 5, 8, and 14 were dislodged after 1st crack.

SP 4

Failure type: 3
Markers 5, 6, 13, and 14 were dislodged after 1st crack.

SP 5

Failure type: 3
Markers 5 and 13 were dislodged after 1st crack.

Batch 13: $f'_c = 6$ ksi; $V_f = 0.75\%$; Fiber: 5D (RC-65/60-BG)

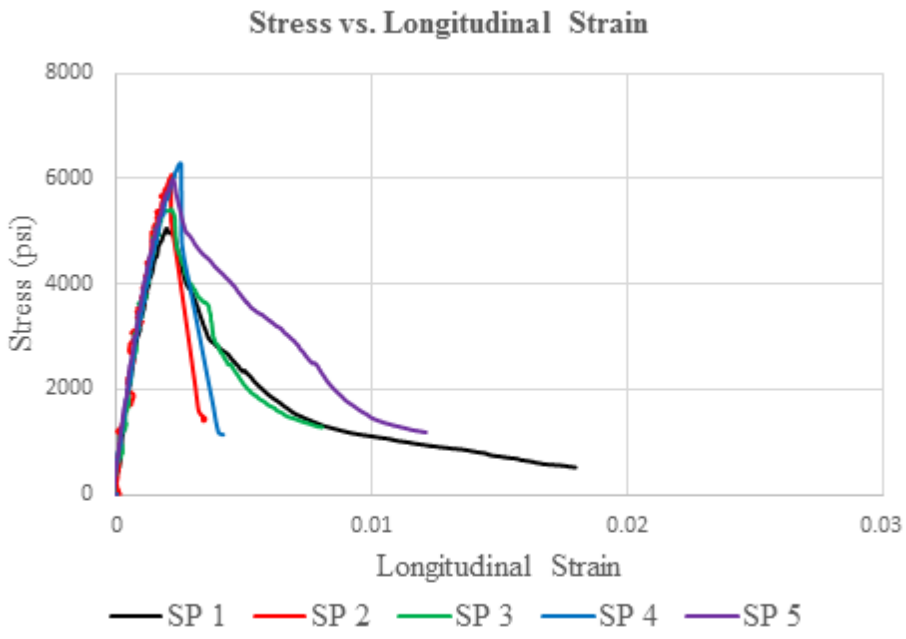

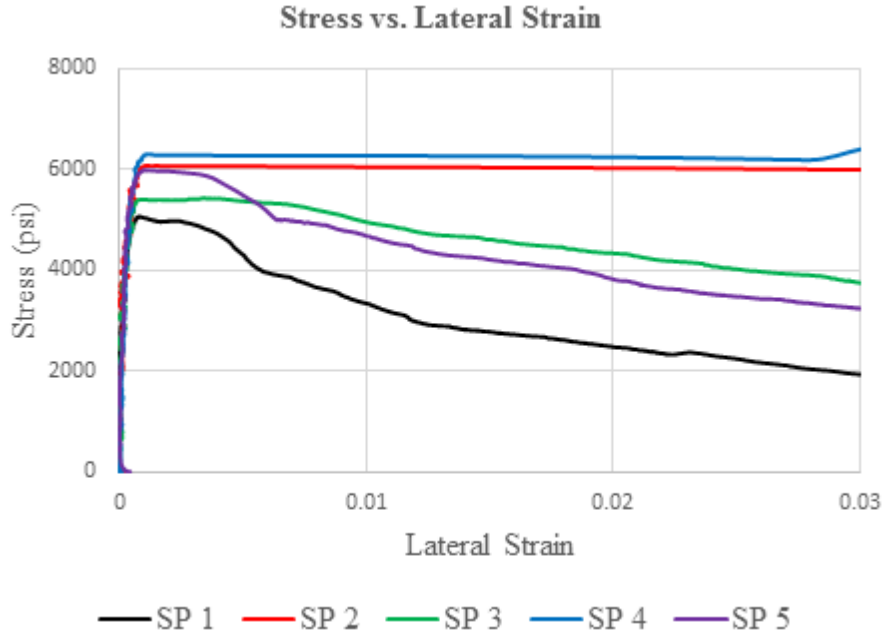

f_{cm} (psi)	$COV(f_{cm})$	$E_c \times 10^3$ (ksi)	$COV(E_c)$	$E_{pp} \times 10^6$ (psi)	$COV(E_{pp})$
5770	8.8%	4.03	8.8%	-2.41	81.9%
Comment:					

SP 1

Failure type: 2

SP 2

Failure type: 3

SP 3

Failure type: 3
Markers 5 and 11 were dislodged after 1st crack.

SP 4

Failure type: 4 or 3
Markers 4, 5, and 6 were dislodged after 1st crack.

SP 5

Failure type: 3
Markers 8, 13, and 14 were dislodged after 1st crack.

Batch 14: $f`_c = 6$ ksi; $V_f = 1.5\%$; Fiber: 5D (RC-65/60-BG)

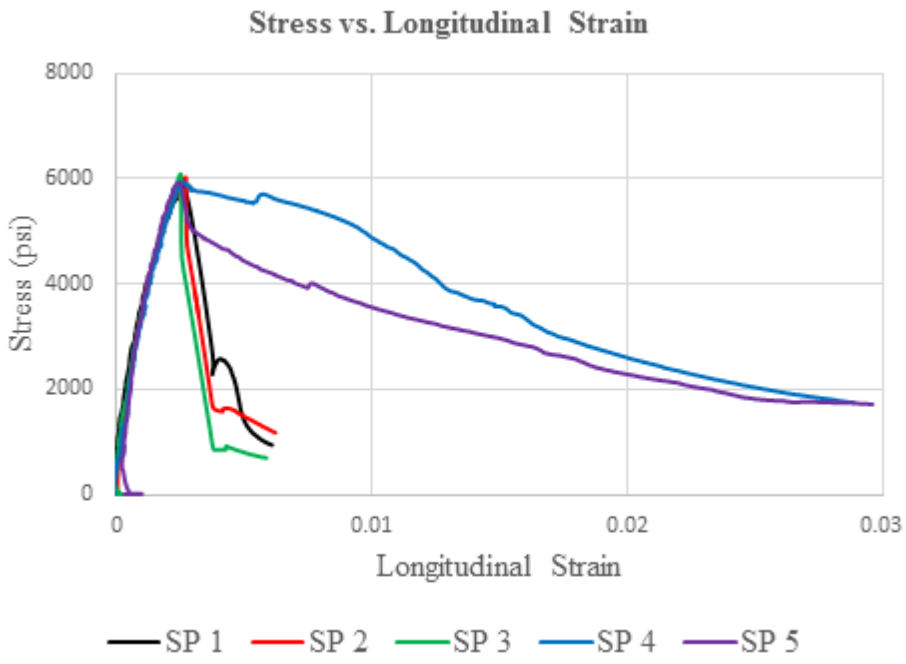

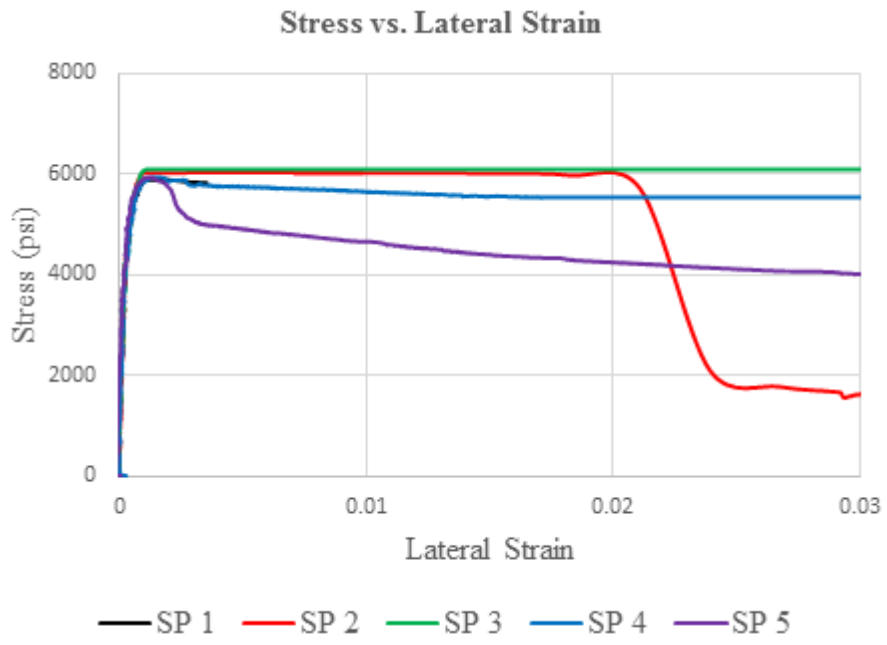

f_{cm} (psi)	$COV(f_{cm})$	$E_c \times 10^3$ (ksi)	$COV(E_c)$	$E_{pp} \times 10^6$ (psi)	$COV(E_{pp})$
5980	1.4%	4.08	11.2%	-0.50	90.1%
Comment: brittle failure.					

SP 1

Failure type: 3
Marker 6 was dislodged after 1st crack.

SP 2

Failure type: 2
Markers 6, 7, and 8 were dislodged after 1st crack.

SP 3

Failure type: 2
Markers 5, 7, and 12 were dislodged after 1st crack.

SP 4

Failure type: 3
Markers 6, 12, and 13 were dislodged after 1st crack.

SP 5

Failure type: 3 or 4
Markers 3, 5, 6, 8, 11, 12, and 4 were dislodged after 1st crack.

Control 2: f'_c = 10 ksi

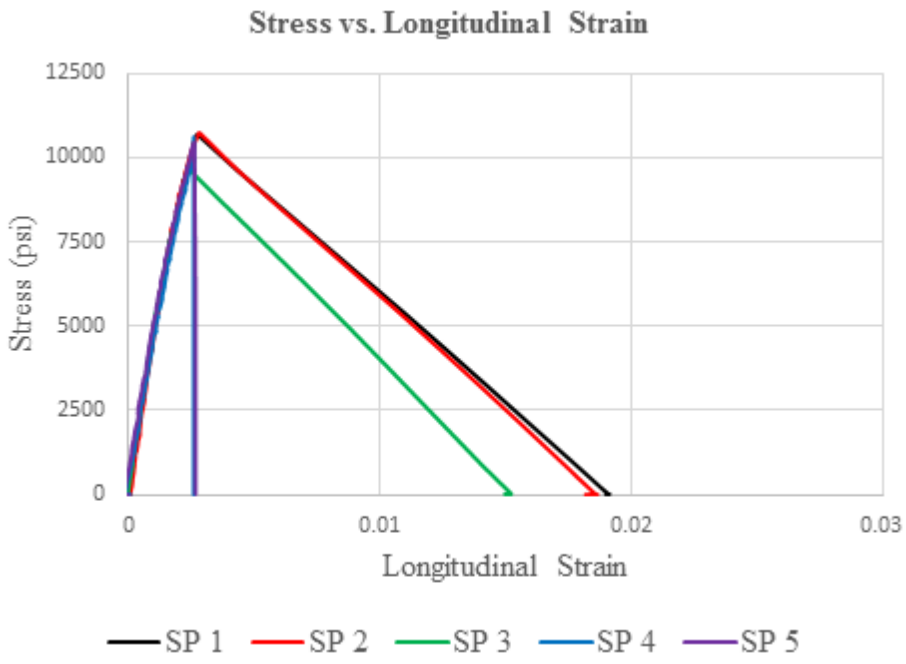

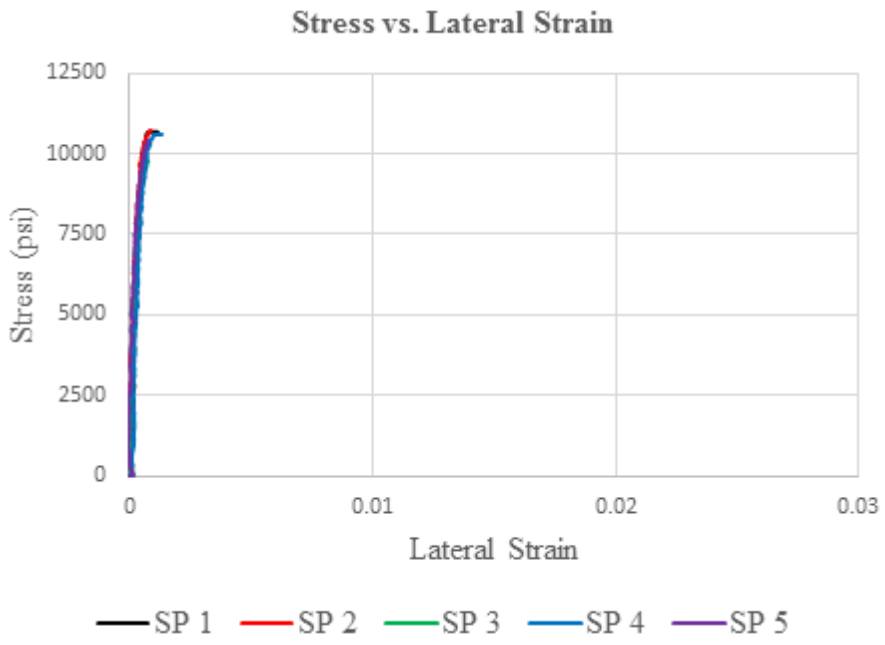

f_{cm} (psi)	$COV(f_{cm})$	$E_c \times 10^3$ (ksi)	$COV(E_c)$	$E_{pp} \times 10^6$ (psi)	$COV(E_{pp})$
10480	3.6%	4.92	6.1%	-16.12	17.7%
Comment: brittle failure, specimens 1,2, and 3 were not used in E_{pp} calculation.					

SP 1

Failure type: 1
Only marker 7 did not dislodge after 1st crack.

SP 2

Failure type: 1
Only marker 4 did not dislodge after 1st crack.

SP 3

Failure type: 1
Only marker 3 did not dislodge after 1st crack.

SP 4

Failure type: 1
Only marker 7 did not dislodge after 1st crack.
Failure type: 2

SP 5

Failure type: 1

Batch 15: $f'_c = 10$ ksi; $V_f = 0.5\%$; Fiber: (RC-80/30-BP)

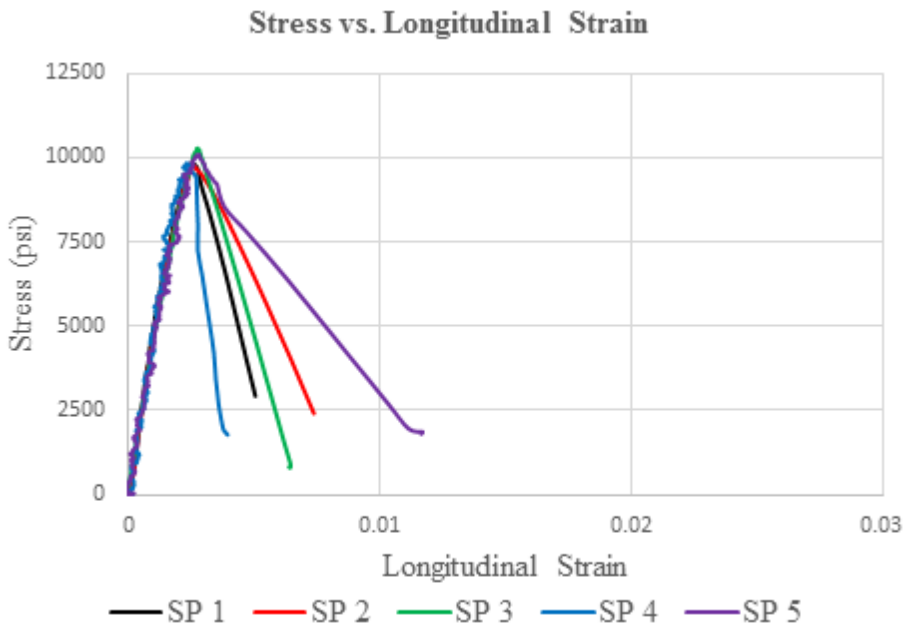

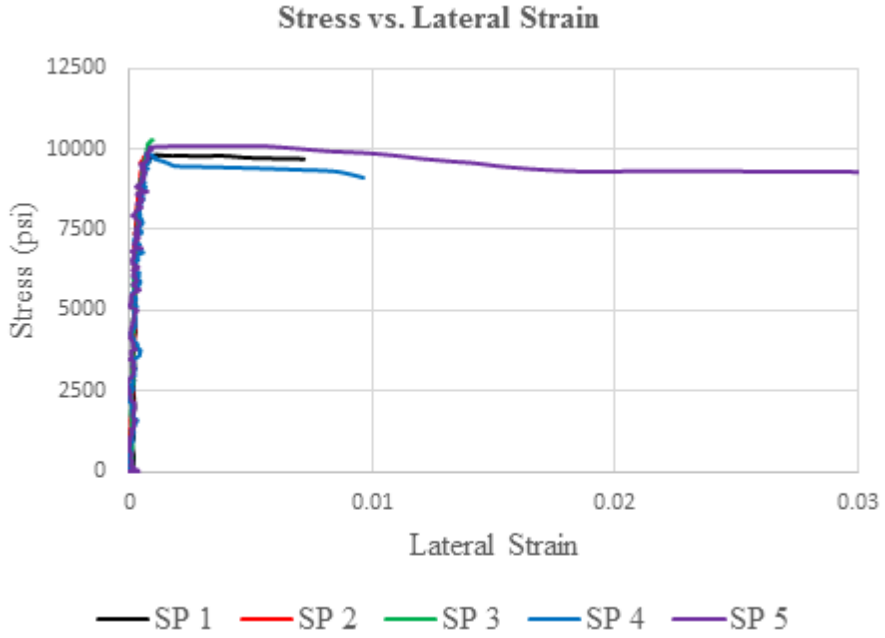

f_{cm} (psi)	$COV(f_{cm})$	$E_c \times 10^3$ (ksi)	$COV(E_c)$	$E_{pp} \times 10^6$ (psi)	$COV(E_{pp})$
9970	2.1%	4.80	4.0%	-3.85	38.2%
Comment: brittle failure, specimens 2 and 5 were not used in E_{pp} calculation.					

SP 1

Failure type: 3
Marker 5 was dislodged after 1st crack.

SP 2

Failure type: 3

SP 3

Failure type: 3

SP 4

Failure type: 3

SP 5

Failure type: 3

Batch 16: $f`_c = 10$ ksi; $V_f = 0.75\%$; Fiber: (RC-80/30-BP)

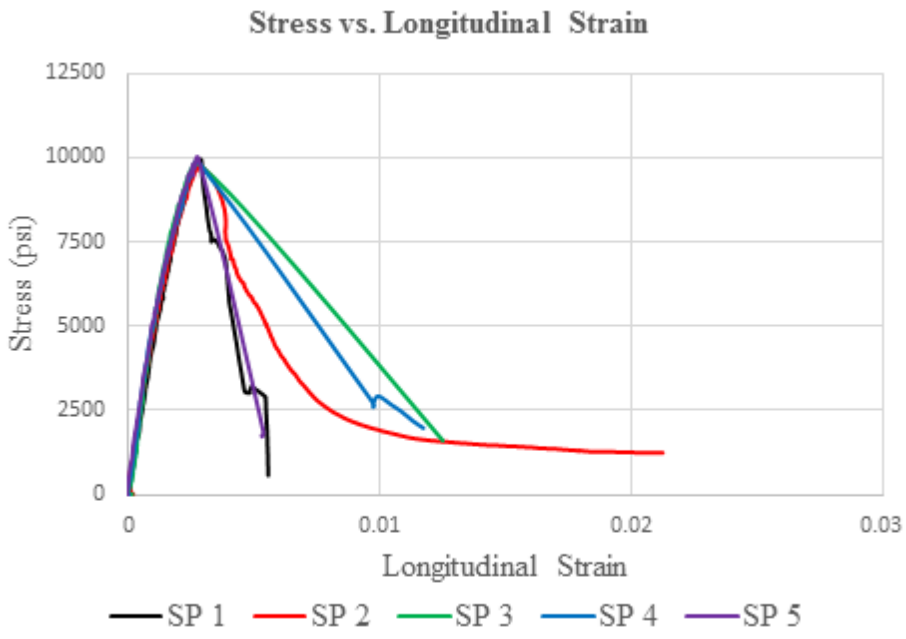

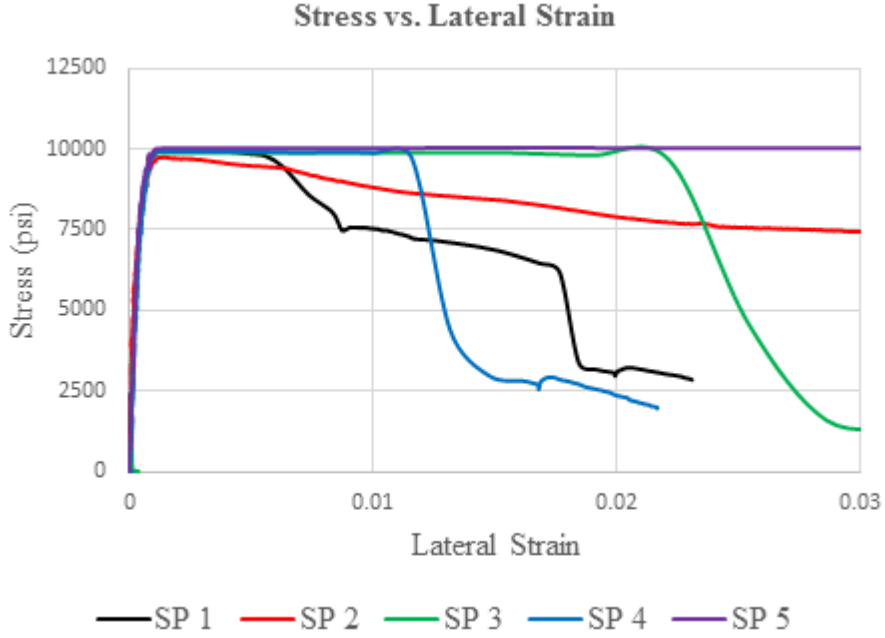

f_{cm} (psi)	$COV(f_{cm})$	$E_c \times 10^3$ (ksi)	$COV(E_c)$	$E_{pp} \times 10^6$ (psi)	$COV(E_{pp})$
9910	1.0%	5.18	8.7%	-2.58	37.2%
Comment: brittle failure, specimens 3 and 4 were not used in E_{pp} calculation.					

SP 1

Failure type: 3

SP 2

Failure type: 3

SP 3

Failure type: 3

SP 4

Failure type: 3

SP 5

Failure type: 3
Marker 12 was dislodged after 1st crack.

Batch 17: $f'_c = 10$ ksi; $V_f = 1.0\%$; Fiber: (RC-80/30-BP)

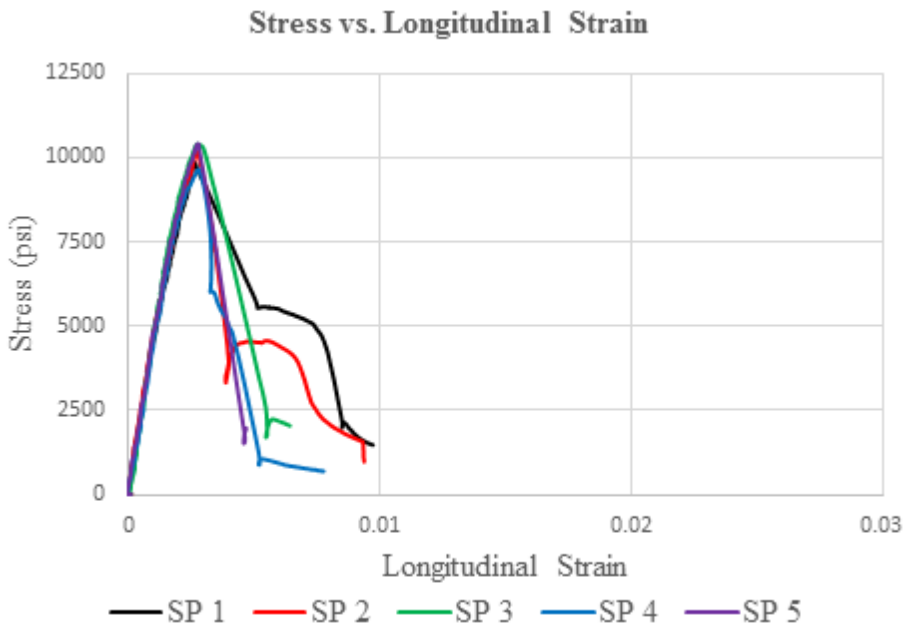

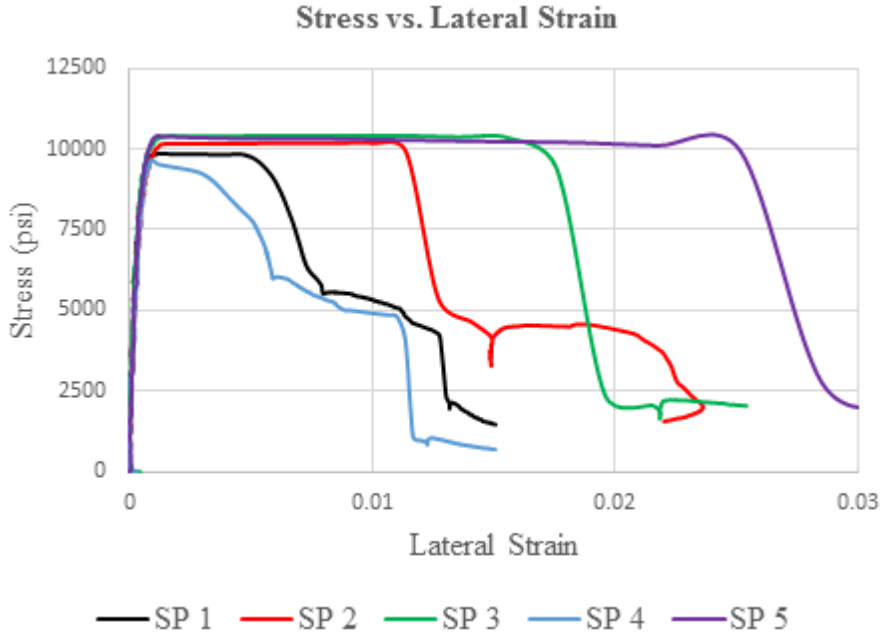

f_{cm} (psi)	$COV(f_{cm})$	$E_c \times 10^3$ (ksi)	$COV(E_c)$	$E_{pp} \times 10^6$ (psi)	$COV(E_{pp})$
10100	3.3%	4.78	4.6%	-1.86	54.2%
Comment: brittle failure.					

SP 1

Failure type: 3

SP 2

Failure type: 3

SP 3

Failure type: 3

SP 4

Failure type: 4 or 3

SP 5

Failure type: 3

Batch 18: $f'_c = 10$ ksi; $V_f = 1.5\%$; Fiber: (RC-80/30-BP)

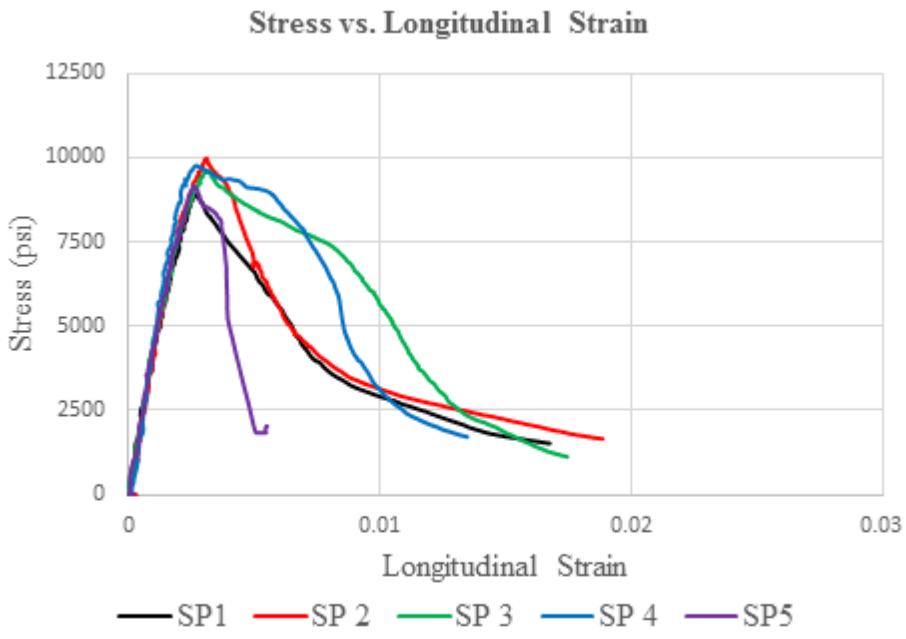

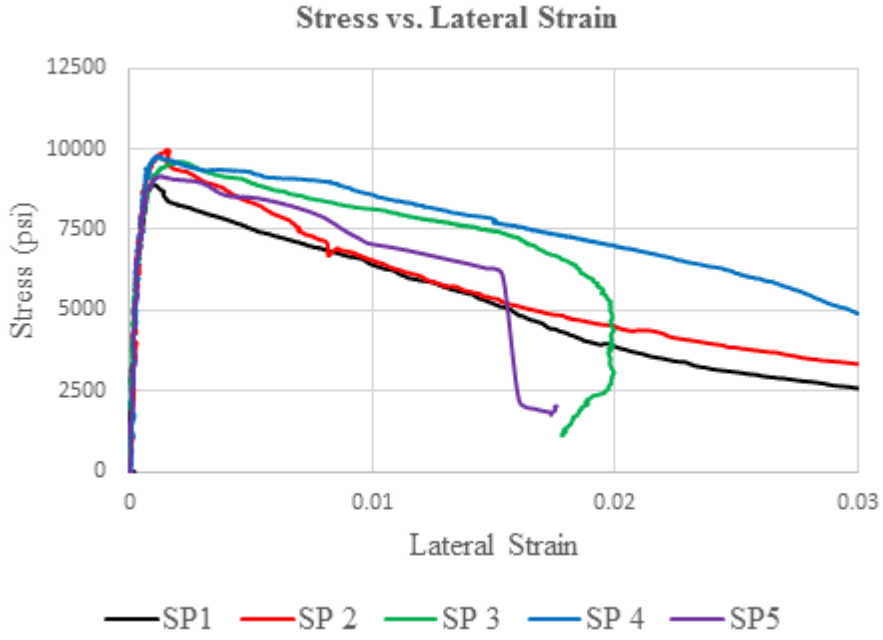

f_{cm} (psi)	$COV(f_{cm})$	$E_c \times 10^3$ (ksi)	$COV(E_c)$	$E_{pp} \times 10^6$ (psi)	$COV(E_{pp})$
9490	4.6%	4.29	4.3%	-0.91	36.6%
Comment: specimen 5 was not used in E_{pp} calculation.					

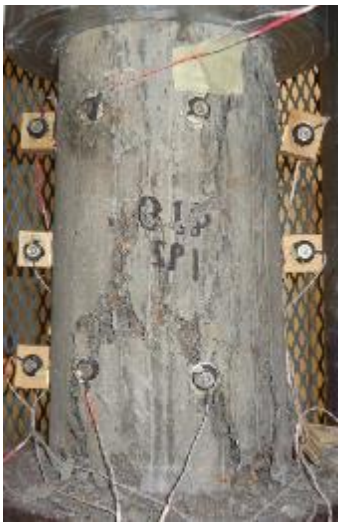

SP 1

Failure type: 3
Marker 4 was dislodged after 1st crack.

SP 2

Failure type: 3

SP 3

Failure type: 3

SP 4

Failure type: 3

SP 5

Failure type: 4

Batch 19: $f`_c = 10$ ksi; $V_f = 0.75\%$; Fiber: 4D (RC-65/60-BG)

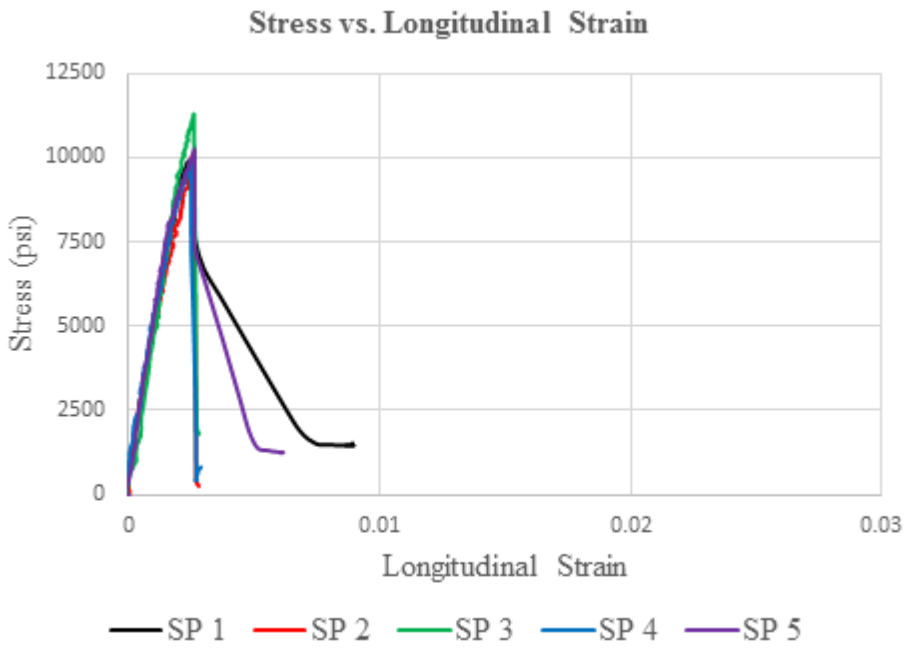

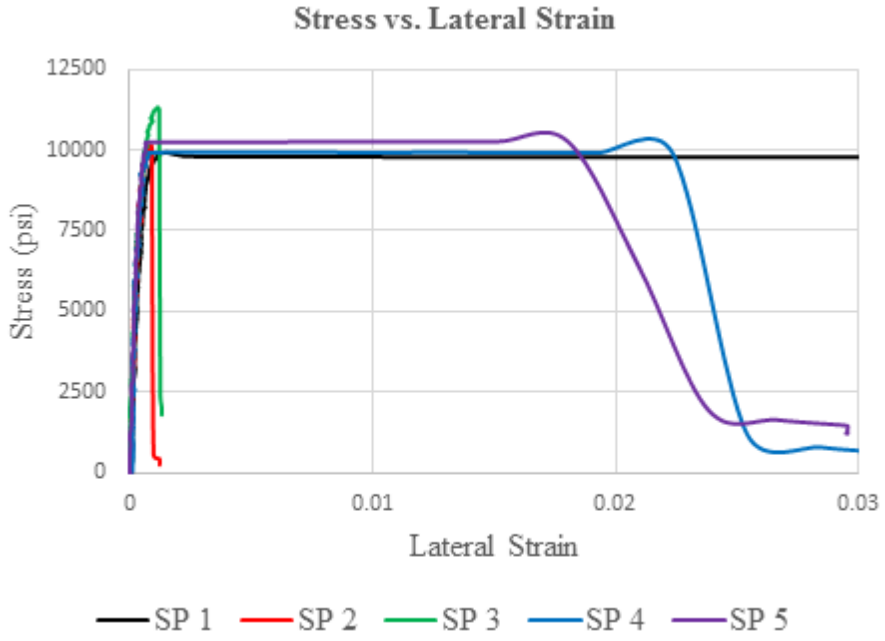

f_{cm} (psi)	$COV(f_{cm})$	$E_c \times 10^3$ (ksi)	$COV(E_c)$	$E_{pp} \times 10^6$ (psi)	$COV(E_{pp})$
10320	5.6%	5.14	7.3%	-8.47	91.3%
Comment: brittle failure.					

SP 1

Failure type: 3
Marker 5 was dislodged after 1st crack.

SP 2

Failure type: 3

SP 3

Failure type: 3
Markers 3, 4, 8, and 11 were dislodged after 1st crack.

SP 4

Failure type: 3

SP 5

Failure type: 3
Markers 3 and 11 were dislodged after 1st crack.

Batch 20: $f`_c = 10$ ksi; $V_f = 1.5\%$; Fiber: 4D (RC-65/60-BG)

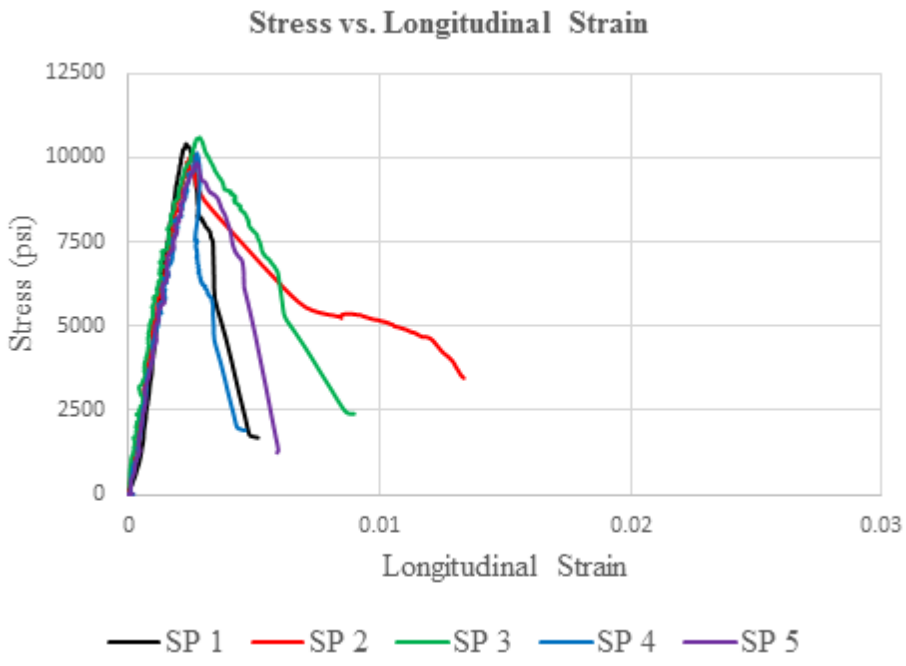

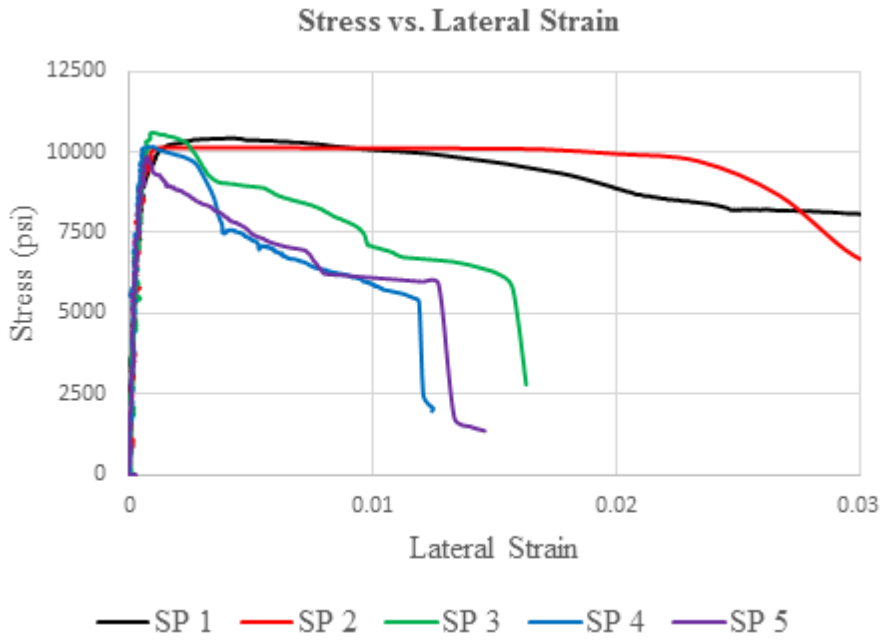

f_{cm} (psi)	$COV(f_{cm})$	$E_c \times 10^3$ (ksi)	$COV(E_c)$	$E_{pp} \times 10^6$ (psi)	$COV(E_{pp})$
10240	2.8%	4.56	13.2%	-1.64	86.6%
Comment:					

SP 1

Failure type: 3
Marker 7 was dislodged after 1st crack.

SP 2

Failure type: 3
Markers 3, 5, 11, and 12 were dislodged after 1st crack.

SP 3

Failure type: 3
Markers 7 and 12 were dislodged after 1st crack.

SP 4

Failure type: 4 or 3

SP 5

Failure type: 4 or 3

Batch 21: $f`_c = 10$ ksi; $V_f = 0.75\%$; Fiber: 5D (RC-65/60-BG)

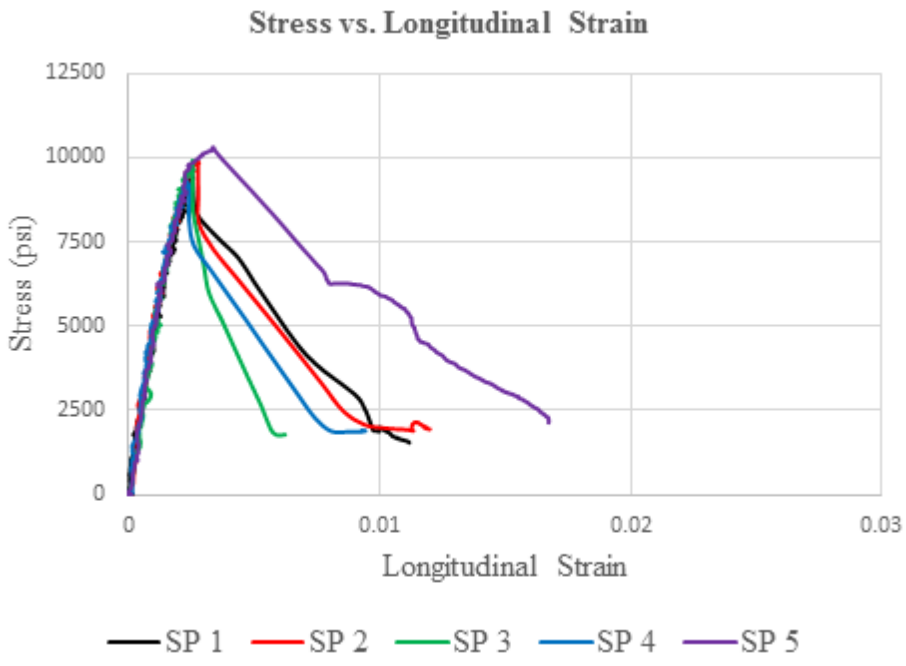

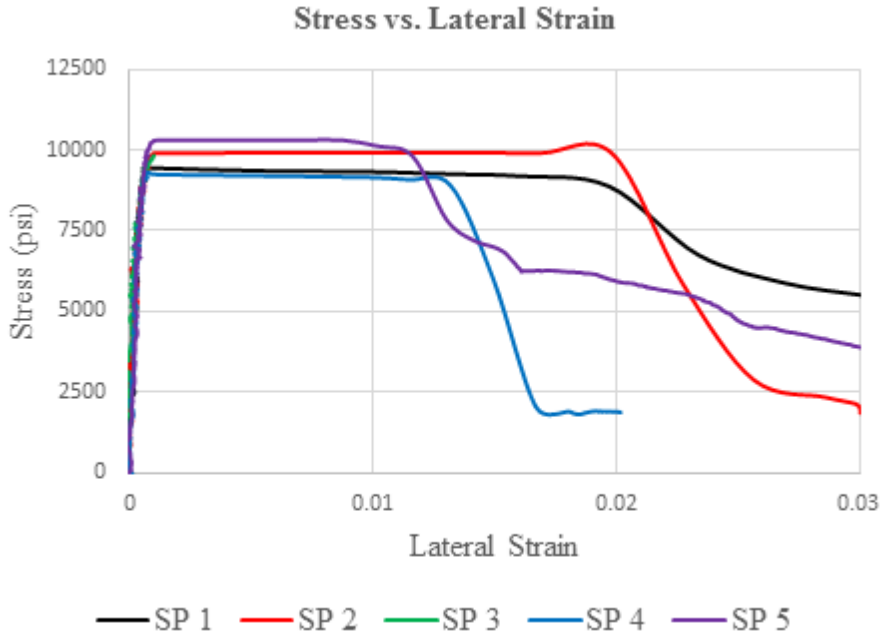

f_{cm} (psi)	$COV(f_{cm})$	$E_c \times 10^3$ (ksi)	$COV(E_c)$	$E_{pp} \times 10^6$ (psi)	$COV(E_{pp})$
9800	4.2%	4.87	8.5%	-3.88	69.1%
Comment: brittle failure.					

SP 1

Failure type: 4
Markers 3, 5, and 7 were dislodged after 1st crack.

SP 2

Failure type: 3
Markers 3 and 4 were dislodged after 1st crack.

SP 3

Failure type: 2
Marker 5 was dislodged after 1st crack.

SP 4

Failure type: 3
Marker 5 was dislodged after 1st crack.

SP 5

Failure type: 3
Marker 3 was dislodged after 1st crack.

Batch 22: $f'_c = 10$ ksi; $V_f = 1.5\%$; Fiber: 5D (RC-65/60-BG)

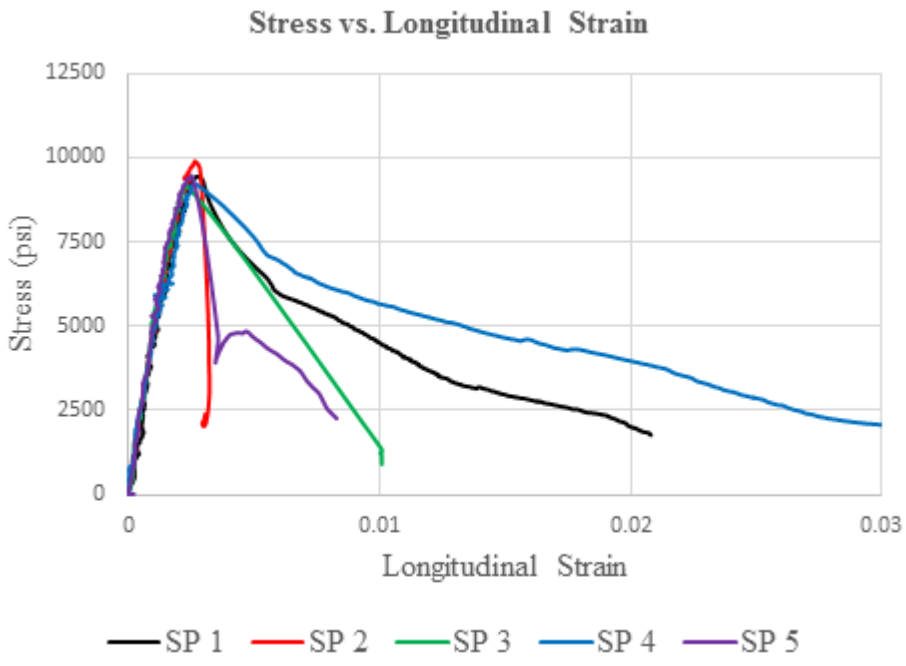

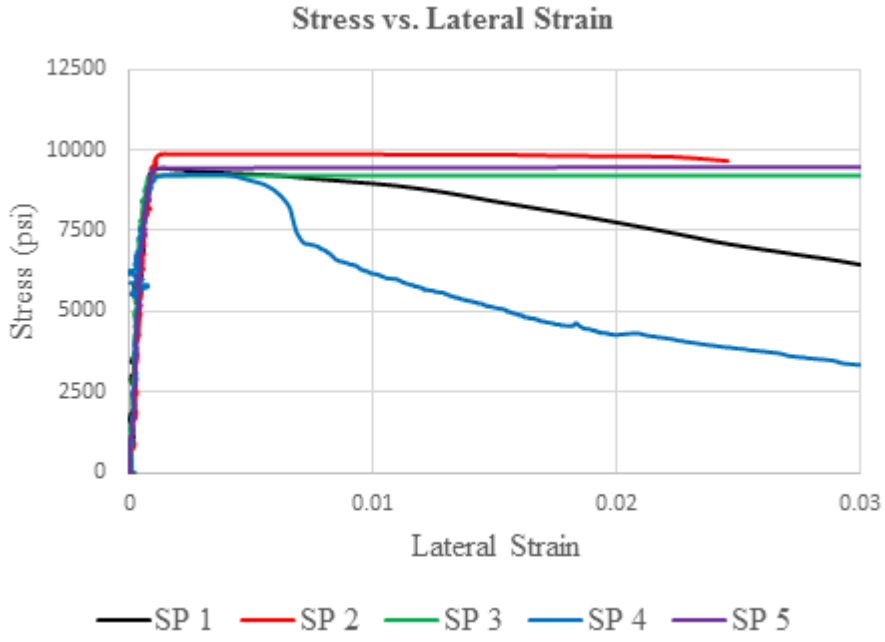

f_{cm} (psi)	$COV(f_{cm})$	$E_c \times 10^3$ (ksi)	$COV(E_c)$	$E_{pp} \times 10^6$ (psi)	$COV(E_{pp})$
9450	2.9%	5.25	15.7%	-0.91	110.0%
Comment: specimen 3 was not used in E_{pp} calculation.					

SP 1

Failure type: 3

SP 2

Failure type: 3

SP 3

Failure type: 4 or 3

SP 4

Failure type: 3

SP 5

Failure type: 4

Appendix C – Summary of Flexure Test Results

This appendix is a presentation of the flexure test results (ASTM C1609). An infrared-based non-contact sensor was used to determine the mid-span net deflection, the primary crack width, and support rotations. These results are plotted in this appendix for each specimen. Figure C.1 illustrates the difference between using an infrared-based non-contact position sensor and the displacement reported by the hydraulic machine for obtaining the mid-span net deflection.

The mean of the first-peak load (P_1), the post-crack peak load (P_{pc}), and their corresponding deflections (δ_1, δ_{pc}) are reported in Table C.1. The post-crack peak load coefficient of variation ($COV(P_{pc})$) and the corresponding primary crack width (ω_{pc}) of the post-crack peak load are also summarized in Table C.1. The loads corresponding to 0.04, 0.08, and 0.12 inch mid-span net deflections ($P_{\delta=0.04\ in.}$, $P_{\delta=0.08\ in.}$, and $P_{\delta=0.12\ in.}$) along with the maximum load (P_{max}) are presented in Table C.2. The mean of the first-peak stress (σ_1), the post-crack peak stress (σ_{pc}), and the corresponding stress of 0.04, 0.08, and 0.12 inch mid-span net deflections ($\sigma_{\delta=0.04\ in.}$, $\sigma_{\delta=0.08\ in.}$, and $\sigma_{\delta=0.12\ in.}$) along with the maximum stress (σ_{max}) are summarized in Table C.3.

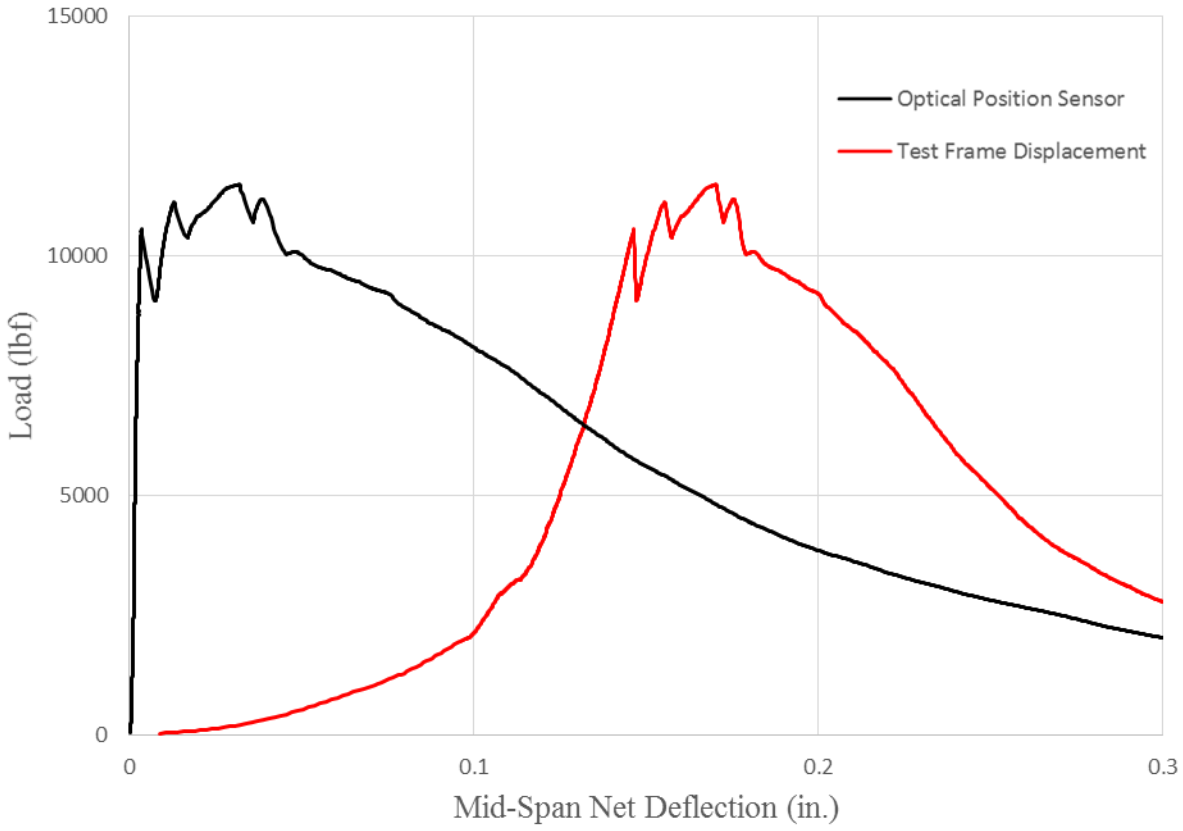

Figure C.1 – Difference between using an infrared-based non-contact position sensor and the test frame displacement to calculate mid-span net deflection.

Table C.1 – First peak and post-crack peak flexural profile.

Batch ID	Fiber type	V_f (%)	P_1 (lbf)	δ_1 (in.)	P_{pc} (lbf)	δ_{pc} (in.)	ω_{pc} (in.)	$COV(P_{pc})$
C 1	N/A	0	8890					0%
B 1	(RC-80/30-BP)	0.5	7540	0	6560	0.03	0.04	41%
B 2	(RC-80/30-BP)	0.75	8900	0	10180	0.03	0.03	14%
B 3	(RC-80/30-BP)	1.0	8700	0.01	11070	0.03	0.03	17%
B 4	(RC-80/30-BP)	1.5	10230	0.01	12200	0.02	0.01	11%
B 5	3D (RC-55/30-BG)	0.5	9760	0	2050	0.06	0.10	84%
B 6	3D (RC-55/30-BG)	0.75	9100	0	4210	0.02	0.04	52%
B 7	3D (RC-55/30-BG)	1.0	9360	0	5500	0.02	0.03	41%
B 8	3D (RC-55/30-BG)	1.5	9080	0	6770	0.02	0.02	13%
B 9	4D (RC-65/60-BG)	0.5	9180	0.01	4360	0.06	0.07	54%
B 10	4D (RC-65/60-BG)	0.75	8890	0	6940	0.03	0.05	60%
B 11	4D (RC-65/60-BG)	1.0	9460	0	9070	0.02	0.04	59%
B 12	4D (RC-65/60-BG)	1.5	9610	0	11760	0.03	0.03	37%
B 13	5D (RC-65/60-BG)	0.75	8390	0.01	7050	0.05	0.05	45%
B 14	5D (RC-65/60-BG)	1.5	9770	0	12720	0.05	0.06	55%
C 2	N/A	0	14820					
B 15	(RC-80/30-BP)	0.5	14460	0.01	13170	0.03	0.03	11%
B 16	(RC-80/30-BP)	0.75	15320	0	16840	0.01	0.01	5%
B 17	(RC-80/30-BP)	1.0	15560	0.01	19520	0.02	0.03	11%
B 18	(RC-80/30-BP)	1.5	15250	0	22730	0.04	0.02	11%
B 19	4D (RC-65/60-BG)	0.75	14700	0.01	14640	0.02	0.02	8%
B 20	4D (RC-65/60-BG)	1.5	15990	0	21360	0.03	0.02	19%
B 21	5D (RC-65/60-BG)	0.75	14420	0.01	16060	0.03	0.03	8%
B 22	5D (RC-65/60-BG)	1.5	15010	0.01	19760	0.03	0.03	23%

Table C.2 – Flexural load profile.

Batch ID	Fiber type	V_f (%)	P_1 (lbf)	P_{pc} (lbf)	$P_{\delta=0.04}$ (lbf)	$P_{\delta=0.08}$ (lbf)	$P_{\delta=0.12}$ (lbf)	P_{max} (lbf)
C 1	N/A	0	8890					8890
B 1	(RC-80/30-BP)	0.5	7540	6560	6020	4700	3360	7540
B 2	(RC-80/30-BP)	0.75	8900	10180	9710	6860	4600	10180
B 3	(RC-80/30-BP)	1.0	8700	11070	10360	7420	5300	11070
B 4	(RC-80/30-BP)	1.5	10230	12200	10310	7400	4960	12200
B 5	3D (RC-55/30-BG)	0.5	9760	2050	4650	1420	860	9760
B 6	3D (RC-55/30-BG)	0.75	9100	4210	3390	1980	1390	9100
B 7	3D (RC-55/30-BG)	1.0	9360	5500	4330	2840	1890	9360
B 8	3D (RC-55/30-BG)	1.5	9080	6770	5150	3260	2160	9080
B 9	4D (RC-65/60-BG)	0.5	9180	4360	5050	3400	2220	9180
B 10	4D (RC-65/60-BG)	0.75	8890	6940	6540	5670	4760	8890
B 11	4D (RC-65/60-BG)	1.0	9460	9070	8100	6550	5140	9460
B 12	4D (RC-65/60-BG)	1.5	9610	11760	10640	8890	7460	11760
B 13	5D (RC-65/60-BG)	0.75	8390	7050	6100	5540	4780	8390
B 14	5D (RC-65/60-BG)	1.5	9770	12720	12310	12290	11720	12720
C 2	N/A	0	14820					14820
B 15	(RC-80/30-BP)	0.5	14460	13170	12730	9510	7140	14460
B 16	(RC-80/30-BP)	0.75	15320	16840	14780	11020	7770	16840
B 17	(RC-80/30-BP)	1.0	15560	19520	18550	14960	11380	19520
B 18	(RC-80/30-BP)	1.5	15250	22730	22140	19270	15860	22730
B 19	4D (RC-65/60-BG)	0.75	14700	14640	13110	9610	7040	14700
B 20	4D (RC-65/60-BG)	1.5	15990	21360	20330	16510	13390	21360
B 21	5D (RC-65/60-BG)	0.75	14420	16060	14590	13270	11360	16060
B 22	5D (RC-65/60-BG)	1.5	15010	19760	18460	16210	12410	19760

Table C.3 – Flexural stresses profile.

Batch ID	Fiber type	V_f (%)	σ_1 (psi)	σ_{pc} (psi)	$\sigma_{\delta=0.04\ in.}$ (psi)	$\sigma_{\delta=0.08\ in.}$ (psi)	$\sigma_{\delta=0.12\ in.}$ (psi)	σ_{max} (psi)
C 1	N/A	0	720					720
B 1	(RC-80/30-BP)	0.5	620	540	500	390	275	620
B 2	(RC-80/30-BP)	0.75	720	730	785	555	370	785
B 3	(RC-80/30-BP)	1.0	730	920	820	590	420	920
B 4	(RC-80/30-BP)	1.5	890	1020	665	460	305	1020
B 5	3D (RC-55/30-BG)	0.5	790	165	375	125	220	785
B 6	3D (RC-55/30-BG)	0.75	755	340	275	160	115	755
B 7	3D (RC-55/30-BG)	1.0	755	445	350	115	155	755
B 8	3D (RC-55/30-BG)	1.5	735	545	420	265	175	735
B 9	4D (RC-65/60-BG)	0.5	740	350	330	215	135	740
B 10	4D (RC-65/60-BG)	0.75	735	570	540	465	310	735
B 11	4D (RC-65/60-BG)	1.0	760	720	645	520	410	760
B 12	4D (RC-65/60-BG)	1.5	775	935	845	705	590	935
B 13	5D (RC-65/60-BG)	0.75	675	565	485	430	355	675
B 14	5D (RC-65/60-BG)	1.50	770	995	965	960	915	995
C 2	N/A	0	1190					1190
B 15	(RC-80/30-BP)	0.5	1160	1055	1020	760	575	1160
B 16	(RC-80/30-BP)	0.75	1230	1345	1180	880	495	1345
B 17	(RC-80/30-BP)	1.0	980	1555	1475	1190	905	1555
B 18	(RC-80/30-BP)	1.5	1215	1810	1765	1535	1265	1810
B 19	4D (RC-65/60-BG)	0.75	1185	1180	1055	775	570	1185
B 20	4D (RC-65/60-BG)	1.5	1285	1715	1630	1325	1075	1715
B 21	5D (RC-65/60-BG)	0.75	1155	1290	1170	1065	910	1290
B 22	5D (RC-65/60-BG)	1.5	1185	1560	1455	1280	985	1560

Batch **page**

Control 1: $f_c^{`} = 6$ ksi

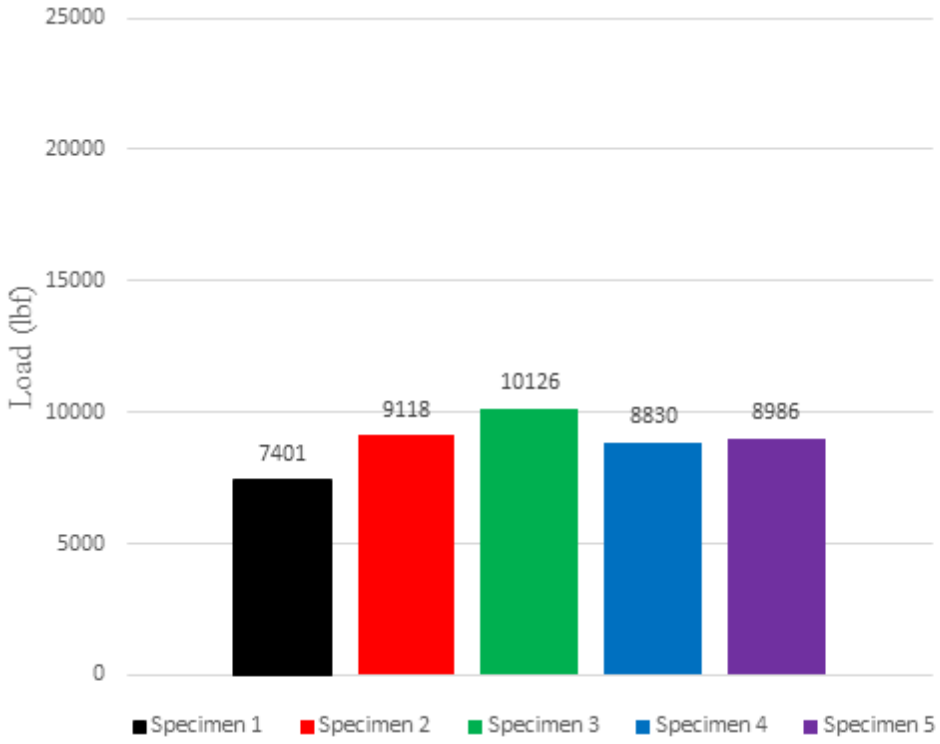

Batch ID		Fiber type			V_f (%)
C 1		N/A			0
P_1 (lbf)	P_{pc} (lbf)	$P_{\delta=0.04\ in.}$ (lbf)	$P_{\delta=0.08\ in.}$ (lbf)	$P_{\delta=0.12\ in.}$ (lbf)	P_{max} (lbf)
8892	0	0	0	0	0
σ_1 (psi)	σ_{pc} (psi)	$\sigma_{\delta=0.04\ in.}$ (psi)	$\sigma_{\delta=0.08\ in.}$ (psi)	$\sigma_{\delta=0.12\ in.}$ (psi)	σ_{max} (psi)
722	0	0	0	0	722
δ_1 (in.)	δ_{pc} (in.)	ω_{pc} (in.)	*COV(Ppc)*		
0	0	0	0%		
Comment: all specimens failed suddenly after first crack (brittle failure).					

SP 1 0 fiber Single crack	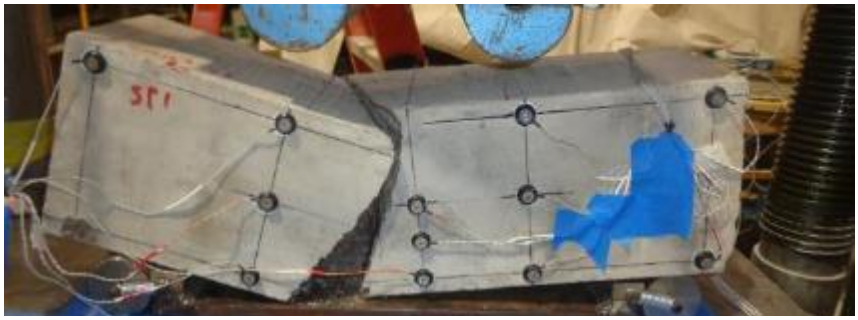
SP 2 0 fiber Single crack	
SP 3 0 fiber Single crack	
SP 4 0 fiber Single crack	
SP 5 0 fiber Wood form Single crack	

Batch 1: $f_c^{`} = 6$ ksi; $V_f = 0.5\%$; Fiber: (RC-80/30-BP)

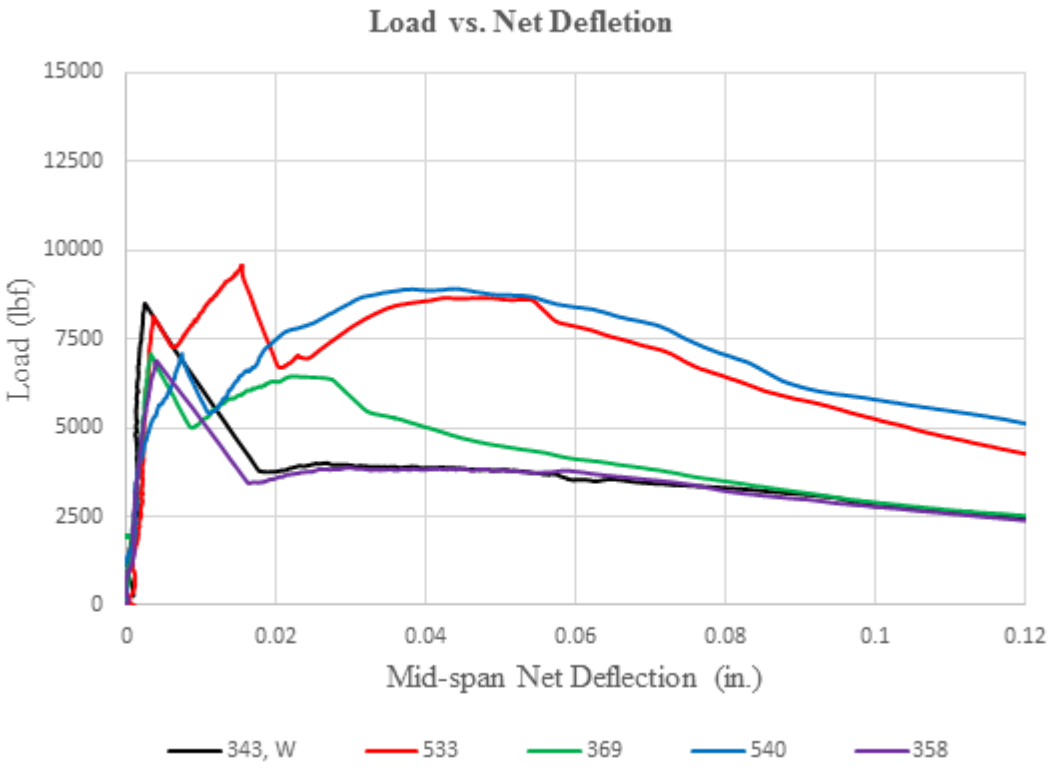

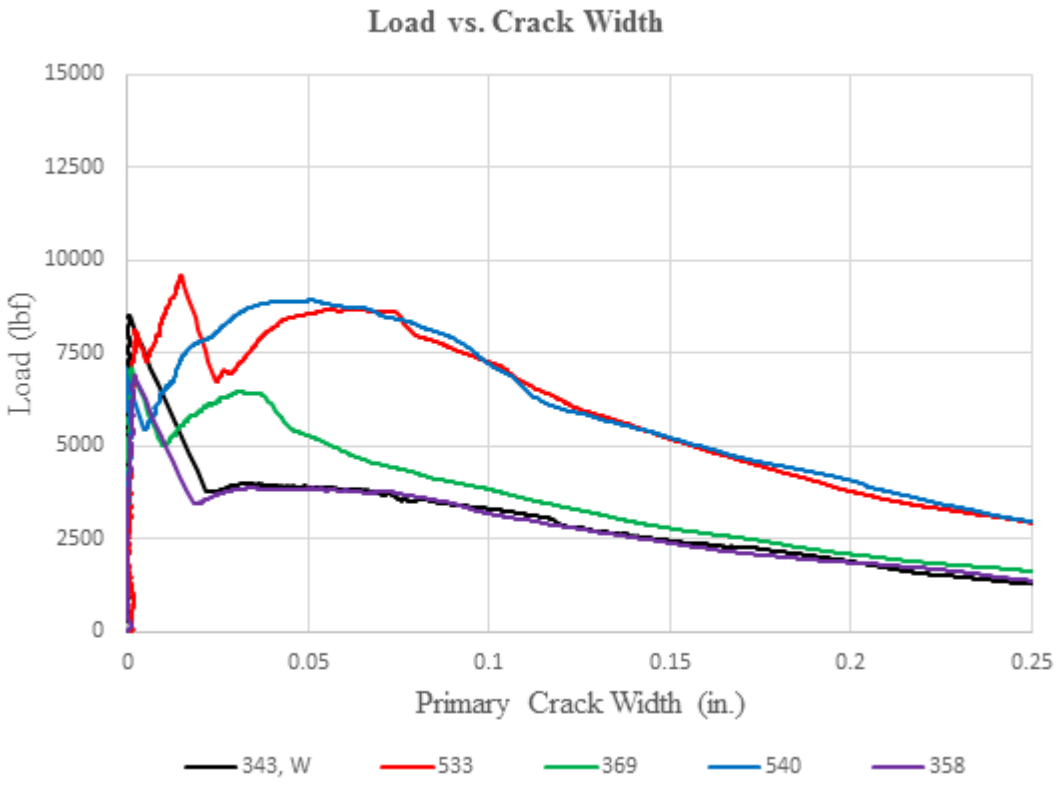

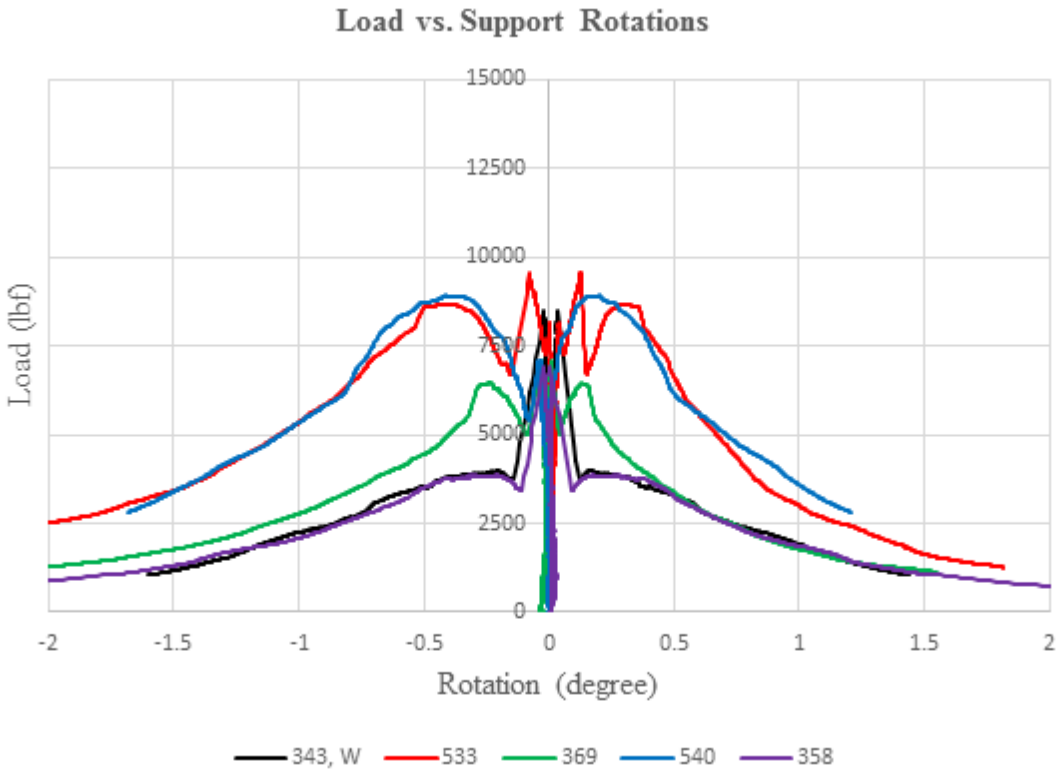

Batch ID		Fiber type			V_f (%)
B 1		(RC-80/30-BP)			0.5
P_1 (lbf)	P_{pc} (lbf)	$P_{\delta=0.04\ in.}$ (lbf)	$P_{\delta=0.08\ in.}$ (lbf)	$P_{\delta=0.12\ in.}$ (lbf)	P_{max} (lbf)
7540	6560	6020	4700	3360	7540
σ_1 (psi)	σ_{pc} (psi)	$\sigma_{\delta=0.04\ in.}$ (psi)	$\sigma_{\delta=0.08\ in.}$ (psi)	$\sigma_{\delta=0.12\ in.}$ (psi)	σ_{max} (psi)
620	540	500	390	275	620
δ_1 (in.)	δ_{pc} (in.)	ω_{pc} (in.)	*COV(Ppc)*		
0.005	0.03	0.04	41%		
Comment: brittle failure, dominated by fiber pullout.					

SP 1 343 fibers Wood form Single crack	
SP 2 533 fibers Multi-crack	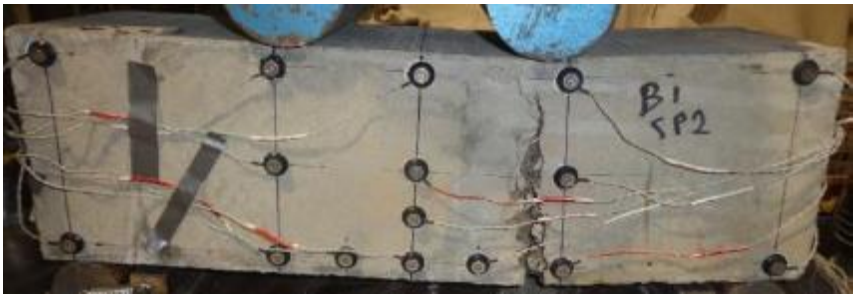
SP 3 369 fibers Single crack	
SP 4 540 fibers Multi-crack	
SP 5 358 fibers Single crack	

Batch 2: $f_c^{`} = 6$ ksi; $V_f = 0.75\%$; Fiber: (RC-80/30-BP)

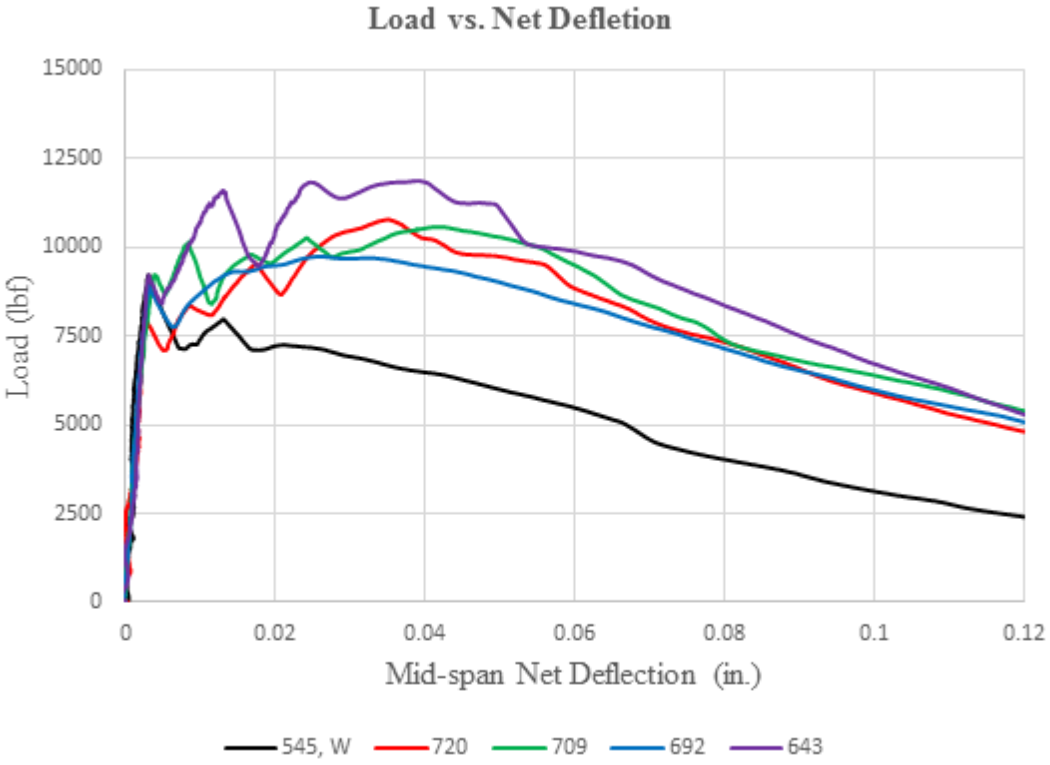

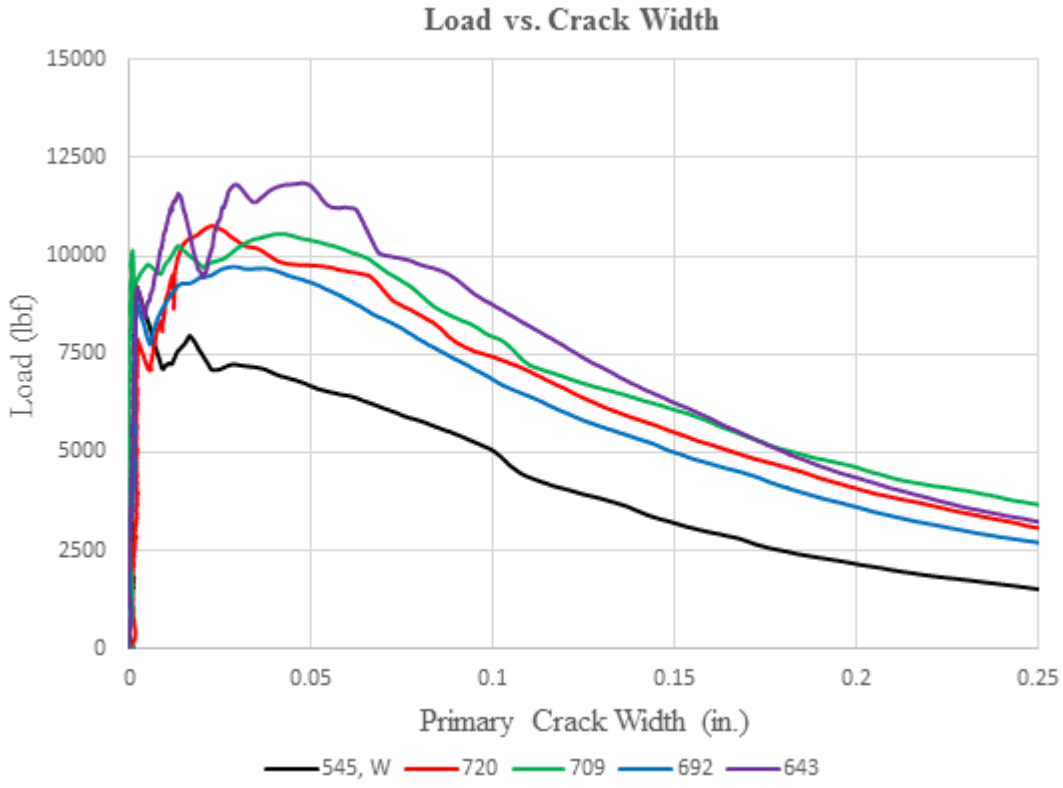

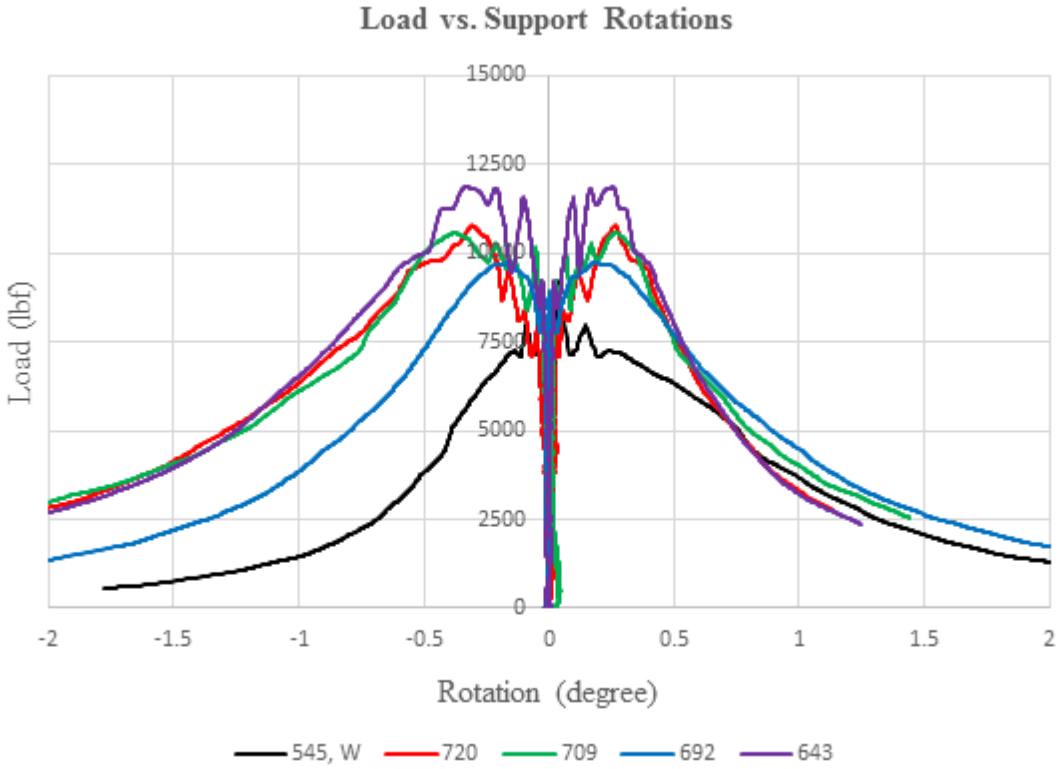

Batch ID		Fiber type			V_f (%)
B 2		(RC-80/30-BP)			0.75
P_1 (lbf)	P_{pc} (lbf)	$P_{\delta=0.04\ in.}$ (lbf)	$P_{\delta=0.08\ in.}$ (lbf)	$P_{\delta=0.12\ in.}$ (lbf)	P_{max} (lbf)
8900	10180	9710	6860	4600	10180
σ_1 (psi)	σ_{pc} (psi)	$\sigma_{\delta=0.04\ in.}$ (psi)	$\sigma_{\delta=0.08\ in.}$ (psi)	$\sigma_{\delta=0.12\ in.}$ (psi)	σ_{max} (psi)
715	730	785	555	370	785
δ_1 (in.)	δ_{pc} (in.)	ω_{pc} (in.)	*COV(Ppc)*		
0.003	0.03	0.03	14%		
Comment: dominated by fiber pullout.					

SP 1 545 fibers Wood form Single crack	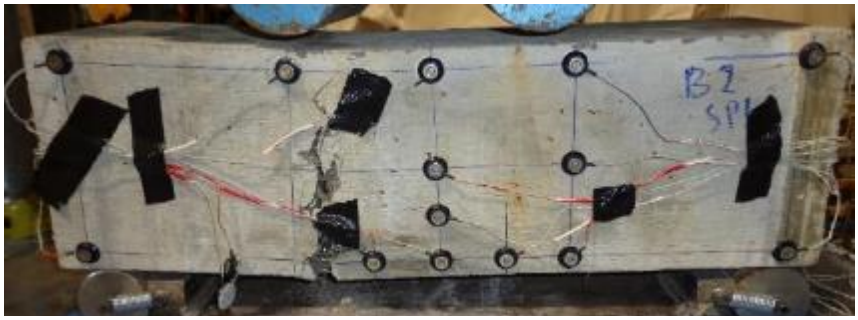
SP 2 720 fibers Multi-crack	
SP 3 709 fibers Single crack	
SP 4 692 fibers Multi-crack	
SP 5 643 fibers Multi-crack	

Batch 3: $f_c^{`} = 6$ ksi; $V_f = 1.0\%$; Fiber: (RC-80/30-BP)

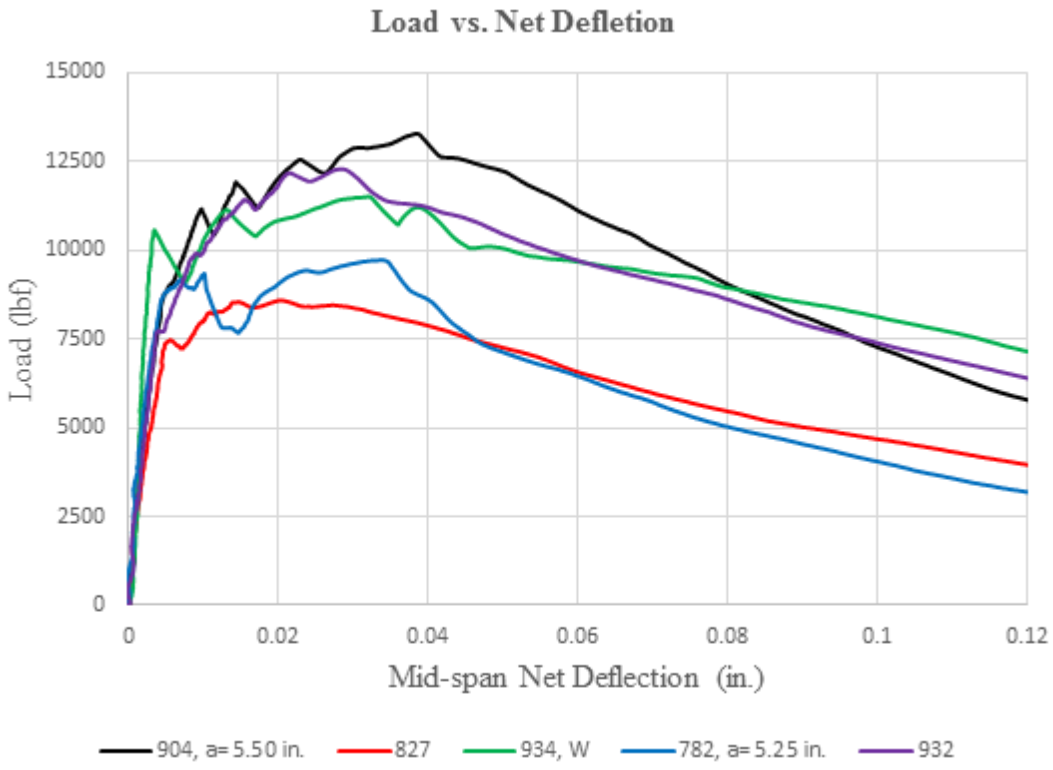

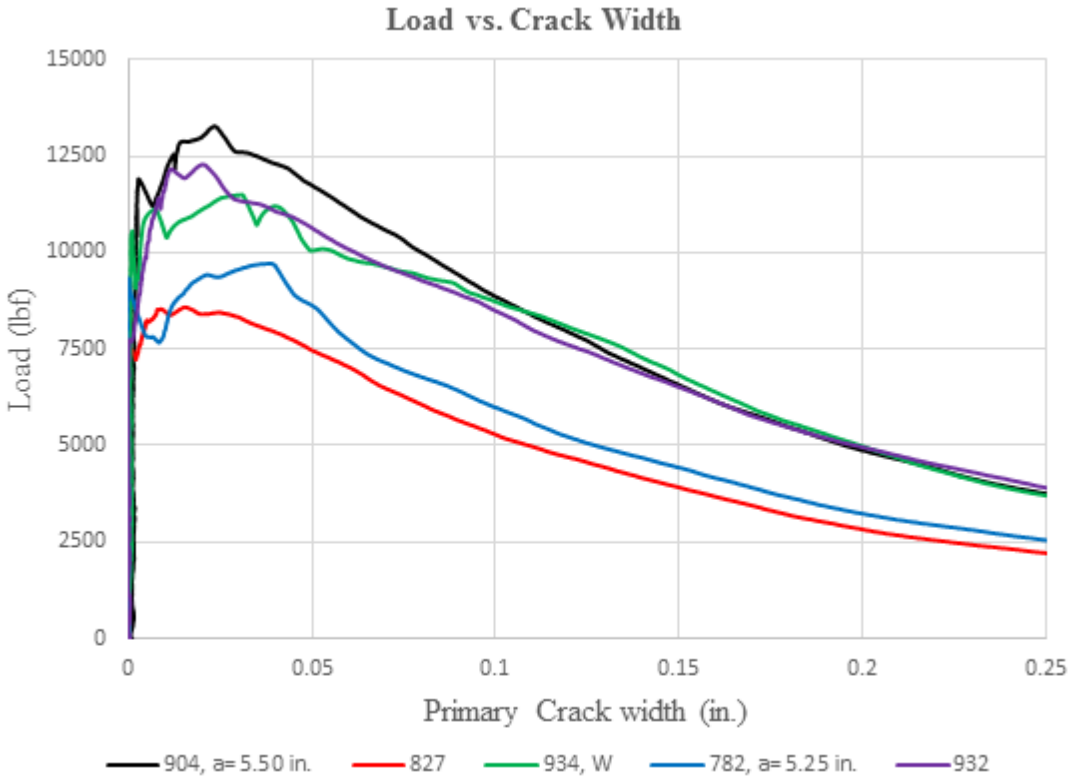

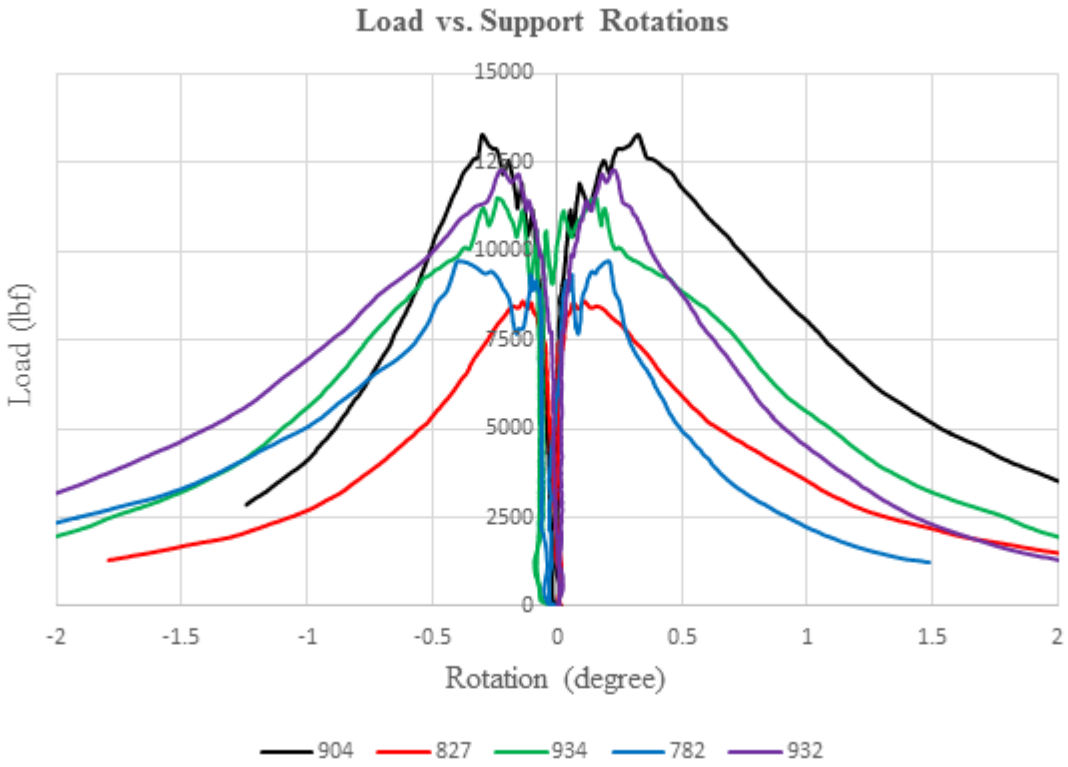

Batch ID		Fiber type			V_f (%)
B 3		(RC-80/30-BP)			1.0
P_1 (lbf)	P_{pc} (lbf)	$P_{\delta=0.04\ in.}$ (lbf)	$P_{\delta=0.08\ in.}$ (lbf)	$P_{\delta=0.12\ in.}$ (lbf)	P_{max} (lbf)
8700	11070	10360	7420	5300	11070
σ_1 (psi)	σ_{pc} (psi)	$\sigma_{\delta=0.04\ in.}$ (psi)	$\sigma_{\delta=0.08\ in.}$ (psi)	$\sigma_{\delta=0.12\ in.}$ (psi)	σ_{max} (psi)
730	920	825	590	420	920
δ_1 (in.)	δ_{pc} (in.)	ω_{pc} (in.)	*COV(Ppc)*		
0.006	0.03	0.03	17%		
Comment: dominated by fiber pullout.					

SP 1 904 fibers Wood form Multi-crack	
SP 2 827 fibers Single crack	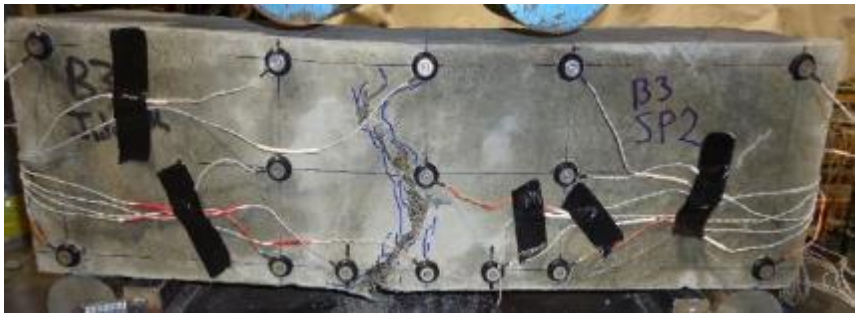
SP 3 934 fibers Wood form Single crack	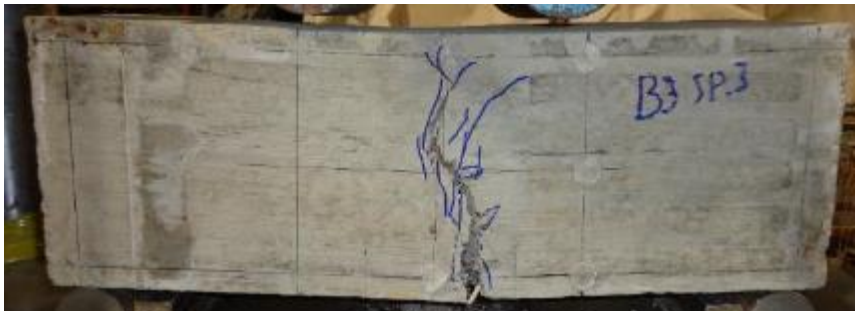
SP 4 782 fibers Single crack	
SP 5 932 fibers Multi-crack	

Batch 4: $f_c^{`} = 6$ ksi; $V_f = 1.5\%$; Fiber: (RC-80/30-BP)

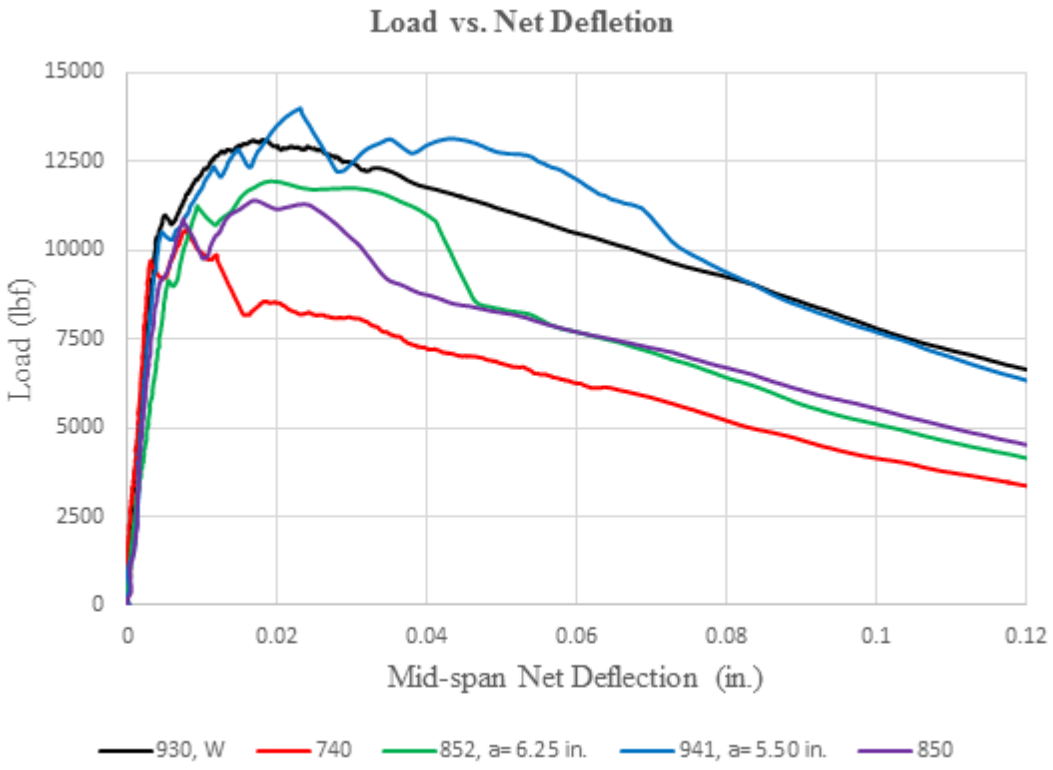

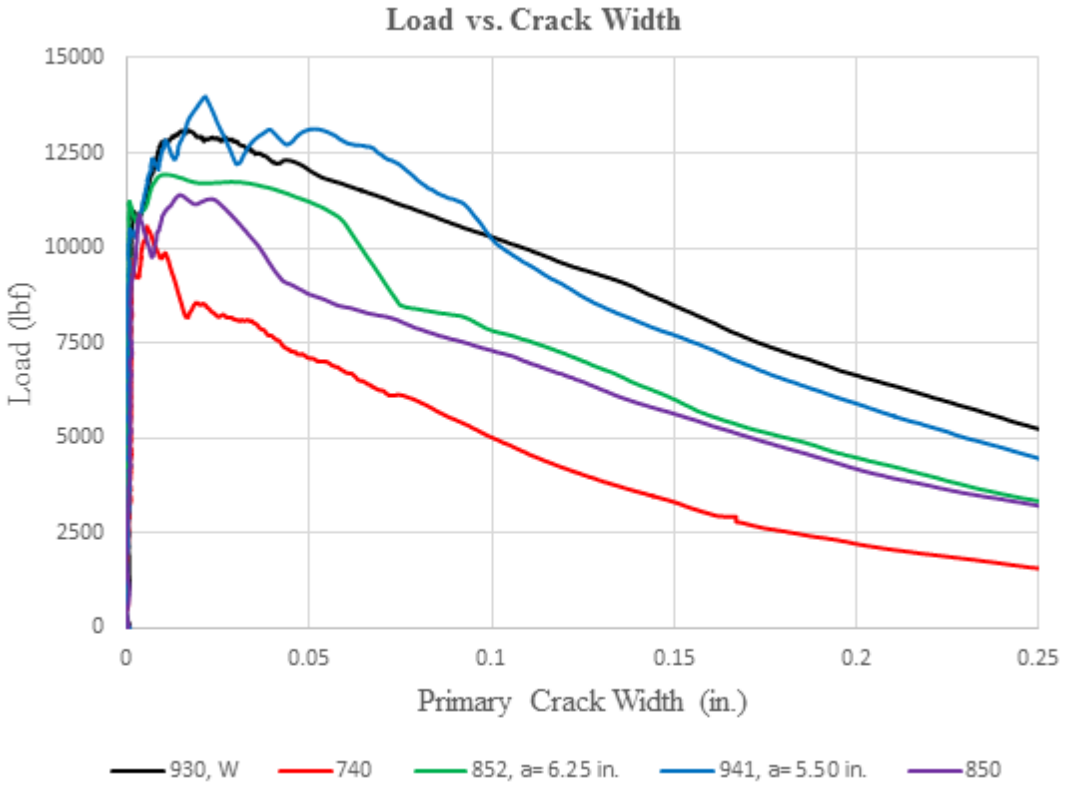

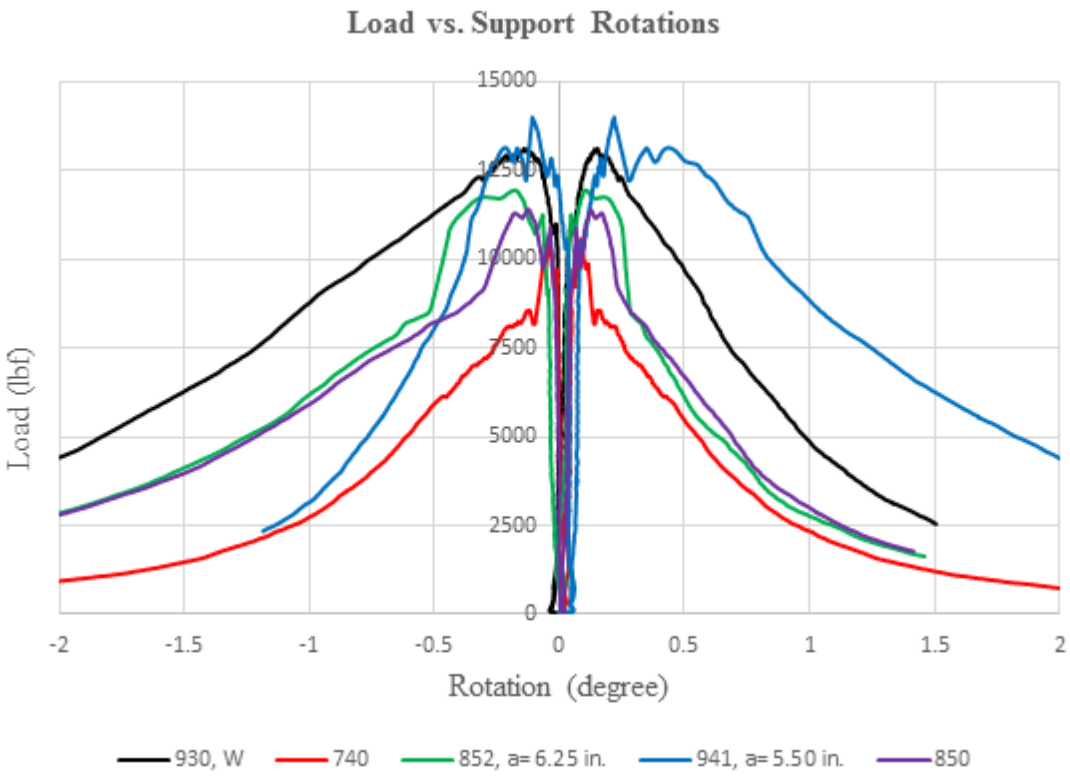

Batch ID		Fiber type			V_f (%)
B 4		(RC-80/30-BP)			1.5
P_1 (lbf)	P_{pc} (lbf)	$P_{\delta=0.04\ in.}$ (lbf)	$P_{\delta=0.08\ in.}$ (lbf)	$P_{\delta=0.12\ in.}$ (lbf)	P_{max} (lbf)
10230	12200	10310	7400	4960	12200
σ_1 (psi)	σ_{pc} (psi)	$\sigma_{\delta=0.04\ in.}$ (psi)	$\sigma_{\delta=0.08\ in.}$ (psi)	$\sigma_{\delta=0.12\ in.}$ (psi)	σ_{max} (psi)
890	1020	665	460	303	1017
δ_1 (in.)	δ_{pc} (in.)	ω_{pc} (in.)	*COV(Ppc)*		
0.006	0.02	0.01	11%		
Comment: multi-crack, dominated by fiber pullout.					

SP 1 930 fibers Wood form Multi-crack	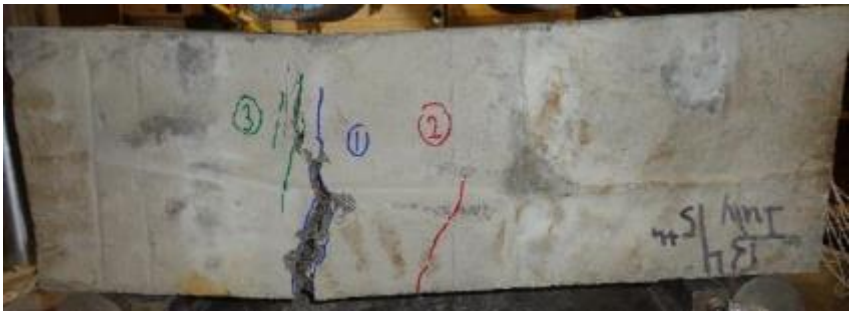
SP 2 740 fibers Multi-crack	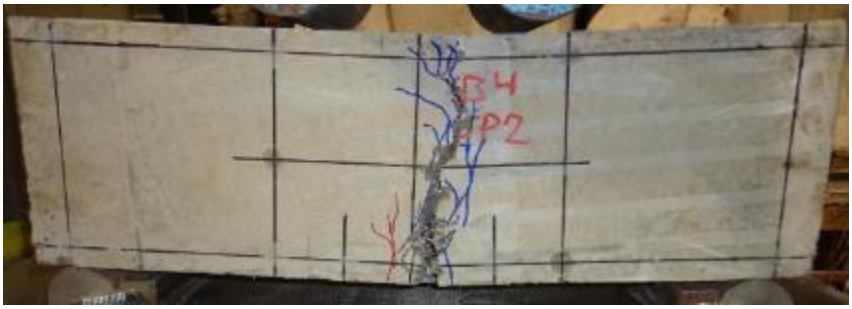
SP 3 852 fibers Multi-crack	
SP 4 941 fibers Multi-crack	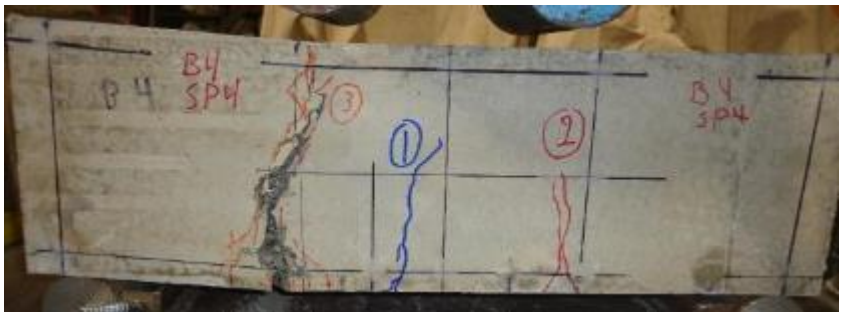
SP 5 850 fibers Single crack	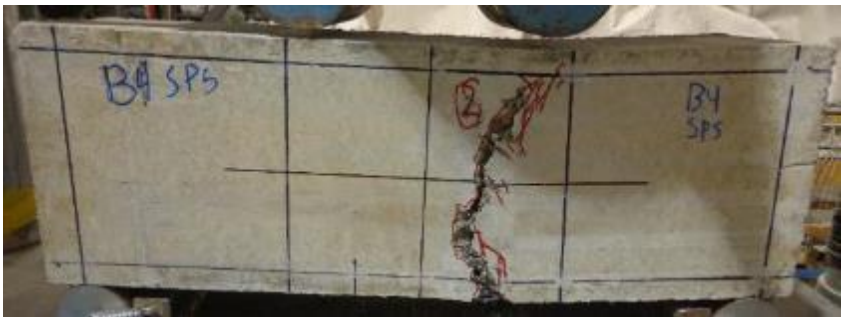

Batch 5: $f_c^{`} = 6$ ksi; $V_f = 0.5\%$; Fiber: 3D (RC-55/30-BG)

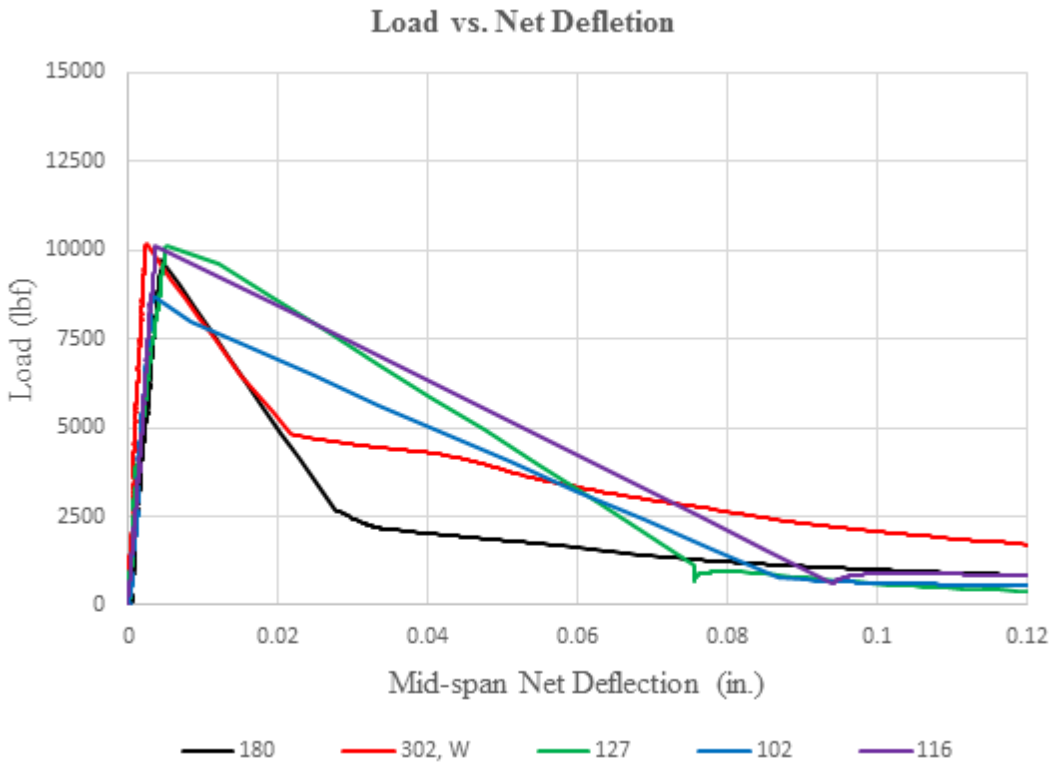

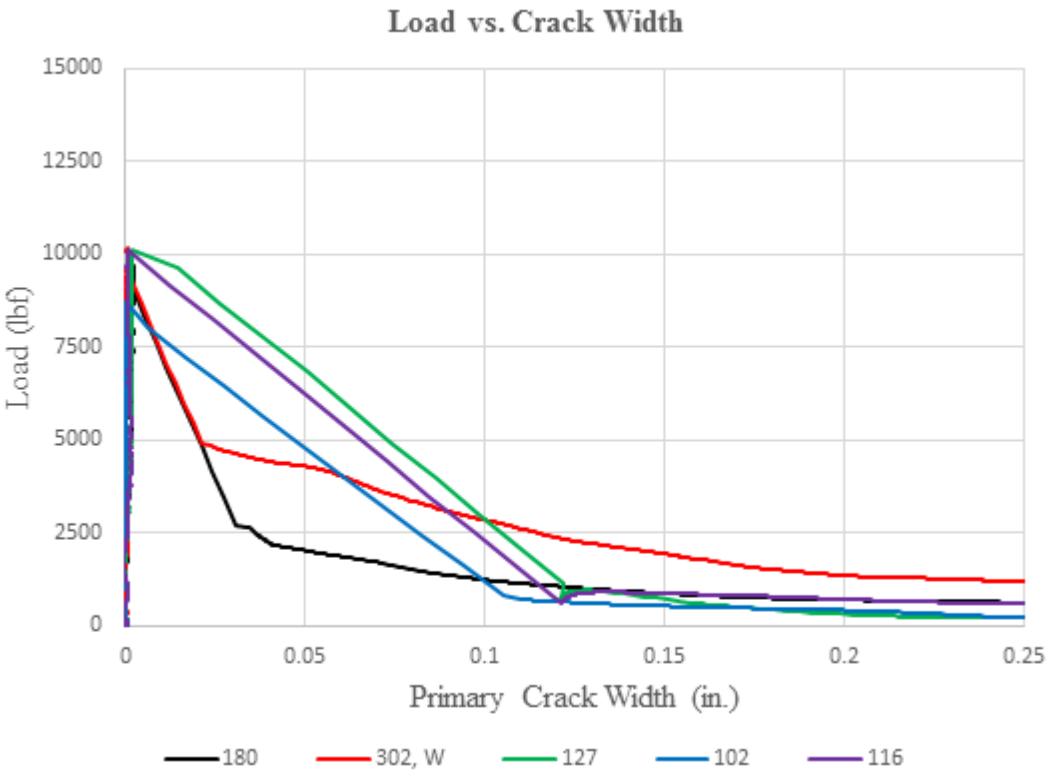

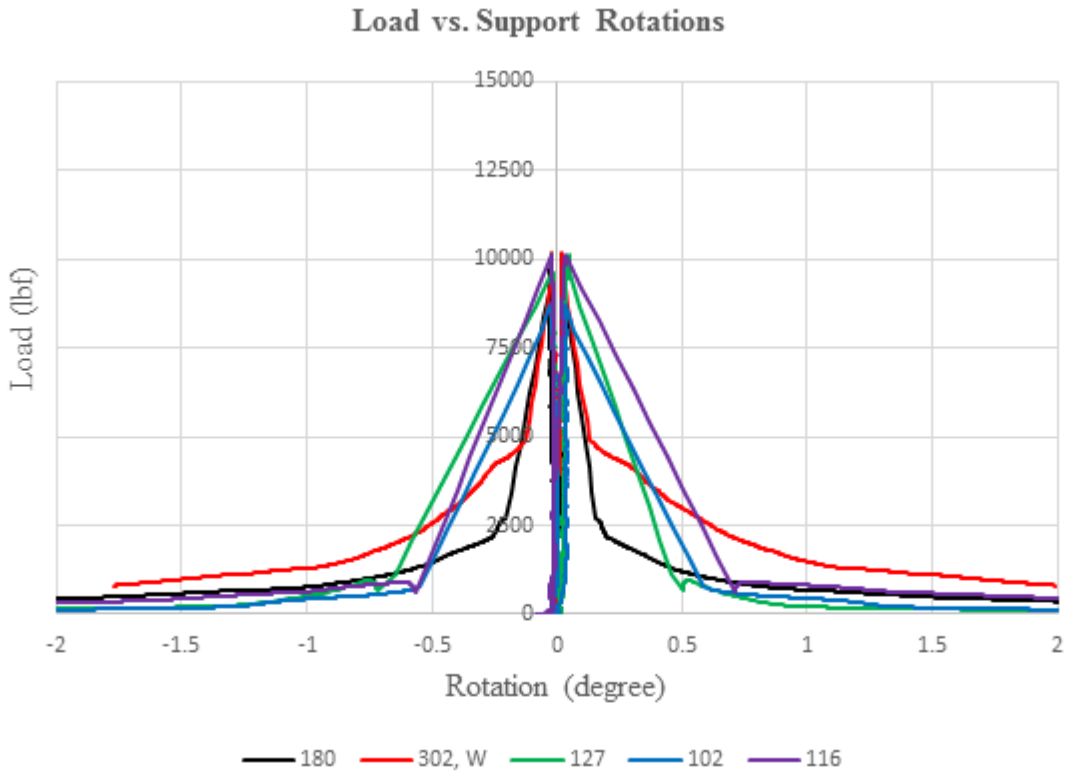

Batch ID		Fiber type			V_f (%)
B 5		3D (RC-55/30-BG)			0.5
P_1 (lbf)	P_{pc} (lbf)	$P_{\delta=0.04\ in.}$ (lbf)	$P_{\delta=0.08\ in.}$ (lbf)	$P_{\delta=0.12\ in.}$ (lbf)	P_{max} (lbf)
9760	2050	4650	1420	860	9760
σ_1 (psi)	σ_{pc} (psi)	$\sigma_{\delta=0.04\ in.}$ (psi)	$\sigma_{\delta=0.08\ in.}$ (psi)	$\sigma_{\delta=0.12\ in.}$ (psi)	σ_{max} (psi)
785	165	375	125	220	785
δ_1 (in.)	δ_{pc} (in.)	ω_{pc} (in.)	*COV(Ppc)*		
0.004	0.06	0.10	84%		
Comment: brittle failure, fiber bundles, dominated by fiber pullout.					

SP 1 180 fibers Single crack	
SP 2 302 fibers Wood form Single crack	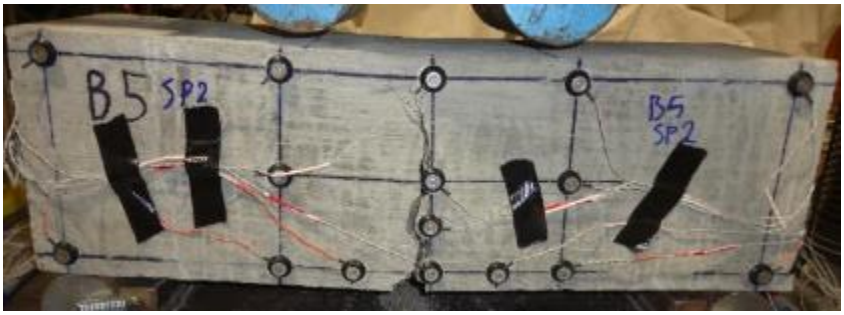
SP 3 127 fibers Single crack	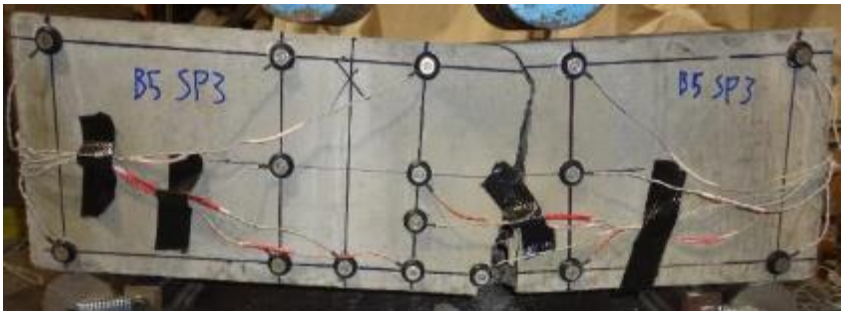
SP 4 102 fibers Single crack	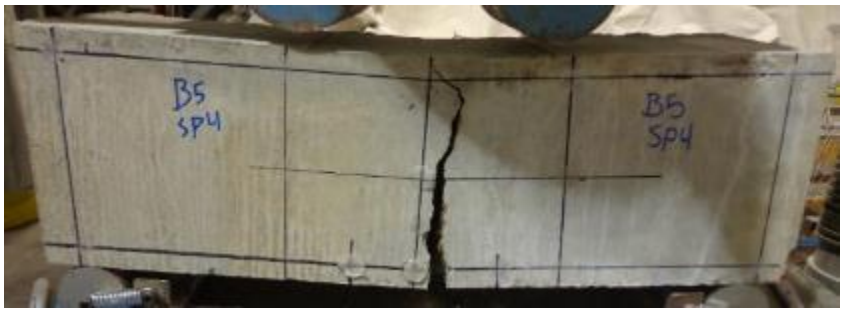
SP 5 116 fibers Single crack	

Batch 6: $f_c^{`} = 6$ ksi; $V_f = 0.75\%$; Fiber: 3D (RC-55/30-BG)

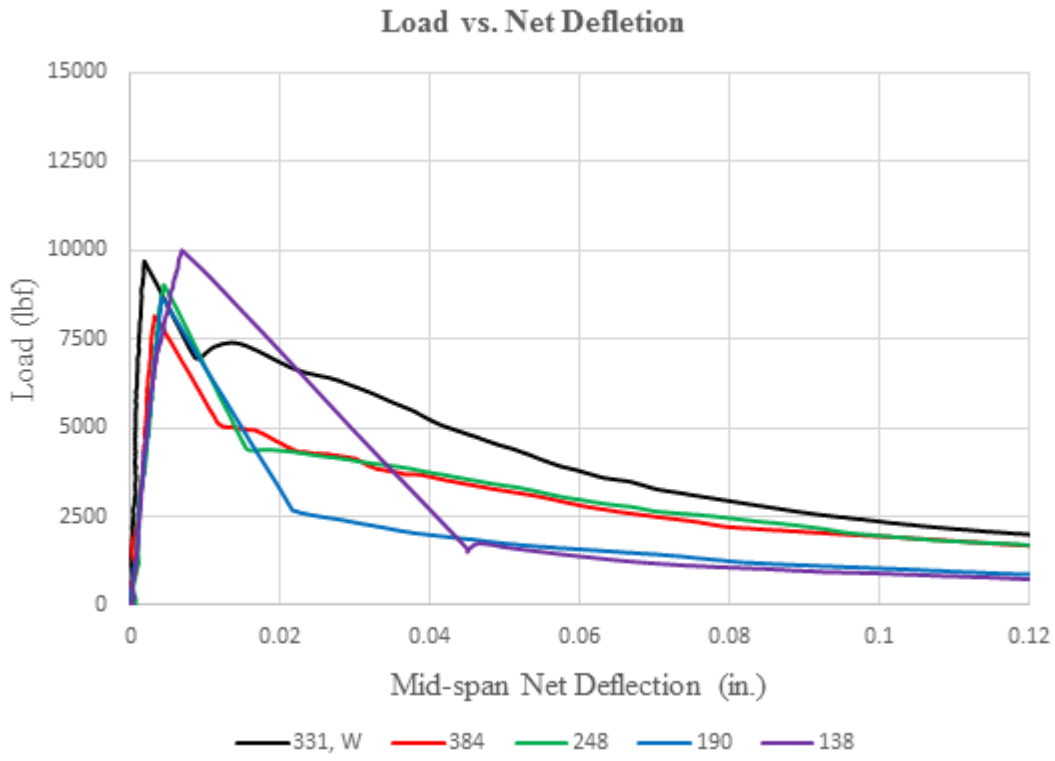

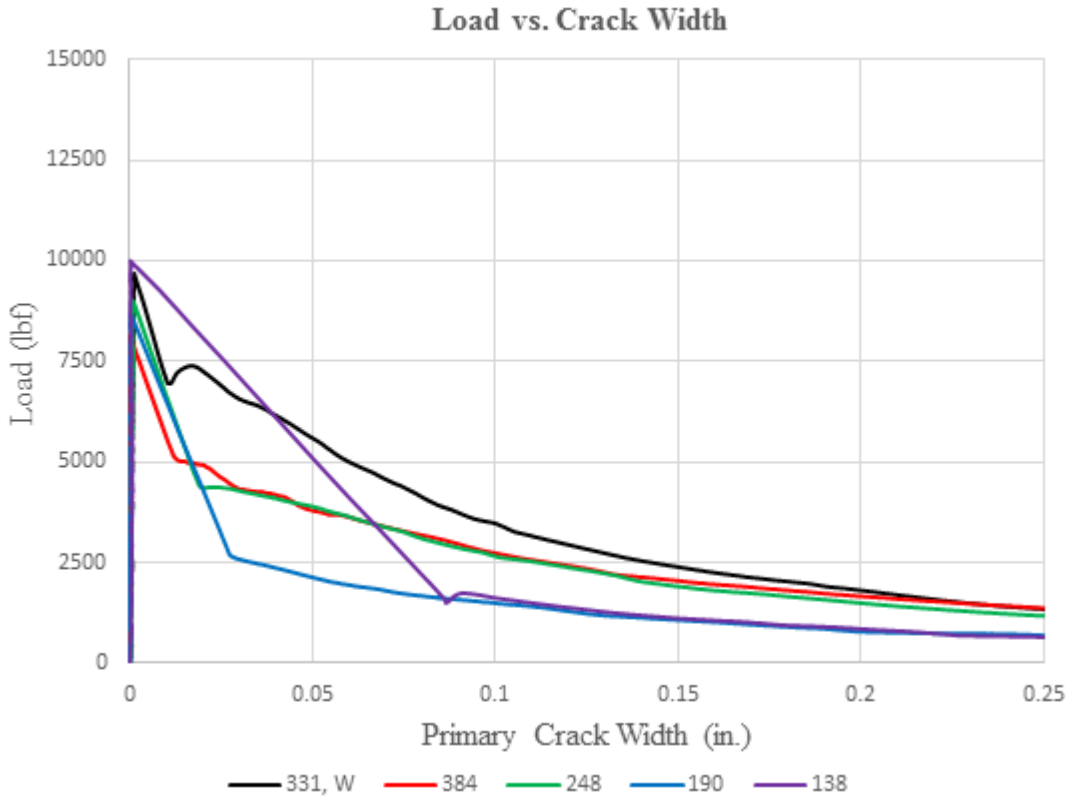

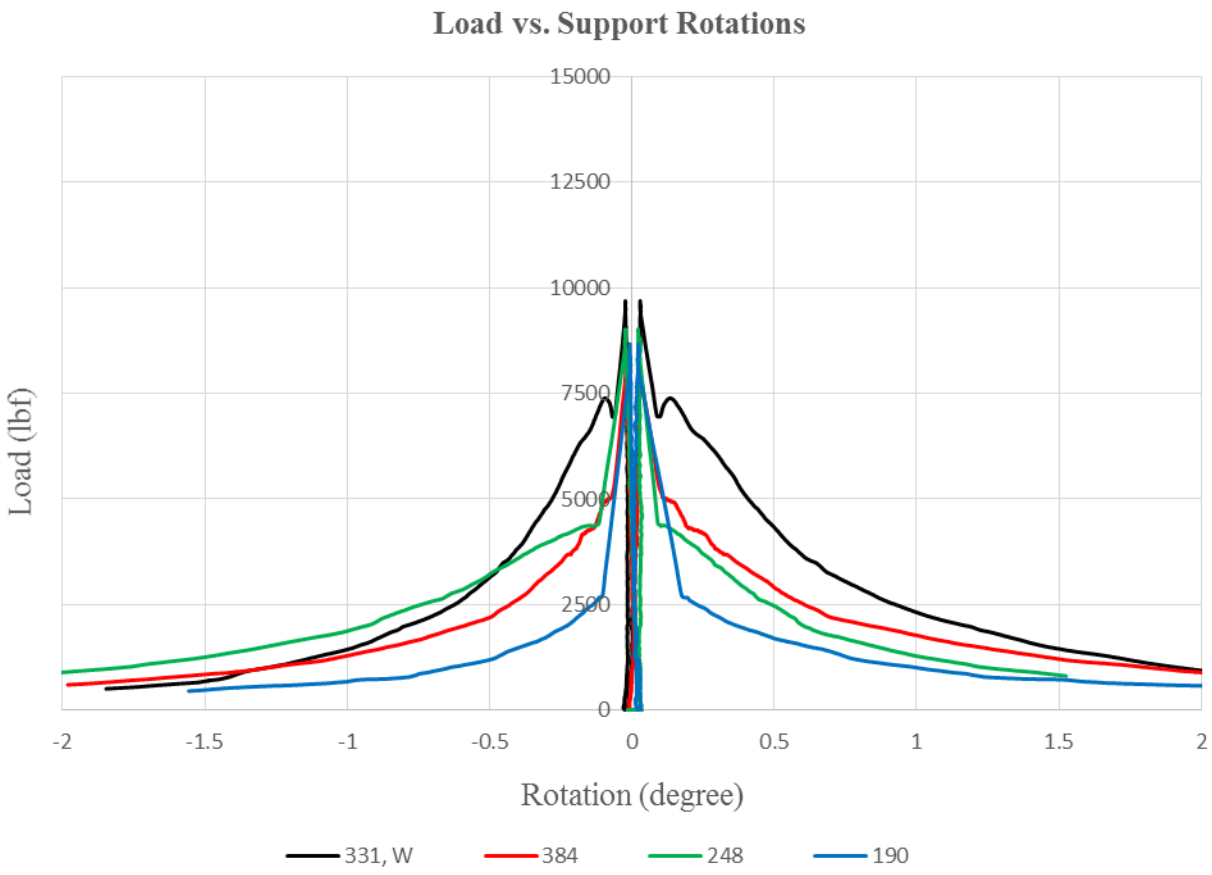

Batch ID		Fiber type			V_f (%)
B 6		3D (RC55/30-BG)			0.75
P_1 (lbf)	P_{pc} (lbf)	$P_{\delta=0.04\ in.}$ (lbf)	$P_{\delta=0.08\ in.}$ (lbf)	$P_{\delta=0.12\ in.}$ (lbf)	P_{max} (lbf)
9100	4210	3390	1980	1390	9100
σ_1 (psi)	σ_{pc} (psi)	$\sigma_{\delta=0.04\ in.}$ (psi)	$\sigma_{\delta=0.08\ in.}$ (psi)	$\sigma_{\delta=0.12\ in.}$ (psi)	σ_{max} (psi)
755	340	280	160	115	755
δ_1 (in.)	δ_{pc} (in.)	ω_{pc} (in.)	$COV(P_{pc})$		
0.004	0.02	0.04	52%		
Comment: brittle failure, fiber bundles, dominated by fiber pullout.					

SP 1 331 fibers Wood form Single crack	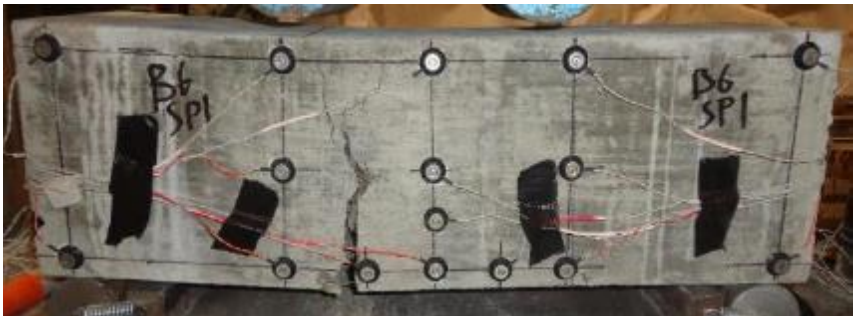
SP 2 384 fibers Single crack	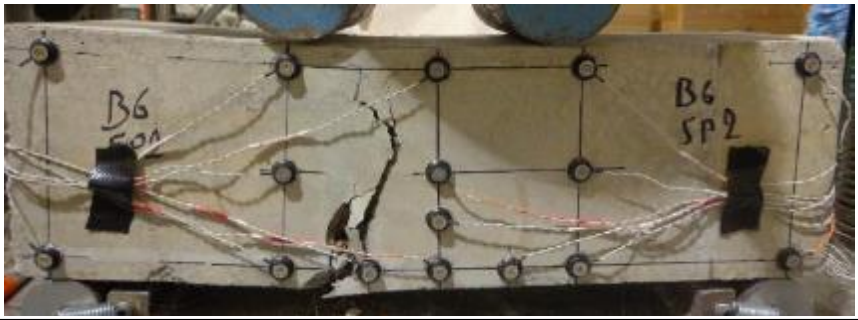
SP 3 248 fibers Single crack	
SP 4 190 fibers Single crack	
SP 5 138 fibers Single crack	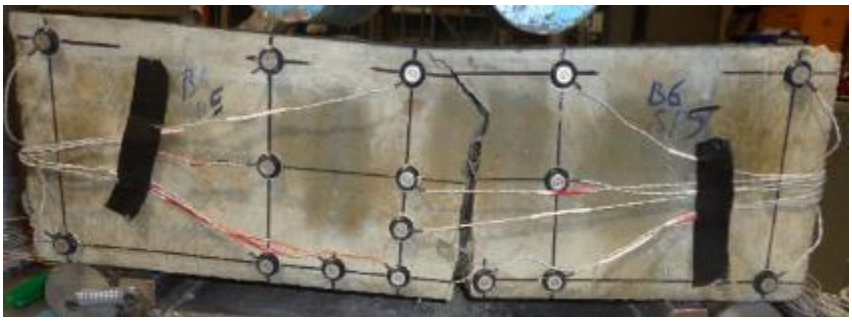

Batch 7: $f_c^{`} = 6$ ksi; $V_f = 1.0\%$; Fiber: 3D (RC-55/30-BG)

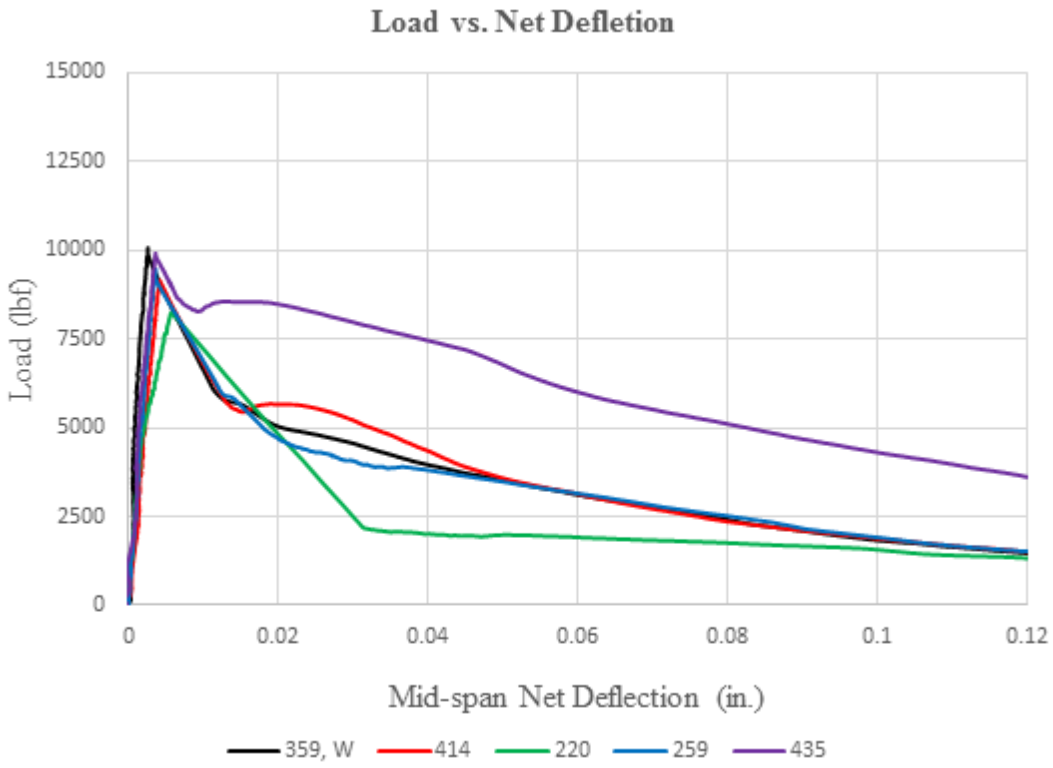

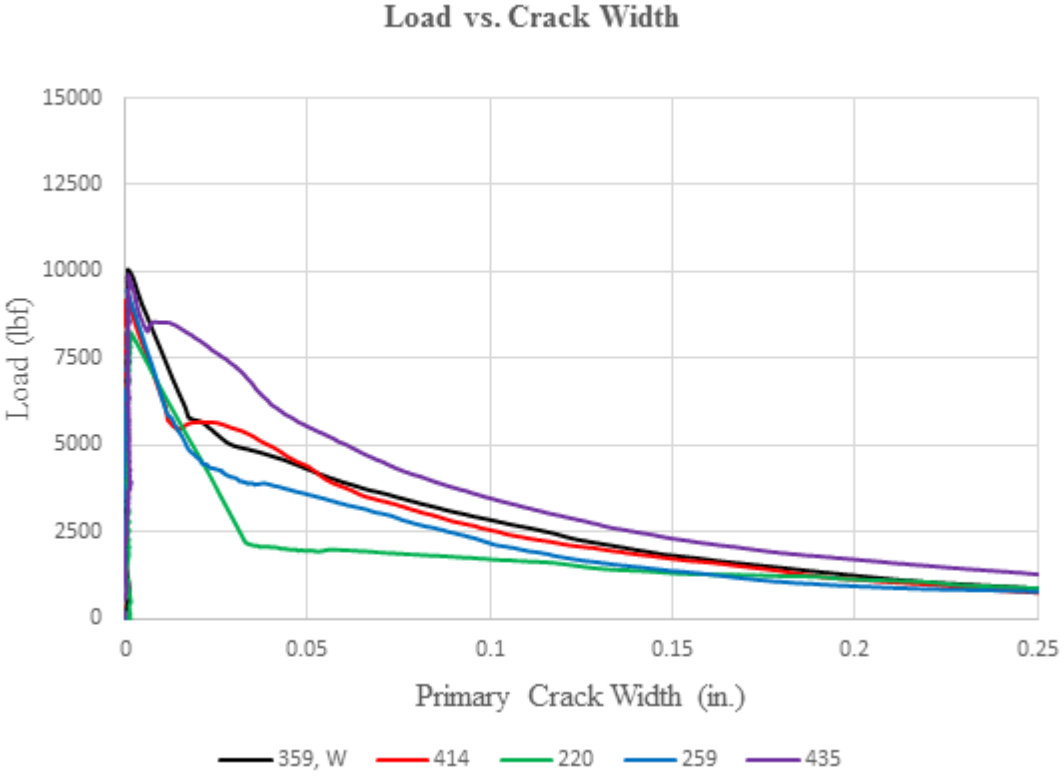

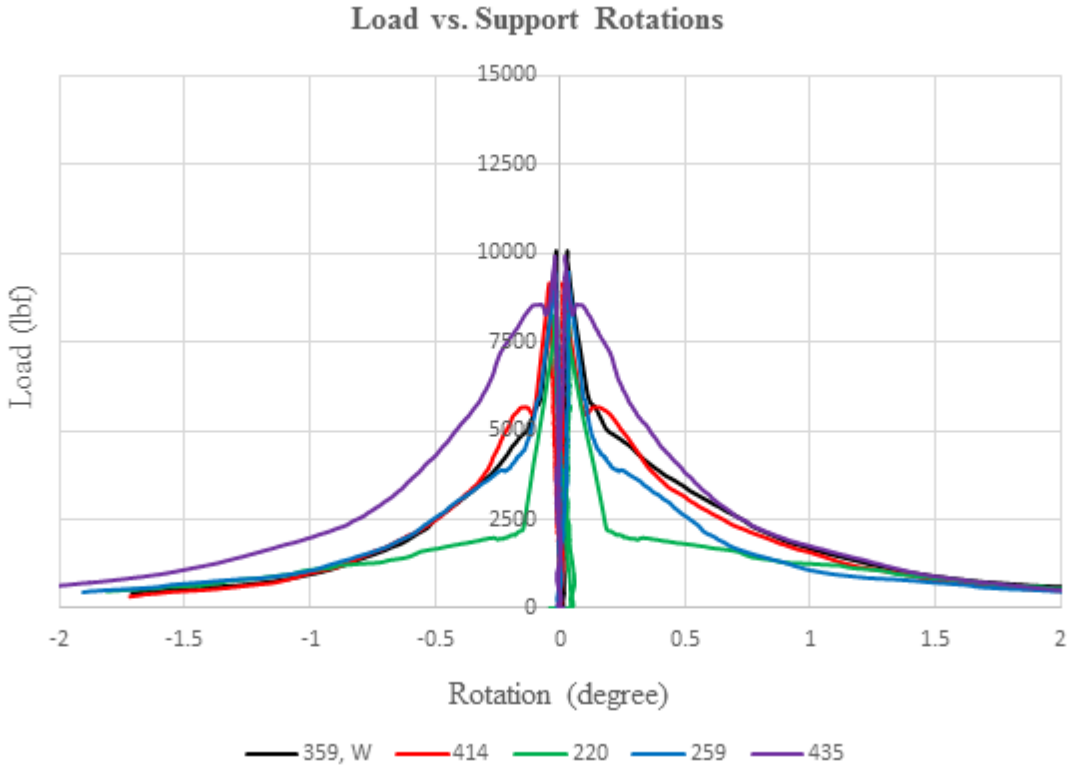

Batch ID		Fiber type			V_f (%)
B 7		3D (RC55/30-BG)			1.0
P_1 (lbf)	P_{pc} (lbf)	$P_{\delta=0.04\ in.}$ (lbf)	$P_{\delta=0.08\ in.}$ (lbf)	$P_{\delta=0.12\ in.}$ (lbf)	P_{max} (lbf)
9360	5500	4330	2840	1890	9360
σ_1 (psi)	σ_{pc} (psi)	$\sigma_{\delta=0.04\ in.}$ (psi)	$\sigma_{\delta=0.08\ in.}$ (psi)	$\sigma_{\delta=0.12\ in.}$ (psi)	σ_{max} (psi)
755	445	350	115	155	755
δ_1 (in.)	δ_{pc} (in.)	ω_{pc} (in.)	$COV(P_{pc})$		
0.004	0.02	0.03	41%		
Comment: brittle failure, fiber bundles, dominated by fiber pullout.					

SP 1 359 fibers Wood form Single crack	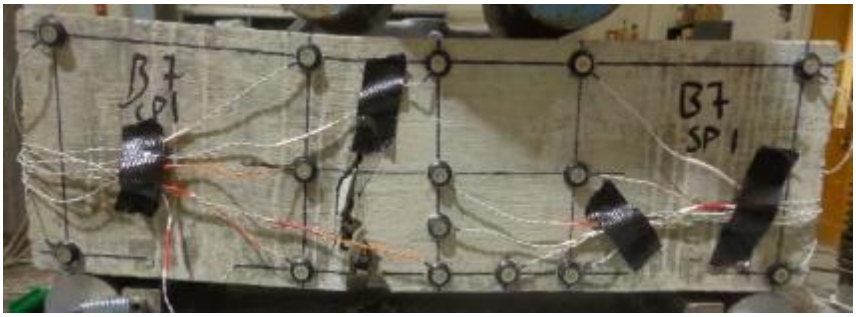
SP 2 414 fibers Single crack	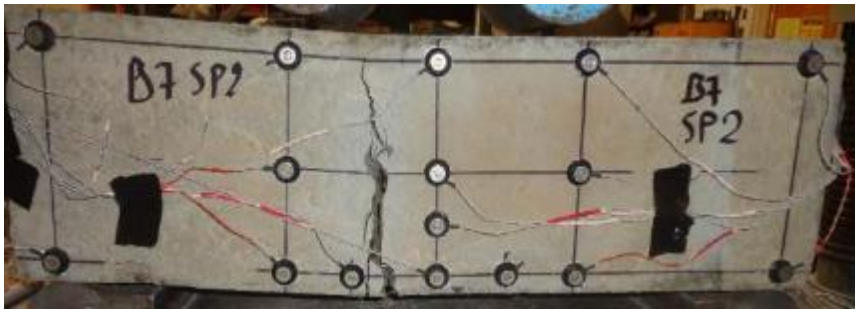
SP 3 220 fibers Single crack	
SP 4 259 fibers Single crack	
SP 5 435 fibers Single crack	

Batch 8: $f_c^{`} = 6$ ksi; $V_f = 1.5\%$; Fiber: 3D (RC-55/30-BG)

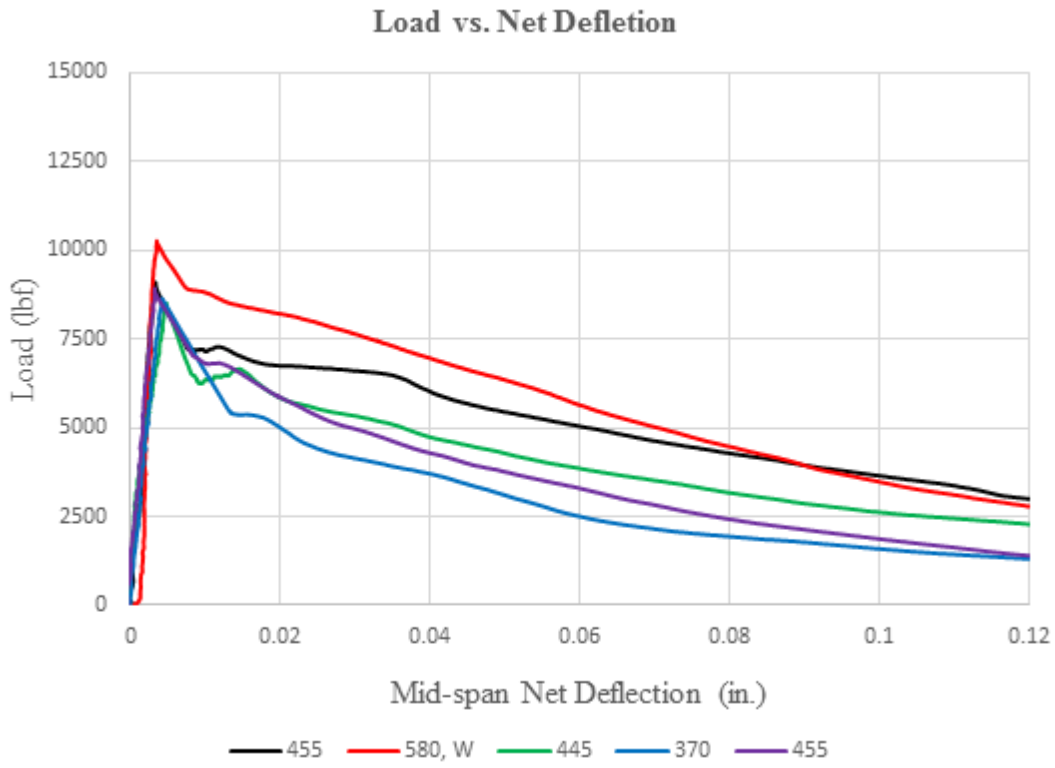

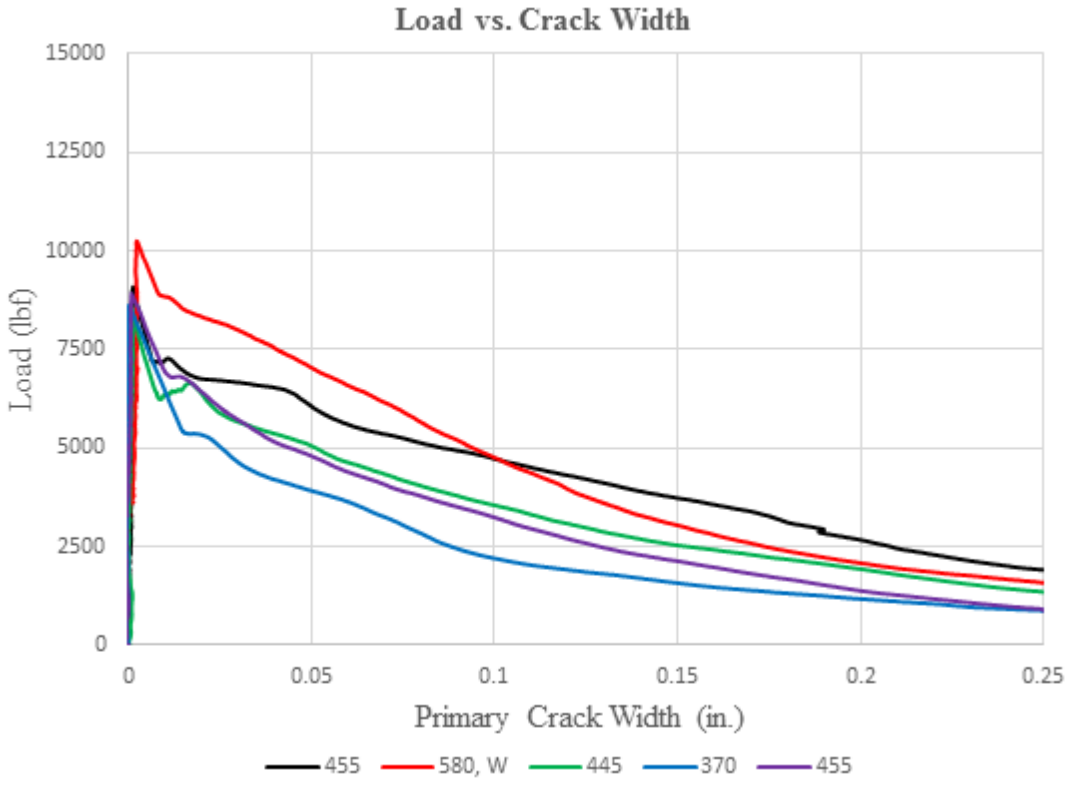

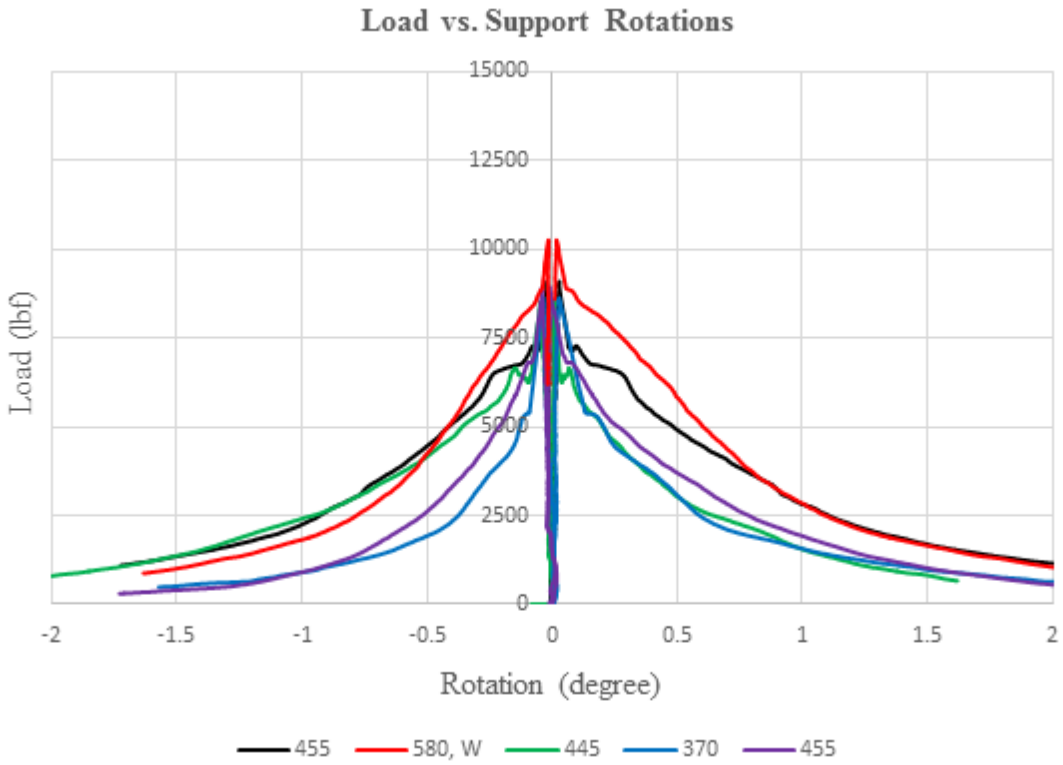

Batch ID		Fiber type			V_f (%)
B 8		3D (RC-55/30-BG)			1.5
P_1 (lbf)	P_{pc} (lbf)	$P_{\delta=0.04\ in.}$ (lbf)	$P_{\delta=0.08\ in.}$ (lbf)	$P_{\delta=0.12\ in.}$ (lbf)	P_{max} (lbf)
9080	6770	5150	3260	2160	9080
σ_1 (psi)	σ_{pc} (psi)	$\sigma_{\delta=0.04\ in.}$ (psi)	$\sigma_{\delta=0.08\ in.}$ (psi)	$\sigma_{\delta=0.12\ in.}$ (psi)	σ_{max} (psi)
735	545	415	265	175	735
δ_1 (in.)	δ_{pc} (in.)	ω_{pc} (in.)	$COV(P_{pc})$		
0.004	0.02	0.02	13%		
Comment: brittle failure, fiber bundles, dominated by fiber pullout.					

SP 1 455 fibers Single crack	
SP 2 580 fibers Wood form Single crack	
SP 3 445 fibers Single crack	
SP 4 370 fibers Single crack	
SP 5 455 fibers Single crack	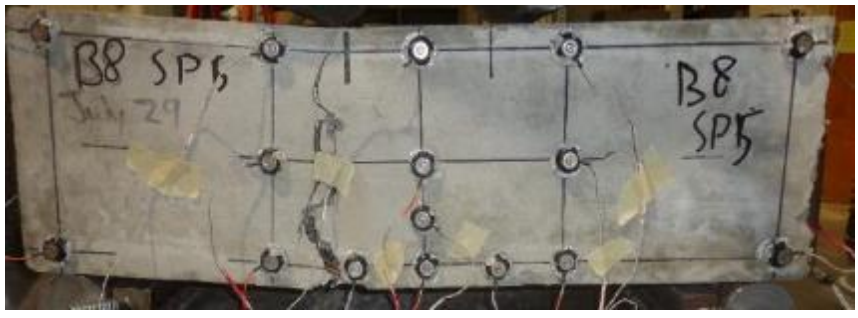

Batch 9: $f_c^{`} = 6$ ksi; $V_f = 0.5\%$; Fiber: 4D (RC-65/60-BG)

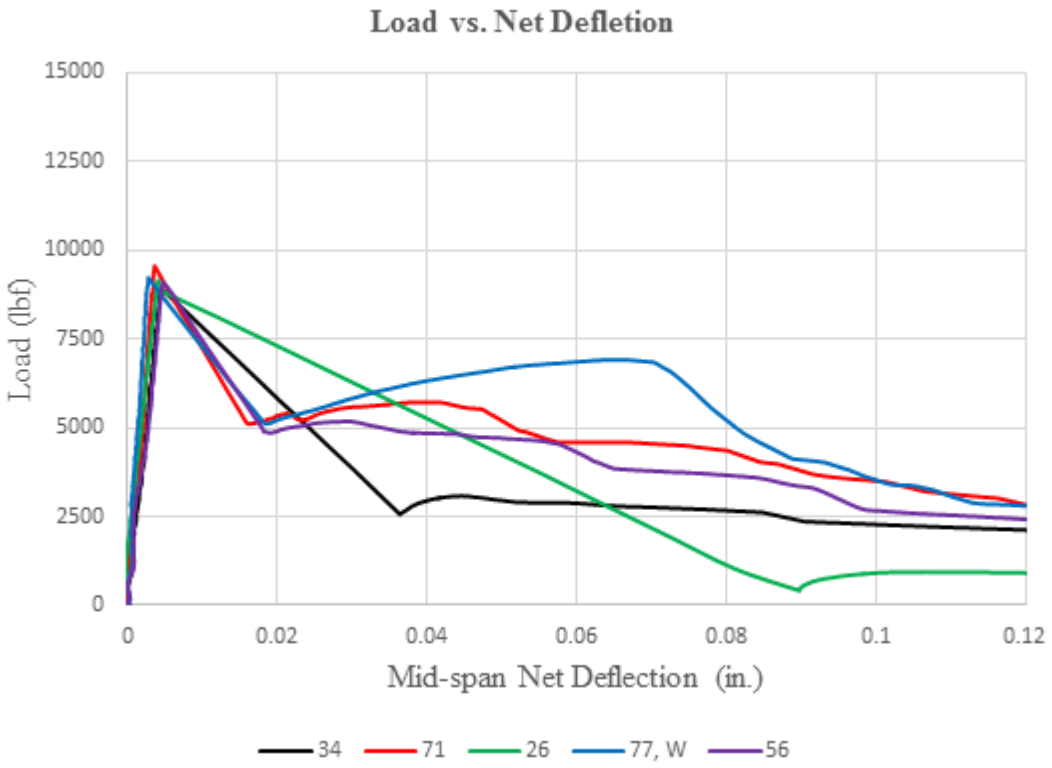

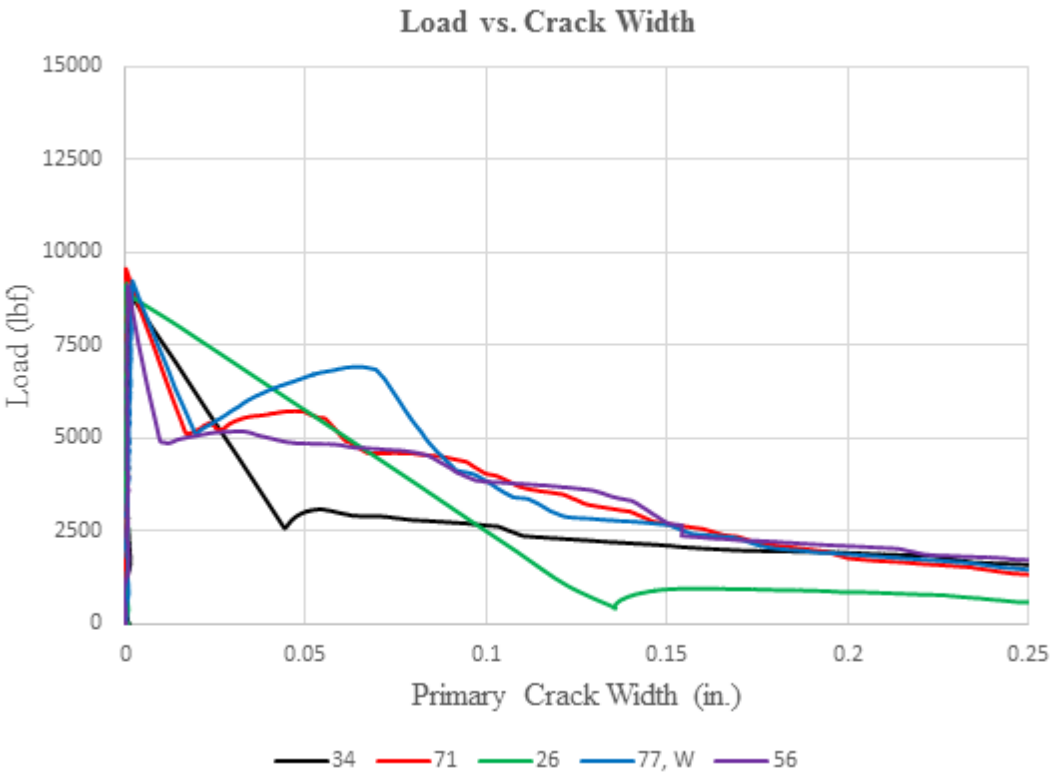

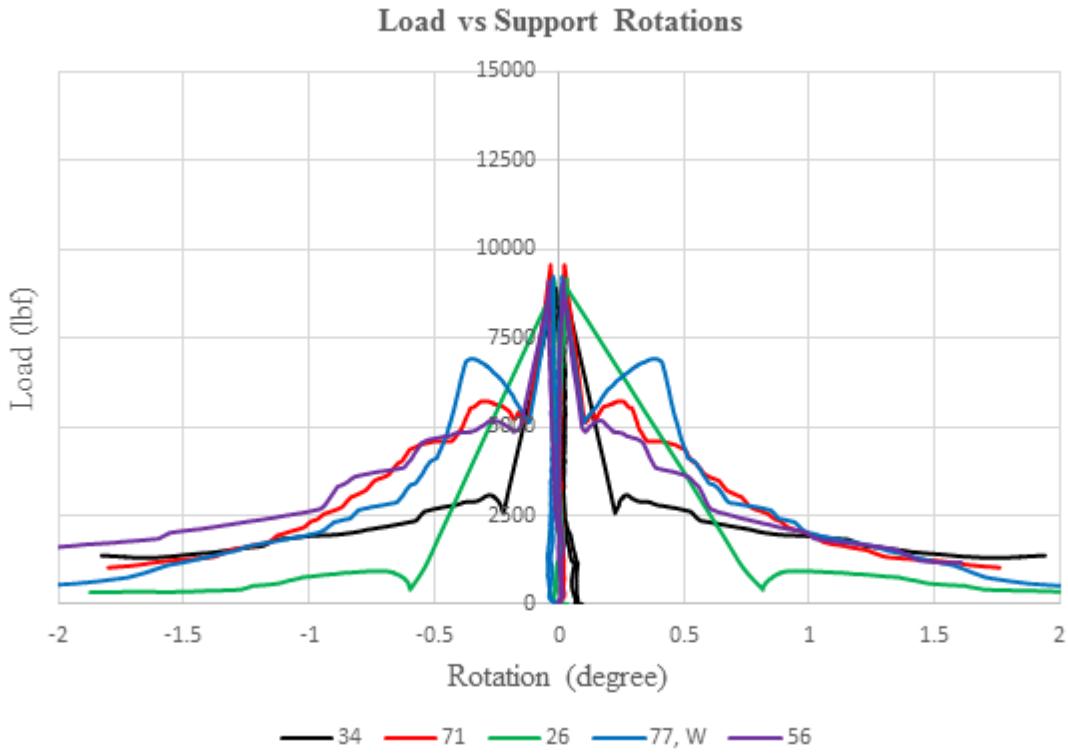

Batch ID		Fiber type			V_f (%)
B 9		4D (RC-65/60-BG)			0.5
P_1 (lbf)	P_{pc} (lbf)	$P_{\delta=0.04\ in.}$ (lbf)	$P_{\delta=0.08\ in.}$ (lbf)	$P_{\delta=0.12\ in.}$ (lbf)	P_{max} (lbf)
9180	4360	5050	3400	2220	9180
σ_1 (psi)	σ_{pc} (psi)	$\sigma_{\delta=0.04\ in.}$ (psi)	$\sigma_{\delta=0.08\ in.}$ (psi)	$\sigma_{\delta=0.12\ in.}$ (psi)	σ_{max} (psi)
740	350	330	215	135	740
δ_1 (in.)	δ_{pc} (in.)	ω_{pc} (in.)	$COV(P_{pc})$		
0.005	0.06	0.07	54%		
Comments: brittle failure, fiber bundles, dominated by fiber pullout and fiber fracture.					

SP 1 34 fibers Single crack	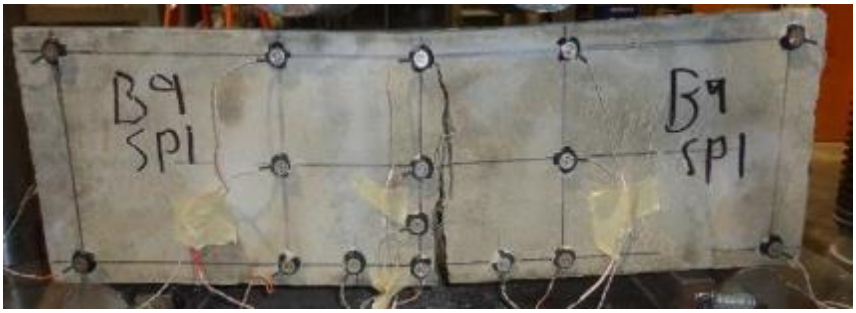
SP 2 71 fibers Single crack	
SP 3 26 fibers Single crack	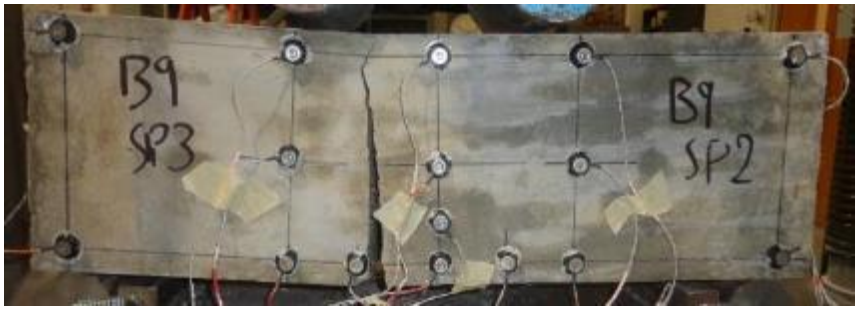
SP 4 77 fibers Wood form Single crack	
SP 5 56 fibers Single crack	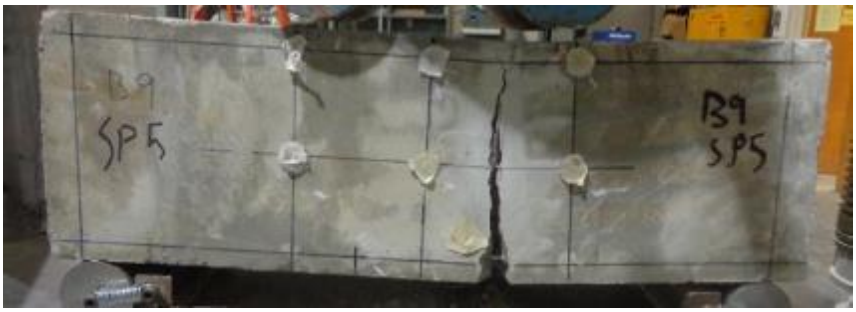

Batch 10: $f_c^{`} = 6$ ksi; $V_f = 0.75\%$; Fiber: 4D (RC-65/60-BG)

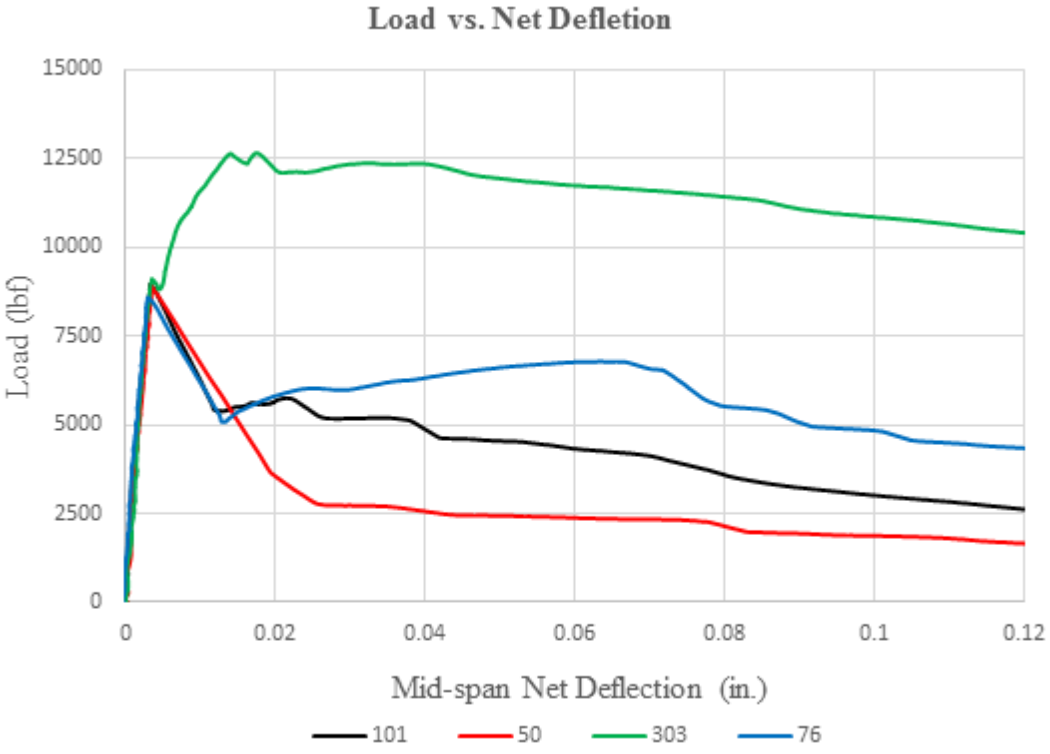

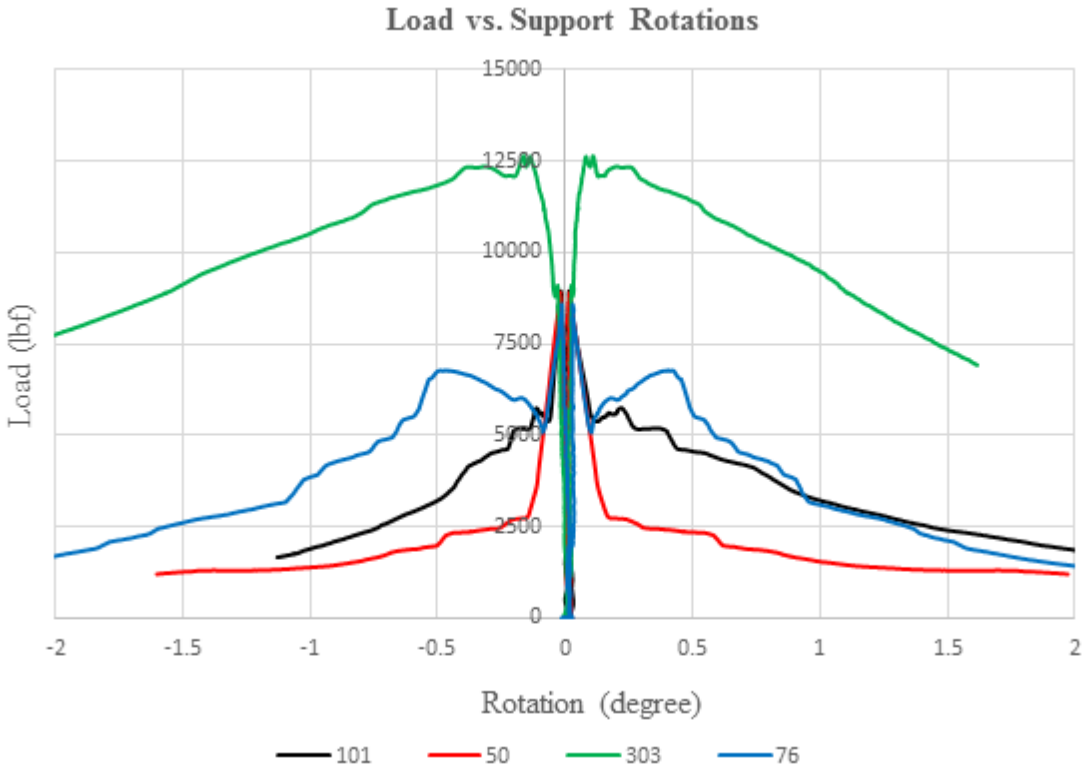

Batch ID		Fiber type			V_f (%)
B 10		4D (RC-65/60-BG)			0.75
P_1 (lbf)	P_{pc} (lbf)	$P_{\delta=0.04\ in.}$ (lbf)	$P_{\delta=0.08\ in.}$ (lbf)	$P_{\delta=0.12\ in.}$ (lbf)	P_{max} (lbf)
8890	6940	6540	5670	4769	8890
σ_1 (psi)	σ_{pc} (psi)	$\sigma_{\delta=0.04\ in.}$ (psi)	$\sigma_{\delta=0.08\ in.}$ (psi)	$\sigma_{\delta=0.12\ in.}$ (psi)	σ_{max} (psi)
735	570	540	465	310	735
δ_1 (in.)	δ_{pc} (in.)	ω_{pc} (in.)	$COV(P_{pc})$		
0.004	0.03	0.05	60%		
Comment: brittle failure, fiber bundles, dominated by fiber pullout and fiber fracture.					

SP 1 101 fibers Single crack	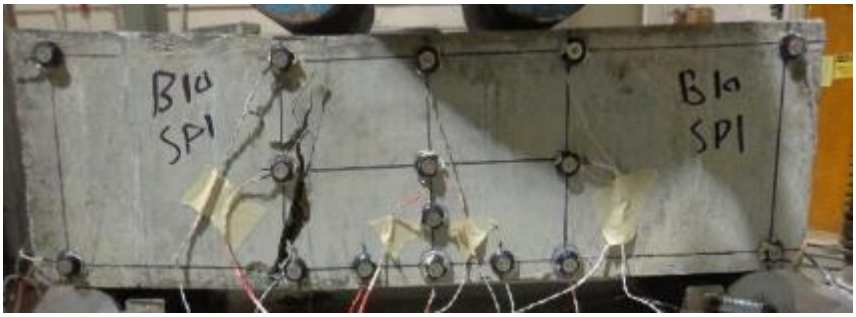
SP 2 50 fibers Single crack	
SP 3 303 fibers Multi-crack	
SP 4 76 fibers Single crack	
SP 5 Wood form Neglected (the test was not completed)	

Batch 11: $f_c^{`} = 6$ ksi; $V_f = 1.0\%$; Fiber: 4D (RC-65/60-BG)

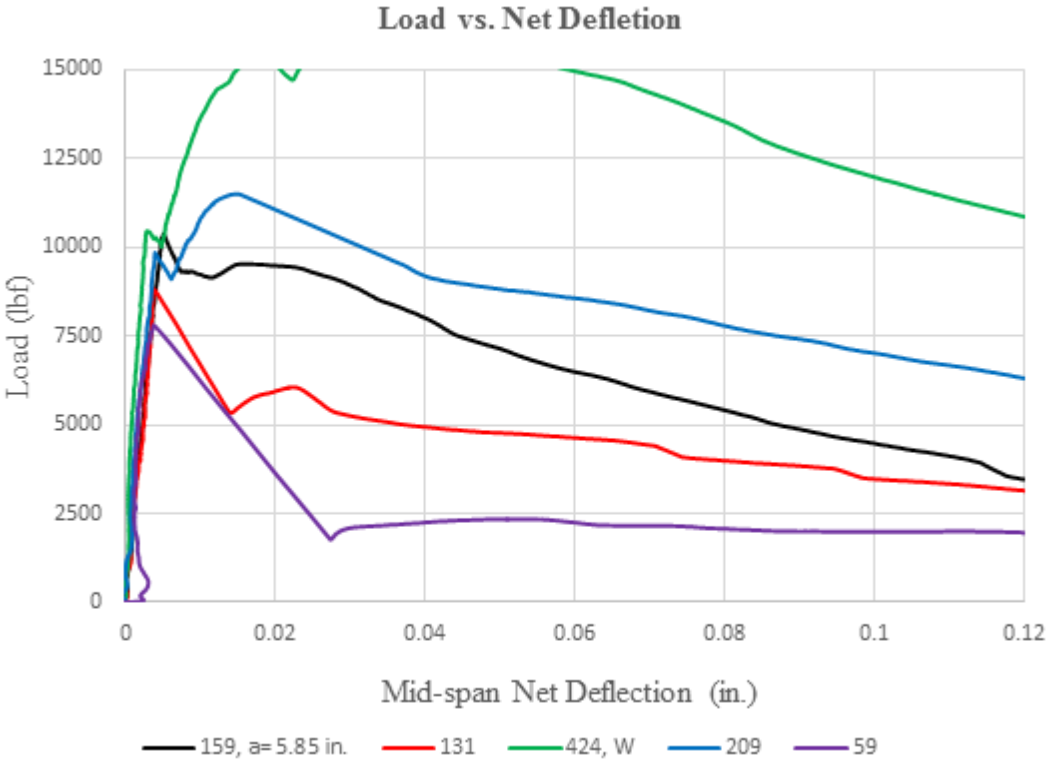

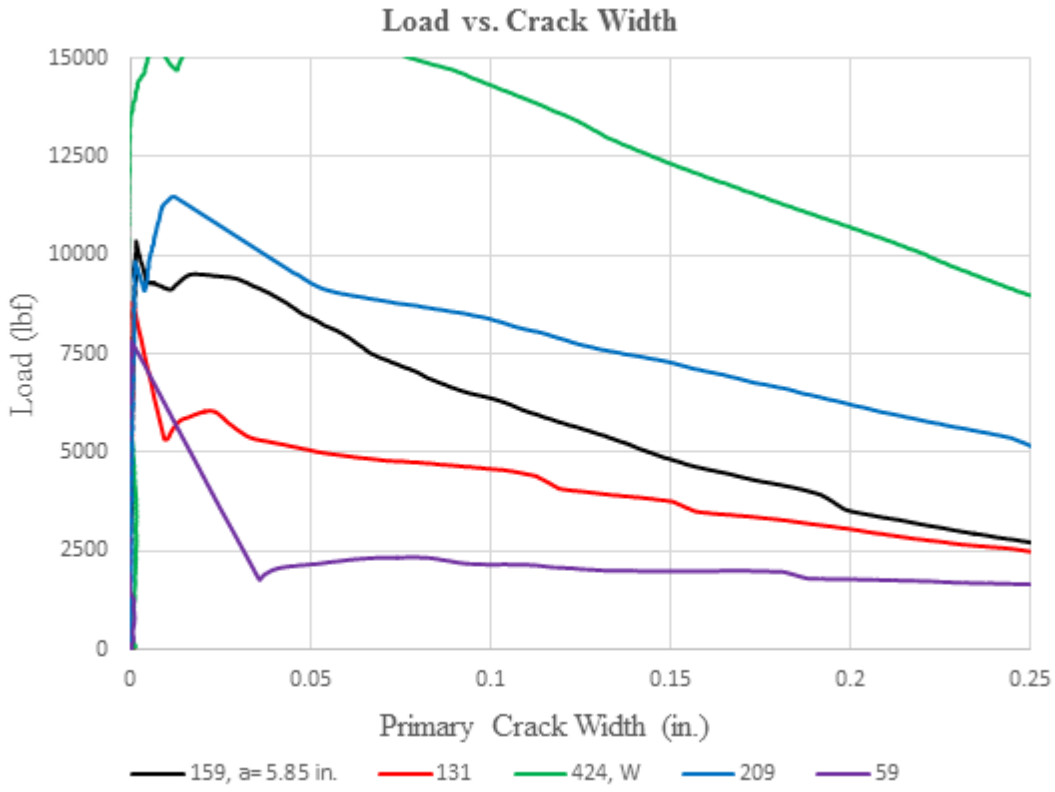

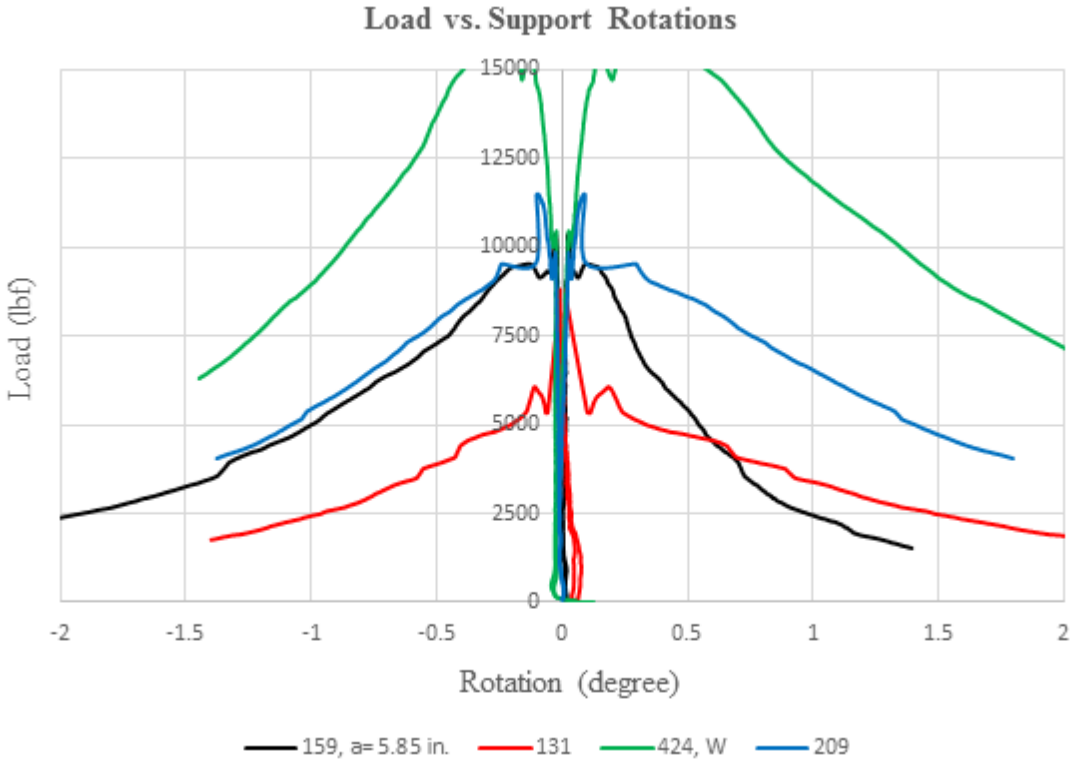

Batch ID		Fiber type			V_f (%)
B 11		4D (RC-65/60-BG)			1.0
P_1 (lbf)	P_{pc} (lbf)	$P_{\delta=0.04\ in.}$ (lbf)	$P_{\delta=0.08\ in.}$ (lbf)	$P_{\delta=0.12\ in.}$ (lbf)	P_{max} (lbf)
9460	9070	8100	6550	5140	9460
σ_1 (psi)	σ_{pc} (psi)	$\sigma_{\delta=0.04\ in.}$ (psi)	$\sigma_{\delta=0.08\ in.}$ (psi)	$\sigma_{\delta=0.12\ in.}$ (psi)	σ_{max} (psi)
760	720	645	520	410	760
δ_1 (in.)	δ_{pc} (in.)	ω_{pc} (in.)	$COV(P_{pc})$		
0.004	0.02	0.04	59%		
Comment: brittle failure, dominated by fiber pullout and fiber fracture.					

SP 1 159 fibers Single crack	
SP 2 131 fibers Single crack	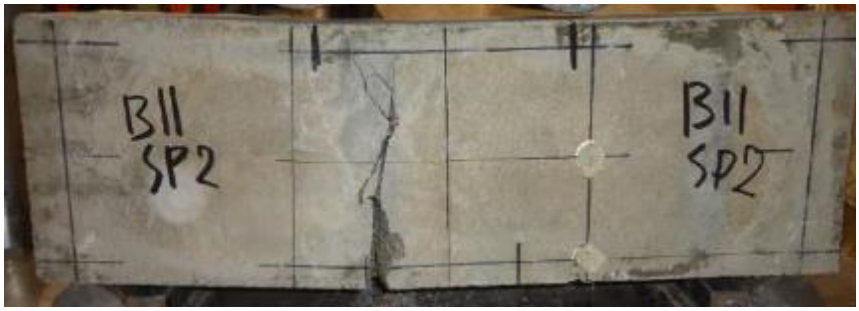
SP 3 424 fibers Wood form Multi-crack	
SP 4 209 fibers Multi-crack	
SP 5 59 fibers Single crack	

Batch 12: $f_c^{`} = 6$ ksi; $V_f = 1.5\%$; Fiber: 4D (RC-65/60-BG)

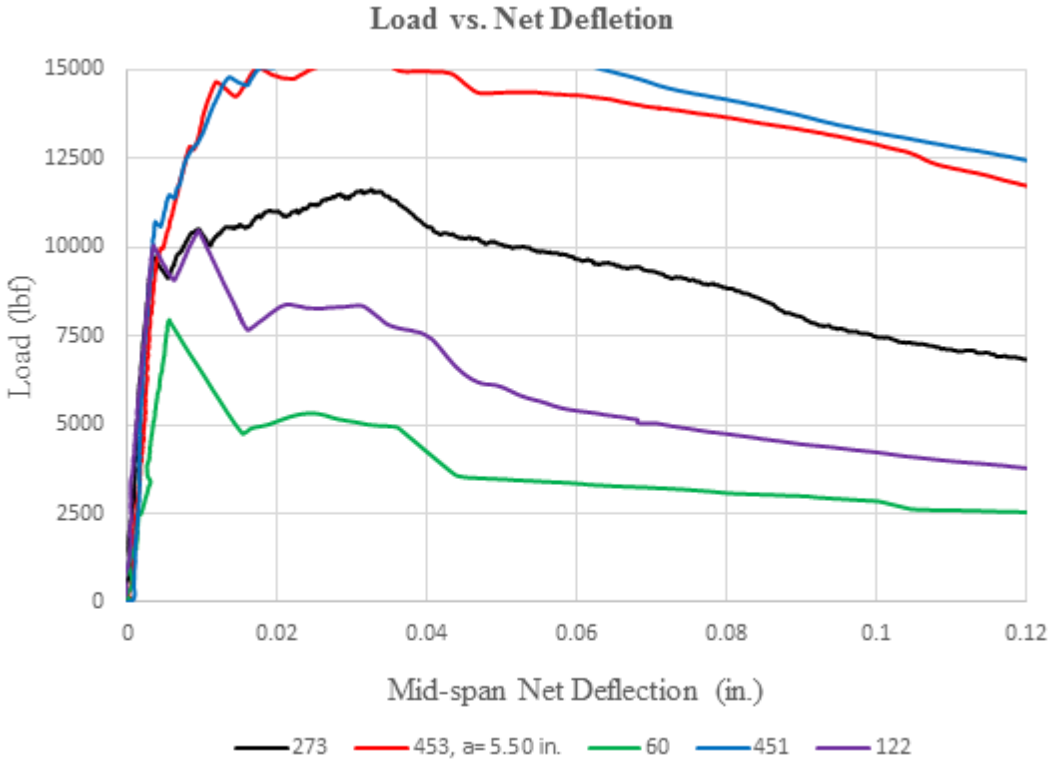

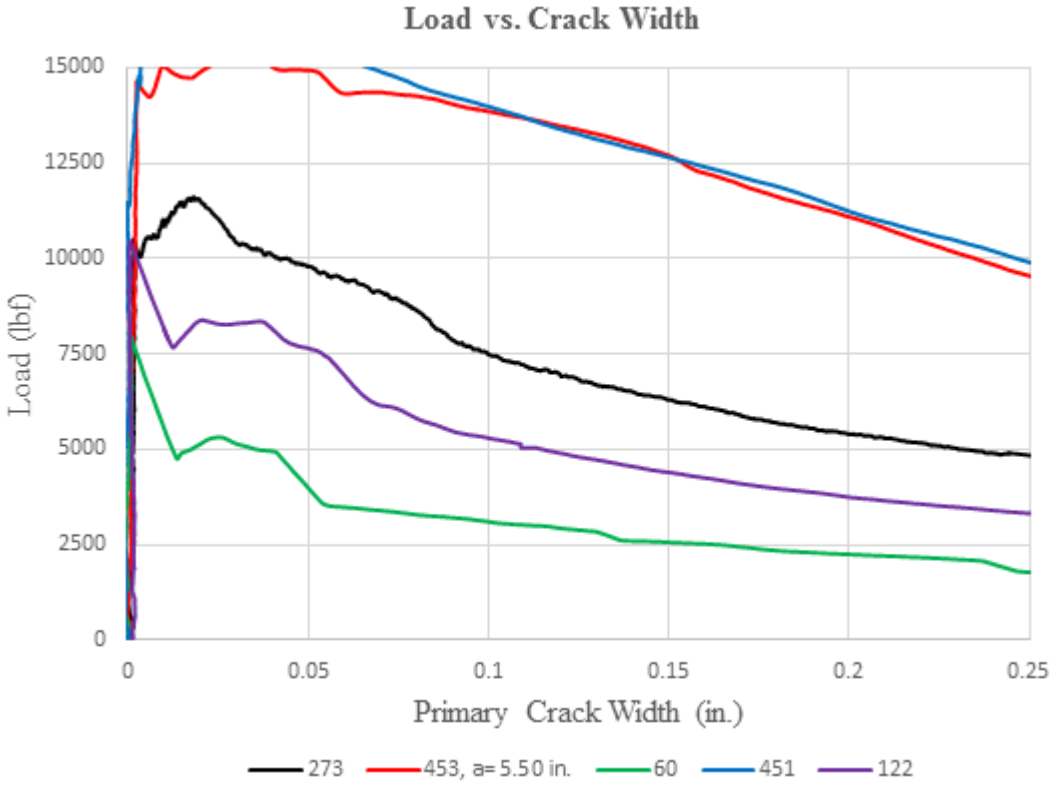

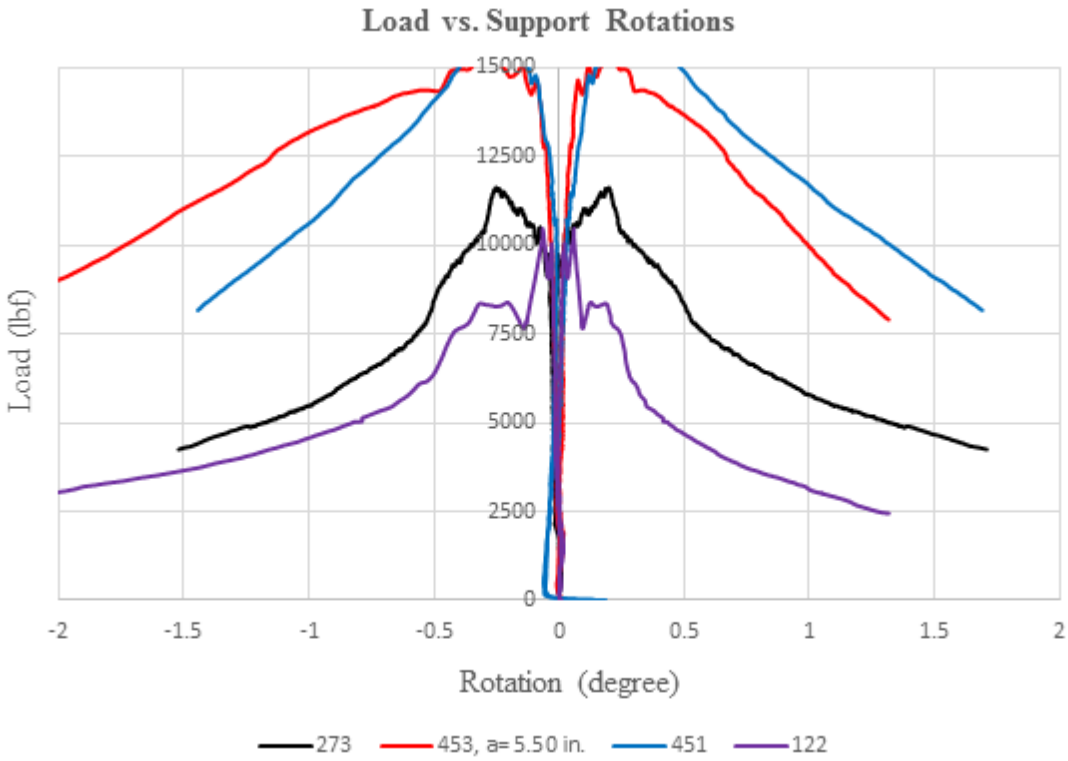

Batch ID		Fiber type			V_f (%)
B 12		4D (RC-65/60-BG)			1.5
P_1 (lbf)	P_{pc} (lbf)	$P_{\delta=0.04\ in.}$ (lbf)	$P_{\delta=0.08\ in.}$ (lbf)	$P_{\delta=0.12\ in.}$ (lbf)	P_{max} (lbf)
9610	11760	10640	8890	7460	11760
σ_1 (psi)	σ_{pc} (psi)	$\sigma_{\delta=0.04\ in.}$ (psi)	$\sigma_{\delta=0.08\ in.}$ (psi)	$\sigma_{\delta=0.12\ in.}$ (psi)	σ_{max} (psi)
775	935	845	705	590	935
δ_1 (in.)	δ_{pc} (in.)	ω_{pc} (in.)	$COV(P_{pc})$		
0.004	0.03	0.03	37%		
Comment: dominated by fiber pullout and fiber fracture.					

SP 1 273 fibers Single crack	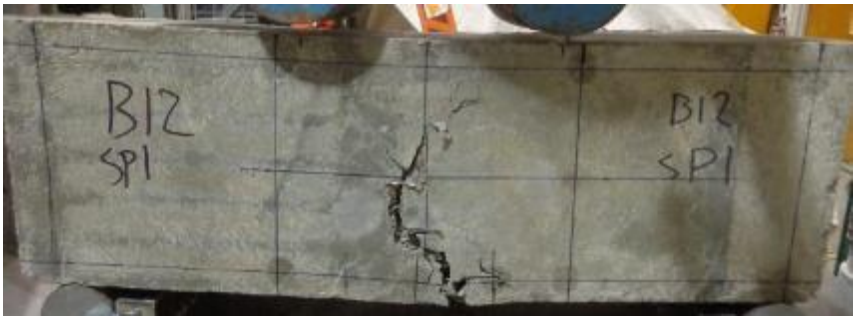
SP 2 453 fibers Multi-crack	
SP 3 60 fibers Single crack	
SP 4 451 fibers Wood form Multi-crack	
SP 5 122 fibers Multi-crack	

Batch 13: $f_c^{`} = 6$ ksi; $V_f = 0.75\%$; Fiber: 5D (RC-65/60-BG)

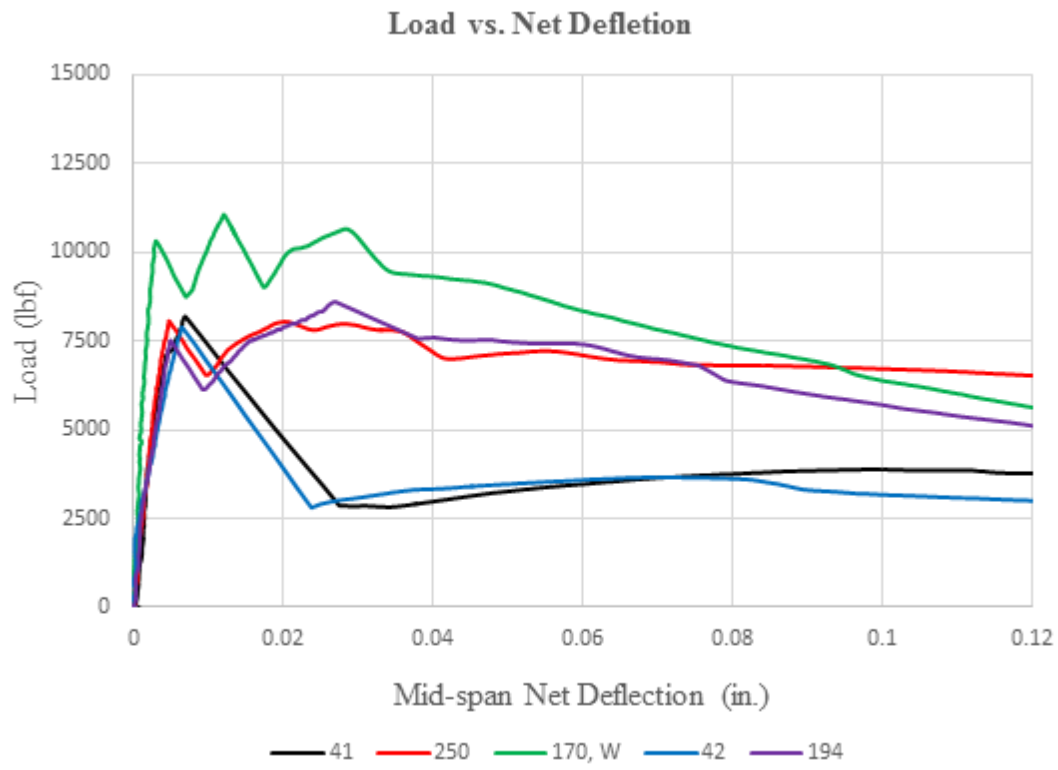

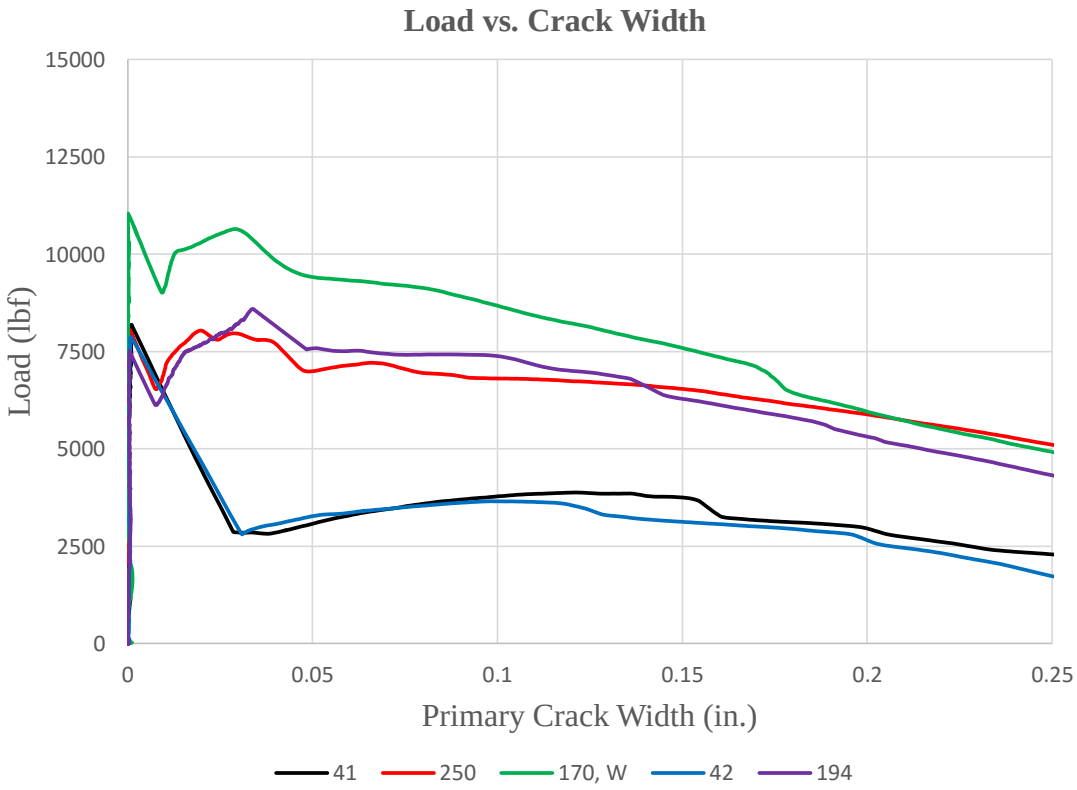

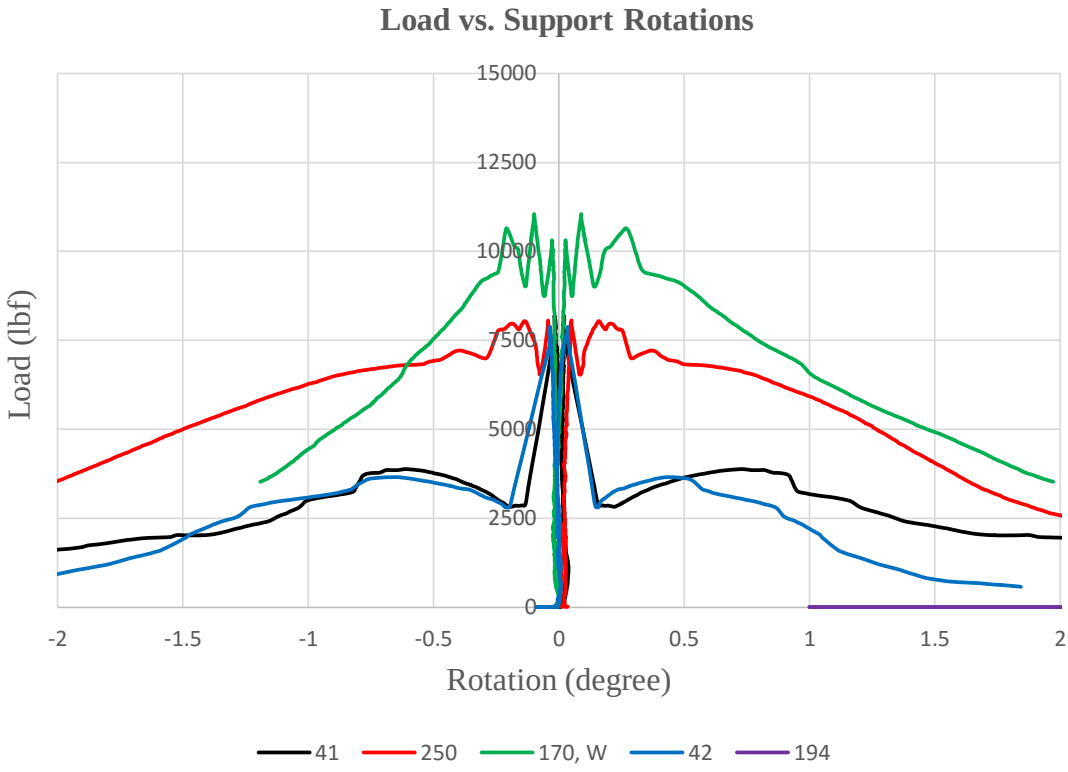

Batch ID		Fiber type			V_f (%)
B 13		5D (RC-65/60-BG)			0.75
P_1 (lbf)	P_{pc} (lbf)	$P_{\delta=0.04\ in.}$ (lbf)	$P_{\delta=0.08\ in.}$ (lbf)	$P_{\delta=0.12\ in.}$ (lbf)	P_{max} (lbf)
8385	7045	6100	5540	4800	8390
σ_1 (psi)	σ_{pc} (psi)	$\sigma_{\delta=0.04\ in.}$ (psi)	$\sigma_{\delta=0.08\ in.}$ (psi)	$\sigma_{\delta=0.12\ in.}$ (psi)	σ_{max} (psi)
675	565	485	430	360	680
δ_1 (in.)	δ_{pc} (in.)	ω_{pc} (in.)	$COV(P_{pc})$		
0.005	0.05	0.05	45%		
Comment: dominated by fiber pullout.					

SP 1 41 fibers Single crack	
SP 2 250 fibers Single crack	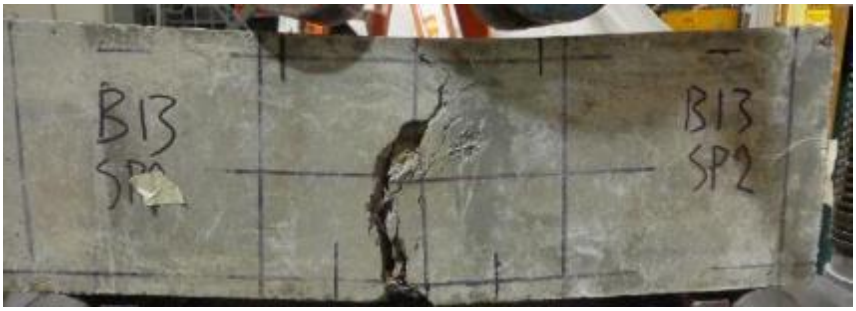
SP 3 170 fibers Wood form Multi-crack	
SP 4 42 fibers Single crack	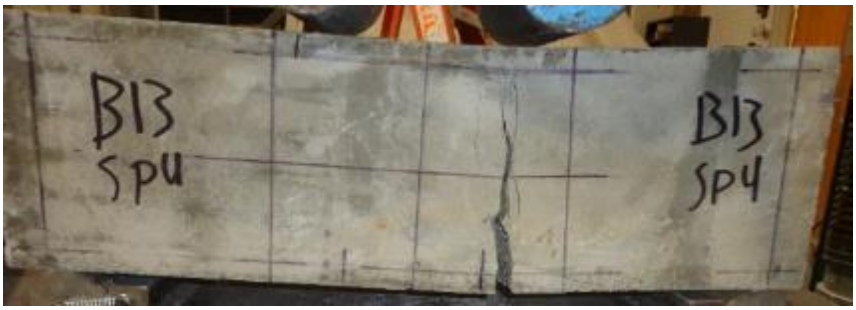
SP 5 194 fibers Single crack	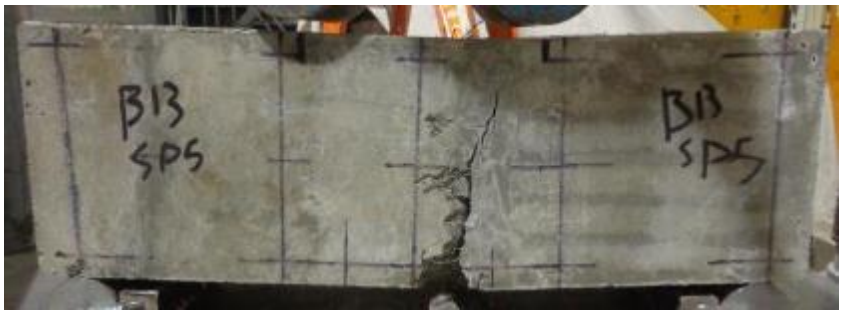

Batch 14: $f_c^{`} = 6$ ksi; $V_f = 1.5\%$; Fiber: 5D (RC-65/60-BG)

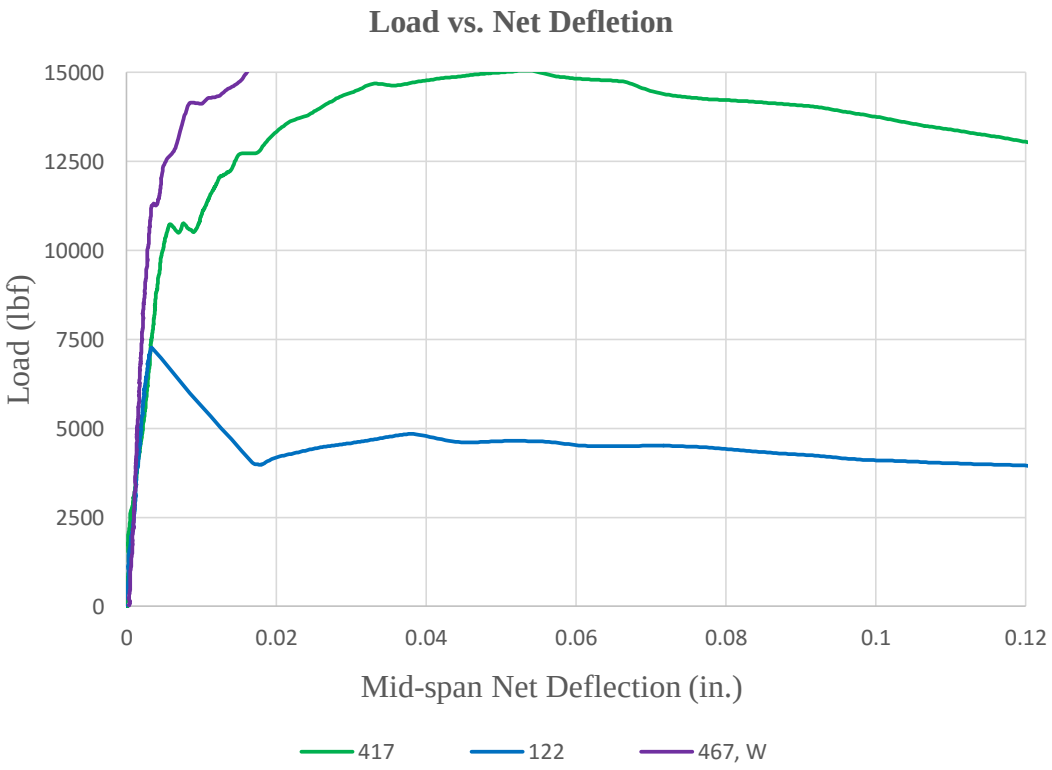

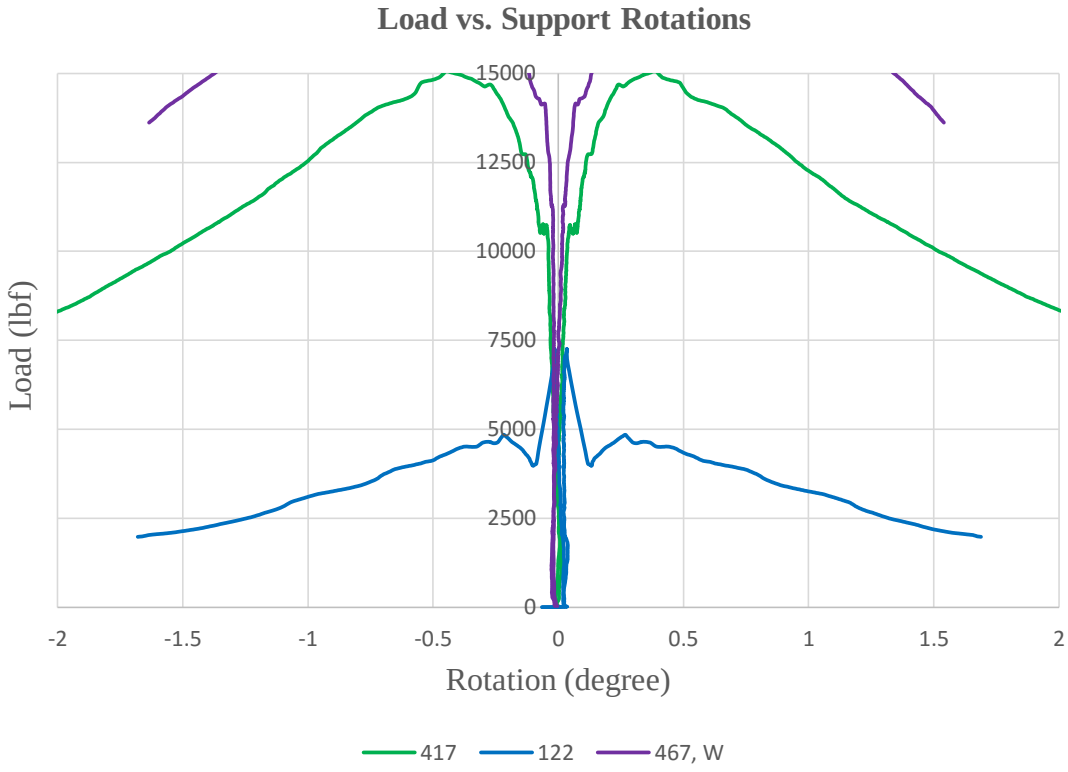

Batch ID		Fiber type			V_f (%)
B 14		5D (RC-65/60-BG)			1.5
P_1 (lbf)	P_{pc} (lbf)	$P_{\delta=0.04\ in.}$ (lbf)	$P_{\delta=0.08\ in.}$ (lbf)	$P_{\delta=0.12\ in.}$ (lbf)	P_{max} (lbf)
9770	12720	12310	12290	11720	12720
σ_1 (psi)	σ_{pc} (psi)	$\sigma_{\delta=0.04\ in.}$ (psi)	$\sigma_{\delta=0.08\ in.}$ (psi)	$\sigma_{\delta=0.12\ in.}$ (psi)	σ_{max} (psi)
770	995	965	960	915	995
δ_1 (in.)	δ_{pc} (in.)	ω_{pc} (in.)	$COV(P_{pc})$		
0.004	0.05	0.06	55%		
Comment: dominated by fiber pullout.					

SP 1 349 fibers Multi-crack Deformation data missing	
SP 2 227 fibers Single crack Deformation data missing	
SP 3 417 fibers Multi-crack	
SP 4 122 fibers Single crack	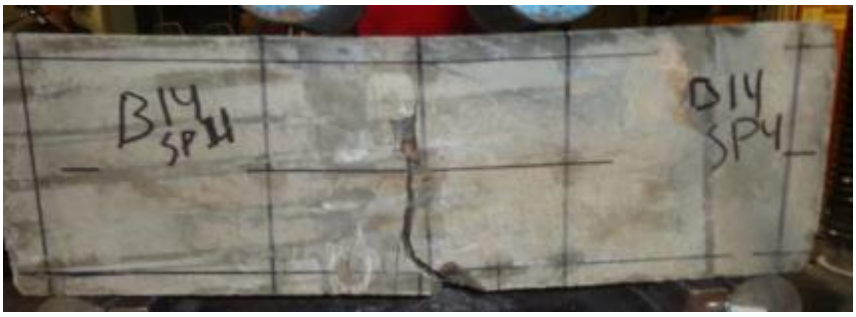
SP 5 467 fibers Wood form Multi-crack	

Control 2: $f_c^{`} = 10$ ksi

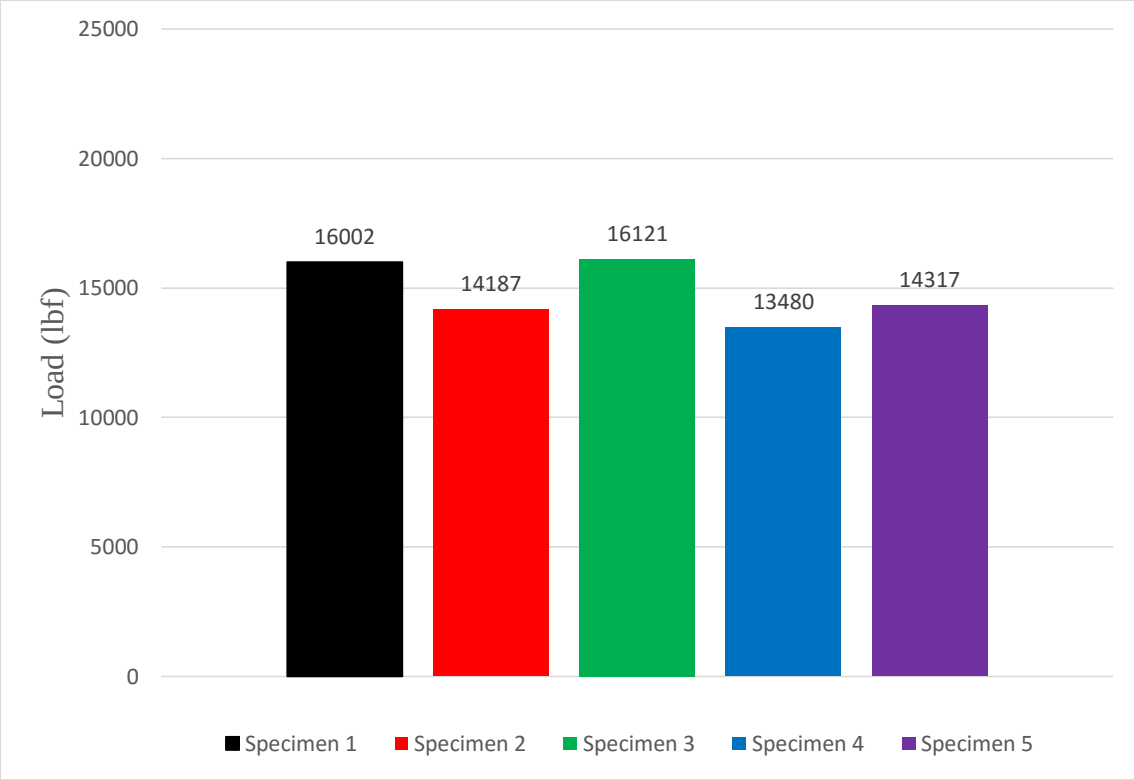

Batch ID		Fiber type			V_f (%)
C 2		N/A			0
P_1 (lbf)	P_{pc} (lbf)	$P_{\delta=0.04\ in.}$ (lbf)	$P_{\delta=0.08\ in.}$ (lbf)	$P_{\delta=0.12\ in.}$ (lbf)	P_{max} (lbf)
14820	0	0	0	0	14820
σ_1 (psi)	σ_{pc} (psi)	$\sigma_{\delta=0.04\ in.}$ (psi)	$\sigma_{\delta=0.08\ in.}$ (psi)	$\sigma_{\delta=0.12\ in.}$ (psi)	σ_{max} (psi)
1190	0	0	0	0	1190
δ_1 (in.)	δ_{pc} (in.)	ω_{pc} (in.)	$COV(P_{pc})$		
0	0	0	0%		
Comment: all specimens failed suddenly after first crack (brittle failure).					

SP 1 0 fiber Single crack Bearing crack Wood form		
SP 2 0 fiber Single crack		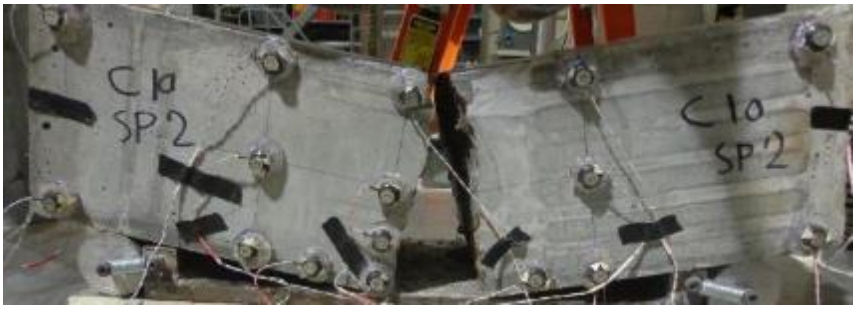
SP 3 0 fiber Single crack Bearing crack		
SP 4 0 fiber Single crack		
SP 5 0 fiber Single crack		

Batch 15: $f_c^{`} = 10$ ksi; $V_f = 0.5\%$; Fiber: (RC-80/30-BP)

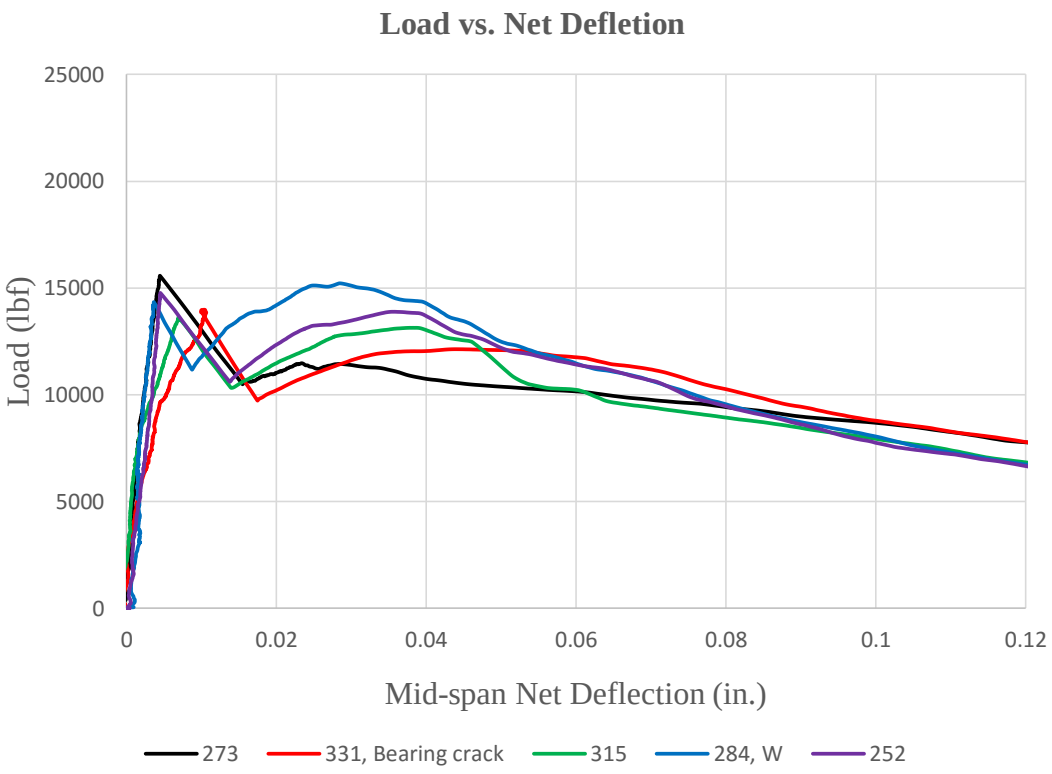

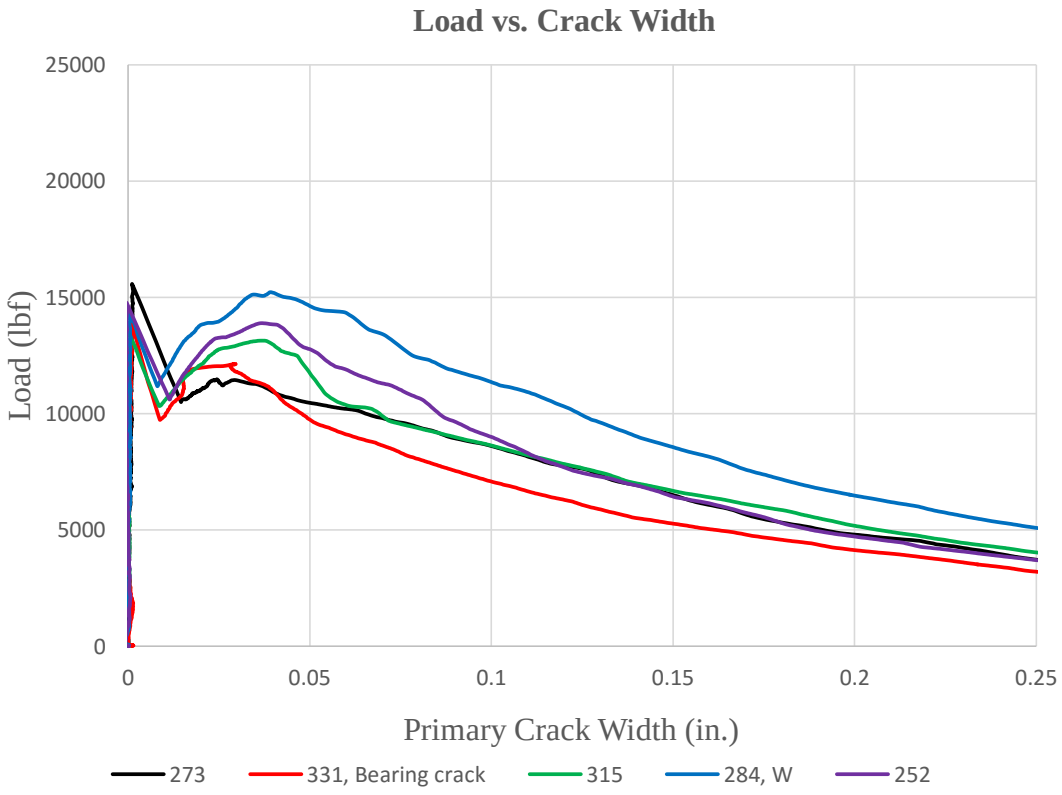

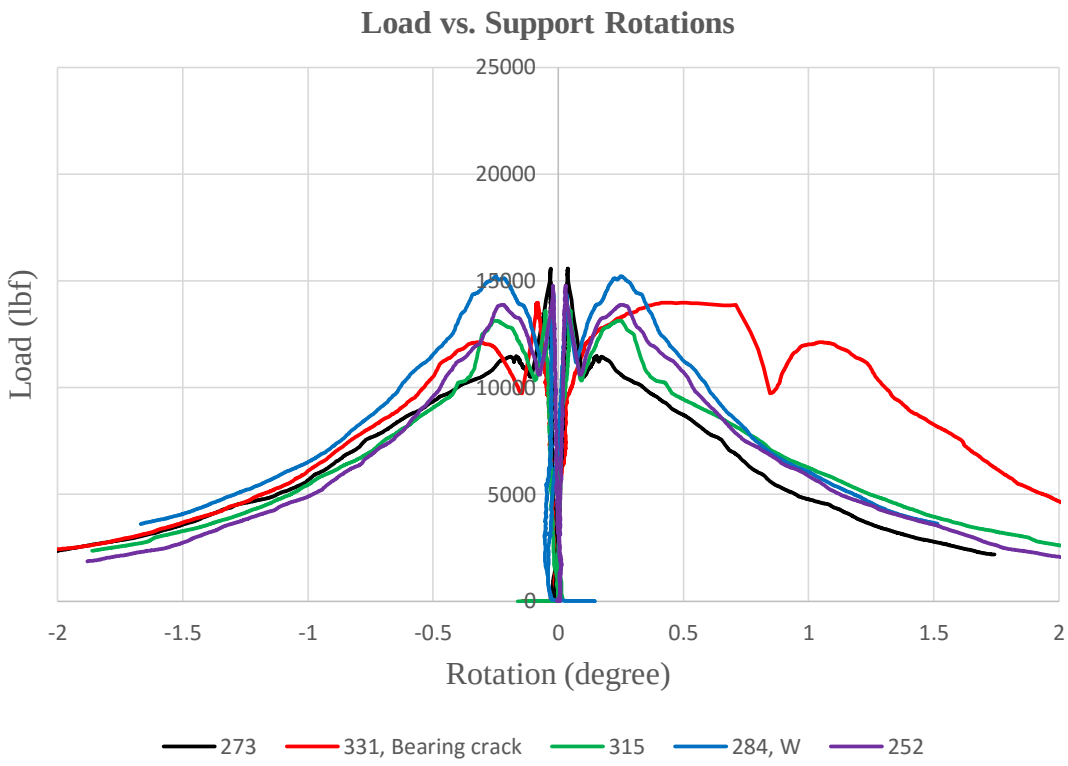

Batch ID		Fiber type			V_f (%)
B 15		(RC-80/30-BP)			0.5
P_1 (lbf)	P_{pc} (lbf)	$P_{\delta=0.04\ in.}$ (lbf)	$P_{\delta=0.08\ in.}$ (lbf)	$P_{\delta=0.12\ in.}$ (lbf)	P_{max} (lbf)
14460	13170	12730	9510	7140	14460
σ_1 (psi)	σ_{pc} (psi)	$\sigma_{\delta=0.04\ in.}$ (psi)	$\sigma_{\delta=0.08\ in.}$ (psi)	$\sigma_{\delta=0.12\ in.}$ (psi)	σ_{max} (psi)
1160	1060	1020	760	570	1160
δ_1 (in.)	δ_{pc} (in.)	ω_{pc} (in.)	$COV(P_{pc})$		
0.006	0.03	0.03	11%		
Comment: brittle failure, dominated by fiber pullout.					

SP 1 273 fiber Single crack		
SP 2 331 fiber Single crack Bearing crack		
SP 3 315 fiber Single crack		
SP 4 284 fiber Single crack Wood form		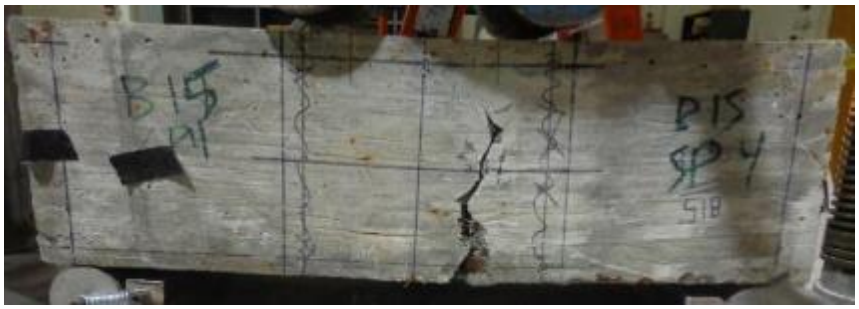
SP 5 252 fiber Single crack		

Batch 16: $f_c^{`} = 10$ ksi; $V_f = 0.75\%$; Fiber: (RC-80/30-BP)

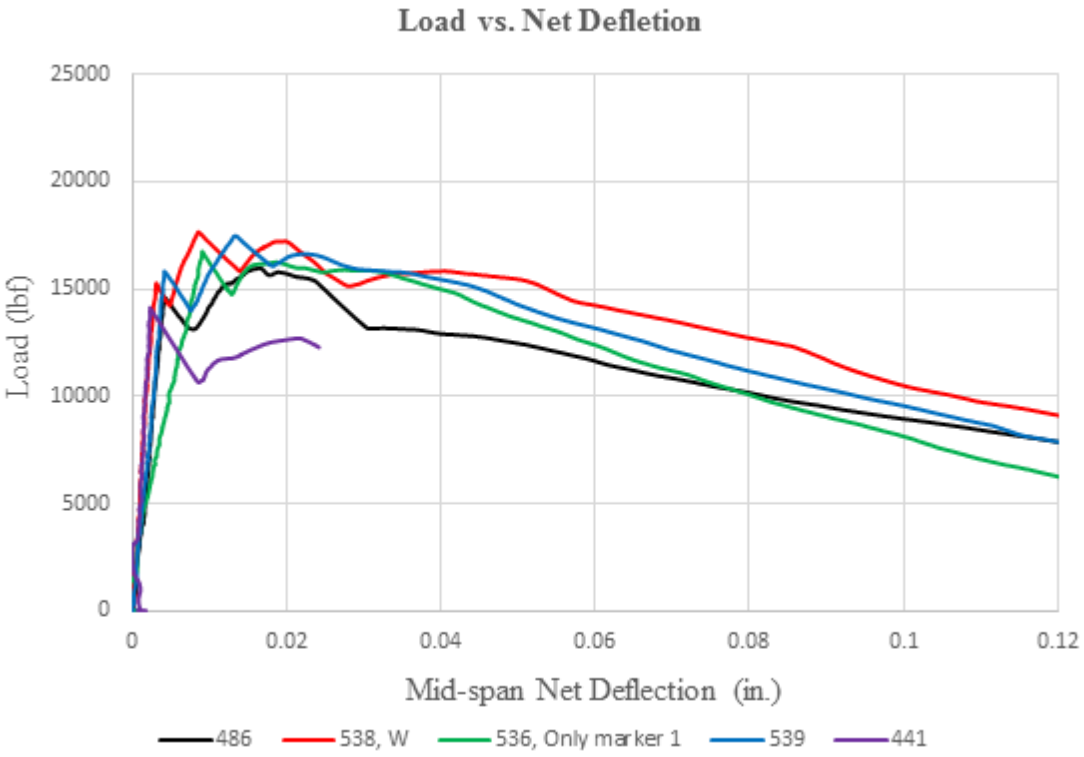

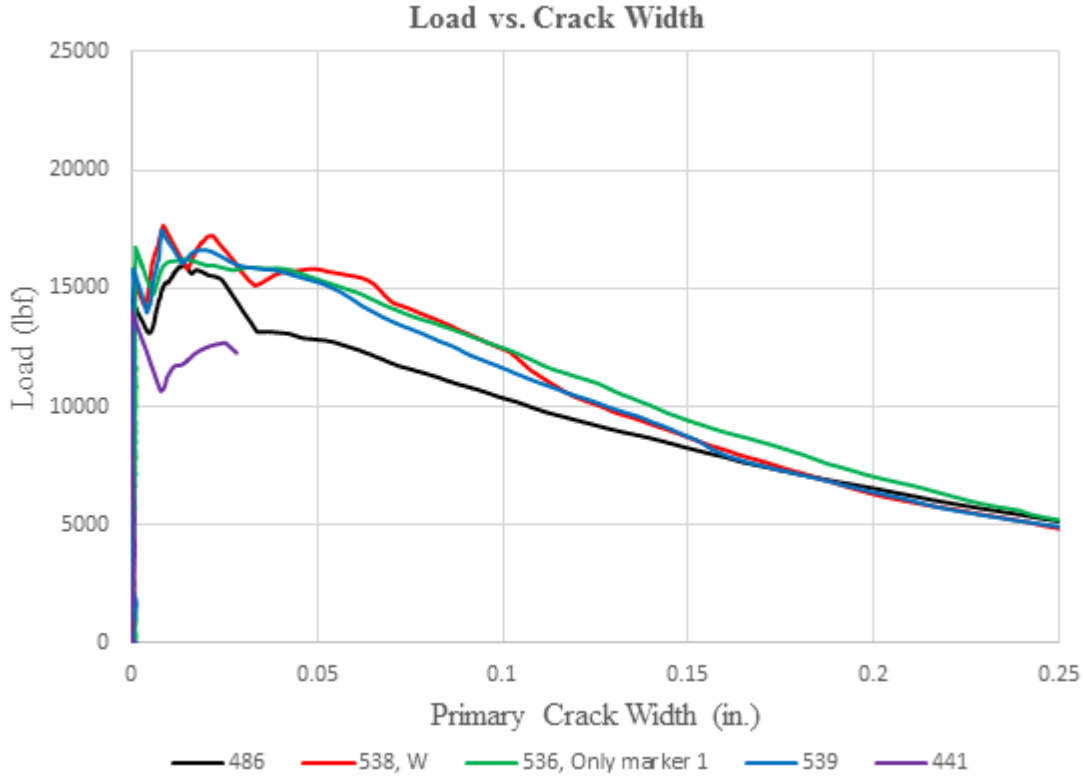

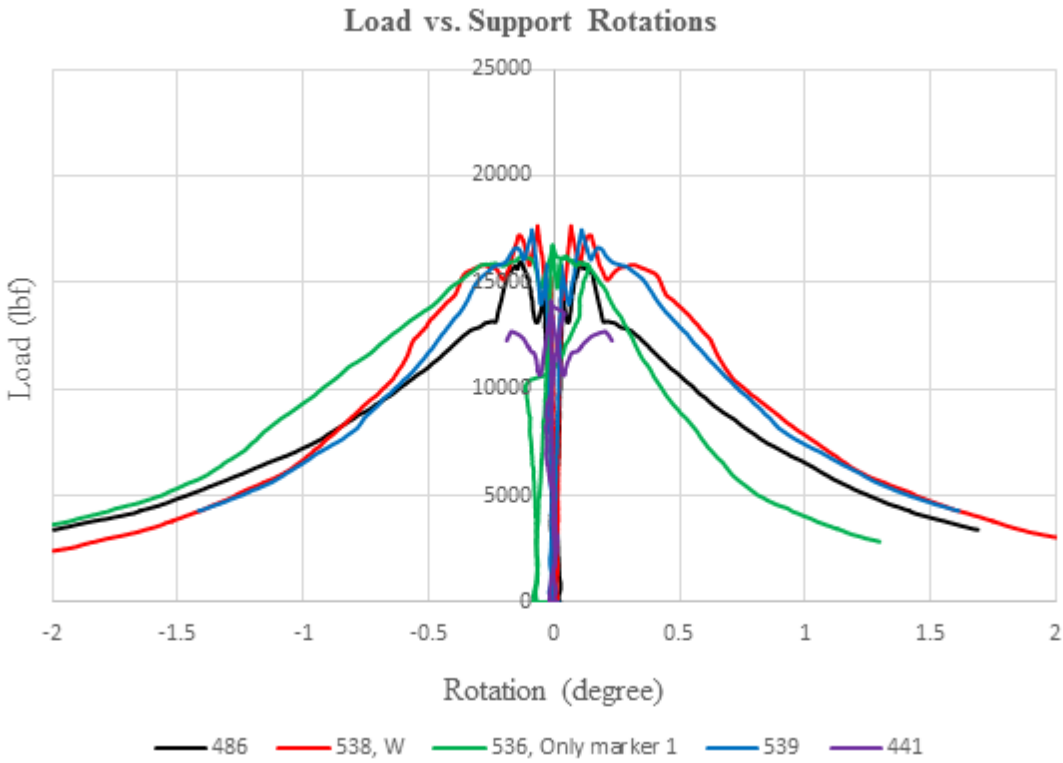

Batch ID		Fiber type			V_f (%)
B 16		(RC-80/30-BP)			0.75
P_1 (lbf)	P_{pc} (lbf)	$P_{\delta=0.04\ in.}$ (lbf)	$P_{\delta=0.08\ in.}$ (lbf)	$P_{\delta=0.12\ in.}$ (lbf)	P_{max} (lbf)
15320	16840	14780	11020	7770	16840
σ_1 (psi)	σ_{pc} (psi)	$\sigma_{\delta=0.04\ in.}$ (psi)	$\sigma_{\delta=0.08\ in.}$ (psi)	$\sigma_{\delta=0.12\ in.}$ (psi)	σ_{max} (psi)
1230	1345	1180	880	495	1345
δ_1 (in.)	δ_{pc} (in.)	ω_{pc} (in.)	$COV(P_{pc})$		
0.005	0.01	0.01	5%		
Comment: brittle failure, dominated by fiber pullout.					

SP 1 486 fiber Single crack	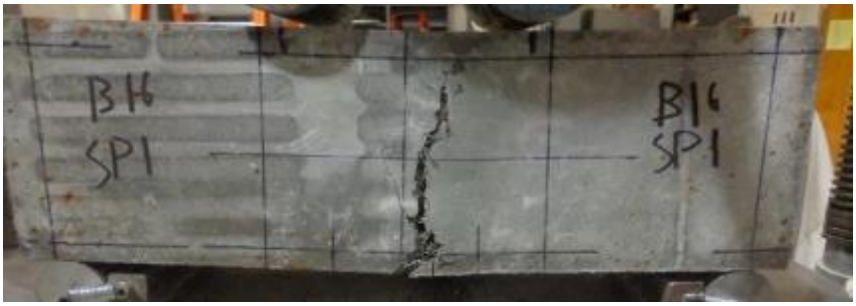
SP 2 538 fiber Single crack Wood form	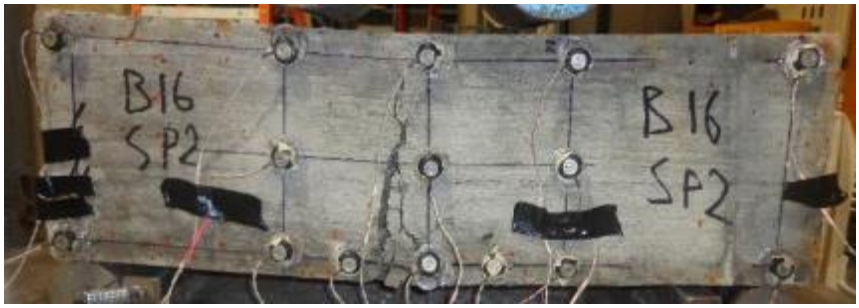
SP 3 536 fiber Single crack	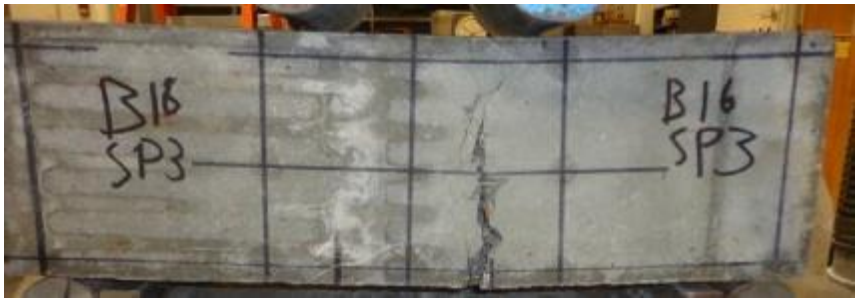
SP 4 539 fiber Single crack	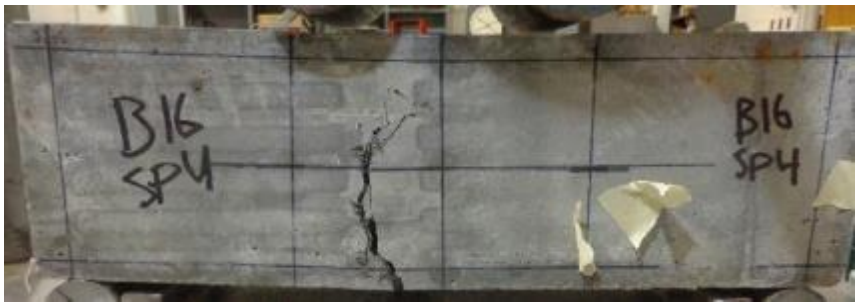
SP 5 441 fiber Single crack	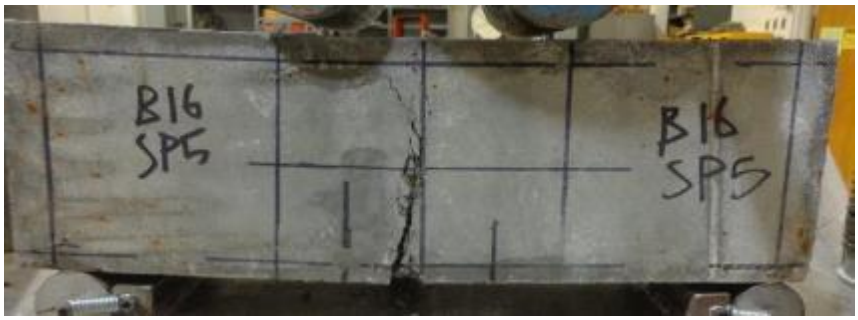

Batch 17: $f_c^{`} = 10$ ksi; $V_f = 1.0\%$; Fiber: (RC-80/30-BP)

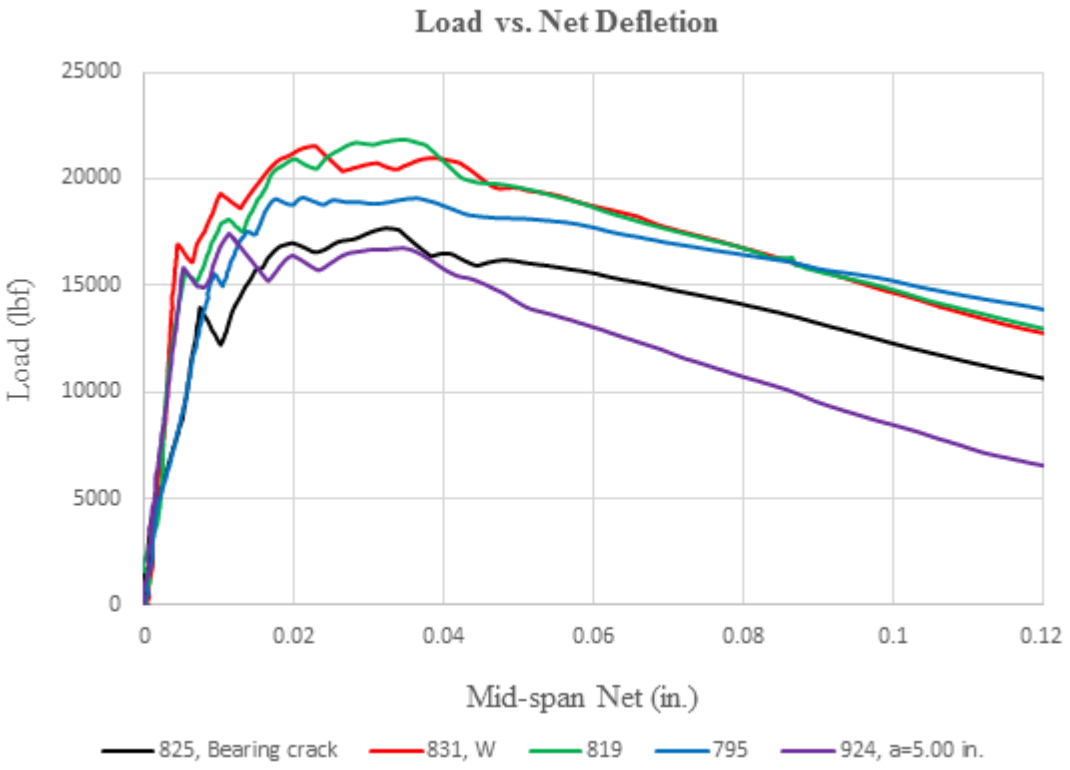

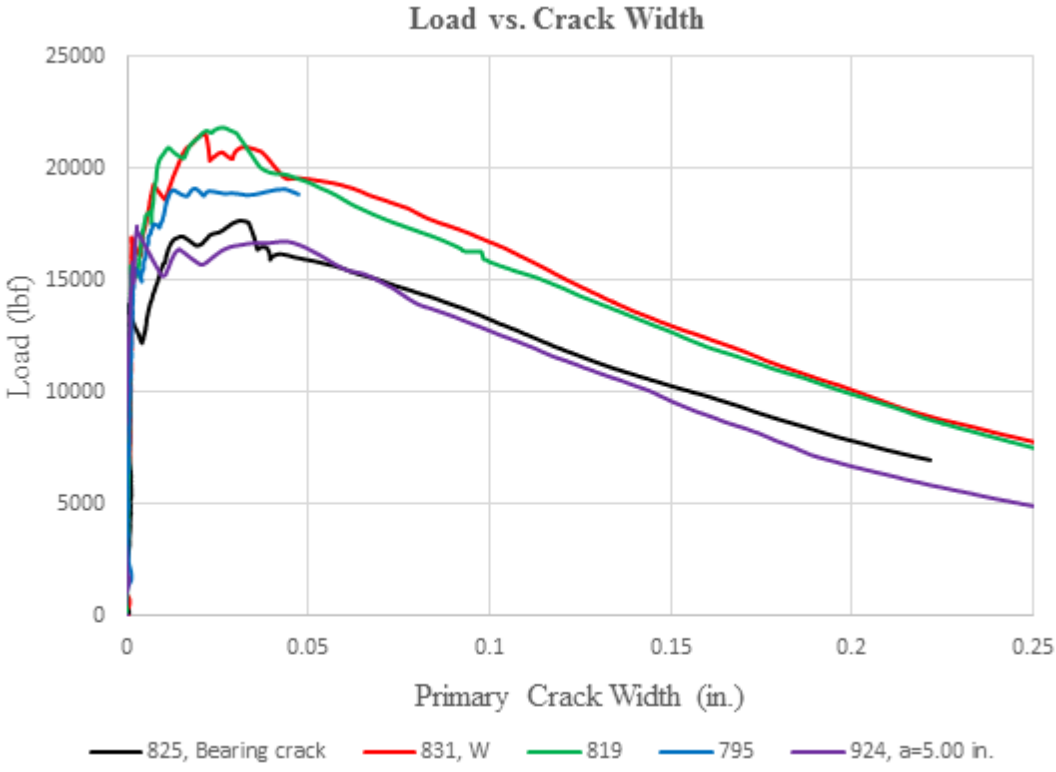

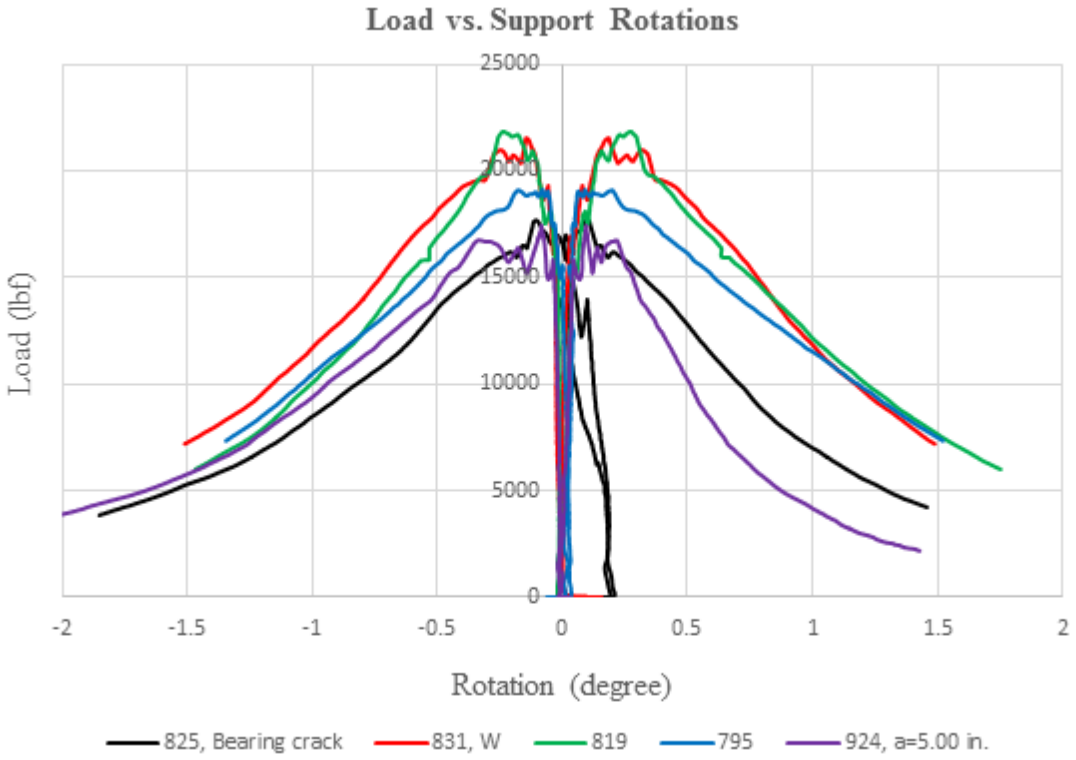

Batch ID		Fiber type			V_f (%)
B 17		(RC-80/30-BP)			1.0
P_1 (lbf)	P_{pc} (lbf)	$P_{\delta=0.04\ in.}$ (lbf)	$P_{\delta=0.08\ in.}$ (lbf)	$P_{\delta=0.12\ in.}$ (lbf)	P_{max} (lbf)
15560	19520	18550	14960	11380	19520
σ_1 (psi)	σ_{pc} (psi)	$\sigma_{\delta=0.04\ in.}$ (psi)	$\sigma_{\delta=0.08\ in.}$ (psi)	$\sigma_{\delta=0.12\ in.}$ (psi)	σ_{max} (psi)
980	1555	1475	1190	905	1555
δ_1 (in.)	δ_{pc} (in.)	ω_{pc} (in.)	$COV(P_{pc})$		
0.005	0.02	0.03	11%		
Comment: dominated by fiber pullout.					

SP 1 825 fiber Single crack Bearing crack		
SP 2 831 fiber Single crack Wood form		
SP 3 819 fiber Single crack		
SP 4 795 fiber Single crack		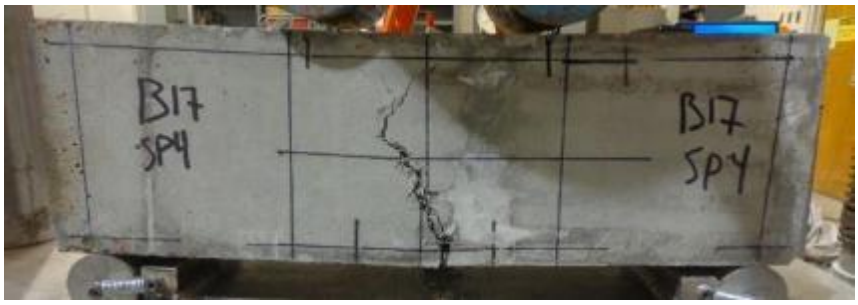
SP 5 924 fiber Single crack		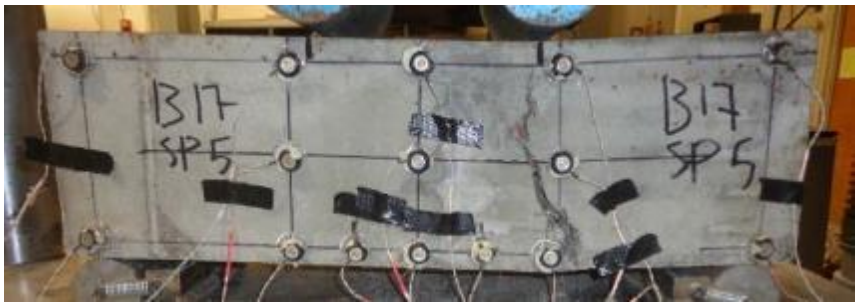

Batch 18: $f_c^{`} = 10$ ksi; $V_f = 1.5\%$; Fiber: (RC-80/30-BP)

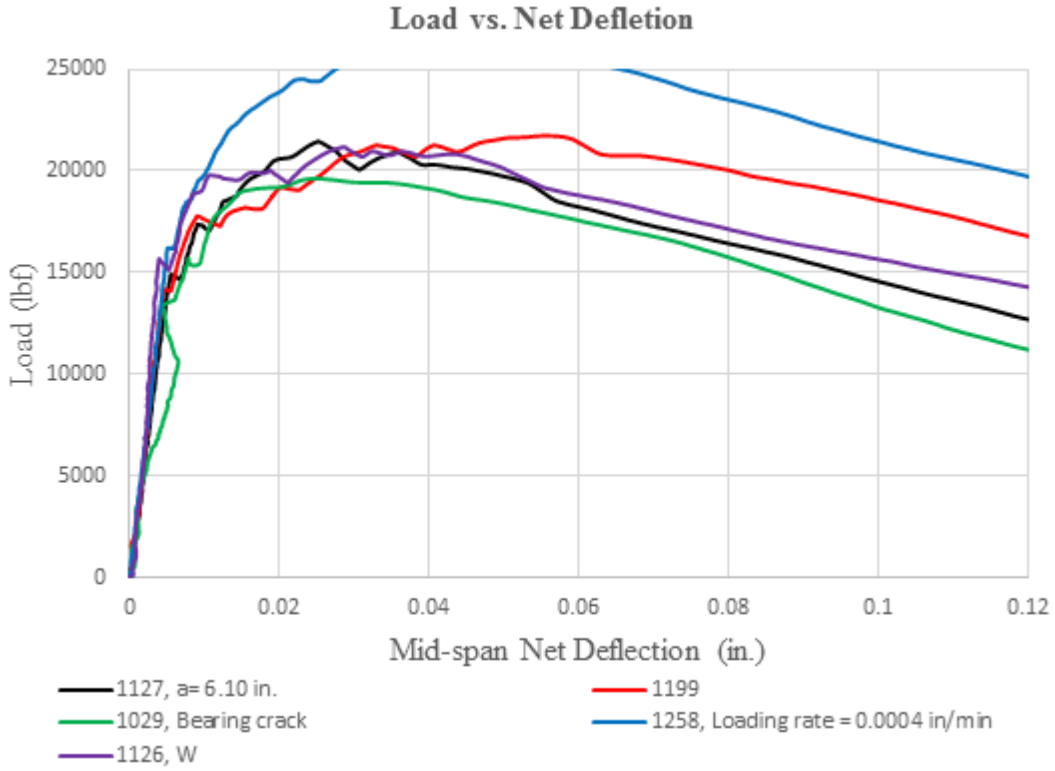

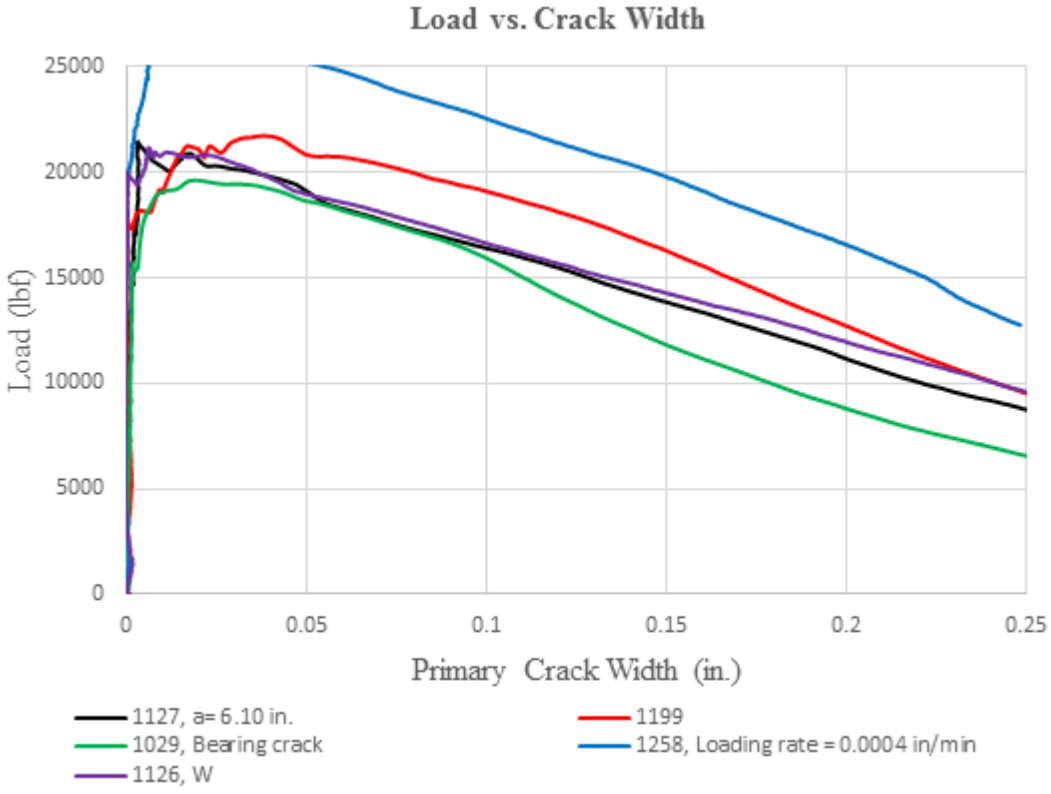

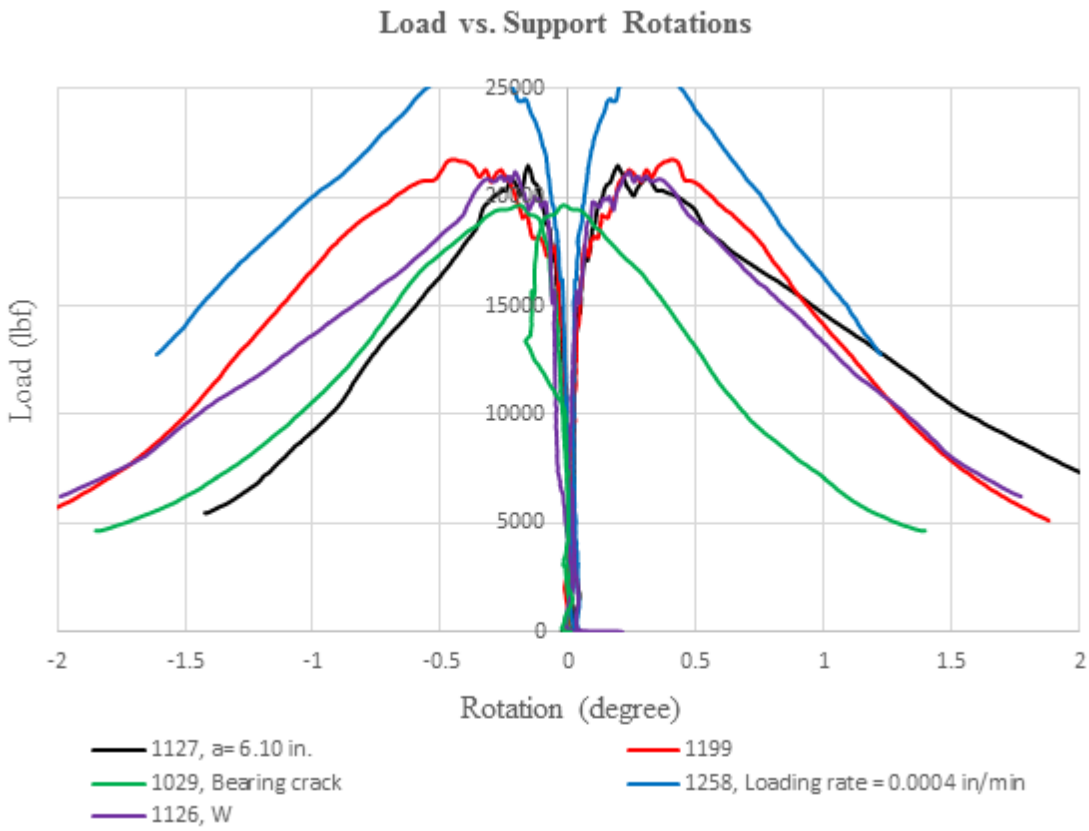

Batch ID		Fiber type			V_f (%)
B 18		(RC-80/30-BP)			1.5
P_1 (lbf)	P_{pc} (lbf)	$P_{\delta=0.04\ in.}$ (lbf)	$P_{\delta=0.08\ in.}$ (lbf)	$P_{\delta=0.12\ in.}$ (lbf)	P_{max} (lbf)
15250	22730	22140	19270	15860	22730
σ_1 (psi)	σ_{pc} (psi)	$\sigma_{\delta=0.04\ in.}$ (psi)	$\sigma_{\delta=0.08\ in.}$ (psi)	$\sigma_{\delta=0.12\ in.}$ (psi)	σ_{max} (psi)
1215	1810	1765	1535	1265	1810
δ_1 (in.)	δ_{pc} (in.)	ω_{pc} (in.)	$COV(P_{pc})$		
0.005	0.04	0.02	11%		
Comment: multi-crack dominated by fiber pullout.					

SP 1 1127 fiber Multi-crack		
SP 2 1199 fiber Multi-crack		
SP 3 1029 fiber Single crack Bearing crack		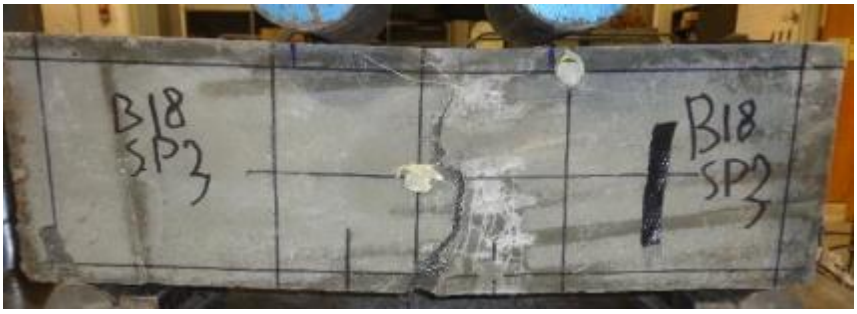
SP 4 1258 fiber Multi-crack		
SP 5 1126 fiber Multi-crack Wood form		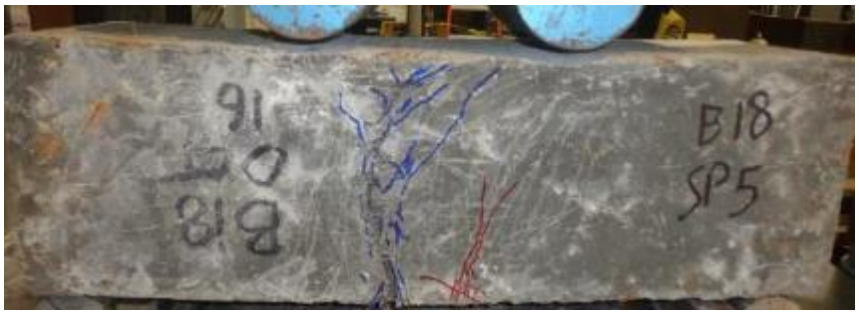

Batch 19: $f_c^{`} = 10$ ksi; $V_f = 0.75\%$; Fiber: 4D (RC-65/60-BG)

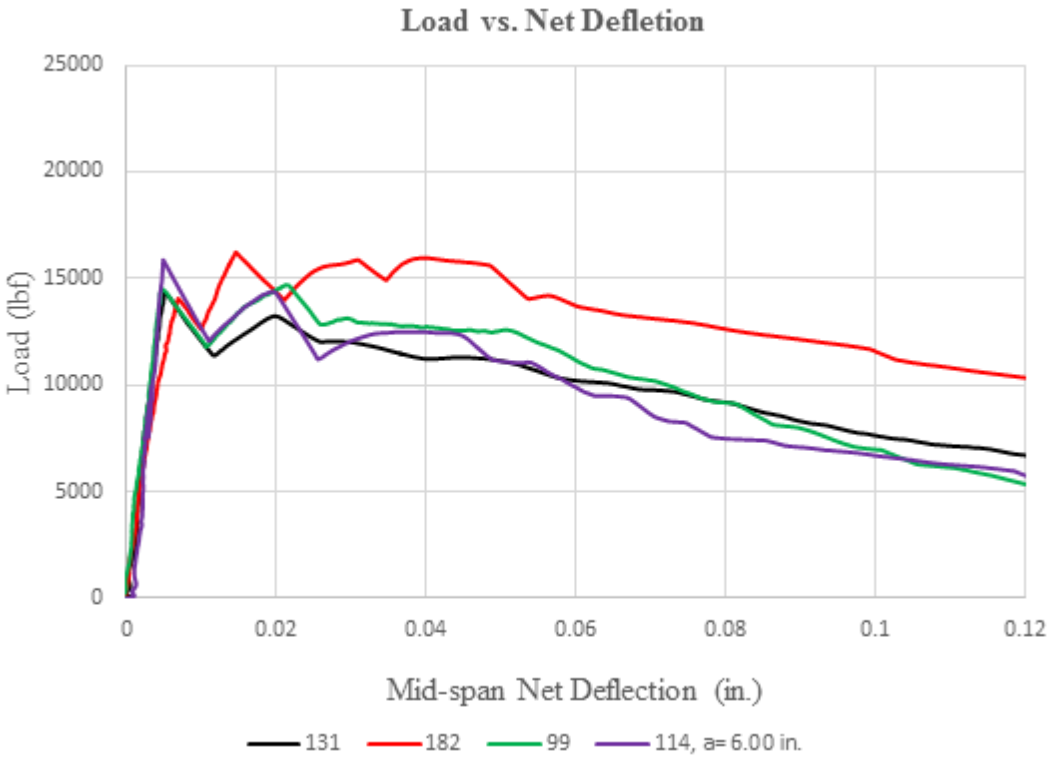

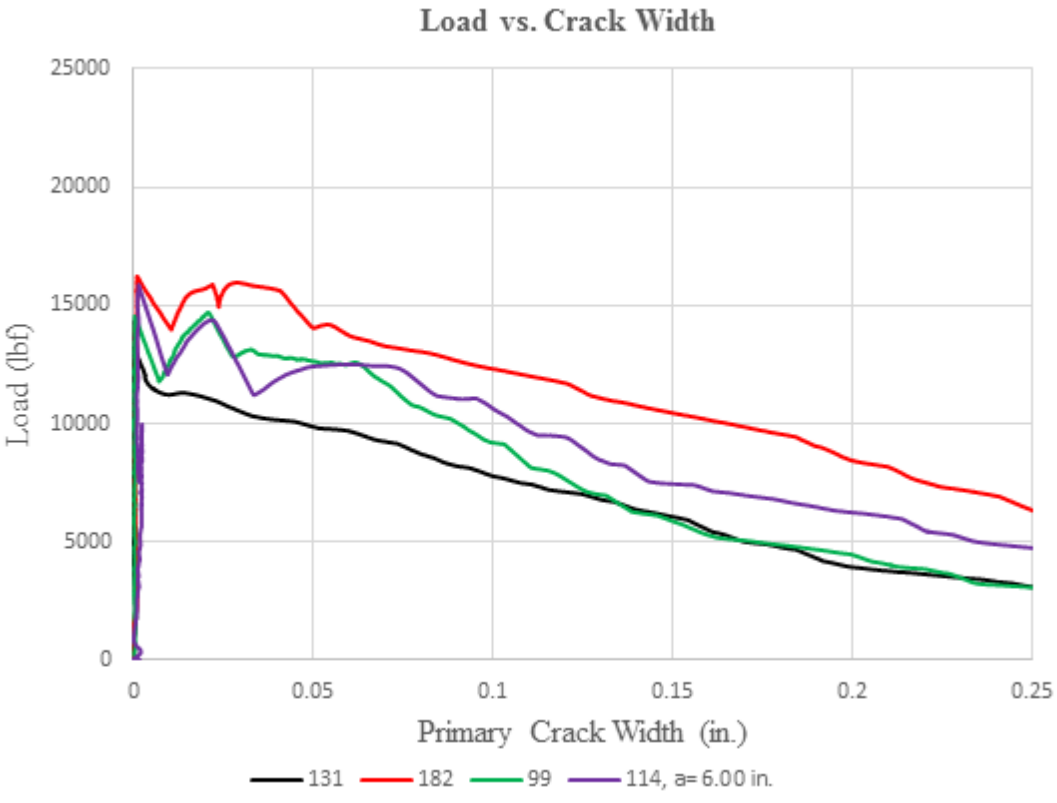

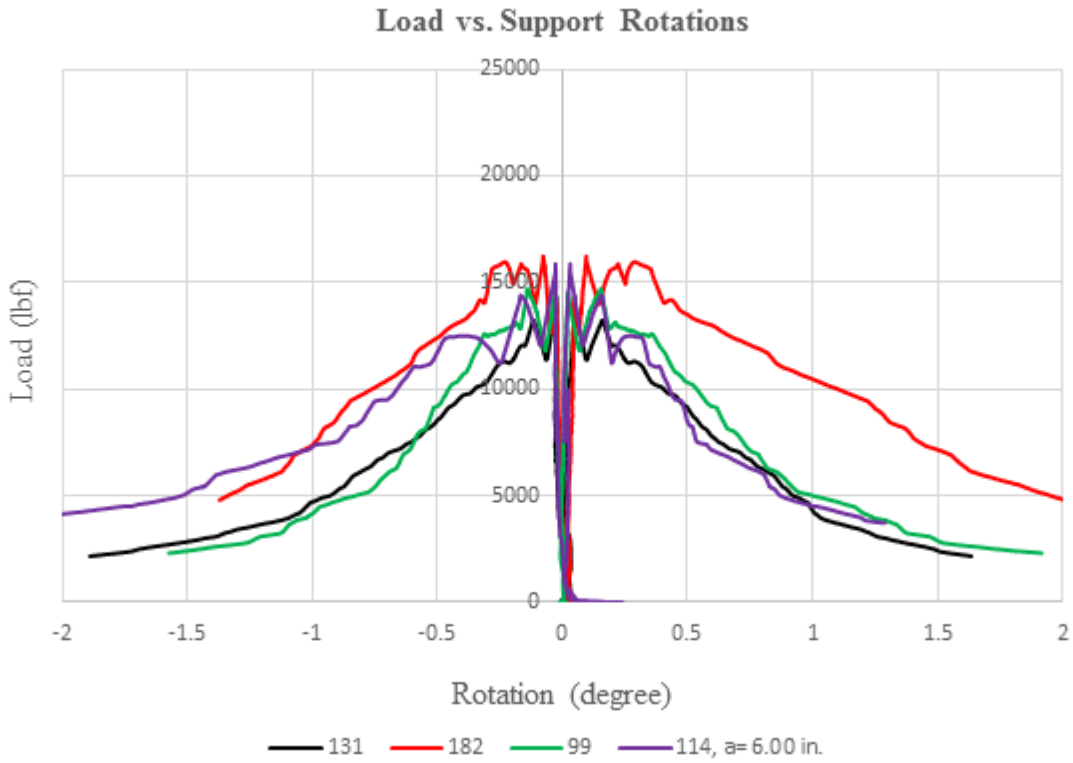

Batch ID		Fiber type			V_f (%)
B 19		4D (RC-65/60-BG)			0.75
P_1 *(lbf)*	P_{pc} *(lbf)*	$P_{\delta=0.04\ in.}$ *(lbf)*	$P_{\delta=0.08\ in.}$ *(lbf)*	$P_{\delta=0.12\ in.}$ *(lbf)*	P_{max} *(lbf)*
14700	14640	13110	9610	7040	14700
σ_1 (psi)	σ_{pc} (psi)	$\sigma_{\delta=0.04\ in.}$ (psi)	$\sigma_{\delta=0.08\ in.}$ (psi)	$\sigma_{\delta=0.12\ in.}$ (psi)	σ_{max} (psi)
1185	1180	1055	775	570	1185
δ_1 (in.)	δ_{pc} (in.)	ω_{pc} (in.)	*COV*(P_{pc})		
0.005	0.02	0.02	8%		
Comment: brittle failure, dominated by fiber pullout and fiber fracture.					

SP 1 131 fiber Single crack		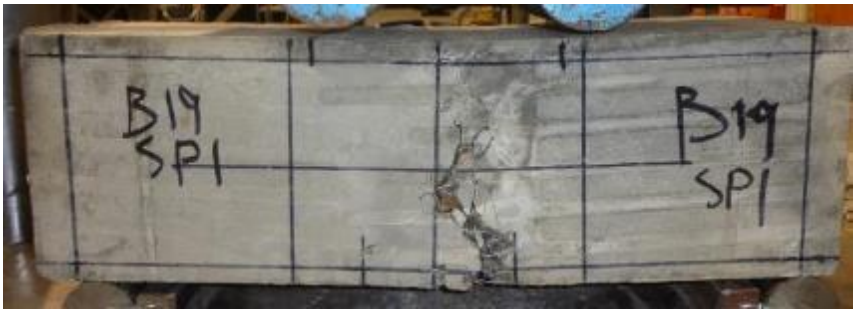
SP 2 182 fiber Single crack		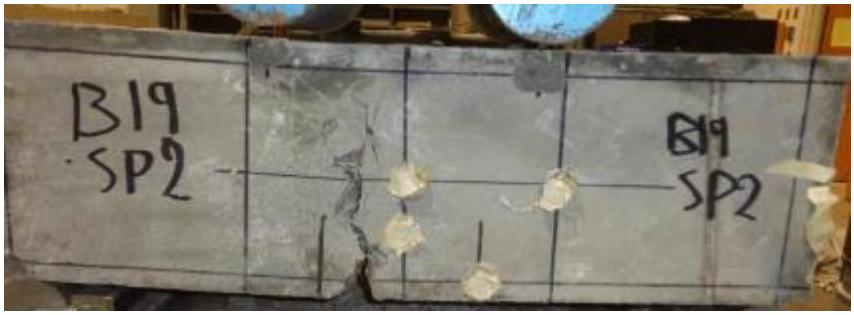
SP 3 99 fiber Single crack		
SP 4 106 fiber Multi-crack Bearing crack		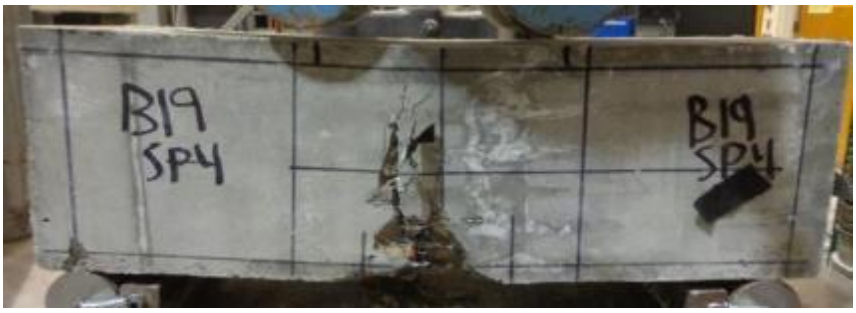
SP 5 114 fiber Multi-crack Bearing crack Wood form		

Batch 20: $f_c^{`} = 10$ ksi; $V_f = 1.5\%$; Fiber: 4D (RC-65/60-BG)

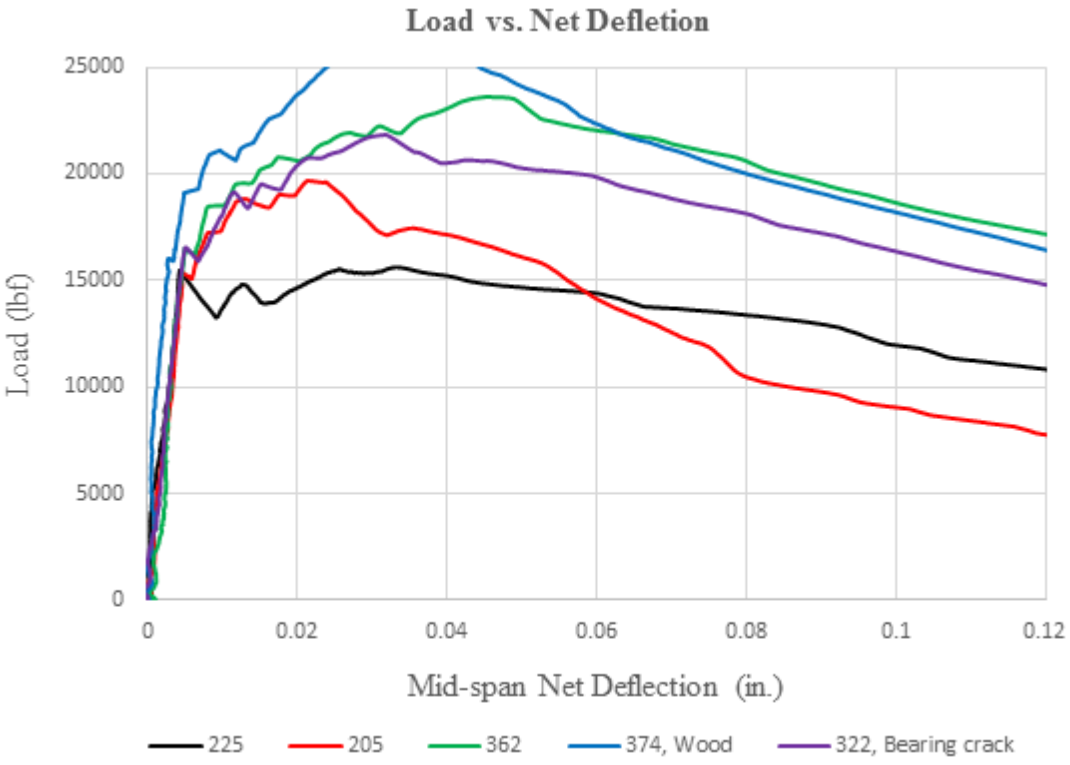

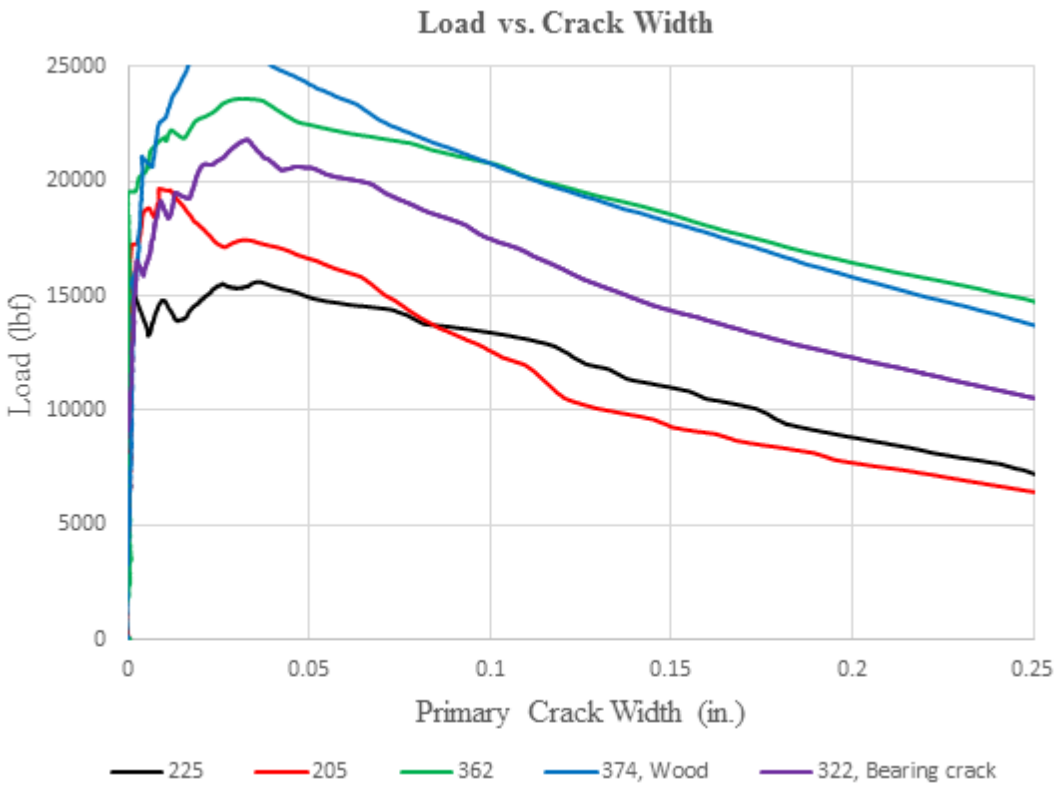

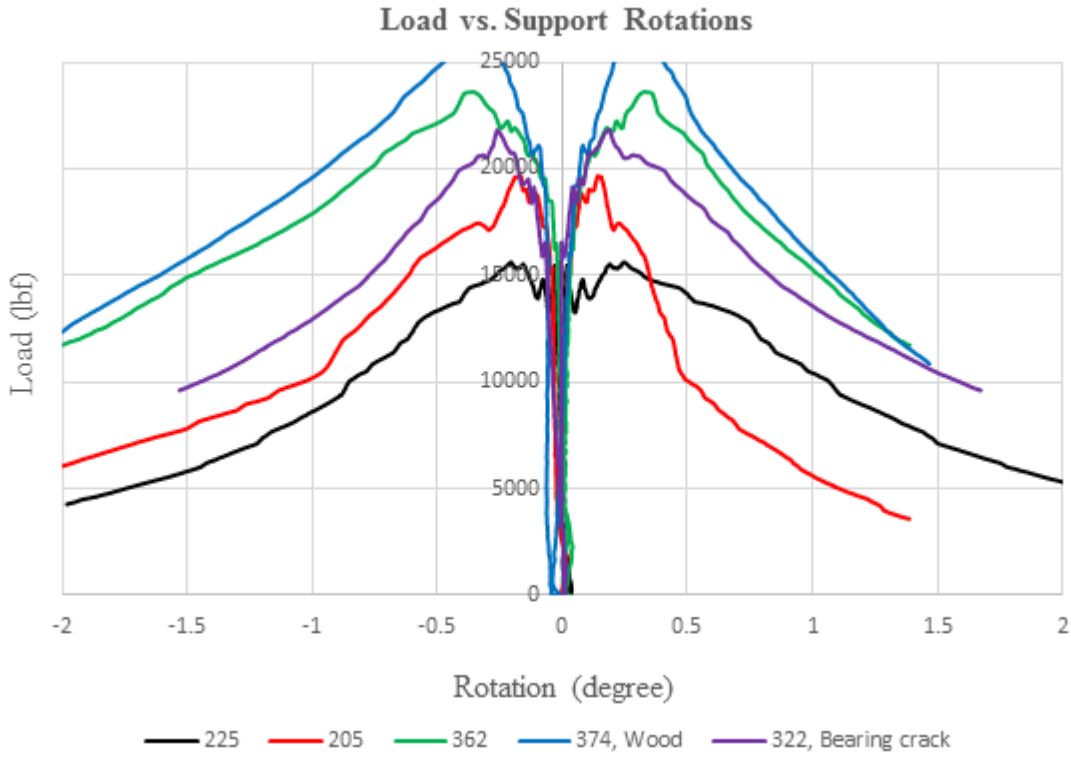

Batch ID		Fiber type			V_f (%)
B 20		4D (RC-65/60-BG)			1.5
P_1 (lbf)	P_{pc} (lbf)	$P_{\delta=0.04\ in.}$ (lbf)	$P_{\delta=0.08\ in.}$ (lbf)	$P_{\delta=0.12\ in.}$ (lbf)	P_{max} (lbf)
15990	21360	20330	16510	13390	21360
σ_1 (psi)	σ_{pc} (psi)	$\sigma_{\delta=0.04\ in.}$ (psi)	$\sigma_{\delta=0.08\ in.}$ (psi)	$\sigma_{\delta=0.12\ in.}$ (psi)	σ_{max} (psi)
1285	1715	1630	1325	1075	1715
δ_1 (in.)	δ_{pc} (in.)	ω_{pc} (in.)	$COV(P_{pc})$		
0.004	0.03	0.02	19%		
Comment: dominated by fiber pullout and fiber fracture.					

SP 1 225 fiber Single crack		
SP 2 205 fiber Multi-crack		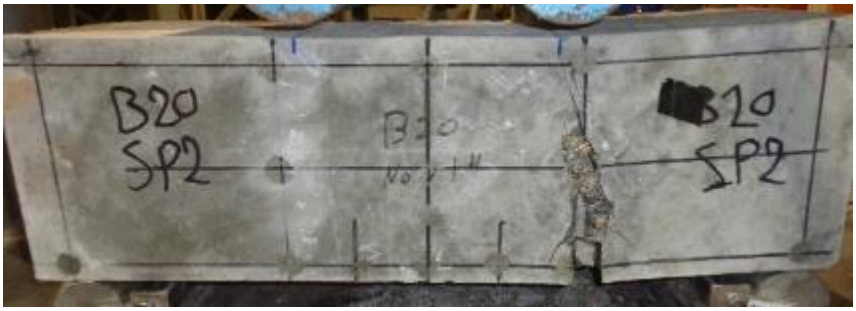
SP 3 362 fiber Multi-crack		
SP 4 374 fiber Multi-crack Wood form		
SP 5 322 fiber Multi-crack Bearing crack		

Batch 21: $f_c^{`} = 10$ ksi; $V_f = 0.75\%$; Fiber: 5D (RC-65/60-BG)

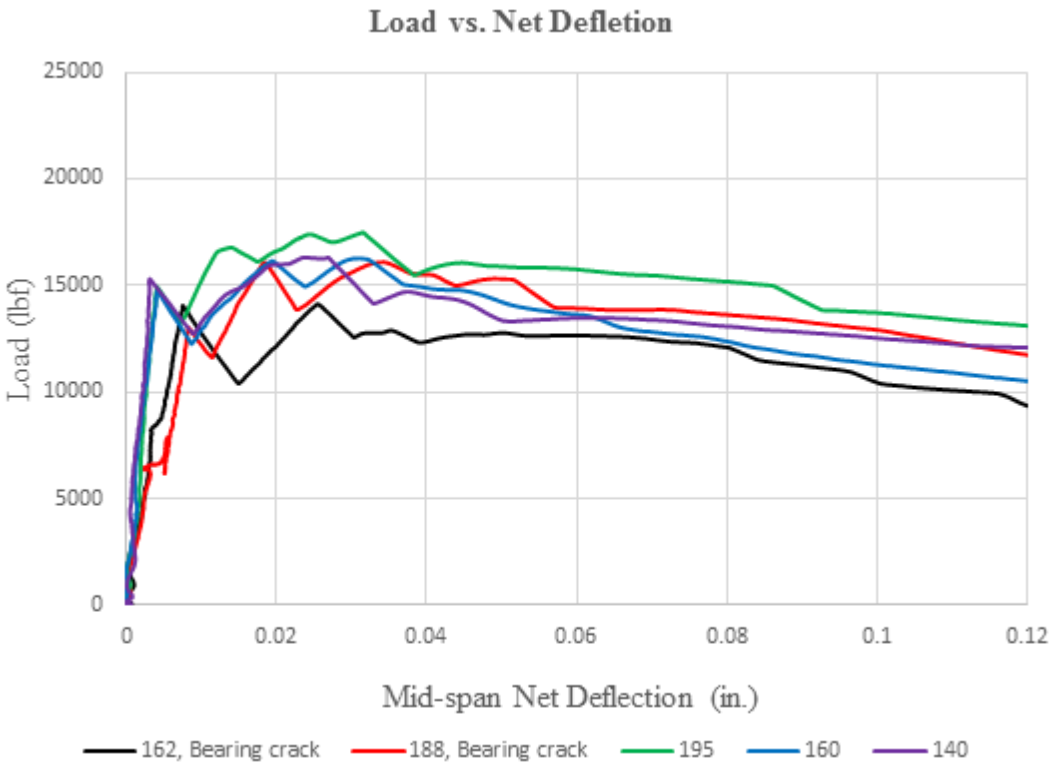

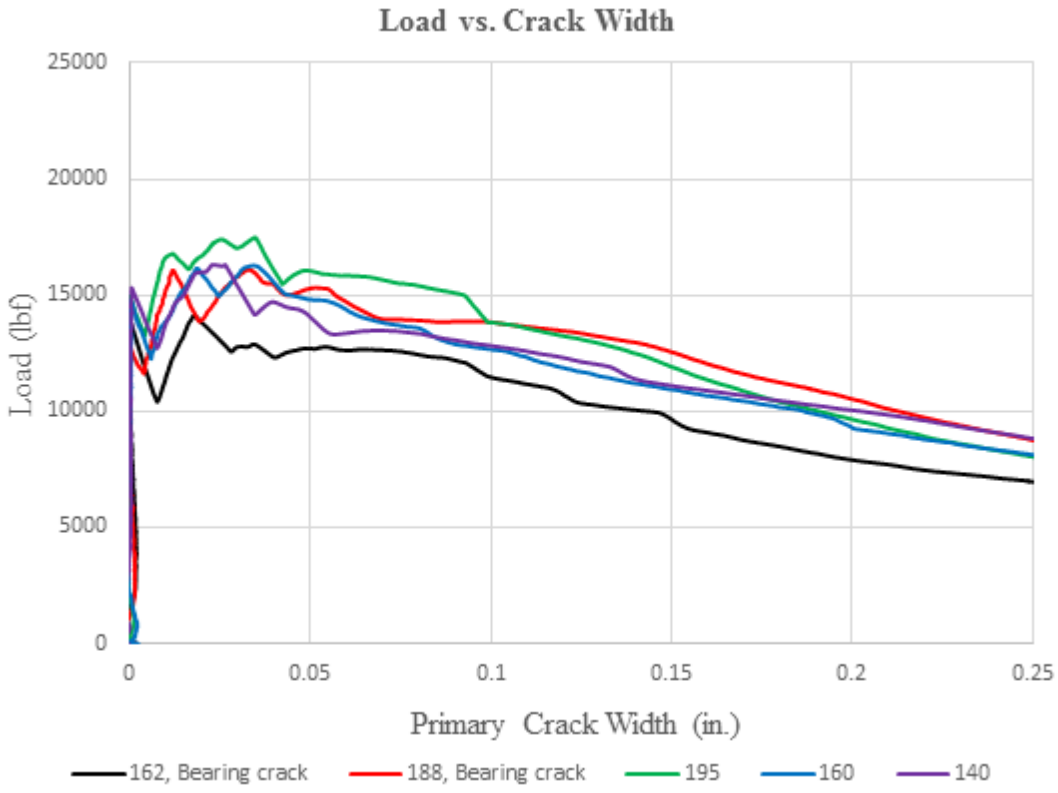

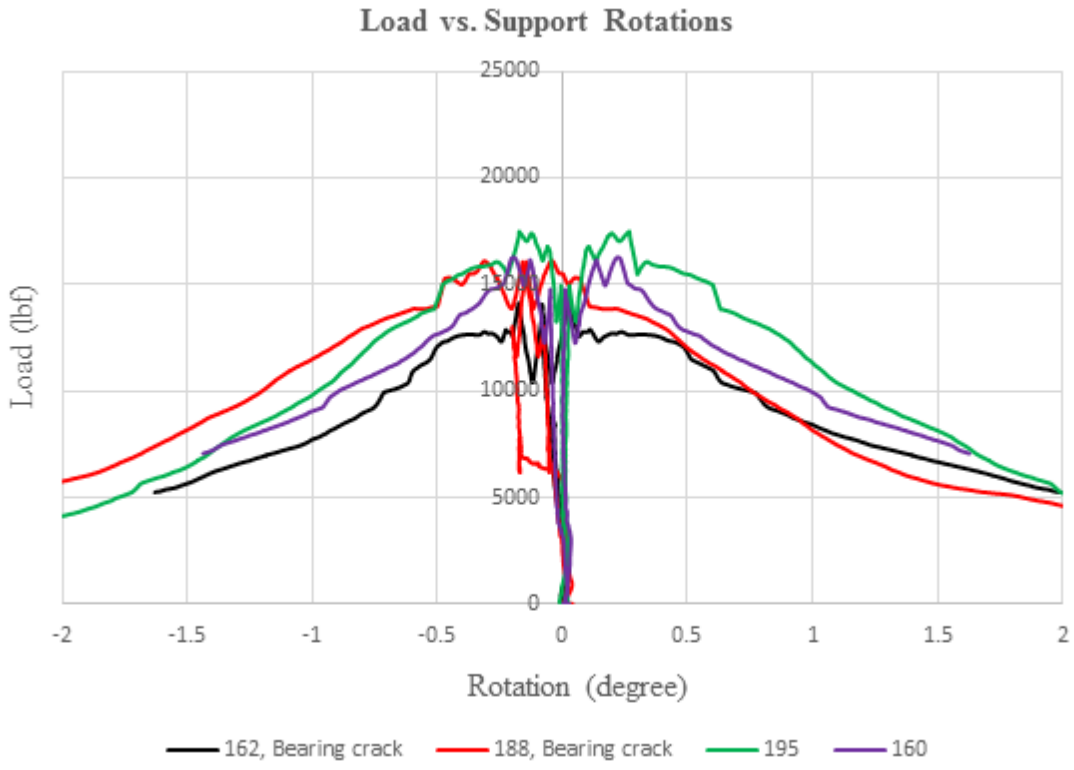

Batch ID		Fiber type			V_f (%)
B 21		5D (RC-65/60-BG)			0.75
P_1 (lbf)	P_{pc} (lbf)	$P_{\delta=0.04\ in.}$ (lbf)	$P_{\delta=0.08\ in.}$ (lbf)	$P_{\delta=0.12\ in.}$ (lbf)	P_{max} (lbf)
14420	16060	14590	13270	11360	16060
σ_1 (psi)	σ_{pc} (psi)	$\sigma_{\delta=0.04\ in.}$ (psi)	$\sigma_{\delta=0.08\ in.}$ (psi)	$\sigma_{\delta=0.12\ in.}$ (psi)	σ_{max} (psi)
1155	1290	1170	1065	910	1290
δ_1 (in.)	δ_{pc} (in.)	ω_{pc} (in.)	$COV(P_{pc})$		
0.005	0.03	0.03	8%		
Comment: brittle failure, dominated by fiber pullout.					

SP 1 162 fiber Multi-crack Bearing crack		
SP 2 188 fiber Single crack Bearing crack		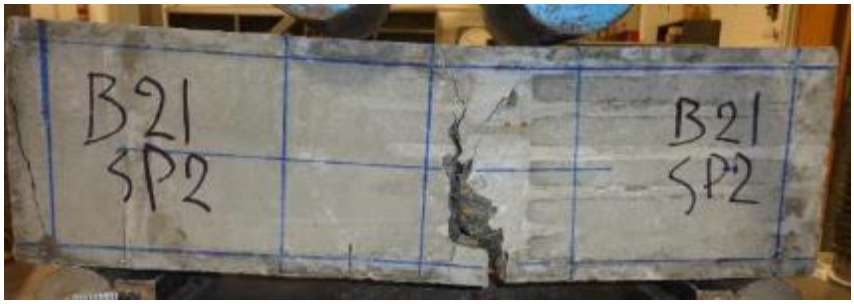
SP 3 195 fiber Multi-crack		
SP 4 160 fiber Single crack		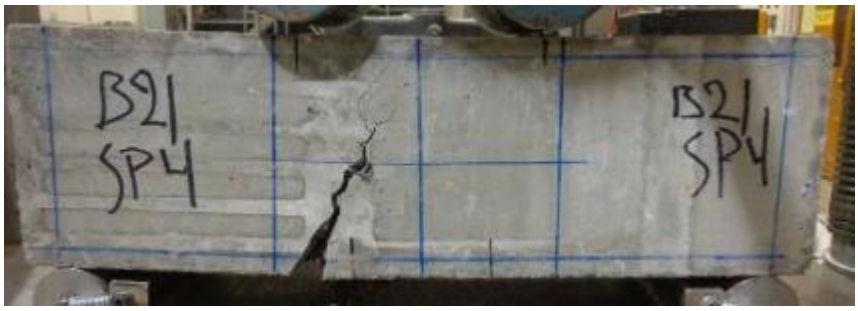
SP 5 140 fiber Multi-crack Bearing crack Wood form		

Batch 22: $f_c^{`} = 10$ ksi; $V_f = 1.5\%$; Fiber: 5D (RC-65/60-BG)

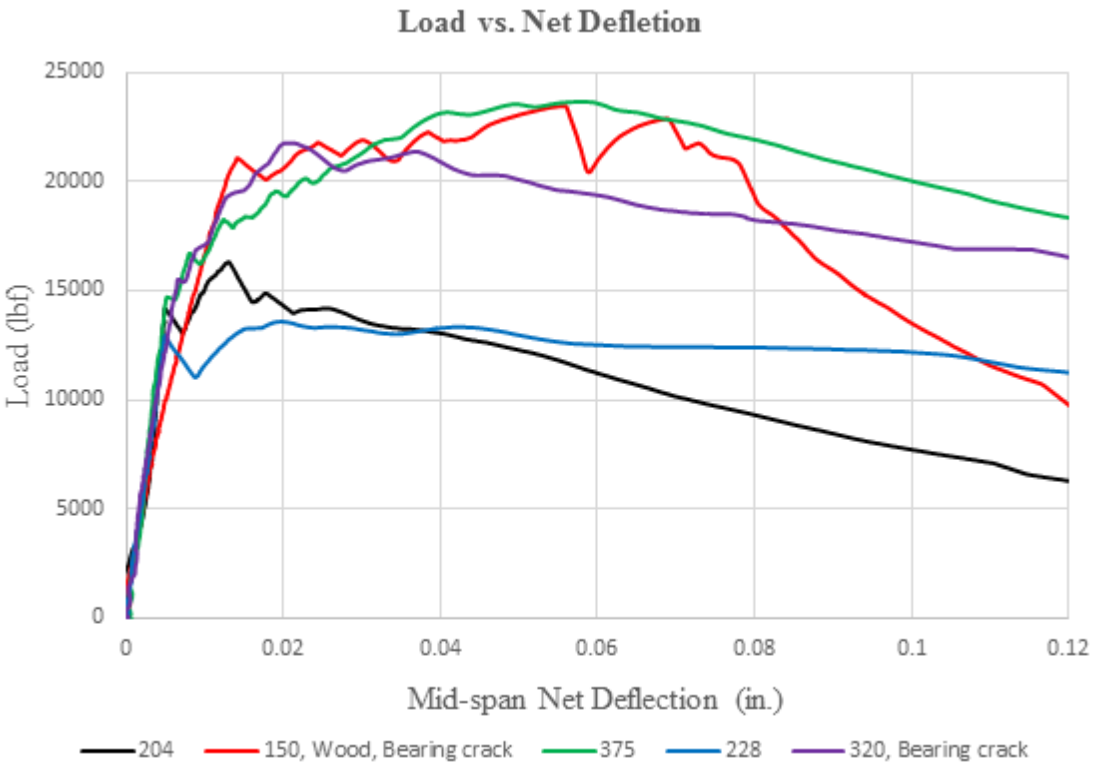

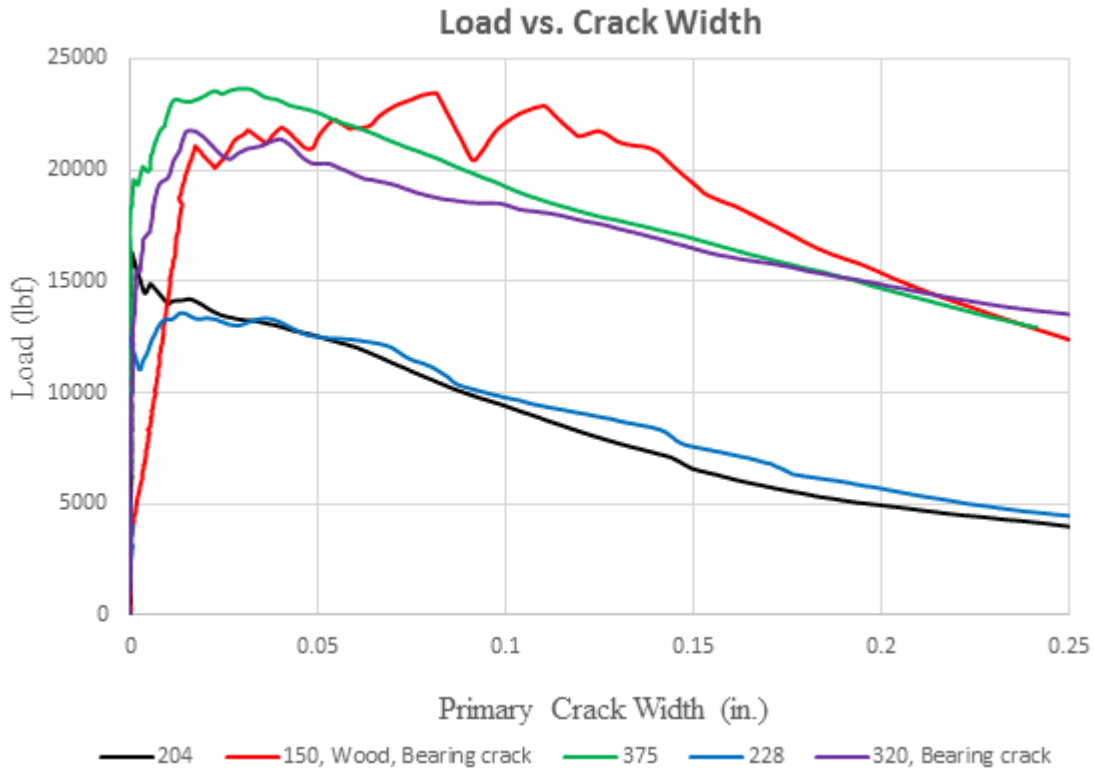

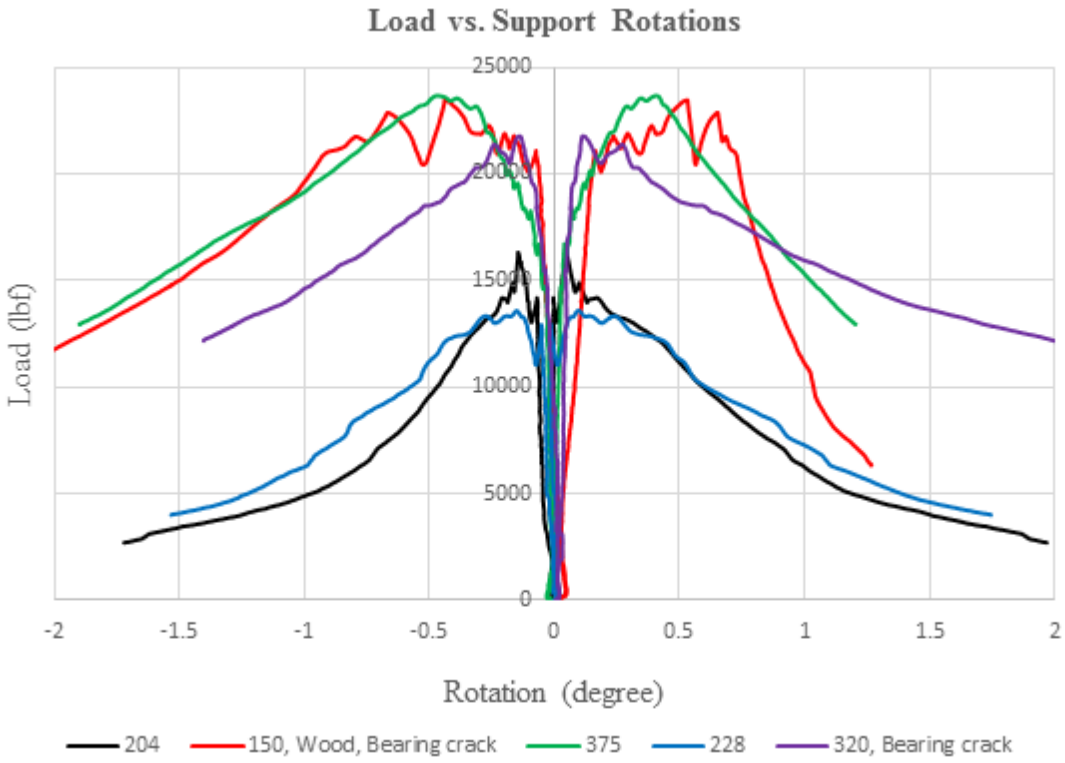

Batch ID		Fiber type			V_f (%)
B 22		5D (RC-65/60-BG)			1.5
P_1 (lbf)	P_{pc} (lbf)	$P_{\delta=0.04\ in.}$ (lbf)	$P_{\delta=0.08\ in.}$ (lbf)	$P_{\delta=0.12\ in.}$ (lbf)	P_{max} (lbf)
15010	19760	18460	16210	12410	19760
σ_1 (psi)	σ_{pc} (psi)	$\sigma_{\delta=0.04\ in.}$ (psi)	$\sigma_{\delta=0.08\ in.}$ (psi)	$\sigma_{\delta=0.12\ in.}$ (psi)	σ_{max} (psi)
1185	1560	1455	1280	985	1560
δ_1 (in.)	δ_{pc} (in.)	ω_{pc} (in.)	$COV(P_{pc})$		
0.006	0.03	0.03	23%		
Comment: dominated by fiber pullout.					

SP 1 204 fiber Multi-crack		
SP 2 150 fiber Multi-crack Wood form Bearing crack		
SP 3 375 fiber Multi-crack		
SP 4 228 fiber Multi-crack		
SP 5 320 fiber Multi-crack Bearing crack		

Appendix D – Summary of Tension Test Results

This appendix provides the tensile test results. The mean of the first-peak stress (σ_1), the post-crack peak stress (σ_{pc}), and the maximum stress ($\sigma_{\max}$) along with the coefficient of variation and the corresponding crack width of the post-crack peak stress (σ_{pc}) are summarized in table D.1. The residual stresses corresponding to crack width of 0.05, 0.10, 0.15, and 0.25 inch for each batch are summarized in Table D.2. Finally, plots of stress versus crack width of each batch along with some observations are presented in this appendix. As with previous test results, crack widths are based on results from the non-contact position sensor. Figure D.1 illustrates the difference between using the infrared-based non-contact sensor and the test frame displacement to determine crack widths.

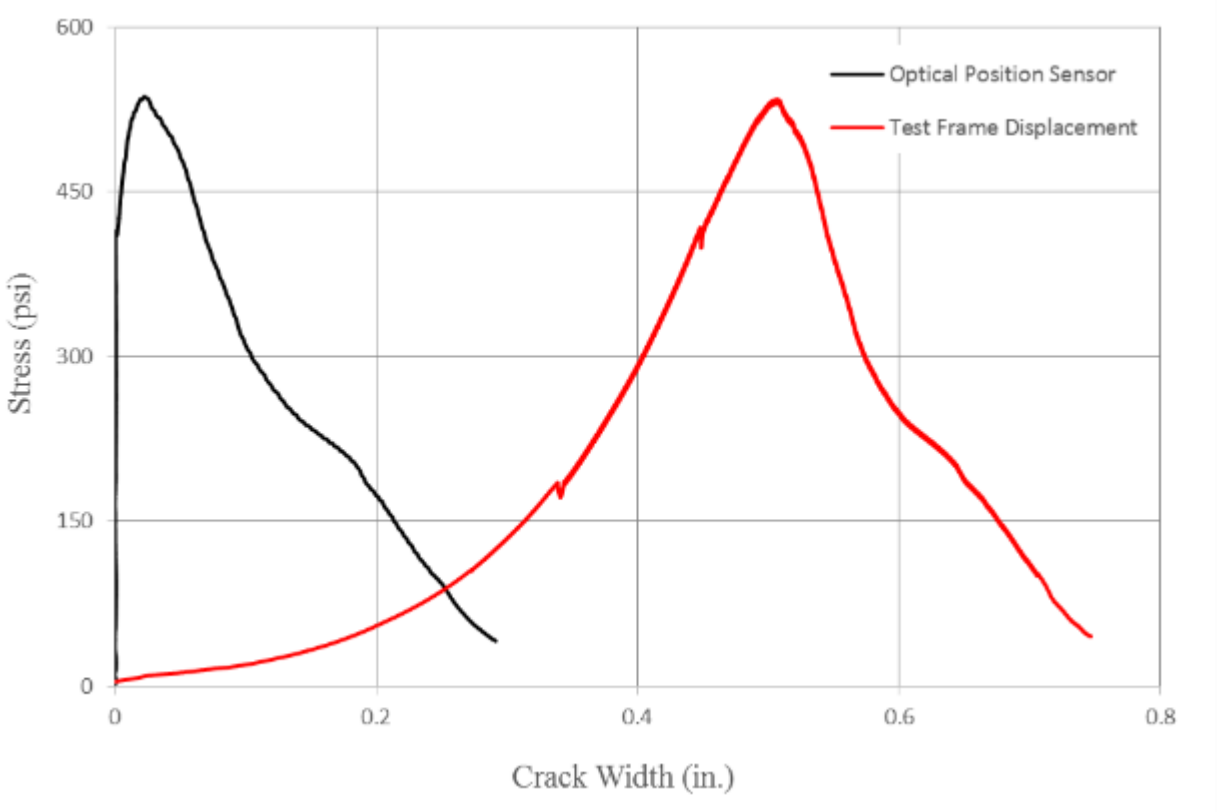

Figure D.1 – The difference between using an infrared-based non-contact sensor and the test frame displacement to determine crack width.

Table D.1 – First peak and post-crack peak profile.

Batch ID	Fiber type	V_f (%)	σ_1 (psi)	σ_{pc} (psi)	$COV(\sigma_{pc})$	ω_{pc} (in.)	σ_{max} (psi)
C 1	N/A	0	465				465
B 1	(RC-80/30-BP)	0.5	410	225	35%	0.04	410
B 2	(RC-80/30-BP)	0.75	465	455	9%	0.02	465
B 3	(RC-80/30-BP)	1.0	440	460	11%	0.02	460
B 4	(RC-80/30-BP)	1.5	405	535	3%	0.02	535
B 5	3D (RC-55/30-BG)	0.5	465	60	126%	0.06	465
B 6	3D (RC-55/30-BG)	0.75	420	130	39%	0.03	420
B 7	3D (RC-55/30-BG)	1.0	420	215	49%	0.02	420
B 8	3D (RC-55/30-BG)	1.5	420	255	54%	0.01	420
B 9	4D (RC-65/60-BG)	0.5	390	285	25%	0.04	390
B 10	4D (RC-65/60-BG)	0.75	420	380	20%	0.03	420
B 11	4D (RC-65/60-BG)	1.0	455	475	23%	0.03	475
B 12	4D (RC-65/60-BG)	1.5	430	590	27%	0.03	590
B 13	5D (RC-65/60-BG)	0.75	395	265	47%	0.05	395
B 14	5D (RC-65/60-BG)	1.5	405	470	36%	0.03	470
C 2	N/A	0	685				685
B 15	(RC-80/30-BP)	0.5	745	490	10%	0.03	745
B 16	(RC-80/30-BP)	0.75	755	545	9%	0.02	755
B 17	(RC-80/30-BP)	1.0	820	885	5%	0.02	885
B 18	(RC-80/30-BP)	1.5	745	865	9%	0.02	865
B 19	4D (RC-65/60-BG)	0.75	750	595	31%	0.03	750
B 20	4D (RC-65/60-BG)	1.5	760	790	33%	0.03	790
B 21	5D (RC-65/60-BG)	0.75	775	720	12%	0.03	775
B 22	5D (RC-65/60-BG)	1.5	710	835	13%	0.04	835

Table D.2 – Tensile stress profile.

Batch ID	Fiber type	V_f (%)	σ_1 (psi)	σ_{pc} (psi)	$\sigma_{\omega=0.05\ in.}$ (psi)	$\sigma_{\omega=0.10\ in.}$ (psi)	$\sigma_{\omega=0.15\ in.}$ (psi)	$\sigma_{\omega=0.25\ in.}$ (psi)
C 1	N/A	0	465					
B 1	(RC-80/30-BP)	0.5	410	225	215	170	115	455
B 2	(RC-80/30-BP)	0.75	465	455	390	270	200	65
B 3	(RC-80/30-BP)	1.0	440	460	400	255	190	80
B 4	(RC-80/30-BP)	1.5	405	535	500	355	260	170
B 5	3D (RC-55/30-BG)	0.5	465	60	65	45	25	75
B 6	3D (RC-55/30-BG)	0.75	420	130	105	85	65	45
B 7	3D (RC-55/30-BG)	1.0	420	215	145	100	70	55
B 8	3D (RC-55/30-BG)	1.5	420	255	220	155	110	85
B 9	4D (RC-65/60-BG)	0.5	390	285	265	145	125	75
B 10	4D (RC-65/60-BG)	0.75	420	380	345	255	210	160
B 11	4D (RC-65/60-BG)	1.0	455	475	440	335	245	200
B 12	4D (RC-65/60-BG)	1.5	430	590	550	460	390	340
B 13	5D (RC-65/60-BG)	0.75	395	265	230	180	140	95
B 14	5D (RC-65/60-BG)	1.5	405	470	440	370	295	215
C 2	N/A	0	685					
B 15	(RC-80/30-BP)	0.5	745	490	310	215	175	130
B 16	(RC-80/30-BP)	0.75	755	545	415	285	215	175
B 17	(RC-80/30-BP)	1.0	820	885	800	540	365	290
B 18	(RC-80/30-BP)	1.5	745	865	790	480	305	240
B 19	4D (RC-65/60-BG)	0.75	750	595	475	310	225	160
B 20	4D (RC-65/60-BG)	1.5	760	790	755	610	465	305
B 21	5D (RC-65/60-BG)	0.75	775	720	615	455	330	290
B 22	5D (RC-65/60-BG)	1.5	710	835	795	685	540	415

Batch **page**

Control 1: $f_c^{`} = 6$ ksi

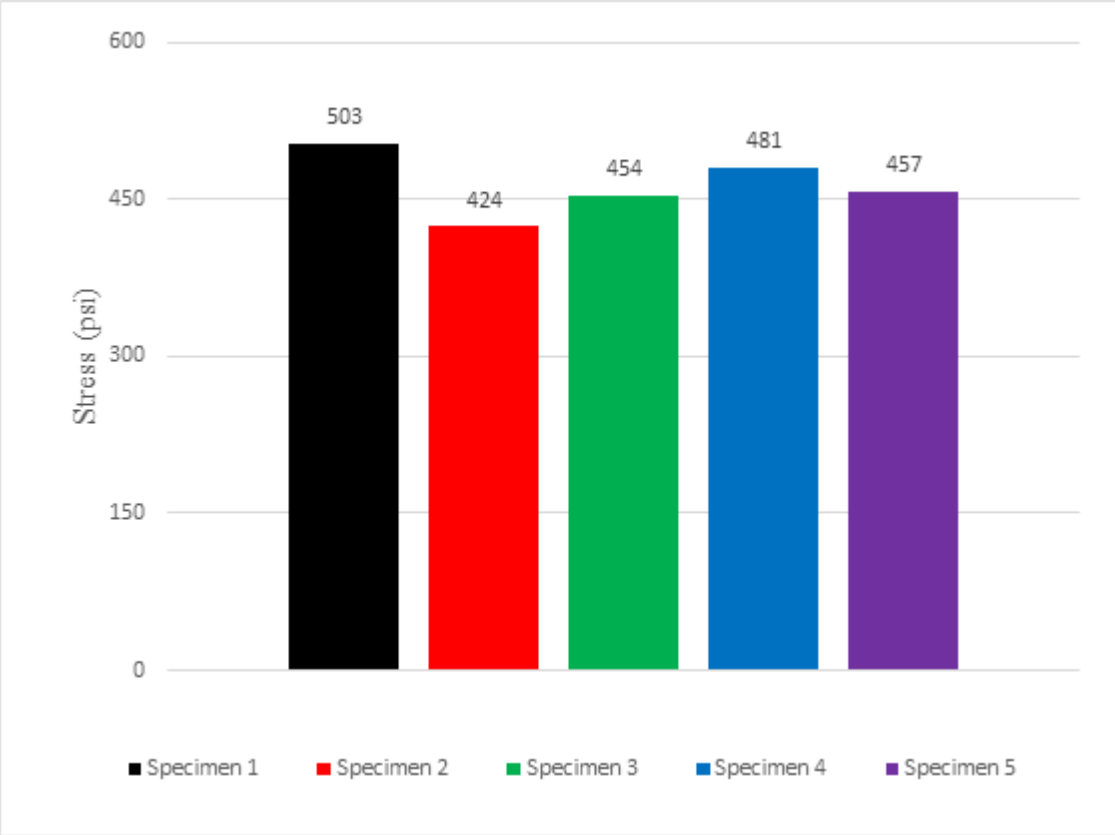

Batch ID	Fiber type				V_f (%)
C 1	N/A				0
σ_1 (psi)	ω_1 (in.)	σ_{pc} (psi)	ω_{pc} (in.)	$COV(\sigma_{pc})$	σ_{max} (psi)
465	0	0	0	0%	465
σ_2 (psi)	ω_2 (in.)	$\sigma_{\omega=0.05\ in.}$ (psi)	$\sigma_{\omega=0.10\ in.}$ (psi)	$\sigma_{\omega=0.15\ in.}$ (psi)	$\sigma_{\omega=0.25\ in.}$ (psi)
0	0	0	0	0	0
Comment: all specimens failed suddenly after first crack.					

SP 1 0 fiber	
SP 2 0 fiber	
SP 3 0 fiber	
SP 4 0 fiber	
SP 5 0 fiber	

Batch 1: $f_c^{`} = 6$ ksi; $V_f = 0.5\%$; Fiber: (RC-80/30-BP)

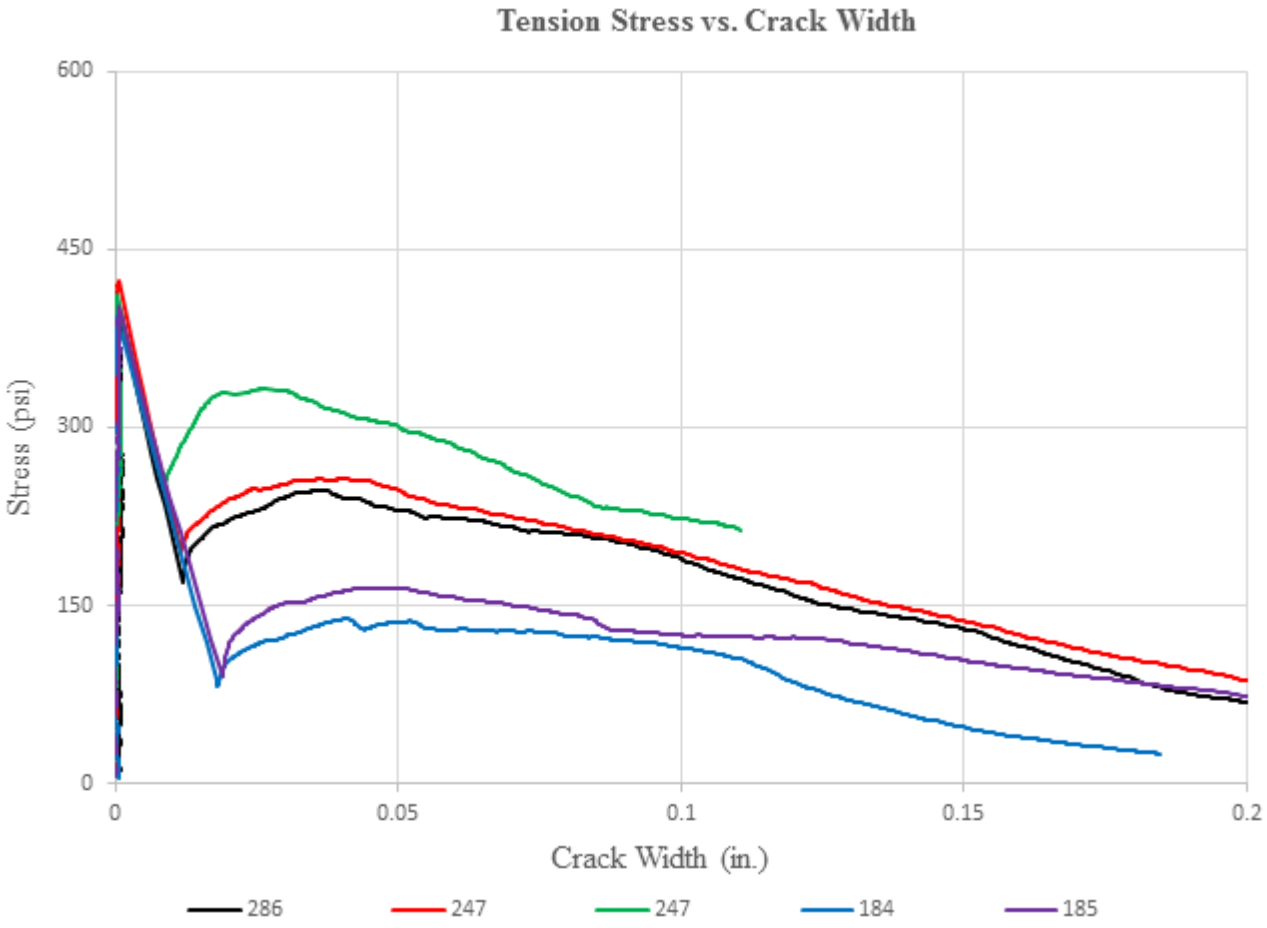

Batch ID	Fiber type				V_f (%)
B 1	(RC-80/30-BP)				0.5
σ_1 (psi)	ω_1 (in.)	σ_{pc} (psi)	ω_{pc} (in.)	$COV(\sigma_{pc})$	σ_{max} (psi)
410	0.001	225	0.039	35%	410
σ_2 (psi)	ω_2 (in.)	$\sigma_{\omega=0.05\ in.}$ (psi)	$\sigma_{\omega=0.10\ in.}$ (psi)	$\sigma_{\omega=0.15\ in.}$ (psi)	$\sigma_{\omega=0.25\ in.}$ (psi)
160	0.014	215	170	115	45
Comment: brittle failure, dominated by fiber pullout.					

SP 1 286 fibers	
SP 2 247 fibers	
SP 3 288 fibers	
SP 4 184 fibers	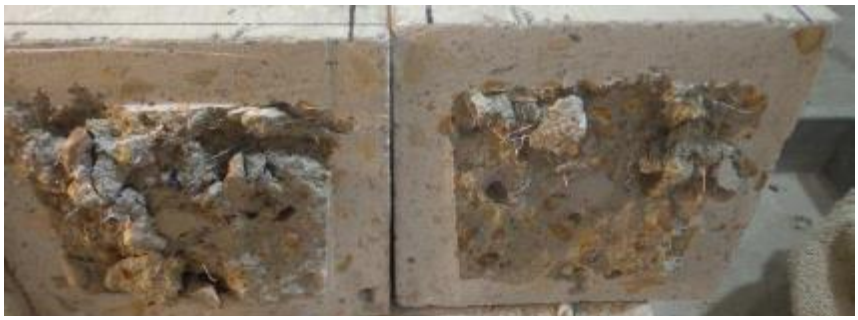
SP 5 185 fibers	

Batch 2: $f'_{c,\text{spec.}} = 6$ ksi; $V_f = 0.75\%$; Fiber: (RC-80/30-BP)

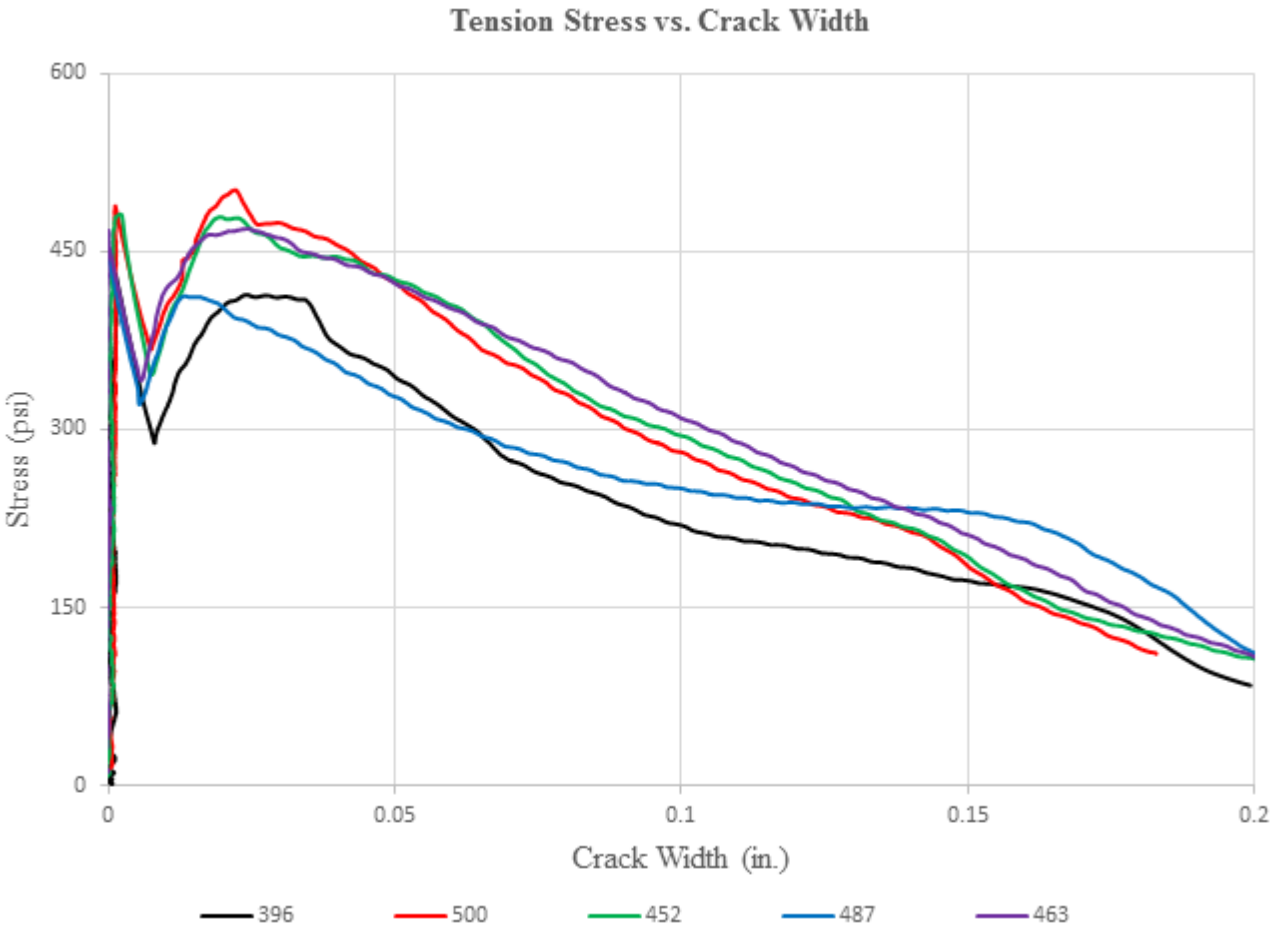

Batch ID	Fiber type				V_f (%)
B 2	(RC-80/30-BP)				0.75
σ_1 (psi)	ω_1 (in.)	σ_{pc} (psi)	ω_{pc} (in.)	$COV(\sigma_{pc})$	σ_{max} (psi)
465	0.001	455	0.021	9%	465
σ_2 (psi)	ω_2 (in.)	$\sigma_{\omega=0.05\ in.}$ (psi)	$\sigma_{\omega=0.10\ in.}$ (psi)	$\sigma_{\omega=0.15\ in.}$ (psi)	$\sigma_{\omega=0.25\ in.}$ (psi)
335	0.007	390	270	200	65
Comment: brittle failure, dominated by fiber pullout.					

SP 1 396 fibers	
SP 2 500 fibers	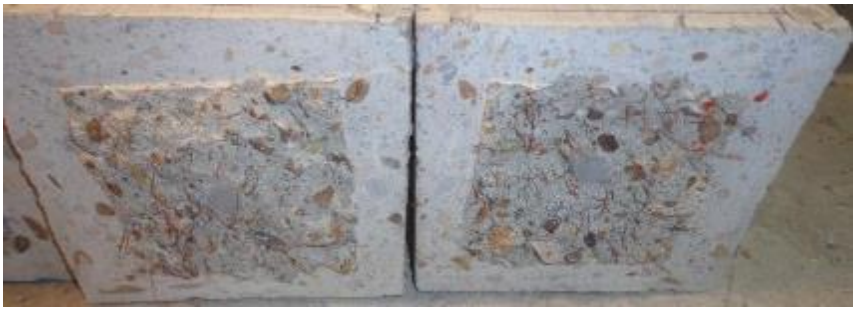
SP 3 452 fibers	
SP 4 487 fibers	
SP 5 463 fibers	

Batch 3: $f_c^{`} = 6$ ksi; $V_f = 1.0\%$; Fiber: (RC-80/30-BP)

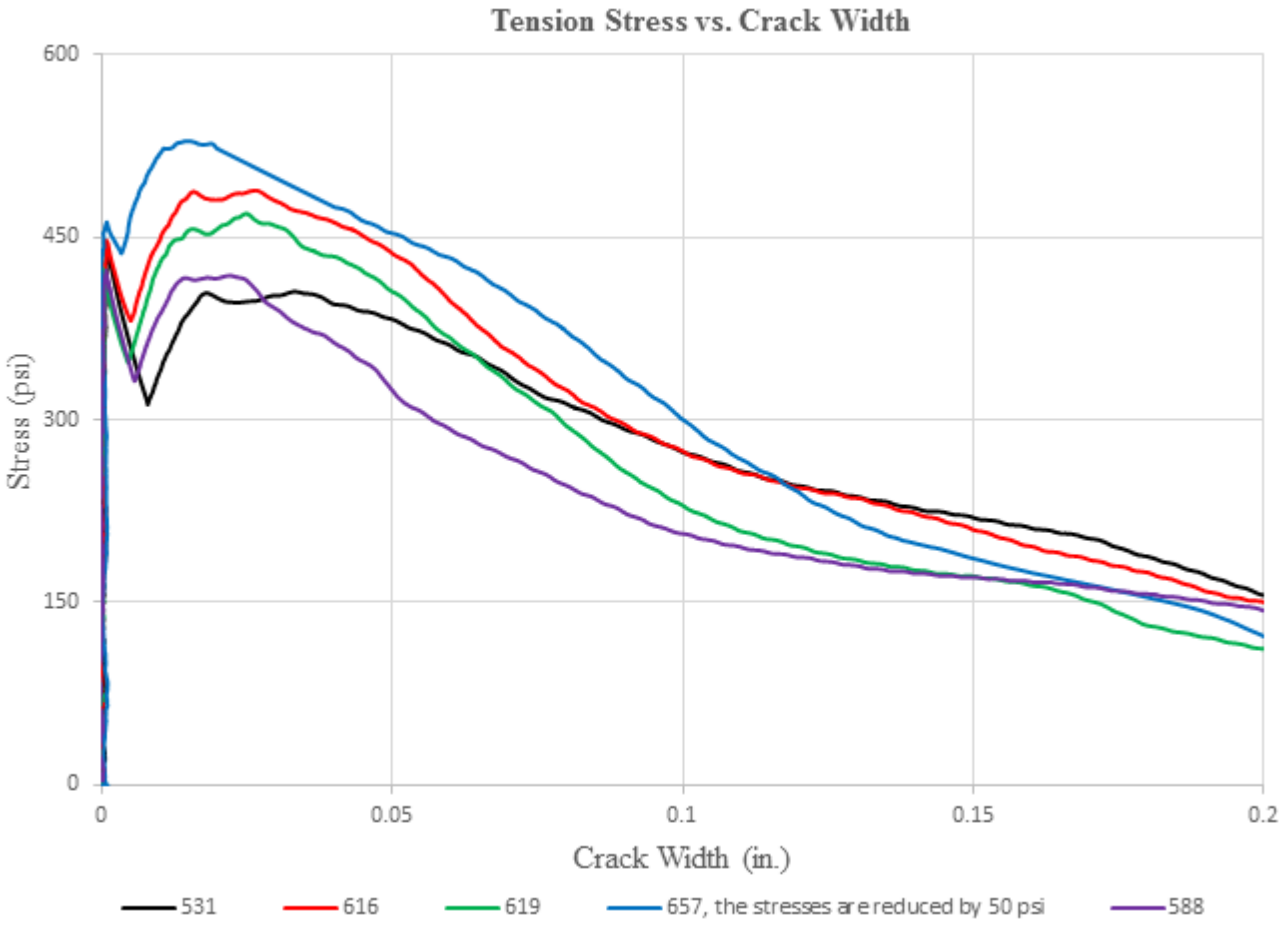

Batch ID	Fiber type				V_f (%)
B 3	(RC-80/30-BP)				1.0
σ_1 (psi)	ω_1 (in.)	σ_{pc} (psi)	ω_{pc} (in.)	$COV(\sigma_{pc})$	σ_{max} (psi)
440	0.001	460	0.025	11%	460
σ_2 (psi)	ω_2 (in.)	$\sigma_{\omega=0.05\ in.}$ (psi)	$\sigma_{\omega=0.10\ in.}$ (psi)	$\sigma_{\omega=0.15\ in.}$ (psi)	$\sigma_{\omega=0.25\ in.}$ (psi)
360	0.005	400	255	190	80
Comment: dominated by fiber pullout.					

SP 1 531 fibers	
SP 2 616 fibers	
SP 3 619 fibers	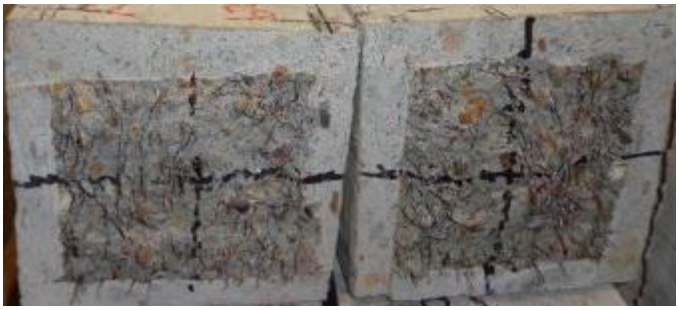
SP 4 657 fibers	
SP 5 588 fibers	

Batch 4: $f_c^{`} = 6$ ksi; $V_f = 1.5\%$; Fiber: (RC-80/30-BP)

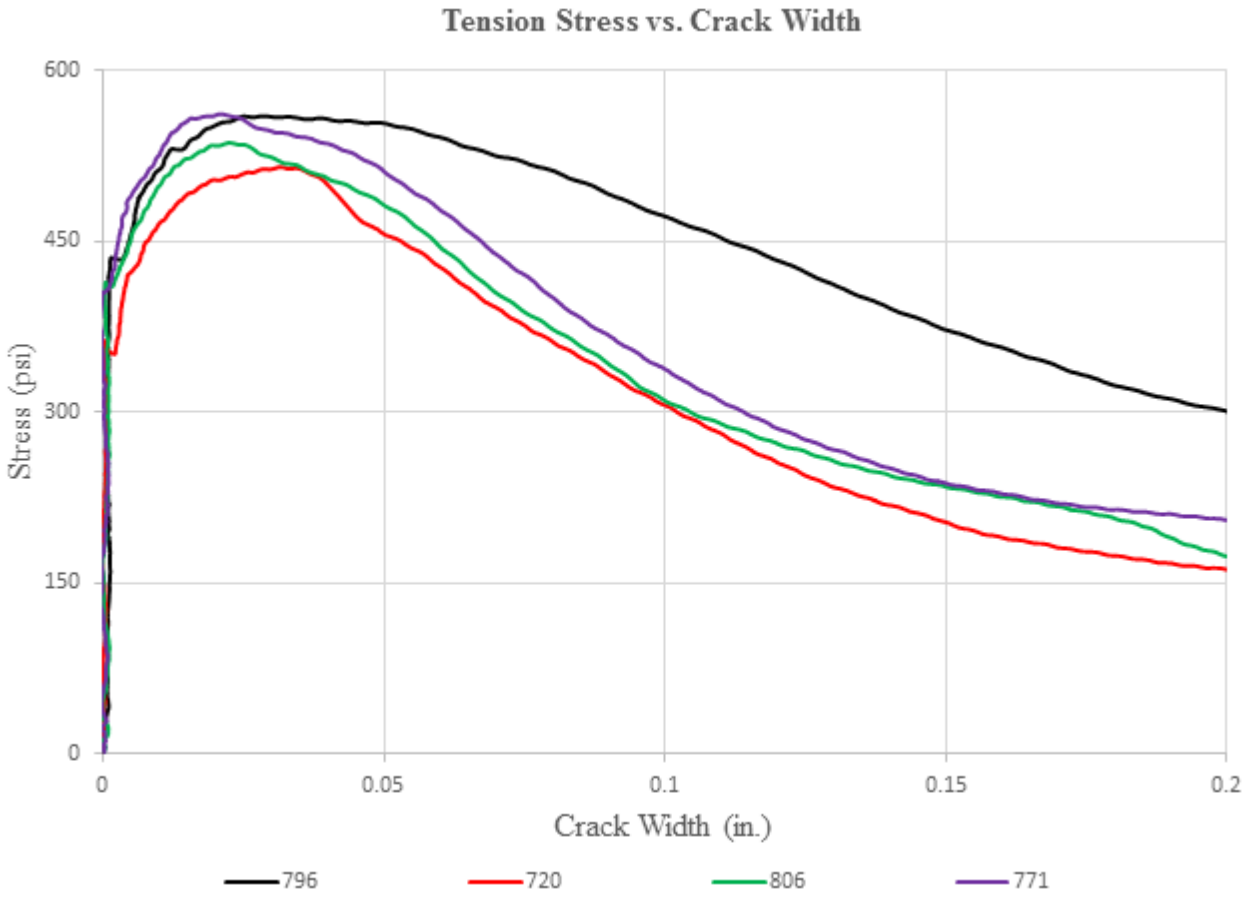

Batch ID	Fiber type				V_f (%)
B 4	(RC-80/30-BP)				1.5
σ_1 (psi)	ω_1 (in.)	σ_{pc} (psi)	ω_{pc} (in.)	$COV(\sigma_{pc})$	σ_{max} (psi)
405	0.001	535	0.025	3%	535
σ_2 (psi)	ω_2 (in.)	$\sigma_{\omega=0.05\ in.}$ (psi)	$\sigma_{\omega=0.10\ in.}$ (psi)	$\sigma_{\omega=0.15\ in.}$ (psi)	$\sigma_{\omega=0.25\ in.}$ (psi)
440	0.002	500	355	260	170
Comment: dominated by fiber pullout.					

SP 1 796 fibers	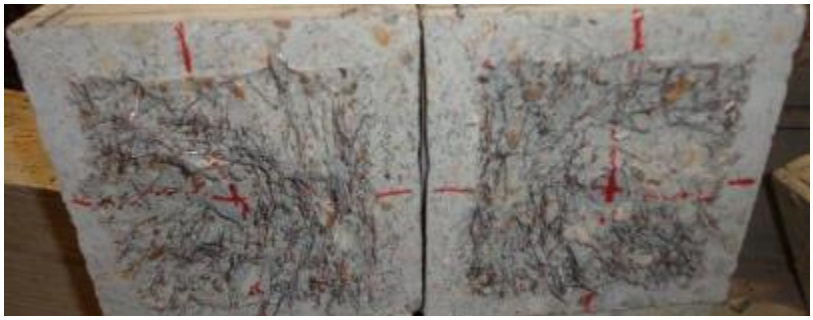
SP 2 720 fibers	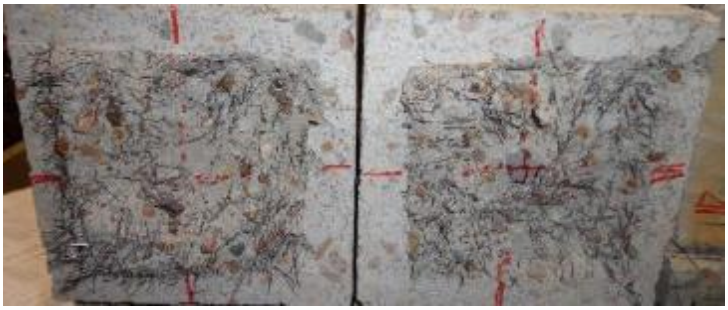
SP 3 806 fibers	
SP 4 910 fibers The reinforcing bar was not located at the failure section.	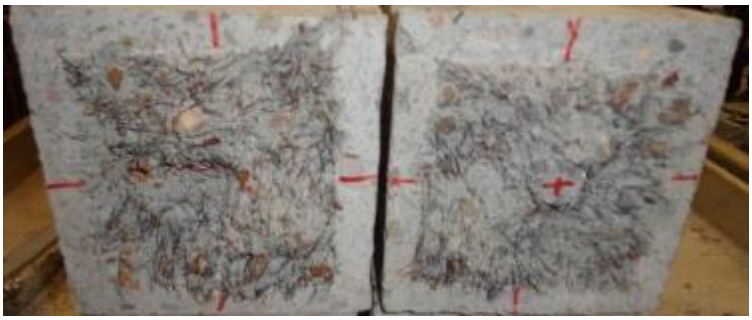
SP 5 771 fibers	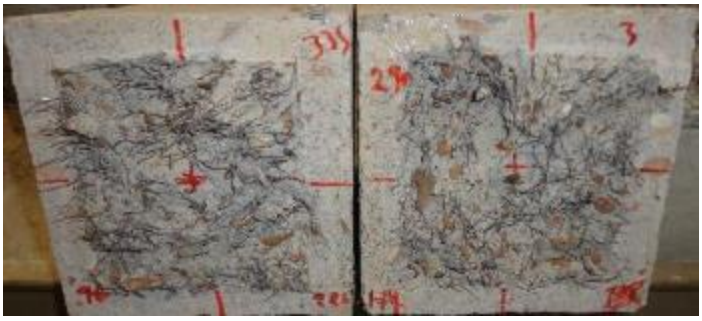

Batch 5: $f_c^{`} = 6$ ksi; $V_f = 0.5\%$; Fiber: 3D (RC-55/30-BG)

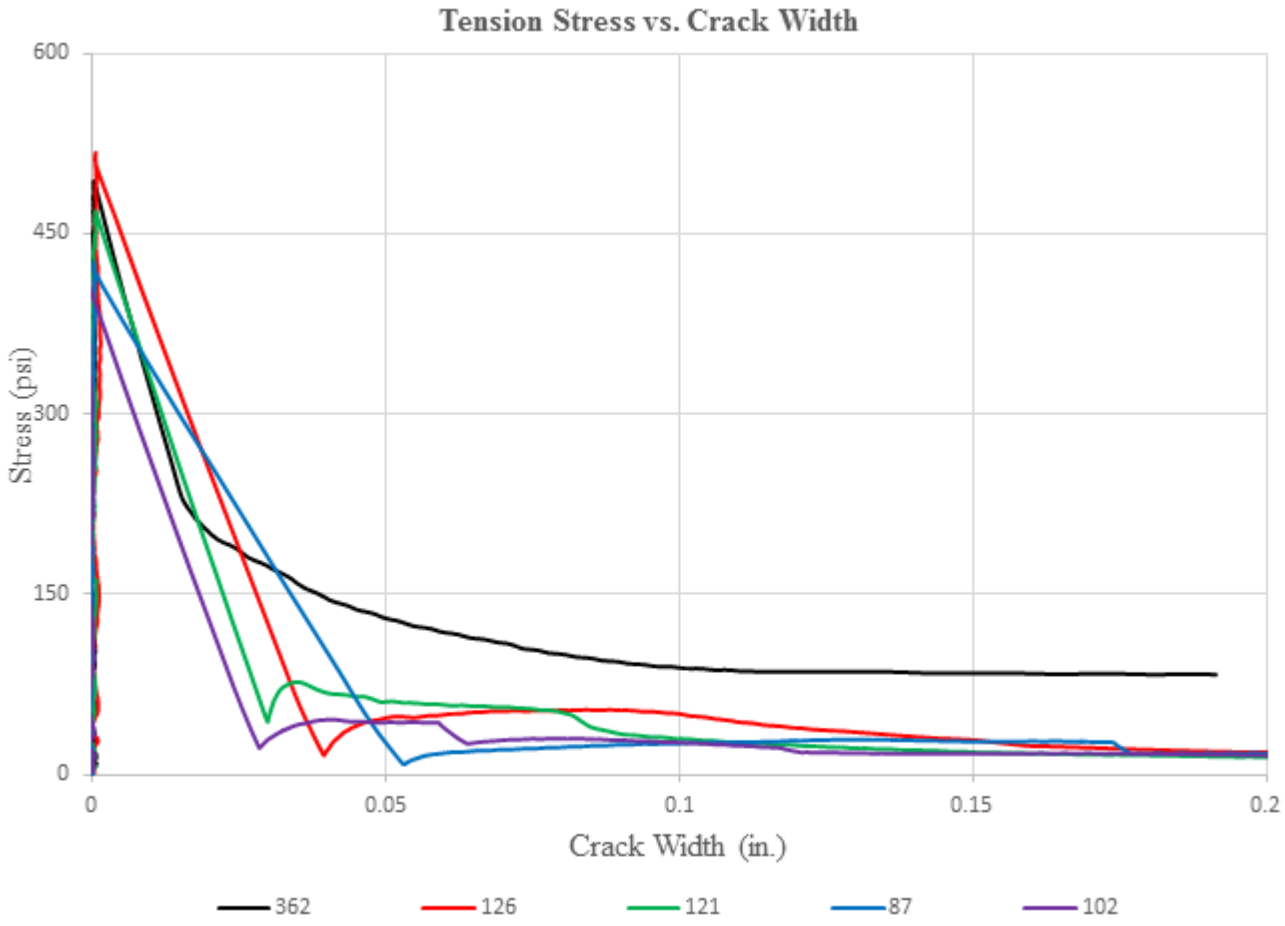

Batch ID	Fiber type				V_f (%)
B 5	3D (RC-55/30-BG)				0.5
σ_1 (psi)	ω_1 (in.)	σ_{pc} (psi)	ω_{pc} (in.)	$COV(\sigma_{pc})$	σ_{max} (psi)
465	0	60	0.064	126%	465
σ_2 (psi)	ω_2 (in.)	$\sigma_{\omega=0.05\ in.}$ (psi)	$\sigma_{\omega=0.10\ in.}$ (psi)	$\sigma_{\omega=0.15\ in.}$ (psi)	$\sigma_{\omega=0.25\ in.}$ (psi)
60	0.03	65	45	25	75
Comment: brittle failure, fiber bundles, dominated by fiber pullout.					

SP 1 362 fibers	
SP 2 126 fibers	
SP 3 121 fibers	
SP 4 87 fibers	
SP 5 102 fibers	

Batch 6: $f_c^{`} = 6$ ksi; $V_f = 0.75\%$; Fiber: 3D (RC-55/30-BG)

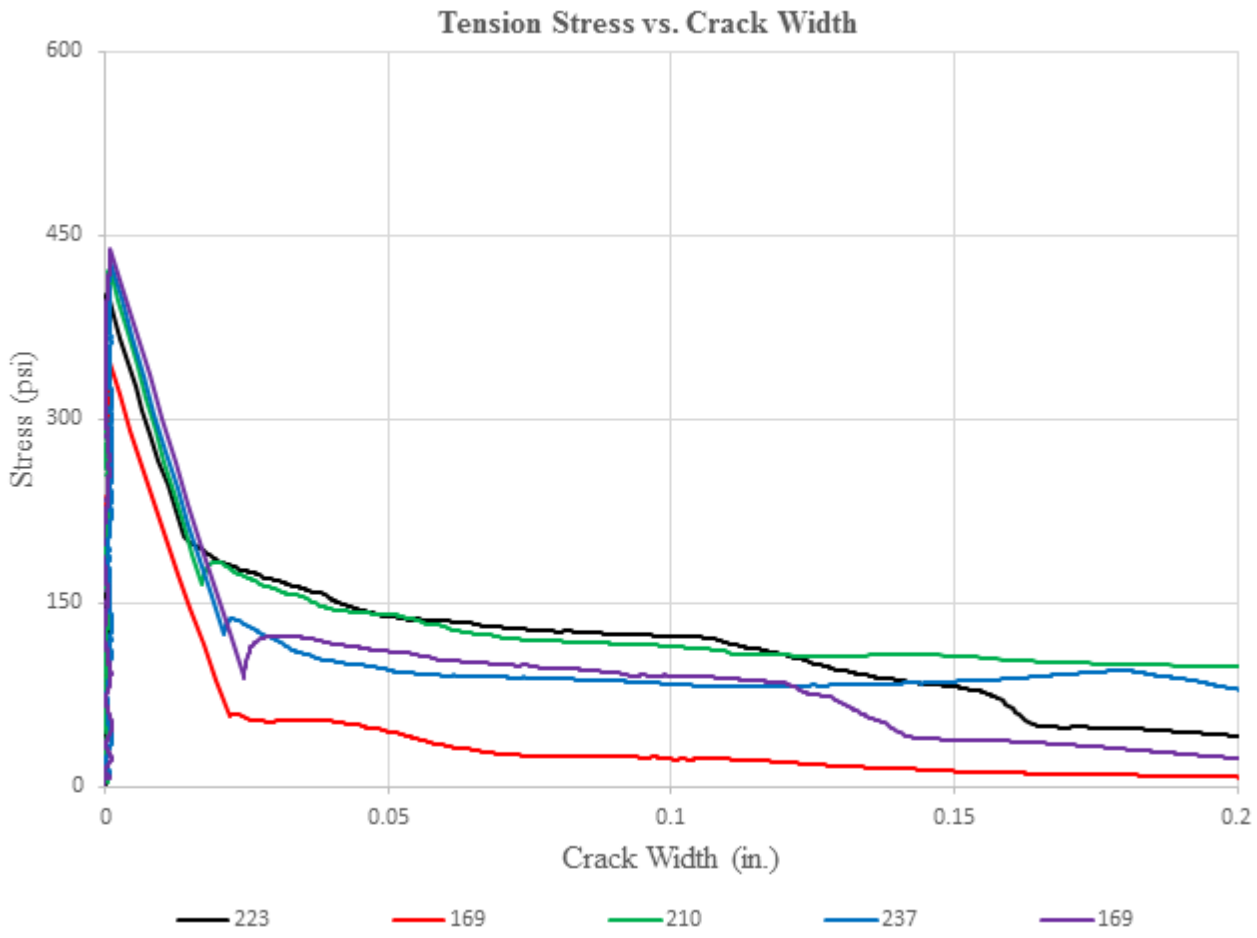

Batch ID	Fiber type				V_f (%)
B 6	3D (RC-55/30-BG)				0.75
σ_1 (psi)	ω_1 (in.)	σ_{pc} (psi)	ω_{pc} (in.)	$COV(\sigma_{pc})$	σ_{max} (psi)
420	0.001	130	0.026	39%	420
σ_2 (psi)	ω_2 (in.)	$\sigma_{\omega=0.05\ in.}$ (psi)	$\sigma_{\omega=0.10\ in.}$ (psi)	$\sigma_{\omega=0.15\ in.}$ (psi)	$\sigma_{\omega=0.25\ in.}$ (psi)
125	0.019	105	85	65	45
Comment: brittle failure, fiber bundles, dominated by fiber pullout and fiber fracture.					

SP 1 223 fibers	
SP 2 169 fibers	
SP 3 210 fibers	
SP 4 237 fibers	
SP 5 169 fibers	

Batch 7: $f_c^{`} = 6$ ksi; $V_f = 1.0\%$; Fiber: 3D (RC-55/30-BG)

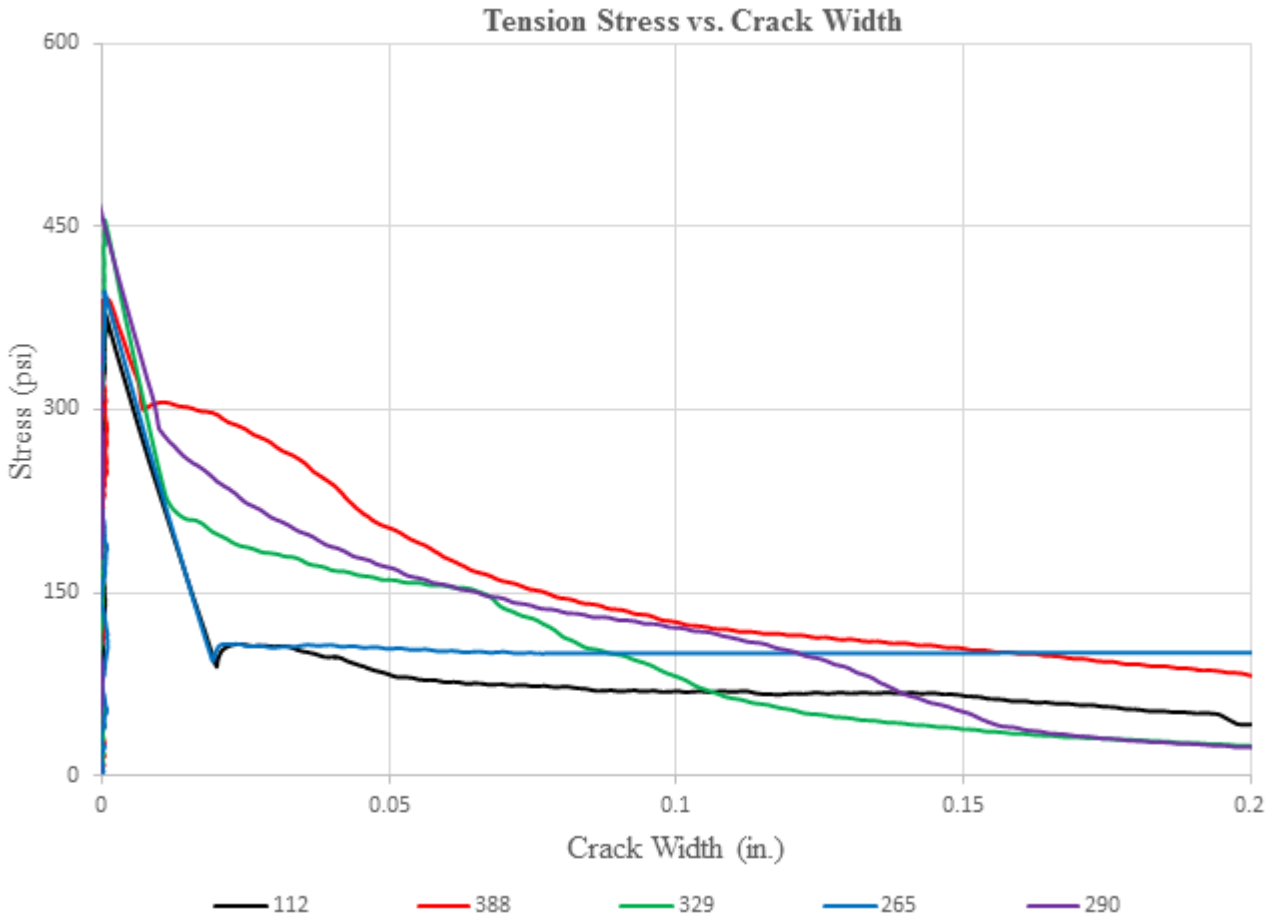

Batch ID	Fiber type				V_f (%)
B 7	3D (RC-55/30-BG)				1.0
σ_1 (psi)	ω_1 (in.)	σ_{pc} (psi)	ω_{pc} (in.)	$COV(\sigma_{pc})$	σ_{max} (psi)
420	0	215	0.020	49%	420
σ_2 (psi)	ω_2 (in.)	$\sigma_{\omega=0.05\ in.}$ (psi)	$\sigma_{\omega=0.10\ in.}$ (psi)	$\sigma_{\omega=0.15\ in.}$ (psi)	$\sigma_{\omega=0.25\ in.}$ (psi)
200	0.013	145	100	70	55
Comment: brittle failure, fiber bundles, dominated by fiber pullout and fiber fracture.					

SP 1 112 fibers	
SP 2 388 fibers	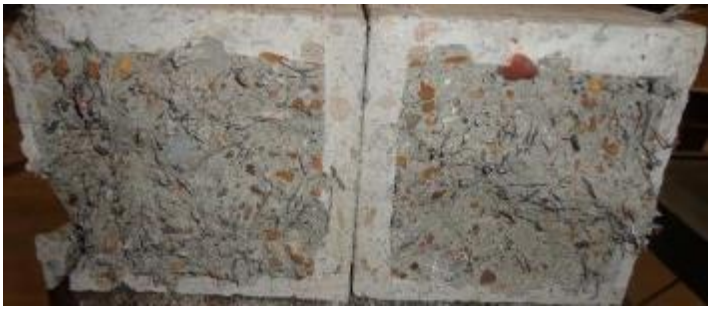
SP 3 329 fibers	
SP 4 265 fibers	
SP 5 290 fibers	

Batch 8: $f_c^{`} = 6$ ksi; $V_f = 1.5\%$; Fiber: 3D (RC-55/30-BG)

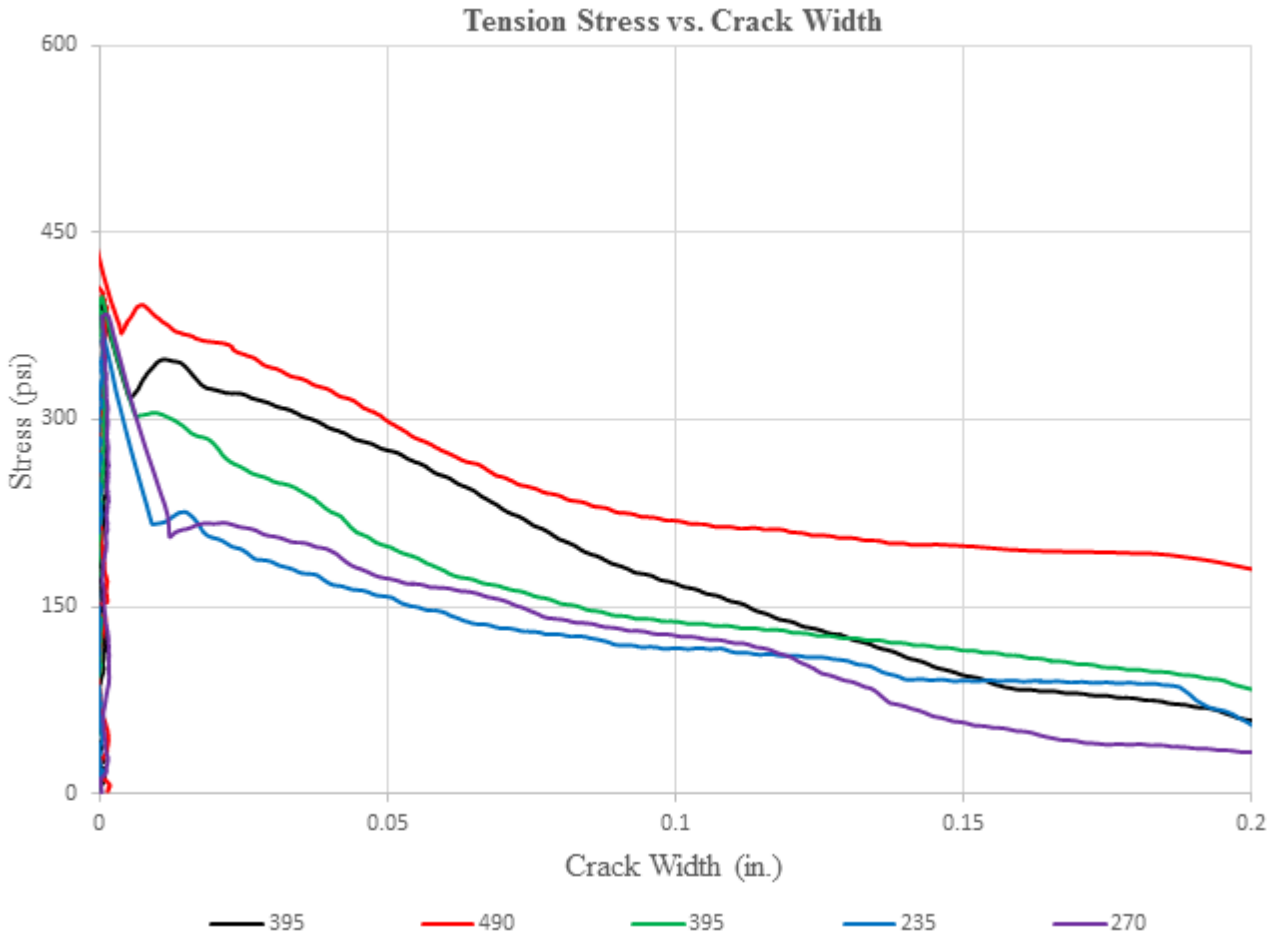

Batch ID	Fiber type				V_f (%)
B 8	3D (RC-55/30-BG)				1.5
σ_1 (psi)	ω_1 (in.)	σ_{pc} (psi)	ω_{pc} (in.)	$COV(\sigma_{pc})$	σ_{max} (psi)
420	0	255	0.015	54%	420
σ_2 (psi)	ω_2 (in.)	$\sigma_{\omega=0.05\ in.}$ (psi)	$\sigma_{\omega=0.10\ in.}$ (psi)	$\sigma_{\omega=0.15\ in.}$ (psi)	$\sigma_{\omega=0.25\ in.}$ (psi)
285	0.008	220	155	110	85
Comment: brittle failure, fiber bundles, dominated by fiber pullout and fiber fracture.					

SP 1 395 fibers	
SP 2 490 fibers	
SP 3 395 fibers	
SP 4 235 fibers	
SP 5 270 fibers	

Batch 9: $f_c^{`} = 6$ ksi; $V_f = 0.5\%$; Fiber: 4D (RC-65/60-BG)

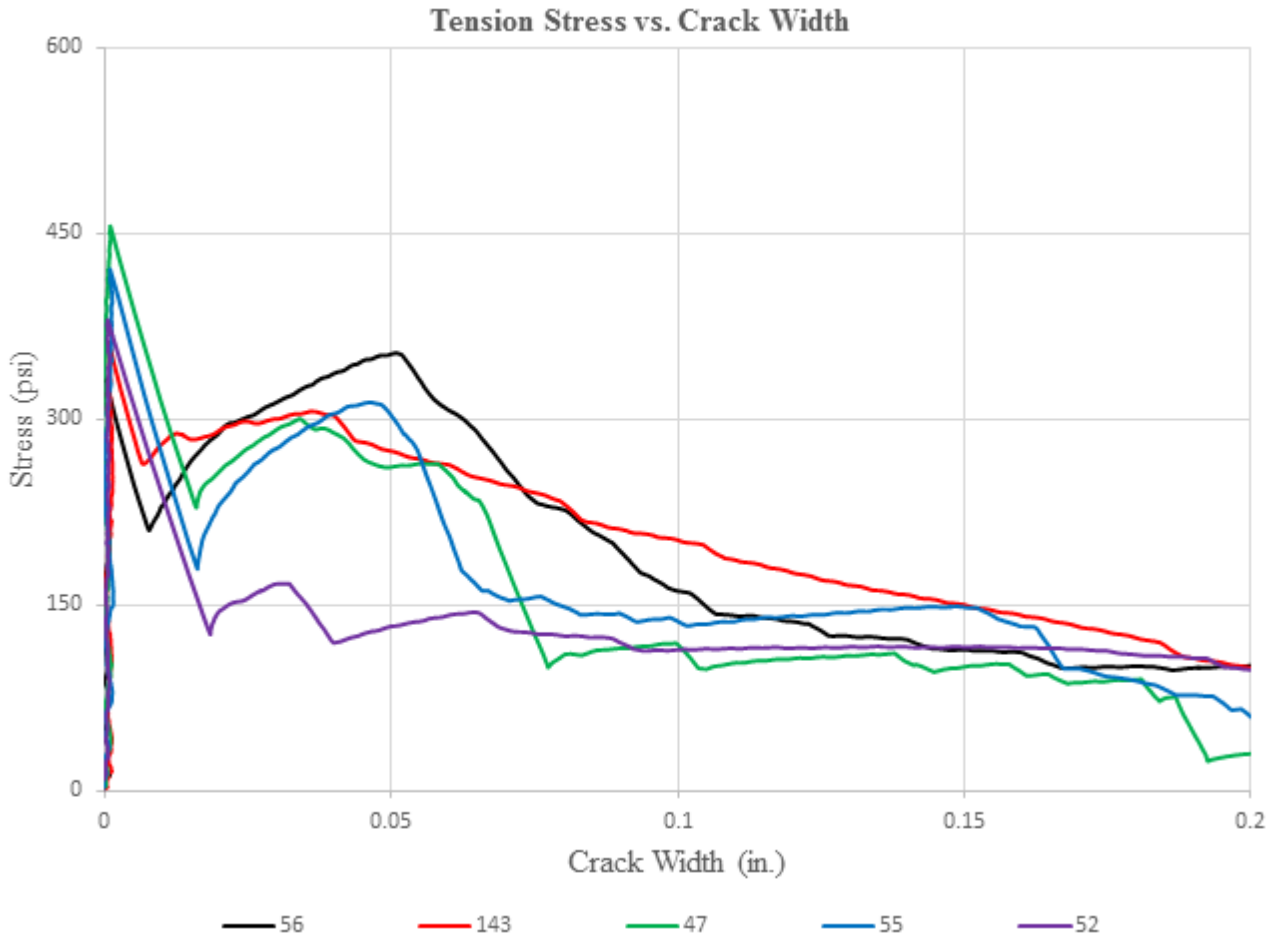

Batch ID	Fiber type				V_f (%)
B 9	4D (RC-65/60-BG)				0.5
σ_1 (psi)	ω_1 (in.)	σ_{pc} (psi)	ω_{pc} (in.)	$COV(\sigma_{pc})$	σ_{max} (psi)
390	0.001	285	0.04	25%	390
σ_2 (psi)	ω_2 (in.)	$\sigma_{\omega=0.05\ in.}$ (psi)	$\sigma_{\omega=0.10\ in.}$ (psi)	$\sigma_{\omega=0.15\ in.}$ (psi)	$\sigma_{\omega=0.25\ in.}$ (psi)
200	0.013	265	145	125	75
Comment: brittle failure, dominated by fiber pullout and fiber fracture.					

SP 1 56 fibers	
SP 2 143 fibers	
SP 3 47 fibers	
SP 4 55 fibers	
SP 5 52 fibers	

Batch 10: $f_c^{`} = 6$ ksi; $V_f = 0.75\%$; Fiber: 4D (RC-65/60-BG)

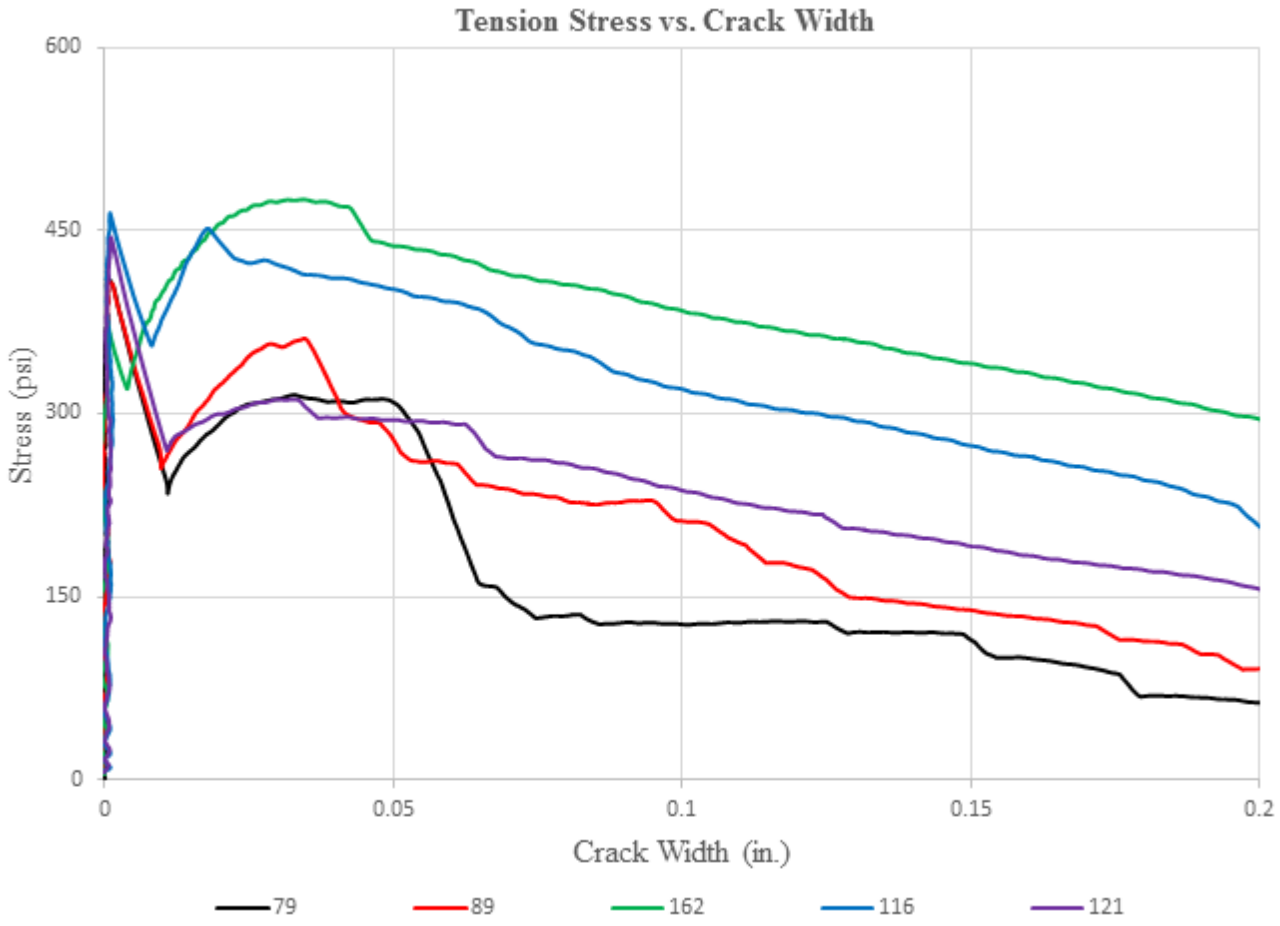

Batch ID	Fiber type				V_f (%)
B 10	4D (RC-65/60-BG)				0.75
σ_1 (psi)	ω_1 (in.)	σ_{pc} (psi)	ω_{pc} (in.)	$COV(\sigma_{pc})$	σ_{max} (psi)
420	0.001	380	0.03	20%	420
σ_2 (psi)	ω_2 (in.)	$\sigma_{\omega=0.05\ in.}$ (psi)	$\sigma_{\omega=0.10\ in.}$ (psi)	$\sigma_{\omega=0.15\ in.}$ (psi)	$\sigma_{\omega=0.25\ in.}$ (psi)
285	0.009	345	255	210	160
Comment: brittle failure, dominated by fiber pullout and fiber fracture.					

SP 1 79 fibers	
SP 2 89 fibers	
SP 3 162 fibers	
SP 4 116 fibers	
SP 5 121 fibers	

Batch 11: $f_c^{`} = 6$ ksi; $V_f = 1.0\%$; Fiber: 4D (RC-65/60-BG)

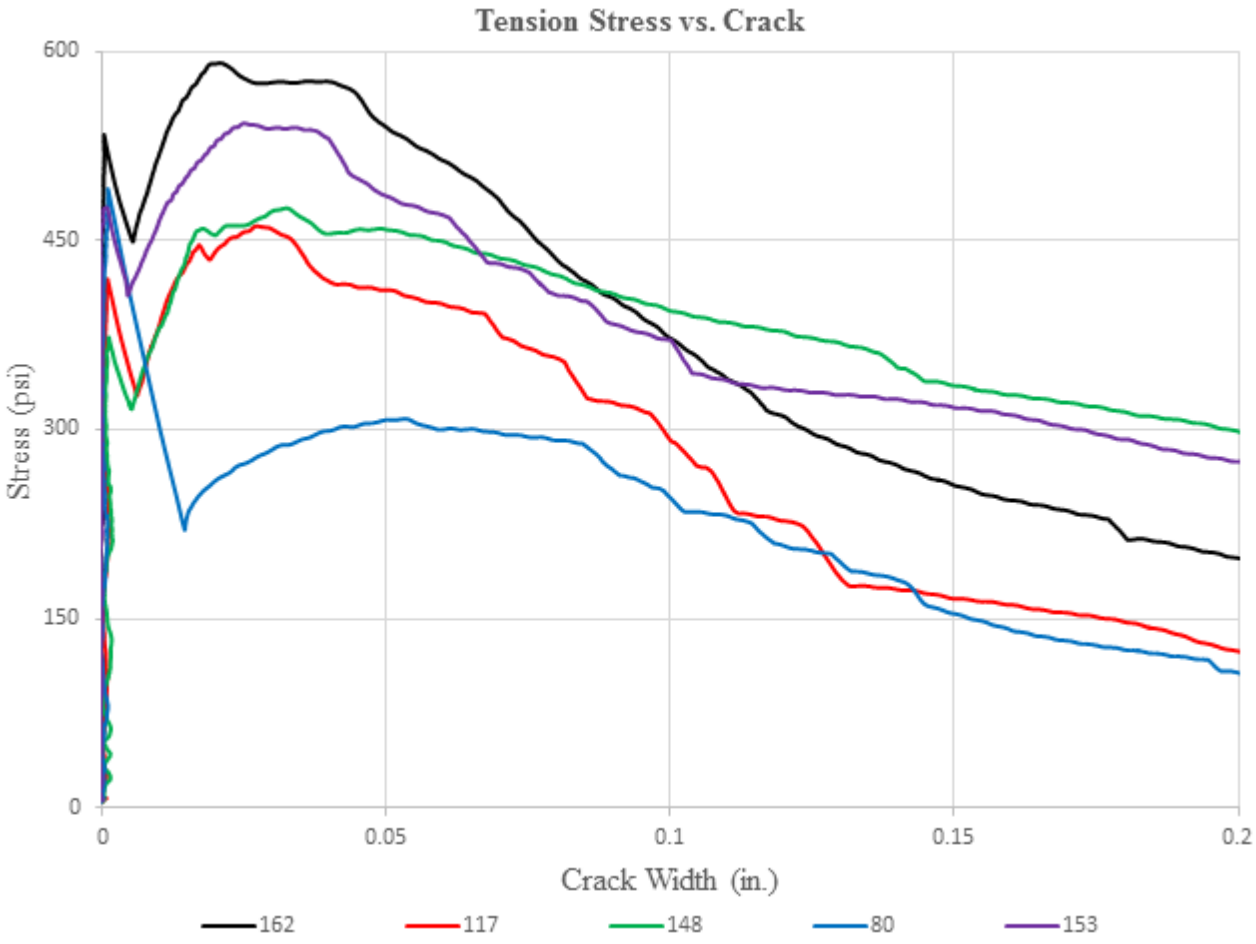

Batch ID	Fiber type				V_f (%)
B 11	4D (RC-65/60-BG)				1.0
σ_1 (psi)	ω_1 (in.)	σ_{pc} (psi)	ω_{pc} (in.)	$COV(\sigma_{pc})$	σ_{max} (psi)
455	0.001	475	0.027	23%	475
σ_2 (psi)	ω_2 (in.)	$\sigma_{\omega=0.05\ in.}$ (psi)	$\sigma_{\omega=0.10\ in.}$ (psi)	$\sigma_{\omega=0.15\ in.}$ (psi)	$\sigma_{\omega=0.25\ in.}$ (psi)
355	0.007	440	335	245	195
Comment: dominated by fiber pullout and fiber fracture.					

SP 1 162 fibers	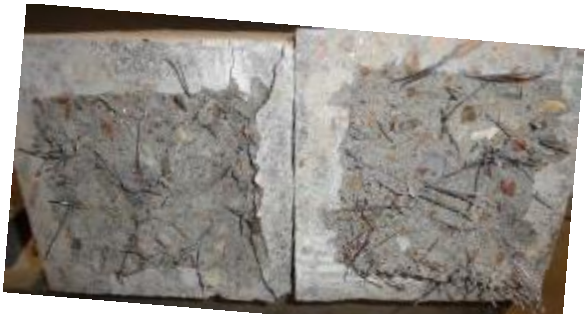
SP 2 117 fibers	
SP 3 148 fibers	
SP 4 80 fibers	
SP 5 153 fibers	

Batch 12: $f_c^{`} = 6$ ksi; $V_f = 1.5\%$; Fiber: 4D (RC-65/60-BG)

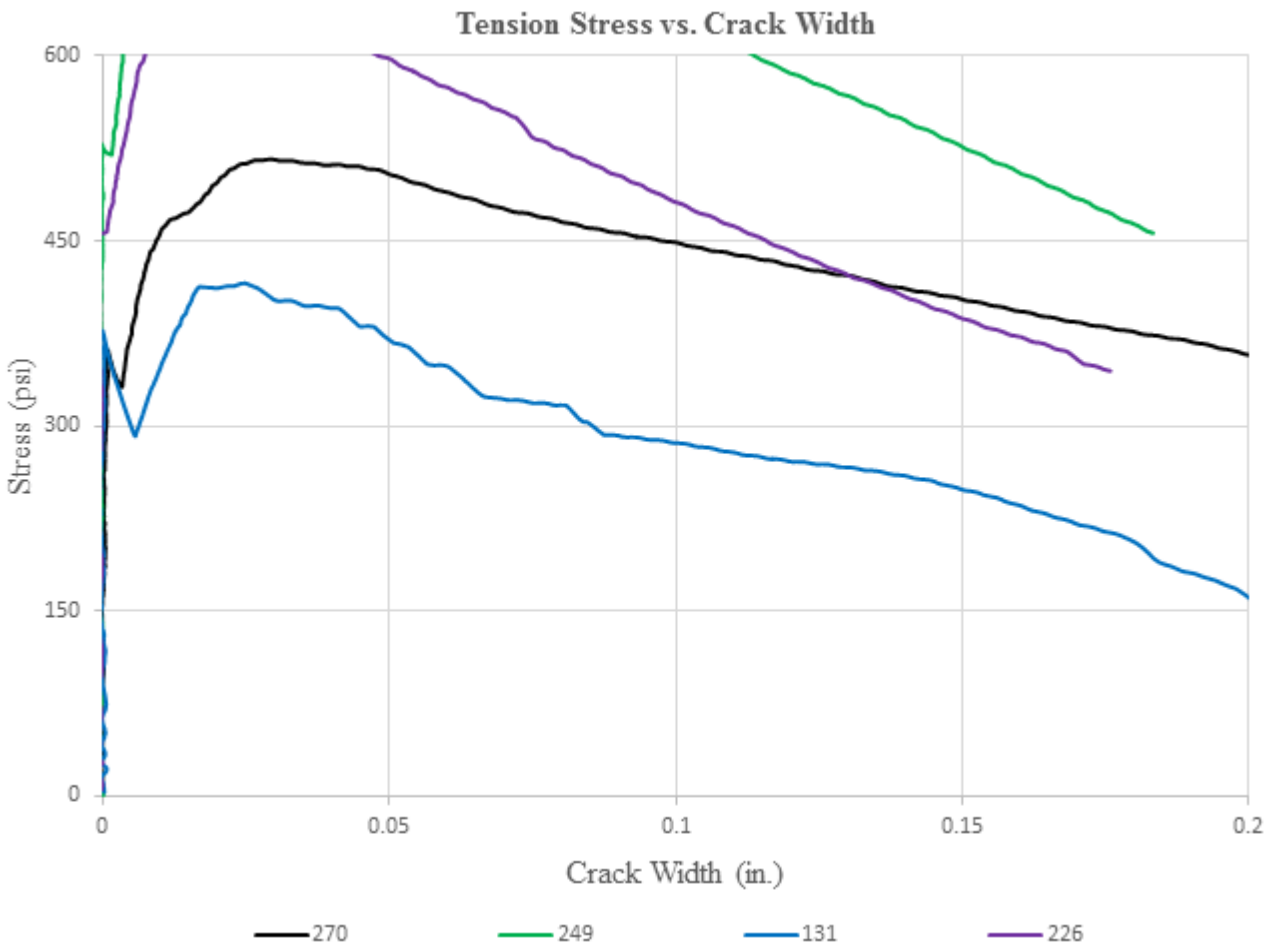

Batch ID	Fiber type				V_f (%)
B 12	4D (RC-65/60-BG)				1.5
σ_1 (psi)	ω_1 (in.)	σ_{pc} (psi)	ω_{pc} (in.)	$COV(\sigma_{pc})$	σ_{max} (psi)
430	0.000	590	0.028	27%	590
σ_2 (psi)	ω_2 (in.)	$\sigma_{\omega=0.05\ in.}$ (psi)	$\sigma_{\omega=0.10\ in.}$ (psi)	$\sigma_{\omega=0.15\ in.}$ (psi)	$\sigma_{\omega=0.25\ in.}$ (psi)
400	0.003	550	460	390	340
Comment: dominated by fiber pullout and fiber fracture.					

SP 1 270 fibers	
SP 2 291 fibers	
SP 3 249 fibers	
SP 4 131 fibers	
SP 5 226 fibers	

Batch 13: $f_c^{`} = 6$ ksi; $V_f = 0.75\%$; Fiber: 5D (RC-65/60-BG)

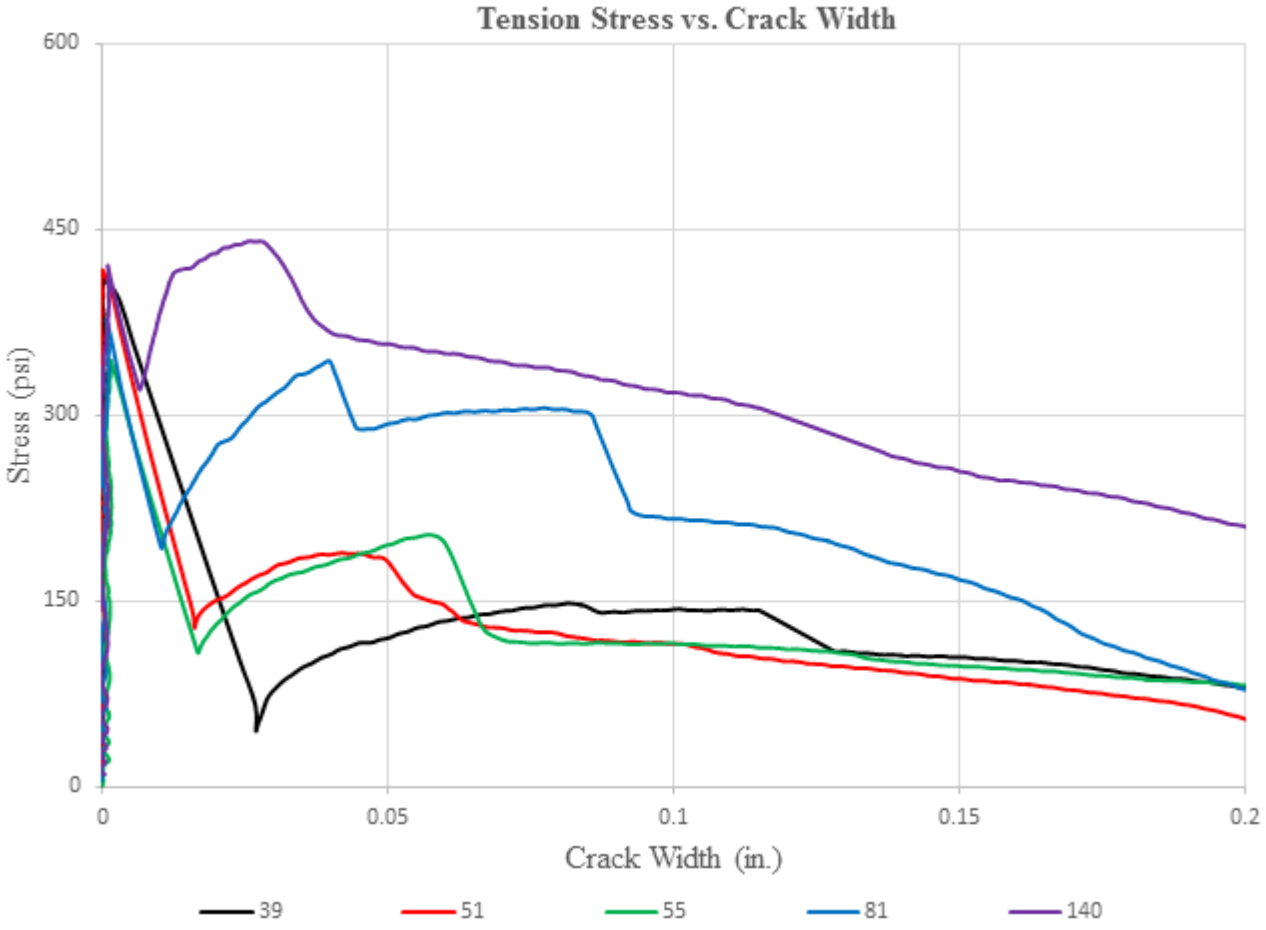

Batch ID	Fiber type				V_f (%)
B 13	5D (RC-65/60-BG)				0.75
σ_1 (psi)	ω_1 (in.)	σ_{pc} (psi)	ω_{pc} (in.)	$COV(\sigma_{pc})$	σ_{max} (psi)
395	0.000	265	0.05	47%	395
σ_2 (psi)	ω_2 (in.)	$\sigma_{\omega=0.05\ in.}$ (psi)	$\sigma_{\omega=0.10\ in.}$ (psi)	$\sigma_{\omega=0.15\ in.}$ (psi)	$\sigma_{\omega=0.25\ in.}$ (psi)
160	0.015	230	180	140	95
Comment: brittle failure, some fiber bundles, dominated by fiber pullout and fiber fracture.					

SP 1 39 fibers	
SP 2 51 fibers	
SP 3 55 fibers	
SP 4 81 fibers	
SP 5 140 fibers	

Batch 14: $f_c^{`} = 6$ ksi; $V_f = 1.5\%$; Fiber: 5D (RC-65/60-BG)

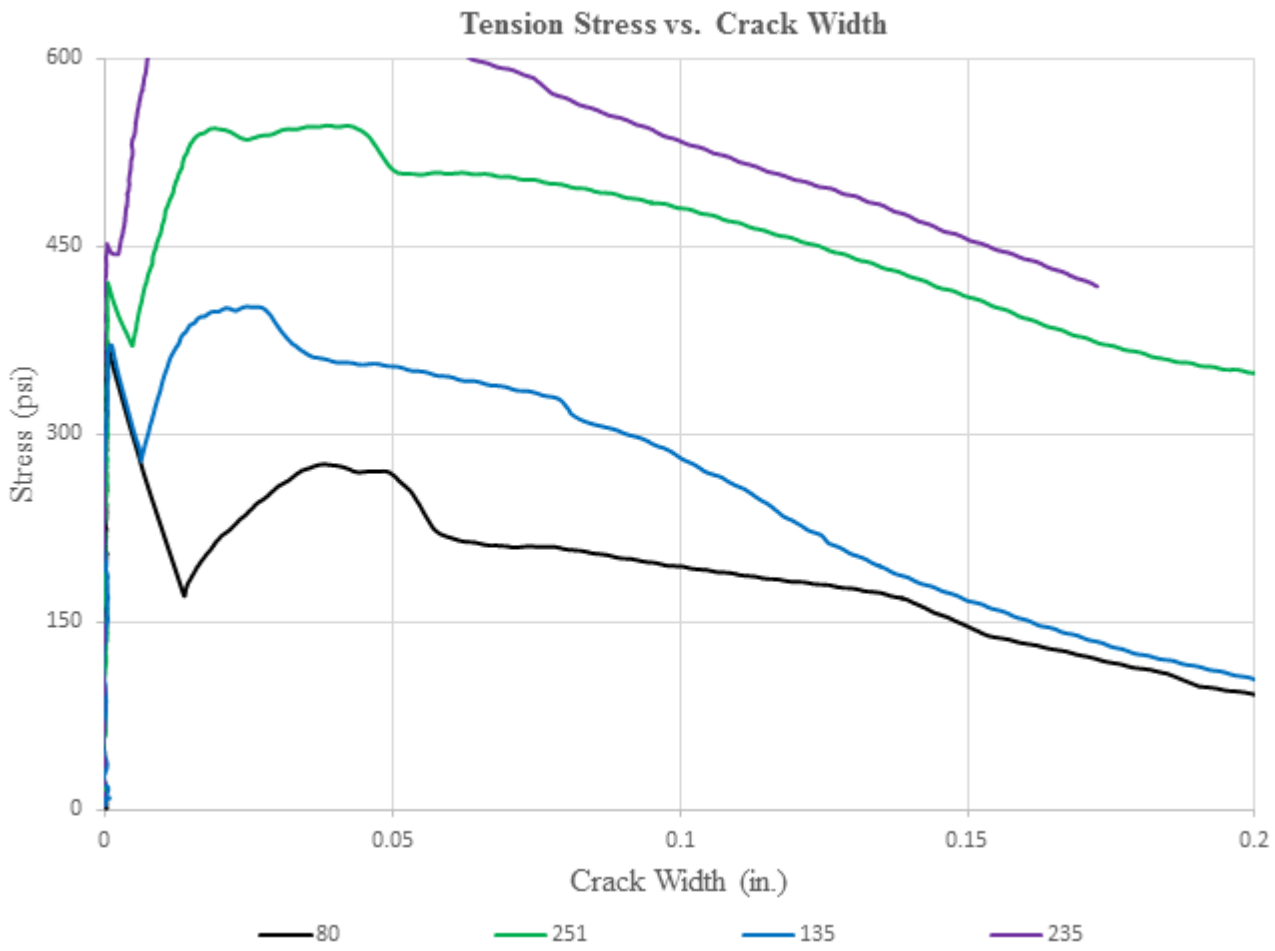

Batch ID	Fiber type				V_f (%)
B 14	5D (RC-65/60-BG)				1.5
σ_1 (psi)	ω_1 (in.)	σ_{pc} (psi)	ω_{pc} (in.)	$COV(\sigma_{pc})$	σ_{max} (psi)
405	0.001	470	0.033	36%	470
σ_2 (psi)	ω_2 (in.)	$\sigma_{\omega=0.05\ in.}$ (psi)	$\sigma_{\omega=0.10\ in.}$ (psi)	$\sigma_{\omega=0.15\ in.}$ (psi)	$\sigma_{\omega=0.25\ in.}$ (psi)
315	0.007	440	370	295	215
Comment: some fiber bundles, dominated by fiber pullout and fiber fracture.					

SP 1 80 fibers	
SP 2 250 fibers	
SP 3 251 fibers	
SP 4 135 fibers	
SP 5 235 fibers	

Control 2: $f_c^{`} = 10$ ksi

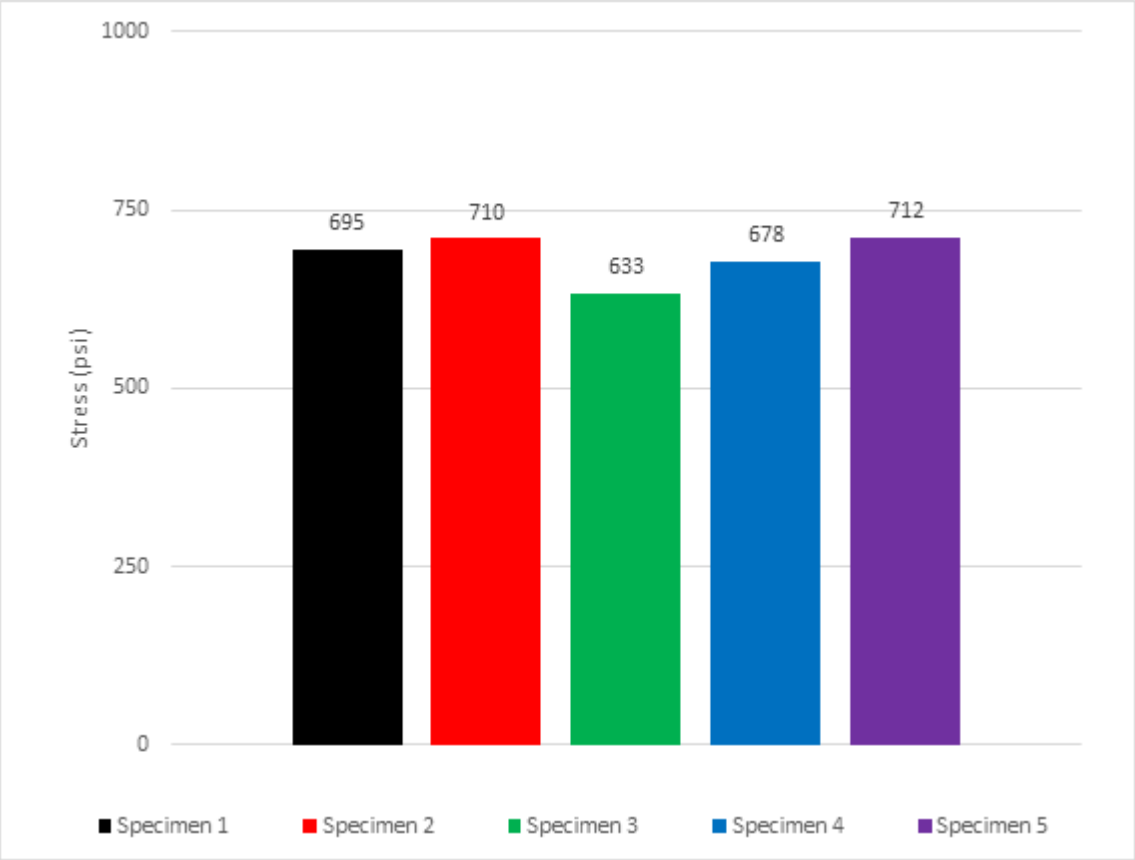

Batch ID	Fiber type				V_f (%)
C 2	N/A				0
σ_1 (psi)	ω_1 (in.)	σ_{pc} (psi)	ω_{pc} (in.)	$COV(\sigma_{pc})$	σ_{max} (psi)
685	0	0	0	0%	685
σ_2 (psi)	ω_2 (in.)	$\sigma_{\omega=0.05\ in.}$ (psi)	$\sigma_{\omega=0.10\ in.}$ (psi)	$\sigma_{\omega=0.15\ in.}$ (psi)	$\sigma_{\omega=0.25\ in.}$ (psi)
0	0	0	0	0	0
Comment: all specimens failed suddenly after first crack.					

SP 1 0 fiber	
SP 2 0 fiber	
SP 3 0 fiber	
SP 4 0 fiber	
SP 5 0 fiber	

Batch 15: $f_c^{`} = 10$ ksi; $V_f = 0.5\%$; Fiber: (RC-80/30-BP)

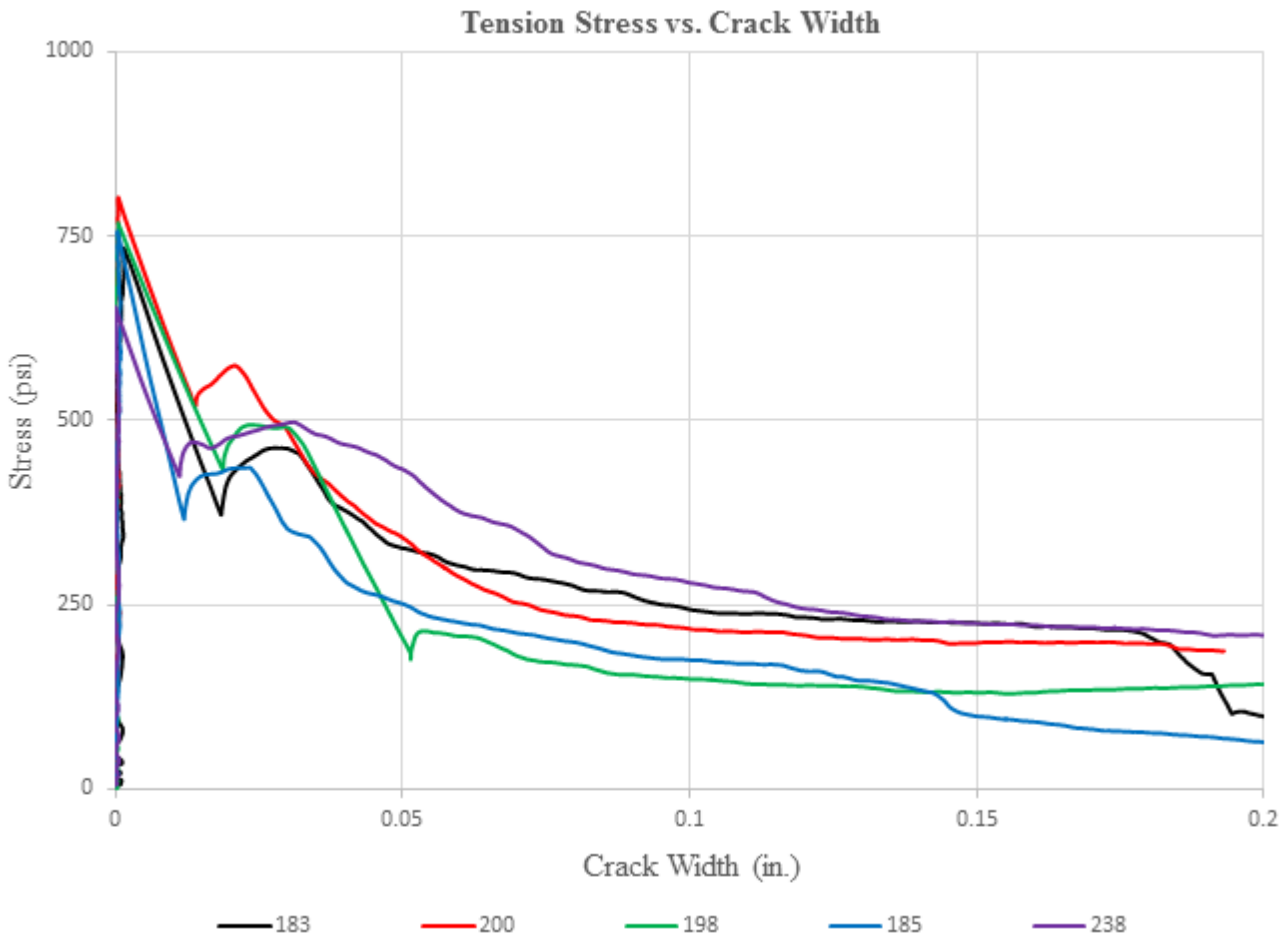

Batch ID	Fiber type				V_f (%)
B 15	(RC-80/30-BP)				0.5
σ_1 (psi)	ω_1 (in.)	σ_{pc} (psi)	ω_{pc} (in.)	$COV(\sigma_{pc})$	σ_{max} (psi)
745	0.001	490	0.028	10%	745
σ_2 (psi)	ω_2 (in.)	$\sigma_{\omega=0.05\ in.}$ (psi)	$\sigma_{\omega=0.10\ in.}$ (psi)	$\sigma_{\omega=0.15\ in.}$ (psi)	$\sigma_{\omega=0.25\ in.}$ (psi)
420	0.015	310	215	175	130
Comment: brittle failure, dominated by fiber pullout.					

SP 1 183 fibers	
SP 2 200 fibers	
SP 3 198 fibers	
SP 4 185 fibers	
SP 5 238 fibers	

Batch 16: $f_c^{`} = 10$ ksi; $V_f = 0.75\%$; Fiber: (RC-80/30-BP)

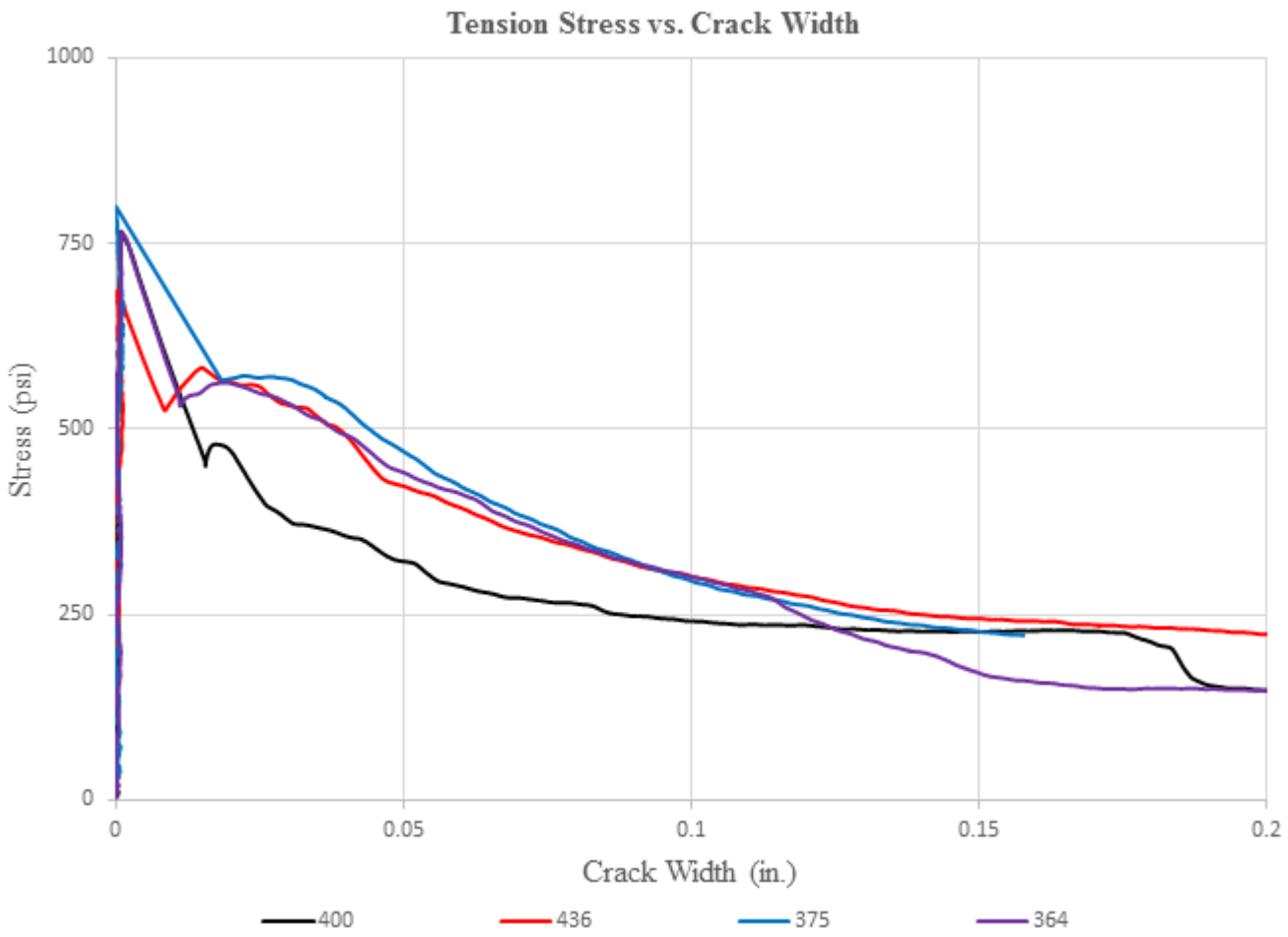

Batch ID	Fiber type				V_f (%)
B 16	(RC-80/30-BP)				0.75
σ_1 (psi)	ω_1 (in.)	σ_{pc} (psi)	ω_{pc} (in.)	$COV(\sigma_{pc})$	σ_{max} (psi)
755	0.001	545	0.021	9%	755
σ_2 (psi)	ω_2 (in.)	$\sigma_{\omega=0.05\ in.}$ (psi)	$\sigma_{\omega=0.10\ in.}$ (psi)	$\sigma_{\omega=0.15\ in.}$ (psi)	$\sigma_{\omega=0.25\ in.}$ (psi)
500	0.011	415	285	215	175
Comment: brittle failure, dominated by fiber pullout.					

SP 1 400 fibers	
SP 2 436 fibers	
SP 3 419 fibers	
SP 4 375 fibers	
SP 5 364 fibers	

Batch 17: $f_c^{`} = 10$ ksi; $V_f = 1.0\%$; Fiber: (RC-80/30-BP)

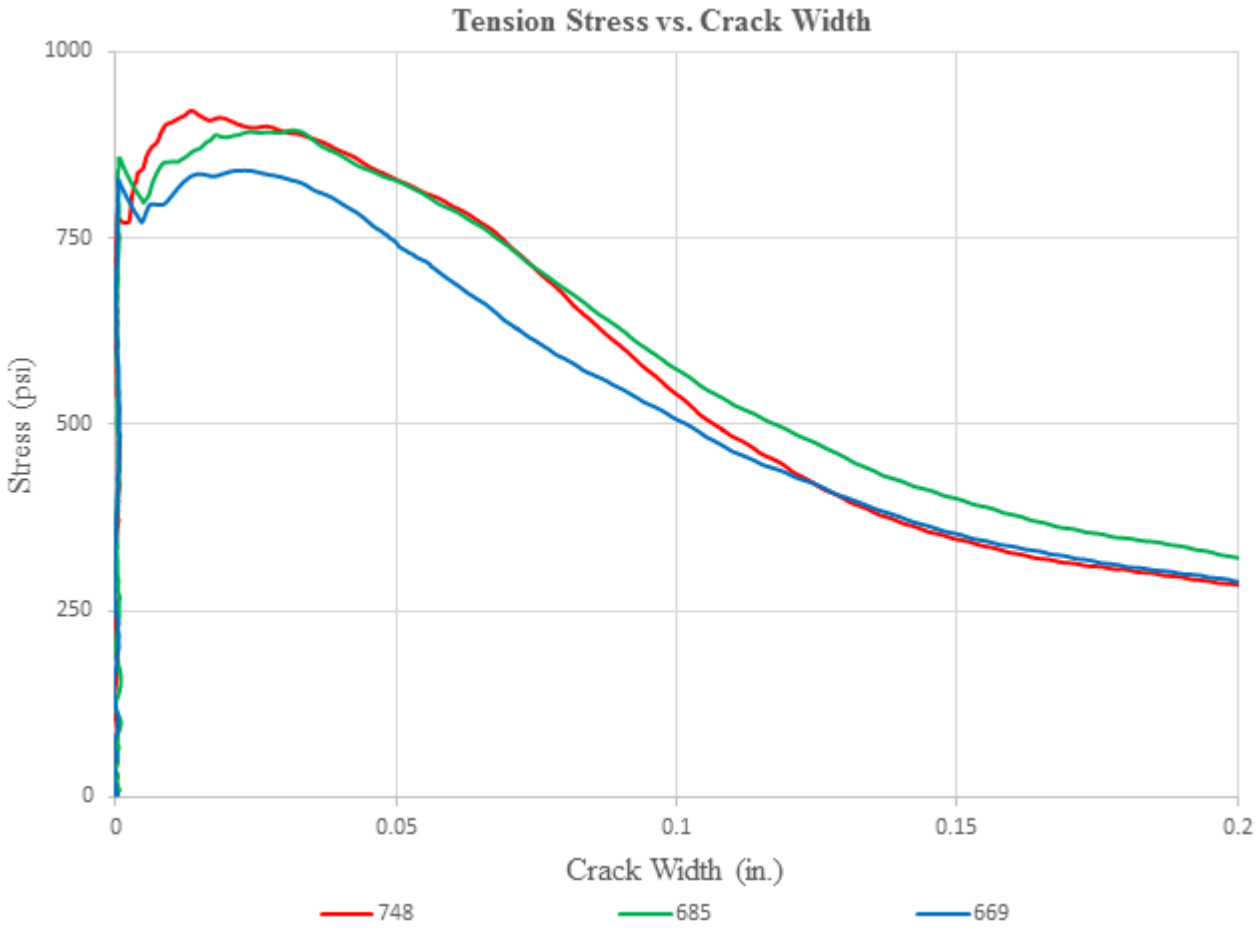

Batch ID	Fiber type				V_f (%)
B 17	(RC-80/30-BP)				1.0
σ_1 (psi)	ω_1 (in.)	σ_{pc} (psi)	ω_{pc} (in.)	$COV(\sigma_{pc})$	σ_{max} (psi)
820	0.001	885	0.023	5%	885
σ_2 (psi)	ω_2 (in.)	$\sigma_{\omega=0.05\ in.}$ (psi)	$\sigma_{\omega=0.10\ in.}$ (psi)	$\sigma_{\omega=0.15\ in.}$ (psi)	$\sigma_{\omega=0.25\ in.}$ (psi)
785	0.004	800	540	365	290
Comment: dominated by fiber pullout.					

SP 1 637 fibers	
SP 2 748 fibers	
SP 3 685 fibers	
SP 4 669 fibers	
SP 5 588 fibers	

Batch 18: $f_c^{`} = 10$ ksi; $V_f = 1.5\%$; Fiber: (RC-80/30-BP)

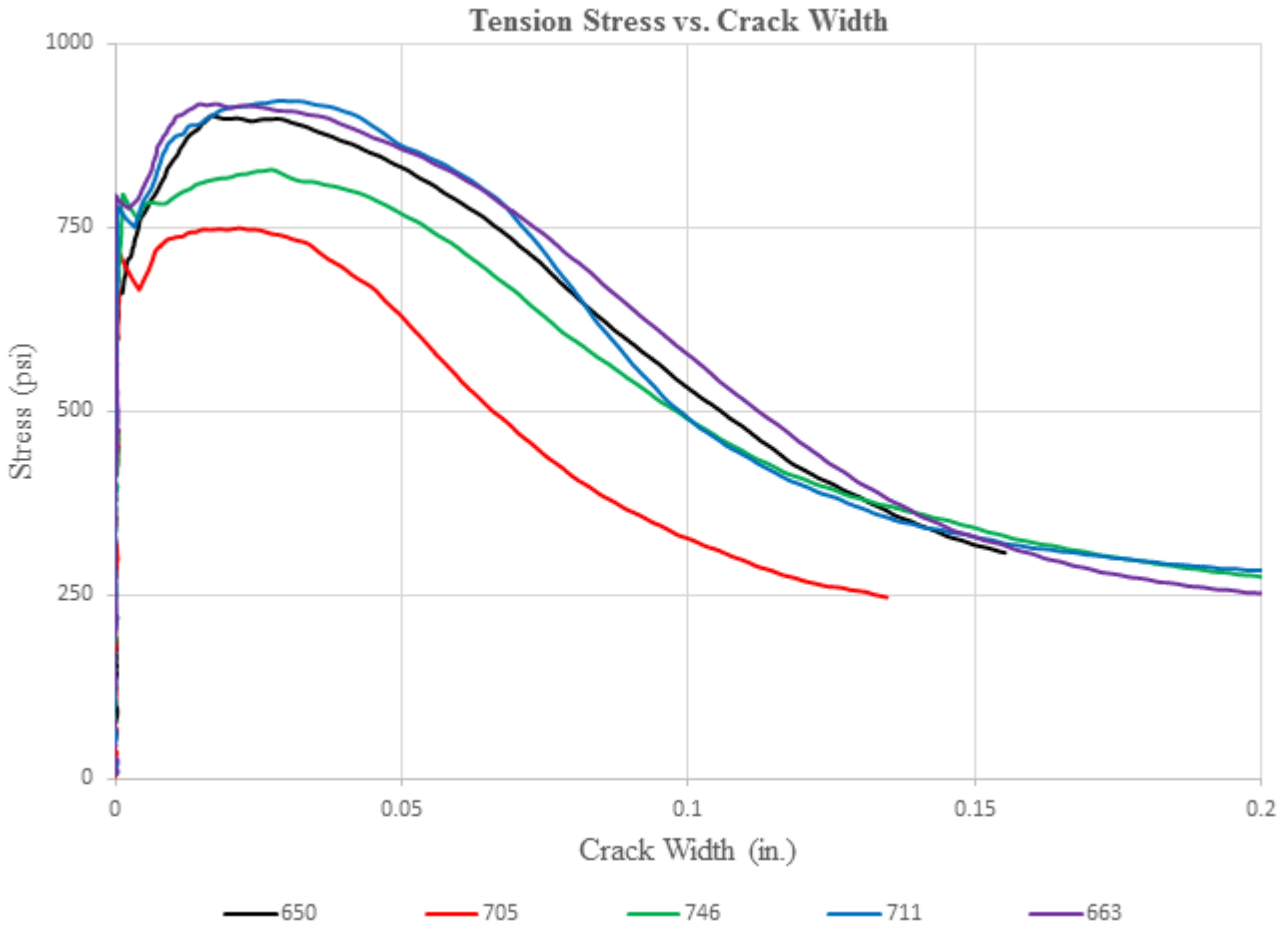

Batch ID	Fiber type				V_f (%)
B 18	(RC-80/30-BP)				1.5
σ_1 (psi)	ω_1 (in.)	σ_{pc} (psi)	ω_{pc} (in.)	$COV(\sigma_{pc})$	σ_{max} (psi)
745	0.001	865	0.023	9%	865
σ_2 (psi)	ω_2 (in.)	$\sigma_{\omega=0.05\ in.}$ (psi)	$\sigma_{\omega=0.10\ in.}$ (psi)	$\sigma_{\omega=0.15\ in.}$ (psi)	$\sigma_{\omega=0.25\ in.}$ (psi)
720	0.003	790	480	305	240
Comment: dominated by fiber pullout.					

SP 1 650 fibers	
SP 2 705 fibers	
SP 3 746 fibers	
SP 4 711 fibers	
SP 5 663 fibers	

Batch 19: $f_c^{`} = 10$ ksi; $V_f = 0.75\%$; Fiber: 4D (RC-65/60-BG)

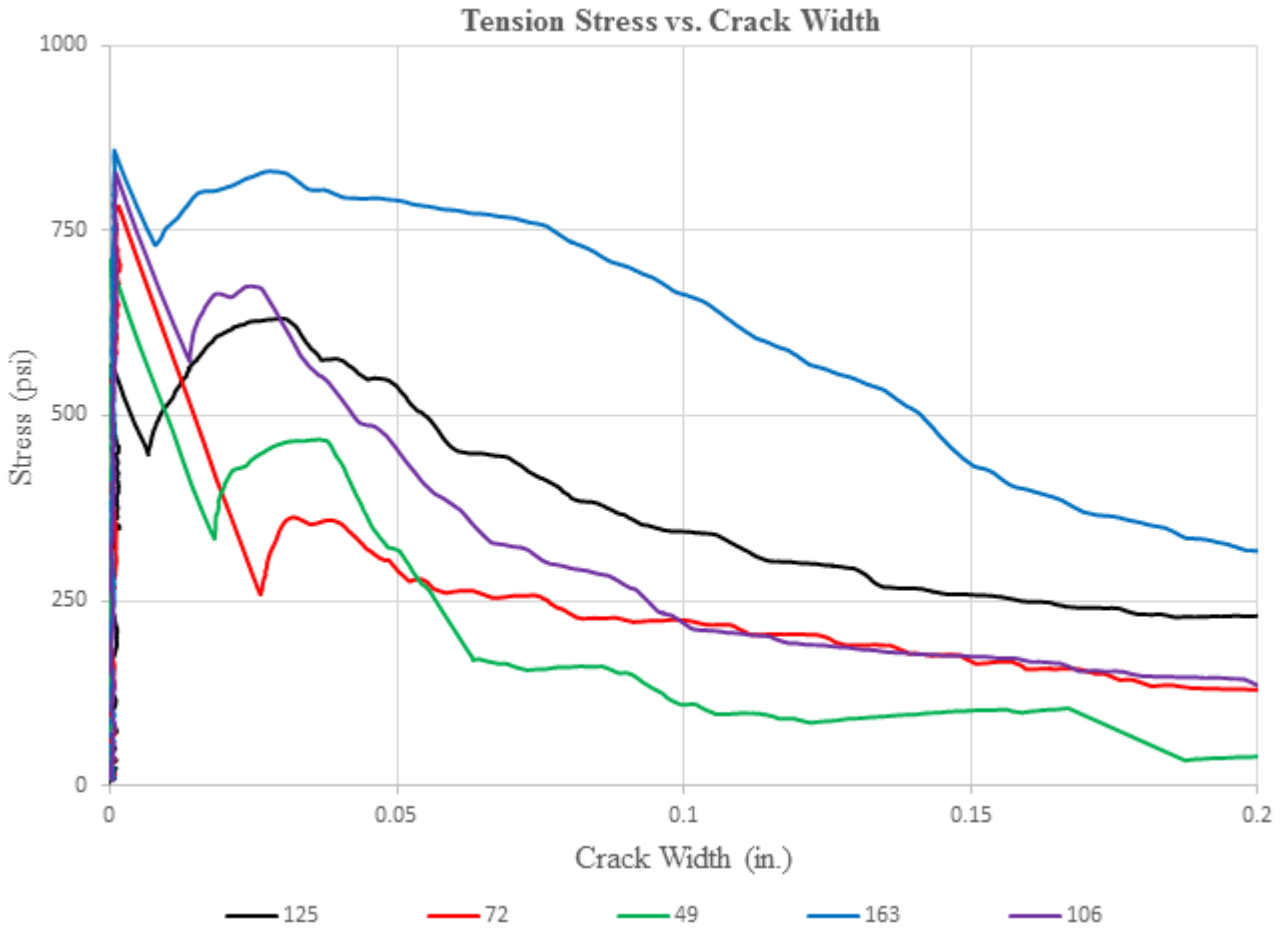

Batch ID	Fiber type				V_f (%)
B 19	4D (RC-65/60-BG)				0.75
σ_1 (psi)	ω_1 (in.)	σ_{pc} (psi)	ω_{pc} (in.)	$COV(\sigma_{pc})$	σ_{max} (psi)
750	0	595	0.03	31%	750
σ_2 (psi)	ω_2 (in.)	$\sigma_{\omega=0.05\ in.}$ (psi)	$\sigma_{\omega=0.10\ in.}$ (psi)	$\sigma_{\omega=0.15\ in.}$ (psi)	$\sigma_{\omega=0.25\ in.}$ (psi)
470	0.015	475	315	225	160
Comment: brittle failure, dominated by fiber pullout and fiber fracture.					

SP 1 125 fibers	
SP 2 72 fibers	
SP 3 49 fibers	
SP 4 163 fibers	
SP 5 106 fibers	

Batch 20: $f_c^{`} = 10$ ksi; $V_f = 1.5\%$; Fiber: 4D (RC-65/60-BG)

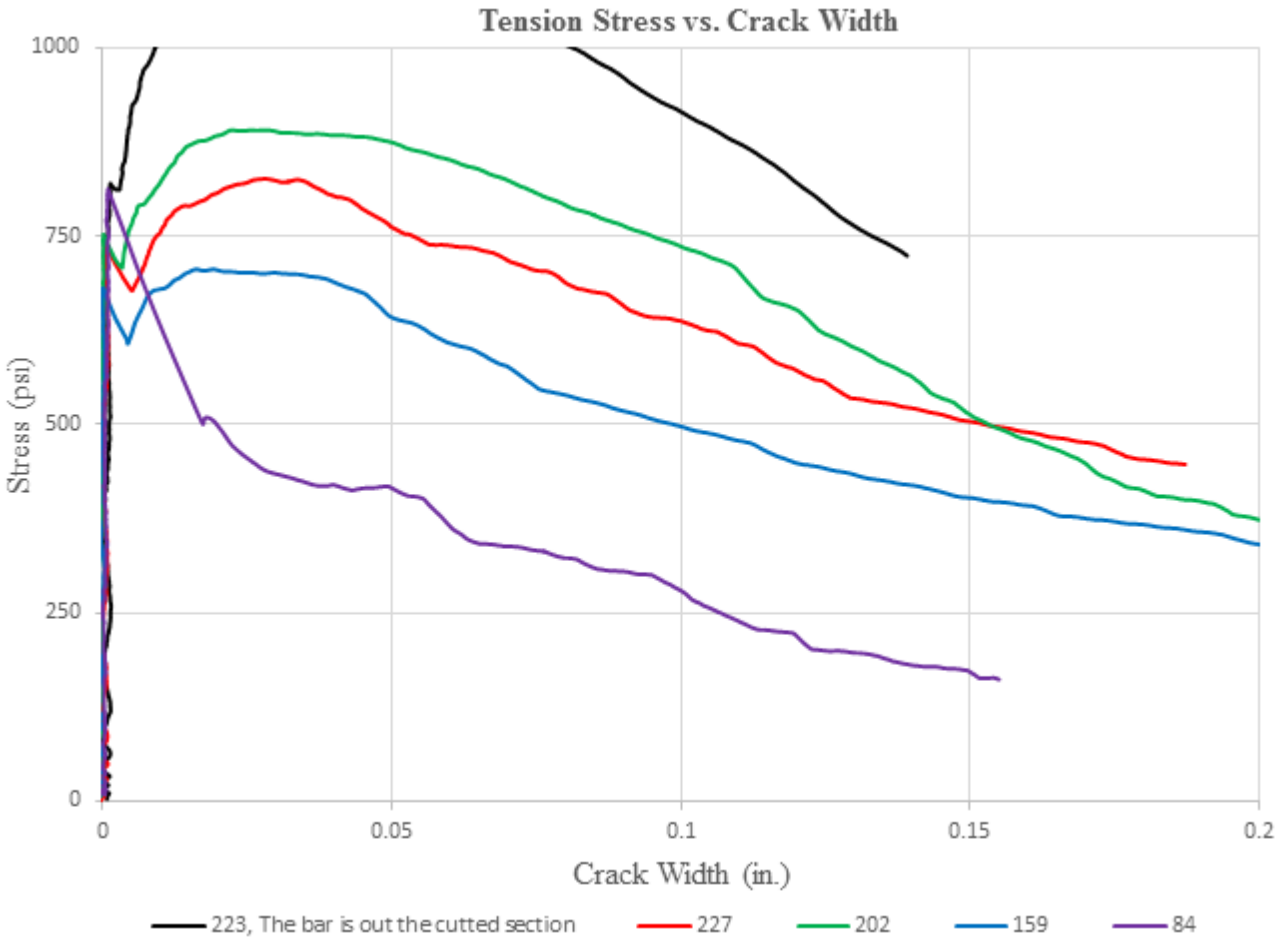

Batch ID	Fiber type				V_f (%)
B 20	4D (RC-65/60-BG)				1.5
σ_1 (psi)	ω_1 (in.)	σ_{pc} (psi)	ω_{pc} (in.)	$COV(\sigma_{pc})$	σ_{max} (psi)
760	0	790	0.030	33%	790
σ_2 (psi)	ω_2 (in.)	$\sigma_{\omega=0.05\ in.}$ (psi)	$\sigma_{\omega=0.10\ in.}$ (psi)	$\sigma_{\omega=0.15\ in.}$ (psi)	$\sigma_{\omega=0.25\ in.}$ (psi)
660	0.006	755	610	465	305
Comment: dominated by fiber pullout and fiber fracture.					

SP 1 223 fibers	
SP 2 227 fibers	
SP 3 202 fibers	
SP 4 159 fibers	
SP 5 84 fibers	

Batch 21: $f_c^{`} = 10$ ksi; $V_f = 0.75\%$; Fiber: 5D (RC-65/60-BG)

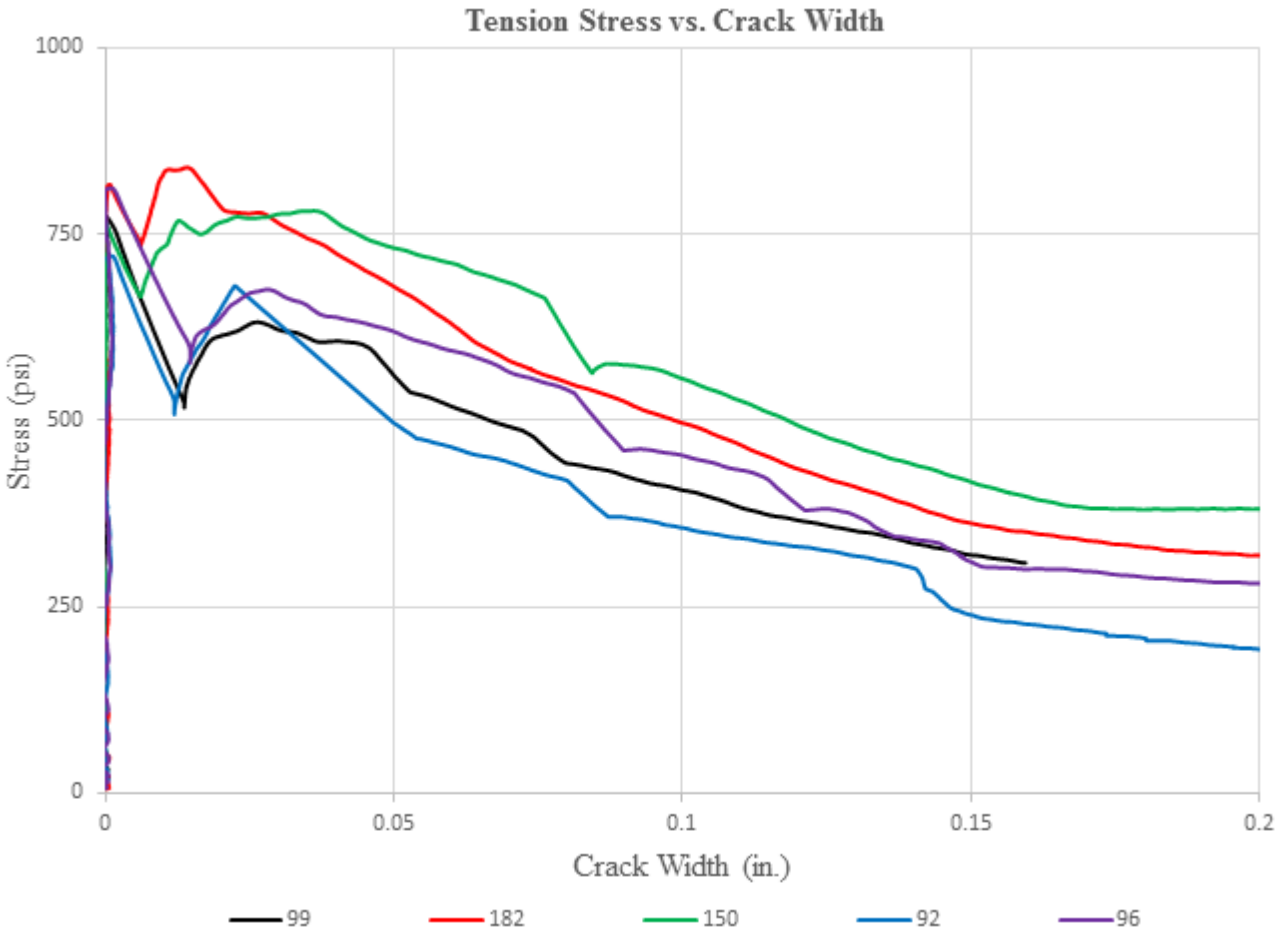

Batch ID	Fiber type				V_f (%)
B 21	5D (RC-65/60-BG)				0.75
σ_1 (psi)	ω_1 (in.)	σ_{pc} (psi)	ω_{pc} (in.)	$COV(\sigma_{pc})$	σ_{max} (psi)
775	0.001	720	0.025	12%	775
σ_2 (psi)	ω_2 (in.)	$\sigma_{\omega=0.05\ in.}$ (psi)	$\sigma_{\omega=0.10\ in.}$ (psi)	$\sigma_{\omega=0.15\ in.}$ (psi)	$\sigma_{\omega=0.25\ in.}$ (psi)
600	0.010	615	455	330	290
Comment: dominated by fiber pullout.					

SP 1 99 fibers	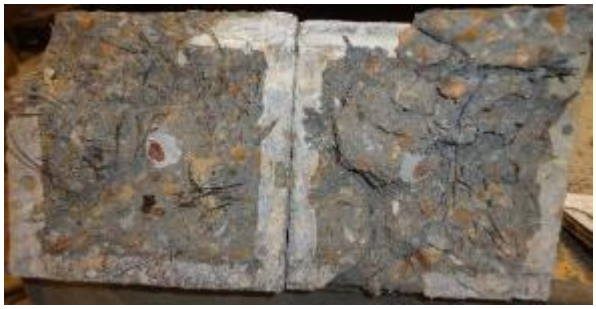
SP 2 182 fibers	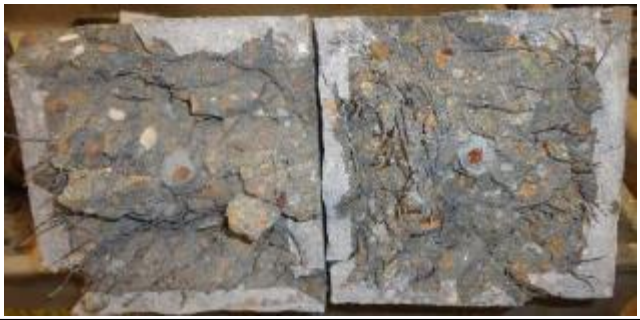
SP 3 150 fibers	
SP 4 92 fibers	
SP 5 96 fibers	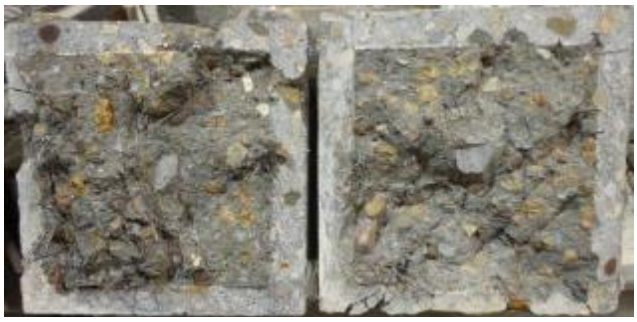

Batch 22: $f_c^{`} = 10$ ksi; $V_f = 1.5\%$; Fiber: 5D (RC-65/60-BG)

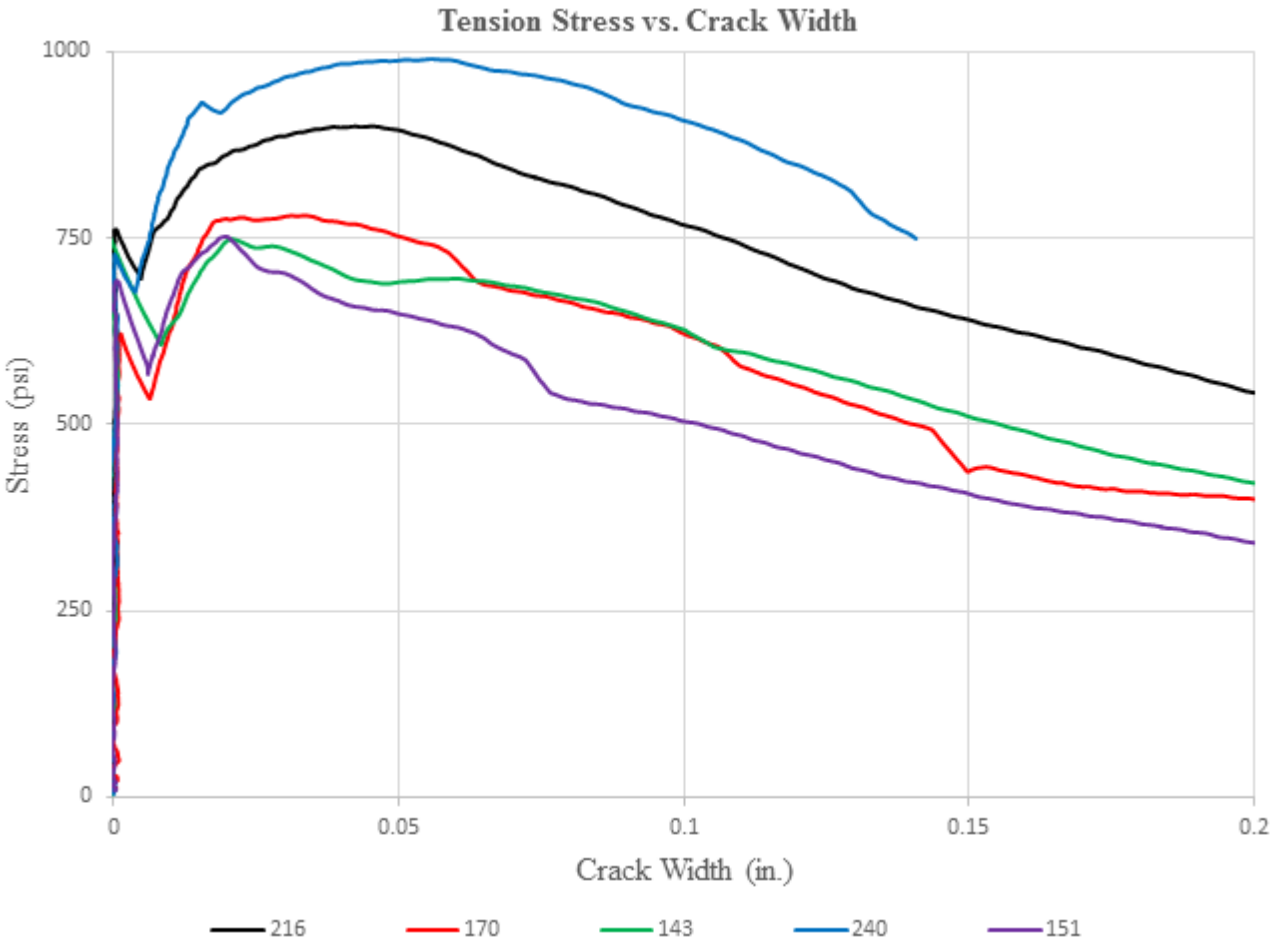

Batch ID	Fiber type				V_f (%)
B 22	5D (RC-65/60-BG)				1.50
σ_1 (psi)	ω_1 (in.)	σ_{pc} (psi)	ω_{pc} (in.)	$COV(\sigma_{pc})$	σ_{max} (psi)
710	0.001	835	0.036	13%	835
σ_2 (psi)	ω_2 (in.)	$\sigma_{\omega=0.05\ in.}$ (psi)	$\sigma_{\omega=0.10\ in.}$ (psi)	$\sigma_{\omega=0.15\ in.}$ (psi)	$\sigma_{\omega=0.25\ in.}$ (psi)
615	0.006	795	685	540	415
Comment: dominated by fiber pullout					

SP 1 216 fibers	
SP 2 170 fibers	
SP 3 143 fibers	
SP 4 240 fibers	
SP 5 151 fibers